

Duurzaamheid en milieu-impact van beton met hoge volumes vliegas

Durability and Sustainability of Concrete with High Volumes of Fly Ash

Philip Van den Heede

Promotor: prof. dr. ir. N. De Belie
Proefschrift ingediend tot het behalen van de graad van
Doctor in de Ingenieurswetenschappen: Bouwkunde

Vakgroep Bouwkundige Constructies
Voorzitter: prof. dr. ir. L. Taerwe
Faculteit Ingenieurswetenschappen en Architectuur
Academiejaar 2013 - 2014



ISBN 978-90-8578-715-0
NUR 955
Wettelijk depot: D/2014/10.500/61

Supervisor

prof. dr. ir. Nele De Belie

Research institute

Magnel Laboratory for Concrete Research
Department of Structural Engineering
Faculty of Engineering and Architecture
Ghent University, Belgium

Examination committee

prof. dr. ir. Luc Taerwe (chairman)
Ghent University
Faculty of Engineering and Architecture
Department of Structural Engineering

prof. dr. ir. Geert De Schutter (secretary)
Ghent University
Faculty of Engineering and Architecture
Department of Structural Engineering

dr. ir. Elke Gruyaert
Ghent University
Faculty of Engineering and Architecture
Department of Structural Engineering

prof. arch. Jan Moens
Ghent University
Faculty of Engineering and Architecture
Department of Architecture and Urban Planning

prof. dr. ir. Veerle Boel
Ghent University
Faculty of Engineering and Architecture
Department of Industrial Technology and Construction

prof. dr. Guillaume Habert
ETH Zürich (Switzerland)

dr. Jeanette Visser
TNO Delft (the Netherlands)

Research funding

As assistant I would like to thank Ghent University for the financial support.

Copyright © Philip Van den Heede 2014

All rights reserved. No part of this publication may be reproduced, stored in a retrieval system or transmitted in any form or by any means, electronic, mechanical, photocopying, recording or otherwise, without prior written permission of the author and his supervisor.

Alle rechten voorbehouden. Dit werk of delen ervan, mogen onder geen enkele voorwaarde en ook niet voor persoonlijk gebruik worden uitgeleend, gekopieerd of op één of andere manier vermenigvuldigd, zonder voorafgaande, schriftelijke toestemming van de auteur en zijn promotor.

My inspiration for perseverance in difficult times during my PhD research:

General McAuliffe's single-word reply to the
German ultimatum to surrender and give up Bastogne:

NUTS!

General Anthony Clement 'Nuts' McAuliffe,
Commander of the 101st Airborne Division troops defending Bastogne, Belgium,
December 22nd 1944.

We've never lost an American in space,
we're sure as hell not gonna lose one on my watch!

Failure is not an option.

Eugene Francis 'Gene' Kranz,
NASA flight director for the Apollo 13 mission (April 11-17th 1970),
in Ron Howard's Apollo 13 (Universal Pictures, 1995).

Dankwoord

Nu mijn doctoraatsproefschrift quasi volledig geschreven is, rest me nog één ding, namelijk het schrijven van een gepast dankwoord. Tijdens mijn onderzoek heb ik kunnen rekenen op de hulp en steun van heel wat mensen. Zonder hun helpende hand was dit proefschrift er wellicht nooit gekomen. Daarom wil ook de tijd nemen om iedereen uitdrukkelijk te bedanken.

Vooreerst wil ik dat uiteraard doen ten aanzien van mijn promotor professor Nele De Belie. Nele, Ik ben u veel dank verschuldigd omdat u mij destijds de kans hebt geboden om te doctoreren aan het Laboratorium Magnel voor Betononderzoek. Ik ben u zeer dankbaar voor de steun die u mij daarbij de voorbije jaren bood. Daarnaast ben ik u ook heel erkentelijk omdat ik in het kader van mijn onderzoek een mooi stukje van de wereld heb mogen zien. Dit alles stimuleerde mij om telkens opnieuw voor de maandelijkse celvergadering een poging te doen om voor de dag te komen met een originele en liefst grappige “attention getter” bij het begin van mijn presentaties. Dit was een beetje mijn manier om steeds weer dankuwel te zeggen. Dankzij uw aanstekelijk enthousiasme ben ik immers tot op het einde in mijn onderzoek blijven geloven. Het was mij dan ook een waar genoegen om tot op heden deel te kunnen uitmaken van de onderzoeksgroep Beton & Milieu.

Een bijzonder woord van dank wil ik richten tot Elke en Gert, mijn twee thesisbegeleiders van weleer. Jullie waren de eersten die me in mijn masterproefjaar wegwijs hebben gemaakt in de wondere wereld van het wetenschappelijk onderzoek. Jullie tips en adviezen zijn zonder twijfel een grote hulp geweest. Ze hebben mij dan ook gesterkt in mijn keuze om voor een doctoraat te gaan. Daarbij heb ik de mogelijkheid gehad om jullie niet alleen als begeleiders, maar ook als toffe collega's te leren kennen. Toch zullen jullie altijd een beetje mijn twee begeleiders blijven naar wie ik steeds zal opkijken. Elke, ik vond het dan ook een hele eer dat jij deel wou uitmaken van mijn examencommissie!

Aan alle andere leden van de examencommissie (prof. Luc Taerwe, prof. Geert De Schutter, prof. Jan Moens, prof. Veerle Boel, prof. Guillaume Habert en dr. Jeanette Visser) wil ik eveneens mijn dank betuigen omdat ze bereid waren om binnen een relatief kort tijdsbestek mijn volledig proefschrift grondig door te nemen. Jullie interessante commentaren, adviezen

en vragen hebben zeer zeker hun waarde gehad bij de verdere optimalisatie van dit proefschrift.

Mijn dank gaat ook uit naar het voltallige ZAP-kader van ons laboratorium. Ik ben professor Luc Taerwe dankbaar omdat ik gedurende al deze jaren kon vertoeven in een prachtig laboratorium met een grote verscheidenheid aan apparatuur die in weinig andere labo's voorhanden is. Meermaals heb ik tijdens mijn proeven die niet zelden tot na de uren duurden, rondgedwaald doorheen het labo. Ik heb me toen gerealiseerd wat voor een aangename werkplek dit wel is. De professoren Geert De Schutter en Stijn Matthys wil ik bedanken voor hun vele deskundige raadgevingen, niet alleen met betrekking tot mijn onderzoek, maar ook aangaande wetenschappelijke dienstverlening en onderwijs. Ook professor Robby Caspeele wil ik uitdrukkelijk vermelden. Robby, bij jou kon ik steeds terecht als ik met statistische en probabilistische vragen zat. Meermaals heb je mijn onderzoek op dat vlak een flink stuk vooruit geholpen, waarvoor mijn beste dank!

Dit doctoraatsproefschrift was er überhaupt niet gekomen zonder de hulp van al het technisch personeel dat werkzaam is binnen ons laboratorium. Tommy, Bart D.W., Sandra, Jan, Peter V.d.b., Nicolas C., Dieter, Peter L., Tom, Nathan, Stefan en Marc, zonder jullie bijstand was er van mijn vrij uitgebreid proefprogramma wellicht niet veel in huis gekomen. Alleszins bedankt daarvoor! Peter V.d.b. wil ik ook expliciet bedanken voor zijn expertise bij de niet alledaagse fenderproeven in het verre Balen. Peter, in jouw aanwezigheid was ik er altijd vrij gerust in dat alles in orde zou komen. Een extra dikke merci ook aan Bart D.W. om in de eindfase van mijn doctoraat de gecrashte harde schijf van mijn laptop alsnog te redden. Uiteraard heb ik niet alleen lovende woorden voor al jullie geleverde inspanningen op technisch vlak. Ik ben ook uitermate dankbaar voor de gezellige praatjes tussendoor over gedeelde interesses (film, muziek, oldtimers, geschiedenis, sport, quizen, huisdieren, ...). Dergelijke gesprekken hebben er dikwijls voor gezorgd dat een op het eerste zicht tegenvallende dag toch nog de moeite waard bleek. Hetzelfde geldt trouwens ook voor de mensen van het administratief personeel. Viviane, Marijke en Christel, jullie hebben me dikwijls bijgestaan bij administratieve rompslomp allerhande (de aankoop van materiaal, het boeken van dienstreizen, het finaal afhandelen van kalibraties, ...). Daarnaast waren jullie echter ook fantastische collega's waarmee je al eens een gezellig babbeltje kon slaan!

Tijdens mijn onderzoek ben ik ook verschillende keren gaan aankloppen bij andere departementen binnen onze universiteit. Ik denk daarbij vooral aan de Vakgroep Anorganische en Fysische Chemie en de Vakgroep Analytische Chemie van de Faculteit Wetenschappen. Binnen de eerste vakgroep wil ik vooral Els, Koen, Kenny en Glenn bedanken voor de geleverde hulp bij de TGA-analyses. Binnen de tweede vakgroep gaat mijn dank vooral uit naar de onderzoeksgroep van prof. Annemie Adriaens. Alice en Michel, bedankt omdat jullie zoveel geduld hebben geïfend bij mijn langdurige corrosiepotentiaalmetingen!

Terloops ben ik ook ten rade kunnen gaan bij mensen die geen deel uitmaakten van onze universiteit. Zo ben ik onder meer terecht gekomen bij het WTCB in Limelette voor carbonatatieproeven bij 1% CO₂. Ik kon er mijn proefstukken telkens toevertrouwen aan de

goede zorgen van de heer Patrick Van Huffel, waarvoor mijn oprechte dank. Naar aanleiding van mijn maandelijks uitstap richting Limelette om proefstukken op te halen heb ik zelfs het prachtige meer van Genval mogen ontdekken. Deze locatie was me voordien totaal onbekend. Het illustreert eens te meer dat de uitdrukking ‘ken uw land’ wel degelijk steek houdt.

Ik wil ook prof. Rob Polder van TU Delft en ir. Joost Gulikers van Rijkswaterstaat in Utrecht danken omwille van hun deskundig advies inzake corrosiepotentiaalmetingen en levensduurvoorspellingen in een chloride-omgeving.

Ook ben ik de zes scriptiestudenten die ik in de afgelopen jaren heb mogen begeleiden, erkentelijk. Mieke, Jan, Christophe, Jamie, Laurens en Renée, jullie hebben deels bijgedragen tot het welslagen van mijn onderzoek. Mijn welgemeende dank daarvoor! Het was zeker ook een meerwaarde om jullie visie te horen in het hele vliegverhaal. Ik ben ook trots op het feit dat ik althans één van jullie heb weten te motiveren om net als ik te kiezen voor een doctoraat. Mieke, je was een thesisstudente uit de duizend!

Uiteraard mag ik ook mijn eerste bureaugenoten niet vergeten. Toen ik in september 2008 als doctoraatsstudent begon, kreeg ik meteen een plek toegewezen in het beruchte eerste bureau op de gang, toen bezet door grapjassen van dienst Lander en Willem. Al snel bleek dat we op heel wat punten op dezelfde golflengte zaten. We hebben dan ook in die beginperiode heel wat afgelachen tussen het werken door en vooral op vrijdagnamiddag. Willem, ik zou je speciaal willen bedanken voor het organiseren van de eerste quiz van “VK De Flamingo’s”. Daarmee heb je ervoor gezorgd dat ik mijn eerste stappen heb gezet in het quizmilieu. Samen met Tommy, Christel en Nicolas R. ben ik toen naar Waarschoot getrokken om er de eer van het labo met hand en tand te verdedigen. Het smaakte direct naar meer en de stichting van quizploeg “De Betondraaiers” was meteen een feit. Sindsdien zijn we deze hobby blijven beoefenen, waarvoor ik jullie dankbaar ben. Ook dank aan alle andere “Betondraaiers” die sindsdien de uitdaging hebben aangegaan om verder mee te quizen. Ik denk aan Brenda, Peter D., Pieter, Mieke, Didier, Pieterjan, Peter L., Tim, Tom, Mathias,... Het waren telkens zeer aangename quizavonden!

De bureaubezetting is echter niet altijd dezelfde gebleven. Lander ging en er kwam iemand uit het verre oosten in de plaats: Jianyun! Together with Nele we went to our first conference in Ancona, Italy. Afterwards, we stayed a bit longer because we both wanted to visit Rome while we were in the neighbourhood. It was truly an unforgettable travel experience! A genuine Roman holiday! Thank you so much! You will always be a very good friend! I will never forget about you!

Mathias was de andere nieuwe bureaugenoot. In het kader van wetenschappelijke congressen zijn we samen naar Wenen en Kyoto getrokken. Mathias, in jouw gezelschap was het daar telkens zeer aangenaam vertoeven, waarvoor mijn oprechte dank. Ook bedankt voor de altijd leuke en interessante nabeschouwingen na het weekend over wellicht de twee meest belangrijke bijzaken ter wereld (althans in België), namelijk wielrennen en voetbal. Het was iets om naar uit te kijken op maandag. Het was ook goed dat ik steeds met jou kon overleggen als ik vast zat met mijn onderzoek. Een oplossing werd misschien niet altijd meteen

gevonden, maar het feit dat ik gewoon al eens mijn problemen kwijt kon, betekende al veel voor mij.

De meest recente nieuwkomer was Ali. Ali, thank you very much for all the interesting talks we had about the history of your home country Iran. Thank you as well for sharing your delicious cookies and nuts in the office!

Enkel mijn bureaugenoten bedanken is uiteraard niet voldoende. Daarvoor was het net iets te aangenaam vertoeven binnen de onderzoeksgroep ‘Beton & Milieu’. Gert, Willem, Nicolas R., Elke, Anibal, Pepa, Pavel, Frederik, Kim, Jianyun, Mieke, Didier, Mathias, Joris, Sandra, Hugo, João, Adelaide, Arn, Eleni, Yusuf, Romy, Ali, Desirée and Julia, ik wil jullie allemaal bedanken voor de celvergaderingen die we samen wisten te overleven in een opperbste sfeer. Ook wil ik me nog eens speciaal richten tot Mieke. Zoals je je wellicht nog herinnert, zijn we ongeveer in dezelfde periode aan de slag gegaan met het schrijven van ons doctoraatsproefschrift. Je bemoedigende woorden in periodes dat ik het niet altijd meer zag zitten waren van onschatbare waarde! Hartelijk dank voor je onvoorwaardelijke steun!

Ook de andere collega’s mag ik zeker niet vergeten. Zij zorgden mee voor de aangename sfeer tijdens de vele middagpauzes, recepties, barbecues, enz. Tim, Pieterjan, Katrien, Dimitri, Nicky, Peter D.P., Brenda, Emmanuel, Pieter, Bart C., Geoffrey, Jeroen, Ruben, Farid en Serge, bedankt voor alles! Dorleta, Aniello, Lucy, Gao, Corina, Florent, Dirk, Elena, Tina, Kubo, Hai Dang, Raul, Jiang Wei, Kai Wu, Yang, Lijie, Kunpeng, Chris and Joshua, thank you very much for all the good times we spent together!

I also want to thank some of the Chinese colleagues in particular. I’m thinking of Qian, Liu, Tan and Mu. I remember all the interesting talks we had in the lab about movies, Western and Chinese culture, travel, etc. Liu and Mu, I will never forget the conference in Hong Kong we attended together. You both were excellent guides! Liu, the football match AA Gent – KV Mechelen we went to see together will also be kept in my memories forever!

Tot slot kan ik niet nalaten om even stil te staan bij mijn naaste familie. Mijn broers Patrick en Pieter hebben er zeker en vast voor gezorgd dat ik de rompslomp van het dagdagelijks schrijven tijdens de afgelopen maanden af en toe eens kon vergeten. Jullie eigenzinnige commentaren bij de nieuws- en sportfeiten van de dag tijdens het journaal zitten daar zeker voor iets tussen. Na zo eens goed te hebben gelachen, kon ik er dikwijls weer met volle moed tegenaan. Ook onze gezamenlijke bezoeken aan de cinema, (hard)rockconcerten, bokswedstrijden, gitaarlessen en andere evenementen stelde ik altijd ten zeerste op prijs. Zelfs op momenten waarop er minder tijd was voor ontspanning, hielpen de goede herinneringen hieraan me telkens weer vooruit. Heel erg bedankt daarvoor!

Daarnaast ben ik mijn ouders ook bijzondere dank verschuldigd voor alle goede zorgen tijdens de afgelopen jaren. Papa, je hebt het zelf ook meegemaakt, een doctoraatsonderzoek loopt niet altijd over rozen. Het is een lange weg met veel “ups” en “downs” waarbij de morele weerbaarheid soms sterk op de proef wordt gesteld. Op zo’n momenten waren onze bezoeken aan oldtimerbeurzen en “historical war wheel”-evenementen of ritjes met onze eigen oldtimers voor mij een ware verademing. Ik ben je dan ook dankbaar dat we er samen

zo nu en dan op uit trokken zodat ik de negatieve energie opnieuw in iets positief kon ombuigen.

Mama en papa, ik heb van jullie alle kansen gekregen om te studeren en jullie hebben mij altijd onvoorwaardelijk gesteund tijdens mijn studies en mijn doctoraatsonderzoek. Bij jullie kon ik steeds en op gelijk welk ogenblik met al mijn problemen terecht. Zonder jullie was dit allemaal niet mogelijk geweest, vandaar een heel dikke merci!

Philip,

Ouwegem, 31 juli 2014

Table of contents

| | |
|-------------------------|-------|
| Dankwoord | i |
| Table of contents | vii |
| Notation index | xvii |
| Summary | xxiii |
| Samenvatting | xxix |

PART I: GENERAL INTRODUCTION

| | |
|--|-----------|
| 1. Fly ash as partial cement replacement in concrete | 3 |
| 1.1. Origin and basic properties | 3 |
| 1.1.1. Origin | 3 |
| 1.1.2. Basic properties | 4 |
| 1.1.3. Motives for its use in concrete | 6 |
| 1.1.3.1. Technological motives | 6 |
| 1.1.3.2. Environmental motives | 6 |
| 1.1.3.3. Economic motives | 6 |
| 1.2. The concept of high-volume fly ash (HVFA) concrete | 6 |
| 1.2.1. General definition | 6 |
| 1.2.2. Reasons for its still limited use in practice | 7 |
| 1.2.2.1. Existing regulations on the use of fly ash | 7 |
| 1.2.2.2. Limited proof of durability in severe environments | 7 |
| 1.2.2.3. Limited quantitative proof of a reduced environmental impact | 7 |
| 2. Life cycle assessment as tool for quantifying sustainability | 9 |
| 2.1. General principle | 9 |
| 2.2. Past and current use of the life cycle assessment methodology | 9 |
| 2.3. Existing bottlenecks when performing life cycle assessment of concrete | 11 |
| 2.3.1. Functional unit choice | 11 |

| | | |
|--------------------------------|---|-----------|
| 2.3.2. | Data collection..... | 11 |
| 2.3.3. | Choice of the allocation of impacts..... | 11 |
| 2.3.4. | Identification of the relevant environmental issues..... | 12 |
| 3. | A twofold research purpose..... | 13 |
| 3.1. | Quantifying the sustainability of HVFA and FA+SF concrete using LCA..... | 13 |
| 3.2. | Optimizing the LCA framework for sustainability studies of concrete | 15 |
| PART II: DURABILITY | | |
| <hr/> | | |
| 4. | Concrete mixtures | 19 |
| 4.1. | Materials applied..... | 19 |
| 4.1.1. | Ordinary Portland cement | 19 |
| 4.1.2. | Fly ash | 20 |
| 4.1.3. | Silica fume..... | 21 |
| 4.1.4. | Sand and aggregates | 22 |
| 4.1.5. | Superplasticizer | 23 |
| 4.1.6. | Air entraining agent..... | 23 |
| 4.2. | Evaluation of the previously developed HVFA concrete mixtures..... | 23 |
| 4.2.1. | Compositions of previously developed HVFA concrete..... | 23 |
| 4.2.2. | Comparison with OPC references | 25 |
| 4.2.3. | Comparison with FA concrete conforming to the k-value concept | 28 |
| 4.3. | Optimization approach 1: Increasing binder content / lowering W/B ratio..... | 30 |
| 4.3.1. | Preparatory study..... | 30 |
| 4.3.2. | Mixtures chosen for durability assessment | 31 |
| 4.4. | Optimization approach 2: Introduction of a third powder | 33 |
| 4.4.1. | Preparatory study..... | 33 |
| 4.4.2. | Mixtures chosen for durability assessment | 36 |
| 5. | Resistance to carbonation | 39 |
| 5.1. | Characterization of the deterioration mechanism and the environment..... | 39 |
| 5.1.1. | Literature review on the deterioration mechanism..... | 39 |
| 5.1.2. | Characterization of the concrete environment | 42 |
| 5.2. | Research methodology | 44 |
| 5.3. | Curing and sample preparation..... | 45 |
| 5.4. | Carbonation testing..... | 45 |
| 5.4.1. | Accelerated carbonation testing at 10% CO ₂ | 45 |
| 5.4.2. | Critical evaluation of accelerated carbonation testing | 46 |
| 5.4.3. | Comparative carbonation testing at 1% and 10% CO ₂ | 48 |
| 5.4.4. | Colorimetric measurement details | 48 |

| | |
|--|-----------|
| 5.4.5. Microscopic measurement details | 49 |
| 5.4.6. Carbonation rate and resistance..... | 50 |
| 5.5. Assessment of carbonation-induced changes in microstructure..... | 50 |
| 5.5.1. Thermogravimetric analysis (TGA) | 50 |
| 5.5.2. X-ray diffraction analysis (XRD)..... | 54 |
| 5.5.3. Mercury intrusion porosimetry (MIP)..... | 54 |
| 5.6. Results and discussion..... | 55 |
| 5.6.1. Colorimetrically versus microscopically assessed carbonation depths..... | 55 |
| 5.6.2. Colorimetrically measured accelerated and field carbonation coefficients... | 58 |
| 5.6.3. Influence of the applied CO ₂ concentration during carbonation testing | 62 |
| 5.6.3.1. Effect on the carbonation coefficient | 62 |
| 5.6.3.2. Effect on the chemistry of the carbonation reaction..... | 64 |
| 5.6.3.3. Effect on the mineralogical phases formed | 68 |
| 5.6.3.4. Effect on the pore structure | 73 |
| 5.6.3.5. Discussion | 75 |
| 5.7. Conclusions | 76 |
| 6. Resistance to chloride ingress..... | 77 |
| 6.1. Characterization of the deterioration mechanism and the environment..... | 77 |
| 6.1.1. Literature review on the deterioration mechanism..... | 77 |
| 6.1.1.1. Chloride-induced corrosion initiation and propagation | 77 |
| 6.1.1.2. Chloride diffusion | 78 |
| 6.1.1.3. Chloride migration | 79 |
| 6.1.1.4. Influencing factors related to the tested concrete compositions | 79 |
| 6.1.2. Characterization of the concrete environment | 80 |
| 6.2. Research methodology | 82 |
| 6.3. Curing, sample preparation and crack verification..... | 82 |
| 6.3.1. Uncracked concrete | 82 |
| 6.3.2. MBE mortar with an artificial crack | 83 |
| 6.3.3. Microscopic verification of the obtained crack widths | 84 |
| 6.4. Experimental assessment of concrete's resistance to chloride ingress | 85 |
| 6.4.1. The chloride migration test cf. NT Build 492 | 85 |
| 6.4.2. The accelerated chloride diffusion test cf. NT Build 443 | 85 |
| 6.4.3. A 'Natural' chloride diffusion test | 88 |
| 6.4.4. Potentiometric titration versus rapid chloride test..... | 88 |
| 6.5. Results and discussion..... | 89 |
| 6.5.1. Chloride migration coefficients..... | 89 |
| 6.5.2. Influencing factors of chloride diffusion testing | 91 |
| 6.5.3. Accelerated chloride diffusion coefficients and surface concentrations | 94 |
| 6.5.3.1. Chloride diffusion coefficients..... | 94 |
| 6.5.3.2. Chloride surface concentrations | 96 |

| | | |
|-------------|--|------------|
| 6.5.4. | ‘Natural’ chloride diffusion coefficients and surface concentrations | 98 |
| 6.5.4.1. | Chloride diffusion coefficients | 98 |
| 6.5.4.2. | Chloride surface concentrations | 99 |
| 6.5.5. | Causes of variation in chloride surface concentration..... | 101 |
| 6.5.6. | Time dependent decrease of the chloride diffusion coefficient | 105 |
| 6.5.7. | Resistance to chloride ingress of artificially cracked MBE mortars | 106 |
| 6.5.7.1. | Microscopic verification of cracks and crack widths | 106 |
| 6.5.7.2. | Chloride migration coefficients of the uncracked MBE mortars ... | 109 |
| 6.5.7.3. | Determination of the maximum crack width allowed | 109 |
| 6.6. | Conclusions | 110 |
| 7. | Resistance to freeze/thaw with deicing salts | 113 |
| 7.1. | Characterization of the deterioration mechanism and the environment | 113 |
| 7.1.1. | Literature review on the deterioration mechanism..... | 113 |
| 7.1.2. | Characterization of the concrete environment | 116 |
| 7.2. | Research methodology | 119 |
| 7.3. | Curing and sample preconditioning | 120 |
| 7.4. | Characterization of the concrete’s air void system | 121 |
| 7.4.1. | Evaluation in the fresh state: time dependent monitoring of air content | 121 |
| 7.4.2. | Evaluation using microscopic analysis on thin sections | 122 |
| 7.4.3. | Evaluation using automated air void analysis | 122 |
| 7.5. | Salt scaling resistance..... | 123 |
| 7.6. | Transport properties | 124 |
| 7.6.1. | Capillary sorption | 124 |
| 7.6.2. | Permeable porosity and degree of saturation | 125 |
| 7.6.3. | Gas permeability | 126 |
| 7.7. | Results and discussion..... | 128 |
| 7.7.1. | AEA dosage and initial air content in fresh state | 128 |
| 7.7.2. | Air void system in hardened state (thin section analysis) | 130 |
| 7.7.3. | Air void system in hardened state (automated air void analysis)..... | 131 |
| 7.7.4. | Salt scaling resistance..... | 137 |
| 7.7.5. | Capillary water sorption and degree of saturation | 140 |
| 7.7.6. | Permeable porosity | 143 |
| 7.7.7. | Gas permeability | 147 |
| 7.8. | General discussion..... | 149 |
| 7.8.1. | Relation: AEA dosage, air void system and salt scaling resistance | 149 |
| 7.8.2. | Relation: AEA dosage, air void system and transport properties | 152 |
| 7.9. | Conclusions | 153 |

PART III: SERVICE LIFE PREDICTION

| | |
|--|------------|
| 8. Service life prediction for carbonation-induced corrosion | 159 |
| 8.1. Choosing an appropriate prediction model and failure event | 159 |
| 8.2. First order probabilistic estimation of the corrosion initiation period | 160 |
| 8.2.1. Limit state function | 160 |
| 8.2.2. Field carbonation coefficient..... | 161 |
| 8.2.3. Concrete cover..... | 161 |
| 8.3. Second order probabilistic estimation of the corrosion initiation period | 162 |
| 8.3.1. Original limit state function of <i>fib</i> Bulletin 34..... | 162 |
| 8.3.2. Environmental function..... | 162 |
| 8.3.3. Execution transfer parameter | 163 |
| 8.3.4. Inverse effective carbonation resistance under natural conditions..... | 163 |
| 8.3.5. Weather function | 164 |
| 8.3.6. Applied limit state function based on <i>fib</i> Bulletin 34..... | 164 |
| 8.3.7. Summarizing overview of the model input parameters..... | 164 |
| 8.4. Semi-probabilistic estimation of the corrosion propagation period | 165 |
| 8.4.1. Limit state function of DuraCrete | 165 |
| 8.4.2. Corrosion penetration necessary to produce a crack..... | 166 |
| 8.4.3. Tensile splitting strength | 166 |
| 8.4.4. Occurring corrosion penetration..... | 167 |
| 8.4.5. Corrosion rate | 167 |
| 8.4.6. Potential electrolytical resistivity | 168 |
| 8.4.7. Summarizing overview of the model input parameters..... | 170 |
| 8.5. Results and discussion | 171 |
| 8.5.1. First order estimation of the corrosion initiation period | 171 |
| 8.5.2. Second order estimation of the corrosion initiation period | 172 |
| 8.5.3. Influence of the selected failure event..... | 174 |
| 8.6. Conclusions | 175 |
| 9. Service life prediction for chloride-induced corrosion | 177 |
| 9.1. Choosing an appropriate prediction model and failure event | 177 |
| 9.2. First order probabilistic estimation of the corrosion initiation period | 178 |
| 9.2.1. Limit state function of <i>fib</i> Bulletin 34..... | 178 |
| 9.2.2. Chloride migration coefficient | 178 |
| 9.2.3. Apparent chloride diffusion coefficient | 179 |
| 9.2.4. Environmental transfer variable | 179 |
| 9.2.5. Experimental transfer parameter and ageing exponent | 179 |
| 9.2.6. Concrete cover..... | 181 |
| 9.2.7. Initial chloride content | 181 |
| 9.2.8. Chloride content at the substitute surface | 182 |

| | |
|--|------------|
| 9.2.9. Critical chloride content | 183 |
| 9.2.10. Summarizing overview of the default model input parameters | 187 |
| 9.3. Second order probabilistic estimation of the corrosion initiation period | 188 |
| 9.3.1. Determination of the experimental transfer parameter | 188 |
| 9.3.2. Determination of the ageing exponent | 190 |
| 9.3.3. Determination of the critical chloride content..... | 192 |
| 9.3.4. Summarizing overview of the default and mix specific input parameters .. | 197 |
| 9.4. Semi-probabilistic estimation of the corrosion propagation period | 198 |
| 9.4.1. Limit state function of DuraCrete | 198 |
| 9.4.2. Summarizing overview of the model input parameters..... | 198 |
| 9.5. Results and discussion..... | 199 |
| 9.5.1. First order estimation of the corrosion initiation period | 199 |
| 9.5.2. Second order estimation of the corrosion initiation period | 200 |
| 9.5.3. Influence of the selected failure event..... | 201 |
| 9.6. Conclusions | 202 |

PART IV: LIFE CYCLE ASSESSMENT

| | |
|--|------------|
| 10. Literature review on life cycle assessment of traditional and ‘green’ concretes | 207 |
| 10.1. Introduction | 207 |
| 10.2. Environmental impact of concrete..... | 208 |
| 10.2.1. Composition | 208 |
| 10.2.1.1. Cement | 208 |
| 10.2.1.2. Cementitious materials | 211 |
| 10.2.1.3. Water | 214 |
| 10.2.1.4. Admixtures | 214 |
| 10.2.1.5. Fine and coarse aggregates..... | 215 |
| 10.2.2. Workability..... | 217 |
| 10.2.3. Strength and mechanical loading | 217 |
| 10.2.4. Durability, environment and service life prediction..... | 218 |
| 10.2.4.1. Environment specific durability based design approaches | 218 |
| 10.2.4.2. Service life prediction | 219 |
| 10.3. Life cycle assessment of concrete | 220 |
| 10.3.1. Definition of goal and scope | 221 |
| 10.3.1.1. Functional unit choice | 222 |
| 10.3.1.2. Other system boundaries | 223 |
| 10.3.1.3. Data quality | 223 |
| 10.3.2. Inventory analysis | 223 |
| 10.3.2.1. Data collection..... | 223 |
| 10.3.2.2. Allocation | 224 |
| 10.3.3. Impact analysis | 226 |

| | |
|--|------------|
| 10.3.3.1. The IPCC approach | 227 |
| 10.3.3.2. The Eco-indicator 99 approach | 227 |
| 10.3.3.3. The CML 2001 approach | 228 |
| 10.3.4. Interpretation | 228 |
| 10.4. Conclusions | 233 |
| 11. Applied LCA methodology | 235 |
| 11.1. Definition of goal and scope..... | 235 |
| 11.1.1. Functional unit choice | 235 |
| 11.1.1.1. One m ³ of concrete | 235 |
| 11.1.1.2. Concrete amount per unit of strength and service life..... | 235 |
| 11.1.1.3. Concrete column with a given load and service life | 236 |
| 11.1.1.4. Concrete slab with a given load and service life | 236 |
| 11.1.2. System boundaries..... | 237 |
| 11.2. Inventory analysis | 239 |
| 11.2.1. Inventory data for cement CEM I 52.5 | 239 |
| 11.2.2. Inventory data for fly ash | 241 |
| 11.2.3. Inventory data for silica fume | 245 |
| 11.2.4. Inventory data for mixing water | 247 |
| 11.2.5. Inventory data for superplasticizers | 248 |
| 11.2.6. Inventory data for sand and aggregates | 249 |
| 11.2.7. Inventory data for transport | 251 |
| 11.2.8. Inventory data for concrete manufacturing at a concrete plant..... | 252 |
| 11.2.9. Inventory data for reinforcing steel | 254 |
| 11.3. Impact analysis | 255 |
| 11.3.1. The IPCC 2007 global warming potential impact method..... | 255 |
| 11.3.2. The CML 2001 impact method | 255 |
| 11.3.3. The Eco-Indicator 99 impact method | 256 |
| 11.4. Interpretation | 256 |
| 12. Environmental impact of HVFA and FA+SF concrete..... | 257 |
| 12.1. Impact of 1 m³ of concrete | 257 |
| 12.1.1. Summary of the LCA input in SimaPro | 257 |
| 12.1.2. Global warming potential per m ³ | 258 |
| 12.2. Impact of the concrete volume per unit of strength and service life | 261 |
| 12.2.1. Summary of the LCA input in SimaPro | 261 |
| 12.2.2. Global warming potential of the required concrete volume..... | 263 |
| 12.2.2.1. In exposure class XC3/4..... | 263 |
| 12.2.2.2. In exposure class XS2 | 264 |
| 12.2.3. Global warming potential including transport and production | 266 |
| 12.2.4. Other problem oriented impacts of the required concrete volume | 267 |

| | |
|--|------------|
| 12.2.5. Damage oriented impacts of the required concrete volume | 276 |
| 12.3. Impact of a concrete column with a given load and service life..... | 278 |
| 12.3.1. Summary of the LCA input in SimaPro | 278 |
| 12.3.2. Global warming potential of the concrete column | 279 |
| 12.3.2.1. In exposure class XC3/4..... | 279 |
| 12.3.2.2. In exposure class XS2 | 281 |
| 12.4. Impact of a concrete slab with a given load and service life | 282 |
| 12.4.1. Summary of the LCA input in SimaPro | 282 |
| 12.4.2. Global warming potential of the concrete slab..... | 284 |
| 12.4.2.1. In exposure class XC3/4..... | 284 |
| 12.4.2.2. In exposure class XS2 | 285 |
| 12.4.3. Influence of active crack width control..... | 286 |
| 12.5. Conclusions | 287 |

PART V: CONCLUSIONS

| | |
|---|------------|
| 13. Main research findings | 293 |
| 13.1. HVFA and FA+SF concrete | 293 |
| 13.2. Resistance to carbonation | 294 |
| 13.3. Resistance to chloride ingress..... | 294 |
| 13.4. Resistance to freeze/thaw with deicing salts | 295 |
| 13.5. Service life prediction..... | 296 |
| 13.5.1. Carbonation-induced corrosion | 296 |
| 13.5.2. Chloride-induced corrosion..... | 297 |
| 13.6. Life cycle assessment | 298 |
| 14. Future research perspectives..... | 301 |
| 14.1. Resistance to carbonation | 301 |
| 14.2. Resistance to chloride ingress..... | 301 |
| 14.3. Resistance to freeze/thaw with deicing salts | 302 |
| 14.4. Service life prediction..... | 302 |
| 14.5. Life cycle assessment | 303 |

BIBLIOGRAPHY, APPENDICES, CURRICULUM VITAE

| | |
|---|------------|
| Bibliographical references | 307 |
| Appendix A | 325 |
| Appendix B | 327 |

| | |
|-------------------------------|------------|
| Appendix C | 329 |
| Appendix D | 331 |
| Curriculum vitae | 337 |

Notation index

Abbreviations

| | | | |
|--------|--|-------|--|
| A | Air entrained | FESEM | Field Emission Scanning Electron Microscope |
| A/P | Air-to-Paste ratio | | |
| AC | Acid-soluble Chloride | FORM | First Order Reliability Method |
| ADEME | Agence de l'Environnement et de la Maîtrise de l'Energie | FU | Functional Unit |
| ADP | Abiotic Depletion Potential | GGBFS | Ground Granulated Blast-Furnace Slag |
| AEA | Air Entraining Agent | GHG | Greenhouse Gas |
| AP | Acidification Potential | GWP | Global Warming Potential |
| B | Binder | HSR | High Sulfate Resistant |
| BE | Ecoinvent data for Belgium | HTP | Human Toxicity Potential |
| BET | Brunauer, Emmett and Teller | HVFA | High-Volume Fly Ash |
| BFS | Blast-Furnace Slag | I | Ecoinvent Infrastructure process |
| CANMET | Canada Centre for Mineral and Energy Technology | IEB | Indirect Energy Bound |
| CH | Ecoinvent data for Switzerland | IPCC | Intergovernmental Panel on Climate Change |
| CKD | Cement Kiln Dust | ISO | International Organization for Standardization |
| DALY | Disability Adjusted Life Years | KMI | Koninklijk Meteorologisch Instituut (Royal Meteorological Institute) |
| DEB | Direct Energy Bound | LCA | Life Cycle Assessment |
| EDX | Energy Dispersive X-ray spectroscopy | LCI | Life Cycle Inventory |
| EFCA | European Federation Concrete Admixtures | LCIA | Life Cycle Impact Assessment |
| EP | Eutrophication Potential | LOI | Loss On Ignition |
| EPA | Environmental Protection Agency | MAETP | Marine Aquatic Ecotoxicity Potential |
| EPD | Environmental Product Declaration | MBE | Mortier du Béton Equivalent (concrete equivalent mortar) |
| ER | Environmental Report | MIP | Mercury Intrusion Porosimetry |
| erf(.) | Error function | MW | Molecular Weight |
| F/T | Freeze/Thaw | NO | Ecoinvent data for Norway |
| FA | Fly Ash | ODP | Ozone Depletion Potential |
| FA/B | Fly Ash-to-Binder ratio | OPC | Ordinary Portland Cement |
| FAETP | Freshwater Aquatic Ecotoxicity Potential | PAF | Potentially Affected Fraction |

| | | | |
|--------|---|------|--|
| PDF | Potentially Disappeared Fraction | SP | Superplasticizer |
| POCP | Photochemical Ozone Creation Potential | TEM | Two-Electrode Method |
| POO | Probability of Occurrence | TETP | Terrestrial Ecotoxicity Potential |
| RCT(W) | Rapid Chloride Test (Water) | TGA | Thermogravimetric Analysis |
| RER | Ecoinvent data representing a European average | TPE | Three Parameter Equation |
| RH | Relative Humidity | U | Ecoinvent Unit Process |
| RM | Raw Material | ULS | Ultimate Limit State |
| SCC | Self-Compacting Concrete | vac1 | Vacuum saturation prior to oven drying |
| SCE | Saturated Calomel Electrode | vac2 | Vacuum saturation after oven drying |
| SCM | Supplementary Cementitious Material | W/B | Water-to-Binder-ratio |
| SEM | Scanning Electron Microscope | W/C | Water-to-Cement ratio |
| SETAC | Society of Environmental Toxicology and Chemistry | WC | Water-soluble Chloride |
| SF | Silica Fume | WL | Weight Loss |
| SF/B | Silica Fume-to-Binder ratio | WS | Weather Station |
| SLS | Service Limit State | XRD | X-Ray Diffraction |
| SM | Stereo Microscope | YLD | Years Lived Disabled |
| | | YLL | Years of Life Lost |

Cement chemistry

| | | | |
|--------|----------------------------------|---------|---------------------------------------|
| A | Aluminium oxide (Al_2O_3) | C_4AF | Tetracalcium aluminoferrite (Ferrite) |
| AF_t | Trisulfate hydrates (Ettringite) | CC | Calcium carbonate ($CaCO_3$) |
| C | Calcium oxide (CaO) | CH | Calcium hydroxide ($Ca(OH)_2$) |
| C_2S | Dicalcium silicate (Belite) | C-S-H | Calcium silicate hydrates |
| C_3A | Tricalcium aluminate (Celite) | F | Iron oxide (Fe_2O_3) |
| C_3S | Tricalcium silicate (Alite) | S | Silicium oxide (SiO_2) |

Greek symbols

| | | | |
|------------------------|--|-----------------|---|
| α | Effective ratio of the moduli of elasticity of steel and concrete, in Chapter 11 (–) | Δx | Depth of the convection zone (mm) |
| α | Specific surface, in Chapter 7 (mm^{-1}) | ε | Dielectric permittivity (F/m) |
| α_1 | Ageing exponent estimated from migration coefficients (–) | ε_t | Error term for inverse effective carbonation resistance (($mm^2/years$)/(kg/m^3)) |
| α_2 | Ageing exponent estimated from apparent diffusion coefficients (–) | κ | Debye constant (m^{-1}) |
| α^c | Characteristic pitting factor (–) | μ | Dynamic viscosity of O_2 ($2.02 \times 10^{-2} Nsm^{-2}$) |
| β | Reliability index (–) | ρ_0^c | Characteristic potential electrolytical resistivity (Ωm) |
| γ_b | Partial factor for b^c (–) | ρ^c | Characteristic resistivity (Ωm) |
| γ_v | Partial factor for the corrosion rate (–) | ρ_{dr} | Dry density (kg/m^3) |
| Δd | Safety margin for the cover thickness (mm) | ρ_{TEM} | Bulk resistivity (Ωm) |
| $\Delta f_{sand\ 0/4}$ | Gravel equivalent mass fraction sand 0/4 (kg) | σ_s | Steel stress (N/mm^2) |
| Δm | Mass loss per unit area (kg/m^2) | τ | Parameter TPE (–) |
| | | Φ | Diameter of the rebar (mm) |
| | | φ | Permeable porosity (%) |

Roman symbols (lowercase)

| | | | |
|---------------------------|--|---------------------------------|---|
| a | Parameter TPE, in Chapter 5 (–) | $k_{cl,res}^c$ | Characteristic value for presence of chloride (–) |
| a | Ageing exponent, in Chapter 9 (–) | | |
| a_c | Amount of carbonatable material per unit volume (kg/m^3) | k_e | Environmental function, relative humidity, in Chapter 8 (–) |
| a_w | Exposed area, capillary sorption test (mm^2) | k_e | Environmental transfer variable, temperature, in Chapter 9 (–) |
| a_{Wenner} | Probe spacing of the four-point Wenner probe (5.0 cm) | $k_{RH,res}^c$ | Characteristic humidity factor for resistivity (–) |
| a_1 | Regression parameter for p_0^d (μm) | k_t | Regression parameter for inverse effective carbonation resistance, in Chapter 8 (–) |
| a_2 | Regression parameter for p_0^d (μm) | | |
| a_3 | Regression parameter for p_0^d ($\mu\text{m}/\text{MPa}$) | k_t | Experimental transfer parameter for the migration coefficient, in Chapter 9 (–) |
| b | Parameter expressing age dependence (–) | | |
| b^c | Characteristic parameter for the position of rebar ($\text{mm}/\mu\text{m}$) | k_t | Factor for load duration, in Chapter 11 (–) |
| b_c | Exponent of regression with respect to concrete curing (–) | $k_{T,res}^c$ | Characteristic temperature factor for resistivity (–) |
| b_e | regression variable temperature dependence (K) | l | Length (m) |
| b_w | Exponent of regression for the weather function (–) | l_m | Average chord length (mm) |
| c | Ionic concentration of the bulk solution (mol/l) | m_0 | Constant for corrosion rate versus resistivity ($\mu\text{m}\cdot\Omega\text{m}/\text{year}$) |
| c_{acce} | CO_2 concentration during the carbonation test (%) | m_d | Mass after oven drying (g) |
| c_{field} | CO_2 concentration in the field (%) | m_l | Mass under water (g) |
| c_s | CO_2 concentration at the concrete surface (kg/m^3) | m_s | Water saturated mass (g) |
| d | Concrete cover (mm) | m_{Sx} | Mass at drying step x (1, 2 or 3) (g) |
| d_c | Average carbonation depth (mm) | m_t | Change in specimen mass (g) |
| d_w | Density of water ($0.001 \text{ g}/\text{mm}^3$) | m_{tDoS} | Sample mass at time t (g) |
| $f_{c,sp}^d$ | Tensile splitting strength (MPa) | n | Number of samples / number of measurements (–) |
| f_{ck} | Characteristic compressive strength (N/mm^2) | n_{res}^c | Age factor for electrolytical resistivity (–) |
| $f_{ct,eff}$ | Effective tensile strength of concrete (N/mm^2) | p | Paste content (%) |
| f_e | Constant parameter, relative humidity (–) | p_0^d | Design value corrosion penetration necessary to produce a crack (μm) |
| $f_{\text{gravel } 2/8}$ | Mass fraction gravel 2/8 (kg) | p^d | Design value occurring corrosion penetration (μm) |
| $f_{\text{gravel } 8/16}$ | Mass fraction gravel 8/16 (kg) | p_{SR} | Probability of driving rain (–) |
| g_e | Constant parameter, relative humidity (–) | t | Time (years, h or s) |
| k_1 | Coefficient for bond properties reinforcing steel (–) | t_0 | Time of reference (years) |
| k_2 | Coefficient for strain distribution (–) | t_c | Period of curing (days) |
| k_a | Apparent gas permeability (m^2) | $t_{\text{crack}_1 \text{ mm}}$ | Time to unacceptable corrosion-induced cracking (years) |
| k_c | Execution transfer parameter (–) | t_{end} | End exposure period (days) |
| $k_{c,res}^c$ | Characteristic curing factor for resistivity (–) | t_{exp} | Exposure period (days) |
| | | t_{hydr} | Age of the concrete at maximum hydration (year) |
| | | t_i^d | Design value time to steel depassivation (years) |

| | | | |
|----------------|---|----------|---|
| t_{SL} | Service life (years) | w^d | Design value of the actual crack width (mm) |
| t_{start} | Start exposure period (days) | w_k | Characteristic crack width (mm) |
| w | Weather exponent (–) | w_t | Relative time of wetness (–) |
| w_0 | Width of the initial visible crack (0.050 mm) | x | Penetration depth / profiling depth (mm) |
| w_b | Bound water content (g/100 g cement) | $x_c(t)$ | Carbonation depth at time t (mm) |
| $w_{b,\infty}$ | Ultimate bound water content (g/100 g cement) | x_d | Average value of the penetration depth (mm) |
| w_{cr} | Critical crack width (1.0 mm) | | |

Roman symbols (uppercase)

| | | | |
|--------------------|---|------------------|---|
| A | Cross-section (m ²) | $D_{ai,0}$ | Instantaneous chloride diffusion coefficient at time t_0 (mm ² /years) |
| $A_{\%}$ | Air content (%) | $D_{app,C}$ | Apparent coefficient of chloride diffusion (mm ² /years) |
| A_{acce} | Accelerated carbonation coefficient (mm/ $\sqrt{\text{weeks}}$) | D_c | Diffusion coefficient of CO ₂ (m ² /s) |
| $A_{c,eff}$ | Effective cross-sectional area of the concrete in the tensile zone (mm ²) | D_{cl} | Average diffusion (or migration) coefficient (m ² /s) |
| A_{field} | Field carbonation coefficient (mm/ $\sqrt{\text{years}}$) | D_e | Effective chloride transport coefficient (m ² /s) |
| $A_{gravel\ 2/8}$ | Water absorption coefficient gravel 2/8 (–) | $D_{e(acce)}$ | Accelerated chloride diffusion coefficient (m ² /s) |
| $A_{gravel\ 8/16}$ | Water absorption coefficient gravel 8/16 (–) | $D_{e(nat)}$ | ‘Natural’ chloride diffusion coefficient (m ² /s) |
| A_s | Cross-sectional area of the steel (mm ²) | D_{max} | Nominal maximum aggregate size (mm) |
| $A_{sand\ 0/4}$ | Water absorption coefficient sand 0/4 (–) | D_{nssm} | Non-steady state chloride migration coefficient (m ² /s) |
| $C(x, t)$ | Chloride concentration at depth x and time t (m%/binder) | DoS | Degree of saturation, capillary sorption test (%) |
| C_0 | Initial chloride content (m%/binder) | $D_{RCM,0}$ | Non-steady state chloride migration coefficient (mm ² /years) |
| C_{crit} | Critical chloride content (m%/binder) | $E(\text{corr})$ | Corrosion potential (mV vs SCE) |
| C_e | Economic allocation coefficient (–) | E_{cm} | Modulus of elasticity of concrete (N/mm ²) |
| C_m | Mass allocation coefficient (–) | E_s | Design value modulus of elasticity of steel (N/mm ²) |
| C_s | Chloride surface concentration (m%/binder) | F | Faraday constant (9.648×10^4 J/(V·mol)) |
| $C_{s(acce)}$ | Accelerated chloride surface concentration (m%/binder) | F_{cl}^c | Characteristic chloride corrosion rate factor (–) |
| $C_{s(nat)}$ | ‘Natural’ chloride surface concentration (m%/binder) | H | Height (mm) |
| C_S | Atmospheric CO ₂ concentration (kg/m ³ or %) | I | Water absorption (mm) |
| $C_{S,\Delta x}$ | Chloride content at depth Δx (m%/binder) | K_c | Characteristic temperature dependency factor (–) |
| D | Pore diameter (μm) | L | Thickness of the specimen (m or mm) |
| D_a | Apparent chloride diffusion coefficient (mm ² /years) | L_S | Spacing factor (μm) |
| | | N | Total number of air void chord lengths (–) |

| | | | |
|--------------------------|--|---------------------------|--|
| \emptyset | Diameter (mm) | $S_{\text{gravel } 8/16}$ | Specific surface area gravel 8/16 (m ² /kg) |
| P | Absolute inlet pressure (2 bar) | S_i | Initial rate of water absorption (mm/ \sqrt{s}) |
| P_a | Atmospheric pressure (bar) | S_s | Secondary rate of water absorption (mm/ \sqrt{s}) |
| P_f | Probability of failure (–) | $S_{\text{sand } 0/4}$ | Specific surface area sand 0/4 (m ² /kg) |
| Q | Gas flow rate (ml/s) | S_x | Degree of saturation of specimens for gas permeability test (%) |
| R | Gas constant (8.314 J/(mol·K)) | T | Temperature (°C or K) |
| $R_{\text{ACC},0}^{-1}$ | Inverse effective accelerated carbonation resistance ((mm ² /years)/(kg/m ³)) | T_a | Total chord length of air voids (mm) |
| R_{carb} | Carbonation resistance ((kg/m ³)/(m ² /s)) | ToW | Time of wetness (–) |
| RH_{real} | Realistic relative humidity of the concrete environment (%) | T_p | Total chord length of paste (mm) |
| RH_{ref} | Reference relative humidity (%) | T_{real} | Temperature of the structural element or the ambient air (K) |
| R_{lower} | Resipod reading for the foam insert of the lower electrode (k Ω cm) | T_{ref} | Standard test temperature (K) |
| R_{meas} | Resistance measured with the Proceq Resipod resistivity meter (k Ω cm) | T_{tot} | Total surface distance traversed (mm) |
| $R_{\text{NAC},0}^{-1}$ | Inverse effective natural carbonation resistance ((mm ² /years)/(kg/m ³)) | U | Absolute value of the applied voltage (V) |
| R_{TEM} | Resistance measured with the two-electrode method (Ω) | V^d | Design value corrosion rate ($\mu\text{m}/\text{years}$) |
| R_{upper} | Resipod reading for the foam insert of the upper electrode (k Ω cm) | V_x | Variation coefficient (–) |
| S | Specific surface area (m ² /kg) | W(t) | Weather function for exposure to carbonation, in Chapter 8 (–) |
| $S_{\text{gravel } 2/8}$ | Specific surface area gravel 2/8 (m ² /kg) | W(t) | Subfunction that considers ageing in presence of chlorides, in Chapter 9 (–) |

Summary

The concept of high-volume fly ash concrete

It is commonly known that substantial amounts of CO₂ are emitted in the clinkering phase of ordinary Portland cement production. One ton of ordinary Portland cement has a carbon footprint of a little less than one ton CO₂ equivalent. Given the abundant use of cement and concrete in the construction industry worldwide it is not surprising that researchers are aiming at reducing the cement related CO₂ emissions through partial cement replacement. The development of high-volume fly ash (HVFA) concrete in the 1980s counts as an extreme example of this practice. In this concrete no less than 50% of the cement is replaced by pozzolanic fly ash (FA), a by-product of coal fired electricity production. As such, the material was considered 'green' by definition. Until now, it has mainly been used in less demanding applications in non-aggressive environments. This research aimed at verifying whether HVFA concrete could also be applied in environments subject to carbonation- and chloride induced corrosion of embedded reinforcing steel and freeze/thaw attack in combination with deicing salts. Because of the slow nature of the pozzolanic fly ash reaction, it is difficult to achieve the same 28-day strength of traditional concrete that is normally used in these more critical environments. Simply increasing the total binder content and lowering the water-to-binder ratio cannot solve this problem. For this reason, 10% silica fume (SF) was introduced as third powder. Both the moderate strength HVFA concrete (C30/37-C35/45) and the high strength FA+SF concrete (C50/60-C55/67) were fully characterized in terms of durability and sustainability.

Durability performance

For the three demanding concrete environments under investigation, the equivalent performance of HVFA and FA+SF concrete in comparison with the applicable OPC and k-value conforming FA (15% FA) reference concrete types was evaluated in accordance with NBN B15-100 (2008). In addition, extra carbonation, chloride migration and diffusion tests were performed at different ages to enable a mix specific service life prediction for carbonation- and chloride-induced corrosion. Moreover, for the environment with exposure to freeze/thaw in combination with deicing salts, the air content in the fresh state as well as the

air void system in the hardened state of HVFA and FA+SF concrete were studied to come up with guidelines for proper artificial air entrainment of these alternative concrete types. The effects of air entrainment on the porosity and transport properties were also investigated. The overall durability assessment led to the following research findings per concrete environment:

- Resistance to carbonation (exposure class XC3/4) – In comparison with the applicable traditional reference concrete types, both HVFA and FA+SF concrete show no equivalent carbonation resistance after 28 days of optimal curing. This was concluded from colorimetric and microscopic carbonation depth measurements. The latter often indicated a higher carbonation depth. In exposure class XC3, the field carbonation rate at 0.05% CO₂ of HVFA concrete was around three times as high. FA+SF concrete performed slightly better with a field carbonation rate only twice as high as for the reference. However, the carbonation resistance of both concrete types was found to be susceptible to suboptimal curing in the first 28 days. Moreover, the accelerated carbonation test at 10% CO₂ in combination with a simple conversion model tends to underestimate the estimated field carbonation coefficient with no less than 45% and 43%, respectively. In addition, it was found that the carbonation mechanism itself changed in particular between exposure to 0.03% and 1% CO₂ and not so much between exposure to 1% and 10% CO₂. In the simulated exposure class XC4, the field carbonation coefficients of HVFA concrete were also higher than those of the applicable references. Still, they remained very low because the intermittent wetting of the concrete had an important pore blocking effect.
- Resistance to chloride ingress (exposure class XS2) – Equivalent performance in terms of chloride resistance exists for both alternative concrete types in comparison with the applicable references. Comparative chloride migration, accelerated and ‘natural’ chloride diffusion tests performed after 28, 91, 273 or 364 days all led to this conclusion. In sharp contrast with OPC concrete, the HVFA concrete showed an excellent ageing behaviour. Migration coefficients of more than 17×10^{-12} m²/s after 28 days decreased to only 2.0-3.0 $\times 10^{-12}$ m²/s after one year. FA+SF concrete already showed migration coefficients in this range after 28 days. From then on a further decrease could still be recorded. Only the chloride migration coefficient of the HVFA concrete was found to be susceptible to suboptimal curing in the first 28 days. The improved chloride resistance with prolonged curing also resulted from the accelerated and ‘natural’ diffusion tests. In this case, the time dependent decrease in diffusion coefficient was less pronounced. For the submerged exposure condition, the chloride surface concentration obtained from chloride profile fitting cannot be considered as constant. A time dependent build-up in chloride surface concentration is expected which varies with the concrete composition.
- Resistance to freeze/thaw with deicing salts (exposure class XF4) – The salt scaling resistance of air entrained HVFA and FA+SF concrete does not meet the equivalent performance criterion of NBN B15-100 (2008). Nevertheless, their mass loss per unit area after 28 severe freeze/thaw cycles did not exceed the 1 kg/m² criterion of NBN EN 1339 (2003). To achieve this goal a substantially increased dosage of air entraining agent of no less than 7.0 ml/kg binder was required for the HVFA concrete. This dosage compensated for any occurring adsorption phenomena. It guaranteed an adequate air-to-paste ratio exceeding 18-20% and a well-developed air void system in hardened state in terms of total

air content ($> 7\%$), spacing factor ($\leq 200 \mu\text{m}$), specific surface ($25\text{-}45 \text{ mm}^{-1}$) and average chord length ($\sim 0.100 \text{ mm}$). Much less air entraining agent ($2.5\text{-}3.0 \text{ ml/ kg binder}$) was needed to achieve an air void system with similar properties for the FA+SF concrete. The presence of a well-developed system of normally isolated air bubbles had an effect on the porosity and transport properties of the concrete. When properly air entrained, the permeable porosity and apparent gas permeability of both concrete types were found to be substantially higher. The capillary sorption behaviour was less clearly affected by the incorporation of an air entraining agent.

Service life performance

- Carbonation-induced depassivation and corrosion – Although characterized by a lower carbonation resistance, probabilistic service life prediction for exposure class XC3 (concrete cover: 35 mm) indicated corrosion initiation periods of 100 years or more for HVFA and FA+SF concrete when based on accelerated carbonation tests at 10% CO_2 after at least 28 days of optimal curing. The same holds true for HVFA concrete when located in exposure class XC4 (concrete cover: 40 mm). However, suboptimal curing in the first 28 days after manufacture can shorten the corrosion initiation period for HVFA concrete to 71 years in exposure class XC3. After additional correction for the fact that an accelerated carbonation test at 10% CO_2 underestimates the field carbonation rate substantially, the time to steel depassivation was reduced even more to only 21 years. The corrosion initiation period of FA+SF concrete still amounted to 71 years after correction for the applied CO_2 concentration and curing conditions. These findings resulted from a simplified square-root-time relation in which the field carbonation rate and the concrete cover were the only load and resistance variables (1st order prediction). It did not account for the concrete's curing behaviour and the meteorological conditions in practice. The latter two items were included in the more advanced limit state function of the *fib* model code for service life design (2nd order prediction). Longer corrosion initiation periods were recorded with this model. The unfavourable Belgian weather conditions for carbonation (relative humidity: $79\pm 9\%$ RH, time of wetness: 0.31) can mainly be held responsible for this. Still, a corrosion initiation period of only 72 years occurred for HVFA concrete in a sheltered outdoor environment (exposure class XC3) after correction for the CO_2 concentration and curing conditions. The calculations did not indicate any problems for the FA+SF concrete. The resistivity, a concrete property which is inversely related to the corrosion rate of embedded reinforcing steel, indicates that the time between onset of active corrosion and unacceptable cracking would be at least 50 years for the HVFA and the FA+SF concrete.
- Chloride-induced depassivation and corrosion – The measured chloride migration coefficients and a set of default values for the experimental transfer parameter, the ageing exponent and the critical chloride threshold level can be used to estimate the time to steel depassivation in accordance with the limit state function of *fib* Bulletin 34 (1st order prediction). This model is based on the solution of Fick's second law of diffusion and involves the typical error function. This prediction approach assigns a very short corrosion initiation period to the OPC reference (< 5 years), while (much) longer durations were estimated for the k-value conforming FA reference cf. NBN B15-001 (2004) (± 30 years),

the HVFA concrete (± 20 years) and the FA+SF concrete (+1000 years) after 28 days optimal curing. After implementation of experimentally determined transfer parameters based on comparative migration and diffusion tests, mix specific ageing exponents estimated from diffusion tests at multiple ages and experimentally verified critical chloride contents from corrosion potential monitoring and subsequent potentiometric titration, the prediction outcome changed significantly (2nd order prediction). Corrosion initiation periods increased substantially mainly due to the much higher value of the critical chloride content (1.9 m%/binder instead of 0.6 m%/binder). Still, the prediction remained in favor of the fly ash containing concrete mixtures, even when the HVFA and FA+SF concrete were suboptimally cured in the first 28 days after casting. Their corrosion initiation period easily exceeded 1000 years, while steel depassivation of the OPC concrete was still expected within less than 50 years. The more substantial reduction in chloride diffusion coefficient with time and the resulting high value for the ageing exponent explain this behaviour. Ageing exponents of the k-value conforming FA reference cf. NBN B15-001 (2004), the HVFA concrete and the FA+SF concrete amounted to 0.53, 0.70 and 0.55, respectively, while this was only 0.15 for the OPC reference. In contrast with carbonation-induced corrosion, the corrosion propagation period estimated from concrete resistivity measurements was very short (< 5 years).

A major drawback of the currently considered prediction models is that they do not account for the presence of cracks in concrete. They simply require experimental input obtained from tests done on uncracked concrete specimens. This condition is seldomly observed in practice. The absence of correction factors for concrete cracking probably explains why often very long service lives (+ 1000 years) were recorded until now.

Life cycle assessment

Life cycle assessment (LCA) is a methodology that allows for an objective quantification of the environmental impact of a product over the entire life cycle. It traditionally consists of four major steps, i.e. the definition of goal and scope, the inventory analysis, the impact analysis and the interpretation. Although originally developed for the environmental evaluation of simple consumer goods, LCA can be used to quantify the ‘greenness’ of HVFA and FA+SF concrete. This LCA study aimed at quantifying the actual reduction in greenhouse gas emissions possible by replacing large portions of the cement by industrial by-products such fly ash and silica fume. However, attention was also paid to other environmental issues, i.e. acidification, eutrophication, abiotic depletion, freshwater/marine aquatic ecotoxicity, terrestrial ecotoxicity, human toxicity, ozone depletion, photochemical oxidation, etc. The conducted LCA calculations specifically relate to the situation in Belgium, where fly ash is becoming less readily available and where silica fume is not being produced. A different outcome is expected if similar LCA calculations would be executed for countries like China and India where there is a still lot of coal fired electricity production and thus also a lot of fly ash available.

The LCA calculations were done for functional units that account for the strength and service life performance of these alternative concrete types in comparison with more traditional concrete, i.e. OPC and k-value conforming FA references for the applicable exposure classes.

Inclusion of these concrete properties is of importance because they govern the structure dimensions and required number of rehabilitation actions over time and thus the total concrete volume needed over the entire life cycle. The required concrete volume per unit of strength and service life or simple structural elements with a given design load and service life qualify as suitable functional units for environmental impact calculations. Life cycle inventory data on the use of raw materials and energy, the emissions to air, water and soil, and the waste production associated with the applied concrete constituents were collected from the renowned Ecoinvent database and combined for the modelling of each concrete composition under investigation in the LCA software SimaPro. Special attention was paid to the allocation of impacts for the by-products fly ash and silica fume and their effects on the environmental score of HVFA and FA+SF concrete in comparison with more traditional concrete types. Since fly ash and silica fume are no longer mere waste products cf. European Union directive 2008/98/EC (2008), it is not sufficient to take only the impact of their basic treatment after production into account. The impacts associated with the primary production processes, i.e. coal fired electricity and Si-metal production, also need to be partially assigned to them. The preference goes to economic allocation, although its susceptibility to price fluctuations remains an issue. Based on the current by-product / main product mass and price ratios, the economic allocation coefficients for fly ash and silica fume equaled 2.9% and 6.1%, respectively. Given the fact that only small amounts of fly ash and silica fume are produced per kWh of electricity (0.052 kg) and per kg of Si-metal (0.15 kg), these relatively small allocation coefficients still impose important impacts to the by-products.

Environmental impact

When considering the required concrete volume per unit of strength and service life as functional unit, the reduction in greenhouse gas emissions achievable with HVFA and FA+SF concrete depends a lot on the studied exposure class.

- Exposure class XC3/4 – HVFA concrete shows little or no potential for the reduction of greenhouse gas emissions. This is mainly due to the moderate strength performance of the material at early age. Moreover, first and second order service life prediction indicated that service life of HVFA concrete can be less than 100 years. On the other hand, the FA+SF composition could be a more environmentally friendly alternative to the OPC reference for exposure class XC3 as its global warming potential was 28 to 36% lower.
- Exposure class XS2 – As both the HVFA and FA+SF concrete show a much better service life performance than the OPC reference, there is an evident reduction in greenhouse gas emissions possible (HVFA: GWP –25-35%, FA+SF: GWP –55-60%). In comparison with a k-value conforming FA reference, there is much less benefit, because its service life is of the same order of magnitude. Reductions in global warming potential are only possible then for FA+SF concrete (GWP –19-21%). In this exposure class, k-value conforming FA concrete with a fly ash content of only 15% actually seemed a better alternative to OPC concrete (GWP –45-50%) than concrete with high cement replacement levels.

A closer look at the other environmental issues besides the effects on global warming indicates that the incorporation of large portions of fly ash and silica fume is far from an environmentally friendly practice. Coal fired electricity and Si-metal production rely just like

cement production very much on the exploitation and combustion of fossil fuels which is accounted for heavily in the acidification, eutrophication, abiotic depletion, freshwater/marine aquatic ecotoxicity, terrestrial ecotoxicity, human toxicity, ozone depletion and photochemical ozone creation potentials. Given the low by-product/main product mass ratios, the economically allocated impacts assigned to 1 kg of fly ash and silica fume remain huge.

Concrete columns or slabs with a given design load and service life were also tested as functional unit to quantify the possible reduction in greenhouse gas emissions with HVFA and FA+SF concrete. The conclusions drawn for the column were similar to those obtained for the required concrete volume per unit of strength and service life. The evaluation of concrete slabs shows a different picture. The use of a high strength concrete for the slab design, e.g. the FA+SF concrete, cannot reduce the slab thickness and thus the required concrete volume in an important way without increasing the required amount of reinforcing steel in the tensile zone. In other words, the strength property of the concrete cannot be fully valorized. In addition, the incorporation of extra reinforcing steel to minimize the crack width in the tensile zone to a possible seemingly uncracked condition (< 0.05 mm) can increase the global warming potential of the slab with another 25-37%.

Samenvatting

Het concept hoog-volume vliegasbeton

Het is algemeen gekend dat aanzienlijke hoeveelheden CO₂ worden uitgestoten tijdens het klinkerproces bij de productie van portlandcement. Eén ton portlandcement heeft een CO₂-voetafdruk van iets minder dan één ton CO₂ equivalent. Gezien het veelvuldig gebruik van cement en beton in de bouwsector is het geen verrassing dat onderzoekers proberen om de cement gerelateerde CO₂-emissies te doen dalen door een deel van het cement in beton te vervangen. Hoog-volume vliegasbeton (HVFA-beton), een betontype dat werd ontwikkeld in de jaren tachtig van vorige eeuw kan gezien worden als een voorbeeld van doorgedreven cementvervanging. In een dergelijk beton wordt niet minder dan 50% van het cement vervangen door puzzolaan vliegas (FA), een bijproduct van kolengestookte elektriciteitscentrales. Op die manier wordt het materiaal als bij definitie voor ‘groen’ aanzien. Tot op heden werd HVFA-beton vooral aangewend voor minder veeleisende toepassingen in weinig agressieve omgevingen. Dit onderzoek had tot doel om na te gaan of HVFA-beton ook zonder problemen kan worden toegepast in omgevingen waarin carbonatatie- en chloridegeïnduceerde corrosie van wapeningsstaal ingebed in beton kan optreden en in omgevingen onderhevig aan vorst/dooi in combinatie met dooizouten. Aangezien de puzzolane vliegasreactie eerder traag verloopt, is het moeilijk om op 28 dagen ouderdom dezelfde sterkte te halen als bij het traditioneel beton dat normaal gebruikt wordt in deze meer kritieke betonomgevingen. Het gewoonweg verhogen van het totale bindmiddelgehalte en het verlagen van de water-bindmiddelfactor biedt geen oplossing voor dit probleem. Om die reden werd 10% silica fume (SF) geïntroduceerd als derde bindmiddel. Zowel voor het HVFA-beton met een eerder matige sterkte (C30/37-C35/45) als voor het FA+SF-beton met een hoge sterkte (C50/60-C55/67) werd het duurzaamheidsgedrag en de milieu-impact volledig nagegaan.

Duurzaamheid

De geschiktheid van HVFA-beton en FA+SF-beton in vergelijking met het geldende referentiebeton op basis van portlandcement en het referentiebeton met 15% vliegas cfr. het waarde concept voor de drie bestudeerde betonomgevingen werd geëvalueerd in

overeenstemming met NBN B15-100 (2008). Daarenboven werden bijkomende carbonatatie-, chloride migratie- en diffusietesten uitgevoerd op verschillende leeftijden om een levensduurvoorspelling op maat van elke betonsamenstelling bij blootstelling aan carbonatatie- en chloride-geïnduceerde corrosie mogelijk te maken. Daarenboven werd in het geval van blootstelling aan vorst-dooi in combinatie met dooizouten het luchtgehalte in verse toestand en het luchtholtesysteem in verharde toestand bestudeerd. Zo konden richtlijnen worden vastgelegd betreffende de optimale dosering van luchtbelvormers in HVFA- en FA+SF-beton, dit om een adequaat luchtholtesysteem in verharde toestand te realiseren. De effecten van de aanwezigheid van een dergelijk systeem op de porositeit en de transporteigenschappen van het beton werden eveneens nagegaan. Het duurzaamheidsgedrag kan per betonomgeving als volgt worden gekarakteriseerd:

- Weerstand tegen carbonatatie (blootstellingsklasse XC3/4) – In vergelijking met het geldende referentiebeton vertoonden het HVFA- en FA+SF-beton geen equivalente weerstand tegen carbonatatie na 28 dagen nabehandeling onder optimale omstandigheden. Dit kon worden besloten uit zowel de colorimetrisch als de microscopisch opgemeten carbonatatedieptes. De microscopische opmetingen resulteerden vaak in een grotere carbonatatediepte. In blootstellingsklasse XC3 was de in situ carbonatatiesnelheid bij 0,05% CO₂ van HVFA-beton ongeveer drie keer zo hoog als bij het referentiebeton. Daarentegen was het FA+SF-beton iets beter bestand tegen carbonatatie. De in situ carbonatatiesnelheid was maar twee keer zo hoog als bij het referentiebeton. Desondanks werd de carbonatatiweerstand van beide betontypes negatief beïnvloed door nabehandeling onder suboptimale omstandigheden. Door uit te gaan van een versnelde carbonatatieproef bij 10% CO₂ in combinatie met een eenvoudig omzettingsmodel bleek ook de werkelijke in situ carbonatatiesnelheid van HVFA- en FA+SF-beton met niet minder dan 45% en 43% te worden onderschat. Daarnaast bleek ook dat het carbonatatiemechanisme zelf vooral wijzigde tussen blootstelling aan 0,03% en 1% CO₂, en niet zozeer tussen blootstelling aan 1% en 10% CO₂. Ook in de gesimuleerde blootstellingsklasse XC4 waren de in situ carbonatatiesnelheden hoger dan die van de verschillende types referentiebeton. Ze bleven evenwel zeer laag aangezien het cyclisch bevochtigen van het beton de poriën tijdelijk ontoegankelijk maakt voor verdere indringing van CO₂.
- Weerstand tegen chloride-indringing (blootstellingsklasse XS2) – De alternatieve betontypes vertoonden wel degelijk een gelijkaardige weerstand tegen chloride-indringing als de verschillende types referentiebeton. Dit werd bevestigd door middel van vergelijkende chloride migratietesten en versnelde en ‘natuurlijke’ diffusietesten na 28, 91, 273 of 364 dagen optimale nabehandeling. In tegenstelling tot traditioneel portlandcement beton, vertoonde het HVFA-beton een uitstekend verouderingsgedrag. De gemeten migratiecoëfficiënten daalden van meer dan 17×10^{-12} m²/s na 28 dagen tot slechts 2.0-3.0 $\times 10^{-12}$ m²/s na 1 jaar. Bij FA+SF-beton werden deze laatste zeer lage migratiecoëfficiënten reeds geregistreerd op een leeftijd van 28 dagen. Bovendien werd daarna nog een zeer sterke daling in migratiecoëfficiënt waargenomen. Nabehandeling onder suboptimale omstandigheden in de eerste 28 dagen na vervaardiging had enkel een uitgesproken negatief effect op de migratiecoëfficiënt van het HVFA-beton. De verbeterde weerstand

tegen chloride-indringing met toenemende nabehandeling kon ook worden waargenomen in de resultaten van de versnelde en de ‘natuurlijke’ chloride diffusietesten. Alleen was in dat geval de daling in diffusiecoëfficiënt minder uitgesproken. In geval van permanente onderdompeling, bleek dat de chloride oppervlakteconcentratie die werd bekomen uit het fitten van het chlorideprofiel, niet als constante kan worden beschouwd. Er wordt verwacht dat de chloride oppervlakteconcentratie toeneemt in functie van de blootstellingstijd. De mate van deze toename hangt wellicht nauw samen met de betonsamenstelling.

- Weerstand tegen vorst/dooi in combinatie met doozouten (blootstellingsklasse XF4) – De doozoutbestandheid van HVFA- en FA+SF-beton met luchtbelvormer voldoet niet aan het geschiktheidscriterium van NBN B15-100 (2008). De hoeveelheid afschilfering per eenheid van oppervlakte is evenwel niet meer dan de maximum toegelaten waarde van 1 kg/m² zoals vastgelegd in NBN EN 1339 (2003). Om daaraan te kunnen voldoen moet een sterk verhoogde dosis luchtbelvormer van niet minder dan 7.0 ml/kg bindmiddel worden toegepast in het geval van HVFA-beton. Een dergelijke dosering kan compenseren voor eventueel optredende adsorptiefenomenen. Deze 7.0 ml/kg bindmiddel garandeerde ook een voldoende groot luchtgehalte relatief ten opzichte van de aanwezige cementpasta van meer dan 18-20% en een uitgesproken luchtholtesysteem in verharde toestand qua totaal luchtgehalte (> 7%), afstandsfactor ($\leq 200 \mu\text{m}$), specifiek oppervlak ($25\text{-}45 \text{ mm}^{-1}$) en gemiddelde koordlengte ($\sim 0.100 \text{ mm}$). Bij FA+SF-beton was er veel minder luchtbelvormer nodig (2.5-3.0 ml/kg bindmiddel) om een luchtholtesysteem met gelijkaardige eigenschappen te realiseren. De aanwezigheid van een goed ontwikkeld systeem van normaliter geïsoleerde luchtballen had wel een invloed op de porositeit en de transporteigenschappen van het beton. Het deed de open porositeit en de schijnbare gasdoorlatendheid van beide betontypes sterk toenemen. De capillaire wateropsorping werd minder beïnvloed door de toevoeging van een luchtbelvormer.

Levensduur

- Carbonatatie-geïnduceerde depassivatie en corrosie – Ondanks de verminderde carbonatatiweerstand van HVFA- en FA+SF-beton, resulteerde een probabilistische levensduurvoorspelling voor blootstellingsklasse XC3 (betondekking: 35 mm) toch in een initiatieduur van 100 jaar of meer voor beide betontypes. Een versnelde carbonatatieproef bij 10% CO₂ na 28 dagen optimale nabehandeling vormde de experimentele basis voor deze voorspelling. Hetzelfde geldt voor HVFA-beton in blootstellingsklasse XC4 (betondekking: 40 mm). Desondanks kan nabehandeling onder suboptimale omstandigheden in de eerste 28 dagen na vervaardiging de duur van de initiatieperiode in blootstellingsklasse XC3 verkorten tot 71 jaar. Na bijkomende correctie voor het feit dat de in situ carbonatatiesnelheid aanzienlijk wordt onderschat op basis van een versnelde carbonatatieproef bij 10% CO₂, zou het nog slechts 21 jaar duren vooraleer depassivatie van het wapeningsstaal optreedt. Na correctie voor de aangewende CO₂ concentratie tijdens de carbonatatieproef en de eraan voorafgaande nabehandeling, kan voor FA+SF-beton nog steeds een initiatieperiode van 71 jaar worden genoteerd. Al deze voorspellingen werden gedaan uitgaande van een eenvoudig wortel-tijd-verband waarbij de in situ carbonatatiecoëfficiënt en de aangenomen betondekking de enige twee belastings- en

weerstandsvARIABLEN waren (voorspelling van 1^{ste} orde). Deze benadering hield geen rekening met het nabehandelingsgedrag van het beton en de meteorologische omstandigheden eigen aan de betonomgeving. Daarmee kon pas worden rekening gehouden door gebruik te maken van de meer geavanceerde grenstoestandsfunctie beschreven in de *fib* richtlijn voor levensduurontwerp (voorspelling van 2^{de} orde). Berekeningen op basis van dit model gaven aan dat het langer duurt vooraleer er depassivatie optreedt. De ongunstige Belgische weersomstandigheden voor carbonatatie (relatieve vochtigheid: 79±9% RH, duur nattigheid: 0,31) zijn hier voornamelijk verantwoordelijk voor. Desondanks bleef een initiatieperiode van slechts 72 jaar mogelijk in het geval van HVFA-beton in een beschutte buitenomgeving (blootstellingsklasse XC3). Dit was het geval na correctie voor de toegepaste CO₂ concentratie tijdens de carbonatatieproef en de voorafgaande nabehandeling. De resistiviteit, een betoneigenschap die zich omgekeerd evenredig verhoudt tot de corrosiesnelheid van het aanwezige wapeningsstaal, gaf aan dat het bij HVFA- en FA+SF-beton minstens 50 jaar duurt vooraleer deze betontypes onaanvaardbare corrosie-geïnduceerde scheuren beginnen te vertonen.

- Chloride-geïnduceerde depassivatie en corrosie – De opgemeten chloride migratiecoëfficiënten en een reeks aangenomen waarden voor de experimentele overgangparameter, de verouderingsexponent en het kritiek chloridegehalte werden gebruikt als input voor de grenstoestandsfunctie om de depassiveringstijd te kunnen inschatten overeenkomstig *fib* Bulletin 34 (voorspelling van 1^{ste} orde). Dit model is gebaseerd op de tweede wet van Fick voor diffusie en gaat uit van de typische foutfunctie. Een dergelijke voorspelling kent een zeer korte initiatieperiode (< 5 jaar) toe aan het referentiebeton op basis van portlandcement. In het geval van een referentiebeton in overeenstemming met het k-waarde concept van NBN B15-001 (2004), een HVFA- en een FA+SF-beton duurt het (veel) langer vooraleer depassivatie optreedt, m.n. ± 30 jaar, ± 20 jaar en meer dan 1000 jaar, en dit telkens na 28 dagen optimale nabehandeling. Levensduurvoorspelling na implementatie van gemeten experimentele overgangparameters, verouderingsexponenten en een experimenteel geverifieerd kritiek chloridegehalte leverde heel andere resultaten op (voorspelling van 2^{de} orde). Voor de bepaling van de experimentele overgangparameter werden vergelijkende migratie- en diffusieproeven uitgevoerd. Verouderingscoëfficiënten werden ingeschat op basis van diffusietesten op meerdere leeftijden. Het kritiek chloridegehalte van beton werd geverifieerd door de corrosiepotentiaal van een ingebedde wapeningstaaf te monitoren tot aanvang van actieve corrosie. Vervolgens werd het kritiek chloridegehalte ter hoogte van de wapening bepaald met behulp van een potentiometrische titratie. Een sterke toename van de geschatte initiatieperiode vloeide voornamelijk voort uit het aannemen van een hoger kritiek chloridegehalte (1,9 m%/bindmiddel in plaats van 0,6 m%/bindmiddel). De levensduurvoorspellingen bleven evenwel in het voordeel van de betonmengsels met vliegglas, zelfs bij een suboptimale nabehandeling van het HVFA- en FA+SF-beton in de eerste 28 dagen na vervaardiging. Zo zou het bij HVFA- en FA+SF-beton gemakkelijk meer dan 1000 jaar duren vooraleer depassivering van het wapeningsstaal optreedt. Bij traditioneel portlandcement beton wordt depassivering van het wapeningsstaal nog altijd binnen de 50 jaar verwacht. De meer uitgesproken vermindering van de diffusiecoëfficiënt in functie van de tijd voor de alternatieve betontypes en de

daaruit voortvloeiende hoge waarde voor de verouderingsexponent verklaren dit. De geschatte verouderingsexponenten voor het vliegaskbeton in overeenstemming met het k-waarde concept van NBN B15-001 (2004), het HVFA-beton en het FA+SF-beton bedroegen respectievelijk 0,53, 0,70 en 0,55. Daarentegen bedroeg de verouderingsexponent van het referentiebeton op basis van portlandcement slechts 0,15. In tegenstelling tot bij carbonatatie-geïnduceerde corrosie, kan op basis van resistiviteitsmetingen worden besloten dat de propagatieperiode in een chloride-omgeving eerder kort zal zijn (< 5 jaar).

Merk op dat er een groot nadeel is verbonden aan de levensduurmodellen die tot nu toe in acht werden genomen. Ze houden geen rekening met de aanwezigheid van scheuren in het beton. De experimentele input tot deze modellen is eenvoudigweg gebaseerd op testresultaten van proeven op ongescheurd beton. Deze ongescheurde toestand komt in de praktijk zelden voor. Het ontbreken van correctiefactoren hiervoor verklaart wellicht waarom nu vaak zeer lange levensduren van 1000 jaar of meer werden bekomen.

Levenscyclusanalyse

Levenscyclusanalyse (LCA) is een methodologie die toelaat om op een objectieve manier de milieu-impact van een product over de volledige levenscyclus te begroten. Voor een levenscyclusanalyse moeten vier belangrijke stappen worden doorlopen, m.n. de definitie van doel en bereik, de inventarisatie, de impactanalyse en de interpretatie. Hoewel de methodologie oorspronkelijk werd ontwikkeld om de milieu-impact van eenvoudige consumptiegoederen te kunnen evalueren, kan LCA ook worden ingezet om het milieuvoordeel van HVFA- en FA+SF-beton te quantificeren. De uitgevoerde levenscyclusanalyse beoogde de werkelijke vermindering in uitstoot van broeikasgassen te bepalen voortvloeiend uit het vervangen van aanzienlijke hoeveelheden cement door industriële bijproducten zoals vliegask en silica fume. Er moet echter ook aandacht worden besteed aan andere milieuproblemen, m.n. verzuring, vermesting, abiotische uitputting, zoetwater/marine aquatische ecotoxiciteit, aardse ecotoxiciteit, toxiciteit voor de mens, afbraak van de ozonlaag, fotochemische oxidatie, enz. De uitgevoerde levenscyclusanalyses zijn specifiek van toepassing op de situatie in België waar vliegask steeds minder voor handen is en waar geen silica fume wordt geproduceerd. Er wordt verwacht dat soortgelijke levenscyclusanalyses voor landen zoals China en India tot heel andere conclusies zullen leiden. Deze landen hangen nog heel sterk af van kolengestookte elektriciteitsproductie en produceren dus wel nog veel vliegask.

De berekeningen werden uitgevoerd voor functionele eenheden die rekening houden met de sterkte en de levensduur van de alternatieve betontypes in vergelijking met meer traditioneel beton geschikt voor de bestudeerde blootstellingsklassen, m.n. portlandcement beton en vliegaskbeton in overeenstemming met het k-waarde concept. Het is van belang om deze betoneigenschappen in beschouwing te nemen omdat ze de dimensies van een betonstructuur alsook het aantal herstellingen in functie van de tijd bepalen. Met andere woorden, deze eigenschappen leggen de totale betonhoeveelheid vast die nodig is tijdens de volledige levenscyclus van de desbetreffende betonstructuur.

De vereiste betonhoeveelheid per eenheid van sterkte en levensduur, alsook eenvoudige structurele elementen met een gegeven ontwerpbelasting en levensduur kunnen worden

gezien als geschikte functionele eenheden voor de berekening van de ermee gepaard gaande milieu-impacten. Inventarisatie van het gebruik van grondstoffen, de emissies naar lucht, water en bodem en de afvalproductie eigen aan de productie van ieder betonbestanddeel werden gehaald uit de gerenommeerde Ecoinvent database. Op basis daarvan werd dan iedere bestudeerde betonsamenstelling gemodelleerd in de LCA software SimaPro. Daarbij werd bijzondere aandacht besteed aan de allocatie van milieu-impacten ten aanzien van de industriële bijproducten vliegias en silica fume. Tevens werden de effecten van allocatie op de milieuscore van HVFA- en FA+SF-beton in vergelijking met meer traditioneel beton nagegaan. Aangezien vliegias en silica fume niet langer als afvalproducten kunnen worden beschouwd in overeenstemming met Europese Richtlijn 2008/98/EC (2008), is het niet voldoende om enkel de impacten gerelateerd aan de basisbewerkingen na productie in rekening te brengen. Impacten die betrekking hebben op de primaire productieprocessen, m.n. de productie van kolengestookte elektriciteit en metallurgisch silicium, moeten ook deels worden toegekend aan de vliegias en de silica fume. De voorkeur gaat daarbij uit naar economische allocatie, hoewel de gevoeligheid van een dergelijk allocatieprincipe voor sterke prijsfluctuaties toch een probleem blijft. Op basis van de huidige bijproduct / hoofdproduct massa- en prijsverhoudingen, zouden de economische allocatiecoëfficiënten respectievelijk 2,9% en 6,1% bedragen. Gezien het feit dat er slechts kleine hoeveelheden vliegias en silica fume per kWh elektriciteit (0,052 kg) en per kg metallurgisch silicium (0,15 kg) worden geproduceerd, leggen vrij kleine allocatiecoëfficiënten nog steeds belangrijke milieu-impacten op aan de bijproducten.

Milieu-impact

Wanneer het vereiste betonvolume per eenheid van sterkte en levensduur als functionele eenheid wordt aangenomen, hangt de mogelijke reductie in uitstoot van broeikasgassen voor HVFA- en FA+SF-beton nauw samen met de beschouwde blootstellingsklasse.

- Blootstellingsklasse XC3/4 – In deze betongeving is het niet mogelijk om met HVFA-beton een belangrijke reductie in broeikasgassen te realiseren. Dit komt vooral door de eerder gematigde sterkte-eigenschappen van dit betontype op jonge leeftijd. Bovendien gaven de levensduurvoorspellingen van eerste en tweede orde aan dat de levensduur van HVFA-beton minder dan 100 jaar kan zijn. Aan de andere kant kan het FA+SF-beton wel een milieuvoordeel opleveren in vergelijking met het referentiebeton op basis van portlandcement voor blootstellingsklasse XC3. Door gebruik te maken van dit betontype kan de uitstoot van broeikasgassen met 28 à 36% worden verminderd.
- Blootstellingsklasse XS2 – Daar HVFA- en FA+SF-beton allebei worden gekenmerkt door een veel langere levensduur dan het referentiebeton op basis van portlandcement, is een reductie in uitstoot van broeikasgassen vrij vanzelfsprekend (HVFA: –25-35%, FA+SF: –55-60%). In vergelijking met het referentiebeton op basis van vliegias conform het k-waarde concept, is er veel minder voordeel te halen, en dit omwille van de vergelijkbare levensduurprestaties van dit beton met de alternatieve betontypes. Een verminderd effect op de opwarming van de aarde is dan enkel mogelijk voor het FA+SF-beton (uitstoot broeikasgassen: –19-21%). In deze blootstellingsklasse lijkt het beton met slechts 15% vliegias conform het k-waarde concept een beter alternatief voor traditioneel portlandcement

beton (uitstoot broeikasgassen: -45-50%) dan beton met een veel meer doorgedreven cementvervanging.

Wanneer gekeken wordt naar andere milieueffecten buiten de klimaatverandering, dan is het vrij duidelijk dat het gebruik van grote hoeveelheden vlieg-as en silica fume in beton allesbehalve milieuvriendelijk is. De productie van kolengestookte elektriciteit en metallurgisch silicium is net als de cementproductie sterk afhankelijk van de ontginning en de verbranding van fossiele brandstoffen. Dergelijke praktijken wegen vrij zwaar door in de impactcategorieën die betrekking hebben op verzuring, vermesting, abiotische uitputting, zoetwater/marine aquatische ecotoxiciteit, aardse ecotoxiciteit, afbraak van de ozonlaag en fotochemische oxidatie. Gezien de lage bijproduct / hoofdproduct massaverhoudingen blijven de impacten die door middel van economische allocatie worden toegekend aan 1 kg vlieg-as en silica fume aanzienlijk.

Betonnen kolommen en platen met een gegeven ontwerpbelasting en levensduur werden ook getest als functionele eenheid om de mogelijke vermindering in uitstoot aan broeikasgassen bij HVFA- en FA+SF-beton te begroten. Het aannemen van ofwel een betonnen kolom ofwel het vereiste betonvolume per eenheid van sterkte en levensduur als functionele eenheid leidde min of meer tot dezelfde conclusies betreffende de haalbare vermindering in uitstoot van broeikasgassen. Dit was niet het geval bij de betonnen platen. Het gebruik van een beton met een vrij hoge sterkte, bijvoorbeeld het FA+SF-beton, resulteert niet in een sterke vermindering van de plaatdikte en dus een verminderd betonvolume zonder dat de vereiste hoeveelheid wapeningstaal in de trekzone van de plaat sterk toeneemt. Met andere woorden, het voordeel qua betonsterkte kan niet volledig worden benut. Daarenboven doet het extra wapeningsstaal nodig om de scheurwijdte in de trekzone van de plaat te beperken tot een schijnbaar ongescheurde toestand (< 0.05 mm), de plaat gerelateerde uitstoot aan broeikasgassen nog eens toenemen met 25 à 37%.

PART I

GENERAL INTRODUCTION

Fly ash as partial cement replacement in concrete

1.1. Origin and basic properties

1.1.1. Origin

Fly ash is an industrial by-product of coal fired electricity production. Traditionally, it is the result of burning pulverized coal at a power plant. As this fuel type travels through the high temperature zone of the furnace, its volatile matter and carbon content are burned off, while the non-combustible impurities present in the coal (e.g. clay, shale, quartz, feldspar, dolomite and limestone) are carried away in the flue gases. Most of the latter ashlike particles become fused in the combustion zone of the furnace. From the moment they leave this zone, the molten ash cools down rapidly from around 1500°C to 200°C in a few seconds and solidifies into spherical, glassy particles. Only a small portion of agglomerated fused matter remains as bottom ash in the furnace. For environmental reasons, the much larger portion of non-agglomerated spherical particles, also known as fly ashes, cannot be emitted to air. Therefore, they are captured from the flue gases by means of a set of mechanical separators followed by electrostatic precipitators or bag filters [Malhotra and Mehta (2005)].

It must be said that the properties of fly ash can differ depending on the underlying technology for coal fired electricity production. For instance, Pietersen (1993) mentions four different furnaces for the combustion of pulverized coal: the ‘wet bottom’ type operating at around 1800°C, the ‘dry bottom’ type with a flame temperature of around 1400-1600°C, a low-NO_x furnace conditioned at 1300-1500°C and a fluidized bed combustor in which the burning temperatures can be reduced to 900-1000°C. Fly ashes produced with the first furnace type normally comprise the most spherical particles with the highest glass content.

Apart from the evolving combustion technology, the fuel composition has also somewhat changed in the course of time. Nowadays, the number of power plants that still entirely rely on the combustion of pulverized coal has decreased a lot. The burning of co-combustion materials (e.g. biomass) in combination with hard coal is becoming more and more common practice. According to van der Sloot and Cnubben (2000), the use of high portions of co-combustion materials could negatively affect the quality of the fly ash in terms of water demand when applied in concrete or could cause increased leaching when landfilled afterwards. However, when used on a more limited basis in correspondence with the criteria

imposed by the European standard NBN EN 450-1 (2012), fly ashes from co-combustion are still suitable for use in concrete. The minimum percentage of coal by dry mass cannot be less than 60% or 50% in case the co-combustion material only originates from green wood. In addition, the maximum proportion of ash derived from co-combustion materials cannot be more than 30% by dry mass.

1.1.2. Basic properties

Fly ash can be identified as an artificial pozzolan. A material has pozzolanic properties when its constituents react with Ca^{2+} or $\text{Ca}(\text{OH})_2$ and form new binding compounds in the presence of water [Takemoto and Uchikawa (1980) as cited by Baert (2009)]. As it is obtained in an industrial instead of a natural way, it is classified as artificial. A fly ash with purely pozzolanic properties is always the result of burning bituminous coal in the furnace. It typically has a low CaO content ($< 10\%$) and essentially consists of SiO_2 and Al_2O_3 . In accordance with ASTM C618-12a (2012), it can be classified as a class F fly ash. A class C fly ash also exists. It is produced in power plants that burn subbituminous or lignite coal and has a CaO content exceeding 10%. This fly ash has both hydraulic and pozzolanic properties. Now, the few coal fired power plants that remain in Belgium only produce the Class F fly ash. Logically, this research only focuses on the use of this fly ash type.

The pozzolanic activity of a fly ash mainly depends on its glass content which ranges between 60 and 90% according Malhotra and Mehta (2005). Lutze and vom Berg (2010) mention a very similar glass content range which lies between 60 and 85%. For a class F fly ash this glass content consists of aluminosilicates. The remaining crystalline minerals in the fly ash are quartz, mullite, sillimanite, hematite and magnetite. These phases do not contribute to the pozzolanic activity. A small portion of residual carbon is also always present in the fly ash. It is present in the form of porous particles with a high specific surface area. According to Lane and Best (1982), the loss on ignition (LOI) of fly ash is a good measure for the unburned carbon content. A high residual carbon content is not desirable because it increases the water demand and the required dosage of chemical admixtures in concrete. Therefore, NBN EN 450-1 (2012) specifies a maximum allowed loss on ignition for three classes of fly ash (A: $\text{LOI} \leq 5.0\%$ by mass, B: $\text{LOI} \leq 7.0\%$ by mass, C: $\text{LOI} \leq 9.0\%$ by mass).

As a pozzolan, fly ash can partially replace cement in concrete. It reacts with the $\text{Ca}(\text{OH})_2$, one of the hydration products of the remaining cement, and water. In the beginning, the SiO_2 – Al_2O_3 framework of the glassy content is broken down by the OH^- ions. From the moment a sufficient number of Si–O–Si or Si–O–Al bonds have been broken, the free silicate and aluminate anions are detached from the network and react with the calcium hydroxide and water to form an amorphous calcium silicate aluminate phase. This is just one of the major hydration products of the fly ash reaction. Several other aluminate hydrates are being formed as well. For more details on that matter and on the physico-chemical interactions between the fly ash and the cement we refer to the literature review conducted by Baert (2009).

Fly ash is not just capable of replacing part of the cement. When used, its presence also influences the properties of the concrete. In the fresh state, these effects are normally more dependent on the physical characteristics of the fly ash than on the chemical and mineralogical composition [Malhotra and Mehta (2005)]. According to Lutze and vom Berg

(2010) the particle shape and particle size distribution are key governing parameters at this stage. The latter property is normally not fully specified for a fly ash. It is sufficient to determine the amount of material retained on a 45 μm sieve after wet sieving. As such NBN EN 450-1 (2012) distinguishes two classes of 45 μm fineness (N: $\leq 40\%$ by mass, S: $\leq 12\%$ by mass). As already mentioned, the larger part of the fly ash consists of fine spherical particles. These can either have a closed surface, be hollow (cenospheres) or be hollow and filled with other particles (plerospheres). According to Malhotra and Mehta (2005), the spherical morphology and smooth surface help to reduce the inner-particle friction in the fresh concrete. In addition, the fine fly ash particles get adsorbed on the oppositely-charged cement particles. As such, less flocculation of the cement particles occurs which can entrap large volumes of mixing water. Moreover, the fine particle size range of fly ash induces a particle packing effect. Mainly its lower density and higher volume per unit mass makes fly ash a better void filler than cement. As a consequence, a lower paste volume is needed to sufficiently plasticize the concrete. All three mechanisms normally contribute to the lower water demand of concrete with fly ash. However, Baert (2009) mentions that the achievable reduction in unit water content for a given consistency, can still differ considerably depending on the mix proportions of the concrete, the particle shape and fineness of the fly ash, the cement replacement level, the grading of the fine and coarse aggregates, etc. An additional benefit in the fresh state exists which is inherent to the lower required water content in presence of fly ash. As such, bleeding can be reduced considerably. In hardened state, the water reducing property of fly ash reduces drying shrinkage and the resulting cracking phenomena [Malhotra and Mehta (2005)]. Besides this benefit, there is the advantage of a lower autogeneous temperature rise because less cement is present. As such, the risk of thermal cracking is reduced significantly.

According to Baert (2009), the use of fly ash also has some undesirable effects. For instance, Ravina (1986) found that initial and final setting is delayed in presence of class F fly ash. Moreover, the unburned carbon present in the fly ash causes an increased adsorption of chemical admixtures such air entraining agents (AEAs). Due to this phenomenon, the required AEA dosage for a given air content in the fresh state needs to be increased substantially. Still, even then a loss in air content of the fresh concrete still remains possible [Gebler and Klieger (1983)].

In hardened state, the effects of fly ash additions on the concrete strength are certainly of importance. Since the pozzolanic fly ash reaction requires the presence of $\text{Ca}(\text{OH})_2$, one of the hydration products of the remaining cement, the strength development of a fly ash concrete is known to be slower than for a traditional concrete. In the beginning, the present fly ash can merely contribute as filler material by establishing an enhanced particle packing. However, with the current availability of high range superplasticizers the slow strength development can easily be compensated for by reducing the water content of the concrete. As such, an acceptable early age strength can be guaranteed [Mehta (1998)]. Despite the more critical early age strength performance of fly ash concrete, its ultimate strength after the pozzolanic fly ash reaction has taken place, is usually higher than for traditional concrete due to a pronounced densification of the pore structure.

Incorporation of fly ash also has an influence on the durability performance of the concrete. Its effect can be either beneficial or detrimental depending on the deterioration mechanisms in

play. Three major durability problems have been studied in the course of this research, i.e. carbonation, chloride ingress and salt scaling in presence of deicing salts. The way fly ash affects each of these mechanisms has been discussed more in detail in Chapters 5, 6 and 7.

1.1.3. Motives for its use in concrete

1.1.3.1. Technological motives

One of the primary aims of using fly ash in concrete since the 1930s was to reduce the heat of hydration in massive concrete structures such as dams. The resulting low early age strength was not seen as problem because an adequate strength could be achieved at the time the full mechanical loads were applied at 90 days to 1 year [Malhotra and Mehta (2005)]. The Hungry Horse Dam in Montana, USA, is a good example of this practice. For its construction in 1948, 35% of the Portland cement in about 3 million m³ of concrete was replaced with fly ash [Lutze and vom Berg (2010)]. Although the previous section clearly indicates that the application of fly ash in concrete has quite some additional technical advantages, these are seldomly mentioned as justification for its use in the early days. This is probably due to the fact that other fly ash properties were still not fully understood at that time.

1.1.3.2. Environmental motives

Already in the early days, there was some kind of an environmental motive involved. By incorporating fly ash in concrete, a useful destination was found for the increasing amounts of this waste produced at the numerous coal fired power plants. In Germany, this became one of the dominant aims from the mid 1970s onwards [Lutze and vom Berg (2010)]. Another environmental motive came by later on. Once concrete technologists started to realize that cement related CO₂ emissions could be reduced significantly by replacing considerable portions of the cement by a waste product, this motive gained more and more importance. It led to the development of high-volume fly ash concrete at CANMET (Canada Centre for Mineral and Energy Technology) in the 1980s [Malhotra and Mehta (2005)]. Since then, the latter advantage has become the major environmental motive for using fly ash in concrete.

1.1.3.3. Economic motives

Besides the technological and environmental motives, there has always been an economic motive for replacing part of the cement with fly ash. Especially in the beginning, when fly ash was still considered as a mere waste product, the artificial pozzolan was much cheaper than ordinary Portland cement (OPC). Its economic value may have increased since it is being seen as a valuable by-product. Still, its price is less than half the price of OPC.

1.2. The concept of high-volume fly ash (HVFA) concrete

1.2.1. General definition

The term high-volume fly ash (HVFA) concrete has originally been introduced by Malhotra at CANMET [Giaccio and Malhotra (1988)]. Every concrete type with a very low water content and at least 50% of the OPC by mass replaced with a class F or C fly ash, meets the

requirements to be identified as such. More details about its specific characteristics follow in Chapter 4. In this research the focus was on a Class F HVFA concrete.

1.2.2. Reasons for its still limited use in practice

1.2.2.1. Existing regulations on the use of fly ash

In Europe, the partial replacement of OPC by fly ash is strictly regulated by the k-value concept of the European concrete standard NBN EN 206-1 (2000) and corresponding national implementations of this standard (e.g. the Belgian standard NBN B15-001 (2004)). This concept simply does not allow a cement replacement level of 50% or more. The only way to get approval for using this concrete type in Belgium is by proving its equivalent performance in comparison with an appropriate reference concrete for the applicable concrete environment. The underlying test procedures for the equivalent performance concept have been described in NBN B15-100 (2008). More information with respect to both the k-value and equivalent performance concept follow in Chapters 3, 4, 5, 6 and 7.

1.2.2.2. Limited proof of durability in severe environments

Until now, HVFA concrete has been used mainly in less demanding concrete applications (e.g. underground foundations, etc.). For the more demanding concrete applications there is much less field experience. A full assessment of HVFA concrete's equivalent performance in comparison with traditional concrete for various severe concrete environments requires the execution of a full scale experimental test program. The setup for this evaluation may even need to go beyond the original framework of the procedures mentioned in NBN B15-100 (2008) to allow for an additional service life estimation of the concrete. As equivalent performance may not always exist for every environment, it needs to be investigated whether the service life performance of HVFA concrete may still be acceptable. For the moment, all this information is still not sufficiently available. As a consequence, concrete manufacturers are not really encouraged to move further in this direction.

1.2.2.3. Limited quantitative proof of a reduced environment impact

Although it is said that the concept of HVFA concrete holds the potential of reducing cement related greenhouse gas emissions significantly, this has never been verified in an objective way. Without this quantitative proof, it is understandable that this potentially 'green' concrete has not been used yet on a larger scale. In the past, it may have been difficult to determine the actual environmental benefit of the material because the necessary tools were missing. However, the further development of the renowned life cycle assessment methodology could certainly serve this purpose (Chapter 2).

Life cycle assessment as tool for quantifying sustainability

2.1. General principle

In general, Life Cycle Assessment (LCA) can be defined as an assessment tool to quantify the environmental impact of products generated over their entire life cycle. The evaluation addresses all relevant activities necessary to make a product function. Each life phase of the product (extraction of resources, production, use, disposal, etc.) is normally considered [Desmyter and Martin (2001)]. The value of this methodology must be understood in view of the increasing importance of sustainable development, which can be identified as development that meets the needs of the present without endangering those of future generations [World Commission on Environment and Development (1987)]. Within this context, also the construction industry, and more in particular the concrete industry, should aim for a higher sustainability from an environmental perspective. Also in this sector, the LCA framework could certainly serve this goal.

2.2. Past and current use of the life cycle assessment methodology

It must be said that the LCA framework was not originally developed for the construction industry. Moreover, in the beginning it was far from a well-developed methodology. The study of environmental impact of consumer products began in the late 1960s and early 1970s when environmental issues like resource and energy efficiency, pollution control and solid waste became issues of broad public concern [Guinée et al. (2011), Assies (1992)]. Initially, those studies were not much more than simple comparisons between products to see which one was better. Soon it was recognized that for many of these products the largest portion of the environmental impact was not caused by its use, but by its production, transportation or disposal [Guinée et al. (2011)]. One of the first published examples of system analysis quantifying the resource requirements, emission loadings and waste flows of a production chain from ‘cradle-to-grave’, dates back from 1974. The study was conducted by the Midwest Research Institute for the US Environmental Protection Agency [Hunt et al. (1974)]. In fact, it was a follow-up of a study performed by the same institute for the Coca Cola Company in 1969 already to enable an environmental comparison between different beverage containers. Guinée et al. (2011) see the period 1970-1990 mainly as the period of conception for LCA. At

that time there was not much uniformity among the evaluation approaches, terminologies and results which prevented LCA from becoming a generally accepted assessment tool. Thus, there was a growing need for more standardization. The first steps in that direction followed from the 1990s onwards. The Society of Environmental Toxicology and Chemistry (SETAC) took a leading role in the continuous improvement and harmonization of the LCA framework, terminology and methodology and finally came up with the SETAC Code of Practice [Consoli et al. (1993)]. On the other hand, the International Organization for Standardization ISO looked after the standardization of methods and procedures. This resulted in the publication of four international standards:

- ISO 14040 (1997): LCA – Principles and framework.
- ISO 14041 (1998): LCA – Goal and scope definition and inventory analysis.
- ISO 14042 (2000): LCA – Life cycle impact assessment.
- ISO 14043 (2000): LCA – Interpretation.

Later on, these four standards were combined into only two standards, i.e. ISO 14040 (2006) and ISO 14044 (2006). In compliance with these standards, the ultimate definition of LCA was ‘the compilation and evaluation of inputs, outputs and potential environmental impacts of a product system throughout its life cycle. The proposed methodology comprised four major steps: (i) the definition of goal and scope, (ii) the inventory analysis, (iii) the impact assessment and (iv) the interpretation (Figure 2.1).

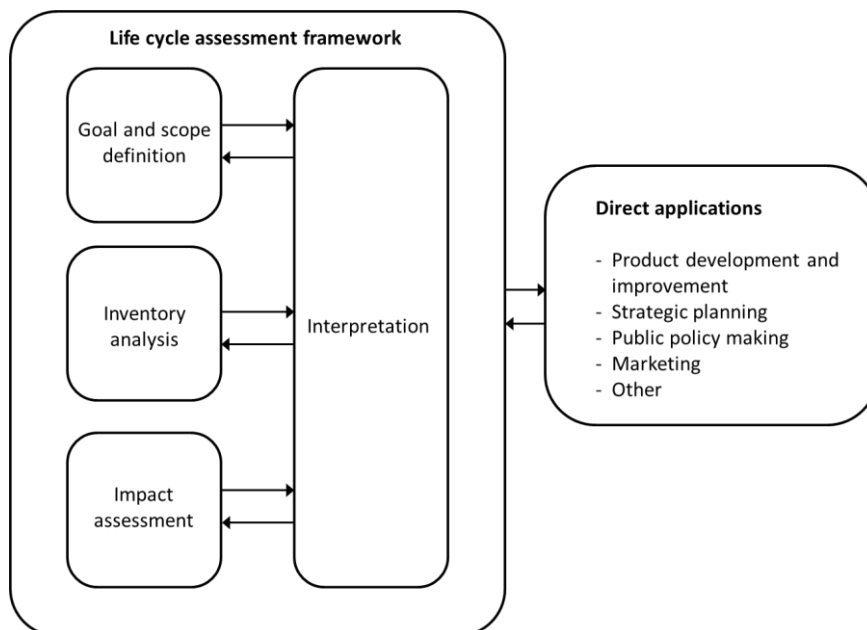


Figure 2.1. The four-step LCA methodology cf. ISO 14040-14044 (2006).

In the 1990s several well-known impact assessment methods for step (iii) were also developed, e.g. the problem oriented CML 1992 method [Heijungs et al. (1992)] and the damage oriented Eco-indicator 99 method [Goedkoop and Spriensma (1999)]. Updated versions of both methods are still in use today.

The extensive efforts done to harmonize and standardize LCA can be held responsible for the substantial attention the methodology gained by the first decade of the 21st century. It is also

in this period that LCA drew the attention of the construction sector [Desmyter and Martin (2001)]. Moreover, environmental policy all over the world started to become more and more life cycle based, especially with respect to carbon footprinting. However, this growing attention for LCA also revealed some problems. Worries started to rise about the correctness and the robustness of the carbon footprint indicators, the neglectance of other environmental impacts and the mere focus on microscopic functional unit related scenarios instead of on more realistic macroscopic scenarios. In addition, the increasing demand for LCA in many different sectors caused a renewed divergence of the methodology again at the expense of the earlier efforts for harmonization and standardization. This is especially true for the choice of the system boundaries, allocation methods, calculation procedures, etc. [Guinée et al. (2011)]. Apparently, each sector has certain ideas on the procedures to follow for adequate LCA. The same goes for the concrete industry.

2.3. Existing bottlenecks when performing life cycle assessment of concrete

To enable a proper environmental impact calculation for concrete with high volumes of the cement replaced by fly ash, several aspects of the general harmonized and standardized LCA methodology will need to be addressed quite thoroughly. Several of these aspects have been introduced briefly below. More information on these and other important issues can be found in the literature review on LCA of traditional and ‘green’ concretes (Chapter 10).

2.3.1. Functional unit choice

In compliance with the LCA methodology, environmental impacts of the concrete should be quantified for a unit that accounts for all the functionalities of the material. In contrast with simple consumer products like for instance the earlier mentioned beverage containers, the use of concrete in construction can cover several functionalities at once (providing shelter, bearing mechanical loads, etc.). A wide range of unit definitions is possible. This can go from a unit concrete volume to a whole concrete structure as built. More clarity is needed on the most appropriate functional unit choice for this type of material.

2.3.2. Data collection

Concrete is a composite material. It is a mixture of cement, water, sand, aggregates, mineral additions (e.g. fly ash) and chemical admixtures (e.g. superplasticizers). Practically all constituents are processed materials originating from nature and thus belong to the technosphere. The use of resources and energy, the emissions to air, water and soil and the waste streams need to be documented and verified for all of them to enable an environmental impact calculation for the composite. Given the number of industrial sectors involved, this is quite a task.

2.3.3. Choice of the allocation of impacts

A mineral addition such as fly ash is an industrial by-product. This means that environmental impact assigned to it, is an allocated impact of coal fired electricity production. The ISO

14040-14044 (2006) standards mention different allocation principles. The suitability of the different allocation approaches needs to be verified.

2.3.4. Identification of the relevant environmental issues

The replacement of large portions of cement by fly ash in concrete mainly aims at reducing the cement related greenhouse gas emissions. The efficiency of this practice can be evaluated through carbon footprinting. However, as the cement replacing materials may play a role in other environmental issues, the mere focus on carbon footprinting is insufficient. Other relevant environmental issues need to be identified. The most suitable impact methods to quantify the corresponding impacts should be chosen accordingly.

A twofold research purpose

3.1. Quantifying the sustainability of HVFA and FA+SF concrete using LCA

Since the development of HVFA concrete in the late eighties of the previous century, introduction sections of the numerous scientific articles and books published on the material include often nothing more than a rather vague general justification for the research conducted. Usually, their authors state that because at least 50% of the OPC is replaced with pozzolanic fly ash, a by-product of coal fired electricity production, cement related greenhouse gas emissions can be reduced substantially. However, the environmental benefit that is aimed for is almost never quantified in an objective way. Or even worse, it is roughly estimated that the reduction in environmental burden in terms of percentage should more or less resemble the cement replacement level. The latter approach totally disregards important differences between HVFA concrete and traditional OPC concrete in terms of strength and durability, which can result in higher concrete amounts needed for the former or latter concrete type to construct and maintain infrastructure carrying a given mechanical load for given predefined time span. The current absence of a reliable quantitative environmental score for HVFA concrete mainly originates from the fact that the above mentioned differences still have not yet been sufficiently documented. Given the abundant amount of literature available on fly ash concrete in general and HVFA concrete in particular, this statement may seem surprising. Yet, it must be said that the majority of the studies conducted in the past mainly dealt with HVFA concrete for use in less demanding applications (e.g. massive unreinforced concrete volumes, foundations, etc.) where differences in strength and durability are much less an issue. The studies available on the performance of HVFA concrete in environments where for instance corrosion of the embedded rebars is at risk or where freeze/thaw cycles in combination with deicing salts can induce severe salt scaling, are not extensive enough. They usually do not allow for at least a proper equivalent performance evaluation in comparison with the proper reference concrete and at best for a proper service life prediction that gives a good idea of the expected number of required rehabilitation actions in time. As a consequence, it remains impossible for the moment to calculate a durability related environmental score.

Within the framework of this PhD thesis, the necessary experimental program has been set up and executed to include mainly durability, hence service life performance and strength aspects into environmental impact calculations for HVFA concrete while using the well-accepted life cycle assessment (LCA) methodology as prescribed by ISO 14040-14044 (2006). Concrete in which 50% of the cement is replaced by a combination of fly ash (FA) and silica fume (SF) was studied in the same way. This FA+SF concrete could be a better alternative to OPC concrete than HVFA concrete. All compositions under investigation were designed based on the knowledge gained from earlier HVFA compositions that have been studied at the Magel Laboratory for Concrete Research (Chapter 4).

The durability performance of the proposed HVFA and FA+SF concrete in three demanding concrete environments was studied prior to the actual environmental impact calculations for these materials: environments where (i) carbonation-induced corrosion (Chapter 5: exposure classes XC3 and XC4) or (ii) chloride-induced corrosion (Chapter 6: exposure class XS2) of the reinforcing steel is at risk and environments where (iii) freeze/thaw attack in combination with deicing salts could cause serious salt scaling (Chapter 7: exposure class XF4). The necessary comparison was made with the durability performance of suitable reference compositions for the exposure classes under investigation. The applied methodology was similar to the one described in NBN B15-100 (2008) for the assessment and validation of less conventional binders for concrete. This Belgian standard particularly deals with concrete containing cements and/or additions of type II for which the standard NBN EN 206-1 (2000) and its national annex NBN B15-001 (2004) provide no or insufficient application rules. Concrete with a binder system consisting of a specific cement type combined with a specific addition of type II (e.g. fly ash) belongs to this category of compositions. With large portions of the cement replaced by fly ash (and silica fume), the studied HVFA and FA+SF concrete compositions need to be evaluated in accordance with this standard because they are not in agreement with the k-value concept of NBN EN 206-1 (2000) and NBN B15-001 (2004). In NBN B15-100 (2008) a standard procedure is given for determining both the general and specific fitness of non-conventional binder systems. Durability issues are normally dealt with within the assessment of the specific fitness. The reference concrete to be used for this should have a composition that would normally be prescribed for the specific application field such as the above mentioned exposure classes. It needs to be subjected to the same durability tests as the concrete compositions under investigation to see whether the applicable equivalent performance criteria of NBN B15-100 (2008) can be met. The evaluation approach in this research was similar. The prescribed durability tests and the criteria of acceptance per test have been mentioned further on in the chapters on carbonation (Chapter 5), chloride ingress (Chapter 6) and freeze/thaw with deicing salts (Chapter 7).

For the environments with exposure to carbonation- and chloride-induced corrosion, the results of the durability tests were implemented in available service life prediction models (Chapter 8 and 9). Because adequate prediction models are not really available for freeze/thaw attack in combination with deicing salts this step could not be included for exposure class XF4.

The knowledge gained during the experimental and modeling phase enabled a fulfillment of the first main research purpose of this thesis: an objective quantification of the sustainability of HVFA and FA+SF concrete using LCA (Chapter 10, 11 and 12).

3.2. Optimizing the LCA framework for sustainability studies of concrete

Within the development process of any new potentially 'green' concrete type, it is at all-time imperative to keep an eye on its expected environmental impact. While the mix design of HVFA and FA+SF concrete requires an in-depth evaluation of the actual reduction in cement related greenhouse gas emissions, other potentially 'green' new concrete types may require a slightly different approach.

In case the 'greenness' of other concrete types comes from reducing concrete's negative effect on global warming by replacing large portions of the OPC with other industrial by-products apart from fly ash (e.g. blast-furnace slag), the methodology will remain in essence the same. A full experimental characterization of the concrete's durability and strength will be required first before the actual life cycle assessment can be conducted.

Nevertheless, other concrete types, not characterized by high cement replacement levels, also exist. For instance, there is the example of completely recyclable and self-healing concrete, two concrete types which have been studied extensively at Magnel Laboratory for Concrete Research since 2007-2008.

With respect to the former concrete type, its composition should be conceived in such a way that the debris obtained after demolition at the end of its service life can be used directly as raw material for Portland cement production. This strategy would avoid further exploitation of natural resources and provide a useful destination for the debris which would otherwise be destined for landfill. Given the concept of completely recyclable concrete, it is quite clear that a mere understanding of the concrete's durability, service life and strength is not enough to conduct a proper LCA. The possible end-of-life scenarios (recycling versus landfill) and possible avoided environmental issues that could result from recycling (e.g. leaching, land use, etc.) obviously need to be implemented in the LCA as well.

When looking at self-healing concrete on the other hand, the strategy to follow could be similar to one that will be discussed in this thesis for concrete with high cement replacement levels, with one exception. Since self-healing concrete relies on embedded healing agents of various origins (microbial, polymeric, etc.) that are triggered upon crack occurrence, the underlying experimental durability assessment for LCA purposes will need to be quite extensive. It means that the experimental methods involved will need to allow for a determination of the expected time to unacceptable concrete cracking. This is in contrast with the bulk of the service life predictions that have been conducted in literature for environments with exposure to rebar corrosion, one of the major future fields of application for self-healing concrete. There, the time to steel depassivation is often set to correspond with the end of service life. This definition can no longer be used if one wants to estimate the environmental benefits that can be achieved with self-healing concrete in comparison with cracked concrete. With inclusion of the corrosion propagation period, a proper LCA seems very well possible.

Thus, potentially 'green' concrete compositions will always require an experimental characterization of the material's performance in time (i.e. a notion of durability and service life) prior to the actual LCA. Evidently, little information on this performance in time is readily available in the early stages of product development and this for two reasons. (i) The new material has not been applied yet in any real structure that could be regularly inspected for damage. (ii) Accelerated laboratory durability tests that allow for adequate service life

prediction are time consuming. True, some basic durability tests exist of which the outcome can be used directly for a first estimation of service life on the short term. However, these tests and the resulting preliminary service life predictions are usually not one hundred percent representative for the deterioration mechanisms and concrete compositions under investigation. Moreover, they do not take into account the often very relevant meteorological conditions of the concrete's future environment. Logically, an experimental quantification of these influencing factors asks for more effort and time within the product development process. Both items will be addressed only if a first rough service life and sustainability assessment based on rather easy-to-obtain data already gives promising results. Only then, the developers of the new material may want to spend the extra effort. The consequences of this gradual shift from a rudimentary (first order) towards a more advanced (second order) service life prediction on the environmental score of concrete will be demonstrated in this thesis for HVFA and FA+SF concrete (Chapters 10, 11 and 12). Moreover, the LCA of HVFA and FA+SF concrete in all its details can be seen as a case study to optimize the combined experimental program and LCA framework to allow for adequate environmental impact calculations for concrete in general. It is seen as the second main research purpose of this thesis.

In the course of this PhD research, a considerable portion of the results obtained have already been published. As such, several of the chapters in this PhD thesis are to a large extent based on the content of published journal papers. The bibliographical references to these journal papers together with an indication of the chapters in which their content was used are given below:

- Van den Heede P, Maes M, Gruyaert E, De Belie N (2012). Full probabilistic service life prediction and life cycle assessment of concrete with fly ash and blast-furnace slag in a submerged marine environment: A parameter study. *Int J Environ Sust Dev*;11(1):32-49.
(Chapters 4, 6, 9)
- Van den Heede P, De Belie N (2012). Environmental impact and life cycle assessment (LCA) of traditional and 'green' concretes: Literature review and theoretical calculations. *Cem Concr Compos*;34(4):431-442.
(Chapter 10)
- Van den Heede P, Fumiere J, De Belie N (2013). Influence of air entraining agents on deicing salt scaling resistance and transport properties of high-volume fly ash concrete. *Cem Concr Compos*;37(3):293-303.
(Chapters 4, 7)
- Van den Heede P, De Belie N (2014). A service life based global warming potential for high-volume fly ash concrete exposed to carbonation. *Constr Build Mater*;55(3):183-193.
(Chapters 4, 5, 8)
- Van den Heede P, Maes M, De Belie N (2014). Influence of active crack width control on the chloride penetration resistance and global warming potential of concrete slabs made with fly ash + silica fume concrete. *Constr Build Mater*;67(Part A):74-80.
(Chapter 4, 6, 9)

PART II

DURABILITY

Concrete mixtures

4.1. Materials applied

4.1.1. Ordinary Portland cement

Within all tested concrete, mortar and paste mixtures, the applied cement type was an Ordinary Portland Cement (OPC) CEM I 52.5 N, complying with NBN EN 197-1 (2011). In total, cement from eight different deliveries to the laboratory was used. Their loss on ignition (LOI), Blaine fineness, density and chemical composition as determined in accordance with NBN EN 196-2 (2005) and NBN EN 196-6 (2010) are given in Table 4.1.

Table 4.1. Loss on ignition (%), Blaine fineness (m²/kg), density (kg/m³) and chemical composition (%) of the eight deliveries of CEM I 52.5 N.

| Cement | CEM I 52.5 N | | | | | | | |
|--------------------------------|---------------------|----------|----------|----------|----------|----------|----------|----------|
| Delivery | 1 | 2 | 3 | 4 | 5 | 6 | 7 | 8 |
| LOI | 1.51 | 1.78 | 1.74 | 1.35 | 1.33 | 1.89 | 1.45 | 1.82 |
| Blaine fineness | 353 | 429.3 | 382.6 | 352 | – | 402.5 | 396.2 | 370 |
| Density | 3122 | 3107 | 3062 | 3033 | – | 3092 | 3137 | 3126 |
| CaO | 63.37 | 63.48 | 62.04 | 62.91 | 62.56 | 62.16 | 62.77 | 62.30 |
| SiO ₂ | 18.90 | 19.61 | 18.99 | 18.50 | 18.81 | 18.54 | 18.51 | 18.77 |
| Al ₂ O ₃ | 5.74 | 5.96 | 5.97 | 5.94 | 5.74 | 6.04 | 6.24 | 6.00 |
| Fe ₂ O ₃ | 4.31 | 4.13 | 4.23 | 4.15 | 4.24 | 4.27 | 4.12 | 4.06 |
| MgO | 0.89 | 0.92 | 0.96 | 0.97 | 1.07 | 1.03 | 1.08 | 1.07 |
| K ₂ O | 0.73 | 0.64 | 0.66 | 0.69 | 0.61 | 0.71 | 0.64 | 0.58 |
| Na ₂ O | 0.47 | 0.49 | 0.46 | 0.46 | 0.51 | 0.46 | 0.50 | 0.51 |
| SO ₃ | 3.34 | 2.72 | 3.18 | 3.28 | 3.21 | 3.21 | 3.44 | 3.35 |
| CO ₂ | 0.50 | 0.83 | 0.88 | 0.47 | 0.62 | 0.99 | 0.65 | 0.60 |
| Insoluble residue | 0.41 | 0.36 | 0.80 | 0.64 | 0.53 | 0.91 | 0.91 | 0.41 |

When comparing the different batches of cement, it is clear that they are very much alike in chemical and physical properties. From the measured CaO (C), SiO₂ (S), Al₂O₃ (A) and Fe₂O₃ (F) contents for each cement, the corresponding mineralogical compositions could be calculated using the well-known calculation method proposed by Bogue for $A/F \geq 0.64$

(Equation 4-1). The theoretical C_3S , C_2S , C_3A and C_4AF contents obtained per batch of cement are summarized in Table 4.2.

$$C_3S = 4.07 \cdot C - (7.6 \cdot S + 6.72 \cdot A + 1.43 \cdot F + 2.85 \cdot SO_3) \quad (4-1)$$

$$C_2S = 2.87 \cdot S - 0.754 \cdot C_3S$$

$$C_3A = 2.65 \cdot A - 1.69 \cdot F$$

$$C_4AF = 3.04 \cdot F$$

Table 4.2. The theoretical mineralogical compositions (%) of the eight cement CEM I 52.5 N deliveries as obtained using the Bogue calculation method.

| Cement Delivery | CEM I 52.5 N | | | | | | | |
|--------------------|--------------|-------|-------|-------|-------|-------|-------|-------|
| | 1 | 2 | 3 | 4 | 5 | 6 | 7 | 8 |
| C_3S | 60.02 | 55.62 | 52.95 | 60.24 | 57.88 | 56.24 | 57.17 | 55.24 |
| C_2S | 8.99 | 14.34 | 14.58 | 7.67 | 10.34 | 10.80 | 10.02 | 12.22 |
| C_3A | 7.93 | 8.81 | 8.67 | 8.73 | 8.05 | 8.79 | 9.57 | 9.04 |
| C_4AF | 13.10 | 12.56 | 12.86 | 12.62 | 12.89 | 12.98 | 12.52 | 12.34 |

4.1.2. Fly ash

Low calcium fly ashes (Class F) from two different sources were used. For fly ash F(1) there were three deliveries to the laboratory, while only two for fly ash F(2) (Table 4.3).

Table 4.3. Loss on ignition (%), 45 μm fineness (%), density (kg/m^3) and chemical composition (%) per batch of fly ashes F(1) and F(2).

| Fly ash Delivery | F(1) | | | F(2) | |
|---------------------------------|-------|---------|-------|-------|-------|
| | 1 | 2 | 3 | 1 | 2 |
| LOI | 4.8 | 3.38 | 3.60 | 4.4 | 1.84 |
| 45 μm fineness | 13.2 | 12.8 | 11.5 | 26.6 | 16.4 |
| Density | 2230 | – | 2221 | 2260 | 2136 |
| CaO | 2.80 | 4.82 | 3.56 | 7.58 | 3.02 |
| SiO ₂ | 48.54 | 50.51 | 51.37 | 50.83 | 54.19 |
| Al ₂ O ₃ | 33.34 | 29.06 | 28.71 | 20.45 | 23.50 |
| Fe ₂ O ₃ | 3.52 | 4.59 | 5.10 | 7.52 | 7.92 |
| MgO | 0.72 | 0.95 | 1.01 | 1.77 | 1.92 |
| K ₂ O | 1.54 | 1.37 | 1.77 | 1.69 | 3.38 |
| Na ₂ O | 0.34 | 0.39 | 0.29 | 1.00 | 1.08 |
| SO ₃ | 0.80 | 0.82 | 1.11 | 0.68 | 0.94 |
| CO ₂ | – | – | 1.16 | – | – |
| Cl ⁻ | 0.002 | < 0.001 | 0.001 | 0.004 | 0.003 |
| Free CaO | < 0.1 | 0.4 | < 0.1 | 0.8 | 0.1 |
| Reactive SiO ₂ | 34.44 | 35.78 | 37.48 | 35.65 | 41.86 |
| Na ₂ O _{eq} | 1.36 | 1.29 | 1.46 | 2.12 | 3.31 |
| P ₂ O ₅ | 0.86 | 1.13 | 0.64 | 2.99 | 0.27 |

It is clear that all batches of fly ash meet the main requirements specified in NBN EN 450-1 (2012) to qualify for use in concrete: the loss on ignition was lower than 5% (Category A) and

the 45 μm fineness (the fraction retained on a 45 μm sieve during a wet sieving test cf. NBN EN 451-2 (1995)) was less than 40% (Category N). Also, the former property turned out similar for both fly ashes (except for fly ash F(2), Delivery 2), while the latter indicates that fly ash F(1) was always finer than fly ash F(2). Moreover, it must be said that the 45 μm fineness measured for each delivery of fly ash F(1) (13.2%, 12.8% and 11.5% retained, respectively) more or less corresponded with the general maximum limiting value of 12% for a very fine Category S fly ash. When looking at the single result conformity criterion for the 45 μm fineness ($\leq 13\%$ retained) as specified in NBN EN 450-1 (2012), then it turns out that only Delivery 1 of fly ash F(1) is actually not a Category S fly ash. For Category S fly ashes normally the water requirement should be verified experimentally and not exceed 95% of that for the corresponding test cement. Since all the fly ashes were originally classified as a Category N fly ash by their corresponding manufacturers, this value was never determined. The chemical properties of all fly ashes were in agreement with the criteria imposed by NBN EN 450-1 (2012). The chloride and sulphate content were never greater than 0.10% and 3.0% by mass, respectively. The free CaO oxide content (%) was at all times lower than 1.5% by mass. The reactive SiO₂ content (%) always exceeded 25% by mass. The sum of the SiO₂, Al₂O₃ and Fe₂O₃ content (%) was never less than 70% by mass. The total content of alkalis (calculated as Na₂O_{eq}, %), the MgO content (%) and the content of total phosphate (P₂O₅, %) were never greater than 5.0%, 4.0% and 5.0% by mass, respectively.

4.1.3. Silica fume

Silica fume (SF) from three different deliveries was applied in the FA + SF concrete compositions under investigation (Section 4.4). Table 4.4 gives a general overview of the measured loss on ignition or LOI (%), BET surface area (m²/g), density (kg/m³) and overall chemical composition (%) of the silica fume from deliveries 1 en 2.

Table 4.4. Loss on ignition (%), BET surface area (m²/g), density (kg/m³) and chemical composition (%) of the applied silica fume per batch.

| Silica fume Delivery | SF | |
|--------------------------------|-------|-------|
| | 1 | 2 |
| LOI | 1.66 | 1.86 |
| BET surface area | 17.76 | 15.51 |
| Density | 2232 | 2232 |
| CaO | 0.23 | 0.20 |
| SiO ₂ | 95.60 | 94.73 |
| Al ₂ O ₃ | 0.34 | 0.36 |
| Fe ₂ O ₃ | 0.11 | 0.71 |
| MgO | 0.37 | 0.39 |
| K ₂ O | 0.92 | 0.90 |
| Na ₂ O | 0.28 | 0.20 |
| SO ₃ | 0.28 | 0.27 |
| CO ₂ | 0.15 | 0.24 |
| Insoluble residue | 66.94 | 67.88 |

For both deliveries, the amorphous SiO_2 content ($> 85\%$), the LOI ($< 4.0\%$) and the BET surface area ($> 15 \text{ m}^2/\text{g}$) were in compliance with NBN EN 197-1 (2011). The materials were also in agreement with NBN EN 13263-1+A1 (2009), the European standard on silica fume for concrete. Since all properties shown were very similar for both silica fumes, the full characterization was not done for the third delivery of silica fume.

4.1.4. Sand and aggregates

In total, sand and aggregates from seven deliveries of natural river sand 0/4, four deliveries of rounded gravel 2/8 and five deliveries of rounded gravel 8/16 were used in the course of this research. The particle size distributions of all of them are shown in Figure 4.1. In general, the particle size distributions for the different batches of sand and aggregates look more or less similar. The most significant variations could usually be observed for the percentages of material passing through the lower sieve mesh sizes per sand and aggregate (e.g. sand 0/4: 0.25 mm, gravel 2/8: 4 mm).

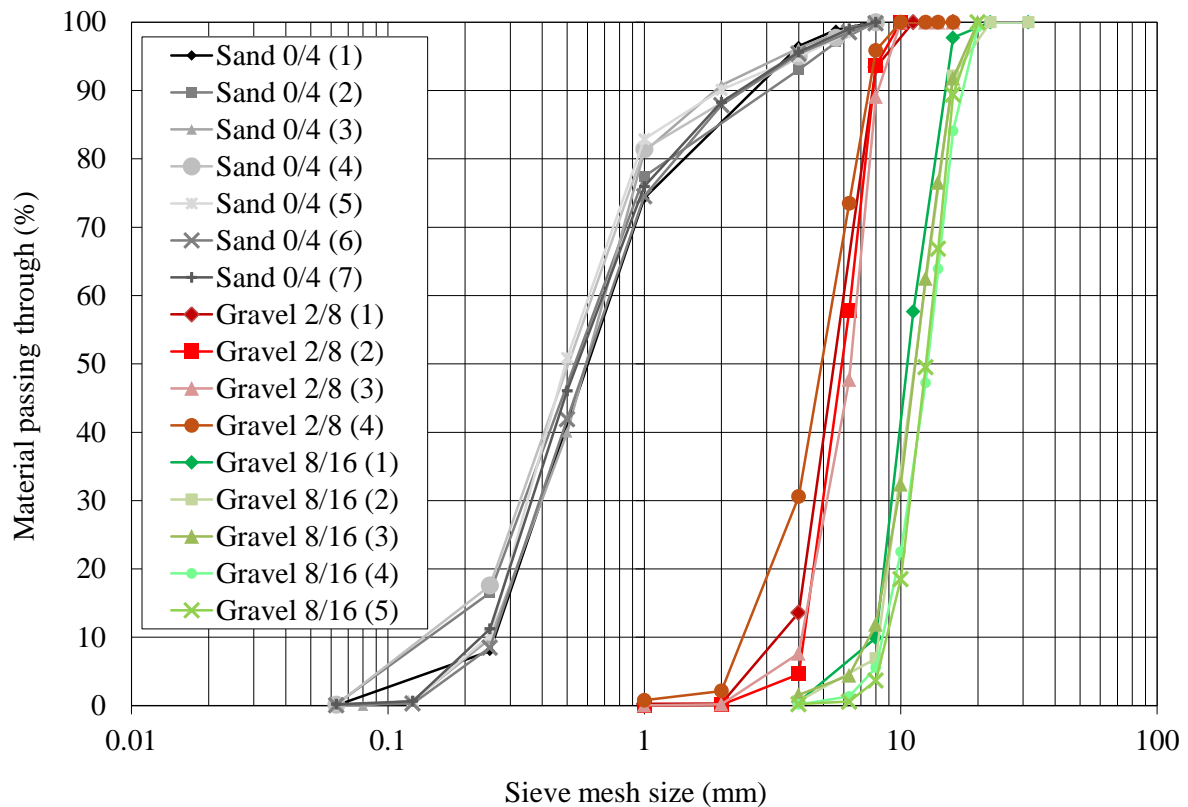


Figure 4.1. Particle size distributions of the applied deliveries of natural river sand 0/4, rounded gravel 2/8 and gravel 8/16.

Apart from its application in concrete, sand 0/4 (5) was used for the manufacturing of concrete representative mortars complying with the Concrete Equivalent Mortar (MBE) method by Schwartzentruber and Catherine (2000). Therefore, the specific surface areas S and water absorption coefficients A (as determined in accordance with EN 1097-6 (2000)) of this sand and the coarse aggregates it replaces in the MBE mortar (being gravel 2/8 (3) and gravel 8/16 (4)) need to be known. The obtained specific surface areas S for sand 0/4 (5), gravel 2/8

(3) and gravel 8/16 (4) amounted to 4.889 m²/kg, 0.398 m²/kg and 0.194 m²/kg, respectively. The corresponding water absorption coefficients A were 0.008, 0.018 and 0.011, respectively. More details regarding the calculation of the MBE mortar mixture proportions based on the values of the specific surface areas and the water absorption coefficients can be found in Section 4.4.1.

4.1.5. Superplasticizer

To improve the workability of the studied concrete mixtures, often characterized by low water-to-binder (W/B) ratios of around 0.35, a commercially available polycarboxylic ether-based superplasticizer (SP) (dry matter mass percentage: 35%, density at 20°C: 1100 kg/m³) was used. The corresponding product information indicates that the optimal dosage for this SP ranges between 400 and 1200 cc per 100 kg of cement. The SP is preferably added after the mixing water and all other concrete constituents. It is said to be compatible with the proposed air entraining agent (Section 4.1.6).

4.1.6. Air entraining agent

To improve concrete's resistance against freeze/thaw attack in presence of deicing salts, an air entraining agent (AEA) can be added. A commercially available fatty acid/polyglycol based AEA (dry matter mass percentage: 4%, density at 20 °C: 1000 kg/m³) was incorporated in the concrete compositions designed for use in exposure class XF4. According to the product specifications, the use of this chemical admixture ensures that artificial air bubbles can be successfully entrained, stabilized and maintained in concrete that contains fly ash or high percentages of fine materials. The admixture dosage necessary to achieve this goal normally ranges between 50 to 550 cc per 100 kg of cement. The AEA needs to be added to the mixing water before being added to the binder, sand and aggregates. When applied, its presence has been indicated within the mixture names of the applicable concrete compositions by means of the letter 'A'.

4.2. Evaluation of the previously developed HVFA concrete mixtures

4.2.1. Compositions of previously developed HVFA concrete

The original definition as proposed by Malhotra in the 1980s suggests the following basic requirements for a concrete composition to qualify as high-volume fly ash concrete [Malhotra and Mehta (2005)]:

- Minimum 50 m% of the binder (B = cement + FA) content consists of ASTM Class F or Class C fly ash.
- The cement content is low, generally no more than 200 kg/m³.
- The water content is low, usually less than 130 kg/m³.
- To obtain a 28-day compressive strength of at least 30 MPa and a slump value exceeding 150 mm for a W/B ratio of 0.35 or less, a superplasticizer is required.
- In case of exposure to freeze and thaw, the use of an air entraining agent (AEA) resulting in an adequate air-void spacing factor, is mandatory.

Apart from a general definition for HVFA concrete, Malhotra and Mehta (2005) also provided typical mixture proportions for the concrete type. To achieve a moderate strength (30 MPa) at 28 days, the water content, the ASTM Type I/Type II cement content and the ASTM Class F fly ash content should amount to 115-125 kg/m³, 155-160 kg/m³ and 215-220 kg/m³, respectively. This means that the corresponding total binder contents, fly ash-to-binder (FA/B) and water-to-binder (W/B) ratios of the suggested concrete compositions should equal 370-380 kg/m³, 58% and 0.31-0.33, respectively. When aiming for a high strength (40 MPa) at 28 days, the water content, the ASTM Type I/Type II cement content and the ASTM Class F fly ash content of the HVFA concrete should range between 115-120 kg/m³, 180-200 kg/m³ and 220-225 kg/m³, respectively. The resulting total binder contents, FA/B and W/B ratios are 400-425 kg/m³, 55-53% and 0.29-0.28.

HVFA concrete has also been investigated at the MagneL Laboratory for Concrete Research since 2003 within the framework of the PhD thesis by Gert Baert [Baert (2009)] and the master theses by Stijn Lammertijn [Lammertijn (2007)] and Philip Van den Heede [Van den Heede (2008)] which were either part of or a continuation of the experimental program initially set up by Kathelijin Cox. When looking at these HVFA mixtures some differences regarding the initial definition of HVFA concrete and the suggested mix proportions by Malhotra and Mehta (2005) can be observed. Two different FA/B ratios for HVFA concrete were considered at that time, i.e. 50% and 67%. The concrete compositions made with these two fly ash contents always had a total binder (B = cement + FA) content of 400 kg/m³ and a W/B ratio of 0.40. The experimental strength and durability of these mixtures was always compared with the corresponding properties of an ordinary Portland cement concrete (FA/B = 0%) and a concrete containing 35% fly ash (FA/B = 35%), both with the same binder content and water-to-binder ratio as the HVFA mixtures. Table 4.5 summarizes the mixture proportions of these concrete mixtures.

The compositions with AEA (*) are the ones studied in Lammertijn (2007), Cox and De Belie (2007) and Lammertijn and De Belie (2008) while the corresponding mixtures without AEA (**) are the ones that were investigated in Van den Heede (2008) and Van den Heede et al. (2010). The experimental strength classes of the concrete compositions shown in Table 4.5 were obtained from compressive strength tests (cf. NBN B15-220 (1990)) performed on a varying number of cubes (Table 4.5: n = 6-12) with a 150 mm side after 28 days of optimal curing at 20 °C and 95% relative humidity (RH). The 5% characteristic compressive strength value needed to determine the strength class was calculated cf. NBN EN 1990 (2002), while assuming the variation coefficient V_X unknown from prior knowledge. This approach was adopted for every composition studied in this thesis.

Note that the cement content of HVFA concrete compositions F50W40 and F67W40 is in agreement with the maximum cement content limit of 200 kg/m³ suggested by Malhotra and Mehta (2005). On the other hand, the applied water content (160 kg/m³) is higher than the proposed 130 kg/m³ criterion. As a consequence, the W/B ratios of these mixtures exceed the required 0.35 to achieve a 28-day compressive strength of at least 30 MPa (as measured on 150 × 300 mm concrete cylinders). Since it is not clear in Malhotra and Mehta (2005) whether this 30 MPa refers to a mean or characteristic strength value, both options were considered. When making the comparison between a desired characteristic cylinder strength of 30 MPa and the characteristic cylinder strengths of the non-air entrained mixtures F50W40 and

F67W40 (Table 4.5: the first figure in the nomenclature of their corresponding strength classes, C25/30^{**} and C16/20^{**}), the latter two compositions cannot really be identified as high-performance HVFA concrete, at least not at early age. In case the 30 MPa indicates a mean compressive strength, the corresponding characteristic strength value is normally around 8 MPa lower, i.e. 22 MPa. In that case only mixture F50W40 may just comply. For the HVFA concrete compositions in which an AEA was applied to achieve a better freeze-thaw resistance their strength is problematic anyhow. Evidently, the compressive strength of air entrained concrete is considerably lower. Usually, every extra percentage of (entrained) air results in a decrease of the concrete's compressive strength with around 5% [Taerwe and De Schutter (1996-2006), Mehta (2001)]. With respect to HVFA mixtures F50W40 and F67W40, the (actually relatively small) dosages of AEA (1.0 ml/kg B) applied resulted in a strength decrease of one strength class to C20/25^{*} and C12/15^{*}, respectively. For a total binder content and W/B ratio of 400 kg/m³ and 0.40 respectively, only the mixture with a cement replacement of 35% (mixture F35W40) seems to meet the 30 MPa cylinder strength criterion. Yet, given its limited cement replacement level, this mixture cannot be seen as a HVFA concrete composition.

Table 4.5. General mixture proportions of the (HVFA) concrete compositions with (*) and without (**) AEA studied by Cox and De Belie (2007) and Van den Heede (2008).

| | F0W40 | F35W40 | F50W40 | F67W40 |
|-------------------------------------|---|--|---|---|
| Sand 0/4 (kg/m ³) | 686 | 668 | 660 | 652 |
| Aggregate 2/8 (kg/m ³) | 451 | 437 | 432 | 427 |
| Aggregate 8/16 (kg/m ³) | 694 | 678 | 668 | 660 |
| CEM I 52.5 N (kg/m ³) | 400 | 260 | 200 | 132 |
| Fly ash (kg/m ³) | 0 | 140 | 200 | 268 |
| Water (kg/m ³) | 160 | 160 | 160 | 160 |
| SP (ml/kg B) | 2.7 [*] /1.9 ^{**} | 1.2 [*] /2.0 ^{**} | 1.2 [*] /2.5 ^{**} | 0.9 [*] /1.9 ^{**} |
| AEA (ml/kg B) | 0.7 [*] /0.0 ^{**} | 0.9 [*] /0.0 ^{**} | 1.0 [*] /0.0 ^{**} | 1.0 [*] /0.0 ^{**} |
| W/B (-) | 0.40 | 0.40 | 0.40 | 0.40 |
| FA/B (%) | 0 | 35 | 50 | 67 |
| Slump (-) ⁺ | S4 [*] /S1 ^{**} | S4 [*] /S3 ^{**} | S4 [*] /S4 ^{**} | S3 [*] /S2 ^{**} |
| Air content (%) | 3.3 [*] /1.6 ^{**} | 4.2 [*] /2.0 ^{**} | 4.3 [*] /1.9 ^{**} | 4.2 [*] /2.5 ^{**} |
| Strength class (-) ⁺⁺ | C45/55 [*] (n = 9) C50/60 ^{**} (n = 9) | C30/37 [*] (n = 7) C35/45 ^{**} (n = 12) | C20/25 [*] (n = 7) C25/30 ^{**} (n = 6) | C12/15 [*] (n = 7) C16/20 ^{**} (n = 6) |

⁺ S1 (10-40 mm), S2 (50-90 mm), S3 (100-150 mm), S4 (160-210), S5 (≥ 220 mm).

⁺⁺ Based on the 5% characteristic compressive strength cf. NBN EN 1990 (2002) (n = varies, V_x: unknown).

4.2.2. Comparison with OPC references

Nevertheless, in comparison with the strength class of OPC concrete composition F0W40 (C45/55^{*} and C50/60^{**}), the strength of all the fly ash containing concrete compositions is several strength classes lower. Obviously, their strength class defining 28-day compressive strength is too low. Still, this observation may also be partly explained by the fact that the strength of the chosen OPC reference may be too high. When designing a new concrete composition for a particular concrete environment, one needs to keep in mind the three basic concrete properties (minimum cement content, maximum water-to-cement (W/C) ratio and

indicative minimum strength class) for the exposure class under investigation as imposed by the European and Belgian concrete standards NBN EN 206-1 (2000) and NBN B15-001 (2004). For the studied exposure classes (XC3, XC4, XS2 and XF4), the suggested minimum cement contents of the applicable reference concrete types are always considerably lower than 400 kg/m³, while the maximum allowed W/C ratios are higher than 0.40 (Table 4.6). As a result, their indicative minimum strength classes are substantially lower than the one obtained experimentally for F0W40. This means that the latter OPC concrete composition is actually too good for the considered environments. Its rather high total cement content also implicates that the environmental benefit that could be gained by replacing a large portion of this cement (200 kg/m³ or more) is overestimated, because the total cement content of the commonly used OPC concrete mixtures for these environments usually does not exceed 340 kg/m³ in practice. Therefore, it was decided to study also the performance of the OPC concrete types for exposure classes XC3, XC4, XS2 and XF4, either as suggested by NBN B15-001 (2004) or NBN EN 206-1 (2000). This resulted in the manufacturing of concrete types T(0.55), T(0.50), T(0.45) and T(0.45)A of which the mixture proportions are given in Table 4.7. Several batches of each composition were made. The applied SP and AEA dosages, slump, air content and strength class per batch are shown in Table 4.8.

Table 4.6. Concrete properties for exposure classes XC3, XC4, XS2 and XF4 cf. NBN EN 206-1 (2000) and NBN B15-001 (2004).

| NBN EN 206-1 | XC3 | XC4 | XS2 | XF4 |
|--|------------|------------|------------|---|
| Max. W/C ratio (–) | 0.55 | 0.50 | 0.45 | 0.45 |
| Min. cement content (kg/m ³) | 280 | 300 | 320 | 340 |
| Min. indicative strength class (–) | C30/37 | C30/37 | C35/45 | C30/37 |
| Min. air content (%) | n.a. | n.a. | n.a. | 4 ^a |
| NBN B15-001 | XC3 | XC4 | XS2 | XF4 |
| Concrete type (–) | T(0.55) | T(0.50) | T(0.45) | T(0.45) / T(0.50)A |
| Max. W/C ratio (–) | 0.55 | 0.50 | 0.45 | 0.45 / 0.50 |
| Min. cement content (kg/m ³) | 300 | 320 | 340 | 340 / 320 |
| Min. indicative strength class (–) | C25/30 | C30/37 | C35/45 | C35/45 / C25/30 |
| Min. air content (%) | n.a. | n.a. | n.a. | n.a./4 ^b /5 ^c /6 ^d |

^a In case the concrete is not air entrained, the performance of the concrete should be tested according to an appropriate test method in comparison with a concrete for which freeze/thaw resistance for the relevant exposure class is proven.

^b For nominal maximum aggregate size D_{\max} : $20 \text{ mm} \leq D_{\max} \leq 31.5 \text{ mm}$.

^c For nominal maximum aggregate size D_{\max} : $11.2 \text{ mm} \leq D_{\max} \leq 16 \text{ mm}$.

^d For nominal maximum aggregate size D_{\max} : $5.6 \text{ mm} \leq D_{\max} \leq 10 \text{ mm}$.

Mixtures T(0.55), T(0.50), and T(0.45) were made in accordance with the guidelines of NBN B15-001 (2004), while mixture T(0.45)A was manufactured in compliance with the criteria NBN EN 206-1 (2000). Mixture T(0.45)A was selected as air entrained reference for exposure XF4 instead of mixture T(0.50)A, because it enabled a better comparison with the performance of the non-air entrained reference T(0.45) for the same exposure class. As such, the effect of the applied AEA on the concrete's deicing salt scaling resistance could be evaluated in a better way, since the only difference between the two mixtures is then the

presence of the chemical admixture in question. Otherwise, the difference in performance could also to some (unknown) extent be attributed to the difference in W/C ratio.

Table 4.7. General mixture proportions of the OPC reference compositions suitable for use in exposure classes XC3, XC4, XS2 and XF4.

| Compositions Batch | T(0.55) a-b-c | T(0.50) a-b | T(0.45) a-b-c-d | T(0.45)A a-b-c-d |
|-------------------------------------|--------------------------|------------------------|----------------------------|-----------------------------|
| Sand 0/4 (kg/m ³) | 715 | 714 | 715 | 715 |
| Aggregate 2/8 (kg/m ³) | 516 | 515 | 515 | 515 |
| Aggregate 8/16 (kg/m ³) | 672 | 671 | 671 | 671 |
| CEM I 52.5 N (kg/m ³) | 300 | 320 | 340 | 340 |
| Water (kg/m ³) | 165 | 160 | 153 | 153 |
| SP (ml/kg B) | Table 4.8 | Table 4.8 | Table 4.8 | Table 4.8 |
| AEA (ml/kg B) | 0.0 | 0.0 | 0.0 | Table 4.8 |
| W/C (-) | 0.55 | 0.50 | 0.45 | 0.45 |

Table 4.8. SP dosage, AEA dosage, slump, initial air content and strength class of OPC references T(0.55), T(0.50), T(0.45) and T(0.45)A.

| Composition | Batch | SP (ml/kg B) | AEA (ml/kg B) | Slump⁺ (-) | Air content (%) | Strength class⁺⁺ (-) |
|--------------------|--------------|-------------------------|--------------------------|----------------------------------|----------------------------|--|
| T(0.55) | a | 0.0 | 0.0 | S3 | 1.6 | C30/37 (n = 3) |
| | b | 2.0 | 0.0 | S4 | 2.3 | C30/37 (n = 3) |
| | c | 2.0 | 0.0 | S3 | 2.8 | C35/45 (n = 4) |
| | | | | | | C30/37 (n = 10) |
| T(0.50) | a | 0.0 | 0.0 | S1 | 2.6 | C45/55 (n = 3) |
| | b | 5.0 | 0.0 | S3 | 1.7 | C45/55 (n = 3) |
| | | | | | | C45/55 (n = 6) |
| T(0.45) | a | 4.9 | 0.0 | S2 | 2.8 | C50/60 (n = 3) |
| | b | 4.9 | 0.0 | S2 | 2.8 | C50/60 (n = 3) |
| | c | 3.0 | 0.0 | S4 | 2.2 | C40/50 (n = 3) |
| | d | 4.0 | 0.0 | S3 | 1.6 | C50/60 (n = 4) |
| | | | | | | C45/55 (n = 13) |
| T(0.45)A | a | 4.4 | 1.5 | S2 | 5.6 | C40/50 (n = 3) |
| | b | 4.9 | 2.2 | S3 | 6.6 | C35/45 (n = 3) |
| | c | 4.0 | 2.0 | S5 | 6.8 | C35/45 (n = 3) |
| | d | 3.0 | 2.0 | S4 | 5.8 | C35/45 (n = 3) |
| | | | | | | C35/45 (n = 12) |

⁺ S1 (10-40 mm), S2 (50-90 mm), S3 (100-150 mm), S4 (160-210), S5 (≥ 220 mm).

⁺⁺ Based on the 5% characteristic compressive strength cf. NBN EN 1990 (2002) (n = varies, V_x: unknown).

When the comparison is made between the experimental strength classes (Table 4.8) of mixtures T(0.55), T(0.50), T(0.45) and T(0.45)A and the indicative strength classes for these reference concrete types as given in either NBN B15-001 (2004) or NBN EN 206-1 (2000) (Table 4.6), the former are always higher than the latter. This observation is no surprise because the minimum indicative strength classes mentioned in the concrete standards must be seen as absolute lower boundaries for expected strength performance. The fact that concrete meets these strength classes per exposure class, must just be seen as an indication that the

concrete does not go against the criteria with respect to the required minimum cement content and the maximum W/C ratio allowed. The given minimum indicative strength classes per exposure class do not imply that concrete cannot have a higher strength class.

Note that the cement type used for all OPC reference mixtures was always a CEM I 52.5 N. This was in part done because this was also the cement type used for the OPC reference that was considered in previous research (see Table 4.5). However, it should be mentioned that the Belgian standard NBN B15-100 (2008) does not prescribe the use of just this cement type for a reference concrete when assessing the specific fitness in terms of durability of a binder system with type II additions. Depending on the concrete environment other cement types can be used as well. For instance, in an environment with exposure to carbonation a CEM III/B could also be used.

4.2.3. Comparison with FA concrete conforming to the k-value concept

The above mentioned reference concrete types are all OPC compositions. It must be said that for each of the exposure classes under investigation a reference concrete composition with FA is also possible.

True, the k-value concept of NBN EN 206-1 (2000) strongly limits the maximum FA content ($FA/cement \leq 0.33$) for such a concrete. When calculating the total binder (cement + FA) content for such a concrete composition, the FA amount needs to be multiplied with a k-factor of 0.4 (in case of CEM I 42.5 or higher), or 0.2 (in case of CEM I 32.5). Moreover, the minimum cement content required for the relevant exposure class may only be reduced by a maximum amount of $k \times (\text{minimum cement content} - 200) \text{ kg/m}^3$ and additionally the amount of (cement + FA) shall not be less than the minimum cement content required in accordance with NBN EN 206-1 (2000). According to NBN B15-001 (2004), it is the amount of (cement + $k \times FA$) that shall not be less than the minimum cement content required which is even a stricter criterion. When combined with a CEM I 52.5 N – as was done in this research – the k-factor for the FA amounts to 0.4.

Nevertheless, if in agreement with all the relevant criteria inherent to the k-value concept, such concrete compositions with FA can also be seen as a proper reference concrete for the corresponding exposure classes. Choosing an OPC concrete or FA concrete conforming to the k-value concept as reference will of course have its consequences when quantifying the environmental benefit of a potentially ‘green’ HVFA or FA+SF concrete. Therefore, some of k-value conforming FA references were also made to study their strength and durability performance. Their mixture proportions are shown in Table 4.9. Each composition was made twice: once with fly ash F(1) and once with fly ash F(2). More information regarding the differences between the two fly ashes can be found in Section 4.1.2.

Within compositions F(1)15_{XC4} and F(2)15_{XC4} the minimum cement content for exposure class XC4 (320 kg/m³) was reduced with the maximum allowable $0.4 \times (320 - 200) = 48 \text{ kg/m}^3$. To meet also the criterion that the (Cement + $k \times FA$) content should equal at least the minimum cement content for exposure class XC4 (320 kg/m³) cf. NBN B15-001 the remaining cement content of the concrete composition still amounts to 300.8 kg/m³. As a result, $FA/(C + k \times FA)$ and $FA/(C + FA)$ ratios are obtained of 15% and 14%, respectively. With 160 kg/m³ water present, the resulting water/(cement + $k \times FA$) ratio equals 0.50 which

corresponds with the maximum W/C ratio for exposure class XC4. The earlier defined W/B ratio or W/(C + FA) ratio is evidently somewhat lower (= 0.46). No extra water was added to compensate for water absorption by the sand and aggregates.

Note that this fly ash content is quite low. The k-value concept allows for a higher amount of fly ash as binder material. However, for a given exposure class the total content of cementitious materials (cement + fly ash) would then also increase. In view of comparative environmental impact calculations, it is important to keep the binder content of the reference concrete as low as possible in order not to overestimate the environmental impacts of the reference. A FA percentage of 15% counts as the maximum FA amount for a minimum total binder content. More fly ash could have been added as filler material. Nevertheless, the latter design approach was not considered in this research.

Table 4.9. Mixture proportions of the concrete compositions with fly ash F(1) and F(2) conforming to the k-value concept and suitable either for use in exposure class XC4 or XS2.

| Composition | F(1)15 _{XC4} | F(2)15 _{XC4} | F(1)15 _{XS2} | F(2)15 _{XS2} |
|-------------------------------------|-----------------------|-----------------------|-----------------------|-----------------------|
| Sand 0/4 (kg/m ³) | 698 | 698 | 696 | 696 |
| Aggregate 2/8 (kg/m ³) | 503 | 503 | 502 | 502 |
| Aggregate 8/16 (kg/m ³) | 656 | 656 | 654 | 654 |
| CEM I 52.5 N (kg/m ³) | 300.8 | 300.8 | 317.6 | 317.6 |
| Fly ash (kg/m ³) | 48 | 48 | 56 | 56 |
| Water (kg/m ³) | 160 | 160 | 153 | 153 |
| SP (ml/kg B) | 2.0 | 3.0 | 2.0 | 3.0 |
| W/(C + k × FA) (–) | 0.50 | 0.50 | 0.45 | 0.45 |
| W/(C + FA) (–) | 0.46 | 0.46 | 0.41 | 0.41 |
| FA/(C + k × FA) | 15 | 15 | 16 | 16 |
| FA/(C + FA) (%) | 14 | 14 | 15 | 15 |
| Slump (–) ⁺ | S3 | S4 | S4 | S4 |
| Air content (%) | 2.7 | 1.5 | 2.5 | 1.8 |
| Strength class (–) ⁺⁺ | C45/55 (n = 3) | C45/55 (n = 3) | C40/50 (n = 3) | C45/55 (n = 3) |

⁺ S1 (10-40 mm), S2 (50-90 mm), S3 (100-150 mm), S4 (160-210), S5 (≥ 220 mm).

⁺⁺ Based on the 5% characteristic compressive strength cf. NBN EN 1990 (2002) (n = varies, V_x: unknown).

Compositions F(1)15_{XS2} and F(2)15_{XS2} were designed to be a representative reference for exposure class XS2. The higher minimum cement content for this exposure class (= 340 kg/m³) was considered when the FA content (= 56 kg/m³) and remaining cement content (= 317.6 kg/m³) of compositions F(1)15_{XS2} and F(2)15_{XS2} were determined. As such, their total binder (B) or (C + FA) content and W/B or W/(C + FA) ratio amounted to 373.6 kg/m³ and 0.41, respectively. Note that no air entrained versions of mixtures F(1)15_{XS2} and F(2)15_{XS2} were made as reference for exposure class XF4. Given the already extensive experimental program, it was not possible to study their deicing salt scaling resistance as well.

Apart from mixture F(1)15_{XS2} (C40/50), the experimental strength classes of all the studied compositions conforming to the k-value concept are similar to the ones obtained for their corresponding OPC reference concrete types, either T(0.50) (C45/55) or T(0.45) (C45/55). Now, comparing the strength classes of HVFA compositions F50W40 or F67W40 (Table 4.5) with those of the OPC or k-value concept conforming references proposed in Tables 4.8 and 4.9, clearly shows that their 28-day characteristic compressive strength is far from sufficient

to compete on a structural basis at early age. Given the fact that their total binder content of 400 kg/m³ was already higher than the (cement (+ FA)) content of these references and that their W/(C +FA) content of 0.40 was lower, it is clear that a HVFA composition with an acceptable early age strength can never have the same total binder content and W/B ratio as its references. This observation suggests a first optimization approach to achieve a more high performance HVFA concrete: applying an even higher total binder content and an even lower W/B ratio (Section 4.3)

4.3. Optimization approach 1: Increasing binder content / lowering W/B ratio

4.3.1. Preparatory study

Within the preparatory study of this optimization approach the total binder content of the HVFA compositions reported in Table 4.5 was maintained at 400 kg/m³ while the W/B ratio was lowered to 0.35 (Table 4.10). The mixture proportions of the resulting compositions F50W35 and F67W35 are shown in Table 4.10.

Table 4.10. Mixture proportions of HVFA concrete compositions with a total binder content of 400 kg/m³ and a W/B ratio of 0.35.

| Composition | F50W35 | F67W35 |
|-------------------------------------|----------------|----------------|
| Sand 0/4 (kg/m ³) | 783 | 671.8 |
| Aggregate 2/8 (kg/m ³) | 420 | 439.9 |
| Aggregate 8/16 (kg/m ³) | 611 | 679.7 |
| CEM I 52.5 N (kg/m ³) | 200 | 132 |
| Fly ash (kg/m ³) | 200 | 268 |
| Water (kg/m ³) | 140 | 140 |
| SP (ml/kg B) | 4.3 | 6.0 |
| AEA (ml/kg B) | 0.0 | 0.0 |
| W/B (-) | 0.35 | 0.35 |
| FA/B (%) | 50 | 67 |
| Slump (-) ⁺ | S1 | S5 |
| Air content (%) | 2.7 | - |
| Strength class (-) ⁺⁺ | C30/37 (n = 3) | C25/30 (n = 3) |

⁺ S1 (10-40 mm), S2 (50-90 mm), S3 (100-150 mm), S4 (160-210), S5 (≥ 220 mm).

⁺⁺ based on the 5% characteristic compressive strength cf. NBN EN 1990 (2002) (n = varies, V_X: unknown.).

Based on compressive strength tests on cubes with a 150 mm side strength classes C30/37 and C25/30 could be assigned to these two compositions. C25/30 is lower than the experimental strength classes of most of the non-air entrained reference concrete types – either OPC based or conforming to the k-value concept – for the exposure classes under investigation. Therefore it was decided to abandon the idea of 67% cement replacement level and to focus on using 50% fly ash. Since the experimental strength class of mixture F50W35 did not exceed C30/37 (which makes it unsuitable for exposure class XS2, at least when working with traditional cements), it was decided to increase the total binder content once more to 450 kg/m³, while maintaining a W/B ratio of 0.35.

4.3.2. Mixtures chosen for durability assessment

Table 4.11 gives a general overview of the HVFA concrete compositions that were studied further on. Both non-air entrained and air entrained versions were considered. Just like for the compositions conforming to the k-value concept, each version was made twice: once with fly ash F(1) and once with fly ash F(2) (see Section 4.1.2). Thus, in total four HVFA compositions were manufactured to be subjected to durability tests representative for exposure classes XC3-XC4, XS2 and XF4. Since quite some batches of each composition were made, the details regarding their admixture dosage, slump, air content and strength class were included in a separate table (Table 4.12).

Table 4.11. Mixture proportions of the HVFA concrete compositions that were subjected to durability tests representative for exposure classes XC3-XC4, XS2 and XF4.

| Composition Batch | F(1)50 a-b-c-d-e-f-g-h | F(1)50A a-b-c-d-e | F(2)50 a-b-c-d-e-f | F(2)50A a-b-c-d |
|-------------------------------------|-----------------------------------|------------------------------|-------------------------------|----------------------------|
| Sand 0/4 (kg/m ³) | 645 | 645 | 645 | 645 |
| Aggregate 2/8 (kg/m ³) | 465 | 465 | 465 | 465 |
| Aggregate 8/16 (kg/m ³) | 606 | 606 | 606 | 606 |
| CEM I 52.5 N (kg/m ³) | 225 | 225 | 225 | 225 |
| Fly ash (kg/m ³) | 225 | 225 | 225 | 225 |
| Water (kg/m ³) | 158 | 158 | 158 | 158 |
| SP (ml/kg B) | Table 4.12 | Table 4.12 | Table 4.12 | Table 4.12 |
| AEA (ml/kg B) | 0.0 | Table 4.12 | 0.0 | Table 4.12 |
| W/B (-) | 0.35 | 0.35 | 0.35 | 0.35 |
| FA/B (%) | 50 | 50 | 50 | 50 |

When looking at the mechanical performance per batch ($n = 3$ or 4) of the non-air entrained composition F(1)50, the achieved strength classes of C40/50 or even C45/55 indicate that a high 28-day compressive strength is possible. This is an improvement in comparison with the HVFA compositions that were tested earlier. However, two batches of the same composition were classified as only a C30/37 concrete. The considerable variation in strength performance per batch resulted in an overall strength class C35/45 ($n = 22$) for the composition in question. For the same composition made with the other fly ash – the coarser fly ash F(2) (see Section 4.1.2) – no strength classes of C40/50 or higher could be recorded. Instead, the strength class per batch ($n = 3$) was either C30/37 or C35/45. As a consequence, the overall strength class of composition F(2)50 was only C30/37. Thus, only composition F(1)50 meets the indicative minimum strength class criterion inherent to each exposure class under investigation (\geq C35/45). Moreover, if the comparison would be made with the experimental strength classes of the applicable reference concrete types, being either OPC concrete (Table 4.8) or fly ash concrete conforming to k-value concept (Table 4.9), the 28-day strength performance of both F(1)50 and F(2)50 would still be insufficient to qualify for use in exposure classes XC4 and XS2, if an equivalent strength performance would be required. This also means that structures made with the proposed HVFA compositions will still have larger structural dimensions than when made with more traditional concrete compositions. To remain environmentally beneficial, the compositions should compensate by performing better in terms of service life.

Table 4.12. SP dosage, AEA dosage, slump, initial air content and strength class of HVFA compositions F(1)50, F(1)50A, F(2)50 and F(2)50A.

| Composition | Batch | SP (ml/kg B) | AEA (ml/kg B) | Slump (-) | Air content (%) | Strength class (-) | |
|-------------|-------|-----------------|------------------|--------------|--------------------|------------------------|-----------------------|
| F(1)50 | a | 7.0 | 0.0 | S5 | 2.6 | C45/55 (n = 3) | |
| | b | 5.0 | 0.0 | S2 | 2.0 | C40/50 (n = 3) | |
| | c | 3.0 | 0.0 | S4 | 2.5 | C30/37 (n = 3) | |
| | d | 4.0 | 0.0 | S3 | 2.5 | C30/37 (n = 3) | |
| | e | 5.0 | 0.0 | S3 | 2.8 | – | |
| | f | 5.0 | 0.0 | S4 | 2.7 | C40/50 (n = 3) | |
| | g | 5.0 | 0.0 | S5 | 2.0 | C40/50 (n = 3) | |
| | h | 5.0 | 0.0 | S3 | 2.7 | C40/50 (n = 4) | |
| | | | | | | C35/45 (n = 22) | |
| F(1)50A | a | 7.0 | 5.0 | S5 | 5.2 | C40/50 (n = 3) | |
| | b | 4.0 | 5.0 | S2 | 4.6 | – | |
| | | | | | | | C40/50 (n = 3) |
| | c | 4.0 | 7.0 | S4 | 7.0 | C25/30 (n = 3) | |
| | d | 4.0 | 7.0 | S2 | 6.1 | C30/37 (n = 3) | |
| e | 4.0 | 7.0 | S1 | 7.6 | C20/25 (n = 3) | | |
| | | | | | | C20/25 (n = 9) | |
| F(2)50 | a | 5.0 | 0.0 | S5 | 2.8 | C35/45 (n = 3) | |
| | b | 5.0 | 0.0 | S5 | 1.6 | C35/45 (n = 3) | |
| | c | 4.0 | 0.0 | S4 | 2.5 | C30/37 (n = 3) | |
| | d | 3.0 | 0.0 | S4 | 2.4 | C30/37 (n = 3) | |
| | e | 3.0 | 0.0 | S3 | 1.8 | C35/45 (n = 3) | |
| | f | 4.0 | 0.0 | S4 | 2.9 | – | |
| | | | | | | C30/37 (n = 15) | |
| F(2)50A | a | 5.0 | 5.0 | S5 | 4.9 | C30/37 (n = 3) | |
| | b | 4.0 | 5.0 | S5 | 4.0 | – | |
| | | | | | | | C30/37 (n = 3) |
| | c | 3.0 | 7.0 | S2 | 8.5 | C16/20 (n = 3) | |
| d | 4.0 | 7.0 | S3 | 6.1 | C20/25 (n = 3) | | |
| | | | | | | C12/15 (n = 6) | |

⁺ S1 (10-40 mm), S2 (50-90 mm), S3 (100-150 mm), S4 (160-210), S5 (≥ 220 mm).

⁺⁺ Based on the 5% characteristic compressive strength cf. NBN EN 1990 (2002) (n = varies, V_x : unknown).

The air entrained versions of compositions F(1)50 and F(2)50 were obviously characterized by a much lower strength. It is clear that the strength difference increases with the difference in (entrained) air content. For the two AEA dosages considered (5.0 ml/kg B and 7.0 ml/kg B), the latter resulted in the highest initial air contents and the lowest overall strength classes (F(1)50A: C20/25 (n = 9), F(2)50A: (C12/15 (n = 6)). This is lower than the indicative minimum for a T(0.45)A reference (C30/37) as defined in NBN EN 206-1 (2000) and lower than the experimental strength class of T(0.45)A (C35/45 (n = 12)). Since a proper deicing salt scaling resistance of concrete depends much more on the presence of a well-developed air void system in the concrete than on its actual strength, the low strength classes of the air entrained HVFA concrete mixtures are not necessarily problematic. On the other hand, even when durable, the larger structural dimensions induced by this very poor strength performance at 28 days may reduce the environmental benefit of the proposed compositions.

In conclusion, the first optimization approach that consisted of increasing the total binder content to 450 kg/m³ and lowering the W/B ratio to 0.35 did not result in a HVFA concrete with a strength class higher than C35/45. The non-equivalent strength performance in comparison with traditional concrete remains an important drawback. Nevertheless, the compositions shown in Table 4.11 were tested further on to characterize their durability performance. A long repair-free service life is as important as a high strength. If the former could be guaranteed despite a lower strength, the composition may still be acceptable from an environmental point of view. At the same time, the search continued to come up with a concrete that has a high cement replacement level ($\geq 50\%$), a high 28-day strength ($\geq C45/55$, cf. T(0.45), $\geq C35/45$ cf. T(0.45)A) and a good durability. Therefore, the possible benefits of adding a third powder, i.e. silica fume, to the concrete were investigated (Section 4.4).

4.4. Optimization approach 2: Introduction of a third powder

4.4.1. Preparatory study

By replacing part of HVFA concrete's 50% fly ash portion by silica fume, a high 28-day strength may be possible without increasing the minimum total binder content of the concrete for a particular exposure class. The possibilities of this strategy were investigated for exposure classes XS2 and XF4. This means that the total binder content of such a concrete should not be below 340 kg/m³ (Table 4.6). From an environmental viewpoint, the binder content should also not be higher than that.

Evidently, the question arises which percentage of the fly ash would need to be replaced with this silica fume in order to achieve the desired early age strength gain. For an OPC concrete, normally no more than 10% of the cement mass is substituted by the material. Two reasons can be given for its addition in rather limited amounts. First of all, silica fume is characterized by a very high specific surface area, which automatically means that its presence will considerably increase the water demand of the concrete. Secondly, it is known to be a very expensive concrete constituent (~0.75 €/kg) (Table 4.13). This is in sharp contrast with common prices for cement (~95 €/ton) and fly ash (~35 €/ton). Since the material cost in construction is preferably as low as possible, a maximum addition of 10% makes sense.

Table 4.13. Unit prices per concrete constituent anno 2012 [source: Pers. Comm. with the manufacturers/suppliers (2012)].

| Constituent | Unit price |
|----------------|-------------|
| Sand 0/4 | 10.32 €/ton |
| Aggregate 2/8 | 19.16 €/ton |
| Aggregate 8/16 | 18.05 €/ton |
| CEM I 52.5 N | 95.00 €/ton |
| Fly ash | 35.00 €/ton |
| Silica fume | 0.75 €/kg |
| Water | 0.004 €/kg |
| SP | 2.22 €/kg |
| AEA | 0.77 €/kg |

During the preparatory study two silica fume percentages (5% and 10% of the total binder mass, 340 kg/m³) in combination with two possible W/B ratios (0.40 and 0.35) were taken into consideration. This gives four FA+SF concrete compositions in total. The effect of the amounts of silica fume on the overall price of the concrete was evaluated while assuming the unit prices reported in Table 4.13 for the different constituents [source: Pers. Comm. with the manufacturers/suppliers (2012)].

Instead of making concrete from the start, equivalent mortar mixtures were manufactured first for the four FA+SF concrete compositions under investigation. An equivalent mortar for OPC reference T(0.45) was also produced. This was done in accordance with the Concrete Equivalent Mortar (MBE) method [Schwartzentruber and Catherine (2000)]. Within a MBE mortar mix, the gravel mass fractions of the corresponding concrete mix – in this case $f_{\text{gravel } 2/8}$ and $f_{\text{gravel } 8/16}$ – are replaced with the amount of sand $\Delta f_{\text{sand } 0/4}$ that has the same specific surface. This sand fraction can be calculated by means of Equation (4-2) in which $S_{\text{gravel } 2/8}$, $S_{\text{gravel } 8/16}$ and $S_{\text{sand } 0/4}$ represent the specific surface areas of the applied coarse aggregates and sand used in the studied concrete mixes.

$$\Delta f_{\text{sand } 0/4} = \frac{f_{\text{gravel } 2/8} \cdot S_{\text{gravel } 2/8} + f_{\text{gravel } 8/16} \cdot S_{\text{gravel } 8/16}}{S_{\text{sand } 0/4}} \quad (4-2)$$

The water amount needs to be adjusted to account for the difference in water absorption between the gravels and the sand. This can be done by using Equation (4-3):

$$\Delta f_{\text{water}} = -f_{\text{gravel } 2/8} \cdot A_{\text{gravel } 2/8} - f_{\text{gravel } 8/16} \cdot A_{\text{gravel } 8/16} + \Delta f_{\text{sand } 0/4} \cdot A_{\text{sand } 0/4} \quad (4-3)$$

with $A_{\text{gravel } 2/8}$, $A_{\text{gravel } 8/16}$ and $A_{\text{sand } 0/4}$ the water absorption coefficients of the coarse aggregates and the sand. The measured water absorption coefficient and the specific surface areas are shown in Table 4.14.

The resulting MBE mortar compositions can be found there as well. The use of MBE mortar instead of concrete normally reduces the material cost and effort [Schwartzentruber and Catherine (2000)]. For each of these MBE mortar compositions three 160 × 40 × 40 mm³ mortar prisms were produced and subjected to a flexural strength and compressive strength test after being cured in water for 28 days cf. NBN EN 196-1 (2005). From the latter test results, the 5% characteristic compressive strength was calculated in correspondence with NBN EN 1990 (2002) (n = 3, V_x = unknown). Only MBE mortar compositions SF10W40 (F(1): 63.51 N/mm²) and SF10W35 (F(1): 67.56 N/mm², F(2): 67.16 N/mm²) were characterized by a characteristic compressive strength higher than the one recorded for OPC reference MBE T(0.45) (62.03 N/mm²). Apparently, applying only 5% SF in presence of 45% fly ash seems to be insufficient to achieve a similar strength at 28 days (56.22 N/mm for W/B = 0.40, 57.03 N/mm² for W/B = 0.35).

When looking at the concrete compositions that correspond with the different MBE mortars, it is clear that even the use of 5% SF in combination with high SP dosages, either 9 or 15.5 ml/kg binder, results in an overall price per m³ (70-76 €/m³) that exceeds the material cost of OPC reference T(0.45) (64 €/m³). Using 10% SF would increase the overall price even more

to 83-88 €/m³. These differences in price still remain after having the price per m³ of concrete normalized to the characteristic compressive strength of the corresponding MBE mortars. As such, the price of the FA+SF concrete compositions would be in the range of 1.25 to 1.33 €/m³/N/mm², while the price of composition T(0.45) would only amount to 1.03 €/m³/N/mm² (Table 4.14).

Table 4.14. Theoretical concrete compositions, specific surface areas and water absorption coefficients of the applied sand and aggregates and MBE mortar mixture proportions.

| Concrete composition | T(0.45) | SF5W40 | SF5W35 | SF10W40 | SF10W35 |
|---|------------------------|-----------------------|-----------------------|------------------------|------------------------------|
| Sand 0/4 (kg/m ³) | 778 | 773 | 791 | 787 | 791 |
| Gravel 2/8 (kg/m ³) | 676 | 671 | 687 | 671 | 687 |
| Gravel 8/16 (kg/m ³) | 447 | 444 | 454 | 444 | 454 |
| CEM I 52.5 N (kg/m ³) | 340 | 170 | 170 | 170 | 170 |
| Fly ash (kg/m ³) | 0 | 153 | 153 | 136 | 136 |
| Silica fume (kg/m ³) | 0 | 17 | 17 | 34 | 34 |
| Water (kg/m ³) | 153 | 136 | 119 | 136 | 119 |
| W/B (-) | 0.45 | 0.40 | 0.35 | 0.40 | 0.35 |
| FA/B (%) | 0 | 45 | 45 | 40 | 40 |
| SF/B (%) | 0 | 5 | 5 | 10 | 10 |
| Sand/aggregate properties | Sand 0/4 | Gravel 2/8 | Gravel 8/16 | | |
| Specific surface area (m ² /kg) | 4.889 | 0.398 | 0.194 | | |
| Absorption coefficient (-) | 0.008 | 0.018 | 0.011 | | |
| MBE Composition | MBE T(0.45) | MBE SF5W40 | MBE SF5W35 | MBE SF10W40 | MBE SF10W35 |
| Sand 0/4 (kg/m ³) | 850.8 | 845.2 | 864.9 | 845.2 | 864.9 |
| CEM I 52.5 N (kg/m ³) | 340 | 170 | 170 | 170 | 170 |
| Fly ash (kg/m ³) | 0 | 153 | 153 | 136 | 136 |
| Silica Fume (kg/m ³) | 0 | 17 | 17 | 34 | 34 |
| Water (kg/m ³) | 136.5 | 119.6 | 102.2 | 119.6 | 102.2 |
| Superplasticizer (ml/kg B) | 3.0 | 9.0 (F(1)) | 15.5 (F(1)) | 9.0 (F(1)) | 15.5 (F(1)) 14.0 (F(2)) |
| W/B (-) | 0.40 | 0.35 | 0.30 | 0.35 | 0.30 |
| FA/B (%) | 0 | 45 | 45 | 40 | 40 |
| SF/B (%) | 0 | 5 | 5 | 10 | 10 |
| 5% characteristic compressive strength (N/mm ²) cf. EN 1990 (2002), (n = 3, V _X unknown) | 62.03 | 56.22 (F(1)) | 57.03 (F(1)) | 63.51 (F(1)) | 67.56 (F(1)) 67.16 (F(2)) |
| Concrete price (€/m ³) | 64 | 70 | 76 | 83 | 88 |
| Concrete price (€/m ³ /N/mm ²) | 1.03 | 1.25 | 1.33 | 1.31 | 1.30-1.31 |

However, if the comparison would be made with the price per m³ per unit of characteristic cube strength of F(1)50 (60 €/m³ divided by 45.81 N/mm² = 1.31 €/m³/N/mm²) or F(2)50 (60.16 €/m³ divided by 43.43 N/mm² = 1.38 €/m³/N/mm²), one can conclude that the material costs of the earlier proposed HVFA compositions and the now considered FA+SF concrete compositions are actually quite similar (Table 4.14). Thus, despite the fact that the price of the former is about 4 €/m³ cheaper than the price of OPC reference T(0.45), the economic benefit completely disappears because of the rather poor 28-day strength of the HVFA concrete. The

strength aspect will be much less an issue for FA+SF concrete. As a consequence, a better durability performance for this concrete type in comparison with traditional concrete would not need to compensate anymore for the larger structural dimensions inherent to a cheaper concrete with a lower early age strength. Instead, this proof of durability could serve as a means to convince people that a somewhat higher production price of the concrete can be worth it. In other words, an optimization approach that consists of introducing 10% silica fume as third powder still holds potential if a good durability performance could be guaranteed. Within the framework of this PhD thesis, the durability of the FA + SF concrete composition with the highest MBE mortar strength (SF10W35) was therefore evaluated experimentally by means of (accelerated) tests representative for the environments in which it would be used.

4.4.2. Mixtures chosen for durability assessment

Similar to the general HVFA concrete formulation that was described in Section 4.3.2, the non-air entrained FA+SF concrete composition SF10W35 was manufactured in twofold: once with a new batch of fly ash F(1) and once with a new batch of fly ash F(2). From now on these mixtures will be identified as F(1)SF and F(2)SF, respectively. Air entrained versions of both mixtures (F(1)SFA and F(2)SFA) were produced as well. The general mixture proportions of all four compositions can be found in Table 4.15. Several batches of each composition were made in which the admixture dosage, slump, initial air content and experimental strength class per batch varied to some extent (Table 4.16). From the overall strength classes based on the strength results of all batches per composition, it is immediately clear that the 28-day mechanical performance of this concrete type is much better when compared with HVFA concrete. The overall strength classes of the non-air entrained F(1)SF and F(2)SF mixtures equal C50/60 and C55/67, respectively. This is higher than the overall strength class of T(0.45) (Table 4.8: C45/55).

Table 4.15. Mixture proportions of the FA+SF concrete compositions that were subjected to durability tests representative for exposure classes XC3, XS2 and XF4.

| Composition Batch | F(1)SF a-b-c-d | F(1)SFA a-b-c-d-e | F(2)SF a-b | F(2)SFA a-b-c |
|-------------------------------------|---------------------------|------------------------------|-----------------------|--------------------------|
| Sand 0/4 (kg/m ³) | 791 | 791 | 791 | 791 |
| Aggregate 2/8 (kg/m ³) | 687 | 687 | 687 | 687 |
| Aggregate 8/16 (kg/m ³) | 454 | 454 | 454 | 454 |
| CEM I 52.5 N (kg/m ³) | 170 | 170 | 170 | 170 |
| Fly ash (kg/m ³) | 136 | 136 | 136 | 136 |
| Silica fume (kg/m ³) | 34 | 34 | 34 | 34 |
| Water (kg/m ³) | 119 | 119 | 119 | 119 |
| SP (ml/kg B) | Table 4.16 | Table 4.16 | Table 4.16 | Table 4.16 |
| AEA (ml/kg B) | 0.0 | Table 4.16 | 0.0 | Table 4.16 |
| W/B (-) | 0.35 | 0.35 | 0.35 | 0.35 |
| FA/B (%) | 40 | 40 | 40 | 40 |
| SF/B (%) | 10 | 10 | 10 | 10 |

Air entrainment obviously induces strength loss. However, the applied AEA dosages that will be used further on to achieve an adequate salt scaling resistance (F(1)SFA: 2.5 ml/kg B, F(2)SFA: 3.0 ml/kg B) resulted in a considerable initial air content (5.3-6.3% and 6.5%) without an unacceptable decrease in strength. The overall experimental strength classes obtained for mixtures F(1)SFA (C40/50) and F(2)SFA (C35/45) are not lower than the strength class measured for the applicable OPC reference T(0.45)A (C35/45).

Table 4.16. SP dosage, AEA dosage, slump, initial air content and strength class of FA+SF compositions F(1)SF, F(1)SFA, F(2)SF and F(2)SFA.

| Composition | Batch | SP (ml/kg B) | AEA (ml/kg B) | Slump (-) | Air content (%) | Strength class (-) |
|-------------|-------|-----------------|------------------|--------------|--------------------|------------------------|
| F(1)SF | a | 14.0 | 0.0 | S4 | 2.1 | C45/55 (n = 3) |
| | b | 14.0 | 0.0 | S4 | 2.6 | C50/60 (n = 3) |
| | c | 12.0 | 0.0 | S4 | 2.7 | C50/60 (n = 3) |
| | d | 14.0 | 0.0 | S4 | 2.5 | C50/60 (n = 4) |
| | | | | | | C50/60 (n = 13) |
| F(1)SFA | a | 12.0 | 5.0 | S5 | 6.4 | C30/37 (n = 3) |
| | b | 12.0 | 3.0 | S5 | 6.7 | C40/50 (n = 3) |
| | c | 10.0 | 1.0 | S2 | 4.1 | C50/60 (n = 3) |
| | d | 12.0 | 2.5 | S4 | 6.3 | C40/50 (n = 3) |
| | e | 12.0 | 2.5 | S4 | 5.3 | C40/50 (n = 3) |
| | | | | | | C40/50 (n = 6) |
| F(2)SF | a | 12.0 | 0.0 | S4 | 3.0 | C50/60 (n = 3) |
| | b | 12.0 | 0.0 | S4 | 3.4 | C55/67 (n = 3) |
| | | | | | | C55/67 (n = 6) |
| F(2)SFA | a | 12.0 | 2.0 | S5 | 6.4 | C35/45 (n = 3) |
| | b | 10.0 | 1.0 | S4 | 5.5 | C35/45 (n = 3) |
| | c | 10.0 | 3.0 | S4 | 6.5 | C35/45 (n = 3) |
| | | | | | | C35/45 (n = 3) |

⁺ S1 (10-40 mm), S2 (50-90 mm), S3 (100-150 mm), S4 (160-210), S5 (≥ 220 mm).

⁺⁺ Based on the 5% characteristic compressive strength cf. NBN EN 1990 (2002) (n = varies, V_x : unknown).

Resistance to carbonation

5.1. Characterization of the deterioration mechanism and the environment

5.1.1. Literature review on the deterioration mechanism

In general, corrosion of steel embedded in concrete consists of two major phases, being the corrosion initiation and propagation period. During the first phase, neither the steel rebar nor the surrounding concrete are visibly deteriorating yet. The actual damage to both the steel and the concrete only occurs during the second phase. It involves formation of more voluminous and porous corrosion reaction products, gradual loss of effective steel cross-section, cracking and spalling of the concrete cover due to the increased volume of the corroding steel and in the end failure of the entire reinforced concrete element/structure due to unacceptable concrete cracking or complete loss of the required steel cross-section [*fib* Bulletin 34 (2006)].

To understand fully what happens during the corrosion initiation period, one must know more about one of concrete's main properties. Under normal conditions, the highly alkaline environment ($\text{pH} \geq 13$) of the concrete is responsible for the formation of a thin oxide and hydroxide layer on top of the steel rebars [Thiery et al. (2007)]. This passivation layer protects the steel against the actual corrosion phenomenon in presence of oxygen and moisture. The above mentioned initiation period corresponds with the time to depassivation of the steel.

Carbonation of the surrounding concrete is one of the mechanisms that can cause this event. Especially in urban and industrial areas and in tropical countries where environmental pollution results in a significant concentration of carbon dioxide, this particular mechanism has the upper hand [da Silva et al. (2009)]. From a chemical viewpoint it is a neutralization reaction of the basic compounds of hydrated cement (in essence $\text{Ca}(\text{OH})_2$ (CH) and calcium silicate hydrates (C–S–H)) by carbonic acid originating from the penetrating CO_2 [Houst and Wittmann (2002), Johannesson and Utgenannt (2001)]. The resulting loss in hydroxide concentration of the pore solution destroys the passive protective oxide film on the steel reinforcements [Papadakis et al. (1991)]. The above mentioned mechanisms indicate that the carbonation resistance of a concrete composition basically depends on two aspects, i.e. the concrete's susceptibility to diffusion of CO_2 and the amount of carbonatable matter available. This dependence is clear from the well-known square-root-time relation (Equation 5-1) for carbonation mentioned in Visser (2012).

$$x_c = \sqrt{\frac{2 \cdot D_c \cdot c_s \cdot t}{a_c}} = \sqrt{\frac{2 \cdot c_s \cdot t}{R_{\text{carb}}}} \quad (5-1)$$

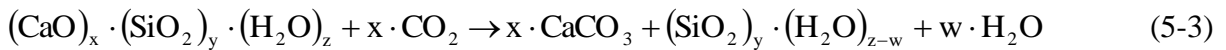
With x_c , the carbonation depth (m), D_c , the diffusion coefficient of CO_2 (m^2/s), c_s , the CO_2 concentration at the concrete surface (kg/m^3), a_c , the amount of carbonatable material per unit volume (kg/m^3), t , the time (s) and $R_{\text{carb}} (= a_c/D_c)$, the carbonation resistance ($(\text{kg}/\text{m}^3)/(\text{m}^2/\text{s})$). Most commonly known is the carbonation process during which the present CH phase reacts with CO_2 . As CO_2 from the surrounding air enters concrete's cement matrix through diffusion it dissolves in the pore water as carbonic acid H_2CO_3 which in turn dissociates as HCO_3^- and CO_3^{2-} ions. On the other hand, the dissolution of solid CH, one of the reaction products of cement hydration, comprises the release of calcium Ca^{2+} and hydroxyl OH^- ions. The reaction between the CO_3^{2-} and the Ca^{2+} ions results in the precipitation of CaCO_3 [Thiery et al. (2007), Borges et al. (2010)]. Equation 5-2 gives a summarizing overview of the chemical reactions involved with CH carbonation [Gruyaert (2011)].



One of the major effects of CH carbonation is a reduction in porosity of the cement matrix. This phenomenon can be explained by the fact that the volume of the Calcite formed is 11-12% greater than the volume of the original CH [Borges et al (2010)].

Thiery et al. (2007) see carbonation of $\text{Ca}(\text{OH})_2$ as only one type of carbonation. Other hydrated compounds can react with CO_2 as well. According to Borges et al. (2010), Parrot (1987) shares a similar opinion. The HCO_3^- and CO_3^{2-} ions present in the pore solution react with the Ca^{2+} ions originating from not only calcium hydroxide (CH), but also from calcium silicate hydrates (C-S-H) and hydrated calcium aluminates and ferro-aluminates. The precipitated reaction products comprise various forms of calcium carbonate, silica gel and hydrated aluminium and iron oxides.

Specifically with respect to C-S-H carbonation, the reaction products are CaCO_3 and a silica gel [Sauman (1971), Slegers and Rouxhet (1976), Suzuki et al. (1985), Kobayashi et al. (1994), as cited by Thiery et al. (2007)]. Equation 5-3 shows the reaction mechanisms associated with C-S-H carbonation [Gruyaert (2011)].



Note that there is evidence that CO_2 reacts simultaneously with the CH and the C-S-H [Groves et al. (1991)]. This statement is also confirmed by Thiery et al. (2007). According to the latter, CH carbonation is initially more rapid than carbonation of the C-S-H gel, but this situation soon reverses because of the formation of a layer of CaCO_3 microcrystals on the surface of CH crystals.

The microstructural consequences of C-S-H carbonation are believed to be very different from the porosity reducing effect of CH carbonation [Borges et al. (2010)]. The removal of interlayer calcium during C-S-H carbonation creates an excess of negative charges, which are

balanced through subsequent formation of Si–OH groups. Condensation of the neighbouring Si–OH groups to Si–OH–Si linkages then forms silica gel [Chen et al. (2006)]. This condensation increases the mean silicate chain length and forms bridges between neighbouring regions. As a result, these regions are being pulled together leading to shrinkage. In other words, the polymerization of the silicate chains in C–S–H may cause a volumetric decrease as well as cracking and a coarsening of the pore structure. This effect is quite in contrast with the decrease in porosity induced by CH carbonation.

Another difference between CH and C–S–H carbonation relates to the mineralogical phases formed in the process. According to Thiery et al. (2007) CH carbonation precipitates mainly well-crystallized Calcite, while its amorphous and metastable polymorphs are more likely the result of C–S–H carbonation. Moreover, the same authors observed a link between the different phases of CaCO₃ and the temperature range in which they decompose during thermogravimetric analysis (550-680°C: the amorphous phase; 680-780°C: the metastable phase, being Vaterite and Aragonite; 780-990°C: the stable phase, being well-crystallized Calcite). In addition, note that Breen et al. (2007) observed a link between the type of metastable calcium carbonate polymorph and the CaO:SiO₂ molar ratio (C/S). Vaterite was found to be present when $C/S \geq 0.67$ while Aragonite occurred when $C/S \leq 0.50$. Borges et al. (2010) associated the presence of Aragonite in carbonated BFS:OPC pastes after decarbonation at lower temperatures with a low CH content prior to carbonation.

Finally, one should be aware that Ettringite carbonation also exists. According to Xiantuo and Ruizhen (1994), Zhou and Glasser (2000) and Houst and Wittmann (1994) Ettringite (or trisulfate hydrates AF₁) decompose into CaCO₃, gypsum and alumina gel. It remains for the moment unclear what kind of effect Ettringite carbonation has on the microstructure of the cement matrix.

Given the different carbonation phenomena, the question arises which mechanism turns out more dominant for a particular binder system. With respect to OPC concrete, there is general agreement upon the fact that the CH carbonation mechanism is prevailing. The resulting formation of more voluminous Calcite easily compensates for any decalcification shrinkage phenomena inherent to C–S–H carbonation [Sisomphon et al. (2010)]. On the other hand, cementitious materials of which the binder fraction consists of cement and mineral additions (e.g. blast-furnace slag, fly ash or silica fume) are usually characterized by a higher porosity after carbonation [De Ceukelaire and Van Nieuwenburg (1993)]. Within blended cement pastes, less CH is initially present because only the OPC fraction of the binder produces CH. Moreover, the CH is being consumed during hydration of the mineral additions. As a result, carbonation of C–S–H is more of an issue for these materials. According to Borges et al. (2010), their susceptibility to C–S–H carbonation highly depends on the permeability of the pastes. Rapid decalcification shrinkage is expected for highly permeable pastes. The process will be accelerated even more for C/S ratios lower than 1.2 [Chen et al. (2006)]. However, if CO₂ ingress is hindered because of a low permeability, C–S–H carbonation might not be a problem, even if the C/S ratio of the blended paste is low [Borges et al. (2010)]. Thus, in case of the former scenario, the decrease in porosity induced by carbonation of the remaining CH cannot compensate for the coarsening of the pore structure attributable to C–S–H carbonation. In case of the latter scenario, the undesirable effects of carbonation might be somewhat less dominant.

5.1.2. Characterization of the concrete environment

Within this part of the research, it has been investigated whether HVFA and FA+SF concrete can be considered useful for steel reinforced concrete applications. Whenever concrete contains reinforcements or other embedded metals and is exposed to a combination of oxygen and moisture, carbonation-induced corrosion is supposed to be at risk. As a result, the studied concrete types need to be optimized for exposure classes XC1 to XC4 in accordance with NBN EN 206-1 (2000). The more critical exposure classes are the ones involving sufficient contact with both water/moisture and oxygen. In other words, the focus should be on exposure classes XC3 and XC4. The first exposure class corresponds with a moderately humid environment with exposure to carbonation-induced steel corrosion. Examples of concrete applications belonging to this exposure class are:

- concrete inside buildings with moderate or high air humidity
- external concrete sheltered from rain.

The second exposure class also represents an environment with exposure to carbonation-induced steel corrosion, but now in combination with wet/dry cycles. During a wet cycle there is direct contact with water. In this perspective, a pertinent remark made by Houst and Wittmann (2002) is worth mentioning here. Concrete exposed outdoors but sheltered from rain carbonates more quickly than concrete that is not sheltered because periodic exposure to rain induces pore blocking. Due to temporary excess presence of water, it is more difficult for the CO₂ to penetrate. In this perspective, exposure class XC3 can be considered as more stringent than exposure XC4.

To develop a better understanding of the typical Belgian exposure conditions, daily relative humidity (RH), precipitation and wind direction data measured between January 1999 and December 2008 at five weather stations (Koksijde (WS1), Kleine Brogel (WS2), Zaventem (WS3), Florennes (WS4) and Luxembourg (WS5)) were analysed. The data were provided by the Royal Meteorological Institute (KMI). A summary of the analysis is shown in Table 5.1. The mean relative humidity for the Belgian climate is clearly rather high (around 80 ± 10% RH) with minima and maxima ranging between around 37% up to 100% RH. A mean value of 80% RH only just still corresponds with the upper limit of the 50-80% humidity range that is considered optimal for the carbonation reaction process [Fernández Bertos et al. (2004)]. The number of days per year that the relative humidity is within this optimal range amounts to 171-212. Thus, humidity conditions are in favor of the carbonation process for only 47-58% of the time. Some literature sources mention a lower upper RH limit for optimal carbonation conditions, i.e. 60% RH (cf. Rozière et al. (2009), Papadakis et al. (1991), Rougeau (1997)) or 70% RH (cf. Audenaert (2006)). In case these values are valid, the time period with an optimal humidity is even shorter. Although no specific RH ranges are mentioned in NBN EN 206-1 (2000), the qualitative definition of exposure class XC3 seems to correspond well with what was observed in terms of air humidity at the five considered locations.

With respect to unsheltered concrete other meteorological conditions such as the amount of precipitation and the wind direction are important as well to assess the concrete's susceptibility to carbonation. Therefore, the time of wetness (ToW) and the probability of driving rain (p_{SR}) were calculated from precipitation and wind direction data provided by the KMI. The first parameter relates to the average number of days per year during which the

amount of precipitation exceeds 2.5 mm. The corresponding ToW value is obtained by dividing this number by the number of days per year during which data were collected. The second parameter gives an indication of the average distribution of the wind direction during such rain events for vertical concrete elements. The p_{SR} parameter corresponds with the number of rainy days (days with precipitation ≥ 2.5 mm) for the most frequently occurring wind direction (usually SW-W) divided by the total number of rainy days for all wind directions. Both ToW and p_{SR} are necessary input to the service life prediction model of *fib* Bulletin 34 (2006) that estimates the time to carbonation-induced corrosion of embedded steel reinforcements. Their effect will be described more in detail in Chapter 8.

Table 5.1. Analysis of daily relative humidity, precipitation and wind direction data measured by the Royal Meteorological Institute (KMI) at five weather stations between 1999 and 2008.

| | WS1 | WS2 | WS3 | WS4 | WS5 |
|--|-------|-------|-------|-------|-------|
| RH _{mean} (%) | 82 | 81 | 79 | 82 | 76 |
| RH _{stdv} (%) | 8 | 11 | 9 | 12 | 14 |
| RH _{min} (%) | 44 | 36 | 40 | 34 | 29 |
| RH _{max} (%) | 100 | 100 | 100 | 100 | 100 |
| Max. number of days per year RH within the optimal 50-80% range | 188 | 178 | 212 | 171 | 207 |
| Average number of days with rainfall ≥ 2.5 mm per year (days) | 115 | 119 | 111 | 124 | 142 |
| ToW (-) | 0.36 | 0.36 | 0.31 | 0.38 | 0.52 |
| p_{SR} (-) | 0.18 | 0.28 | 0.16 | 0.23 | 0.26 |
| Wet period _{mean} (days) | 2 | 2 | 2 | 2 | 3 |
| Wet period _{stdv} (days) | 2 | 2 | 1 | 2 | 3 |
| Wet period _{max} (days) | 12 | 11 | 10 | 10 | 14 |
| Proportioning relative to the mean duration of a wet period (%) | 68-32 | 69-31 | 72-28 | 65-35 | 68-32 |
| Wet period _{median} (days) | 2 | 2 | 2 | 2 | 2 |
| Dry period _{mean} (days) | 5 | 5 | 5 | 4 | 4 |
| Dry period _{stdv} (days) | 5 | 5 | 5 | 5 | 4 |
| Dry period _{max} (days) | 28 | 24 | 28 | 22 | 22 |
| Proportioning relative to the mean duration of a dry period (%) | 72-28 | 72-28 | 74-26 | 72-28 | 72-28 |
| Dry period _{median} (days) | 3 | 3 | 3 | 3 | 2 |

When concrete is being designed for use in exposure class XC4, not only the expected amount of precipitation, but also the duration of rain related wet periods as well as the duration of the preceding and subsequent dry periods are of importance. It would enable the definition of a typical wet/dry cycle for the Belgian climate. Therefore, the durations of the observed wet and dry periods at the different weather stations were also characterized in Table 5.1. It was assumed that a wet period consisted of days with ≥ 2.5 mm precipitation. During a dry period the amount of precipitation per day was considered to be less than 2.5 mm. Table 5.1 includes the mean and maximum values for these durations as well as the standard deviations on the individual values. From these data it can be concluded that dry periods usually last longer

than wet periods. On average, the durations of the dry and wet periods are 4-5 days and 2-3 days, respectively. The corresponding maximum values for each condition amount to 22-28 days and 10-14 days, respectively. The proportioning of the durations lower and higher than the mean durations of the wet and dry periods has also been indicated in terms of percentage (% lower-% higher). Around 70% of dry and wet periods recorded have duration equal or lower than the mean values recorded. This is another indication that the duration of both periods is actually quite short. The reported median values of the wet and dry periods further confirm this, especially with respect to the dry periods.

The required resistance of HVFA and FA+SF concrete (mixtures F(1)50, F(2)50, F(1)SF and F(2)SF) against carbonation-induced corrosion has been tested more or less in correspondence with the equivalent performance approach for non-traditional concrete with type II additions as suggested in NBN B15-100 (2008). According to this standard only the carbonation behaviour of unreinforced concrete needs to be determined in a quantitative way. Thus, a monitoring of the corrosion rate of rebars embedded in the carbonation exposed concrete is not required. NBN B15-100 (2008) suggests an accelerated carbonation test during which the concrete is to be exposed in an atmosphere at 1% CO₂, 20 ± 2 °C and 60 ± 10% RH. Note that the standard does not prohibit carbonation tests at a higher CO₂ concentration. After 28 and 56 days of exposure, the carbonation depth is to be visualized colorimetrically and measured in accordance with paragraph 4.2 of RILEM CPC-18 (1988). Equivalent performance in terms of carbonation resistance is defined by means of Equation 5-4:

$$d_{c, \text{concrete to be tested}} \leq 1.2 \times d_{c, \text{reference concrete}} \quad (5-4)$$

with $d_{c, \text{concrete to be tested}}$ and $d_{c, \text{reference concrete}}$, the average carbonation depths after 56 days of the tested concrete composition with type II additions and the reference concrete. The latter concrete should normally be a traditional composition that can be used in exposure classes XC3 and/or XC4, i.e. OPC reference concrete types T(0.55) and T(0.50) (Section 4.2.2) or k-value conforming FA-references, e.g. F(1)15_{XC4}, F(2)15_{XC4} (Section 4.2.3).

5.2. Research methodology

The carbonation resistance of HVFA and FA+SF concrete in comparison with the appropriate OPC and k-value conforming FA references has been evaluated experimentally with a twofold purpose. First of all, this characterization is necessary to evaluate whether the equivalent performance criterion of NBN B15-100 (2008) for carbonation resistance can be met. Secondly, in case this criterion is not met it would be most interesting to know what this means in terms of the concrete's service life. Therefore, the experimental program was organized as such that its output enabled not only a rudimentary but also an advanced service prediction. Moreover, a multi-level test approach was adopted to assess the sensitivity of the service life estimation to different varying test conditions and different measuring techniques. Within a first research step, the effect of the applied technique to determine carbonation depth was investigated. A comparison was made between the fast and accessible colorimetric measurements with phenolphthalein and the more labor intensive, yet more accurate

microscopic measurements on thin sections. The effect of the applied CO₂ concentration (1% or 10%) during the accelerated carbonation test was studied as well.

Within a second research step the experimentally obtained carbonation rates for the studied HVFA and FA+SF compositions were determined at different testing ages in order to characterize the effect of the concrete's curing behaviour. This is necessary input for a mixture specific advanced service life prediction.

5.3. Curing and sample preparation

The carbonation resistance was assessed for the following compositions: T(0.55), T(0.50), F(1)15_{XC4}, F(2)15_{XC4}, F(1)50, F(2)50, F(1)SF, F(2)SF, F(1)SFA and F(2)SFA. Per concrete mixture, cubes with a 100 mm side were cast. After casting, the cubes were kept at a constant temperature and relative humidity (RH) of 20 °C and 95%, respectively. These curing conditions were considered as optimal. Demoulding took place the next day whereupon the specimens were stored again under the same conditions until the age of 21, 84 or 175 days. At that moment, 5 of the 6 cube surfaces were treated with an impermeable coating to ensure a unidirectional flow of CO₂ throughout the samples during the experiment. The untreated side was always a cast surface of the cube.

With respect to exposure class XC3, the effect of suboptimal curing was also investigated, be it on a more limited scale. Small batches (40 l) of concrete mixtures F(1)50 and F(1)SF were made. The concrete cubes obtained were optimally cured for only 7 days. From then on they were stored in a climate room at 20°C and 60% RH for 21 days. The impermeable coating was applied at the end of this preconditioning period. Only the 28-day testing age was considered for the suboptimally cured specimens of mixtures F(1)50 and F(1)SF.

5.4. Carbonation testing

5.4.1. Accelerated carbonation testing at 10% CO₂

Per testing age (28, 91 and 182 days), the accelerated carbonation test involved exposing three coated concrete cubes to an atmosphere containing 10% CO₂ at 20 °C and 60% RH cf. [Audenaert (2006), Gruyaert et al. (2013)]. Apart from the CO₂ concentration, these test conditions were thought to be representative for exposure class XC3. After 3, 6, 10, 14 and 18 weeks of exposure the carbonation depth was measured on saw cuts of the cubes.

Another three cubes of each concrete mixture apart from OPC reference T(0.55) were alternately submerged in water for one week and exposed to the same test conditions (10% CO₂, 20 °C and 60% RH) for another week to simulate exposure class XC4 cf. Audenaert (2006). The carbonation depth was determined on saw cuts of the three cubes after 2, 4, 6, 8 and 10 wet/dry cycles. It should be noted that the suggested wet and dry period each with a fixed duration of one week, may not exactly correspond with a realistic wet/dry cycle (Section 5.1.2). The durations of both periods may already be slightly too long. On average, they should last less than one week (dry period: 4-5 days, wet period: 2-3 days). Moreover, varying durations are not being simulated this way. However, because the carbonation chamber could only be opened once a week to guarantee steady exposure conditions in terms of CO₂ concentration, relative humidity and temperature, these requirements could not easily be met. As a consequence the procedure proposed by Audenaert (2006) was followed anyway.

The last saw cuts taken from each test series subjected to the accelerated carbonation tests (either after 18 weeks or after 10 wet/dry cycles) were not only tested for carbonation using the colorimetric method, but also by means of microscopic analysis on thin sections. This was only done for the samples tested at 28 and 91 days. The carbonation resistance after 182 days of optimal curing was only assessed colorimetrically.

A very similar test procedure was adopted to evaluate the carbonation resistance of the FA+SF concrete compositions. One of the main differences was that no slices were sawn anymore from the test cubes at different time intervals. Instead, more cubes – twelve in total – were cast per concrete mixture. After 4, 8, 12 and 16 weeks of exposure, three cubes were split to enable colorimetric carbonation assessment on fractured surfaces instead of on saw cuts. This change in procedure was decided because an experimental estimation of the carbonation depth by means of the phenolphthalein dyeing method (Section 5.4.2) is preferably done on fractured surfaces according to RILEM CPC-18 (1988). However, Gruyaert et al. (2013) compared carbonation coefficients when calculated from colorimetric measurements done on broken and sawn surfaces. The differences turned out negligible for OPC and BFS concrete. The same conclusions are probably also valid for HVFA and FA+SF concrete indicating that the experimental output of the two approaches can be compared with each other. Another difference relates to the investigated exposure classes. Since the service life predictions initially done for HVFA concrete (Chapter 8) indicated that carbonation-induced depassivation is much less an issue for the simulated exposure class XC4 cf. Audenaert (2006) than for exposure class XC3, the suitability of FA+SF concrete for exposure class XC4 was no longer studied.

5.4.2. Critical evaluation of accelerated carbonation testing

Note that the adopted CO₂ concentration during an accelerated carbonation test can vary considerably with the chosen test method. For instance, NBN B15-100 (2008) suggests a CO₂ concentration of 1% during the carbonation test for equivalent performance assessment of concrete with type II additions, but gives the freedom to work with other CO₂ concentrations as well. According to *fib* Bulletin 34 (2006) concrete needs to be stored in a carbonation cabinet at 2% CO₂ for 28 days to determine its inverse effective carbonation resistance. Lo and Lee (2002) applied the same CO₂ concentration. NT Build 357 (1989) on the other hand specifies an atmosphere of 3% CO₂ and Borges et al. (2010) expose concrete to a CO₂ concentration of 5% to accelerate carbonation. In our research, the applied CO₂ concentration was 10% by volume cf. Audenaert (2006) and Gruyaert et al. (2013). Literature survey also shows that still higher CO₂ concentrations are inherent to some test methods for accelerated carbonation. For instance, a CO₂ concentration of 20% was applied in Chang and Chen (2006). The AFPC-AFREM procedure on accelerated carbonation testing is even more extreme as it requires a carbonation chamber conditioned at 50% CO₂ [Rozière et al. (2007)]. Thus, it is clear that there is not much uniformity among the available carbonation test methods. Nevertheless, some researchers are convinced that increasing the CO₂ concentration too much will result in important chemical changes of the concrete's paste fraction that would not occur if the concrete could naturally carbonate at 0.03% CO₂. Castellote et al. (2009) found that the polymerisation of the calcium silicate hydrate (C-S-H) after carbonation of

OPC pastes increases with the increase of the CO₂ concentration applied. When carbonating at 0.03% CO₂ and 3% CO₂ there is remaining C–S–H gel, although with a lower Ca/Si ratio than that of an uncarbonated sample (Ca/Si = 1.87), but still with the characteristics of this phase. The obtained Ca/Si ratios for the C–S–H gels of samples carbonated at 0.03% CO₂ and 3% are quite similar and amount to 1.23 and 1.18, respectively. When carbonating at 10% and 100% CO₂ the C–S–H gel completely disappears. It is completely transformed into polymerised Ca-modified silica gel. In a CO₂ atmosphere of 3% or less, this transformation is only partial. The presence of remaining unhydrated cement and Ettringite also highly depends on the imposed CO₂ concentration. After carbonation at 0.03% CO₂ and 3% CO₂, unhydrated cement and Ettringite are still there. Testing at 10% CO₂, makes the Ettringite completely disappear and leaves only a small amount of unhydrated cement. A CO₂ concentration of 100% results in a complete disappearance of both the Ettringite and the unhydrated cement. Based on these findings Castellote et al. (2009) conclude that the maximum allowable CO₂ concentration for acceleration of the carbonation process is 3%. Only under these conditions, a dramatical change in microstructure of the pastes is avoided. Nevertheless, they emphasize that these observations only hold true for OPC pastes and they advise that their validity should also be checked for pastes consisting of alternative binder materials (e.g. FA).

Borges et al. (2010) studied the carbonation behaviour of pastes containing high amounts of blast-furnace slag (BFS) by exposing them at 5% CO₂. When dealing with OPC+BFS pastes attention needs to be paid to both the carbonation of calcium hydroxide (CH) and C–S–H, and their corresponding specific effects on the microstructure as indicated in Section 5.1.1. The same probably goes for blended pastes consisting of OPC and FA.

Yet, when considering the findings of Castellote et al. (2009), at least part of the shrinkage due to the carbonation of C–S–H observed by Borges et al. (2010) may also be attributed to the fact that the carbonation test was performed in an atmosphere with 5% CO₂ instead of the proposed maximum value of 3%. Performing carbonation tests at a CO₂ concentration above 3% may overestimate the carbonation of C–S–H, the coarsening of the microstructure and thus the measured carbonation depths and rates that result from it.

However, this effect does not take into account another phenomenon inherent to carbonation. The production of calcium carbonate always coincides with the release of water. When carbonating concrete at a high CO₂ concentration, the amount of water produced could be more than the porous matrix is capable of expelling in the same time interval. The time needed to establish a condition of equilibrium again is believed to slow down the propagation of the carbonation depth [da Silva et al. (2009), Saetta and Vitaliani (2004)]. Da Silva et al. (2009) also mention that CO₂ solubility is low when high CO₂ concentrations are used. The penetrating CO₂ first needs to transform into acid in the presence of water before the actual carbonation reaction can take place and the amount of CO₂ capable of dissolving in water is limited. If these mechanisms would turn out more dominant than the coarsening of the pore structure due to the carbonation shrinkage attributable to the acceleration of the carbonation test, applying a high CO₂ concentration would rather underestimate the carbonation depth and rate under field conditions.

Thus, depending on the prevailing mechanism – either the increase in permeability due to carbonation shrinkage [Borges et al. (2010)] or the blocking effect of the water released during carbonation [Saetta and Vitaliani (2004)] together with the limited solubility of CO₂ in

water [da Silva et al. (2009)] – experimentally estimated field carbonation rates from highly accelerated tests either over- or underestimate the carbonation resistance and expected service life of a concrete with a high content of supplementary cementitious materials (SCMs) in its natural environment. Life cycle assessment based on this service life assessment may attribute a higher or lower environmental burden to the material than when the service life assessment would be based on a more natural carbonation test (Chapter 8, Chapter 12).

5.4.3. Comparative carbonation testing at 1% and 10% CO₂

To evaluate this effect more quantitatively, another 24 concrete cubes (side: 100 mm) of OPC reference T(0.55), HVFA mixture F(1)50 and FA+SF mixture F(1)SF were cast. Half of the cubes per mixture were subjected to an accelerated carbonation test at 10% CO₂, 20°C and 60% RH, while the other twelve were kept in a carbonation cabinet at 1% CO₂, 20°C and 60% RH for a similar test. According to da Silva et al. (2009) a concentration of 1% CO₂ develops the same reaction products as a normal atmosphere at 0.03% CO₂ and can thus be considered as a more or less natural carbonation process. Exposure started 28 days after the cubes were optimally preconditioned and coated (as described in Section 5.3). Field carbonation rates obtained from both experiments were compared with each other to quantify the effect of the CO₂ concentration applied (10% versus 1%).

Exposing the concrete to 1% CO₂ at 20 °C and 60% RH may be more in agreement with the standard procedure of NBN B15-100 (2008). Nevertheless, some differences remained that need to be mentioned. The test was performed on partially coated cubes instead of on the prescribed uncoated 100 × 100 × 400 mm³ prisms. The samples were not cured in water for 55 days. There was no subsequent sample drying at 50 ± 5 °C for 14 days followed by a 7-day storage at 20 °C and 60° RH prior to exposure. Moreover, the carbonation depth was determined on more than the prescribed two occasions (after 28 and 56 days).

Changes in microstructure induced by carbonation at 1% and 10% were studied on pastes with the same binder compositions and W/B ratios as concrete mixtures T(0.55), F(1)50 and F(1)SF. The pastes were cast in sealable cylindrical moulds (Ø: 46 mm, height: 50 mm) that were kept on rotating stands until the next day in order to prevent bleeding and segregation. Then, the cylinders were cured under water at 20 ± 2 °C until they reached the age of 28 days. Once surface dry, the upper and lower surfaces of the paste cylinders were sealed with an impermeable aluminium tape leaving only the mantle surface for exposure. As such, two cylinders per mixture were stored in the carbonation cabinets at 1% and 10% CO₂ for 12 weeks. Some additional cylinders were crushed into very small pieces (Ø: 1-3 mm). They were kept in a normal environment at 20°C and 60% RH until they were carbonated in a fully natural way. In such an atmosphere, the CO₂ concentration is normally around 0.03%. Another set of cylinders was continuously cured in water for 182 days.

5.4.4. Colorimetric measurement details

Per saw cut treated with phenolphthalein, nine different measurements (one every 10 mm) were done, and this to the nearest millimetre. After spraying the 1% phenolphthalein solution onto the concrete slices or fractured surfaces, the carbonated area will show colourless, while the non-carbonated area will colour purple. The point of transition for phenolphthalein is

situated at around pH 8.0-9.8 [General Chemistry Online (2014)]. Since a pH between 9 and 13 is required to maintain the protective passivation layer upon the steel reinforcements, the colorimetric method gives a more or less adequate estimation of the CO₂ ingress. However, given the pH range for colour transition, there is still a risk for an underestimation of the actual carbonation depth. To evaluate the magnitude of this underestimation, the actual penetration depth was also evaluated on thin sections.

5.4.5. Microscopic measurement details

After 28 and 91 days of optimal curing followed by 16/18 weeks of exposure or 10 wet-dry cycles, a 45×30×15 mm³ prism was sawn from one 15 mm thick slice in such a way that a 45×15 mm² face was the exposed surface. First, one 45 × 30 mm² face was glued onto a glass slide with a thickness of 2.9 mm. Then, the samples were cut and polished until the height of the concrete specimens and the glass equaled 10.1 mm. In a next step, the samples were impregnated under vacuum with a fluorescent epoxy. After impregnation, the excess epoxy was ground away and an object glass was glued onto the polished surface. In a final step, the glass slides were cut off and the concrete samples on the object glasses were polished until thin sections with a 25 μm thickness were obtained. A cover glass was glued onto them for protection.

Note that for the OPC concrete compositions thin sections were made for only one curing age after completion of the accelerated carbonation test. For OPC reference T(0.55) the 28 days curing period was considered, while for mixture T(0.50) thin sections were taken from the concrete that was optimally cured for 91 days.

All thin sections were examined with a Leica DM LP polarizing microscope under crossed polars. The luminous intensity of the polarized light equaled 6.5 on a scale of 10. Images were taken with a Leica DFC295 camera and analysed with the Leica Application Suite v.3.7 software. The carbonated zone was characterized by a lighter brownish stain (Figure 5.1). The number of measurements per thin section ranged between 4 and 8.

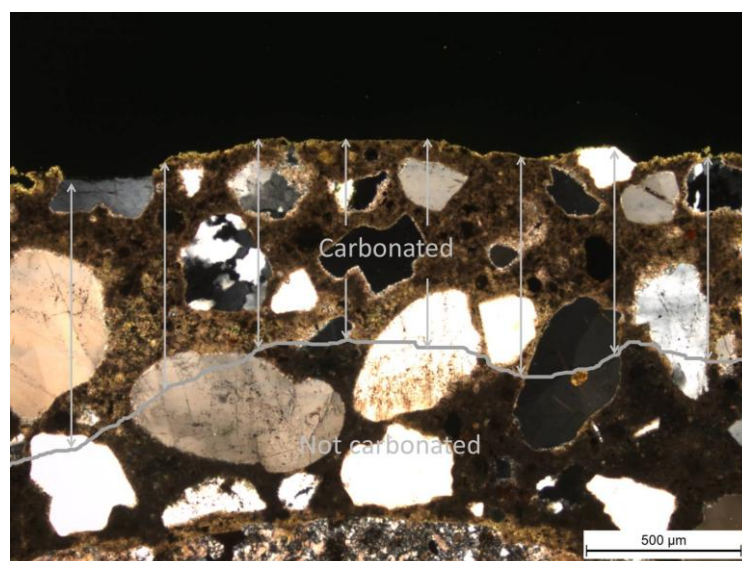


Figure 5.1. The carbonated zone with a lighter stain as observed under the microscope under crossed polars.

5.4.6. Carbonation rate and resistance

For each concrete mixture tested, the measured carbonation depths (in mm) with the phenolphthalein colour indicator were plotted as function of the square root of the exposure time t (in weeks) to determine an experimental (accelerated) carbonation coefficient A_{acce} (in $\text{mm}/\sqrt{\text{weeks}}$). The carbonation rate obtained cannot be considered as a realistic one, because a CO_2 concentration of 10% exceeds the natural CO_2 concentration in air (0.03%) by far. To obtain a first estimation of the corresponding carbonation rate under field conditions from accelerated carbonation tests performed at 10% CO_2 , Audenaert (2006) used a conversion formula that expresses the ratio of the accelerated and field carbonation coefficients (A_{acce} and A_{field}) in terms of their corresponding CO_2 concentrations c_{acce} and c_{field} . The same formula (Equation 5-5) was also used in this research.

$$\frac{A_{\text{acce}}}{A_{\text{field}}} = \frac{\sqrt{c_{\text{acce}}}}{\sqrt{c_{\text{field}}}} \quad (5-5)$$

Note that Sisomphon and Franke (2007) used a very similar conversion formula. Only the CO_2 concentration of their accelerated carbonation test was different (3% instead of 10%). Since literature indicates that 3% CO_2 could be the maximum allowable CO_2 concentration for an accelerated carbonation test (see Section 5.4.2), one could conclude that Equation 5-5 may not be applicable for all values of c_{acce} . We therefore calculated A_{field} of one HVFA mixture (F(1)50), one FA+SF mixture (F(1)SF) and one OPC reference (T(0.55)) from both the outcome of the carbonation test performed at 10% CO_2 and 1% CO_2 (Section 5.6.3.1).

5.5. Assessment of carbonation-induced changes in microstructure

5.5.1. Thermogravimetric analysis (TGA)

Initially, TGA was done on water cured, uncarbonated pastes to evaluate how the CaOH_2 content of the cementitious pastes that represent concrete mixtures T(0.55), F(1)50 and F(1)SF evolved as a function of time. Since the W/B ratios of the OPC paste (W/B: 0.55) and the HVFA and FA+SF pastes (W/B: 0.35) were very different, an additional OPC paste T(0.35) with the same W/B ratio as the latter two mixtures was studied as well. At the age of 1d, 2d, 7d, 14d, 21d, 28d, 56d, 91d and 182d small chunks of the original paste cylinders immersed in water were crushed with mortar and pestle until all material could pass a sieve with a 74 μm mesh size. Around 50 mg of powdery sample was heated from 20°C to 1100°C at a rate of 10°C/min under an inert atmosphere (nitrogen). The mass change as a function of temperature was recorded with a Netzsch Sta 449 F3 Jupiter TGA apparatus.

Later on, powdery samples were also collected from the paste cylinders that were exposed to increased CO_2 concentrations (1% and 10%) in the carbonation cabinets. After 12 weeks of exposure the paste cylinders were split and the carbonation front was visualized with the phenolphthalein colour indicator. In a next step, holes were drilled in the uncarbonated and carbonated zones of the cylinders' fractured surfaces (Figure 5.2). The powders collected as such were subjected to TGA while using the same test procedure as described above. Small pieces of paste (\varnothing : 1-3 mm) that carbonated naturally in an atmosphere at 20°C and 60% RH,

where the CO_2 concentration is expected to be at around 0.03% CO_2 (Section 5.4.3) were crushed and tested as well.

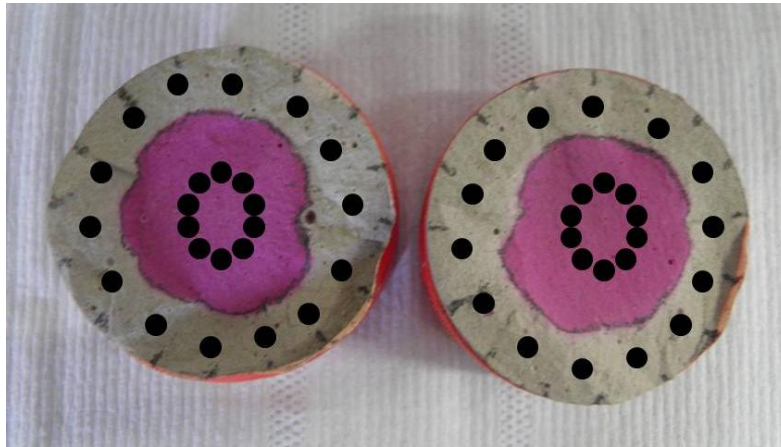


Figure 5.2. Carbonation front visualized with phenolphthalein and indicative location of the drillings on the fractured surfaces of the paste cylinders.

The results of the thermogravimetric measurements were analyzed in the Netzsch-Proteus Analysis software. To enable comparison between the OPC, HVFA and FA+SF pastes under investigation, the recorded mass losses during TGA were expressed in % relative to the residual mass of the powdery sample at 1100°C. Also note that the mass losses recorded during TGA were always corrected for the concurrent dehydration of other hydrated compounds (Figure 5.3). This was done in accordance with Baert (2009).

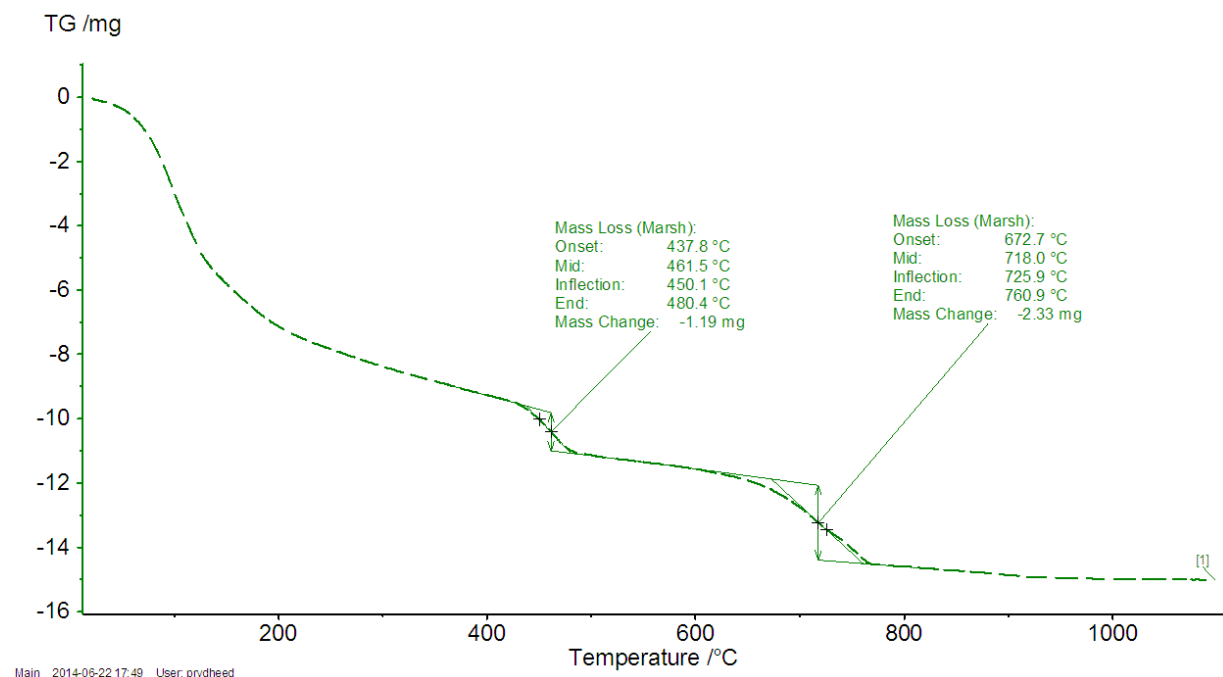


Figure 5.3. Mass losses observed with TGA in the Netzsch-Proteus Analysis software and the necessary corrections for concurrent dehydration of other hydrated compounds when determining the mass losses associated with $\text{Ca}(\text{OH})_2$ and CaCO_3 .

The non-evaporable or the chemically bound water content of all pastes – intentionally carbonated or not – was determined by means of Equations 5-6.

$$w_b = WL_{140^{\circ}\text{C}-1100^{\circ}\text{C}} - WL_{\text{CaCO}_3 \text{ unexposed / exposed}} \quad (5-6)$$

with $WL_{140^{\circ}\text{C}-1100^{\circ}\text{C}}$, mass loss between 140°C and 1100° , $WL_{\text{CaCO}_3 \text{ unexposed / exposed}}$, mass loss attributed to decarbonation at around 650°C of the uncarbonated or intentionally carbonated sample. According to Pane and Hansen (2005), the lower limit of the considered temperature range (140°C) corresponds with the temperature range at which boiling distilled water completely turns into gas. The same authors believe that the free (physically bound) water in paste samples behaves in a similar way.

For the determination of the $\text{Ca}(\text{OH})_2$ (CH) and CaCO_3 (CC) content of the pastes that were not intentionally carbonated, a calculation method similar to the one suggested by Borges et al. (2010) was used. The original method assumes that the presence of any carbonates in the unexposed paste samples as identified by means of TGA under an inert atmosphere solely originates from the initially available CH. In other words, the amount of additional carbonates that originate from any carbonate fractions present in the raw materials of the pastes was considered negligible. However, since the CO_2 content of FA was observed to be almost twice the CO_2 content of OPC, it was decided to correct for the mass loss ($WL_{\text{original CO}_2}$) due to decarbonation of the original cement, fly ash and silica fume present in each paste (see tabulated CO_2 percentages in Tables 4.1, 4.3 and 4.4). Under this assumption the initial CaCO_3 content (%CC) could be calculated from Equation 5-7.

$$\% \text{CC}_{\text{unexposed}} = \left(WL_{\text{CaCO}_3 \text{ unexposed}} - WL_{\text{original CO}_2} \right) \cdot \frac{MW_{\text{CaCO}_3}}{MW_{\text{CO}_2}} \quad (5-7)$$

with $WL_{\text{CaCO}_3 \text{ unexposed}}$, mass loss attributed to decarbonation, MW_{CaCO_3} , molecular weight of CaCO_3 (100 g/mol) and MW_{CO_2} , molecular weight of CO_2 (44 g/mol).

The initial $\text{Ca}(\text{OH})_2$ content could be quantified by means of Equation 5-8. This equation consists of two terms. The first term relates to the still present CH fraction in the paste sample and requires the mass loss due to decomposition of CH in CaO and H_2O (WL_{CH}) at around $400\text{-}500^{\circ}\text{C}$ as input. The second term relates to the small CH fraction that had already carbonated during sample preparation and requires $WL_{\text{CaCO}_3 \text{ unexposed}}$ as input. Further on, this equation depends on the molecular weights of CH (MW_{CH} : 74 g/mol), H_2O ($MW_{\text{H}_2\text{O}}$: 18 g/mol) and CO_2 (MW_{CO_2} : 44 g/mol).

$$\% \text{CH}_{\text{unexposed}} = WL_{\text{CH unexposed}} \cdot \frac{MW_{\text{CH}}}{MW_{\text{H}_2\text{O}}} + \left(WL_{\text{CaCO}_3 \text{ unexposed}} - WL_{\text{original CO}_2} \right) \cdot \frac{MW_{\text{CH}}}{MW_{\text{CO}_2}} \quad (5-8)$$

The CC and CH contents of the intentionally carbonated pastes were not calculated in exactly the same way. For that purpose, Equations 5-9 and 5-10 were used.

$$\%CC_{\text{exposed}} = \left(WL_{\text{CaCO}_3 \text{ exposed}} - WL_{\text{original CO}_2} \right) \cdot \frac{MW_{\text{CaCO}_3}}{MW_{\text{CO}_2}} \quad (5-9)$$

$$\%CH_{\text{exposed}} = WL_{\text{CH exposed}} \cdot \frac{MW_{\text{CH}}}{MW_{\text{H}_2\text{O}}} \quad (5-10)$$

Now, according to Borges et al. (2010) the amount of C–S–H carbonation can be estimated indirectly from the CH and CC contents measured at the start and end of an accelerated carbonation experiment. To achieve this goal the following sequence of calculations needs to be performed:

- (i) Calculation of the %CH that carbonated before and during the carbonation experiment (A) by subtracting the amount of CH remaining after the test from the %CH that was initially available.
- (ii) Calculation of the expected %CC that was formed out of the %CH that had carbonated (B) by multiplying the amount of carbonated CH (A) with $MW_{\text{CaCO}_3}/MW_{\text{Ca(OH)}_2}$.
- (iii) Calculation of the estimated amount of carbonates that were the result of C–S–H carbonation (C) by subtracting the expected %CC that was formed out of the %CH that had carbonated (B) from the %CC that was measured at end of the carbonation test.

This was the overall procedure followed by Borges et al. (2010) to obtain an estimation of the amount of C–S–H carbonation for blended OPC-BFS pastes when subjected to an accelerated carbonation test at the age of 90 days. The considered testing age is evidently very important when studying pastes containing pozzolanic SCMs such as FA and SF. After 90 days, the CH content of such a paste will not change much anymore since most of the pozzolanic hydration reactions have already taken place. However, this is not the case when an increased CO_2 concentration was already applied after 28 days. At that moment, the CH content is still at its highest level because the pozzolanic reactions have not started yet or are still ongoing. Thus, during exposure the CH will not only be consumed by the (accelerated) carbonation reaction, but also by the pozzolanic hydration reaction. As a consequence, when based on the initial CH content at the start of the carbonation experiment cf. Borges et al. (2010), the estimated amount of C–S–H carbonation may be considerably underestimated. For this reason, it was decided to calculate (A), (B) and (C) also from the CH and CC contents of an unexposed paste sample with the same age (~112 days) as the carbonated paste at the end of the test. The suggested alternative approach to estimate the amount of C–S–H carbonation will no longer underestimate the phenomenon. However, it still holds the risk of overestimating it because it is not known whether the carbonation reaction and the pozzolonic hydration reaction simply coexist without affecting each other. If the pozzolonic hydration reaction would be hindered due to the simultaneously occurring carbonation reaction, the SCMs may not hydrate to the same extent as they normally would in an unexposed paste. As such, the CH would be preferentially consumed by the carbonation reaction. This would result in more CH carbonation and less C–S–H carbonation. Being aware of the risks of under- or overestimating the amount of C–S–H carbonation depending on the procedure followed (the method of Borges et al. (2010) or the suggested alternative method), the results of both methods were

taken into consideration. The actual amount of C–S–H carbonation probably ranges between the boundaries set by the two calculation methods.

5.5.2. X-ray diffraction (XRD)

The way of collecting and preparing the powdery samples for XRD analysis was very similar to the methodology described in the section on TGA (Section 5.5.1). Only difference in comparison with the latter was that a 10 m% ZnO internal standard was added to samples to enable absolute phase quantification in accordance with the Rietveld method for whole-powder pattern fitting. The powdery samples were side-loaded into the sample holder for analysis to reduce the effect of a preferential particle orientation. As such, the samples were inserted in a Thermo Scientific ARL X'tra Diffractometer equipped with a Peltier cooled detector and analysed in θ - 2θ geometry over an angular range of 5-70 $^{\circ}2\theta$ (Cu K radiation). The applied step size and counting time amounted to 0.02 $^{\circ}2\theta$ and 1s/step, respectively. Topas Academic V4.1 software was used for the Rietveld Refinement [Coelho (2007)]. The measurement specific or sample displacement error, a cosine Chebyshev function of 12 polynomial terms for background correction, the phase specific scale factors, the unit cell parameters and the Lorentzian peak shape broadening parameters were among the refined parameters. Within the XRD-patterns obtained special attention was paid to the mineralogical phases that specifically relate to uncarbonated and carbonated samples, being Portlandite, Ettringite and Kuzelite in case of the former condition and Calcite, Vaterite and Aragonite in case of the latter. No correction was done for the variation in hydration degree between the powdery samples of the different paste mixtures during quantitative Rietveld Analysis.

5.5.3. Mercury intrusion porosimetry (MIP)

Possible changes in pore properties of the pastes that were exposed to 1% or 10% CO₂ were studied using Mercury Intrusion Porosimetry (MIP). Little pieces of paste taken from the colorimetrically determined carbonated and uncarbonated zones of the paste cylinders were treated with liquid N₂ and then stored in a LTE Scientific Mini Lyotrap freeze-dryer until their masses could be considered constant. The size of the samples did not exceed 14 mm in cross-section in order to make sure they could easily be inserted in the dilatometer of the MIP apparatus (PASCAL 140+440 Series, Thermo Fischer Scientific). For each analysis around 1.3-1.4 g of sample was used. First, the samples were tested in the low pressure unit of the instrument (PASCAL 140 Series). There, the pressure on the mercury filled dilatometer with the sample was gradually increased from 0 to 200 kPa. This intrusion phase was followed by an extrusion phase during which the pressure was lowered again to 100 kPa. Next, the dilatometer was moved to the high pressure unit of the MIP instrument (PASCAL 440 Series) where the samples were subjected to mercury pressures ranging from 0.1 MPa to 200 MPa back to 0.1 MPa. As such, the samples went again through an intrusion and an extrusion phase. Per type of sample two replicates were tested. Afterwards the results were analysed in the software application SOL.I.D [Thermo Fisher Scientific Inc. (2011)]. The obtained pore size distributions and porosities corresponding with the capillary pores (0.01 μm < pore diameter D < 10 μm , cf. Gruyaert (2011), St John (1998)) of completely carbonated paste after exposure to 1% and 10% CO₂ as well as uncarbonated paste were compared with each

other. Within the SOL.I.D software, the accessible porosity is calculated automatically by multiplying the total volume of intruded mercury during the test (in mm^3/g , for pore diameters ranging from approximately $0.007 \mu\text{m}$ to $100 \mu\text{m}$) with the samples' bulk density (which is also measured by the MIP apparatus during the test) in g/mm^3 . The capillary porosity was calculated in the same way, except for the fact that for this porosity only the capillary pore range ($0.01 \mu\text{m} < \text{pore diameter } D < 10 \mu\text{m}$) was considered.

5.6. Results and discussion

5.6.1. Colorimetrically versus microscopically assessed carbonation depths

With respect to the carbonation depths of the OPC references, the k-value conforming FA references and the HVFA mixtures the following conclusions can be drawn (Figure 5.4).

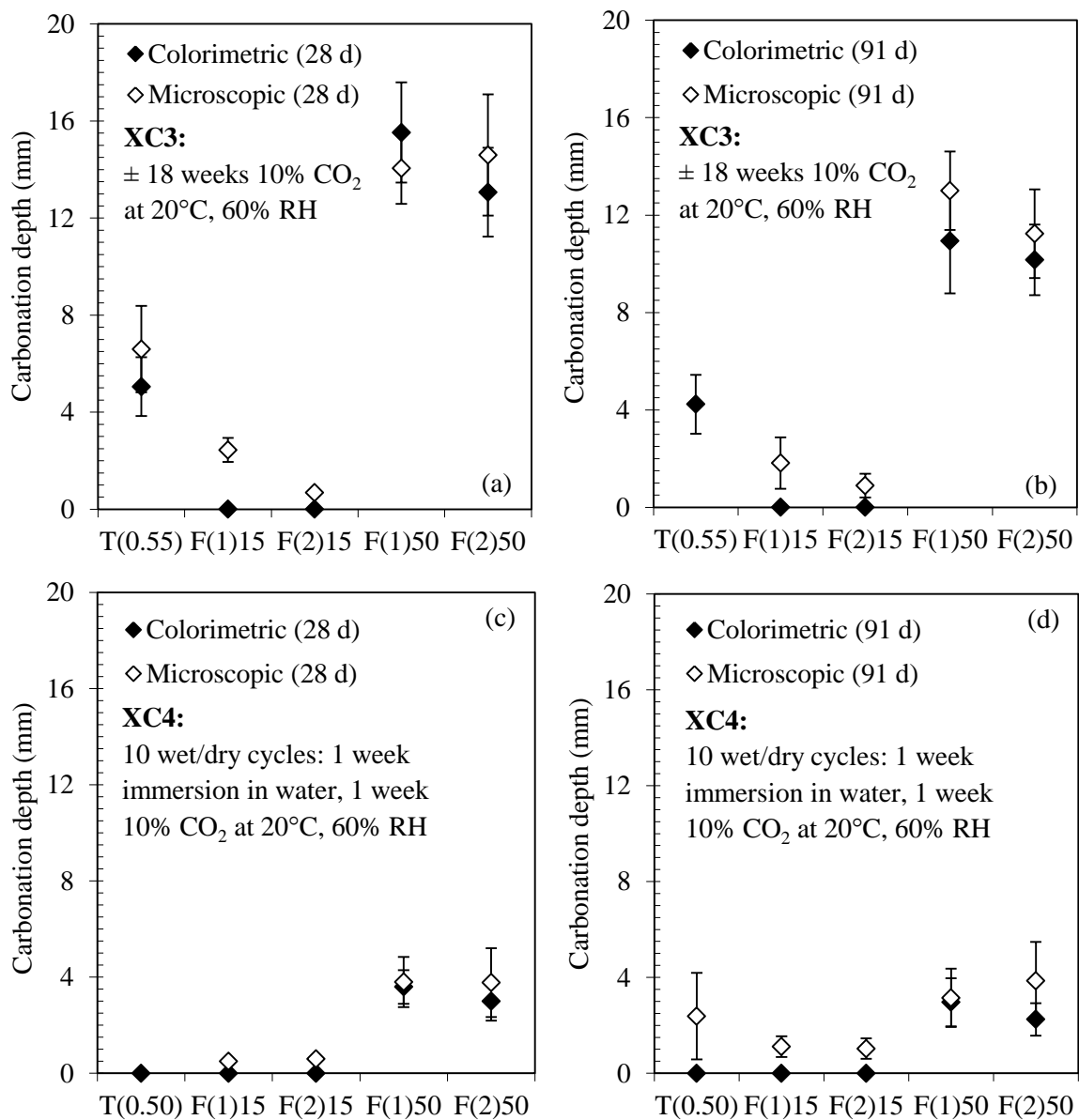


Figure 5.4. Difference between colorimetric and microscopic assessed carbonation depths in simulated XC3 (a, b) and XC4 environments (c, d) for OPC, FA and HVFA concrete.

Microscopic measurements usually resulted in higher carbonation depths than colorimetric measurements with the phenolphthalein colour indicator. This observation holds true for practically every studied concrete mixture after 28 and 91 days of optimal curing followed by either ± 18 weeks of continuous exposure to 10% of CO_2 at 20 °C and 60% RH (simulated exposure class: XC3) or 10 wet/dry cycles (simulated exposure class: XC4). Mixture F(1)50, optimally cured for 28 days and exposed to the simulated XC3 environment, was the only exception. Statistical analysis (Independent Sample T tests, Significance level = 0.05) showed that the recorded differences in carbonation depth were only non-significant for the F(1)50 mixtures destined for exposure class XC4, and this for two curing ages (28 and 91 days).

Since the Leica Application Suite v.3.7 software provides necessary tools for measuring distances, the microscopic technique for measuring the carbonation depth is certainly more precise (accuracy: ± 0.2 mm). This is in contrast with the determination of a phenolphthalein colour change boundary to the nearest millimeter by means of a simple ruler. Moreover, microscopic measurements allow for the detection of incipient carbonation and partially carbonated areas in the vicinity of larger pores or the more porous interfacial transition zone of aggregates. As a consequence, one would expect that a microscopically assessed carbonation depth would always be characterized by a larger standard deviation on the individual values. A statistical homogeneity of variance check (Levene's test, Significance level = 0.01) for the microscopic and colorimetric measurements would then turn out significant for all concrete mixtures. However, this statement only holds true for mixtures T(0.50) at 91d (XC4), F(1)15 at 28 days and 91 days (XC3, XC4), F(2)15 at 28 days and 91 days (XC3, XC4) and F(2)50 at 28 days and 91 days (XC4).

An overall comparison between the different concrete mixtures for exposure class XC3 shows that HVFA compositions F(1)50 and F(2)50 are much more susceptible to carbonation than the concrete mixtures F(1)15 and F(2)15 with only 15% FA and OPC reference T(0.55) (Figure 5.4a and 5.4b). This observation follows from both the colorimetric and microscopic carbonation depth measurements, and this for the two curing ages. When looking at the results for exposure class XC4, the same conclusions can be drawn. Evidently, the cyclic immersion of the concrete in water to simulate a XC4 environment resulted in considerably lower carbonation depths. After each immersion period the concrete needed to dry out before the CO_2 could steadily penetrate the concrete again.

Analysis of the final carbonation depth measurements as obtained for the different FA+SF concrete mixtures led to the following findings (Figure 5.5). First of all, colorimetric and microscopic assessed carbonation depths were not significantly different from each other for most of the considered FA+SF concrete mixtures (Independent sample T test, Significance level = 0.05). Mixture F(2)SF at 91 days was the only exception. This finding is in contrast with the usually significant differences between the colorimetrically and microscopically assessed carbonation depths that were observed for the OPC, FA and HVFA concrete. The variances of the colorimetric and microscopic measurements turned out homogenous for all the FA+SF mixtures tested, except for mixture F(1)SF at 91 days (Levene's test, Significance level = 0.01). Thus, the microscopic method that enables an accurate determination of partially carbonated zones around pores and the more porous interfacial transition zone around aggregates, did not result in a considerably larger standard deviation on the carbonation depth measurements as was sometimes observed for previously studied mixtures.

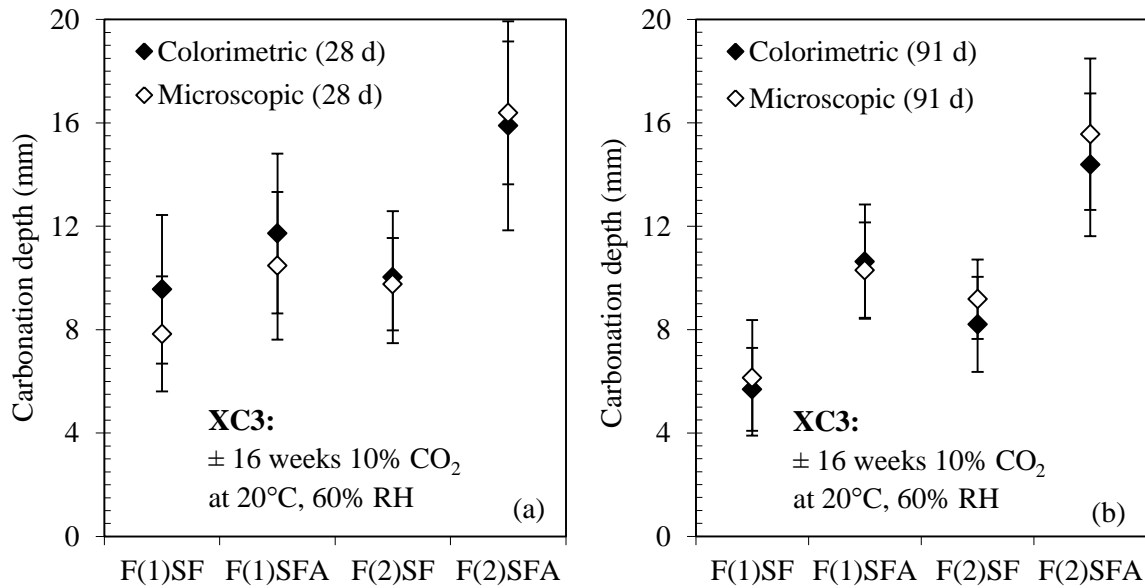


Figure 5.5. Difference between colorimetric and microscopic assessed carbonation depths in a simulated XC3 (a, b) environment for non-air entrained and air entrained FA+SF concrete.

Given the sometimes contrary findings for the different concrete types, the question remains whether the simple colorimetric method can really result in a significant underestimation of the actual carbonation depth as observed on a microscopic scale under crossed polars. For the moment there is no uniform answer to this question. For the OPC, FA and HVFA concrete, basically the findings of Gruyaert et al. (2013) for OPC and BFS concrete remained valid. An exposed OPC concrete that shows no signs of carbonation after applying phenolphthalein, usually has a small carbonated zone that can be detected by means of optical microscopy. In our research, this was also the case for OPC reference T(0.50) and the k-value conforming FA references (F(1)15 and F(2)15). On the other hand, with respect to OPC reference T(0.55) as well as most HVFA mixtures, the microscopic assessed carbonation front was usually located further inwards than the colorimetrically assessed carbonation front. This finding is in agreement with Gruyaert et al. (2013) for BFS concrete. Note that these differences often turned out significant for HVFA concrete. Yet, these significant differences did not exist for FA+SF concrete. It must be said though that the microscopic thin section measurements done on the FA+SF were more difficult because less areas could be found that consisted mainly out of paste matter. There, a clear transition from the lighter to the darker brownish stain is most easily detected. However, on the thin sections of the FA+SF concrete (with a much lower paste content in comparison with the HVFA concrete) these zones seemed much more interrupted by the presence of small and large aggregates, and in case of air entrainment, by the presence of large quantities of round shaped small air voids. The abundant interruptions made it much more difficult to determine the exact location of the carbonation front. This may explain the now non-significant differences between the colorimetric and microscopic assessed carbonation depths.

Based on the measured carbonation depths for FA+SF concrete, one could conclude that air entrainment can affect the carbonation resistance of the concrete in a negative way. Both after 28 and 91 days of optimal curing more carbonation was observed for mixtures F(1)SFA and

F(2)SFA. Apparently, the artificial air void system present in these concrete compositions may provide preferential pathways for CO₂ ingress. This aspect will be discussed more in detail in Chapter 7 after a full characterization of the concrete's air void system and its effect on the porosity and transport properties.

Finally, a comparison can be made between the measured carbonation depths of the non-air entrained HVFA and the FA+SF concrete mixtures. For both curing ages the carbonation depths of mixtures F(1)SF and F(2)SF were significantly lower than those of mixtures F(1)50 and F(2)50. This is a first indication that the suggested FA+SF composition has a better carbonation resistance than the HVFA concrete. A comparison of their carbonation coefficients which are based on measurements taken at different time intervals should bring further confirmation for this statement (Section 5.6.2).

5.6.2. Colorimetrically measured accelerated and field carbonation coefficients

The accelerated carbonation coefficients A_{acce} (Table 5.2) are in line with the individual colorimetric carbonation depths after each carbonation test (Figure 5.4-5.5).

For exposure class XC3, the A_{acce} values of the HVFA mixtures F(1)50 (4.3 ± 0.1 mm/ $\sqrt{\text{weeks}}$) and F(2)50 (3.6 ± 0.1 mm/ $\sqrt{\text{weeks}}$) are around three times the corresponding carbonation coefficient of OPC reference T(0.55) (1.3 ± 0.1 mm/ $\sqrt{\text{weeks}}$) after 28 days of optimal curing prior to exposure. Prolonged optimal curing for 91 days resulted in an important decrease of the carbonation coefficient for HVFA mixtures F(1)50 (2.4 ± 0.1 mm/ $\sqrt{\text{weeks}}$, -44%) and F(2)50 (2.3 ± 0.1 mm/ $\sqrt{\text{weeks}}$, -36%). This time dependent decrease was less pronounced for the OPC reference (1.0 ± 0.1 mm/ $\sqrt{\text{weeks}}$, -23%), which indicates that a considerable part of OPC hydration had already taken place by the age of 28 days. On the other hand, the hydration process of HVFA concrete takes longer, because a sufficient amount of Ca(OH)₂, a hydration product of the remaining OPC, needs to be present first before the FA can start to react. The further densification of the microstructure due to the pozzolanic FA reaction is therefore expected at later age. The significantly improved carbonation resistance after 91 days as reported in Table 5.2 seems to demonstrate this phenomenon. However, when looking at the A_{acce} values obtained after 182 days of optimal preconditioning, a slightly increased carbonation coefficient was recorded for mixtures F(1)50 (2.7 ± 0.1 mm/ $\sqrt{\text{weeks}}$) and F(2)50 (2.6 ± 0.1 mm/ $\sqrt{\text{weeks}}$). This is in contrast with the corresponding carbonation coefficient of OPC reference T(0.55) which had decreased further on to 0.6 ± 0.1 mm/ $\sqrt{\text{weeks}}$. Gruyaert et al. (2013) also observed either a slight increase or decrease in carbonation rate between 3 months (~ 91 days) and 6 months (~ 182 days) of optimal sample preconditioning for concrete in which 50%, 70% or 85% of the cement was replaced with BFS. An additional carbonation test performed by Gruyaert et al. (2013) after 18 months of curing resulted again in a carbonation coefficient similar to the one measured after 91 days. For BFS concrete 91 days is therefore seen as the optimal curing period beyond which the concrete's carbonation resistance will not improve anymore. A similar time span is expected for the studied HVFA concrete compositions and OPC reference T(0.55), although an additional carbonation test at later age would also be advised to find further confirmation for this statement.

Table 5.2. Accelerated carbonation coefficients (A_{acce} , 10% CO_2) and estimated field carbonation coefficients (A_{field} , 0.05% CO_2) measured colorimetrically and microscopically.

| Colorimetric measurements | | | | | | | | | |
|---------------------------|--------------------------|--|----------------|---------|----------------|---|----------------|---|---------|
| Class | Mix | A_{acce} (mm/ $\sqrt{\text{weeks}}$) | | | | | | A_{field} (mm/ $\sqrt{\text{years}}$) | |
| | | 28 d | R ² | 91 d | R ² | 182 d | R ² | 28 d | 91 d |
| XC3 | T(0.55) | 1.3±0.1 | 0.70 | 1.0±0.1 | 0.71 | 0.6±0.1 | 0.97 | 0.7±0.1 | 0.5±0.1 |
| | | 3.4±0.1 ^b | – | – | – | – | – | 1.8±0.1 ^b | – |
| | F(1)15 | 0.0 | – | 0.0 | – | 0.0 | – | 0.0 | 0.0 |
| | F(2)15 | 0.0 | – | 0.0 | – | 0.0 | – | 0.0 | 0.0 |
| | F(1)50 | 4.3±0.1 | 0.99 | 2.4±0.1 | 0.92 | 2.7±0.1 | 0.98 | 2.2±0.1 | 1.3±0.1 |
| | | 5.9±0.1 ^a | – | – | – | – | – | 3.0±0.1 ^a | – |
| | | 7.8±0.1 ^b | – | – | – | – | – | 4.0±0.1 ^b | – |
| | F(1)50 | 10.7±0.1 ^c | – | – | – | – | – | 5.5±0.1 ^c | – |
| | | 3.6±0.1 | 0.98 | 2.3±0.1 | 0.93 | 2.6±0.1 | 0.94 | 1.8±0.1 | 1.2±0.1 |
| | F(1)SF | 2.5±0.1 | 0.90 | 1.6±0.1 | 0.98 | 1.9±0.1 | 0.99 | 1.3±0.1 | 0.8±0.1 |
| | | 3.3±0.1 ^a | – | – | – | – | – | 1.7±0.1 ^a | – |
| | | 4.4±0.1 ^b | – | – | – | – | – | 2.3±0.1 ^b | – |
| | | 5.8±0.1 ^c | – | – | – | – | – | 3.0±0.1 ^c | – |
| | F(1)SFA | 3.3±0.1 | 0.99 | 2.6±0.1 | 0.95 | 3.0±0.1 | 0.89 | 1.7±0.1 | 1.3±0.1 |
| F(2)SF | 2.7±0.1 | 0.99 | 2.1±0.1 | 0.91 | 2.1±0.1 | 0.95 | 1.4±0.1 | 1.1±0.1 | |
| F(2)SFA | 4.5±0.1 | 0.98 | 4.0±0.1 | 0.99 | 3.3±0.1 | 0.98 | 2.3±0.1 | 2.0±0.1 | |
| XC4 | T(0.50) ^{*/**} | 0.0 | – | 0.0 | – | 0.0 | – | 0.0 | 0.0 |
| | F(1)15 ^{*/**} | 0.0 | – | 0.0 | – | 0.0 | – | 0.0 | 0.0 |
| | F(2)15 ^{*/**} | 0.0 | – | 0.0 | – | 0.0 | – | 0.0 | 0.0 |
| | F(1)50 [*] | 1.0±0.1 | 0.97 | 0.9±0.1 | 0.95 | 1.0±0.1 | 0.90 | 0.5±0.1 | 0.5±0.1 |
| | F(1)50 ^{**} | 1.4±0.1 | 0.98 | 1.2±0.1 | 0.96 | 1.4±0.1 | 0.90 | 0.7±0.1 | 0.6±0.1 |
| | F(2)50 [*] | 0.9±0.1 | 0.95 | 0.7±0.1 | 0.85 | 0.7±0.1 | 0.97 | 0.5±0.1 | 0.4±0.1 |
| | F(2)50 ^{**} | 1.4±0.1 | 0.94 | 0.9±0.1 | 0.86 | 1.0±0.1 | 0.97 | 0.7±0.1 | 0.5±0.1 |
| | Microscopic measurements | | | | | | | | |
| Class | Mix | A_{acce} (mm/ $\sqrt{\text{weeks}}$) | | | | A_{field} (mm/ $\sqrt{\text{years}}$) | | | |
| | | 28 d | 91 d | 28 d | 91 d | | | | |
| XC3 | T(0.55) | 1.6±0.5 | – | 0.9±0.3 | – | | | | |
| | F(1)15 | 0.7±0.2 | 0.5±0.3 | 0.4±0.1 | 0.3±0.2 | | | | |
| | F(2)15 | 0.2±0.1 | 0.3±0.2 | 0.1±0.1 | 0.2±0.1 | | | | |
| | F(1)50 | 3.8±0.4 | 3.4±0.5 | 1.9±0.2 | 1.7±0.3 | | | | |
| | F(2)50 | 3.9±0.7 | 3.0±0.5 | 2.0±0.4 | 1.6±0.3 | | | | |
| | F(1)SF | 2.2±0.6 | 1.6±0.6 | 1.1±0.3 | 0.8±0.3 | | | | |
| | F(1)SFA | 3.0±0.8 | 2.8±0.5 | 1.5±0.4 | 1.4±0.3 | | | | |
| | F(2)SF | 2.7±0.5 | 2.5±0.4 | 1.4±0.3 | 0.8±0.3 | | | | |
| | F(2)SFA | 4.4±0.7 | 4.2±0.8 | 2.2±0.4 | 2.1±0.4 | | | | |
| XC4 | T(0.50) [*] | – | 0.6±0.4 | – | 0.3±0.3 | | | | |
| | T(0.50) ^{**} | – | 0.8±0.6 | – | 0.4±0.3 | | | | |
| | F(1)15 [*] | 0.2±0.2 | 0.3±0.2 | 0.1±0.1 | 0.2±0.1 | | | | |
| | F(1)15 ^{**} | 0.2±0.1 | 0.4±0.2 | 0.1±0.1 | 0.2±0.1 | | | | |
| | F(2)15 [*] | 0.2±0.1 | 0.3±0.2 | 0.1±0.1 | 0.2±0.1 | | | | |
| | F(2)15 ^{**} | 0.3±0.1 | 0.4±0.2 | 0.2±0.1 | 0.2±0.1 | | | | |
| | F(1)50 [*] | 1.0±0.3 | 0.9±0.4 | 0.6±0.2 | 0.5±0.2 | | | | |
| | F(1)50 ^{**} | 1.5±0.4 | 1.2±0.5 | 0.8±0.2 | 0.6±0.3 | | | | |
| | F(2)50 [*] | 1.0±0.4 | 1.0±0.5 | 0.6±0.2 | 0.5±0.3 | | | | |
| | F(2)50 ^{**} | 1.5±0.6 | 1.4±0.6 | 0.8±0.3 | 0.8±0.3 | | | | |

* A_{acce} values were calculated with inclusion of the immersion period in water.

** A_{acce} values were calculated with exclusion of the immersion period in water.

^a A_{acce} and A_{field} values for suboptimal curing: 7 days at 20 °C and 95% RH, 21 days at 20 °C and 60% RH.

^b A_{acce} and A_{field} values for optimal curing corrected for the applied CO_2 concentration.

^c A_{acce} and A_{field} values for suboptimal curing^a after correction for the applied CO_2 concentration^b.

The accelerated carbonation coefficients of the non-air entrained FA+SF mixtures are only around twice the carbonation coefficients of OPC reference T(0.55) after 28 and 91 days of curing. As such, mixtures F(1)SF and F(2)SF have a substantially improved carbonation resistance. The decrease in A_{acce} value which is observed between 28 and 91 days of curing ranges between 22-36% which seems somewhat less in comparison with the HVFA mixtures. This could indicate that the secondary pozzolanic hydration reactions inherent to the FA+SF concrete occurred faster in comparison with HVFA concrete. However, this statement requires verification on a microstructural level. This could be done by performing thermogravimetric analyses at multiple testing ages in order to see from which point in time on the consumption of the CH phases start. This aspect will be discussed more in detail within Section 5.6.3.2. Note that more prolonged curing (182 days) sometimes resulted in a slight increase of the carbonation coefficient again. If longer curing periods would have been considered as well, this increase would probably turn out negligible.

The addition of an AEA to create a pronounced artificial air void system to improve the salt scaling properties of the FA+SF concrete was found to have a significant effect on the carbonation resistance of the concrete. The resulting A_{acce} values are comparable to those of non-air entrained HVFA concrete. It completely cancels out the benefit of using 40% FA in combination with 10% SF. This issue will be addressed more thoroughly in Chapter 7.

Note that the R^2 values that correspond with the carbonation coefficients of the HVFA mixtures are closer to unity (R^2 : 0.92-0.99) than the ones reported for mixture T(0.55) after 28 and 91 days (R^2 : 0.70-0.71). This can be explained by the fact that a much more well-defined carbonation front existed for the HVFA mixtures after applying the phenolphthalein colour indicator. The colorimetric determination of the carbonation front for the OPC reference T(0.55) was more difficult because the samples were characterised by a more gradual transition from colourless to purple. This made it difficult to determine the exact location of colour transition. As a consequence, plotting the carbonation depths as a function of the square root of time resulted in a less pronounced linear relation.

With respect to the FA mixtures conforming to the k-value concept of NBN B15-001, no carbonation was recorded using the colorimetric measuring technique. As a result, the accelerated carbonation coefficient of mixtures F(1)15 and F(2)15 is seemingly 0.00 mm/ $\sqrt{\text{weeks}}$. However, the microscopic measuring technique revealed that these two concrete mixtures indeed showed signs of – be it limited – carbonation (Figure 5.4-5.5). The microscopic carbonation measurements obtained after around 16-18 weeks of exposure to 10% CO₂ were also used for the calculation of an accelerated carbonation coefficient. Since only one exposure period (± 16 or 18 weeks) was considered, linear regression could not be used for this purpose. A rudimentary carbonation coefficient was obtained by simply dividing the measured carbonation depth (Figure 5.4-5.5) by $\sqrt{16}$ or $\sqrt{18}$ weeks. Logically, the corresponding standard deviations on the individual values for only one exposure period are considerably higher than the standard deviations on the colorimetric carbonation coefficients obtained by means of linear regression. Nevertheless, the same technique was applied to come up with a microscopic carbonation coefficient for the OPC reference and the HVFA and FA+SF mixtures. Comparison of the two measuring techniques shows that apart from the F(1)50 mixture tested at 28 days, all HVFA mixtures were characterised by slightly higher

microscopic carbonation coefficients. In case of FA+SF concrete quite the opposite was true. However, the difference turned out insignificant.

With respect to the results for exposure class XC4, more or less the same conclusions are valid as for exposure class XC3. Logically, the carbonation coefficients obtained for the former exposure class are much lower relative to the ones obtained for the latter. This is not only the case when the immersion period in water is included (*), but also when it is excluded (**) from the exposure time. Apparently, the amount of water absorbed by keeping the specimens submerged every two weeks is not sufficiently released again from the concrete during each subsequent week of exposure to 10% CO₂. As a result, penetration of CO₂ was hindered substantially. This explains why the A_{acce}^{**} values of HVFA mixtures F(1)50 and F(2)50 for exposure class XC4 still differ significantly from their corresponding A_{acce} values measured in exposure class XC3. When based upon colorimetric measurements, the former coefficients are about 32-49% lower than the latter. The microscopic measuring technique resulted in very similar percentages (34-47%). However, the latter percentages are not valid for mixtures F(1)15 and F(2)15. Sometimes, their low carbonation coefficients recorded for exposure class XC4 were even a little higher than the ones recorded for exposure class XC3 (e.g. F(2)15 at 91 days).

Until now all the results reported related to concrete that had been optimally cured for 28, 91 or 182 days. For one HVFA and one FA+SF mixture a comparison was made between the A_{acce} values obtained after 28 days of optimal curing (28 days at 20°C and 95% RH) and 28 days of suboptimal curing (7 days at 20°C and 95% RH + 21 days at 20°C and 60% RH). Figure 5.6 shows the resulting carbonation depths as a function of the square-root-of-time for the simulated exposure class XC3.

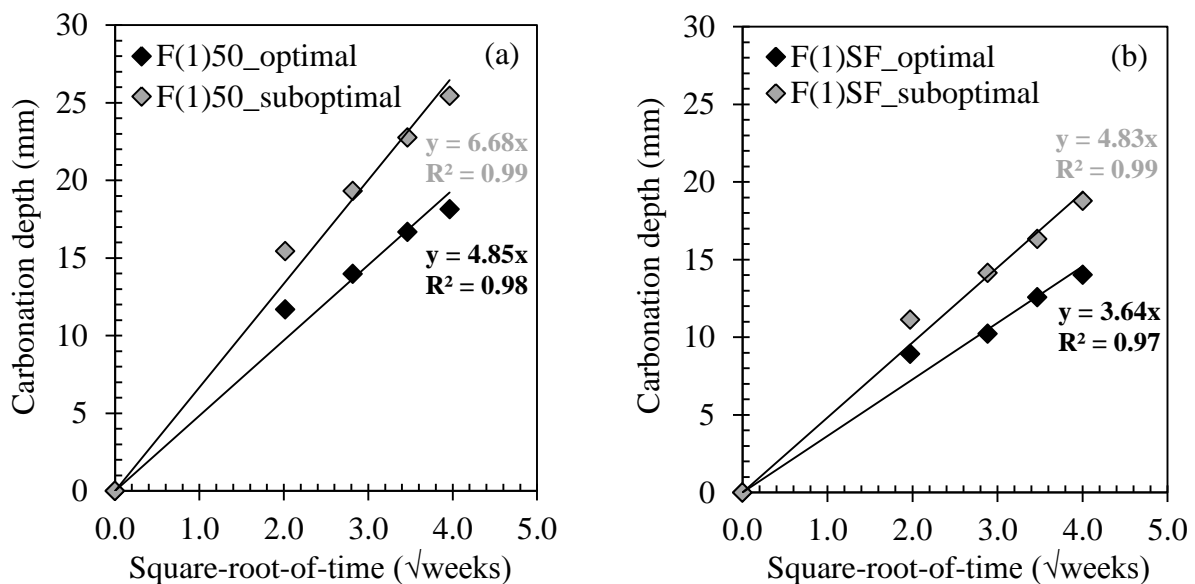


Figure 5.6. Effect of suboptimal curing on the accelerated carbonation coefficient of HVFA mixture F(1)50 and FA+SF mixture F(1)SF.

After 28 days of suboptimal curing the carbonation coefficient of the HVFA composition is 1.38 times higher than after 28 days of optimal curing. For the FA+SF composition the

difference between the two curing conditions can be explained by a very similar factor ($\times 1.33$). Although these additional A_{acce} values for the optimally cured F(1)50 and F(1)SF mixtures slightly differed from the original ones shown in Table 5.2, the same conversion factors were applied to the latter. As such, accelerated carbonation coefficients for suboptimally cured concrete can be evaluated in perspective of the ones that were obtained after prolonged optimal curing (91 and 182 days). Their estimated values have been tabulated in Table 5.2 (^a). For the suboptimal curing conditions, HVFA composition F(1)50 has the lowest carbonation resistance based on a carbonation test involving exposure to 10% CO_2 .

5.6.3. Influence of the applied CO_2 concentration during carbonation testing

5.6.3.1. Effect on the carbonation coefficient

Carbonation coefficients obtained after exposing a certain concrete to 10% CO_2 are expected to be much higher than the carbonation coefficients of the same concrete after being exposed to only 1% CO_2 . In case of the proposed HVFA and FA+SF concrete compositions, an obvious difference in carbonation rate could indeed be observed (Figure 5.7a, b). The OPC reference on the other hand showed a somewhat different behaviour. Exposure to only 1% CO_2 still resulted in the lowest A_{acce} value (1.37 mm/ $\sqrt{\text{weeks}}$). Nevertheless, the difference with the result obtained in a 10% CO_2 atmosphere (1.65 mm/ $\sqrt{\text{weeks}}$) is rather small (Figure 5.7c). There were some doubts whether the carbonation chamber conditioned at 10% CO_2 was working properly while the OPC reference was being tested as there were rather strong fluctuations in relative humidity around the preset value of 60% RH. However, the carbonation coefficient (1.65 mm/ $\sqrt{\text{weeks}}$) did not deviate much from the one that has been recorded for the previously tested batch of T(0.55) concrete (1.30 mm/ $\sqrt{\text{weeks}}$, Table 5.2). Yet, given the lower R^2 values for the latter results due to a not always very distinct colour change boundary, the results of this reference should still be interpreted with caution. Preferably, comparative carbonation testing should be repeated once more for the OPC reference to find further confirmation for the now observed small difference in carbonation coefficient after exposure to 1% and 10% CO_2 .

One of the main reasons for performing these comparative carbonation tests was a validity check of the conversion formula to go from an accelerated to a field carbonation coefficient (Equation 5-5) for CO_2 concentrations higher than 3% (Section 5.4.6). Therefore, the carbonation coefficients corresponding with exposure to 10% CO_2 were implemented in this equation to estimate a carbonation coefficient for a 1% CO_2 environment. By doing so, 1% CO_2 is assumed to be a field concentration. Although seldomly as high, perhaps only in industrial areas [Audenaert (2006)], the carbonation related reaction products should not differ too much from the expected reaction products in a normal atmosphere at 0.03% CO_2 [NBN B15-100 (2008)]. Thus, this assumption is believed to be justified.

If Equation 5-5 would be valid, then the estimated carbonation coefficient for 1% CO_2 should not differ too much from the measured value. This was clearly not the case for neither of the considered concrete types. For mixtures F(1)50, F(1)SF and T(0.55), the estimated values were only 55%, 57% and 38% of the measured values. In other words, the use of Equation 5-5 results in an important underestimation of the field carbonation rate when based upon a carbonation test involving a much higher CO_2 concentration (up to 10% CO_2). This

observation cannot be neglected in perspective of the empirical service predictions that will be performed in Chapter 8. Therefore, a CO₂ concentration related corrected value for the 28-day carbonation coefficients of mixtures F(1)50, F(1)SF and T(0.55) under optimal curing conditions has been included in Table 5.2^(b). The corrected values were obtained by dividing the original A_{acce} values of F(1)50, F(1)SF and T(0.55) by 55%, 57% and 38%, respectively. This increased the corresponding field carbonation coefficients substantially. The highest one was recorded for the HVFA mixture and equals 4.0 mm/ $\sqrt{\text{years}}$. Note that all the field carbonation coefficients reported in Table 5.2 correspond with a CO₂ concentration of 0.05%. The origin of this particular concentration will be discussed more in detail in Chapter 8.

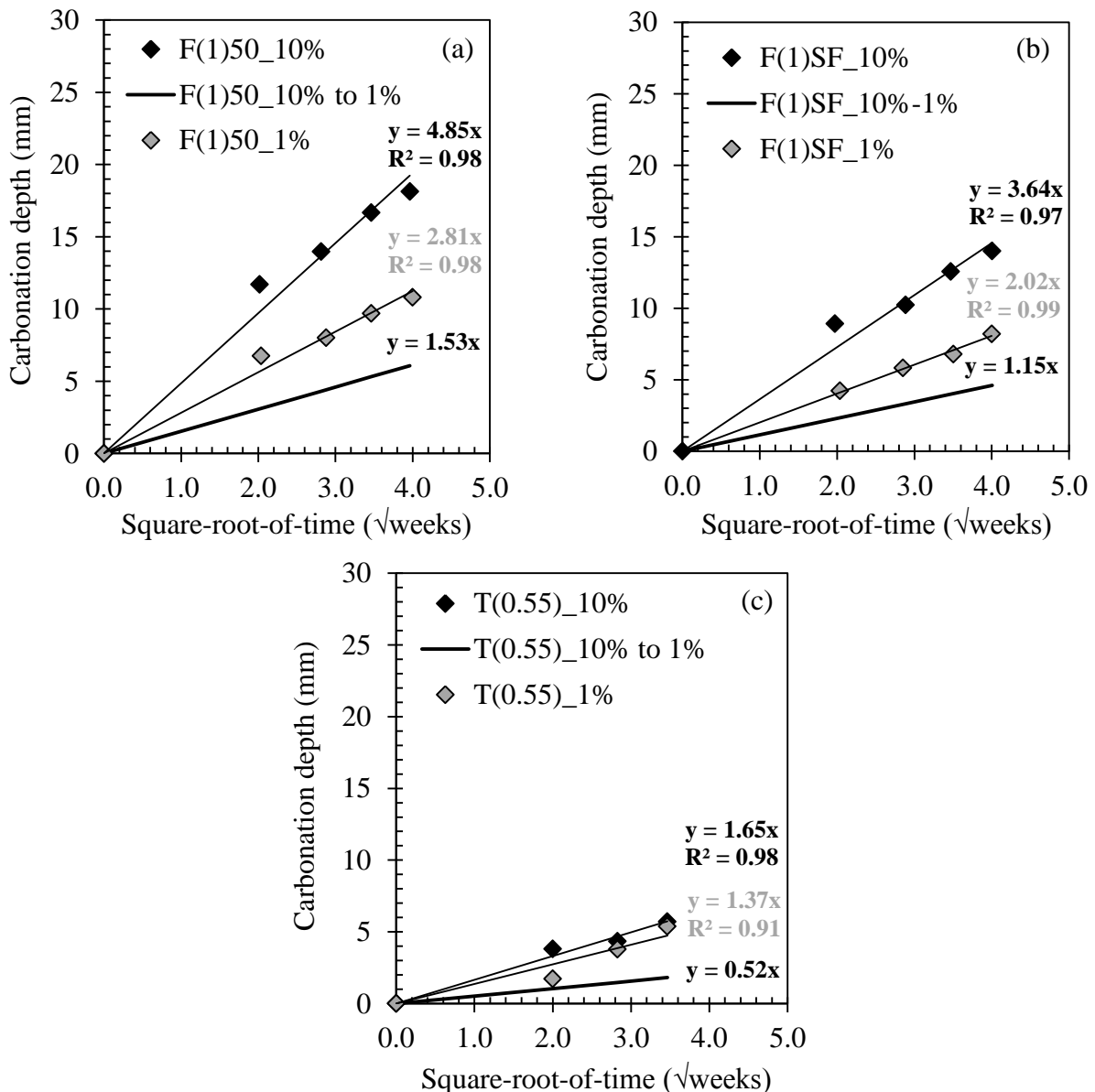


Figure 5.7. Effect of the applied CO₂ concentration on the carbonation coefficient of HVFA mixture F(1)50 and FA+SF mixture F(1)SF and OPC reference T(0.55).

This is just one way of showing the effect of the applied CO₂ concentration during accelerated carbonation testing. Another method based on a comparison of the carbonation resistance

R_{carb} (cf. Equation 5-1) per test has been proposed by Visser (2012). This evaluation approach has been included in Appendix A.

5.6.3.2. Effect on the chemistry of the carbonation reaction

Before going into detail on the effects of the applied CO_2 concentrations during (accelerated) carbonation testing that can be measured with TGA, one should first understand what happens to the unexposed pastes. Time dependent monitoring of the chemically bound water (w_b), the $\text{Ca}(\text{OH})_2$ (CH) and CaCO_3 (CC) contents in g/100 g cement led to the following findings:

- For all studied pastes the w_b content clearly increased with time until the age of 28 days whereafter it gradually stabilizes at around its maximum value at time infinity ($w_{b,\infty}$). The value of $w_{b,\infty}$ was estimated by fitting a three parameter equation (TPE) through the data points using non-linear regression (Equation 5-11).

$$w_b = w_{b,\infty} \cdot \exp\left(-\left(\frac{\tau}{t}\right)^a\right) \quad (5-11)$$

This equation is similar to the one proposed by Pane and Hansen (2005) and was also used by Gruyaert (2011) for the same purpose. The intercept and curvature of the plot obtained with this three parameter equation on a logarithmic scale are governed by its parameters τ and a , respectively. The plots of the estimated three parameter equations for the different pastes were included in Figures 5.8a and 5.8d.

The $w_{b,\infty}$ values of paste mixtures T(0.55), T(0.35), F(1)50 and F(1)SF amounted to 30.8 ± 4.5 g/100 g cement, 22.8 ± 2.4 g/100 g cement, 30.0 ± 6.9 g/100 g cement and 27.4 ± 1.5 g/100 g cement, respectively. The value of OPC paste mixture T(0.35) is well in range with the 23% by mass of the anhydrous material for fully hydrated cement as suggested by Neville (1995). Surprisingly, the $w_{b,\infty}$ value of the other OPC mixture seems higher. However, given the considerable variation on the fitted parameter, the difference with the suggested 23% by mass may not be so large after all. More TGA measurements, especially at later age, are needed for further verification. The same goes for HVFA mixture F(1)50 which was characterized by even more scatter on the ultimate w_b content of 30.8 g/100 g cement. The fitted ultimate bound water content of mixture F(1)SF showed much less variation (1.5 g/100 cement). The $w_{b,\infty}$ value of 27.4 g/100 cement is slightly higher than 23% by mass of the anhydrous material for fully hydrated cement and seems to indicate that a small amount of water is also bound by the SCMs. Still, more TGA measurements at later age are needed to find further verification for this.

- When comparing the measured CH contents it is immediately clear that the OPC pastes and pastes with SCMs behave in a different way (Figure 5.8b and 5.8e). The OPC pastes are characterized by a steadily increasing CH content within the 28-day period after casting up until a value of around 20 g/100 g cement. From then on, the CH content of OPC paste does not seem to change substantially anymore. The highest CH contents were recorded for OPC paste T(0.55) with a W/C ratio of 0.55. If on the other hand the binder fraction of the

paste partially consisted of pozzolanic materials such as FA (and SF), the evolution of the CH content was different.

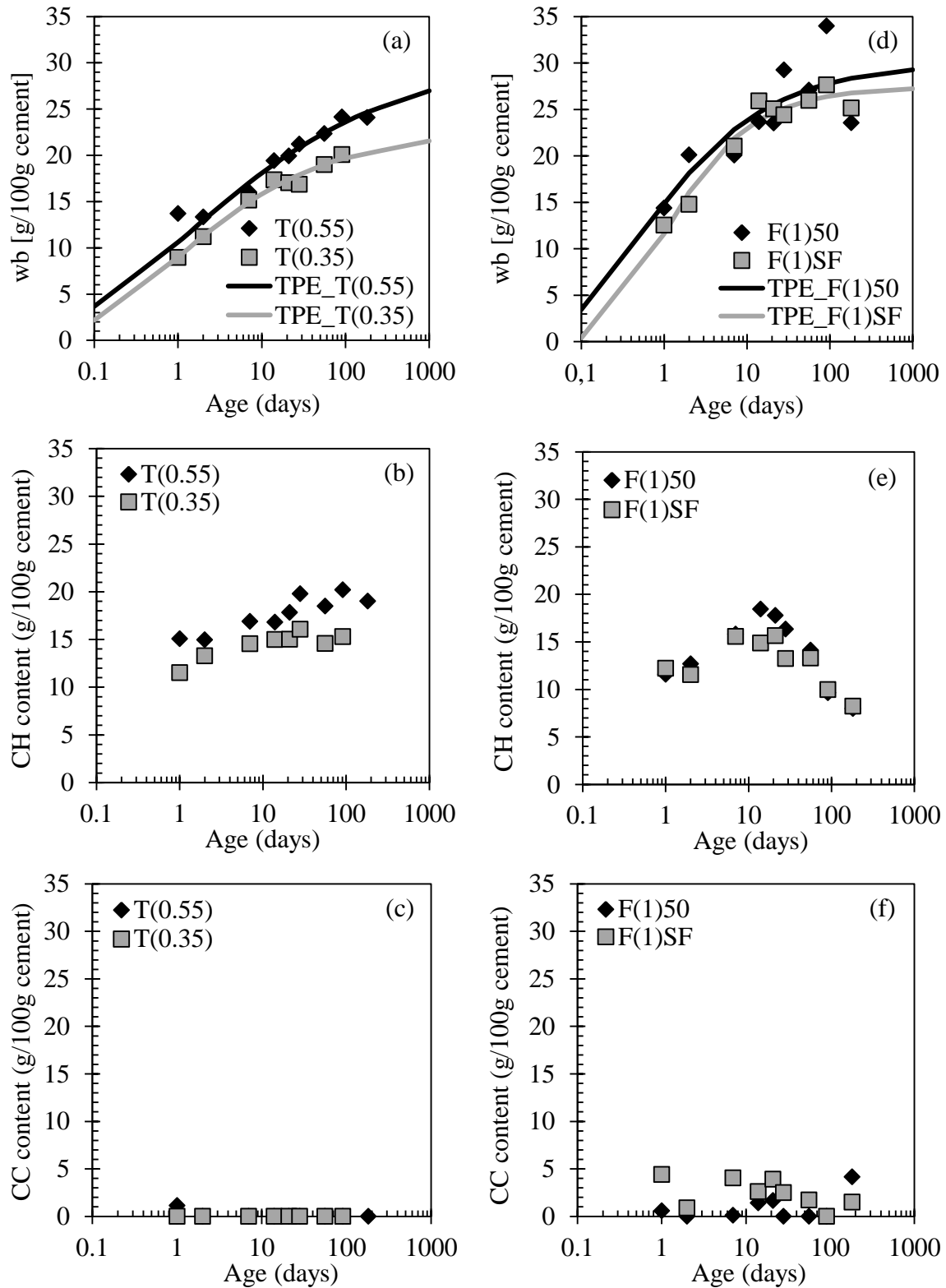


Figure 5.8. Evolution of the bound water (w_b), the $\text{Ca}(\text{OH})_2$ (CH) content and the CaCO_3 (CC) contents of water cured OPC, HVFA and FA+SF pastes as a function of time.

Up until the age of 21 days there was also a build-up in CH content for HVFA paste F(1)50. Yet, the maximum amount reached (18.4 g/100 g cement) was a little lower than the CH content of the OPC pastes at that age. Moreover, from then on the CH content gradually decreased again until only 8.0 g/100 g cement remained after 182 days. Quite a similar trend was observed for paste F(1)SF that contains 40% FA and 10% SF. It must be said though that for a FA+SF binder system the maximum CH content was already reached after 7 days. This maximum CH content (15.6 g/100 g cement) was also found to be slightly lower when compared with the HVFA paste. The final CH content of the FA+SF and HVFA pastes after 182 days of immersion in water were almost identical.

- Despite the precautions taken to prevent carbonation (i.e., continuous immersion in water until the moment of testing) of the pastes that were not deliberately exposed to (increased) CO₂ concentrations, some initial carbonation could not be avoided. The pastes containing SCMs seemed a little more susceptible to the phenomenon (Figure 5.8c, f). This carbonation was mainly due to the atmospheric exposure during sample preparation (i.e. crushing and grinding of the pastes with pestle and mortar) in a non-CO₂ free environment.

This characterization of the optimally cured OPC, HVFA and FA+SF pastes as a function of time by means of TGA not only gives relevant information regarding the ongoing hydration, it also contains necessary experimental input to estimate the amount of C–S–H carbonation after an (accelerated) carbonation test performed at different CO₂ concentrations (0.03% CO₂, 1% CO₂ and 10% CO₂). When calculated in accordance with Borges et al. (2010), the CC and CH contents after 28 days at the start of the experiment together with CC and CH contents of the carbonated pastes at the end of the test (after 112 days) are to be used (Table 5.3).

Table 5.3. Estimation of the extent of C–S–H carbonation as calculated from TGA data (in g/100 g binder) obtained from pastes before and after carbonation cf. Borges et al. (2010).

| Before carbonation (at 28 days) | T(0.55) | | | F(1)50 | | | F(1)SF | | |
|---|----------------|----------|-----------|---------------|----------|-----------|---------------|----------|-----------|
| CC initially present (Equation 5-7) | 0.0 | | | 0.0 | | | 1.3 | | |
| CH initially present (Equation 5-8) | 19.8 | | | 8.2 | | | 6.6 | | |
| After carbonation (at 112 days) | T(0.55) | | | F(1)50 | | | F(1)SF | | |
| CO₂ concentration (%) | 0.03 | 1 | 10 | 0.03 | 1 | 10 | 0.03 | 1 | 10 |
| CC formed (Equation 5-9) | 54.5 | 71.0 | 68.5 | 23.2 | 30.5 | 35.0 | 28.9 | 32.4 | 35.2 |
| CH remaining (Equation 5-10) | 0.0 | 0.0 | 0.0 | 0.5 | 0.0 | 0.0 | 0.0 | 0.0 | 0.0 |
| Carbonated CH (A) | 19.8 | 19.8 | 19.8 | 7.6 | 8.2 | 8.2 | 6.6 | 6.6 | 6.6 |
| CC from carbonated CH (B) | 26.8 | 26.8 | 26.8 | 10.3 | 11.0 | 11.0 | 8.9 | 8.9 | 8.9 |
| CC from C–S–H carbonation (C) | 27.7 | 44.2 | 41.7 | 12.9 | 19.5 | 23.9 | 19.9 | 23.5 | 26.2 |
| % CH carbonation | 49 | 38 | 39 | 44 | 36 | 32 | 31 | 27 | 26 |
| % C–S–H carbonation | 51 | 62 | 61 | 56 | 64 | 68 | 69 | 73 | 74 |

(A) = %CH initially available (Equation 5-8) – %CH remaining (Equation 5-10)

(B) = (A) × MW_{CaCO₃}/MW_{Ca(OH)₂}

(C) = %CC formed (cf. Equation 5-9) – (B)

As such, the highest percentages of C–S–H carbonation were recorded for the FA+SF paste (69-74%). In case of the HVFA paste these percentages were slightly lower (56-68%), while the lowest percentages of C–S–H carbonation were observed for the OPC paste (53-64%). However, the differences between the OPC and HVFA pastes were actually not that

pronounced. The applied CO₂ concentration during carbonation testing also seems to play a role. For every studied paste mixture the estimated amount of C–S–H carbonation increased with increasing CO₂ concentration. The most substantial difference was seen between the pastes that carbonated naturally at 0.03% CO₂ and the pastes that were subjected to an accelerated carbonation test either at 1% and 10% CO₂. The differences in amount of C–S–H carbonation between the latter two test conditions were rather negligible (1-4%).

As already mentioned in Section 5.5.1, this approach probably underestimates the actual amount of C–S–H carbonation for the pastes with FA (and SF) because the pozzolanic reactions have not started yet or are still ongoing after only 28 days. The alternative calculation method does not depend on the amount of CC and CH present at the start of the carbonation test, but on the corresponding amounts present in unexposed pastes with the same age as the carbonated pastes at the end of the test (after 112 days). Except for the fact that the as such obtained percentages of C–S–H carbonation for paste mixtures F(1)50 and F(1)SF are higher, basically all previously drawn conclusions remain valid. If the paste contained FA (and SF), more C–S–H carbonation is observed than when the binder fraction only consisted of OPC. Regarding the applied CO₂ concentration, the most notable difference in amount of C–S–H carbonation (3-5%) again existed between the natural and accelerated carbonation conditions. For the OPC paste a difference of up to 10% was recorded. The differences in amount of C–S–H carbonation after exposure to 1% or 10% CO₂ were insignificant (1%) for all pastes considered.

As explained in Section 5.5.1, the C–S–H carbonation percentages obtained with the alternative calculation method may be somewhat exaggerated for the pastes containing pozzolans. While the method of Borges et al. (2010) underestimates C–S–H carbonation, the alternative method may overestimate it. The actual amounts of carbonates that originate from the C–S–H will range between the outcomes of the two methods. However, the trends observed with each method will probably remain.

Table 5.4. Estimation of the extent of C–S–H carbonation as calculated from TGA data (in g/100 g binder) obtained from uncarbonated and carbonated pastes at the age of 112 days.

| Uncarbonated (at 112 days) | T(0.55) | | | F(1)50 | | | F(1)SF | | |
|---|----------------|----------|-----------|---------------|----------|-----------|---------------|----------|-----------|
| CC normally present (Equation 5-7) | 0.0 | | | 0.1 | | | 0.0 | | |
| CH normally present (Equation 5-8) | 19.0 | | | 4.3 | | | 4.6 | | |
| Carbonated (at 112 days) | T(0.55) | | | F(1)50 | | | F(1)SF | | |
| Applied CO₂ concentration (%) | 0.03 | 1 | 10 | 0.03 | 1 | 10 | 0.03 | 1 | 10 |
| CC formed (Equation 5-9) | 54.5 | 71.0 | 68.5 | 23.2 | 30.5 | 35.0 | 28.9 | 32.4 | 35.2 |
| CH remaining (Equation 5-10) | 0.0 | 0.0 | 0.0 | 0.5 | 0.0 | 0.0 | 0.0 | 0.0 | 0.0 |
| Carbonated CH (A) | 19.0 | 19.0 | 19.0 | 3.8 | 4.3 | 4.3 | 4.6 | 4.6 | 4.6 |
| CC from carbonated CH (B) | 25.7 | 25.7 | 25.7 | 5.1 | 5.8 | 5.8 | 6.3 | 6.3 | 6.3 |
| CC from C–S–H carbonation (C) | 28.8 | 45.3 | 42.8 | 18.1 | 24.7 | 29.1 | 22.6 | 26.1 | 28.9 |
| % CH carbonation | 47 | 36 | 37 | 22 | 19 | 17 | 22 | 19 | 18 |
| % C–S–H carbonation | 53 | 64 | 63 | 78 | 81 | 83 | 78 | 81 | 82 |

(A) = %CH normally present (Equation 5-8) – %CH remaining (Equation 5-10).

(B) = (A) × MW_{CaCO₃}/MW_{Ca(OH)₂}.

(C) = %CC formed (cf. Equation 5-9) – (B).

Finally, it should be noted that only a TGA based calculation of the amount of C–S–H carbonation revealed an influence of the applied CO₂ concentration during carbonation testing. No influence could be detected from a mere analysis of the most basic TGA output, i.e. the thermal decompositions curves of each sample. In contrast with the findings of Thiery et al. (2007) the decarbonation related mass losses did not occur in different temperature ranges depending on the type of calcium carbonate that is decomposing (550-680°C: the amorphous phase; 680-780°C: the metastable phase, being Vaterite and Aragonite; 780-990°C: the stable phase, being well-crystallized Calcite). Usually the thermal decomposition curves of carbonated samples showed a continuous mass loss between 550°C and 990°C.

5.6.3.3. Effect on the mineralogical phases formed

Quantitative Rietveld analysis was done on the X-ray diffractograms of the OPC, HVFA and FA+SF pastes (Figures 5.9, 5.10, 5.11). The results are shown in Tables 5.5, 5.6 and 5.7. Attention was especially paid to the mineralogical phases that are normally present when uncarbonated (Portlandite, Kuzelite, Etringite) and carbonated (Calcite, Vaterite, Aragonite). Apart from those, some of the other phases measured specifically relate to one or more of the binder materials used, e.g. OPC (β -C₂S, C₄AF, Hydrogarnet), FA and SF (Mullite, Quartz_low). The percentages mentioned for ‘Other’ comprise crystalline material present in amounts smaller than the detection limit of the apparatus as well as non-crystalline material. Tables 5.5, 5.6 and 5.7 give three analyses for the pastes that fully carbonated at 10% CO₂. Samples 10%a, 10%b and 10%c were collected from the holes drilled 5-7 mm, 10-12 mm and 18-22 mm from the exposed mantle surfaces of the paste cylinders.

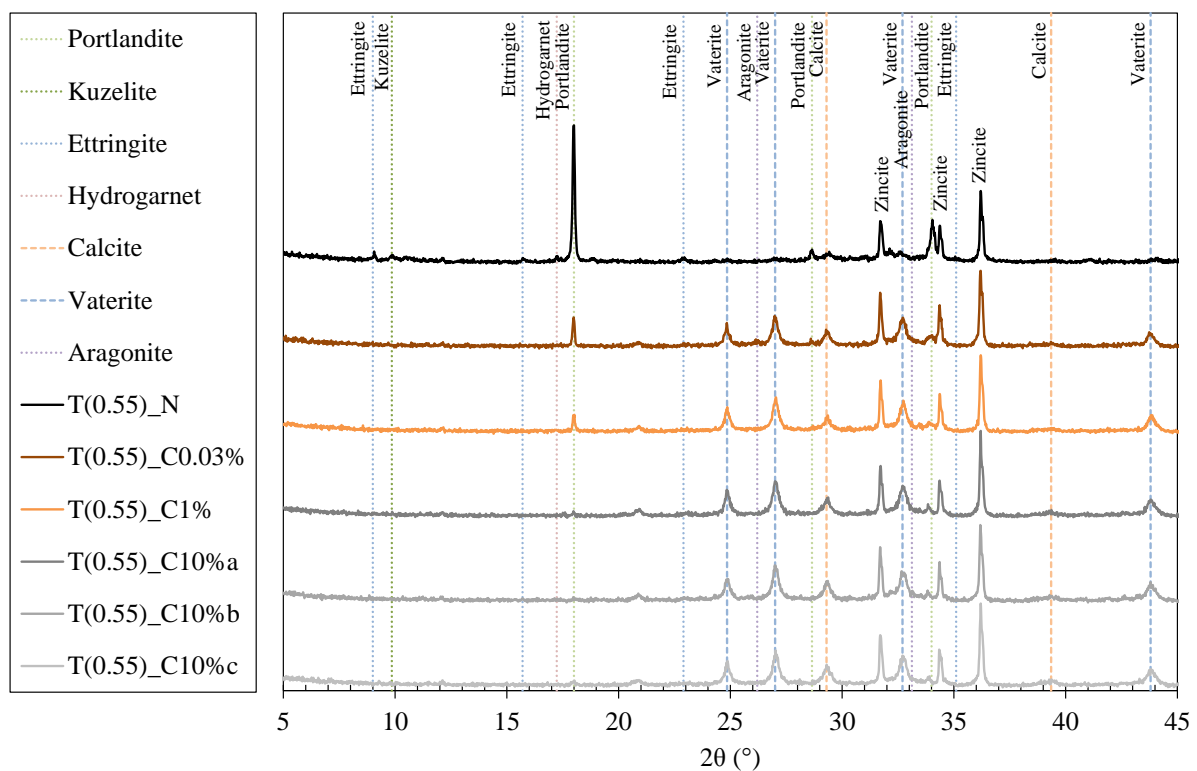


Figure 5.9. X-ray diffractogram of OPC paste T(0.55) in uncarbonated condition (N) and after carbonation at 0.03%, 1% and 10% CO₂.

Table 5.5. Quantitative Rietveld analysis of OPC paste T(0.55) in uncarbonated condition (N) and after carbonation at 0.03%, 1% and 10% CO₂.

| Phase (%) | N | 0.03% | 1% | 10%a | 10%b | 10%c |
|-------------------------------------|-------------|-------------|-------------|-------------|-------------|-------------|
| β-C ₂ S | 6.8 | 2.8 | 2.1 | 2.0 | 2.4 | 1.9 |
| C ₄ AF | 3.6 | 3.4 | 4.0 | 4.3 | 3.9 | 3.5 |
| Mullite | – | – | – | – | – | – |
| Quartz_low | – | – | – | – | – | – |
| Portlandite | 18.5 | 2.9 | 0.4 | 0.3 | 0.1 | 0.1 |
| Kuzelite | 1.4 | – | – | – | – | – |
| Ettringite | 3.0 | 0.7 | 0.4 | 0.4 | 0.6 | – |
| Hydrogarnet | 0.7 | 0.5 | 0.8 | 0.7 | 0.8 | 0.7 |
| Calcite | 1.8 | 3.9 | 4.0 | 5.6 | 6.2 | 6.2 |
| Vaterite | 2.3 | 28.5 | 37.0 | 41.3 | 40.4 | 36.3 |
| Aragonite | – | 2.5 | – | – | – | – |
| Other | 61.9 | 54.9 | 51.3 | 45.5 | 45.6 | 51.3 |
| Calcite+Vaterite+Aragonite | 4.1 | 38.8 | 41.0 | 46.9 | 46.9 | 42.5 |
| Calcite/(Vaterite+Aragonite) | 0.78 | 0.13 | 0.11 | 0.14 | 0.15 | 0.17 |

From the quantitative assesment of the mineralogical phases present in OPC paste T(0.55) the following conclusions can be drawn:

- Since the entire binder content consisted of OPC, β-C₂S, C₄AF and Hydrogarnet were the only binder related phases detected. Mullite and Quartz_low were not present. In uncarbonated condition, the β-C₂S content exceeded the C₄AF content. After carbonation, quite the opposite was true.
- In uncarbonated condition, the paste logically contains a substantial amount (18.5%) of Portlandite (Ca(OH)₂), the main hydration product of the cement. Ettringite and Kuzelite were also present, be it in much smaller amounts (1.4% and 3%, respectively).
- Small amounts of Calcite (1.8%) and Vaterite (2.3%) were measured in the unexposed condition. Their presence is attributed to a slight carbonation of the samples during their preparation in a non-CO₂ free environment
- When carbonated, the remaining amount of Portlandite decreased with an increasing CO₂ concentration. This amount became negligible starting from a CO₂ concentration of 1%. The same goes for the Ettringite content. The Kuzelite fraction already completely disappears starting from a CO₂ concentration of 0.03%.
- After carbonation the metastable Vaterite phase was most abundantly available (28.5-41.3%). This statement holds true for every CO₂ concentration considered. Carbonation at 1% and 10% CO₂ resulted in the highest values. The fraction of stable Calcite was much smaller (3.9-6.2%). Somewhat higher percentages were recorded after carbonation at 10% CO₂. The metastable Aragonite was only measured in the naturally carbonated paste at 0.03% CO₂. The Calcite+Vaterite+Aragonite contents ranged between 38.8- 46.9%. The highest percentages were recorded after exposure to 10% CO₂.
- When considering the Calcite/(Vaterite+Aragonite) ratio no important changes with increasing CO₂ concentration could be observed. Their values ranged between 0.11-0.17 which was much lower when compared with the uncarbonated sample (0.78).

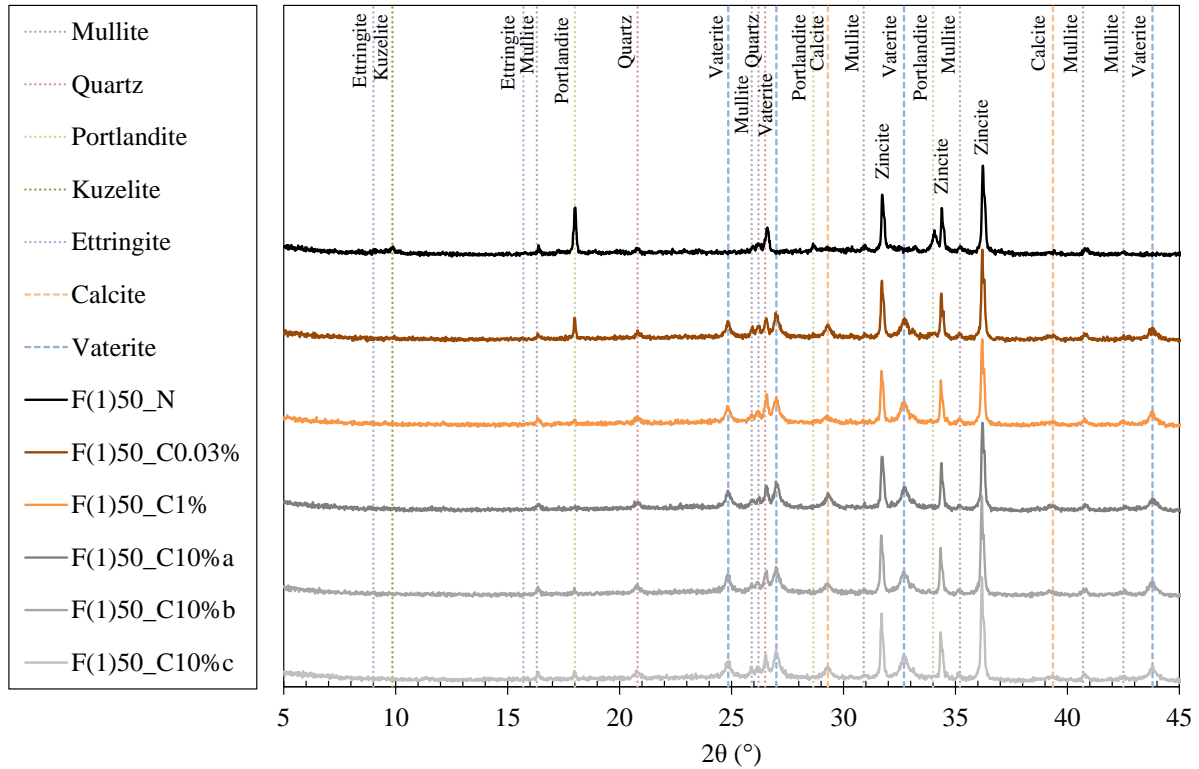


Figure 5.10. X-ray diffractogram of HVFA paste F(1)50 in uncarbonated condition (N) and after carbonation at 0.03%, 1% and 10% CO₂.

Table 5.6. Quantitative Rietveld analysis of HVFA paste F(1)50 in uncarbonated condition (N) and after carbonation at 0.03%, 1% and 10% CO₂.

| Phase (%) | N | 0.03% | 1% | 10%a | 10%b | 10%c |
|-------------------------------------|------------|-------------|-------------|-------------|-------------|-------------|
| β-C ₂ S | 2.7 | 1.9 | 1.6 | 1.5 | 1.4 | 1.4 |
| C ₄ AF | 1.1 | 1.6 | 1.9 | 1.6 | 1.6 | 1.5 |
| Mullite | 4.0 | 3.2 | 4.9 | 3.7 | 3.7 | 3.6 |
| Quartz_low | 7.4 | 8.1 | 9.3 | 7.8 | 8.4 | 8.4 |
| Portlandite | 4.6 | 0.6 | 0.1 | — | — | 0.1 |
| Kuzelite | 1.4 | 0.3 | 0.1 | 0.1 | 0.2 | — |
| Ettringite | 1.1 | 0.2 | 0.5 | 0.2 | 0.3 | 0.1 |
| Hydrogarnet | 0.4 | 0.4 | 0.5 | 0.4 | 0.4 | 0.2 |
| Calcite | 0.5 | 2.7 | 1.1 | 3.2 | 1.9 | 2.2 |
| Vaterite | — | 17.1 | 21.0 | 19.4 | 20.2 | 19.8 |
| Aragonite | — | 0.4 | 0.4 | 0.2 | 0.1 | 0.1 |
| Other | 76.6 | 63.6 | 58.7 | 62.0 | 61.6 | 62.6 |
| Calcite+Vaterite+Aragonite | 0.5 | 20.2 | 22.5 | 22.8 | 22.2 | 22.1 |
| Calcite/(Vaterite+Aragonite) | — | 0.15 | 0.05 | 0.16 | 0.09 | 0.11 |

An in-depth analysis of the results obtained for the HVFA paste led to the following conclusions:

- As 50% of the binder system in this paste consisted of fly ash, a shift in presence of the binder related phases was clearly visible. Substantial amounts of Mullite (3.6-4.9%) and

Quartz_{low} (7.4-9.3%) were now detected, while the β -C₂S and the C₄AF were lower. In uncarbonated condition the β -C₂S content again exceeded the C₄AF content. After carbonation, both contents were more or less similar, which means that mainly the β -C₂S content was affected by carbonation. The low Hydrogarnet fraction remained stable.

- In uncarbonated condition the Portlandite content (4.6%) of the HVFA paste is obviously lower than the Portlandite content of the OPC paste (18.5%) since that phase is consumed by the pozzolanic fly ash reaction. The measured percentages of Kuzelite and Ettringite were much lower (1.4% and 1.1%, respectively).
- After natural (0.03% CO₂) and accelerated (1% and 10% CO₂) carbonation, the remaining amounts of Portlandite, Kuzelite and Ettringite became negligible.
- The carbonation reaction products mainly consisted of metastable Vaterite (17.1-21.0%). Much less stable Calcite was present (1.1-3.2%). The amounts of Aragonite were negligible. No obvious effect of the applied CO₂ concentration could be observed, also when the Calcite + Vaterite + Aragonite contents (20.2-22.8%) and the ratio of the stable and metastable phases (0.05-0.16) were taken into consideration. The total amounts of carbonation reaction products were found to be lower than the corresponding amounts that were recorded for the OPC paste (38.8-46.6%). This was no surprise since there was considerably less Portlandite available for the carbonation reaction.

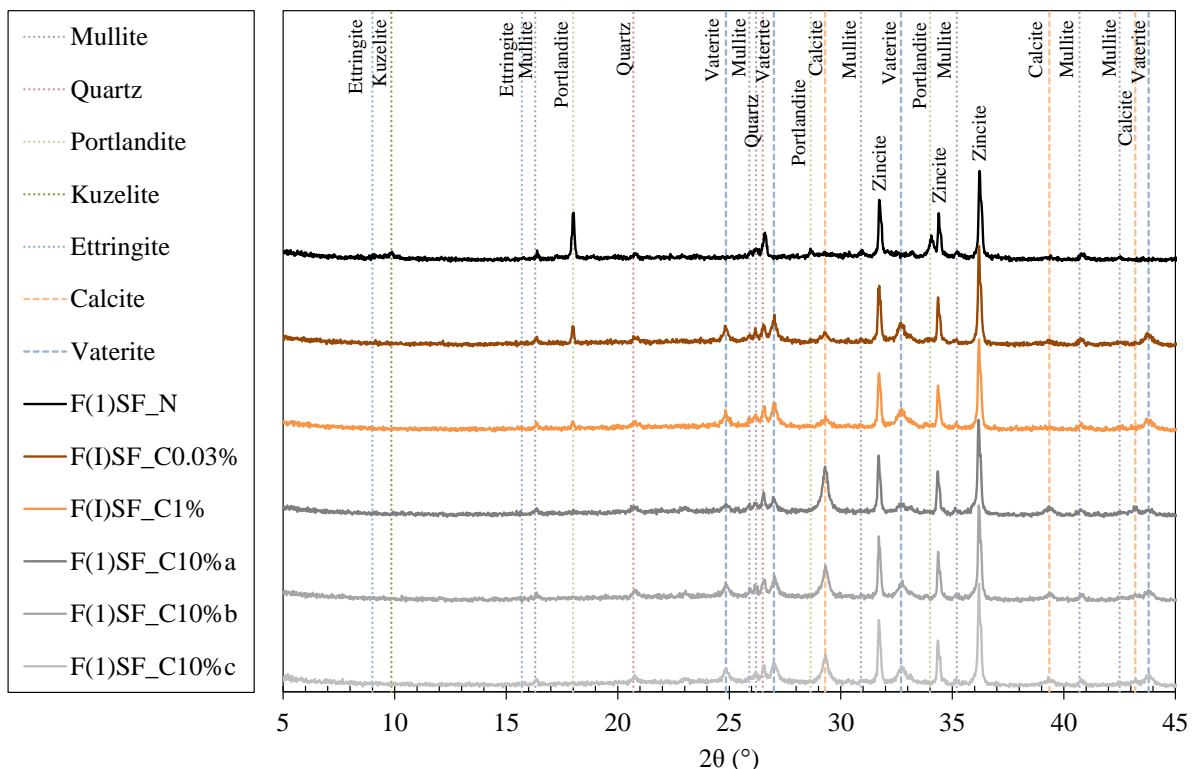


Figure 5.11. X-ray diffractogram of FA+SF paste F(1)SF in uncarbonated condition (N) and after carbonation at 0.03%, 1% and 10% CO₂.

Table 5.7. Quantitative Rietveld analysis of FA+SF paste F(1)SF in the uncarbonated condition (N) and after carbonation at 0.03%, 1% and 10% CO₂.

| Phase (%) | N | 0.03% | 1% | 10%a | 10%b | 10%c |
|-------------------------------------|------------|-------------|-------------|-------------|-------------|-------------|
| β-C ₂ S | 3.2 | 1.6 | 1.9 | 0.4 | 0.5 | 0.7 |
| C ₄ AF | 1.1 | 1.7 | 1.7 | 1.2 | 1.4 | 1.3 |
| Mullite | 2.8 | 2.8 | 3.2 | 2.6 | 2.8 | 2.6 |
| Quartz_low | 6.5 | 6.8 | 6.9 | 6.9 | 6.8 | 6.1 |
| Portlandite | 5.7 | 0.3 | 0.1 | 0.1 | – | – |
| Kuzelite | 0.2 | 0.1 | – | 0.1 | 0.1 | 0.1 |
| Ettringite | 2.3 | 0.4 | 0.3 | 0.2 | 0.3 | 0.4 |
| Hydrogarnet | 0.3 | 0.3 | 0.3 | 0.3 | 0.0 | 0.1 |
| Calcite | 0.8 | 1.8 | 1.8 | 11.5 | 7.4 | 6.3 |
| Vaterite | – | 16.4 | 15.7 | 7.7 | 13.7 | 14.6 |
| Aragonite | – | 0.1 | 1.8 | 0.1 | 0.3 | 0.2 |
| Other | 77.1 | 67.6 | 66.3 | 69.0 | 66.6 | 67.5 |
| Calcite+Vaterite+Aragonite | 0.8 | 18.3 | 19.3 | 19.3 | 21.4 | 21.1 |
| Calcite/(Vaterite+Aragonite) | – | 0.11 | 0.11 | 1.49 | 0.54 | 0.43 |

The main findings of the Rietveld analyses performed on the HVFA and FA+SF pastes were more or less similar:

- Again smaller amounts of β-C₂S (3.2%) and C₄AF (1.1%) were present when uncarbonated. After carbonation, mainly the β-C₂S content decreased. After carbonation at 10% CO₂, the β-C₂S phase almost completely disappeared. This phenomenon was not observed for the HVFA paste. In comparison with the same HVFA paste, Mullite and Quartz_low were present in somewhat smaller amounts. Their contents remained stable at 2.6-3.2% and 6.1-6.9% respectively, regardless the carbonation condition of the sample. A low Hydrogarnet fraction was present which was not affected by carbonation.
- In uncarbonated condition the Portlandite content (5.7%) was again much lower in comparison with OPC paste, because of the occurrence of Portlandite consuming pozzolanic reactions of both the fly ash and the silica fume. Small amounts of Kuzelite and Ettringite were noticed as well. The latter two phases almost completely disappeared after carbonation at any of the studied CO₂ concentrations.
- The total content of carbonation reaction products was similar for all the CO₂ concentrations that were studied and was found to be slightly lower than the corresponding values of the HVFA paste. The major carbonation reaction product was again Vaterite (13.7-14.6%). There was one exception though. The sample carbonated at 10% which was collected 5-7 mm from the exposed surface (C10%a) was characterized by the Vaterite content of only 7.7% while the Calcite content was no less than 11.5%. For the moment this deviating behaviour cannot be explained. Further research on this matter is imperative. The Calcite content seems to depend very much on the applied CO₂ concentration. For low CO₂ concentrations (0.03% and 1%) the Calcite content after carbonation is very small (1.8%). Substantially higher Calcite percentages were recorded after carbonation at 10%. This difference is especially visible when the Calcite/(Vaterite+Aragonite) ratio is considered (0.03-1%: 0.11 versus 10%: 0.43-1.49).

As such, mixture F(1)SF was the paste composition that was most obviously affected by the applied CO₂ concentration during carbonation testing. The OPC and HVFA pastes were barely influenced by this parameter. However, it should be noted that this conclusion is based on the XRD measurements only. There seems to be no link with the estimated amounts of C–S–H carbonation as calculated from the TGA output.

5.6.3.4. Effect on the pore structure

Pore size distributions for the capillary pore range ($0.01 \mu\text{m} < D < 10 \mu\text{m}$) and the corresponding capillary porosities of OPC paste T(0.55), HVFA paste F(1)50 and FA+SF paste F(1)SF are presented in Figure 5.12. The following trends were observed:

- Carbonation at 1% and 10% CO₂ induces a pronounced reduction in capillary porosity of the OPC paste. This reduction was most striking after exposure to the highest CO₂ concentration. When uncarbonated, this porosity amounted to 25.8-26.6%. Carbonation at 1% CO₂ made this porosity decrease to 21.4-24.1%. After carbonation at 10% CO₂, this porosity equaled only 14.5-16.7% anymore. There was also a shift for the major peak in the pore size distribution. When uncarbonated or carbonated at 1% CO₂, this peak corresponded with a pore diameter of around 0.07 μm . Exposure to 10% CO₂ induced a shift of this peak to a pore diameter of only a little more than 0.02 μm , which indicates that the high CO₂ concentration imposed caused serious densification of the pore structure which is normally induced by CH carbonation. The presence of more metastable Vaterite with a higher solubility than Calcite, a phase which was present in much smaller amounts, did not seem to affect this CH carbonation induced densification in a negative way (Section 5.6.3.3). Moreover, it should be noted that the amount of CH carbonation in the pastes carbonated at 1% and 10% CO₂ was rather similar (Section 5.6.3.2). Thus, the increased porosity reduction and pore structure densification of OPC paste with an increasing CO₂ concentration cannot simply be explained by the fact that more CH carbonated. However, the MIP results for OPC paste could explain why a field carbonation coefficient estimated from a carbonation experiment conducted at 10% CO₂ is so much lower than a field carbonation coefficient estimated from a carbonation experiment performed at only 1% CO₂.
- Quite a different trend was observed for the HVFA paste. Carbonation still induces a reduction in capillary porosity. However, this reduction is much less pronounced. While an uncarbonated sample could be characterized by a capillary porosity of 21.9-22.3%, samples carbonated at 1% and 10% CO₂ had capillary porosity of 21.1-21.2% and 18.3-19.6%, respectively. Although smaller, there was still an obvious difference between two CO₂ concentrations considered for accelerated carbonation testing. In contrast with the OPC paste, carbonation caused a slight coarsening of the pore structure. This could be concluded from the peak shift in the pore size distribution from a pore diameter of 0.04 μm in uncarbonated condition (which is lower when compared with the OPC paste) towards a pore diameter of 0.2 μm and 0.3 μm after carbonation at 1% and 10% CO₂. A higher CO₂ concentration seems to have a stimulating effect on the coarsening of the pore structure.

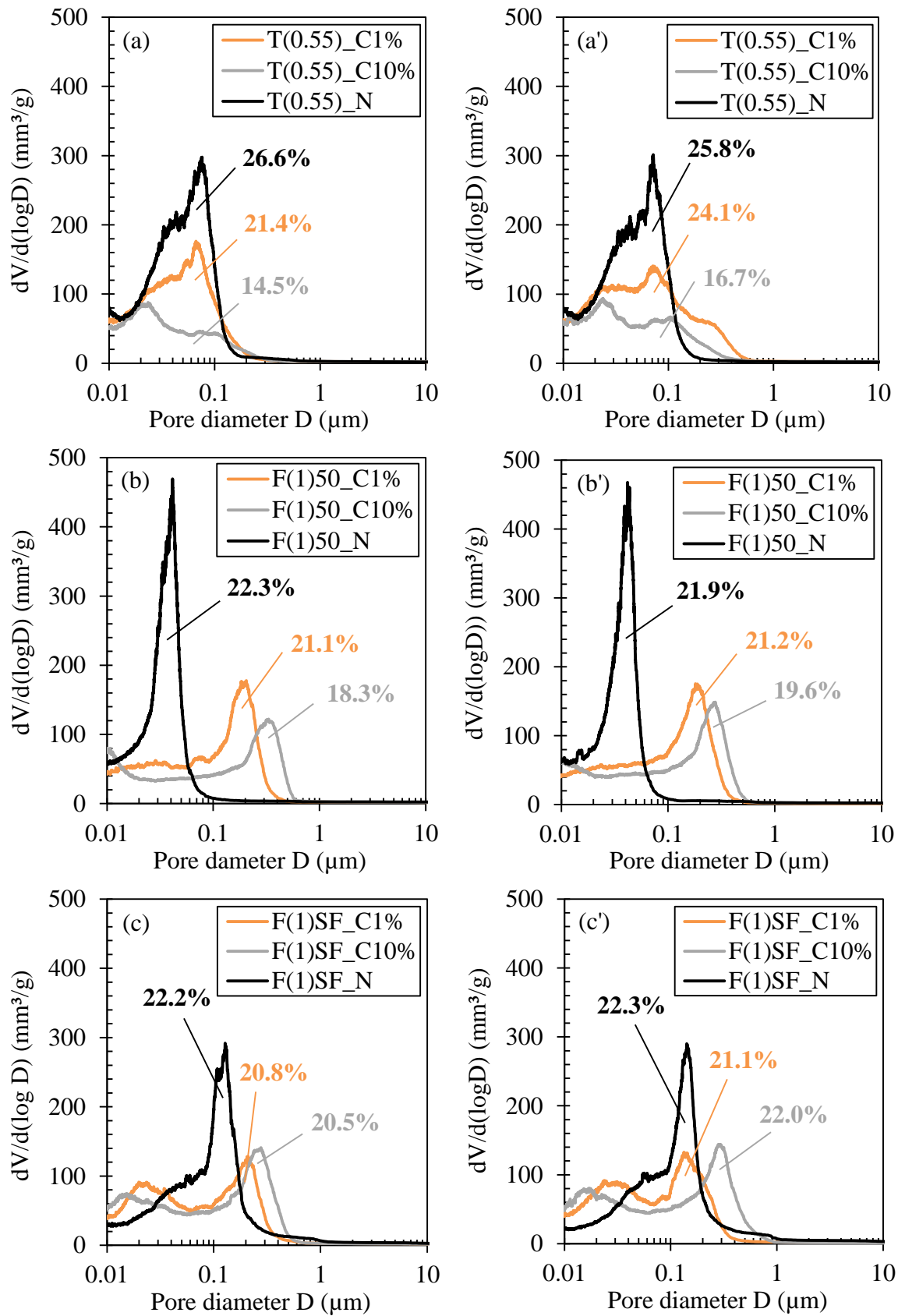


Figure 5.12. Pore size distributions for the capillary pores and capillary porosities (%) of two replicates of each paste studied (T(0.55): a, a'; F(1)50: b, b'; F(1)SF: c, c') in uncarbonated condition (N) and after carbonation at 1% and 10% CO₂.

Since the latter phenomenon is usually attributed to C–S–H carbonation, one would expect a bit more C–S–H carbonation after carbonation at 10% CO₂ instead of at 1% CO₂. This was indeed the case. However, the observed differences seemed rather negligible (Section 5.6.3.2) and thus cannot fully explain an increased coarsening with an increasing CO₂ concentration. In perspective of the estimated field carbonation coefficients from both experiments, the lower values that result from the highly accelerated test (Section 5.6.3.1) can only be supported by its lower capillary porosity and not by the fact that this porosity consisted of larger pores.

- The capillary porosities of the FA+SF paste (22.2-22.3%) in uncarbonated condition were similar to those recorded for the HVFA paste. The main pore diameter (0.15 μm) was considerably different though. This coarser pore structure is rather surprising given the presence of 10% silica fume in paste F(1)SF. Carbonation induced only a slight reduction in capillary porosity. The differences in porosity after carbonation at 1% and 10% CO₂ (20.8-21.1% versus 20.5-22.0%) were not very pronounced. Carbonation induced a coarsening of the pore structure again. Carbonation at 1% and 10% CO₂ induced a shift of the main pore diameter shifted to 0.2 μm and 0.3 μm. Similar shifts were observed for the HVFA paste. The fact that just slightly more C–S–H carbonated at 10% CO₂ (Section 5.6.3.2) seems not enough to explain the shift to 0.3 μm instead of 0.2 μm. An important difference with the HVFA paste is the occurrence of second smaller peak in the pore size distribution for the capillary pore range. These peaks correspond with very small pore diameters, i.e 0.025 μm at 1% CO₂ and 0.015 μm at 10% CO₂. Their occurrence implicates that there was to some extent a densification of the pore structure as well. Now, a similar capillary porosity consisting mainly of larger pores (0.3 μm) and only to some extent of very fine pores (0.015 μm) cannot explain the lower field carbonation rates estimated from a carbonation experiment at 10% CO₂ as opposed to a field carbonation coefficient measured after exposure to just 1% CO₂.

5.6.3.5. Discussion

In fact, neither of the applied investigation techniques (TGA, XRD and MIP) applied on uncarbonated and carbonated samples could reveal the actual cause of the underestimation of the field carbonation coefficients when based on a highly accelerated carbonation test involving exposure to 10% CO₂. True, the observed porosity reduction and strong densification of the pore structure of OPC paste after carbonation at 10% could explain this to some extent, yet not completely. For the HVFA and FA+SF pastes the explanation must be sought elsewhere since these binder systems behaved in a totally different way. Probably, the available conversion formula to go from an accelerated to a field carbonation coefficient (Equation 5-5) is simply not entirely correct. Further research on its improvement is therefore imperative. One of the theories that most certainly must be verified further on is the excessive production of water during carbonation at 10% CO₂ which induces pore blocking, cf. Saetta and Vitaliani (2004).

5.7. Conclusions

- In conclusion, accelerated carbonation testing at 10% CO₂ revealed that HVFA concrete is more susceptible to carbonation than the applicable OPC or k-value conforming FA reference. In case of continuous exposure (cf. exposure class XC3) after 28 days optimal curing, the highest estimations for the corresponding carbonation coefficients in the field amounted to 2.2 mm/ $\sqrt{\text{years}}$. In case of exposure in combination with wet/dry cycles (cf. exposure class XC4), this field carbonation coefficient was reduced with more than half.
- Non-air entrained FA+SF concrete was found to be slightly more resistant to carbonation than HVFA concrete as field carbonation coefficients equaled only 1.4 mm/ $\sqrt{\text{years}}$.
- Especially for HVFA concrete, colorimetric assessment of carbonation usually slightly underestimates the actual carbonation depth which can be observed microscopically under crossed polars. However, this underestimation can be considered as negligible.
- Suboptimal curing in the first 28 days after casting has a negative impact on the carbonation resistance of HVFA and FA+SF concrete in a XC3 environment. It makes their field carbonation coefficients increase to 3.0 and 1.7 mm/ $\sqrt{\text{years}}$, respectively.
- When the field carbonation coefficients are estimated from an accelerated carbonation experiment at 1% CO₂, these coefficients exceed the ones obtained from a carbonation test at 10% CO₂ by far after 28 days of optimal curing. This was the case for OPC, HVFA and FA+SF concrete. As such, the highest field carbonation coefficients recorded for each concrete type in exposure class XC3 amounted to 1.8, 4.0 and 2.3 mm/ $\sqrt{\text{years}}$, respectively. The underestimation inherent to carbonation testing at 10% CO₂ cannot simply be explained by an important reduction in porosity and densification of the pore structure as assessed by means of MIP. On the other hand, the results of the conducted TGA and XRD analyses indicate that the carbonation mechanisms during exposure to 1% and 10% CO₂ are similar. More important differences exist between natural carbonation at 0.03% CO₂ and slightly accelerated carbonation at 1% CO₂. More research is needed to come up with a more accurate formula that adequately converts an accelerated into a field carbonation coefficient.
- The sometimes important changes in field carbonation coefficients depending on the curing and accelerated carbonation test conditions were taken into consideration when performing service life prediction based on the output of these tests (Chapter 8).

Resistance to chloride ingress

6.1. Characterization of the deterioration mechanism and the environment

6.1.1. Literature review on the deterioration mechanism

6.1.1.1. Chloride-induced corrosion initiation and propagation

Besides carbonation, chloride ingress can also induce corrosion of the reinforcing steel in concrete. Just like for carbonation-induced corrosion a distinction can be made between the corrosion initiation and propagation period as suggested by Tuutti (1982) and Browne (1980). In this case the corrosion initiation phase corresponds with the time required for a critical chloride concentration to reach the location of the rebars. Once present in this concentration, the chlorides tend to locally destroy the passivation layer which naturally forms on the steel surface in presence of the highly alkaline environment of the surrounding concrete (pH 9-14). This event marks the end of corrosion initiation and the start of corrosion propagation. As already mentioned in Section 5.1.1, the actual corrosion damage occurs during the second stage. Because of the very high corrosion rates usually observed in marine environments and the difficulty of modelling the corrosion process and its effects, the service life of reinforced concrete in marine environments is often said to correspond with just the corrosion initiation period [Costa and Appleton (1999b)]. Since the chloride-induced corrosion propagation period is usually very short in comparison with the time to steel depassivation, this definition of service life is not seen as a problem [DuraCrete (2000)]. According to Sandberg et al. (1998) the duration of the initiation phase mainly depends on (i) the penetration rate of chloride ions in concrete and (ii) the already mentioned critical concentration needed for depassivation of the reinforcing steel. Within this chapter only the first property has been characterized for the proposed concrete compositions. The second property, i.e. the critical chloride concentration, has been studied more in detail in Chapter 9. A good overview of the influencing factors regarding concrete's resistance to chloride ingress and the test methods available to quantify this resistance has already been given in Yuan (2009) and Gruyaert (2011). In this section, only the factors relevant for the tested concrete compositions and the applied test methods were summarized. Attention was paid to two different forms of chloride transport in hardened concrete, i.e. diffusion and electrical migration.

6.1.1.2. Chloride diffusion

The transport of chloride ions in fully saturated hardened concrete is governed by diffusion. This transport mechanism is a consequence of nature's desire to cancel out concentration differences. When comparing the rates of diffusion through the solid portion of this matrix and the pore solution, the latter obviously has the upperhand by far. As a consequence, whenever a pathway for chloride ions is being blocked by solid phase, further transport of these chloride ions will occur around this phase. Thus, the rate of chloride diffusion through concrete is not only determined by the diffusion coefficient through the pore solution but also by the physical characteristics of the concrete's capillary pore structure [Yuan (2009)]. A distinction is usually made between steady state and non-steady state diffusion. In case of the former, there is no change in chloride concentration with time, while in case of the latter there is. These two different conditions were described by means of Fick's first and second law of diffusion. More mathematical background on both laws can be found in Yuan (2009). Evidently, it is the non-steady state condition that is most often encountered in practice. The chloride profiling method described in NT Build 443 (1995) enables the calculation of a non-steady state diffusion coefficient (see Section 6.4.2).

Depending on the extraction procedure this coefficient relates to either the acid-soluble or the water-soluble chlorides. Literature survey shows that the available procedures for determining each type of chloride can vary [Chaussadent and Arliguie (1999), Pavlik (2000), Andrade et al. (2000), Castellote and Andrade (2001a, 2001b), RILEM TC 178-TMC (2002a, 2002b), Tang and Nilsson (2001)]. The acid-soluble chloride content is said to correspond with the concrete's total chloride content. When the relation between the water-soluble and the actual free chloride content measured in the pore solution is also known, the bound chloride content can be determined by subtracting the estimated free chloride content from the total chloride content. The bound chloride content is a measure for the concrete's capacity to bind chlorides to its hydration products.

In perspective of concrete's resistance to chloride-induced corrosion, a high chloride binding capacity is desirable, and this for several reasons: (i) it reduces the total amount of free chlorides present in the vicinity of the reinforcing steel that can initiate corrosion, (ii) it removes chloride from the diffusion flux and thus slows down chloride ingress and (iii) it results in the formation of Friedel's salt ($3\text{CaO}\cdot\text{Al}_2\text{O}_3\cdot\text{CaCl}_2\cdot 10\text{H}_2\text{O}$) and its analogue that reduces the porosity of the microstructure [Gruyaert (2011), Glasser et al. (2008)]. Apart from this chemical binding (reaction between chloride ions and the C_3A or C_4AF), there is also a phenomenon called physical binding. It comprises the adsorption of chloride ions to the surface of the C-S-H [Yuan (2009)]. Given the fact that bound chlorides cannot initiate corrosion [Kayyali and Haque (1995), Suryavanshi et al. (1998)], a mere determination of the concrete's free chloride content seems sufficient. However, according to Gruyaert (2011) and Yuan (2009) several other researchers, e.g. Glass and Buenfeld (1997), Glass and Buenfeld (2000), Reddy et al. (2002), claim that bound chlorides can be released again as free chlorides due to changes in temperature, pore solution chemistry or carbonation. Thus, it seems safer to consider not only the free but also the total chloride content. In this Chapter both the free chloride content derived from water-soluble chloride content and the total chloride content were considered.

6.1.1.3 Chloride migration

The second chloride transport mechanism requires the presence of an external electrical field as driving force. Several accelerated chloride test methods, e.g. NT Build 492 (1999), rely on this principle. By imposing an electrical field, the chlorides in the exposure solution will move rapidly towards a positive electrode. As such, the penetration of chlorides in concrete goes much faster than when diffusion is the only driving force. As a consequence, the process of chloride binding cannot be completed [Gruyaert (2011)]. For chloride concentrations in the sample lower than 0.14% there seems to be no binding at all, while for higher chloride concentrations the bound chloride content is lower than during a natural chloride diffusion test [Castellote et al. (1999)]. According to Ollivier et al. (1997), as cited by Yuan (2009), no difference in binding capacity after a chloride migration test is seen when the applied voltage ranges between 2-30V. However, it could be that the effect on the binding behaviour already occurred for voltages below 2V. With respect to the applied voltage during a migration test, it should also be mentioned that due to a potential drop between the electrodes and the sample surface, the real potential across the specimen is 1.5-2V lower than the potential imposed between the two electrodes during the test [McGrath (1996)]. The applied voltage needs to be corrected for this when the aim is to calculate a chloride migration coefficient based on all relevant test data. For the mathematical expression describing electrical migration of a specific ion and its derivation we refer to Yuan (2009) and Andrade (1993). The solution of the Nernst-Planck equation with omission of the advection term for non-steady state migration conditions by Tang and Nilsson (1992) has been summarized in Yuan (2009). The end result is a practical equation for calculating a non-steady state chloride migration coefficient of concrete cf. NT Build 492 (1999). More details regarding this equation can be found in Section 6.4.1.

6.1.1.4. Influencing factors related to the tested concrete compositions

Cement composition and content: The chemical binding capacity of OPC is governed by the presence of the alumina-bearing phases C_3A and C_4AF . The more Al_2O_3 and Fe_2O_3 the cement contains, the more of these phases are formed and the more chlorides can chemically bind with them. On the other hand, the extent of physical binding of chloride ions to the C-S-H surface highly depends on the C_3S and C_2S content. The more of these cement minerals present, the more physical binding occurs. The SO_3 content of the cement is known to have a negative impact on the chemical binding capacity because they (preferably) react with C_3A and C_4AF to form Ettringite or monosulfate [Yuan (2009)]. Since in all tested concrete compositions the same cement was applied, a different binding behaviour can only be explained by the fact that in the compositions with high cement replacement levels less of this cement was present. However, the effect of the applied supplementary cementitious materials (fly ash (and silica fume)) must be considered as well.

Supplementary cementitious materials content: According to the majority of literature reviewed by Yuan (2009) the chloride binding capacity increases with increasing fly ash content. Wiens and Schiessl (1997) attribute this behaviour to the alumina content of the fly ash which results in the formation of more Friedel's salt. On the other hand, the presence of silica fume decreases the chloride binding capacity. Literature review by Yuan (2009)

indicates that partial replacement of cement with silica fume may induce three important changes: (i) increase of C–S–H with a lower C/S ratio, (ii) reduction of the pH and (iii) a dilution effect of the C₃A. More C–S–H normally is in favor of more binding. However, when characterized by a low C/S ratio this is not necessarily the case. A reduction in the pH value lowers the amount of Friedel's salt formed and the dilution effect of the C₃A may also have a negative effect on the binding. With respect to the effect of the pH value or the alkalinity of the concrete it must be said that Gruyaert (2011) comes to quite a different conclusion based on several literature findings: the higher the pH, the lower the bound chloride content is.

W/B ratio: Delagrave et al. (1997) and Angst et al. (2009) reported that lowering the W/B ratio normally causes a decrease in chloride binding.

Porosity: Finally, it must be said that the resistance to chloride ingress does not only depend on the concrete's capacity for chloride binding. As already mentioned in Section 6.1.1.2 diffusion of chlorides also depends on the physical characteristics of the capillary pore structure. It is quite generally known that applying a low W/B ratio results in less porous concrete. The same goes for adding silica fume and fly ash, although in case of the latter practice the densification of the pore structure will only be seen at later age. A less porous concrete will be less susceptible to chloride ingress.

6.1.2. Characterization of the concrete environment

Steel reinforced concrete structures assumed to be located in marine environments either belong to exposure class XS1, XS2 or XS3 cf. NBN EN 206-1 (2000) depending on the specific environmental conditions of the concrete:

- XS1: coastal concrete exposed to airborne salt but not in direct contact with sea water
- XS2: concrete permanently submerged in sea water
- XS3: concrete located in the tidal, splash or spray zone

Obviously, XS3 is the most critical exposure class. There is direct contact with chlorides that can induce depassivation of the embedded reinforcing steel once having reached their location. There is also alternating direct contact with both water and oxygen which is a necessary condition for depassivated steel to corrode. However, most of the commonly used test methods to assess the resistance of a certain concrete type to merely chloride ingress – the corrosion propagation period is in most cases not considered – rely on continuous contact with high concentration chloride or simulated sea water solutions because this exposure condition is better defined [Sandberg et al. (1998)]. In other words, the exposure conditions of these experiments actually resemble more exposure class XS2 than XS3. For instance, to evaluate the equivalent performance of concrete with type II additions in terms of resistance to diffusion of chlorides the Belgian standard NBN B15-100 (2008) specifies that this should be assessed experimentally by performing comparative chloride diffusion or migration tests. During chloride diffusion tests conforming to NT Build 443 (1995) concrete cylinders are permanently immersed in 165 g/l aqueous NaCl solutions for at least 35 days, while chloride migration tests conforming to NT Build 492 (1999) usually require that the test cylinders are put continuously in contact with a 10% aqueous NaCl solution for usually 24 hours. Equivalent performance exists if the applicable criterion of acceptance is met (Equation 6-1).

$$D_{\text{cl, concrete to be tested}} \leq 1.4 \times D_{\text{cl, reference concrete}} \quad (6-1)$$

With $D_{\text{cl, concrete to be tested}}$ and $D_{\text{cl, reference concrete}}$ the average chloride diffusion (or migration) coefficients of the tested concrete composition with type II additions and the reference concrete. The latter concrete composition is traditionally an OPC concrete that can be used in the applicable exposure class. The OPC reference concrete type considered in this part of the research is mixture T(0.45) which is seen as the appropriate reference for both exposure class XS2 and XS3. Alternatively, the k-value conforming FA concrete compositions F(1)15_{XS2} and F(2)15_{XS2} could also be seen as suitable reference concretes for these two exposure classes.

The above mentioned references may indeed have a deemed-to-satisfy durability performance in exposure classes XS2 and XS3. However, the issue remains that the exposure conditions during chloride diffusion or migration experiments are not in agreement with the intermittent wetting and drying inherent to the more critical exposure class XS3. The specific environmental conditions of the latter exposure class could be taken into account by applying the necessary correction factors to the experimental output of the chloride diffusion or migration tests. Service life prediction models for chloride-induced corrosion of concrete situated in very specific environments are often based on this approach. In theory, it would thus be possible to focus on exposure class XS3 in this research. However, as the representativeness of all the correction factors proposed in the prediction models is often far from certain and their verification would require a full-scale experimental program of in situ testing, it was decided to focus on exposure class XS2.

With respect to exposure class XS2, the main influencing parameter is the chloride concentration of the sea water. Audenaert (2006) summarized the commonly observed marine chloride concentrations. According to CUR report 100 (1981) ocean water consists of 19.8 grams of chlorides per liter. Within proximity of the coast line, sea water is expected to be more diluted which reduces its salinity. Sea water from the North Sea is characterized by chloride concentrations that range between 18.5 up to 24.9 g/l. To test the potential chloride penetration resistance of concrete in this sea water under laboratory conditions, one basically has three options. The concrete composition under investigation can be exposed to actual sea water or a simulated sea water solution that has the very same ion proportioning as actual sea water or a solution that merely has the same chloride concentration as actual seawater with use of only one salt, e.g. NaCl. For this research, the latter option was chosen. To obtain a solution with a chloride concentration of 19.8 g/l while using NaCl as only chloride source, a ± 33 g/l aqueous NaCl solution needs to be prepared. Note that the chloride concentration of this solution is very similar to the one of the artificial seawater solution proposed in CUR recommendation 48 (1999).

Apart from the chloride concentration of the sea water, also its temperature is of relevance in perspective of the concrete's resistance to chloride ingress. Within service life prediction models such as the one of *fib* Bulletin 34 (2006), the applied chloride migration/diffusion coefficients usually recorded at around 20 °C need to be corrected in order to be applicable for the much lower temperatures of the sea water in practice (± 10 °C).

6.2. Research methodology

The overall experimental program consisted of a vast series of non-steady state chloride migration and diffusion tests for the concrete compositions under investigation at three different testing ages. As such, the program served a twofold research purpose. First of all, it enabled an equivalent performance assessment for the proposed HVFA and FA+SF concrete in comparison with the applicable OPC and k-value conforming FA references. Attention was being paid to possible different outcomes of this evaluation depending on the underlying transport mechanisms (migration versus natural or accelerated diffusion), chloride contents (free versus total chloride content) and measuring techniques (potentiometric titration versus rapid chloride test).

Secondly, since all tests were performed at different testing ages, the evolution of the chloride migration/diffusion coefficients with time could be assessed. It provides relevant information with respect to the concrete's ageing behaviour which can vary considerably with the concrete type. From these data ageing exponents for each studied concrete composition were calculated which were implemented in the prediction models for comparative mixture specific service life estimations (Chapter 9).

Finally, the effect of cracking on the resistance to chloride ingress was evaluated on two concrete representative mortars, i.e. MBE T(0.45) and MBE SF10W35 with fly ash F(2) (Table 4.14). Specimens with artificially induced cracks of varying width (0.1, 0.2 and 0.3 mm) were subjected to an alternative non-steady state chloride migration test for a short time period. This was done to see whether there is a crack width below which the material could be treated as uncracked, possibly due to autogenous healing phenomena. By designing reinforced concrete structures in accordance with this stricter crack width criterion, the available prediction models for uncracked concrete could be used directly (Chapter 9).

6.3. Curing, sample preparation and crack verification

6.3.1. Uncracked concrete

The chloride resistance was assessed for the following concrete compositions: T(0.45), F(1)15_{XS2}, F(2)15_{XS2}, F(1)50, F(2)50, F(1)SF and F(2)SF. In total, 27 cubes with a 150 mm side were cast per concrete mix. After casting, the cubes were kept at a constant temperature and relative humidity (RH) of 20 °C and 95%, respectively. Demoulding took place the next day whereupon the specimens of OPC, FA and HVFA concrete were stored again under the same conditions until the age of 21, 84 or 357 days. In case of the FA+SF concrete the three different preconditioning periods were 21, 84 and 266 days. Then, cores with a diameter of 100 mm were drilled out of each cube. Nine of them were used for the migration tests and the accelerated and more realistic chloride diffusion tests at the age of 28 days, another nine were subjected to the same tests after 91 days, while the last nine provided the specimens for the corresponding tests at the age of 273 or 364 days. The outermost 10 mm, containing the cast surface, was cut from the two ends of each core in correspondence with NT Build 443 (1995). Starting from these saw cuts, two cylindrical specimens with a thickness of 50 mm were taken from each core. As such, six cylindrical samples were available for each test at each testing age. For the chloride migration tests all six of them were used, while only three for the accelerated and 'natural' chloride diffusion tests.

In addition, the effect of suboptimal curing on the 28-day chloride migration coefficient was evaluated on small batches (40 l) of concrete mixtures F(1)50 and F(1)SF. The specimens for these tests were optimally cured for only 7 days. From then on they were stored in a climate room at 20°C and 60% RH for 21 days.

6.3.2. MBE mortar with an artificial crack

15 cylindrical specimens (diameter: 110 mm, height: 53 mm) were made in PVC tube moulds for mixtures MBE T(0.45) and MBE SF10W35 with fly ash F(2) (Table 4.14): 3 samples without crack plus 3×4 samples containing an artificial crack as a result of putting thin metal plates with a nominal thickness of 0.1, 0.2 and 0.3 mm at a depth of 15 mm in the cylindrical moulds just before casting. Figure 6.1 shows a schematic of the mould setup with the metal plate fixed at the desired crack depth cf. Mu (2012).

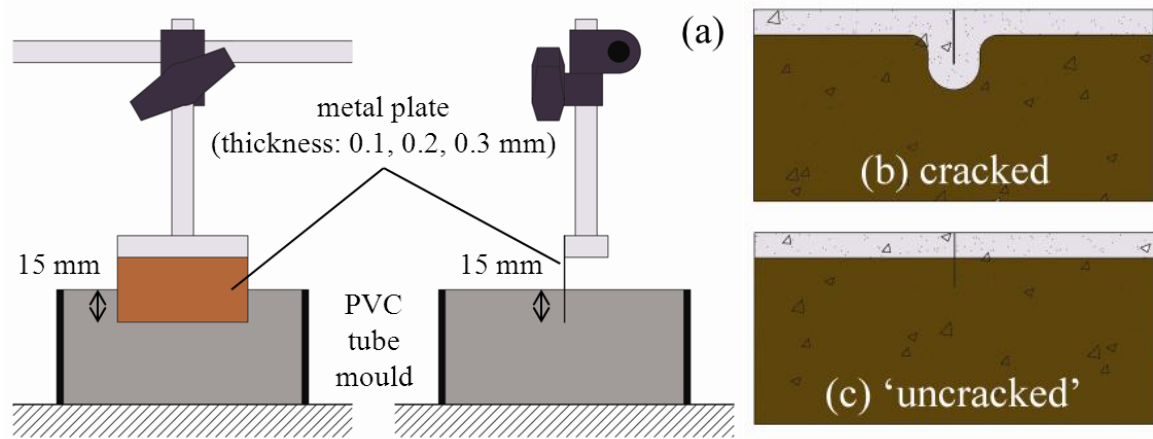


Figure 6.1. Mould setup for creating artificial cracks in mortar samples (a), expected AgNO_3 colour change boundary in a cracked (b) and a seemingly uncracked (c) sample section.

Note that artificial cracks created by means of thin metal plates are different from more natural cracks induced by mechanical loading. Both techniques are in use and have their advantages and disadvantages. By means of thin metal plates it is indeed not possible to reproduce a concrete crack which is realistic in all its properties. However, it is seen as a very convenient way to study the effect of one crack property in particular, being the crack width (which is the main crack property considered in crack controlled structure design). The reproducibility of cracks created as such is high. On the other hand, displacement steered mechanical loading to create more natural cracks does not always guarantee the same predefined crack width. Moreover, with the latter method it is difficult to ensure that the crack does not go all the way through the specimen. This condition is required to be able to conduct the chloride migration test. With thin metal plates fixed at a certain height in the sample mould the crack depth is rather easy to control. Therefore, we adopted the thin metal plate technique.

Nevertheless, one should remain aware of the differences between these artificial cracks and naturally induced cracks. The walls of the voids created with thin metal plates should be considered as cast surfaces. These surfaces are subject to the so-called wall effect which

means that the more fine (usually cementitious) materials will be present in the vicinity of the crack walls. Its unhydrated fraction can still react later on and initiate autogenous healing. However, this may be the only effect that favors this mechanism for the artificial cracks. It is also unknown if the fraction of unhydrated materials near the crack walls is sufficient to induce full closure of the crack. For naturally induced cracks on the other hand, there can be several beneficial effects. There, the crack width can seriously vary over the length of a crack. The crack tortuosity and crack wall roughness will evidently be higher [Akhavan et al. (2012)]. Moreover, cracks will contain more concrete particles broken from the surface due to cracking [Edvardsen (1999)]. All these conditions contribute to a partial blocking of the crack followed by the autogenous healing phenomenon. These favorable conditions are not present in the artificial cracks. Given these differences, a more detailed comparison between artificially and naturally cracked specimens in relation to their autogenous healing capacity would certainly be relevant.

After casting, the specimens were kept at a constant temperature and relative humidity (RH) of 20 °C and 95%, respectively. The metal plates were carefully removed from the samples after approximately 12 h whereupon the cylinders were demoulded. From then on, they were stored again under the same conditions until the age of 28 days.

6.3.3. Microscopic verification of the obtained crack widths

After 28 days, the obtained crack widths were measured after mechanical flattening of the cylinders' troweled surfaces and on a saw cut perpendicular to the crack of the fourth cylinder of each cracked series. The latter samples were only used for the evaluation of the cross-sectional crack width and not exposed to chlorides. All crack width measurements were done on micrographs taken with a Leica S8 APO stereo microscope (SM) (magnification: 20×) while using the LAS 3.7 software.

After the cross-sectional crack width evaluation with the stereo microscope, the cracked area of the non-exposed MBE mortar SF10W35 with the 0.1 mm wide crack was also subjected to scanning electron microscope (SEM) analysis to study the partial closing of the crack more in detail. By then, the sample was 196 days old. Three 20×20×10 mm³ prisms containing a cross-section of the crack, were cut from one cylinder halve and then put in an ultrasonic bath with isopropanol to remove all loose particles inside the crack. Afterwards, the samples were vacuum dried for one week and gold coated by means of a Baltec SCD030 Sputter Coater before being examined in a FEI QUANTA 200F SEM at an accelerating voltage of 20 kV. Secondary electron imaging was used for electron micrography.

Another three uncoated samples of mixture SF10W35 were analyzed with a Jeol JSM-7600F Field Emission Scanning Electron Microscope (FESEM) equipped with AZtecEnergy software [Oxford Instruments (2014)] for EDX mapping of the crack and its surrounding area in cross-section. This method allowed to see whether the chemical composition of the partially closed cracked differed substantially from the composition of the plain mortar matrix. EDX mapping was done for the following elements: Si, Ca, Al, and Fe.

6.4. Experimental assessment of concrete's resistance to chloride ingress

6.4.1. The chloride migration test cf. NT Build 492

The resistance to chloride penetration was evaluated experimentally using the rapid chloride migration test as described in NT Build 492 (1999). This method enables the calculation of a non-steady state chloride migration coefficient. The following test procedure was adopted. First, the cylindrical specimens were vacuum saturated in a 4 g/l $\text{Ca}(\text{OH})_2$ solution. After 18 ± 2 hours of immersion in this solution, the specimens were fixed inside silicon rubber sleeves with a 0.3 N NaOH (anolyte) solution on top. The bottom surface of the samples in the sleeves was brought in contact with a 10% NaCl solution (catholyte). Then, an external electrical potential was applied axially across each cylinder, which forces the chloride ions to migrate into the specimens. After a certain test duration (usually 24 hours) the specimens were removed from the sleeves and split axially, whereupon a 0.1 M silver nitrate solution was sprayed onto the freshly split sections. When the white silver chloride precipitation had become clearly visible, the penetration depth was measured from the center to both edges at intervals of 10 mm. From the chloride ingress obtained, a non-steady state migration coefficient was calculated using the simplified formula of NT Build 492, using a fixed chloride concentration (= 0.07 N) at the colour change boundary (Equation 6-2):

$$D_{\text{nssm}} = \frac{0.0239 \cdot (273 + T) \cdot L}{(U - 2) \cdot t} \left(x_d - 0.0238 \cdot \sqrt{\frac{(273 + T) \cdot L \cdot x_d}{U - 2}} \right) \quad (6-2)$$

where D_{nssm} , U , T , L , x_d and t represent the non-steady state migration coefficient ($\times 10^{-12}$ m^2/s), the absolute value of the applied voltage (V), the average value of the initial and final temperatures in the anolyte solution ($^{\circ}\text{C}$), the thickness of the specimen (mm), the average value of the penetration depths (mm) and the test duration (h), respectively.

The cracked MBE mortar specimens went through the same test procedure except for the fact that the external electrical potential was imposed for only 4 h. This is much less than the normal 24 h test duration. The short test period was chosen to make sure that the overall chloride ingress would not be more than 13 mm, the average depth of the artificially induced cracks. Obviously, in case the crack is too wide, the chloride penetration close to the crack would be higher than 13 mm (Figure 6.1b). The 10% NaCl solution would almost immediately reach the deepest point of the crack and chloride migration would start from there on. For each of the specimens containing a 0.1, 0.2 or 0.3 mm crack, it was evaluated whether the chloride penetration around the crack extended much beyond the deepest point of the crack. If not, the specimen could be considered as uncracked (Figure 6.1c) and the D_{nssm} value measured for the uncracked specimen would be valid. As such, service life prediction could be done using D_{nssm} values measured on uncracked concrete. However, it also means that a concrete structure needs to be designed according to the stricter crack width criterion.

6.4.2. The accelerated chloride diffusion test cf. NT Build 443

Per testing age, three cylinders ($n = 3$), were preconditioned as prescribed in NT Build 443 (1995). Firstly, they were immersed in a saturated $\text{Ca}(\text{OH})_2$ solution until constant mass,

whereafter they were treated with an epoxy coating on all sides except the surface to be exposed. After the epoxy layer had hardened, the samples were stored again in this $\text{Ca}(\text{OH})_2$ solution until constant mass. Then, these cylinders were immersed in an aqueous NaCl solution with a concentration of 165 g/l for 9 weeks. During exposure, the temperature of the NaCl solutions was kept constant at around 20 °C.

Immediately after removal from the aqueous NaCl solutions, 10 concrete powders were collected from the cylinders by grinding material in 2 mm layers parallel to the exposed surface using a Metabo grinding apparatus (Figure 6.2a). By doing so, the average chloride content could be determined at a depth of 1, 3, 5, 7, 9, 11, 13, 15, 17 and 19 mm. For the FA+SF concrete the actual thicknesses of the preset 2 mm layers were checked by measuring the grinding depth with a dial gauge before and after grinding of each layer (Figure 6.2b).

The determination of the total chloride concentration consisted of an acid-soluble extraction in a nitric acid solution followed by a potentiometric titration against silver nitrate cf. Mu (2012). Therefore, it is identified as the acid-soluble chloride concentration (AC (titr.)). First, the powders (passing through a 160 μm sieve) were dried at 80 °C until constant mass. After cooling down to room temperature, 2 g of each powder was weighed in a 150 ml glass beaker. 5 ml of nitric acid (concentration: 0.3 mol/l) and 40 ml deionized water were added. The obtained solutions were stirred carefully and then heated onto a hot plate until they just started to boil. After cooling them down, they were filtered and diluted with water in a 100 ml volumetric flask. From these 100 ml solutions, 10 ml was pipetted for determination of the chloride concentration per powder using a Metrohm MET 702 automatic titration apparatus (Figure 6.2c) with 0.01 mol/l silver nitrate as titration solution. The test solution consisted of the pipetted 10 ml of extract, 10 ml of deionized water and 40 ml of nitric acid (0.03 mol/l).



Figure 6.2. Test setups for profile grinding (a) and grinding depth measurements (b) and the Metrohm MET 702 automatic titration apparatus (c).

The water-soluble chloride concentration (WC (titr. 24h)) as a function of the penetration depth was measured as well. Therefore, 50 ml of deionized water was added to 2.5 g of each powder in a plastic beaker. The resulting solutions were stirred firmly whereafter the beakers were sealed with a lid. After approximately 24 hours, practically all the powders had sank to the bottom of the beakers and 5 ml of solution could easily be extracted from the solution's upper layer with a pipet. This 5 ml of extract was added to 15 ml of deionized water and 40 ml of nitric acid (0.03 mol/l). The solutions obtained were then ready for testing in the

automatic titration apparatus. The suggested procedure was in agreement with Mu (2012). By applying a factor of 0.8 to the measured water soluble chloride contents an estimation of the concrete's free chloride contents as a function of the penetration depth could be obtained. This factor was proposed by Yuan (2009). For further clarification, the link between the different chloride contents measured using the applied potentiometric titration procedures and the total, the bound and free chlorides has been established in Table 6.1.

Table 6.1. Link between the measured acid- and water-soluble chloride concentration (AC (titr.) and WC (titr. 24h)) and the total, bound and free chlorides.

| Measured chloride concentration | Chloride type |
|--|----------------------------------|
| Acid-soluble chloride concentration AC (titr.) | Total (= bound + free chlorides) |
| $0.8^* \times$ Water-soluble chloride concentration WC (titr. 24h) | Free chlorides |

* Correction factor proposed by Yuan (2009)

From the resulting chloride profiles per sample, the surface concentration $C_{s(acce)}$ (m%/binder) and the effective chloride transport coefficient $D_{e(acce)}$ (m²/s) were estimated by fitting equation 6-3 to the measured chloride contents using non-linear regression analysis with omission of the first point of the profile (0-2 mm) if it deviated substantially from the overall shape of the profile.

$$C(x, t) = C_s - (C_s - C_0) \cdot \operatorname{erf}\left(\frac{x}{2 \cdot \sqrt{D_e \cdot t}}\right) \quad (6-3)$$

where $C(x, t)$ is the chloride concentration at depth x and time t , C_0 is the initial chloride concentration and $\operatorname{erf}(\cdot)$ is the error function. Per three samples of each series, the mean values of the diffusion coefficients and surface concentrations, as well as their standard deviations on the individual values were calculated.

In the course of this research it was necessary to evaluate the value of the free chloride surface concentration C_s not only in m%/binder but also in mol/l. This was done by using the conversion formula (Equation 6-4) proposed by Gruyaert (2011) and Maes et al. (2013).

$$C_s\left(\frac{\text{mol}}{\text{l}}\right) = \frac{\rho_{\text{dr}} \cdot C_s(\%)}{MW_{\text{Cl}} \cdot \varphi} \quad (6-4)$$

With ρ_{dr} , the dry density of the concrete in kg/m³, $C_s(\%)$, the chloride surface concentration relative to the mass of the concrete and φ , the permeable porosity in Vol% as calculated from a vacuum saturation experiment in combination with oven drying at 105°C and MW_{Cl} , the molecular weight of Cl. The experimental determination of this porosity has been described more in detail in Section 7.6.2.

6.4.3. A 'Natural' chloride diffusion test

The cylinders used for the 'natural' chloride diffusion test – also three per testing age – were not preconditioned with $\text{Ca}(\text{OH})_2$ nor with water. After applying the epoxy coating, they were stored in an aqueous 33 g/l NaCl solution for 18 weeks (realistic diffusion test). The latter concentration corresponds with the normal Cl^- concentration in sea water according to CUR report 100 (1981). Apart from the omission of the vacuum saturation in a saturated $\text{Ca}(\text{OH})_2$ solution and the subsequent longer immersion period of the samples in a low concentration NaCl solution, the test procedure prior to chloride profiling was very similar to the one applied during the accelerated chloride diffusion test. The main experimental output of the 'natural' tests was again an effective chloride diffusion coefficient $D_{e(\text{nat})}$ (m^2/s) and a surface concentration $C_{s(\text{nat})}$ (m%/binder). Again both the total and the free chloride contents were determined.

6.4.4. Potentiometric titration versus rapid chloride test

Apart from the potentiometric titration technique there are also other methods to determine the total or free chloride content of a collected concrete powder, e.g. the rapid chloride test developed by Germann Instruments. To evaluate the effect of the applied test method, a comparison was made between the chloride concentrations and profiles measured by means of potentiometric titration and the rapid chloride test for one FA+SF concrete, i.e. mixture F(1)SF optimally cured for 273 days.

The latter test actually consists of two extraction methods. First of all, there is the Rapid Chloride Test (RCT) method that results in the determination of the acid soluble chloride content. Therefore, 1.5 g of each powder needs to be dissolved in commercially available RCT vials of Germann Instruments containing 9 ml of extraction liquid. After being shaken for 5 minutes, the vials were left to stand for 24 hours before the actual measurement of the acid-soluble chloride concentration AC (RCT 24h).

Secondly, there is the Rapid Chloride Test Water (RCTW) method to measure a water soluble chloride concentration. For its determination again 1.5 g of powder needed to be dissolved in the commercially available RCTW vials. After shaking the vials for 5 minutes, their contents were filtered into another type of RCTW vials containing 1 ml buffer solution. Once being shaken again, the actual measurement could be conducted. As the measurement of this water-soluble chloride measurement usually takes place after maximum a half hour, it has been identified further on as WC (RCT 1/2h).

After the above mentioned preparatory steps a calibrated electrode was submerged into the applicable vials with solution and the voltage readings on the display of the apparatus were recorded. These voltages were then converted into an acid- or water-soluble chloride content in percentage by concrete weight by means of the calibration curve which was determined prior to the test. This curve could be obtained by submerging the electrode in a set of calibration liquids with known chloride concentration (Figure 6.3). In the end, the values obtained were multiplied with the density ($2391 \text{ kg}/\text{m}^3$) and divided by the binder content ($340 \text{ kg}/\text{m}^3$) of the FA+SF concrete composition under investigation.

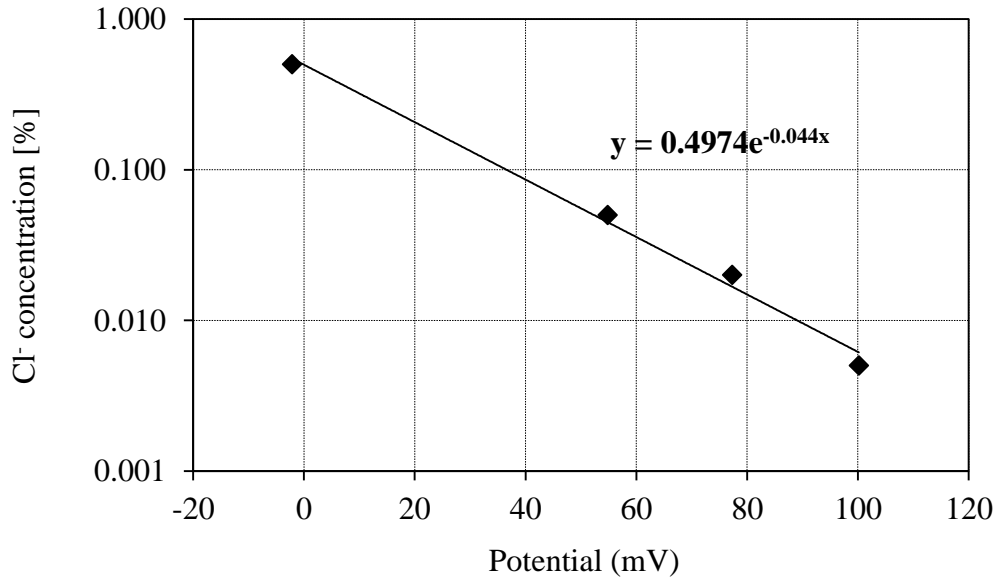


Figure 6.3. Calibration curve obtained by the subsequent immersion of the electrode in the calibration liquids with known Cl⁻ concentration (0.005%, 0.020%, 0.050% and 0.500%).

6.5. Results and discussion

6.5.1. Chloride migration coefficients

Within Figure 6.4 the chloride migration coefficients of HVFA and FA+SF concrete are compared with those of the applicable OPC and k-value conforming FA references (T(0.45), F(1)15 and F(2)15).

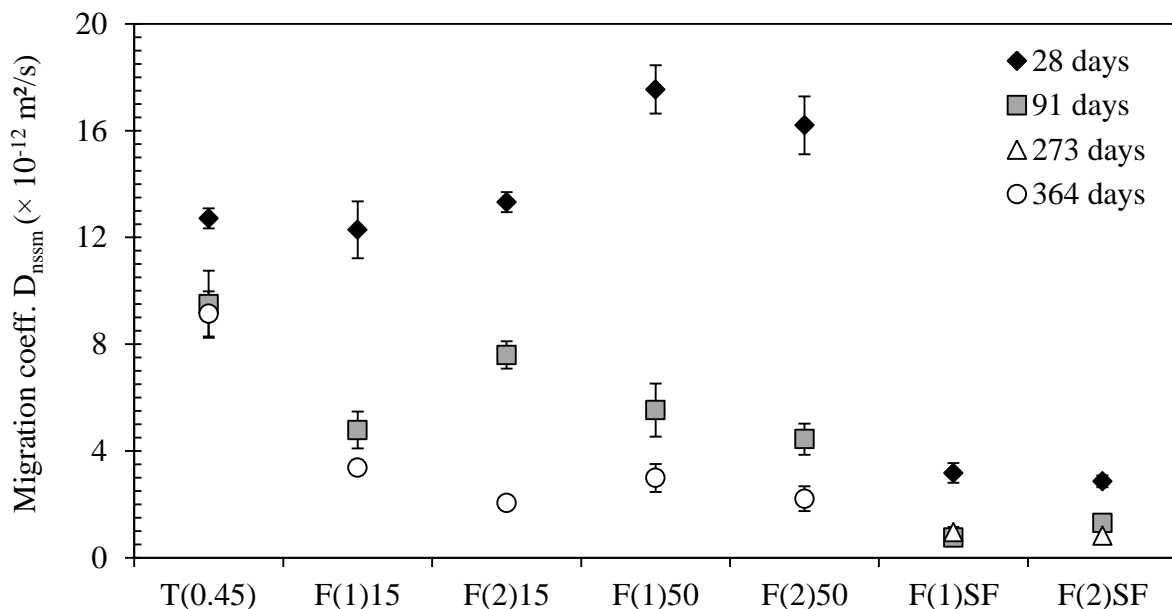


Figure 6.4. Non-steady state chloride migration coefficient D_{nssm} of the different concrete mixtures and its evolution with prolonged curing.

After 28 days of optimal curing all three references performed quite similar (D_{nssm} : 12.7-12.3- 13.3×10^{-12} m²/s). Nevertheless, the evolution of the chloride migration coefficient with time was different. In case of the OPC reference T(0.45), the value of D_{nssm} only decreased to around 9.1×10^{-12} m²/s after about one year (~364 days). The k-value conforming FA references F(1)15 and F(2)15 were found to be much more resistant to chloride migration at the same age (D_{nssm} : $3.4\text{-}2.1 \times 10^{-12}$ m²/s). This different ageing behaviour is of course of importance when estimating the time to chloride-induced steel depassivation using service life prediction models (Chapter 9). In perspective of the equivalent performance assessment of HVFA and FA+SF concrete this is less an issue, since NBN B15-100 (2008) does not impose chloride testing at multiple testing ages.

A validity check of the equivalent performance criterion (Equation 6-1) for HVFA concrete (F(1)50, F(2)50) after 28 days of optimal curing appears to have a quite positive outcome. Although considerably less resistant to chloride migration (D_{nssm} : $17.5\text{-}16.2 \times 10^{-12}$ m²/s), the recorded D_{nssm} values did not exceed 1.4 times the D_{nssm} value of references T(0.45) and F(2)15. The criterion was only just not met if mixture F(1)15 would be seen as the appropriate reference concrete for HVFA mixture F(1)50. Similar to the k-value conforming FA references, the chloride migration coefficients of HVFA concrete (F(1)50, F(2)50) decreased substantially with prolonged curing. After about one year, their values amounted to only 3.0 and 2.0×10^{-12} m²/s, respectively. This means that the equivalent performance criterion is automatically met for these concrete mixtures when 91 or 364 days would be seen as time of reference for equivalent performance assessment.

Among all tested concrete compositions, the FA+SF mixtures (F(1)SF, F(2)SF) were characterized by the lowest chloride migration coefficients. Already after 28 days, their D_{nssm} values ($3.2\text{-}2.9 \times 10^{-12}$ m²/s) were far below those recorded for the reference concrete types. Prolonged curing even caused a further drop in chloride migration coefficient. After 273 days mixtures F(1)SF and F(2)SF were characterized by D_{nssm} values of only 0.9 and 0.8×10^{-12} m²/s, respectively. Obviously, the proposed FA+SF concrete is in agreement with the equivalent performance concept of NBN B15-001 (2008).

Figure 6.5 shows the effect of suboptimal curing (7 days at 20°C and 95% RH, followed by 21 days at 20°C and 60% RH) on the 28-day chloride migration coefficient measured for additional batches of F(1)50 and F(1)SF. The corresponding D_{nssm} value of the same concrete mixtures after 28 days of optimal curing is also shown as reference. With respect to chloride migration, the HVFA concrete is clearly more susceptible to this suboptimal curing than the FA+SF concrete. For the former concrete composition there is a difference of no less than about 7.0×10^{-12} m²/s. In case of the latter, no significant difference in chloride migration coefficient could be observed between the two curing conditions. Finally, it must be said that comparison between Figure 6.3 and Figure 6.4 shows that the chloride migration coefficient of optimally cured F(1)50 and F(1)SF concrete varied quite a bit between two batches of concrete. Nevertheless, a similar difference between optimally and suboptimally cured F(1)50 and F(1)SF concrete is expected for the initial batches of these concrete mixtures.

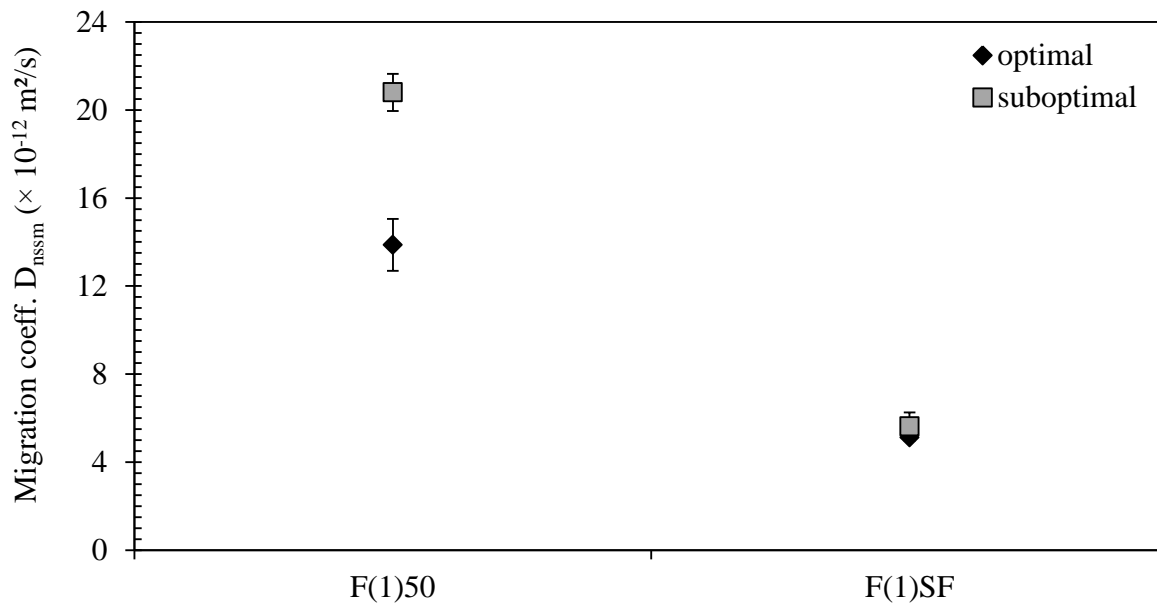


Figure 6.5. Effect of suboptimal curing on the chloride migration coefficient of HVFA mixture F(1)50 and FA+SF mixture F(1)SF.

6.5.2. Influencing factors of chloride diffusion testing

Before quantifying the accelerated and ‘natural’ chloride diffusion coefficients and surface concentrations, some influencing factors that govern the properties of the chloride profiles were investigated. Therefore, the chloride profiles obtained for one concrete were analysed more in detail. Special attention was paid to the effect of the more precise layer depth determination using a dial gauge (Figure 6.2b) on the shape of chloride profile and the value of the parameters that characterize this profile (Figure 6.6a, b). A comparison was also made between the acid- and water-soluble chloride concentration measured by means of the proposed potentiometric method (Section 6.4.2) and the commercial Rapid Chloride Test method (Section 6.4.4) (Figure 6.6c, d). The effect of considering the initial chloride content $C_{s,0}$ of the concrete during chloride profile curve fitting was studied as well (Figure 6.6e, f). The concrete composition under investigation was mixture F(1)SF subjected to the accelerated chloride diffusion test after 273 days of optimal curing. Figure 6.6 shows the graphical output of this parameter study.

Although Figures 6.6a and 6.6b seem to present very similar chloride profiles, there is a difference. When the X-axis is showing the layer depth estimated from the dial gauge readings after grinding each layer of concrete (Figure 6.6b), their values slightly deviate from the default layer depths (1, 3, 5, 7, 9, 11, 13, 15, 17 and 19 mm) set by the operator of the grinding apparatus (Figure 6.6a). Usually the actual layer thickness is a little less than 2 mm. As a consequence, there is a slight shift of the chloride profile to the left in the graphs. Fitting the proposed error function (Equation 6-3) through the data points corresponding with the acid- and water-soluble chloride contents, shows that the estimated chloride diffusion coefficients and surface concentrations were not affected by this slight shift. When working with the default layer depths, the $D_{e(acce)}$ and $C_{s(acce)}$ values that correspond with the acid-soluble chloride content amounted to $1.0 \times 10^{-12} \text{ m}^2/\text{s}$ and 3.2 m%/binder, respectively. The diffusion coefficients and surface concentrations estimated from the water-soluble chloride

profiles equaled 0.9×10^{-12} m²/s and 3.2 m%/binder, respectively. In case the measured layer depths were used for chloride profile fitting, practically the same values were obtained for the acid- and water-soluble chlorides. Thus, it seems that the dial gauge measurements for more exact layer depth determination were not really necessary. The general shape of the profile, which determines the value of $D_{e(\text{acce})}$, is not really altered by the shift. The same goes for the Cl⁻ concentration at depth 0 mm. However, major shifts in surface concentration seem perfectly possible when the entire chloride profile only would slightly move towards depth 0 mm. Concrete with a very high resistance to chloride ingress should be very susceptible to this phenomenon. As its chloride profile has a very steep initial curvature, the slightest shift to the left or right may result in a very different chloride surface concentration. Careful interpretation of the measured surface concentrations is therefore imperative.

Comparison of the profiles obtained for the acid- and water-soluble chlorides shows that the two curves almost completely coincide. True, the measured water-soluble chloride contents per layer still need to be converted to the corresponding free chloride contents. According to Yuan (2009), the former should be multiplied with factor 0.8 to obtain the latter. However, since the acid- and water-soluble chloride profiles almost coincide, one might as well apply the proposed factor to the acid-soluble chloride-content to obtain the free chloride content. Since measuring the water-soluble chloride content seemed completely redundant that way, the correctness of the acid- and water-soluble chloride contents measured by means of the potentiometric titration procedure described in Section 6.4.2 was questioned. Therefore, both types of chloride concentration were also determined for several layers of mixture F(1)SF using the commercially available Rapid Chloride Test (RCT and RCTW).

When using the RCT test procedure, the acid-soluble chloride content AC (RCT) turned out just a little bit lower than the output of the potentiometric titration (AC (titr.)). Figure 6.6c clearly shows this. After chloride profile fitting, the estimated chloride diffusion coefficients and surface concentrations amounted to 0.8×10^{-12} m²/s and 3.1 m%/binder, respectively. Thus, the difference in output between the two test methods is relatively small. The measured acid-soluble chloride content by means of potentiometric titration is very comparable.

As indicated in Figure 6.6d the water-soluble chloride contents WC (RCTW 1/2h) measured with the standard RCTW method were much lower than those obtained by means of potentiometric titration (WC (titr. 24h)). The chloride diffusion coefficients and surface concentrations obtained with the former method amounted to only 0.5×10^{-12} m²/s and 1.8 m%/binder, respectively. Evidently, there is a strong difference in contact time between the powdery test samples and the chloride extraction solution for the two test methods. This could perhaps explain this behaviour. The actual RCTW potential registrations were done maximum a half hour after the addition of the powdery samples to the RCTW vials followed by their filtering into the buffer solutions. In case of potentiometric titration the contact time was around 24 hours, cf. Mu (2012). Given this substantial difference in contact time, it was decided to perform another potentiometric titration after already half an hour of contact time as well (WC (titr. 1/2h)). This resulted in $D_{e(\text{acce})}$ and $C_{s(\text{acce})}$ values of 0.6×10^{-12} m²/s and 2.4 m%/binder, respectively. Additional RCTW measurements after more than 24 hours of contact time were also done (WC (RCTW 24h)). Then, $D_{e(\text{acce})}$ and $C_{s(\text{acce})}$ equaled 0.6×10^{-12} m²/s and 1.8 m%/binder, respectively.

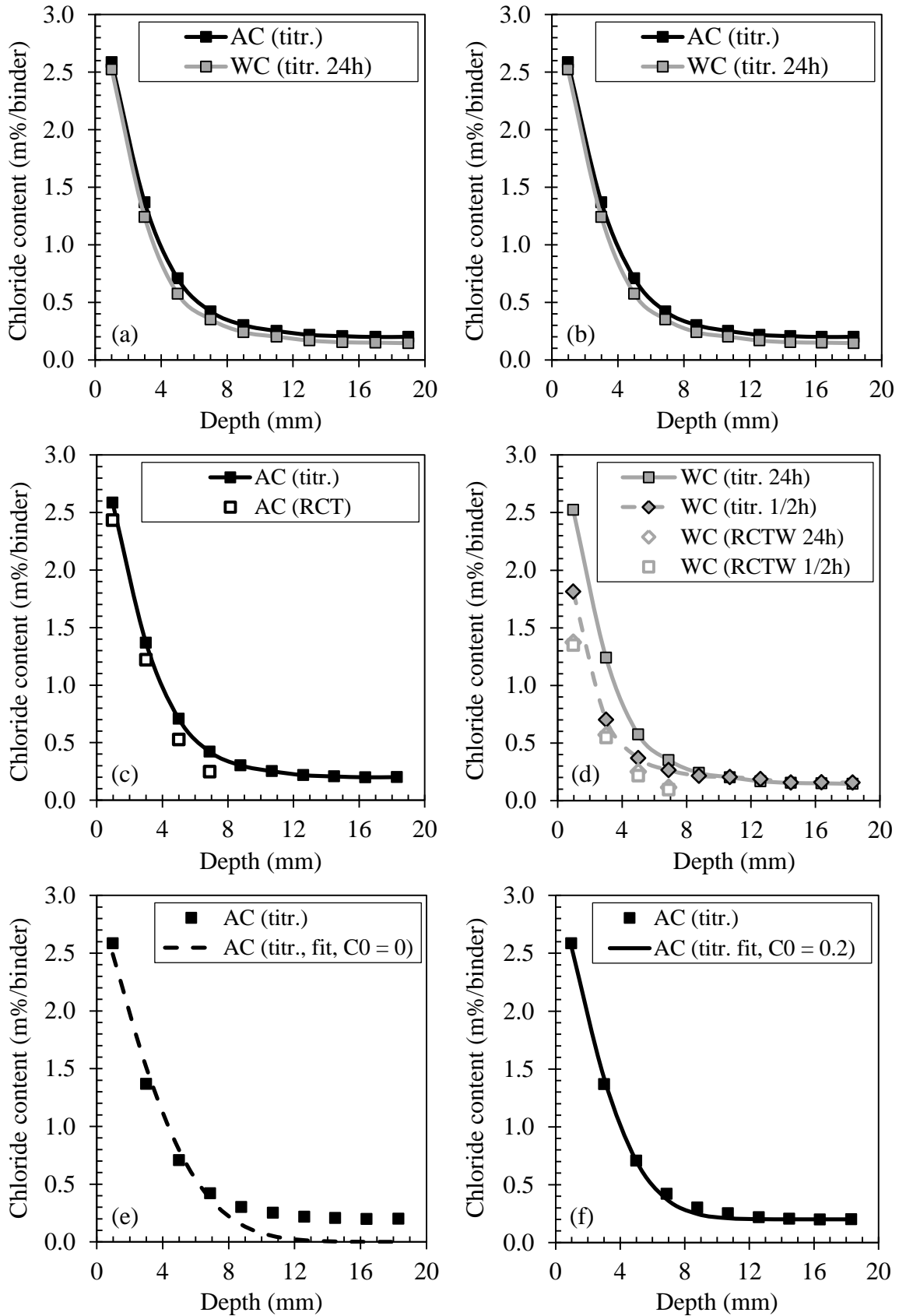


Figure 6.6. Influence of layer depth determination (a, b), applied test method for measuring chloride concentrations (c, d) and the initial chloride content (e, f) on the chloride profiles of mixture F(1)SF after the accelerated chloride diffusion test.

Thus, a shorter contact time prior to potentiometric titration significantly alters the output of the experiment. A prolonged contact time prior to the RCTW measurement did not cause important changes. In other words, depending on the test method the measured water-soluble chloride contents can vary considerably with the contact time for chloride extraction. The estimated free chloride content that relates to this water-soluble chloride content is obviously also affected by this. Different contact times and test methods will require different correction factors to determine the free chloride content correctly. Nevertheless, since several authors claim that bound chlorides can be released again as free chlorides [Glass and Buenfeld (1997), Glass and Buenfeld (2000), Reddy et al. (2002)], the service predictions done in this research were based on the total (= bound + free) chloride contents for safety reasons. This chloride content is known to correspond quite well with the acid-soluble chloride content. As a consequence, optimal contact times for water-soluble chloride extraction and optimal correction factors for estimating the corresponding free-chloride contents were not investigated any further within the framework of this research. Finally, it should be noted that working with the total chloride content for service life prediction may not be that ideal either. True, it gives service life estimations on the safe side. However, since blended binder systems usually have a higher chloride binding capacity than binder systems consisting entirely out of Portland cement, the assumed safety levels can be very different between the two.

The chloride profile fitting itself should also be done with caution. Quite often the initial chloride concentration of concrete prior to exposure is assumed to be negligible. Parameter C_0 in Equation 6-3 is simply set to 0.0 m%/binder without further verification of its actual value. Initially, the very same was done for all studied concrete mixtures. However, Figure 6.6e clearly shows that this approach results in an unsatisfactory curve fit (AC (titr., fit, $C_0 = 0$)). Therefore, it was decided to measure the initial chloride concentration of each concrete composition on powders collected from remaining specimens that were never exposed to chlorides. The initial chloride concentration of composition F(1)SF was 0.2 m%/binder. The chloride contents of the concrete layers collected at high depth, far from the exposed surface were practically the same. Thus, the stable chloride concentration that is reached for deepest layers matches well with the initial chloride concentration. By taking its value into account a much better curve fit is obtained (Figure 6.6f: AC (titr., fit, $C_0 = 0.2$)). Note that considering the initial chloride concentration significantly changes the value of the estimated diffusion coefficient as its value goes from 1.5×10^{-12} m²/s to only 1.0×10^{-12} m²/s. The chloride surface concentration goes from 3.0 m%/binder to 3.2 m%/binder and is thus less affected by this practice. For the results shown in the following sections, the initial chloride concentration was always considered during chloride profiling. The measured acid- and water-soluble chloride concentrations corresponded with AC (titr.) and WC (titr. 24h). When available, the layer depths measured with the dial gauge were used for chloride profiling.

6.5.3. Accelerated chloride diffusion coefficients and surface concentrations

6.5.3.1. Chloride diffusion coefficients

The accelerated diffusion coefficients as estimated from the total and free chloride profiles obtained after immersion in the 165 g/l aqueous NaCl solution are shown in Figure 6.7. These coefficients are usually considerably lower in value than their corresponding non-steady

chloride migration coefficients D_{nssm} (Figure 6.4). There seems to be one exception though. After prolonged optimal curing (91d, 273d) the differences between the migration and diffusion coefficients have become rather small for the FA+SF mixtures.

Little or no difference seems to exist between the diffusion coefficient estimated from the total and free chloride profiles. The former value was always either slightly higher or similar to the latter. This observation supports the safe choice to use mainly the diffusion coefficient that corresponds with the total chlorides for service life prediction purposes.

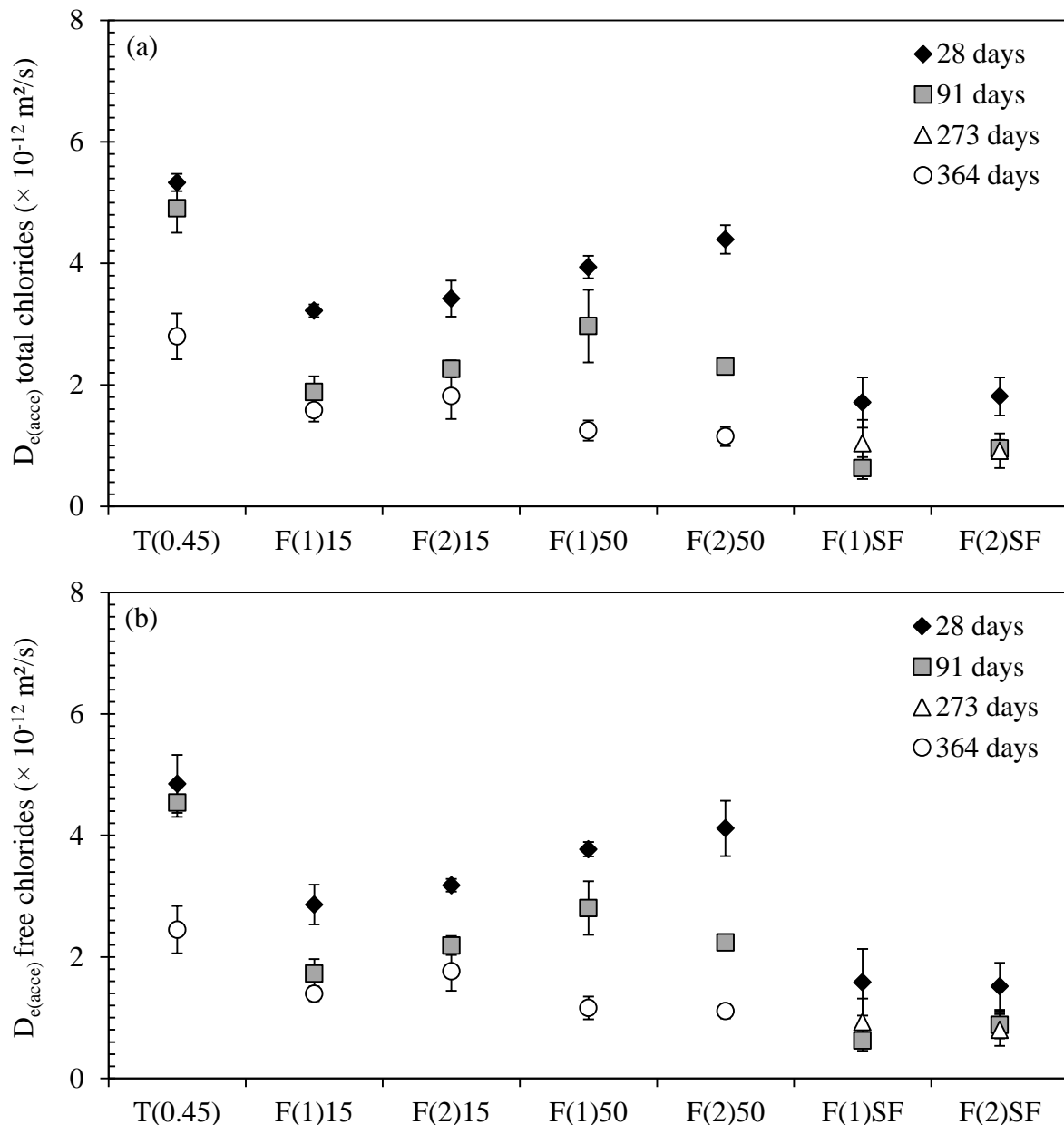


Figure 6.7. Accelerated chloride diffusion coefficients $D_{e(acce)}$ estimated from the total (a) and free (b) chloride profiles after 28, 91 and 273 or 364 days of curing.

When comparing the diffusion coefficients of the different concrete compositions, not all the trends that were previously observed after exposure to chloride migration seem valid again. For instance, HVFA compositions F(1)50 and F(2)50 already seem more resistant to chloride

diffusion than OPC reference T(0.45) after 28 days of optimal curing. This conclusion could not be drawn from the chloride migration test results. There, the equivalent performance criterion (Equation 6-1) was only just met for the 28-day curing condition. Thus, the equivalent performance of OPC and HVFA concrete at early age can be confirmed in a more pronounced way from an accelerated chloride diffusion test instead of from a migration test. However, it must be emphasized that this can be due to a considerable age difference between the concrete specimens that were used for the two tests. Although the curing period was the same for both, the duration of each test was very different. While the whole migration test, with inclusion of the sample preconditioning, lasted for only 2 days, the profile grinding for determination of the diffusion coefficient was done no less than 91 days after curing ended. Thus, the migration coefficient was obtained at an age where the pozzolanic hydration reactions had barely started (Chapter 5). The diffusion coefficient on the other hand was measured at a time that most of the secondary hydration reactions had taken place as well. This explanation is probably also valid for the different chloride migration and diffusion behaviour of the k-value conforming FA references F(1)15 and F(2)15. While their migration coefficients were rather similar to the one of mixture T(0.45) after 28 days of optimal curing, their diffusion coefficients were lower. Apart from the different (secondary) hydration degrees at different ages, the absence of the external electrical field during the diffusion will also have had an effect. Nevertheless, in case mixtures F(1)15 and F(2)15 would be seen as the appropriate reference composition, the equivalent performance criterion for the HVFA mixtures is still met for the 28-day curing period prior to an accelerated diffusion test. Logically, proof of equivalent performance still exists after prolonged curing.

The FA+SF concrete compositions were characterized by very low chloride diffusion coefficients ($1.5-1.6 \times 10^{-12}$ m²/s) from the start. The equivalent performance criterion is evidently met for all curing ages. The difference between the migration and diffusion coefficients after 28 days of optimal curing can probably again be explained by the age difference of the concrete at the end of the corresponding tests.

An important drop in diffusion coefficient could be observed for all fly ash (and silica fume) containing concrete compositions between 28 and 91 days of optimal curing. For the HVFA mixtures an additional drop occurred between 91 and 364 days of optimal curing. This increasing resistance to chloride ingress with time will automatically result in a higher ageing exponent for the concrete and a longer time to chloride-induced steel depassivation of embedded rebars. These exponents were estimated in Chapter 9.

Note that for the OPC concrete also a substantial drop in diffusion coefficient still occurs between 91 and 364 days of optimal curing, which is rather surprising since no slow secondary hydration reactions are expected anymore. The validity of this value will be evaluated further on in view of the measured chloride surface concentrations during this test and the experimental outcome of the natural diffusion test.

6.5.3.2. Chloride surface concentrations

The chloride surface concentration $C_{s(acce)}$ is the other parameter that results from chloride profile fitting. An overview of all measured total and free chloride surface concentrations measured is given in Figure 6.8.

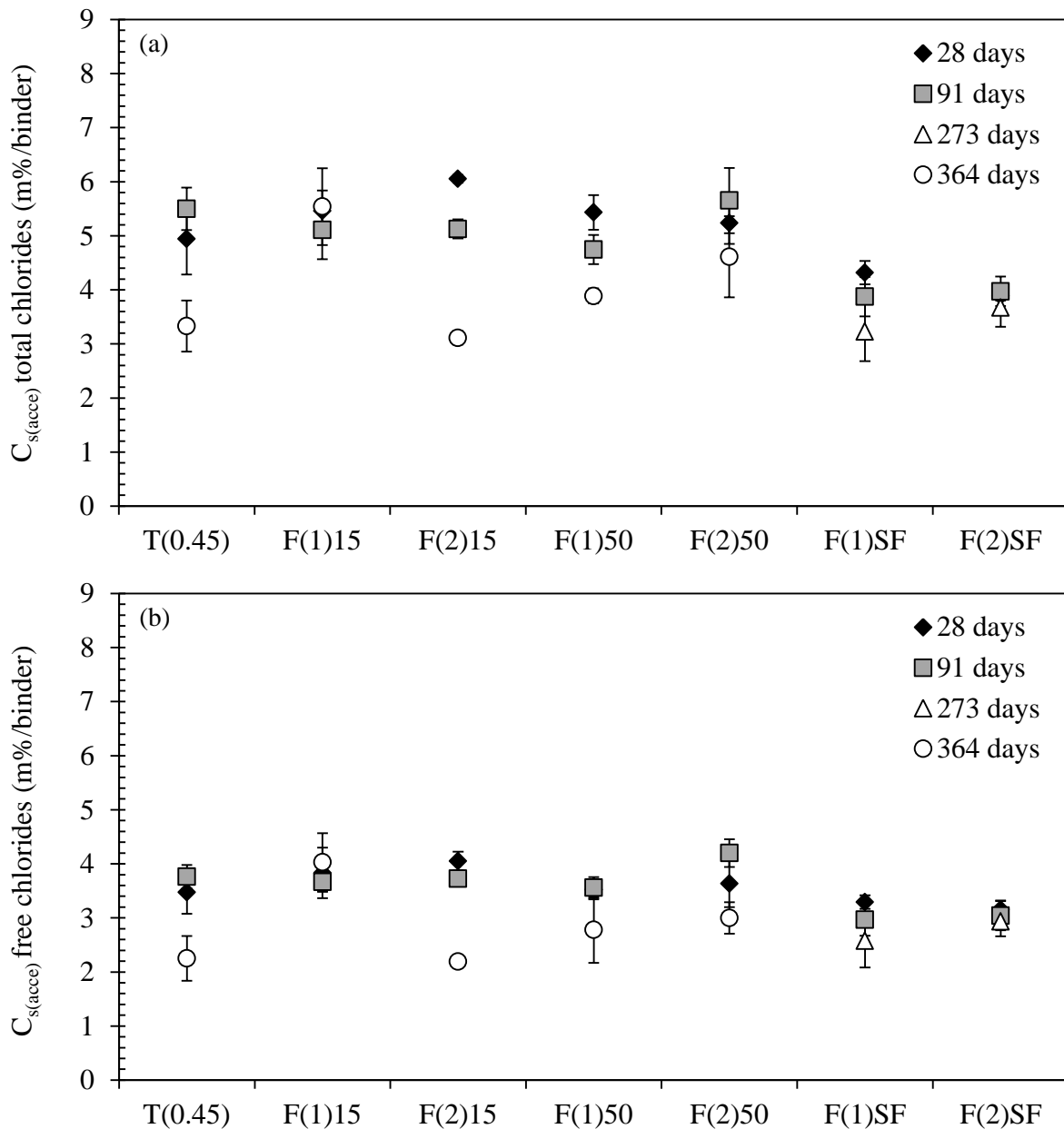


Figure 6.8. Accelerated chloride surface concentrations $C_{s(acce)}$ estimated from the total (a) and free (b) chloride profiles after 28, 91 and 273 or 364 days of curing.

Although the concrete specimens used for these diffusion tests were all immersed in a 165 g/l aqueous NaCl solution, quite some variation in chloride surface concentration seems to be present. This variation in total and free chloride surface concentration exists between the different concrete mixtures and curing ages considered. One would rather expect a more uniform free chloride surface concentration since this concentration most directly relates to the chloride concentration of the original exposure solution. Now, the differences in free chloride surface concentration may have become somewhat smaller, but they did not disappear. A more or less stable concentration of 3.8 m%/binder was found for mixtures T(0.45), F(1)15, F(2)15, F(1)50 and F(2)50 after 28 and 91 days of optimal curing. Yet, this concentration dropped to around 2.6 m%/binder for the 364-day curing period, except for the

surface concentration of composition F(1)15. The FA+SF concrete mixtures were characterized by a $C_{s(\text{acce})}$ value of 3.0 m%/binder for the three curing periods (28, 91 and 273 days). The very small surface concentration for OPC reference T(0.45) after 364 days of optimal curing might in part be responsible for the rather surprising, low diffusion coefficient at the same age. The validity of the latter, which is normally correlated with the former, should therefore be interpreted with caution. A comparison with the 'natural' diffusion coefficients is necessary to see whether the important drop in diffusion coefficient between 91 and 364 days of optimal curing for mixture T(0.45) indeed makes sense.

The fact that the specimens were immersed in a rather highly concentrated, yet far from saturated NaCl solution, could perhaps explain the variations observed. Not all NaCl may have been dissolved completely during the preparation of the test solutions. If so, the undissolved NaCl could have accumulated near the exposed surfaces of concrete specimens. As a consequence, the chloride surface concentration would be higher than when the concrete would have been immersed in a solution with complete dissolution of the NaCl. If this would be the proper explanation for the observed variations, then little variation in free chloride surface concentration should exist after the 'natural' diffusion test as 33 g NaCl per liter is much easier to dissolve completely. This has been verified in Section 6.5.4.2. A more thorough discussion on the possible causes for varying chloride surface concentrations follows in Section 6.5.5.

6.5.4. 'Natural' chloride diffusion coefficients and surface concentrations

6.5.4.1. Chloride diffusion coefficients

The 'natural' diffusion coefficients $D_{e(\text{nat})}$ obtained from the total and free chloride profiles (Figure 6.9a and Figure 6.9b) were very similar to their corresponding accelerated chloride diffusion coefficients $D_{e(\text{acce})}$ (Figure 6.7a and 6.7b). Thus, proof of an equivalent performance for HVFA and FA+SF concrete also exists when the evaluation is based on 'natural' chloride diffusion tests. Both the OPC and k-value conforming FA compositions can be seen as references. This choice does not affect the conclusion of the equivalent performance evaluation using Equation 6-1. Equivalent performance exists for all curing ages considered.

With $D_{e(\text{nat})}$ values ranging between $0.9\text{--}1.1 \times 10^{-12}$ m²/s after 28 days of optimal curing, the FA+SF compositions F(1)SF and F(2)SF can again be classified as compositions with the highest resistance to chloride ingress at early age. A further decrease in diffusion coefficient with prolonged curing time exists, but is not as pronounced as for the other fly ash containing concrete mixtures, e.g. F(1)15, F(2)15, F(1)50 and F(2)50. For the latter four mixtures the diffusion coefficient representing the free chlorides drops from around 3.0×10^{-12} m²/s after 28 days to only 1.0×10^{-12} m²/s after 364 days of optimal curing. For OPC reference T(0.45) $D_{e(\text{nat})}$ does not substantially decrease with prolonged curing time. This is in contrast with the outcome of the accelerated diffusion test and will have its consequences for the concrete's ageing exponent when based upon a 'natural' instead of on an accelerated diffusion test (Chapter 9). Because no additional hydration reactions at latter age except for the still slowly progressing OPC reaction are expected for mixture T(0.45), the observed evolution of the natural diffusion coefficient with time seems more logic. The validity of the substantial drop in accelerated diffusion coefficient between 91 and 364 days of optimal curing looks doubtful.

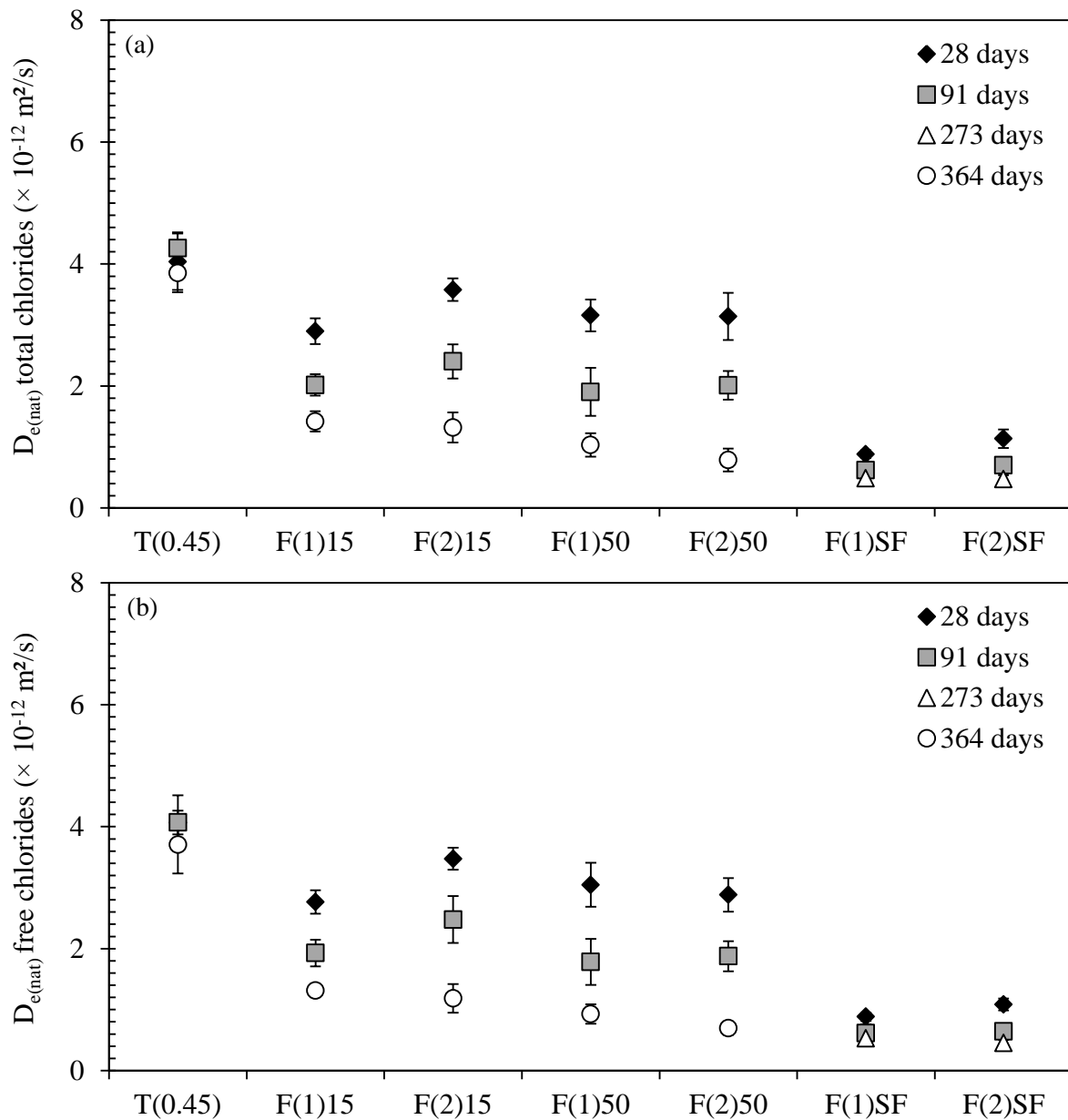


Figure 6.9. 'Natural' chloride diffusion coefficients $D_{e(\text{nat})}$ estimated from the total (a) and free (b) chloride profiles after 28, 91 and 273 or 364 days of curing.

6.5.4.2. Chloride surface concentrations

Surface concentrations measured after a 'natural' diffusion test (Figure 6.10a and 6.10b) seem more stable than those obtained after an accelerated diffusion test (Figure 6.8a and 6.8b). This is especially true for the free chloride surface concentrations. Compositions T(0.45), F(1)15, F(2)15, F(1)50 and F(2)50 all had a free chloride surface concentration of around 2.3 m%/binder on average. FA+SF composition F(1)SF and F(2)SF were still characterized by clearly lower values for $C_{s(\text{nat})}$, i.e. around 1.5 m%/binder on average. Thus, definitely not all variations can be explained by an incomplete dissolution of the NaCl used for the test solutions. The question arises whether this explanation is even valid at all. To verify this, it was decided to convert the now observed free chloride surface concentrations in m%/binder to concentrations in mol/l. This way, a direct comparison can be made with the Cl^- concentration

of the original exposure solutions (Section 6.5.5). Note that the unit conversion could only be performed for the mixtures for which the permeable porosity was measured. This characterization of porosity was done while studying the salt-scaling resistance of (non-) air entrained HVFA and FA+SF concrete (Chapter 7). Since no k-value conforming FA references were investigated as such, the unit conversion was not possible for mixtures F(1)15 and F(2)15. Note that 273 and 364 days of curing were also not considered in Chapter 7, the C_s values in mol/l for these curing ages were calculated based on the porosities obtained after 91 days. Since these porosities were very similar to those obtained after 28 days, it seems reasonable to assume that they will not change much anymore with time.

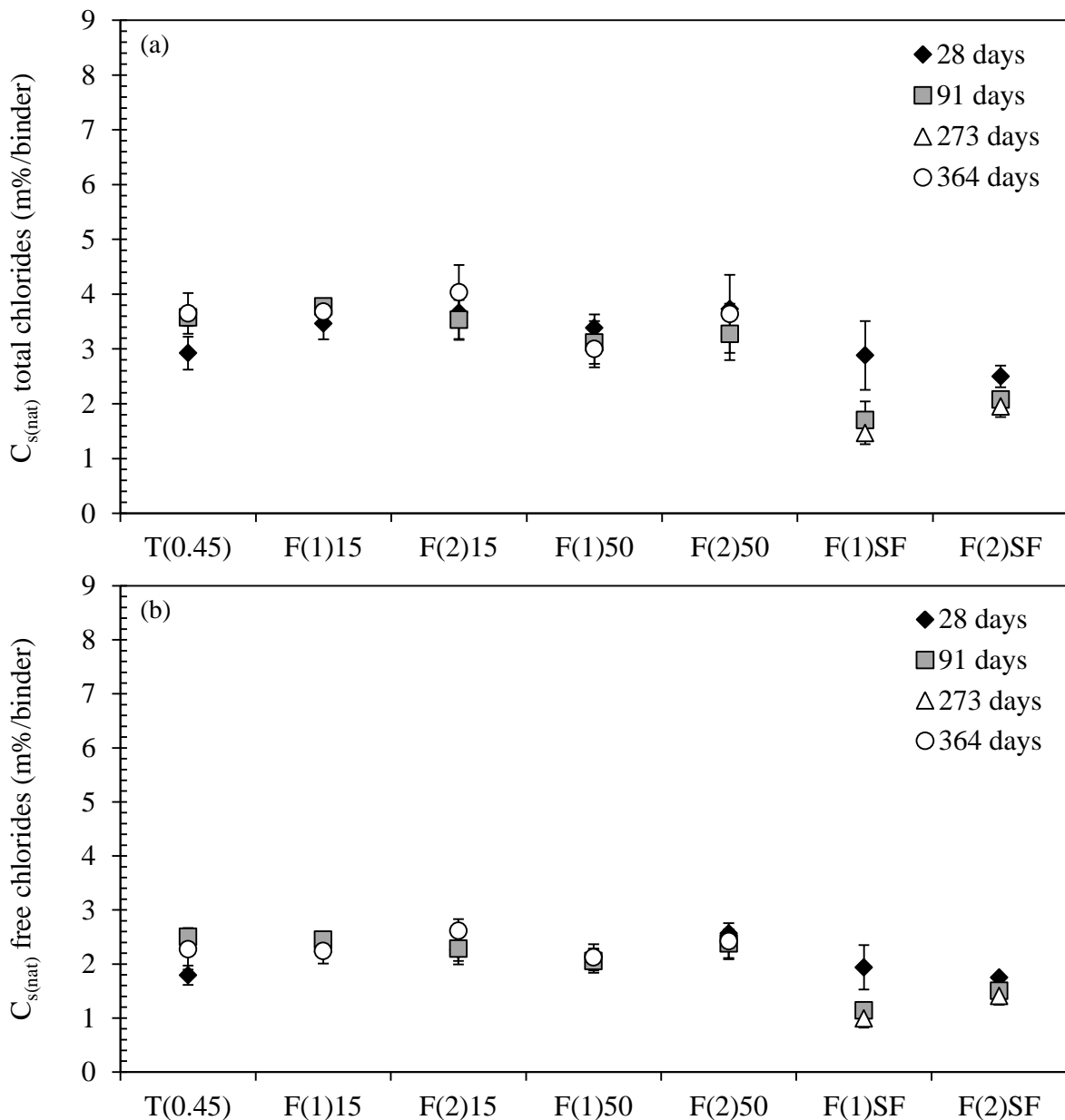


Figure 6.10. 'Natural' chloride surface concentrations $C_{s(nat)}$ estimated from the total (a) and free (b) chloride profiles after 28, 91 and 273 or 364 days of curing.

6.5.5. Causes of variation in chloride surface concentration

After unit conversion to mol/l the earlier observed variations in chloride surface concentration remain, especially with respect to the accelerated chloride diffusion test (Figure 6.11a). There seems to be one major difference though. While the surface concentrations of the FA+SF concrete compositions expressed in m%/binder were the lowest of all mixtures, the same concentrations in mol/l turned out to be highest of them all. This is mainly due to the fact that the conversion to mol/l requires a division of the original concentration by the very low permeable porosities of these mixtures. This effect was less pronounced for the output of the ‘natural’ diffusion test, particularly for mixture F(1)SF after prolonged curing.

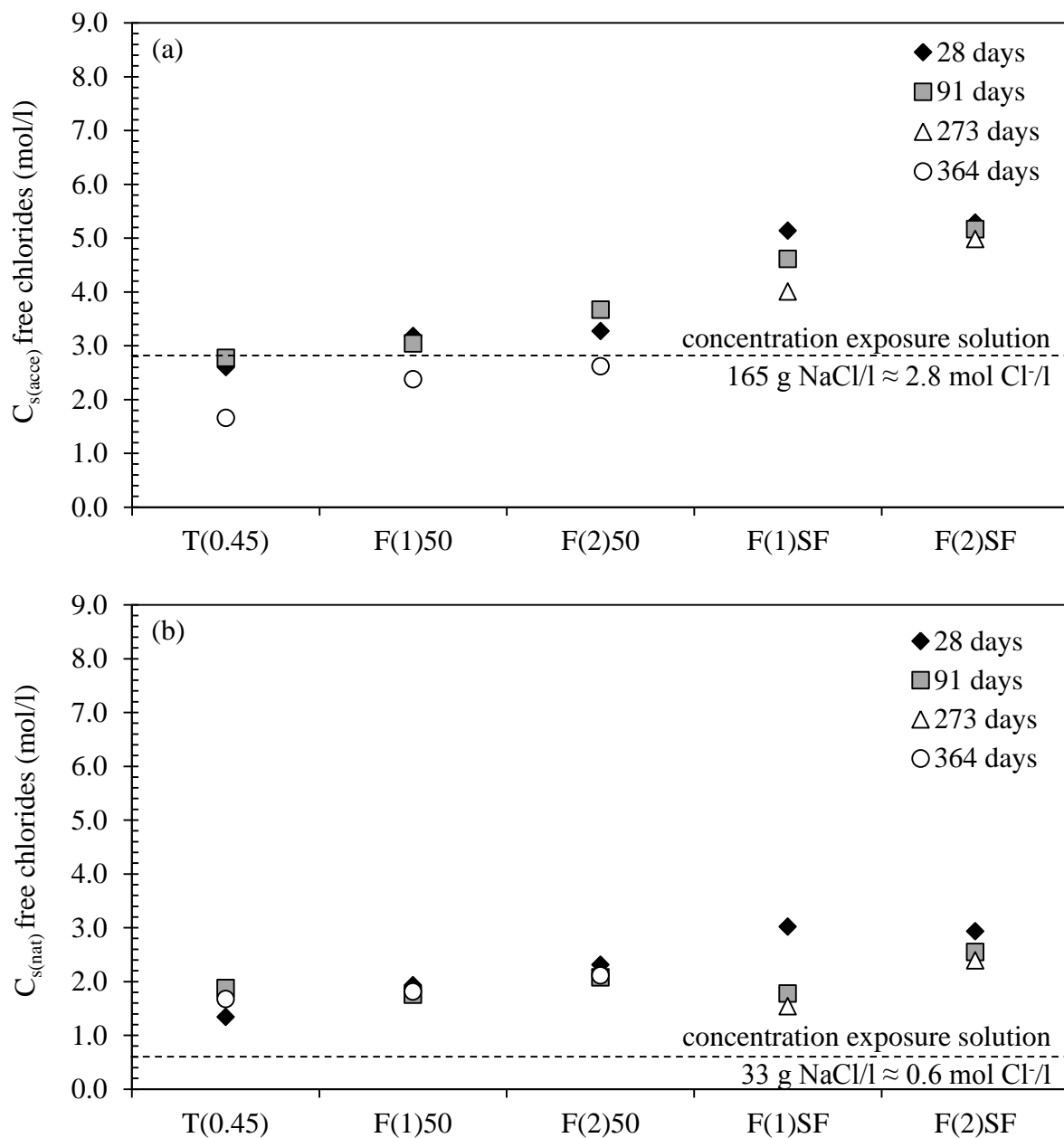


Figure 6.11. Free chloride surface concentrations in mol/l obtained after accelerated (a) and ‘natural’ (b) chloride diffusion tests.

Another important observation after conversion of the chloride surface concentration to mol/l relates to the link between this concentration and the original chloride concentration of the exposure solution. Immersion in a high concentration chloride solution (165 g NaCl per liter or ± 2.8 mol Cl^- per liter), resulted in $C_{s(\text{acce})}$ values that were similar or lower to this concentration for T(0.45). In case of the HVFA mixtures the surface concentration was similar or slightly higher. The FA+SF concrete compositions were characterized by surface concentrations that were 1.5 to 1.8 times higher. After immersion in a solution with a more realistic chloride concentration (33 g NaCl per liter or ± 0.6 mol Cl^- per liter) the measured $C_{s(\text{nat})}$ values were always more than twice the original chloride concentration (Figure 6.11b). This varying behaviour, which seems to depend on the type of concrete tested and the chloride concentration of the exposure solution, requires a more in-depth evaluation.

First of all, it must be emphasized that a surface concentration that exceeds the chloride concentration of the original exposure solution is not an uncommon phenomenon. Moreover, it is seldomly attributed to an incomplete dissolution of the chloride source during preparation of the exposure solution. For instance, Glass et al. (1996) found that the free chloride concentration of pore solution from thin cementitious discs subjected to a pore expression test after 28 days of immersion in a 0.135 mol/l chloride solution was around 30% higher than the concentration of the contact solution. This was attributed to the release of bound chlorides under high pressure. Baroghel-Bouny et al. (2007a, 2007b) observed that the water-soluble chloride content at the concrete surface was almost two times the chloride concentration of the contact solution, i.e. 18.2 g Cl^-/l , due to the condensation phenomenon first described by Nagataki et al. (1993). The research of the latter revealed that after 13 weeks of immersion in an aqueous NaCl solution with a similar chloride concentration as seawater (0.547 mol/l), the free chloride concentration measured after a pore expression test was almost twice that of the contact solution. This difference in concentration was attributed to condensation phenomena induced by the existence of an electrical double layer in the pores of the cement paste.

According to Friedmann et al. (2008) the concept of this layer was first described by Stern in 1924. It consists of a diffuse and a compact layer which are close to the surface solids in contact with an electrolyte solution. The compact layer is the layer that is in direct contact with the solid, in this case the pore wall of the cementitious material. Since the surface of hydrated cement is negatively charged [Chatterji (1992)], positively charged particles will be adsorbed to the pore wall. The compact layer of a chloride exposed cement based material comprises this zone and mainly consists of the ions with a positive charge, e.g. Ca^{2+} , K^+ and Na^+ . The electrical potential that is created that way causes the formation of a diffuse layer mainly consisting of ions with a negative charge, e.g. OH^- and SO_4^{2-} , and Cl^- . As a result, a difference in ionic concentration is established between the diffuse layer and the bulk solution. As such, the concentration of chloride ions in the diffuse layer is much higher than in the bulk solution. According to Nagataki et al. (1993), this condition fully explains why the surface chloride concentration is much higher than the concentration of the exposure solution. However, according to Yuan (2009) this explanation is too simple as it disregards the fact that the extension of the diffuse layer is highly depending on the ionic concentration of the bulk solution. This conclusion follows directly from the Debye Equation (Equation 6-5) which can be derived from the original definition of the Debye constant κ mentioned by Friedmann et al. (2008) and Adamson and Gast (1997).

$$\frac{1}{\kappa} = \frac{1}{\sqrt{\frac{2 \cdot F^2 \cdot c}{R \cdot T \cdot \varepsilon}}} \quad (6-5)$$

With $1/\kappa$, the Debye length (m), F , the Faraday constant (9.648×10^4 J/(V · mol)), c , the ionic concentration of the bulk solution (mol/l), R , the gas constant (8.314 J/(mol · K)), T , the absolute temperature (K) and ε , the dielectric permittivity of the solution (F/m). Friedmann et al. (2008) calculated the Debye length for a bulk solution composed of monovalent anions with a cation concentration of 0.1 mol/l at 25°C using Equation 6-5. The resulting thickness of the diffuse layer amounted to 0.97 nm. Now, since this is much smaller than the normal pore size range of cement based materials ranging from nanometer to millimeter, Yuan (2009) concluded that the pores of cementitious materials usually both contain the diffuse layer and a portion of the bulk solution. Only in the very fine pores (diameter < 2 nm) an overlap of the diffuse layers can occur which means that the bulk solution is not present in these pores. The total volume of solution present in these pores and entirely consisting of the diffuse layer may not be negligible in comparison with the bulk solution if a lot of these pores are present. If so, the free chloride surface concentration can indeed be higher than the concentration of the exposure solution.

However, this statement only holds true for very fine pores in contact with a bulk solution characterized by a low ionic concentration (0.1 mol/l). The concentrations of interest in this study were much higher (33 g NaCl per liter \approx 0.6 mol/l, 165 g NaCl per liter \approx 2.8 mol/l). Given the inverse relation between the ionic concentration of the bulk solution and the Debye length (Equation 6-5), the thickness of the diffuse layer for these exposure solutions will be smaller than for low concentration solutions. As a consequence, more bulk solution should be present in the pores. Thus, the free chloride surface concentration measured after immersion in 33 g/l and 165 g/l aqueous NaCl solutions should be well in agreement with the chloride concentrations of exposure solutions. Yuan (2009) found that the chloride concentration of the pore solution of cement paste discs after 35 and 180 days of immersion indeed corresponded quite well with the concentration of the 0.5 mol/l and 1.0 mol/l exposure solutions and attributed this to the above described double electrical layer effect. On the other hand, the free chloride surface concentrations of concrete after 49 days of immersion in a 165 g/l aqueous NaCl solution was lower than the chloride concentration of the exposure solution (\approx 2.8 mol Cl⁻/l). Yuan (2009) attributed this to the fact that a 49-day immersion period was probably not sufficient to establish an equilibrium state between the surface pore solution and the exposure solution.

In this research, 63- and 125-day immersion periods were applied for the accelerated and ‘natural’ chloride diffusion tests, respectively. The 63 days of immersion in 165 g/l aqueous NaCl solution resulted in free chloride surface concentrations that were similar or lower (e.g. T(0.45), similar or higher (e.g. F(1)50, F(2)50) or considerably higher (e.g. F(1)SF, F(2)SF) than the chloride concentration of the exposure solution (\approx 2.8 mol Cl⁻/l). Thus, except for OPC reference T(0.45) after 364 days of optimal curing, the 63-day immersion period was found to be sufficient to reach at least the equilibrium state. The question remains why the

free chloride surface concentration of the HVFA concrete and especially the FA+SF concrete exceeded 2.8 mol Cl⁻/l. As explained earlier, electrical double layer phenomena play a minor role in case of high concentration exposure solutions and can thus not cause free chloride surface concentrations of more than 2.8 mol Cl⁻/l unless very fine pores would be present in large quantities. The latter condition could unfortunately not be verified from the MIP results shown in Chapter 5 because a quantitative assessment of the very fine pore range requires mercury pressures of over 200 MPa. Such pressures were not applied during the MIP tests. Nevertheless, it is known that the presence of silica fume can indeed cause an important densification of the pore structure. Thus, the presence of very fine pores could be a valid explanation which deserves further attention.

125 days of immersion in 33 g/l aqueous NaCl solution always resulted in free chloride surface concentrations that exceeded the chloride concentration of the exposure solution by far. Thus, the duration of the immersion period was definitely enough to reach the state of equilibrium mentioned by Yuan (2009). The reason why the free surface chloride concentrations were much higher than ± 0.6 mol Cl⁻/l remains unclear. Electrical double layer effects cannot have caused this since the concentration of the exposure solution exceeded the criterion of 0.5 mol Cl⁻/l [Yuan (2009)]. The presence of more very fine pores also looks doubtful as explanation since the OPC mixture behaves in the same way as the fly ash containing mixtures. The same goes for the presence of more very fine pores within the FA+SF compositions, because the surface concentrations of mixture F(1)SF decreased substantially with prolonged curing.

Although a proper physical explanation cannot easily be given for free chloride surface concentrations exceeding the chloride concentration of the contact solution, a build-up in chloride surface concentration with increasing exposure time is often observed in practice. This phenomenon is most documented for concrete in the tidal or spray zone or concrete exposed to airborne chlorides [Costa and Appleton (1999a, 1999b)]. Ann et al. (2009) observed the surface chloride build-up in the tidal and splash zone and for the aerated exposure condition. According to Swamy et al. (1994), as cited by Costa and Appleton (1999b), the chloride surface concentration in all exposure conditions, except for complete immersion, is characterized by a quasi-linear variation with the square root of time. In other words, there is an increase in chloride surface concentration that tends to be attenuated over time. In the submerged zone there is a tendency for a constant value of C_s which is associated with an equilibrium between the chloride concentration in the sea water and in the skin concrete [Costa and Appleton (1999a)].

However, not every literature source supports a constant C_s value in case of complete immersion. For instance, Sandberg et al. (1998) studied a wide range of concrete compositions (OPC mixtures, high-sulfate resistant (HSR) cement mixtures, FA mixtures and SF mixtures with varying W/B ratios) submerged in seawater at a marine field test facility. The authors observed an increase in total chloride surface concentration with increasing exposure time ranging from 0.6-0.8 to 5.1-5.4 years for all tested concrete compositions. The values recorded after 0.6-0.8 year and 5.1-5.4 years were also not similar for all mixtures. Their values after 0.6-0.8 years of exposure ranged between 1.3 and 3.1 m%/binder, while those after 5.1-5.4 years ranged between 2.4 and 5.1 m%/binder. Given the order of magnitude of these concentrations, the corresponding free chloride surface concentration will also be higher than the chloride concentration of the surrounding seawater. True, the chloride

surface concentrations reported in Sandberg et al. (1998) would actually first need to be converted to mol/l and then be compared with the Cl^- concentration of the seawater at the test facility in order to allow for an adequate comparison. Unfortunately, this conversion was not possible because not all necessary input to Equation 6-4 was readily available in Sandberg et al. (1998).

Thus, there is an important surface chloride build-up at the concrete surface beyond the original chloride concentration of the seawater which is not the same for different concrete types. This was also observed for the concrete compositions that were studied in this research. Apparently, for the same exposure time not all concrete compositions are in the same stage of this surface chloride build-up at different ages. To fully characterize this time dependent behaviour, chloride profiling after various exposure times is necessary. This was not done in the course of this research, because the service life prediction model that was used assumed a constant chloride surface concentration as a function of time for the submerged condition. Only the time-dependent decrease of the chloride diffusion coefficient under ideal curing conditions was taken into account by means of an ageing exponent in the model for chloride-induced steel depassivation described in *fib* Bulletin 34 (2006). Obviously, as soon as measurements after various exposure times become available, the model should be corrected for the time-dependent surface chloride build-up in the submerged condition. For now, a higher constant surface concentration could be assumed as safety precaution (see Chapter 9).

6.5.6. Time dependent decrease of the chloride diffusion coefficient

The results shown in Sections 6.5.3-6.5.4 clearly indicated that both the accelerated and ‘natural’ chloride diffusion coefficients of most of the tested concrete compositions – especially the ones containing FA (and SF) – decreased with prolonged optimal curing. Now, the majority of the literature found on the time-dependency of the diffusion coefficient, mention a decrease in diffusion coefficient with increasing exposure time, which is not the same thing. Costa and Appleton (1999a) reported this phenomenon for the tidal zone, the spray zone and the atmospheric zone and attributed it to three main effects:

- The ongoing hydration of the cement, which causes a reduction in concrete porosity, especially at relatively young age.
- The formation of a layer of Brucite on the surface which reduces chloride penetration. This effect is not only of relevance in the tidal zone, but also in the submerged zone.
- The reactions between cement hydration products and ions from the seawater which also cause a reduction in concrete porosity, e.g. the reaction between chlorides and C_3A to form chloroaluminates and the reaction of magnesium and sulphate ions with cement compounds to form Brucite and Ettringite.

Obviously, not all of these effects will have played a role in the decrease of the diffusion coefficient with prolonged curing. Since the period of immersion in aqueous NaCl solution (63 or 125 days) was the same for each considered curing period (28, 91 or 273/364 days), the second and third effect would always have contributed to the same extent. Moreover, since no magnesium and sulfate ions were present in the test solutions, the porosity reducing effects of Brucite and Ettringite formation were simply not present. Thus, mainly the ongoing hydration of the cement/binder system and the increasing availability of aluminate containing hydration

products that react with chlorides can be held responsible for the decrease in diffusion coefficient with prolonged curing. An ageing exponent based on this decrease does not take into account all porosity reducing effects that occur in practice. As a result, this approach will probably underestimate the actual ageing exponent of the concrete in its actual marine environment. A service life prediction based on this exponent will probably be on the safe side. This aspect has been discussed more thoroughly in Chapter 9.

6.5.7. Resistance to chloride ingress of artificially cracked MBE mortars

6.5.7.1. Microscopic verification of cracks and crack widths

Table 6.2 shows that the observed crack widths at the surface did not differ much from the thicknesses of the thin metal plates (0.1, 0.2 and 0.3 mm). The cross-sectional crack widths measured on one cylinder of each cracked series further confirm this good match for both mortar compositions. Note that the cross-sectional crack width observed on the MBE SF10W35 sample with a 0.1 mm crack had a rather high standard deviation on the individual values (stdv.: 0.08 mm). This is mainly due to the fact that the measured crack widths – recorded over the entire crack depth at regular distances of 1 mm – quite often equaled zero. At several places alongside its cross-sectional area, the SM micrographs (age: 28 days) showed crack closure which could not be attributed to a mere filling by loose particles originating from the mechanical surface flattening (Figure 6.12a).

Table 6.2. Microscopic crack width measurements of MBE T(0.45) and MBE SF10W35.

| MBE T(0.45) | | | MBE SF10W35 | | |
|-------------|-------------------|---------------|-------------|-------------------|---------------|
| 0.1 mm | Flattened surface | Cross-section | 0.1 mm | Flattened surface | Cross-section |
| n | 33 | 12 | n | 33 | 12 |
| mean | 0.08 mm | 0.09 mm | mean | 0.13 mm | 0.12 mm |
| stdv. | 0.01 mm | 0.01 mm | stdv. | 0.03 mm | 0.08 mm |
| 0.2 mm | Flattened surface | Cross-section | 0.2 mm | Flattened surface | Cross-section |
| n | 33 | 12 | n | 33 | 12 |
| mean | 0.19 mm | 0.21 mm | mean | 0.21 mm | 0.20 mm |
| stdv. | 0.01 mm | 0.02 mm | stdv. | 0.02 mm | 0.03 mm |
| 0.3 mm | Flattened surface | Cross-section | 0.3 mm | Flattened surface | Cross-section |
| n | 33 | 12 | n | 33 | 12 |
| mean | 0.27 mm | 0.34 mm | mean | 0.29 mm | 0.33 mm |
| stdv. | 0.02 mm | 0.02 mm | stdv. | 0.03 mm | 0.05 mm |

The additional SEM micrographs that were taken afterwards (age: 196 days) further confirm this observation (Figure 6.12b). The (partial) crack closure practically always consisted of a bridging with solid material. In the second SEM micrograph, a very fine crack (< 5 µm in width) seems to be going through the solid crack filling material. Re-cracking was quite often observed during the SEM analysis. This phenomenon was probably induced by the sawing operations done to obtain the 20×20×10 mm³ prismatic SEM samples from the MBE SF10W35_0.1 mm cylinder halve. The fact that this very fine crack is going through the whole local bridging of the crack demonstrates that it was once a solid crack filling material.

EDX mapping performed on the partially closed crack and the adjacent mortar matrix clearly revealed the location of mainly Si containing sand particles (Figure 6.13). Practically no sand grains were present in the crack filling material. If this was the case, the partial closure of the crack could not have been caused by autogenous healing phenomena. Then, the crack simply had closed again shortly after removal of the thin metal plates. With no grains present, the crack filling material must fully consist of hydration products of the binder materials (C–S–H, alumina containing hydrates,...) or CaCO_3 due to possible carbonation. This condition supports the theory of autogenous healing.

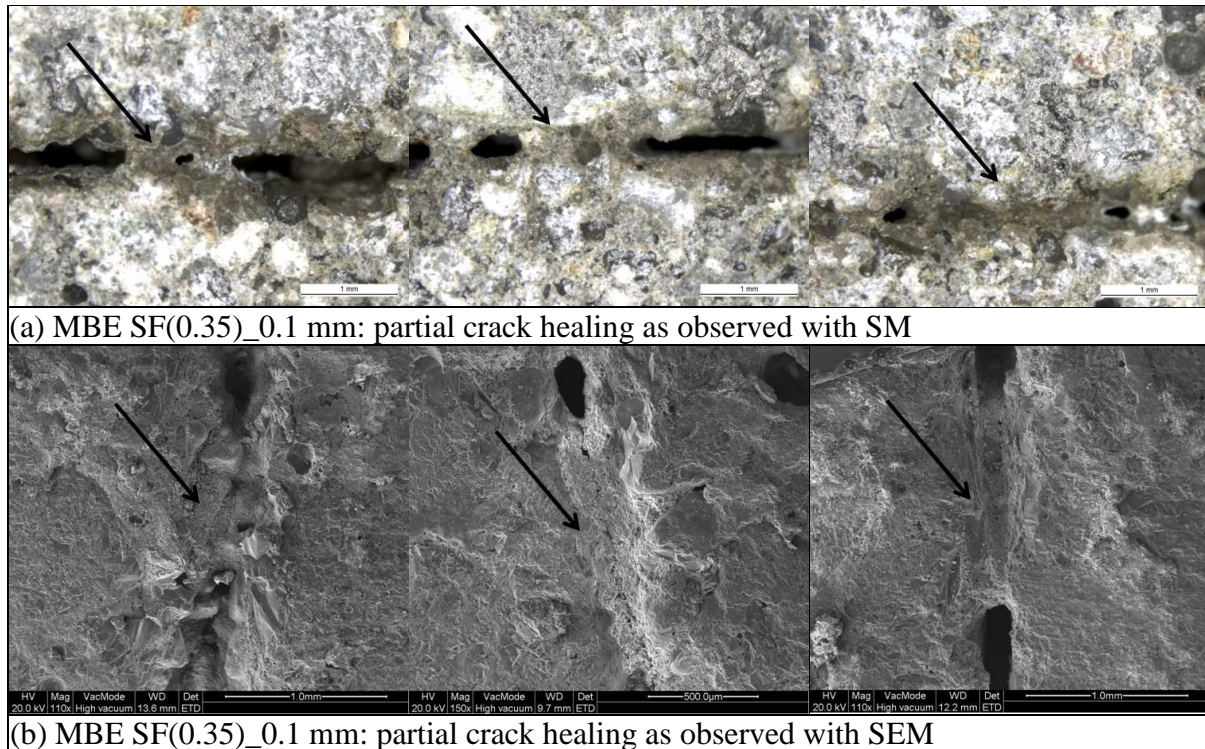


Figure 6.12. Partial crack healing of the 0.1 mm wide crack in MBE SF10W35 as observed on SM and SEM micrographs.

The partial crack closure observed both with SM and FESEM (in combination with EDX) may indicate that for a crack width of ± 0.1 mm, partial autogenous crack healing can occur. Since this phenomenon was not observed on the MBE T(0.45) sample with a 0.1 mm crack, the partial autogenous healing that was detected is most likely induced by further hydration of the unreacted alternative binders (FA and SF) present in MBE SF10W35. Jaroenratanapirom and Sahamitmongkol (2011) reported fast natural healing of cracks ≥ 0.05 mm in OPC mortars with 10% silica fume and without fly ash. Figure 6.12 and Figure 6.13 show that this may also be the case for the MBE SF10W35 mortar containing 50% OPC, 40% FA and 10% SF. Evidently, these preliminary findings should be verified further on. A full-scale investigation of the autogenous healing phenomena that can occur in presence of fly ash and silica fume was outside the scope of this thesis.

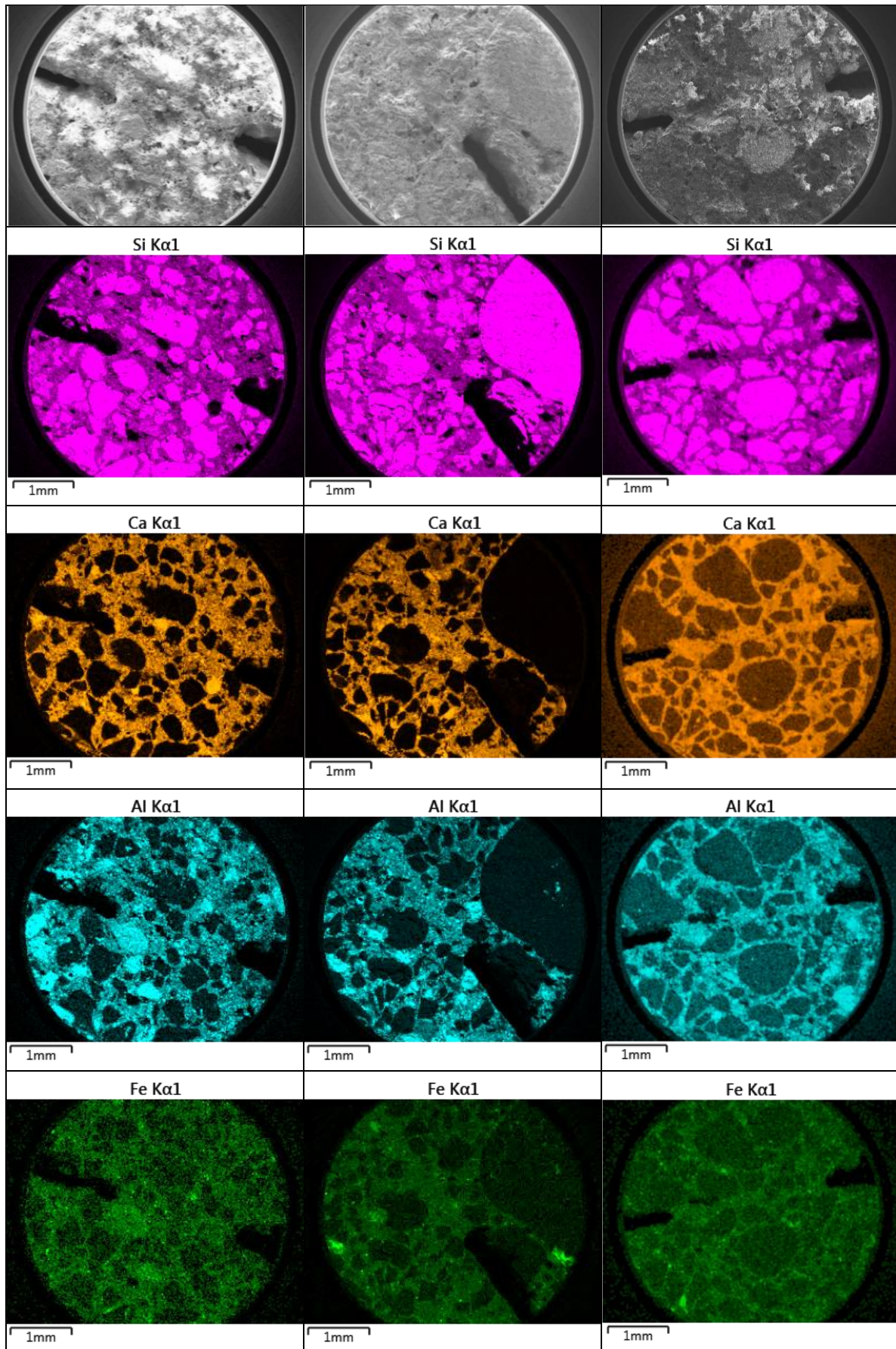


Figure 6.13. FESEM micrograph and EDX mapping of MBE SF10W35_0.1 mm.

6.5.7.2. Chloride migration coefficients of the uncracked MBE mortars

MBE mortar SF10W35 was characterized by a 28-day non-steady state chloride migration coefficient D_{nssm} of $3.4 \pm 0.6 \times 10^{-12} \text{ m}^2/\text{s}$. This is only around one third of the 28-day D_{nssm} value ($10.7 \pm 1.0 \times 10^{-12} \text{ m}^2/\text{s}$) obtained for OPC reference MBE T(0.45). Thus, when uncracked, the former mortar composition is much more resistant to chloride penetration than the latter. Comparison of these results with the migration coefficients of the corresponding concrete mixtures T(0.45) and F(2)SF (Figure 6.4) shows that the difference in chloride resistance between the two binder systems is of the same order of magnitude.

6.5.7.3. Determination of the maximum crack width allowed

Figure 6.14 shows one representative photo of the chloride penetration for each mortar-crack combination after the four hour non-steady state migration test.

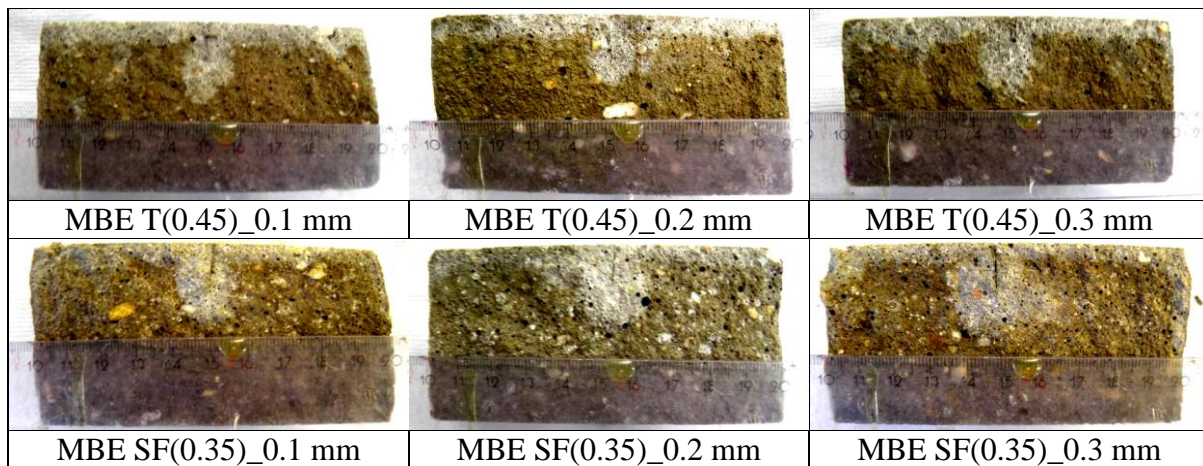


Figure 6.14. Observed AgNO_3 colour change boundary on the cracked samples of MBE T(0.45) and MBE SF10W35.

Per mortar mix and crack width all broken cylinder surfaces ($n = 6$) looked similar. The chloride penetration always extended beyond the deepest point of the crack. This was the case for all three nominal crack widths (0.1, 0.2, 0.3 mm) that were experimentally assessed in this research, also when already some partial autogenous healing had occurred for the 0.1 mm crack of MBE SF10W35. In other words, none of the studied cracked samples could be considered as uncracked cf. Figure 6.1c. This means that for the considered 10% NaCl solution used during the migration test, the maximum crack width allowed should be reduced even more, preferably to a value that ensures complete autogenous healing of the crack, i.e. the 0.05 mm crack width suggested by Jaroenratanapirom and Sahamitmongkol (2011). For the latter crack width, complete crack closure was observed within 12 days, which is much earlier than the age of our cracked samples at the time of inspection with SM (at 28 days) and SEM (at 196 days).

Obviously, it would be interesting to manufacture another series of cracked samples containing a 0.05 mm wide crack and subject them to chloride migration tests as well. However, it is difficult to create these very fine artificial cracks in mortar with the current mould setup (Figure 6.1a). Metal plates with a thickness of only 0.05 mm have almost no

stiffness. As a result, it is practically impossible to maintain them at a fixed position in the fresh mortar. Moreover, their intact removal from the hardened mortar is also not evident. More research is needed on how this could be achieved in the future.

It should also be verified further on whether there is a need for stricter crack width criteria in case of continuous exposure to actual seawater, which is not just an aqueous NaCl solution. For instance, due to the presence magnesium in seawater, a Brucite layer can be formed which can reduce chloride penetration (see Section 6.5.6). For the moment this effect has not been studied yet when defining the most appropriate maximum crack width criterion for concrete in direct contact with seawater.

6.6. Conclusions

- The conducted experimental study revealed that the proposed HVFA and FA+SF concrete compositions both meet the equivalent performance criterion of NBN B15-100 (2008) for chloride resistance when based on migration tests, accelerated diffusion tests and 'natural' diffusion tests performed after 28, 91 and 273 or 364 days.
- While after just 28 days of optimal curing the HVFA concrete is actually almost on the verge of not showing an equivalent performance in terms of chloride migration, the FA+SF concrete most definitely performs much better than the applicable OPC and k-value conforming FA reference. The chloride diffusion behaviour of HVFA concrete after 28 days of optimal curing was found to be less critical, but this was mainly because the required exposure period for a diffusion test is much longer than during a chloride migration experiment. As a consequence, the actual determination of the diffusion coefficient evidently occurs at a much later age. At that time most of the secondary hydration reactions have already taken place.
- The age difference at the time of the actual measurements also in part explains why the decrease in migration coefficient with prolonged curing is much more pronounced than the time-dependent decrease in diffusion coefficient. Other effects such as chemical binding or reactions between the chlorides and the aluminate containing hydration products will have played a less prominent role due to the nature of the migration test. Imposing an electrical field across the concrete implies a very quick transport of chloride ions and thus incomplete binding.
- The decrease in diffusion coefficient after immersion in artificial aqueous NaCl solutions is probably less pronounced than in actual seawater because some porosity reducing effects that require the presence of magnesium and sulfate ions in the exposure solution, simply cannot take place. An ageing exponent based on the tests involving immersion in aqueous NaCl solution will probably be on the safe side.
- The 'natural' diffusion test results suggested that the chloride surface concentration of OPC, FA, HVFA and FA+SF concrete in the submerged condition is probably not constant in time. Just like for the atmospheric, spray, splash and tidal exposure condition, a surface chloride build-up is expected in case of complete immersion. Further confirmation for this behaviour could follow from additional diffusion tests performed at various exposure times. For now, a higher constant surface chloride concentration can be assumed to avoid an overestimation of the expected service life.

-
- When cracks are present with a width lower than the 0.3 mm maximum criterion for reinforced concrete cf. Eurocode 2, the material cannot be treated as uncracked. Even for crack widths lower than 0.1 mm this is not the case. To achieve this goal, the maximum crack width allowed needs to be lowered further on to a value that can ensure autogenous healing of the concrete. A link should exist between the imposed crack width limit and the presence of SCMs (e.g. fly ash, silica fume) in the concrete, since their presence favors autogenous healing. Exposure to actual seawater instead of a highly concentrated aqueous NaCl solution may lead to different conclusions with respect to the maximum crack width allowed as the presence of magnesium can induce a decrease in chloride ingress. These aspects certainly need to be studied further.

Resistance to freeze/thaw with deicing salts

7.1. Characterization of the deterioration mechanism and the environment

7.1.1. Literature review on the deterioration mechanism

Exposure to freeze/thaw cycles in combination with deicing salts can cause scaling or flaking of the concrete surface. Although most researchers agree upon the general definition of this damage form, there is still a lot of discussion about the underlying deterioration mechanism. Boel (2006) gives a good summarizing overview of the existing theories to explain the phenomenon. However, before going into detail on them, it is necessary to give some background on the different mechanisms that play a role when concrete is exposed to freeze/thaw without deicing salts. These have been mentioned in Boel (2006) as well.

Freeze/thaw: First of all, there is the hydraulic pressure mechanism. It is quite generally known that freezing water comes along with an increase in volume of around 9%. As a consequence, the water that has not frozen yet, is being forced to move to other places. If this is not possible the evolving pressures can induce cracking. With the presence of an adequate air void system in the concrete where the still unfrozen water can move to, this problem can be avoided.

Secondly, there is the ice pressure mechanism. In contrast with the previous mechanism, non-frozen water would rather be attracted to the point where freezing occurs first. The freezing point of water in a pore is known for being inversely proportional to the pore radius. This means that the freezing of water will occur first in the larger pores. As soon as the water in a large pore is frozen, additional water is being transported from neighbouring small pores to the larger pores which makes the ice crystal grow in the large pore. The ice crystal can keep on growing due to a pressure difference between the large pore and the neighbouring smaller pores. This pressure difference is a consequence of the surface tension between the water and the ice. The excess pressure in the large pore is inversely proportional to the radius of the neighbouring smaller pore. When the resulting tensile stresses in the cementitious matrix would become too high, it can induce cracking. A lot also depends on the transport rate of the water (vapour) between pores. Normally the excess pressure is not very high in concrete. Thus, the ice pressure mechanism only becomes important in case of long freezing periods. If this

would be the case, the presence of a substantial amount of entrained air voids where the ice crystals can grow logically would avoid cracking.

The above mentioned two mechanisms are considered to be the most important ones for the meteorological conditions in the Netherlands [Visser (2002)]. Boel (2006) expects the same for the Belgium climate. In addition, Boel (2006) still mentions a few other mechanisms, such as the osmotic pressure principle. In accordance with the latter, the freezing of water in the larger air voids increases the alkalinity of the remaining water and an alkali concentration gradient is created. As a result, solution with a lower alkalinity is being attracted which reduces the alkali concentration in the larger air void again. Due to this dilution effect more ice can be formed again. With an adequate air void system present in the concrete, all water can move towards the air voids where it can freeze without problem. If not, the alkali concentration gradient will remain and the osmotic pressures will keep on rising. Eventually, this can cause cracking.

Freeze/thaw with deicing salts: Now, when looking at the available theories that are believed to explain the damage induced by freeze/thaw with deicing salts [Boel (2006), Copuroglu (2006)], there is sometimes a link with previously mentioned mechanisms when deicing salts are absent.

(i) For instance, there is the theory of Powers (1965) stating that salt scaling damage is induced by occurring hydraulic and osmotic pressures in combination with gradients in salt concentration.

(ii) On the other hand, the theory of Hansen (1963) states that the damage is due to an oversaturated salt solution in the larger pores. Salt crystals start to form and more salt molecules are attracted to the larger pores. The ongoing salt crystallization can impose excessive pressures on the cementitious microstructure.

(iii) Furthermore, there is the theory of Snyder (1965) which is based on the variation in freezing point for the water in the concrete due to a salt concentration gradient. Normally, the freezing point decreases with an increasing salt concentration. Logically, the inner part of the concrete contains water with a lower salt concentration and thus has a higher freezing point. As a consequence, both the inner part and the top layer of the concrete can freeze first. As temperature drops further on, the unfrozen layer in between, which contains water with a higher salt concentration will also start to freeze. The remaining unfrozen water comes under pressure and induces scaling of the frozen top layer.

(iv) More recently, the glue-spalling theory [Copuroglu (2006), Valenza and Scherer (2007a, b)] has been introduced. A decrease in temperature of the composite material (concrete + frozen solution) below the freezing point of the solution induces tensile stresses and subsequent cracking of the ice layer. This phenomenon is explained by the fact that the ice layer tends to contract much more than the concrete layer. The cracks in the ice layer penetrate into the underlying concrete and propagate according to a path parallel to the concrete surface [Gruyaert (2011)]. A literature review conducted by Valenza and Scherer (2007a, b) seems to indicate that the glue-spalling theory is the only theory that properly explains all known features (e.g. the existence of a pessimum salt concentration of 3%, the pressures involved, etc.) of salt scaling. A fully adequate explanation does not follow from the more traditional theories involving either hydraulic or crystallization pressures or thermal shock effects. Nevertheless, even the glue-spalling theory still remains subject to criticism

[Gruyaert (2011)]. While for the more traditional theories, the benefit of having an adequate (entrained) air void system in concrete has become quite clear in the meantime, this may be less evident for the glue-spalling theory. According to Valenza and Scherer (2007b), air entrainment improves the salt scaling resistance because it reduces bleeding and thus contributes to a stronger concrete surface. Moreover, the effective use of an air entraining agent has another benefit. Initial freezing in the air voids causes a suction in the pore fluid which compresses the porous matrix. This can reduce the damaging stresses due to the thermal expansion mismatch between the concrete surface and the ice layer on top of it.

Salt scaling resistance of fly ash and/or silica fume concrete: When concrete with fly ash is to be exposed to freeze and thaw in presence of deicing salts, one should keep in mind that any (surface) strength increase induced by the pozzolanic fly ash reaction can only be benefited from after 1-2 months of curing [Valenza and Scherer (2007a)]. It is also quite generally accepted that the presence of fly ash normally hinders the artificial entrainment of air to establish an adequate air void system in the concrete once hardened [Klieger and Gebler (1987), Neville (1996), Gebler and Klieger (1983), Pistilli (1983)]. This problem can normally be solved by increasing the applied dosage of AEA [Klieger and Gebler (1987), Whiting (1989), Gebler and Klieger (1983), Sturup and Hooton (1983), Virtanen (1990)]. However, even with an adequate air void system, the incorporation of fly ash usually has a negative effect on the concrete's salt scaling resistance. Salt scaling can only be reduced if concrete's 28-day strength equals around 40 MPa or if its actual W/C ratio is lower than 0.5 [Bilodeau et al. (1991), Bilodeau and Malhotra (1992)]. The amount of fly ash used also plays an important role. The application of up to 58% FA normally tends to reduce the water demand and postpone the initial setting time of the concrete [Bilodeau and Malhotra (1992)]. The availability of more water implicates that the actual W/C ratio is higher in the beginning which can result in excessive bleeding. The amount of bleeding was observed to increase with increasing fly ash addition [Neuwald et al. (2003)]. In this perspective, a 30% fly ash addition is considered as critical [Afrani and Rogers (1993), Whiting (1989)]. The latter phenomenon affects the surface strength in a negative way and can cause more salt scaling despite an adequate air void system. Given the slow pozzolanic reaction of the fly ash one should realize that this secondary cementitious material does not really belong to the binder system in the beginning. Thus, to evaluate the concrete's susceptibility to bleeding it is indeed the actual W/C ratio that is of importance at this stage and not the W/B ratio. Also note that the concrete's bleeding behaviour may differ with the finishing of the concrete surface. According to Janeva et al. (2002) lateral molded surfaces are less scaling resistant due the presence of extra moisture from bleeding. The scaling behaviour of troweled concrete surfaces was found to be very dependent on the curing precautions taken in the first hours after casting. According to Neuwald et al. (2003) promoting the evaporation of bleeding water in the first six hours after casting before sealing the concrete with plastic sheets normally substantially improves the scaling resistance of the surface. This procedure is far better than an immediate sealing of the concrete because bleeding water that cannot evaporate results in a higher W/C ratio of and thus a lower strength of the surface layer [Afrani and Rogers (1993)]. The effect of incorporating silica fume in the concrete is not unambiguous. Concrete containing this by-product normally has an improved salt scaling resistance which is

attributed to the resulting strength increase [Valenza and Scherer (2007a)]. For concrete with a W/C ratio ≥ 0.4 and strength ≥ 40 -45 MPa, there is significant improvement [Jacobsen et al. (1991), Aitcin and Pigeon (1986)]. If characterized by a W/C ratio < 0.35 and strength of at least 40-45 MPa, the presence of the silica fume does not really have a notable effect on the salt scaling resistance [Sellevold and Farstad (1991), Sorensen (1983), Gagne et al. (1991)]. Increasing the silica fume content in air entrained concrete while maintaining the same workability with a high-range water-reducer causes more scaling. Since the silica fume initially acts as inert filler until the pozzolanic reaction starts, the initial W/C ratio increases with increasing silica fume percentages. As a consequence there will be more bleeding and a weakening of the surface [Valenza and Scherer (2007a)]. As such, SF concrete behaves in a similar way as FA concrete.

Although only mentioned for BFS concrete in Valenza and Scherer (2007a), there is another mechanism that can affect FA and SF concrete's salt scaling resistance in a negative way, being carbonation. Also for the latter concrete types Aragonite and Vaterite, the two polymorphs of CaCO_3 that are 20% and 90% more soluble than Calcite [Plummer and Busenberg (1982)] can be present. Their preferential dissolution when exposed to moisture degrades the surface [Valenza and Scherer (2007a)]. Moreover, CH is being consumed during the pozzolanic FA and SF hydration reactions causing more C-S-H carbonation and a coarsening of the pore structure (Section 5.1.1, Section 5.4.2). Carbonation exposed BFS concrete that is subject to the same phenomena, has a lower salt scaling resistance than carbonation exposed OPC concrete. The depth of scaling was also found to be equivalent to the depth of carbonation which again shows that the surface strength determines the amount of scaling damage [Stark (1997), Utgenannt (1999)].

In conclusion, salt scaling of a well air entrained FA and SF concrete is to a large extent promoted by a weakening of the concrete surface either induced by bleeding or carbonation. Both phenomena need to be kept under control to achieve an adequate salt scaling resistance.

7.1.2. Characterization of the concrete environment

An environment with exposure to freeze-thaw attack in presence of deicing salts normally belongs to either exposure class XF2 or XF4 [NBN EN 206-1 (2000)]. The former exposure class relates to concrete characterized by moderate water saturation in contact with airborne deicing salts, while the latter comprises highly saturated concrete in direct contact with deicing salts. Exposure class XF4 is obviously more critical. Therefore, the proposed HVFA and FA+SF concrete compositions have been specifically designed for this exposure class. With proof of a satisfactory durability performance in the corresponding environment, the suggested compositions could qualify for use in:

- road and bridge decks exposed to deicing salts
- concrete surfaces exposed to direct spray containing deicing salts and freezing
- splash zones of marine structures exposed to freezing

The required durability performance of these non-traditional concrete compositions with type II additions has been evaluated in a way similar to the equivalent performance concept of NBN B15-100 (2008). In other words, the deicing salt scaling resistance of the HVFA and FA+SF concrete compositions has been compared with the salt scaling resistance of a suitable

reference concrete. Therefore, the concrete compositions under investigation and the reference concrete were subjected to an (accelerated) salt scaling test similar to the one described in Annex D of NBN EN 1339 (2003) for conformity control of concrete paving flags. In order to have equivalent performance, the recorded mass losses per unit area (Δm) after 28 severe freeze/thaw cycles should comply with the applicable criterion of acceptance imposed by NBN B15-100 (2008) (Equation 7-1).

$$\Delta m_{\text{concrete to be tested}} \leq 1.2 \times \Delta m_{\text{reference concrete}} \quad (7-1)$$

As already pointed out in Section 4.2.2 concrete compositions T(0.45) and T(0.45)A are considered to be the reference concrete types for exposure class XF4. They were chosen as reference concrete to assess equivalent performance.

Apart from this comparison with a reference concrete, it was decided to verify whether the proposed concrete compositions also meet the criterion of acceptance imposed by NBN EN 1339 (2003) itself. Therefore, the average mass loss at the end of the test should not exceed 1.0 kg/m² and not one individual result can exceed 1.5 kg/m². Note that these are very severe criteria which may not be realistic for every concrete application (e.g. quay walls) apart from the concrete paving flags mentioned in the standard.

Note that the test method applied is an accelerated way of characterizing concrete's salt scaling resistance. Freeze/thaw cycles with temperatures ranging from -18 to 20 °C within a 24 h timeframe are rather severe and do not occur on a regular basis in practice, at least not in Belgium. Hourly air temperature data collected and provided by the Royal Meteorological Institute (KMI) between January 1999 and December 2008 for five weather stations in Belgium (Koksijde (WS1), Kleine Brogel (WS2), Zaventem (WS3), Florennes (WS4) and Luxembourg (WS5)) clearly demonstrate this (Table 7.1). True, the timeframe considered may be rather short. The winters of the last couple of years were less severe, so it probably would have been better to look at a larger time period in order to include more extreme temperatures. Nevertheless, the 10-year time period at least gives a first indication.

The minimum temperature T_{\min} in air never reached -18 °C for neither of the locations considered. Moreover, 28 subsequent freezing days (with T_{\min} in air ≤ 0 °C) or 28 subsequent freeze/thaw (F/T) cycles (with T_{\min} in air ≤ 0 °C and T_{\max} in air > 0) also almost never occur. Knowing that temperatures measured at ground level – the more relevant temperatures with respect to salt scaling – are 3 to 5 °C lower than air temperatures measured ± 1.5 m above ground [KMI (2010)] and that significant salt scaling damage only occurs during F/T cycles with minimum temperatures below -10°C [Valenza and Scherer (2007a)], the provided temperature data were converted to the expected temperatures at ground level and analysed more in detail. Only two out of five weather stations (WS2 and WS5) recorded minimum temperatures at ground level below -18°C. Although a maximum of over 100 F/T cycles were observed at each location per year between 1999 and 2008, the number of subsequent F/T cycles was always less than 28 (max. 19 at WS2). The number of days per year that temperature dropped below the critical -10 °C varied with the geographical location and ranges between 5 and 22. The number of subsequent freezing days with $T_{\min} \leq -10$ °C is even lower (between 3 and 9). A day during which T_{\min} drops below -10 °C does not necessarily correspond with one F/T cycle since thawing may not occur within 24 hours. When

considering only the actual critical F/T cycles at ground level (with $T_{\min} \leq -10$ °C and $T_{\max} > 0$ within 24 hours), it can be concluded that these usually occur once a year and never on a subsequent basis. Thus, it would take no less than 28 years before concrete would be exposed to 28 critical F/T cycles at WS1, WS3, WS4 and WS5. Weather station WS2 seems to be the only location for which this simplified assumption would not be valid.

Table 7.1. Analysis of the temperature data measured by the Royal Meteorological Institute (KMI) at weather stations WS1, WS2, WS3, WS4 and WS5 between 1999 and 2008.

| | WS1 | WS2 | WS3 | WS4 | WS5 |
|---|-------|-------|-------|-------|-------|
| T_{\min} in air | -7.4 | -13.5 | -9.1 | -12.0 | -14.0 |
| Max. number of days per year with T_{\min} in air ≤ 0 °C | 48 | 78 | 57 | 75 | 83 |
| Max. number of subsequent days per year with T_{\min} in air ≤ 0 °C | 14 | 17 | 14 | 21 | 28 |
| Max. number of F/T cycles in air per year with $T_{\min} \leq 0$ °C and $T_{\max} > 0$ | 45 | 70 | 55 | 65 | 69 |
| Max. number of subsequent F/T cycles in air per year with $T_{\min} \leq 0$ °C and $T_{\max} > 0$ | 14 | 14 | 13 | 13 | 14 |
| T_{\min} at ground level (= T_{\min} in air - 5°C) | -12.4 | -18.5 | -14.1 | -17.0 | -19.0 |
| Max. number of days per year with T_{\min} at ground level ≤ 0 °C | 141 | 159 | 135 | 157 | 170 |
| Max. number of subsequent days per year with T_{\min} at ground level ≤ 0 °C | 31 | 67 | 30 | 67 | 83 |
| Max. number of F/T cycles at ground level per year with $T_{\min} \leq 0$ °C | 113 | 122 | 102 | 102 | 105 |
| Max. number of subsequent F/T cycles at ground level per year with $T_{\min} \leq 0$ °C | 16 | 19 | 17 | 13 | 12 |
| Max. number of days per year with T_{\min} at ground level ≤ -10 °C | 5 | 22 | 9 | 16 | 20 |
| Max. number of subsequent days per year with T_{\min} at ground level ≤ -10 °C | 3 | 7 | 5 | 6 | 9 |
| Max. number of F/T cycles at ground level per year with $T_{\min} \leq -10$ °C | 1 | 5 | 1 | 1 | 1 |
| Max. number of subsequent F/T cycles at ground level per year with $T_{\min} \leq -10$ °C | 0 | 2 | 0 | 0 | 0 |

In addition, it must be emphasized that these so-called critical F/T cycles are still less severe than the ones proposed in NBN EN 1339 (2003) with surface temperatures ranging between -18 and 20 °C within 24 h. Nevertheless, although the accelerated laboratory salt scaling test proposed in the European standard turns out unrealistic with respect to the temperature regime applied, proof of equivalent performance cf. NBN B15-100 (2008) for concrete with type II additions not conforming to the k-value concept (e.g. HVFA concrete and FA+SF concrete), can only be delivered by means of this accelerated test method. Realistic field tests are not commonly accepted. In North-America, Malhotra and Mehta (2005) encountered a very

similar problem during documenting the salt scaling resistance of HVFA concrete. HVFA concrete pavement in Wisconsin (US) and sidewalk sections in Halifax (Canada) made with HVFA concrete and subjected to deicing salts, exhibited a good performance in the field [Malhotra and Mehta (2005)]. On the other hand, more salt scaling deterioration has been observed for HVFA concrete under more severe laboratory conditions cf. ASTM C672 (2003). Despite this known discrepancy between the output of field and laboratory testing and given the fact that the latter is the only output currently being accepted, the proposed HVFA and FA+SF concrete compositions were designed to pass the severe laboratory experiment.

7.2. Research methodology

Within the scope of this research, HVFA and FA + SF concrete compositions were developed that should meet the salt scaling criterion of 1 kg/m² based on the chosen air content in its fresh state. Indeed, quite some attention needs to be paid to the initial air content of the concrete compositions under investigation. One should know that quite some differences exist between concrete standards regarding the required minimum air content in the fresh state to achieve an adequate air void system in the hardened state and an acceptable salt scaling resistance. According to the European standard NBN EN 206-1 (2000), concrete exposed to freeze/thaw in combination with deicing salts is preferably air entrained to achieve an air content of at least 4% in the fresh state. According to the Belgian standard NBN B 15-001 (2004) artificial air entrainment is also not mandatory. As a consequence, it is almost never used in Belgium. If applied, it should relate to the maximum aggregate size of the concrete. For a maximum nominal aggregate size of 16 mm, it specifies an air content of at least 5%. The American standard ACI 201.2R (2008) also takes into account the higher air content requirements of concrete mixtures with higher paste contents due to smaller nominal maximum aggregate sizes. However, also the severity of the exposure is of importance in this standard. A distinction is made between moderate and severe exposure. Exposure conditions are considered to be severe whenever deicing salts are present. In such an environment, an air content of 6 to 7% is recommended for a maximum nominal aggregate size of 16 mm, while 5 to 5.5% of air is only sufficient in the case of moderate exposure (excl. deicing salts) for the same aggregate size. Nevertheless, the recommendations of ACI 201.2R (2008) are not binding. Local conditions and experience with specific mixtures and procedures could still warrant other values. According to some authors the air-to-paste (A/P) ratio should be used to evaluate the concrete's air void system and not the air content (which is the air-to-concrete ratio). An air void system having a total volume of about 18 to 20% of the paste volume normally should protect the paste against freeze/thaw damage [Pinto (2001), Mielenz et al. (1958)]. All these different criteria demonstrate that quite some divergence on this matter exists. This issue certainly needs to be addressed before actually exposing the concrete to F/T cycles in combination with deicing salts.

In a first research phase, the air void system in the hardened state (air content, spacing factor, specific surface and average chord length) was characterized by means of microscopic analysis on thin sections and air void analysis conforming to ASTM C457 (2010). It should reveal which of the above mentioned criteria regarding the air content in the fresh state indeed creates an adequate air void system in the hardened state.

In a second research phase, the salt scaling resistance of the concrete's cast surface was tested according to the procedure described in NBN EN 1339 (2003). The effectiveness of the applied air entraining agent (AEA) in combination with fly ash (+ silica fume) was investigated for fly ashes from two different sources.

In a third research phase, it was investigated whether the addition of an AEA can make steel reinforced HVFA and FA+SF concrete more susceptible to other important deterioration mechanisms that strongly depend on the permeability of the concrete, e.g. steel corrosion. In the literature, this impact has seldomly been studied. When located in a XF4 environment, corrosion can be initiated by the chlorides from deicing salts entering the concrete or by concrete carbonation due to a constant exposure to exhaust fumes from motorized traffic. To evaluate the impact of air entrainment on the chloride- or carbonation-induced corrosion resistance, the material needs to be exposed to chlorides and CO₂ concentrations as present in the natural environment. Since this approach is usually quite time consuming, two influencing parameters (water penetrability and gas permeability) were studied instead of performing the required realistic chloride diffusion and carbonation tests. With respect to carbonation-induced corrosion, the accessibility to water and the permeability to air are very relevant parameters to be studied [Lammertijn and De Belie (2008)]. The same holds true for chloride-induced corrosion.

7.3. Curing and sample preconditioning

The following concrete compositions were experimentally tested: mixtures T(0.45), T(0.45)A, F(1)50, F(1)50A, F(2)50, F(2)50A, F(1)SF, F(1)SFA, F(2)SF and F(2)SFA. A series of 400 × 400 × 100 mm³ concrete slabs and cubes with a side length of 150 mm were cast per mixture. After casting, the specimens were kept at a constant temperature and relative humidity of 20 °C and 95%, respectively. Demoulding took place the next day whereupon the slabs and cubes were stored again under the same conditions until the age of testing. All tests were conducted after 28 and 91 days of curing to see whether the formation of additional hydration products due to the fly ash reaction can influence the air void system in the hardened state.

The specimens used for microscopic analysis on thin sections, air void analysis, freeze-thaw testing and measurement of the gas permeability were all taken from the slabs. At the initial stage of the testing program, the vacuum saturation tests were performed on cylinders taken from the cubes, while the capillary sorption tests were done directly on the cubes. However, in the course of the experiments performed on HVFA concrete samples with the given geometries, a more in depth literature survey (Section 7.6.2) on the subject revealed that it would be more interesting to subject cylindrical specimens similar to the ones applied in the freeze-thaw test, to a capillary sorption test first and then perform a vacuum saturation test on the same samples afterwards. As a result, the saturation degree of the samples at the start of the freeze-thaw test as well as its evolution in the course of the capillary sorption test would be known (Section 7.6.2). The latter approach was followed to some extent for the HVFA concrete and fully for the FA+SF concrete.

Depending on the procedure followed, the sample conditioning prior to testing somewhat differed. When following the first approach, the capillary water uptake, the permeable porosity and the gas permeability were measured after oven drying to constant mass (< 0.1%

mass change within 24 hours) at 40 °C. Usually, this took about 14 days. Afterwards, the measurements were repeated on the same specimens after oven drying at 105 °C. The latter drying procedure removes all capillary and gel water from the concrete [Audenaert (2006)]. A pre-drying temperature of 105 °C was also proposed by Boel et al. (2008) to successfully measure concrete's gas permeability at a water saturation degree of 0%. It is noted that drying at 105°C is sometimes subject to criticism as the method may induce pore collapse and a modification of the stoichiometry and density of the calcium silicate hydrate gels (C-S-H) [Thomas et al. (1999), Jennings (2000)]. However, the same drying temperature has been successfully applied to measure the total porosity of concrete by means of a hydrostatic weighing technique after vacuum saturation. This porosity seems to be only slightly higher in comparison with the one deduced from experimental water vapour desorption isotherms [Baroghel-Bouny (2007)]. Compared to total porosities calculated from phase assemblage of the present hydrates, the measured porosities through hydrostatic weighing and oven drying at 110 °C are also only slightly higher [Lothenbach et al. (2008)]. Nevertheless, it needs to be noted that in addition to total porosity, pore connectivity and size are also important for the transport properties of concrete. Despite the successful use of the higher drying temperature according to the literature, it was decided to first measure the capillary water uptake, the permeable porosity and the gas permeability after pre-drying at a lower temperature (40 °C), before measuring the same parameters after pre-drying at 105 °C.

In case of the second testing approach, the cylinders for the combined capillary sorption-vacuum saturation experiment as well as the cylinders for a gas permeability test as a function of the saturation degree were treated in accordance with the pre-conditioning procedure imposed by ASTM C1585-04^e (2007) for the American capillary sorption test. At the proper testing age (either 28 or 91 days), the samples were removed from the curing chamber and stored in a climate room at 50 °C and 80% RH for 3 days. Afterwards, each specimen was placed in a separate sealable container in a way that enables a free flow of air around each specimen. The sealed containers were stored at 20 °C for 18 days until the start of the actual combined capillary sorption-vacuum saturation experiment and the gas permeability test. The output of this gas permeability test is different from the one mentioned earlier on. It measures the apparent gas permeability coefficient as a function of the concrete's saturation degree and not merely after subsequent pre-drying at two temperatures (40 °C and 105 °C).

7.4. Characterization of the concrete's air void system

7.4.1. Evaluation in the fresh state: time dependent monitoring of air content

All the air contents that have been tabulated until now in Tables 4.5, 4.8, 4.9, 4.10, 4.12 and 4.16 are initial air contents. They were recorded approximately 15 min after mixing with a TESTING Air entrainment meter (capacity: 8 l). The test procedure followed was similar to the one described in NBN EN 12350-7 (2009).

Besides the measurement of the initial air content (Tables 4.5, 4.8, 4.9, 4.10, 4.12, 4.16), a time dependent monitoring of the air content was also considered on small batches (40 l) of each air entrained HVFA concrete mixture using the same SP dosage of 4.0 ml/kg B. This was the dosage needed to achieve the highest slump class for at least one of the mixtures that was studied on small scale (a 40 l batch). This dosage was then used for all the other mixtures

as well. For the air entrained FA + SF concrete the time dependent monitoring of the fresh air content was done on the same (large) batches of concrete (175 l batches) that were used for the manufacturing of all the plates and cubes required for further testing in the hardened state. The applied test procedure was similar to the one followed by Zhang (1996). First, the initial air content was determined 15 min after mixing. Then, the remaining concrete was mixed for 5 min and allowed to stand for 5 min. This procedure was repeated twice whereupon the air content (cf. NBN EN 12350-7 (2009)) and slump (cf. NBN EN 12350-2 (2009)) were measured again 60 min after the mixing. In addition, Zhang's experimental procedure was extended with an extra measurement of the air content and slump after 120 min.

7.4.2. Evaluation using microscopic analysis on thin sections

Thin sections were prepared and analyzed in accordance with the procedure described in Section 5.4.5. The microscopic analysis enabled a qualitative study of the air void system. Per concrete mixture and curing period, a series of photos was taken of the thin sections as observed under the microscope. Per thin section, 3 photos were taken near the cast surface and 3 photos near the saw cut surface. This resulted in 6 photos per thin section and thus 18 photos per concrete mixture at each age. Since visual observation showed no obvious differences between them, only one representative photo of each concrete mixture was included in this thesis.

7.4.3. Evaluation using automated air void analysis

A more quantitative air void analysis is possible with the RapidAir 457 apparatus. In accordance with ASTM C457 (2010), the linear traverse method was used to determine the air content and air void distribution of the hardened concrete. The test was performed on cylindrical specimens ($n = 4$, Diameter (\varnothing) = 80 mm, Height (H) = 20 mm). The technique required a careful polishing of the sample surfaces since scratches are to be avoided and air voids must have sharp edges [Jakobsen et al. (2006)]. Therefore, the following polishing procedure was used. First, the sample surfaces were mechanically flattened. Then, the surfaces were subsequently treated with 8 different wet diamond polishing pads (grit 50, 100, 200, 400, 800, 1500, 3000 and 8000). Before using each polishing pad, a raster was drawn onto the surfaces with chalk. Each time, the polishing with one pad continued until the chalk raster had completely disappeared from the surface.

Contrast enhancement was realized as follows: the polished surfaces were coloured with black ink and white BaSO₄ powder (maximum particle size $\leq 2 \mu\text{m}$) was distributed on top to fill the air voids. After removing the excess powder with a steel blade, the specimens were ready for testing. The threshold grey level value for analysis equaled 221 on a 0-256 scale. All samples were analyzed in two perpendicular directions using 10 probe lines per frame with a total traverse length of 17733 mm and a scanned area of $50 \times 50 \text{ mm}$. With the recorded total chord length of air voids T_a (mm) and paste T_p (mm), the total surface distance traversed across T_{tot} (mm), the total number of air void chord lengths N (-) and the paste content p (%) for each concrete composition, the concrete's air void system can be fully characterized. Air contents $A_{\%}$ (%), specific surfaces α (mm^{-1}), spacing factors L_S according to Powers (μm) and average chord lengths l_m (mm) were calculated using Equations 7-2, 7-3, 7-4 and 7-5:

$$A_{\%} = \frac{T_a}{T_{\text{tot}}} \times 100 \quad (7-2)$$

$$\alpha = \frac{4N}{T_a} \quad (7-3)$$

$$L_s = \frac{T_p}{4N} \text{ (for } p/A_{\%} \leq 4.33) \text{ or } L_s = \frac{3}{\alpha} \left[1.4 \left(1 + \frac{p}{A_{\%}} \right)^{1/3} - 1 \right] \text{ (for } p/A_{\%} > 4.33) \quad (7-4)$$

$$l_m = \frac{T_a}{N} \quad (7-5)$$

7.5. Salt scaling resistance

Deicing salt scaling resistance was evaluated in accordance with NBN EN 1339 (2003). Cylinders ($\varnothing = 100$ mm, $H = 50$ mm) were glued into a piece of insulated PVC tube with either the casting surface or troweled surface upwards. A 5 mm thick water layer was put on top of the cylindrical test surfaces for at least 72 h to check for leakages. Next, the water layer was replaced with a 5 mm thick 3% NaCl solution after which the specimens were subjected to 28 severe freeze/thaw cycles in a freezing chamber where temperatures ranged from -18 to 20 °C in 24 h (Figure 7.1). The applied 3% corresponds with the pessimum concentration with respect to salt scaling which is independent of the solute used [Valenza and Scherer (2007a)]. Every 7 d, the scaled material was collected, dried at 105 °C and weighed to determine the mass loss per unit area (Δm).

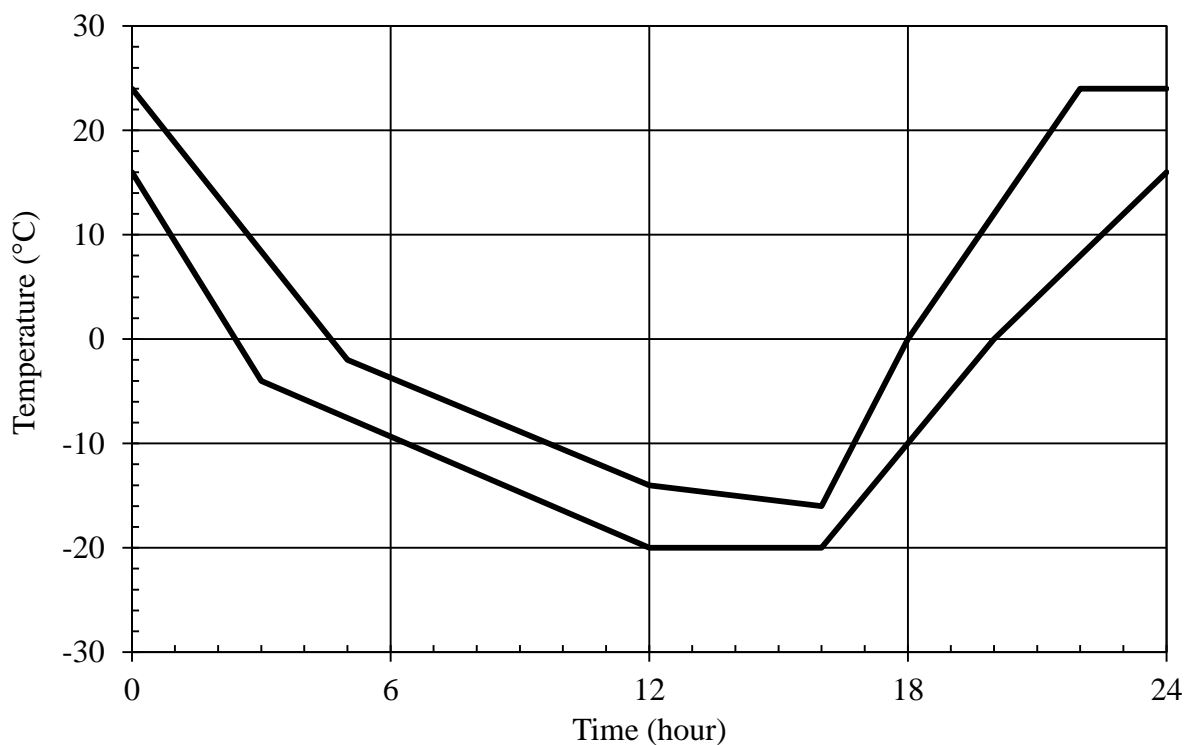


Figure 7.1. Temperature regime of a 24 hour freeze-thaw cycle during an accelerated freeze-thaw test with deicing salts cf. NBN EN 1339 (2003).

7.6. Transport properties

7.6.1. Capillary sorption

The first testing approach implied an investigation of the capillary sorption behaviour of the tested non-air entrained and air-entrained HVFA concrete mixtures by means of a test method similar to the one described in the Belgian Standard NBN B15-217 (1984). Note that the applied 40 °C pre-drying temperature is only slightly different from the pre-drying temperature (50 °C) prescribed in ASTM C 1585 – 04e (2007) to measure capillary sorption. On the other hand, the Belgian standard does not impose restrictions with respect to the relative humidity during pre-drying as the American standard does (80% RH). After weighing the oven dried cubes ($n = 3$, $H = 150$ mm), they were put on rods in a water bath in such a way that they were immersed for 5 mm. To obtain unidirectional flow, the sides adjacent to the inflow face were covered with a self-adhesive aluminium tape. The experiment was carried out in a climate chamber with a constant temperature of 20 ± 2 °C and a relative humidity of $60 \pm 5\%$. For each specimen and pre-drying temperature (40 °C and 105 °C), the mass increase as a function of time (after 1.5h, 3h, 6h, 1d, 2d, 7d, 9d and 14d) was measured and the corresponding capillary water uptake per unit area was calculated. Similar to the calculation approach prescribed by ASTM C 1585 – 04e (2007) an initial and secondary rate of water absorption were calculated. In accordance with the American standard, the absorption parameter I (mm) was obtained by using the following equation (Equation 7-6):

$$I = \frac{m_t}{a_w \cdot d_w} \quad (7-6)$$

with m_t , the change in specimen mass (g) at time t (s), a_w , the exposed area of the specimen (mm^2), d_w , the density of the water with neglectance of its temperature dependency (0.001 g/mm^3). It should be noted that the absorption I does not correspond with the capillary rise in the specimen. To have a first indication of the latter, only the area of the pores present in the exposed specimen surface would need to be considered in Equation 7-6 and not the full area. Even then, a lot would still depend on the original saturation degree of the specimen before an adequate estimation of the capillary rise during the test can be made.

The initial rate of water absorption S_i ($\text{mm}/\sqrt{\text{s}}$) corresponds with the slope of the linear regression line that is obtained by plotting the water absorption I against the square root of time t ($\sqrt{\text{s}}$). To determine this initial rate of absorption all the data points until the measurements after 6h were used. The secondary rate of water absorption S_s ($\text{mm}/\sqrt{\text{s}}$) was also the result of a linear regression, only now performed on the data points collected between 1d to 7d. The properties considered during the comparison between non-air entrained and air entrained HVFA concrete comprise the two rates of water absorption and the water absorption at the end of the test after 14 days, and this both after subsequent pre-drying at 40°C and 105°C.

The second testing approach required a capillary sorption test which corresponded even more with the test method described in ASTM C 1585 – 04e (2007). As already pointed out in Section 7.3 sample pre-conditioning was somewhat different and the sample geometries were no longer cubes with a 150 mm side but small concrete cylinders ($n = 4$, $\varnothing = 100$ mm, $H = 50$

mm) of which either a cast or troweled surface was to be put in contact with water for 9 days. The mantle surfaces of the cylinders were covered with adhesive aluminium tape to ensure unidirectional flow. Their top surfaces were covered with a thin plastic plate during the test. The samples were weighed after 1 min, 5 min, 10 min, 20 min, 30 min, 1h, 2h, 3h, 4h, 5h, 6h, 1d, 2d, 3d, 6d, 7d, 8d and 9d. The output of the experiment comprised again the initial and secondary rate of water absorption as well as the water absorption after 9 days. This test procedure was adopted for another series of non-air entrained HVFA concrete (F(1)50-2, F(2)50-2) and air entrained HVFA concrete (F(1)50A-2, F(2)50A-2). The latter two compositions were believed to have a more adequate air void system and salt scaling resistance than the air entrained HVFA compositions that were tested in the beginning (F(1)50A, F(2)50A). The non-air entrained and air entrained FA + SF concrete compositions were also subjected to the capillary sorption experiment conforming to ASTM C 1585 – 04e (2007).

7.6.2. Permeable porosity and degree of saturation

For the first testing approach, vacuum saturation tests were performed on cylindrical concrete specimens ($n = 9$, $\varnothing = 100$ mm, $H = 50$ mm) of composition T(0.45), T(0.45)A, F(1)50, F(1)50A, F(2)50 and F(2)50A. After measuring the oven dry masses ($m_{d\ 40^{\circ}\text{C}/105^{\circ}\text{C}}$), the samples were put in a tank where a vacuum with a residual pressure of 2.7 kPa was created for 2.5 h. Then, water was introduced at a rate of 50 mm/h until complete submersion of the samples. Subsequently, air pressure was restored and the samples were kept under water for 24 h. A similar vacuum saturation technique is mentioned in ASTM C 1202 – 05 (2005). The procedure described here is in accordance with the Belgian Standard NBN B05-201 (1976) and allows the calculation of a permeable porosity $\varphi_{40^{\circ}\text{C}/105^{\circ}\text{C}}$ (%) using Equation 7-7.

$$\varphi_{40^{\circ}\text{C}/105^{\circ}\text{C}} = \frac{m_{s\ 40^{\circ}\text{C}/105^{\circ}\text{C}} - m_{d\ 40^{\circ}\text{C}/105^{\circ}\text{C}}}{m_{s\ 40^{\circ}\text{C}/105^{\circ}\text{C}} - m_{l\ 40^{\circ}\text{C}/105^{\circ}\text{C}}} \times 100 \quad (7-7)$$

Within this formula, $m_{l\ 40^{\circ}\text{C}/105^{\circ}\text{C}}$ and $m_{s\ 40^{\circ}\text{C}/105^{\circ}\text{C}}$ stand for the mass under water and the water saturated mass after vacuum saturation, respectively. Drying at 105 °C is in correspondence with the drying procedure described in ASTM C 642 – 06 (2006). In the literature, similar hydrostatic weighing techniques have been used successfully to measure porosity [Baroghel-Bouny (2007), Lothenbach et al. (2008)]. All methods required oven drying at an elevated temperature ranging from 105 °C to 110 °C and were published in test method recommendations [AFPC-AFREM (1997)] and national standards [NBN B05-201 (1976), SN 505 262/1 (2003)].

The second testing approach basically consisted of the same experimental procedures. Two major differences are worth mentioning. Firstly, the specimens used for this test are the very same cylinders that were used for the 9-day capillary sorption test conforming to ASTM C 1585 – 04e (2007). Secondly, only one drying temperature, i.e. 105 °C, was taken into consideration. At the end of the capillary sorption test, the self-adhesive aluminium tape was removed from the mantle surfaces of the cylinders. As such, the samples were stored in the vacuum tank where they were vacuum saturated in accordance with the above mentioned

procedure. After determining their mass under water m_1 as well as their water saturated mass m_s on the next day, the samples were dried to constant mass (mass loss $\leq 0.1\%$ in 24h) at 105°C for approximately 10 days whereafter the whole vacuum saturation procedure, including the weighing step after 24h, was repeated. As a result, two different permeable porosities can be calculated using Equation 7-7. The first permeable porosity $\phi_{105^\circ\text{C}}$ (%) was calculated by implementing the m_1 and m_s values measured during the first vacuum saturation (vac1) and thus prior to drying at 105°C in Equation 7-7. The second permeable porosity $\phi_{105^\circ\text{C}}$ (%) was obtained by using the m_1 and m_s values measured during the second vacuum saturation (vac2) and thus after drying at 105°C . Comparison between these two porosities was considered important especially when studying air entrained concrete. If drying at 105°C could induce concrete micro-cracking to some extent, these small cracks could establish pathways between the normally isolated air voids present in a highly air entrained concrete. As a consequence, more water would be absorbed during a vacuum saturation test after pre-drying at 105°C . The corresponding permeable porosity would also be substantially higher.

The main advantage of using the same samples for both the capillary sorption and vacuum saturation experiments lies in the fact that the latter tests enable the calculation of the concrete's degree of saturation (DoS, %) during the capillary sorption measurements. This can be done by means of Equation 7-8:

$$\text{DoS} = \frac{m_{t\text{DoS}} - m_{d105^\circ\text{C}}}{m_{s\ 105^\circ\text{C}} - m_{d105^\circ\text{C}}} \times 100 \quad (7-8)$$

with $m_{t\text{DoS}}$, mass (g) of the sample without the adhesive aluminium tape at time t (s), $m_{d\ 105^\circ\text{C}}$, mass (g) of the sample after oven drying at 105°C , $m_{s\ 105^\circ\text{C}}$, water saturated mass (g) of the sample after the first vacuum saturation. Moreover, the degrees of saturation recorded at the start of the capillary sorption tests will more or less match with the degrees of saturation of the cylinders to be subjected to the accelerated salt scaling test. As mentioned in Section 7.3 their geometry and pre-conditioning was the same. Performing a combined capillary sorption and vacuum saturation test on the same samples to evaluate concrete's degree of saturation at the start of a salt scaling test is a procedure similar to the one proposed by Fagerlund (1977) to determine the critical degree of saturation of a concrete exposed to freeze/thaw (without deicing salts). Unlike the particular deterioration mechanism studied by Fagerlund (1977), damage induced by freeze/thaw attack in combination with deicing salts normally does not depend so much on a critical degree of saturation, but on a critical freezing temperature [*fib* Bulletin 34 (2006), Petersson (2004)]. Nevertheless, it remains worthwhile investigating whether the degree of saturation at the start of the salt scaling test can be considered as similar for non-air entrained and air entrained concrete.

7.6.3. Gas permeability

With respect to the first testing approach, the O_2 flow rate Q (ml/s) and the corresponding apparent oxygen permeability k_a at 2 bar pressure were measured on cylindrical specimens ($n = 3$, $\text{Ø} = 150$ mm, $H = 50$ mm) using the 'Cembureau' permeameter mentioned in RILEM TC 116-PCD (1999). This was done both after pre-drying at 40°C and 105°C .

Before each measurement, a certain waiting period (\pm half hour) was required to obtain a steady gas flow rate Q (ml/s) through the three cylindrical specimens. The apparent gas permeability k_a of each mixture was calculated by means of Equation (7-9) [Boel (2006)], without performing a Klinkenberg correction [Klinkenberg (1941)].

$$k_a = \frac{2Q}{A} \frac{\mu L P_a}{(P^2 - P_a^2)} \quad (7-9)$$

The other parameters in Equation 7-9 are: the cross-sectional area A of the specimen (m^2), the thickness L of the specimen (m), the dynamic viscosity μ of the fluid ($2.02 \times 10^{-5} \text{ Nsm}^{-2}$ for O_2 at 20°C), the atmospheric pressure P_a (bar) and the absolute inlet pressure P (2 bar). The apparent gas permeability after pre-drying at two different temperatures was measured for concrete mixtures T(0.45), T(0.45)A, F(1)50, F(1)50A, F(2)50 and F(2)50A.

The gas permeability of the FA + SF concrete compositions was evaluated in accordance with the second testing approach. After being preconditioned in the same way as the samples used for the combined capillary sorption and vacuum saturation test, the cylindrical specimens ($n = 3$, $\varnothing = 150 \text{ mm}$, $H = 50 \text{ mm}$) were vacuum saturated while following the test procedure and the subsequent weighing steps described in Section 7.6.2. Then, the cylinders were dried in three steps, successively at 80°C (step 1, step 2) and 105°C (step 3), until all capillary and gel water was removed. After each drying phase, the flow rate Q (ml/s) and the corresponding apparent oxygen permeability k_a was measured at 2 bar pressure and calculated from Equation 7-9. The weighing of the samples at each drying step made it possible to calculate their degree of saturation S_x (%) using Equation 7-10.

$$S_x = \frac{m_{Sx} - m_{S3}}{m_s - m_{S3}} \times 100 \quad (7-10)$$

In this equation m_{Sx} , m_s and m_{S3} correspond with the mass (g) at drying step x (1, 2 or 3), the water saturated mass after vacuum saturation and the completely dry mass at drying step 3, respectively. By using Equation 7-9 and 7-10 together, the apparent gas permeability k_a can be expressed as a function of the concrete's saturation degree. A summary of the entire test procedure is shown in Table 7.2. Apart from the sample pre-conditioning, this test procedure is very similar to the method originally developed by Boel (2006). For comparison between mixtures, mainly the apparent gas permeability of the completely dry samples (S_{S3}) was considered.

Table 7.2. Experimental procedure to determine concrete's apparent gas permeability k_a as a function of its saturation degree (cf. Boel (2006) from day 21 on).

| Day | Instruction | Measurement |
|-----|--|-------------|
| 0 | Sample preconditioning at 50°C and 80% RH | |
| 3 | Sample storage in separate sealed containers at 20°C and 60% RH | |
| 21 | Removal from sealed containers, vacuum saturation cf. Section 7.6.2 | |
| 22 | Weighing | m_s |
| | Hydrostatic weighing | m_l |
| | Covering cylinders' mantles with Aluminium foil, weighing, drying at 80 °C | |
| 23 | Covering cylinders completely with Aluminium foil, drying at 80 °C | |
| 24 | Removing from oven, storing in climate room (20 °C and 60% RH) | |
| 25 | Weighing | m_{S1} |
| | First gas permeability test | k_{a1} |
| | Drying at 80 °C | |
| 28 | Covering cylinders completely with Aluminium foil, drying at 80 °C | |
| 29 | Removing from oven, storing in climate room (20 °C and 60% RH) | |
| 30 | Weighing | m_{S2} |
| | Second gas permeability test | k_{a2} |
| | Drying at 105 °C | |
| 35 | Removing from oven, storing in climate room (20 °C and 60% RH) | |
| 36 | Weighing | m_{S3} |
| | Third gas permeability test | k_{a3} |

7.7. Results and discussion

Note that all standard deviations mentioned in tables or shown by means of error bars in figures represent the standard deviations on the individual values, unless indicated otherwise.

7.7.1. AEA dosage and initial air content in fresh state

The incorporation of fly ash in concrete has an impact on the required AEA dosage to achieve an adequate initial air content in the fresh state (Table 7.3). For the reference T(0.45)A, a dosage of 2.0 ml/kg binder was sufficient to have an initial air content (6.8%) conforming to all consulted standards (NBN EN 206-1 (2000), NBN B15-001 (2004), ACI 201.2R (2008)). With respect to the air entrained HVFA mixtures F(1)50A and F(2)50A, a much higher AEA dosage (5.0 ml/kg binder) resulted in an air content that was considerably lower than the 6.8% of the reference: 5.2% for mixture F(1)50A and 4.9% for mixture F(2)50A. As a consequence, the air content criterion of 6-7% imposed by ACI 201.2R (2008) was not met.

In addition, air-to-paste (A/P) ratios were calculated from the initial air contents measured 15 minutes after mixing and included in Table 7.3. The A/P ratio of mixture T(0.45)A exceeded the 18 to 20% range (A/P: 25.7%) recommended by Pinto (2004) and Bielenz et al. (1958), while F(1)50A and F(2)50A had air-to-paste ratios below the optimal range (15.6% and 14.7%, respectively). The optimal initial air content corresponding with the recommended air-to-paste range was calculated for each air entrained concrete mixture. For mixture T(0.45)A

an air content of 4.8-5.3% would be enough, while for F(1)50A and F(2)50A, the air contents should equal 6.0-6.7% and 6.0-6.6%, respectively, as the HVFA concretes had a considerably lower total aggregate volume fraction. However, this higher air content was not achieved for the air entrained HVFA mixtures that were studied initially.

Table 7.3. Applied AEA and SP dosages (ml/kg B), slump classes, initial air contents in the fresh state (%) and corresponding A/P ratios (%).

| Composition | T(0.45) | T(0.45)A | F(1)50(-2) | F(1)50A(-2) | F(2)50(-2) | F(2)50A(-2) |
|------------------------|----------------|-----------------|-------------------|--------------------|-------------------|--------------------|
| AEA dosage (ml/kg B) | 0.0 | 2.0 | 0.0 (0.0) | 5.0 (7.0) | 0.0 (0.0) | 5.0 (7.0) |
| SP dosage (ml/kg B) | 2.0 | 4.0 | 7.0 (5.0) | 7.0 (5.0) | 5.0 (3.0) | 5.0 (3.0) |
| Slump ⁺ (–) | S2 | S5 | S5 (S4) | S5 (S4) | S5 (S3) | S5 (S2) |
| Air content (%) | 2.8 | 6.8 | 2.6 (2.7) | 5.2 (7.0) | 2.8 (1.8) | 4.9 (8.5) |
| A/P (%) | 10.6 | 25.7 | 7.9 (8.1) | 15.6 (20.7) | 8.4 (5.4) | 14.7 (25.2) |
| Composition | | | F(1)SF | F(1)SFA | F(2)SF | F(2)SFA |
| AEA dosage (ml/kg B) | | | 0.0 | 2.5 | 0.0 | 3.0 |
| SP dosage (ml/kg B) | | | 14.0 | 12.0 | 12.0 | 10.0 |
| Slump ⁺ (–) | | | S4 | S4 | S4 | S4 |
| Air content (%) | | | 2.6 | 6.3 | 3.4 | 6.5 |
| A/P (%) | | | 10.2 | 24.7 | 13.4 | 25.5 |

⁺ S1 (10-40 mm), S2 (50-90 mm), S3 (100-150 mm), S4 (160-210), S5 (≥ 220 mm).

Therefore, two additional air entrained HVFA mixtures with an increased AEA dosage (7.0 ml/kg B instead of 5.0 ml/kg B) were made: F(1)50A-2 and F(2)50A-2. Their estimated A/P ratios (F(1)50A-2: 20.7%, F(2)50A-2: 25.2%) were also calculated from the fresh air contents (Table 7.3: F(1)50A-2: 7.0%, F(2)50A-2: 8.5%) and found to be more or less in agreement with or higher than the suggested 18-20% criterion.

When looking at the air entrained FA+SF concrete compositions (F(1)SFA, F(2)SFA), the AEA dosages required (2.5 ml/kg B and 3.0 ml/kg B, respectively) to achieve an initial air content in the fresh state of around 6% were not much higher than the 2.0 ml/kg B used in OPC reference T(0.45)A. The total binder content of both FA+SF mixtures amounted to 340 kg/m³. This is in correspondence with the total cement content of the OPC reference. As a result, the volume fractions of paste present in 1 m³ of each concrete composition are rather similar (T(0.45)A: 0.2647 m³, F(1)SF: 0.2553 m³, F(2)SFA: 0.2549 m³) and considerably lower than the volume fractions of paste present in the adequately air entrained HVFA mixtures (F(1)50A-2: 0.3373 m³, F(2)50A-2: 0.3373 m³). This means that the optimal range for the A/P ratio (18-20%) for the FA+SF concrete could be achieved with a lower initial air content (4.6-5.1% for both F(1)SFA and F(2)SFA) and thus with a lower AEA dosage. As already mentioned earlier, a similar initial air content range (4.8-5.3%) would also be ideal for OPC reference T(0.45)A. The now applied AEA dosages in mixtures T(0.45)A, F(1)SFA and F(2)SFA resulted in initial air contents (6.8%, 6.3% and 6.5%) and A/P ratios (25.7%, 24.7% and 25.5%) that were above optimal. Nevertheless, these above optimal ranges were never a problem in perspective of the concrete's salt scaling resistance (see Section 7.7.4). Lower initial air contents were deliberately not aimed for to have somewhat of a safety margin in case the initial air content in the fresh state would decrease with time (see Section 7.8.1).

7.7.2. Air void system in hardened state (thin section analysis)

A comparison between the different HVFA mixtures with air entrainment, indicates that the use of a rather high dosage of AEA (5.0 ml/kg B) did not result in a very pronounced system of artificial air bubbles inside the concrete matrix for mixture F(1)50A (Figure 7.2).

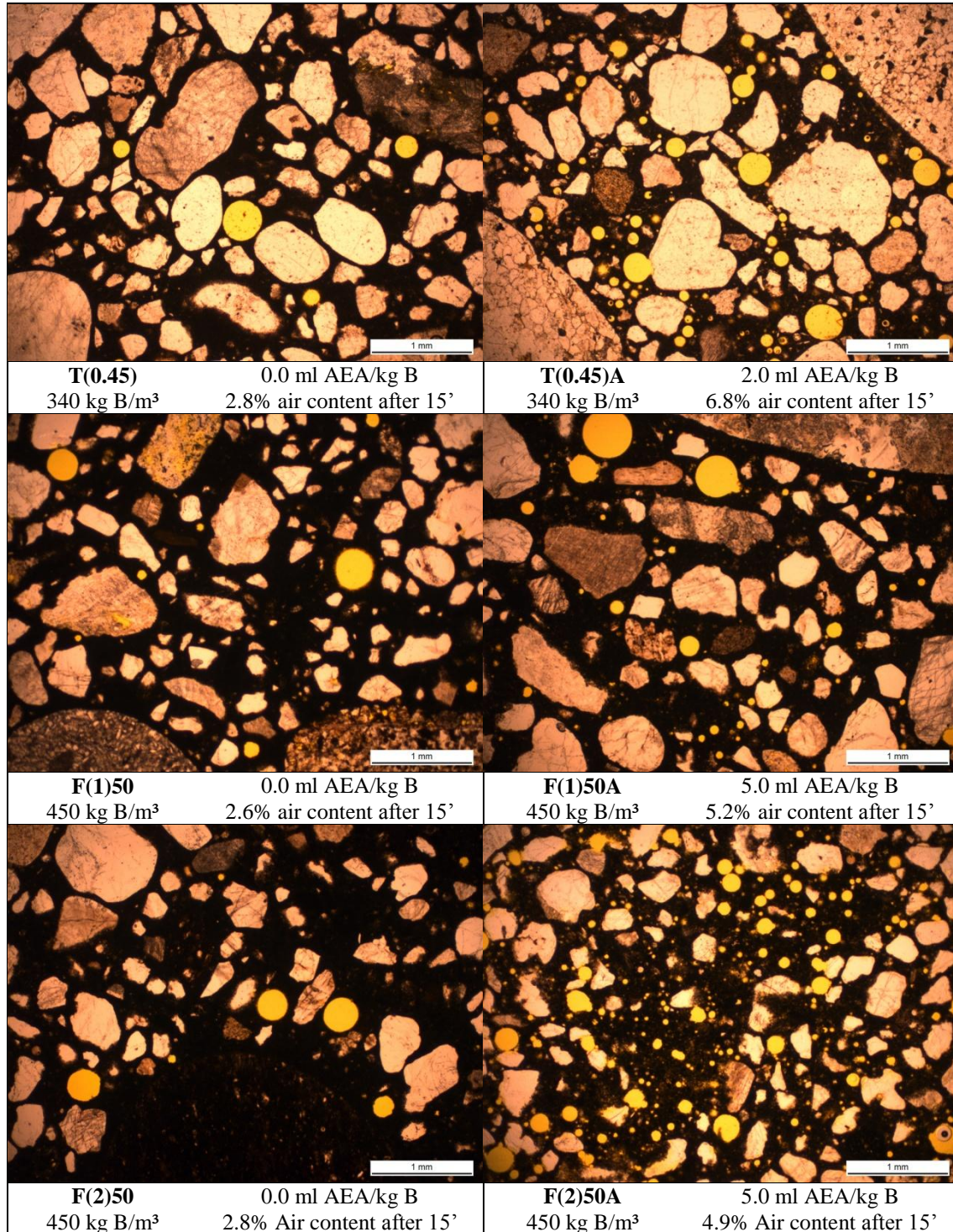


Figure 7.2. Thin section analysis of the air void system (coloured yellow) qualitatively shows the effect of applying an AEA (A) in OPC and HVFA concrete.

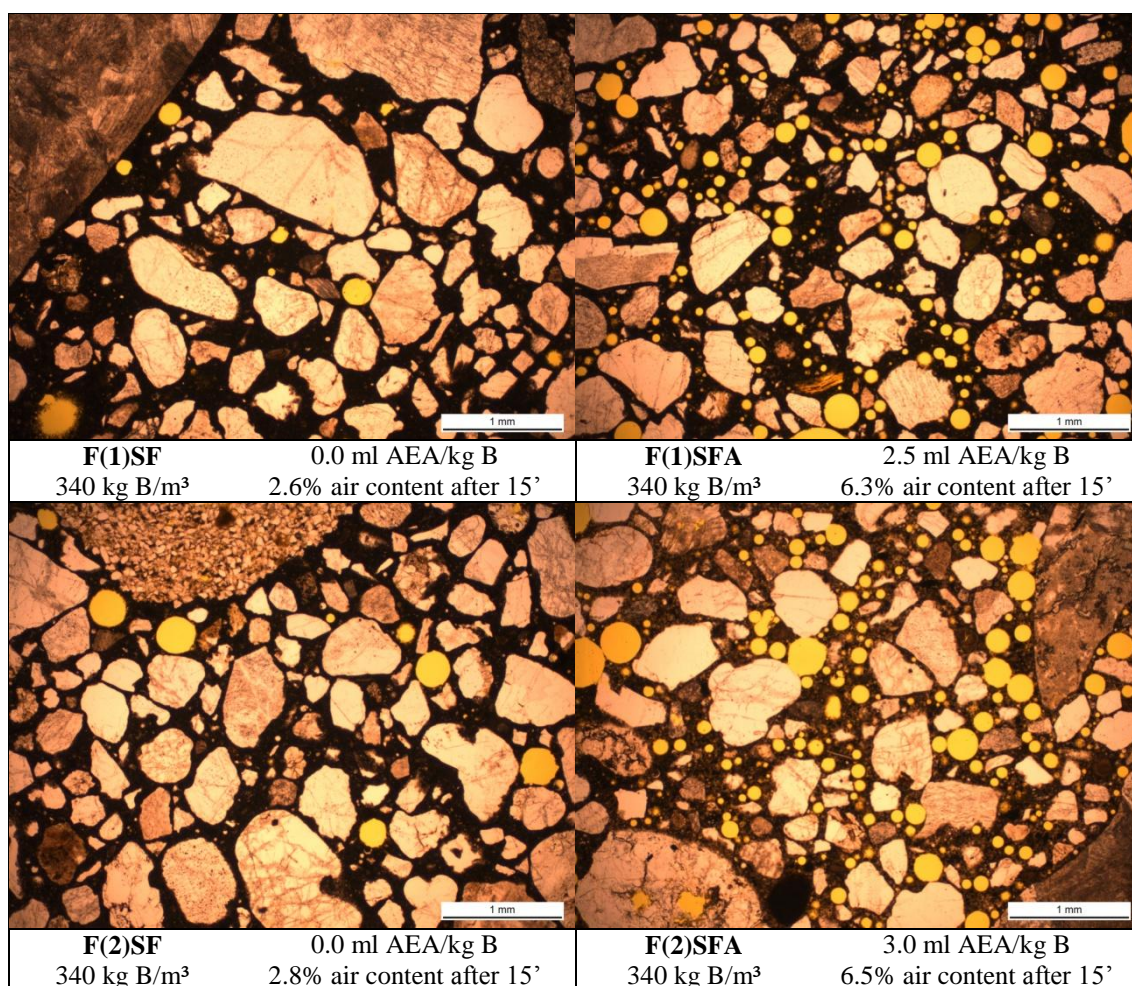
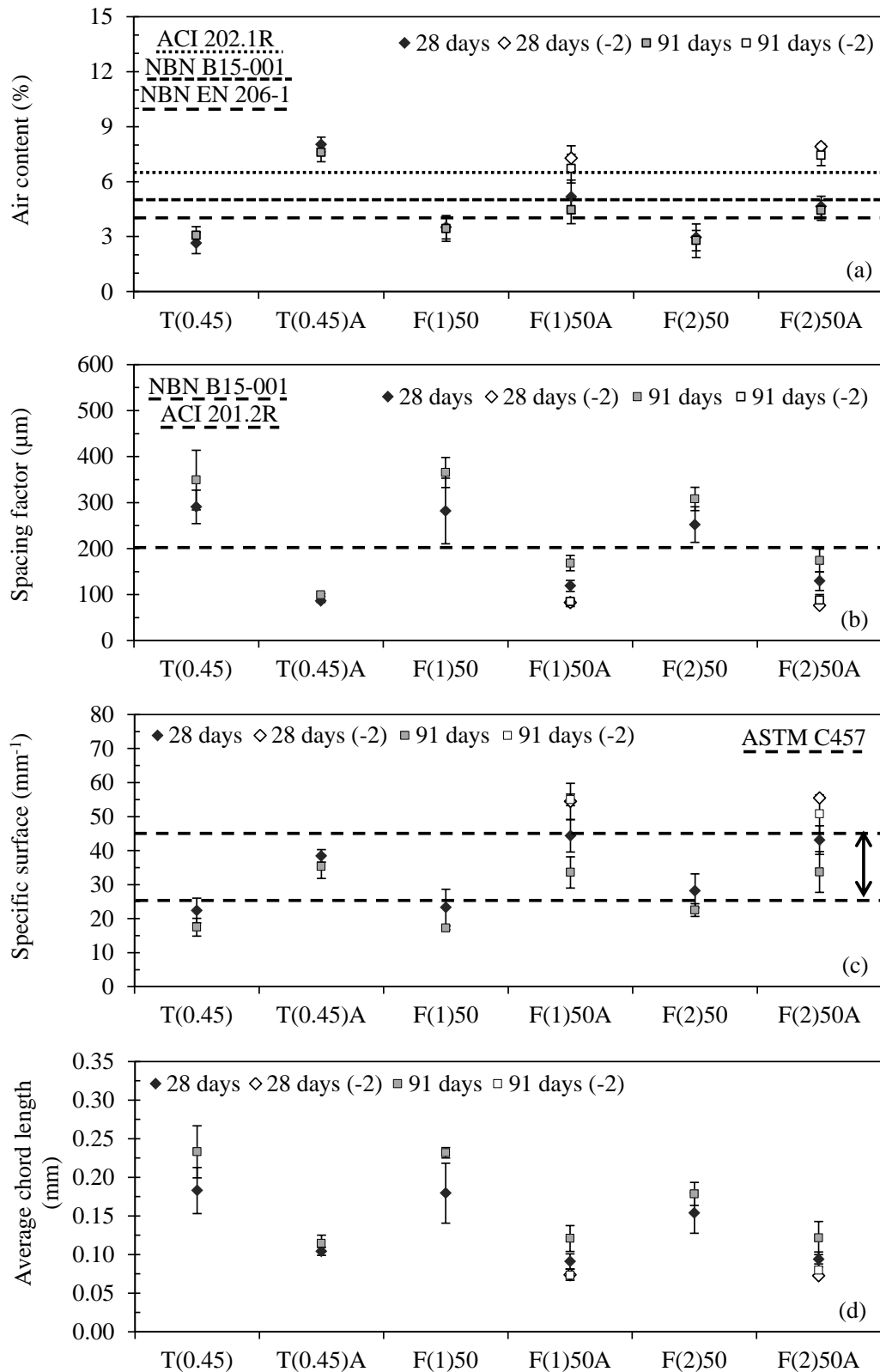


Figure 7.3. Thin section analysis of the air void system (coloured yellow) qualitatively shows the effect of applying an AEA (A) in FA+SF concrete.

7.7.3. Air void system in hardened state (automated air void analysis)

Concrete's total air content is the parameter usually specified since it is easily measurable in the field [ACI 201.2R (2008)]. Although the minimum air contents mentioned in Section 7.2 normally apply to the air content in the fresh state, the values obtained for the hardened concrete were evaluated according to the same criteria (Figure 7.4a).

Compared to T(0.45), the air entrained reference T(0.45)A was characterized by a much higher air content (7.5-8.0%). Note that the higher values for the T(0.45)A reference mixture are somewhat different from its initial air content (6.8%, Table 7.3) in the fresh state. Moreover, it was observed that in addition to the presence of the smaller regular shaped air voids due to air entrainment, all sample surfaces of T(0.45)A contained some larger – more than 1 mm in cross-section – irregular shaped air voids, likely entrapped as opposed to entrained air. There may be two possible explanations for the difference between the air content in fresh and hardened state. Either the entrapped air has evolved after the initial air content measurements, or it was removed more effectively from the fresh concrete that was used for the air content measurements than from the concrete used to cast the concrete specimens (Section 7.3).



| | | | | | | |
|---------------------------------|-----|-----|-----|---------------|-----|---------------|
| B (kg/m^3) | 340 | 340 | 450 | 450 | 450 | 450 |
| AEA ($\text{ml}/\text{kg B}$) | 0.0 | 2.0 | 0.0 | A:5.0/A-2:7.0 | 0.0 | A:5.0/A-2:7.0 |
| Air content (%) after 15' | 2.8 | 6.8 | 2.6 | A:5.2/A-2:7.0 | 2.8 | A:4.9/A-2:8.5 |

Figure 7.4. Influence of AEA use on the air content (a), the spacing factor (b), the specific surface (c) and the average chord length (d) of the reference and the HVFA mixtures as obtained from automated air void analysis after 28 and 91 d of curing.

According to St. John et al. (1998) the maximum diameter of an entrained air void is 1 mm. This criterion could be used to separate the entrained from the entrapped air. Now, the air void analysis technique enables the determination of an air content based on all chord lengths traversed during the analysis and an air content solely based on the traversed chord lengths < 1 mm. Although looking at the latter air content will obviously result in an overestimation of the actual entrained air content (it considers all traversed chord lengths of the voids and not just the diameters), it provides a first rough estimation of the entrained-entrapped air proportions. The total air content of the non-air entrained reference T(0.45) was found to consist of 52-55% for air voids with chord lengths < 1 mm. For T(0.45)A this value increased to 92-93% (Table 7.4). Thus, despite the presence of some larger entrapped air voids, the artificial entrainment of air voids was quite effective after all. It also means that an explanation for the difference between the air contents in fresh and hardened state must be sought elsewhere (Section 7.8.1).

Table 7.4. Difference between the air contents calculated from all traversed chords and the air contents calculated from the traversed chords < 1 mm during an automated air void analysis.

| Air content (%) | T(0.45) | T(0.45)A | F(1)50 | F(1)50A | F(2)50 | F(2)50A |
|------------------------|----------------|-----------------|---------------|------------------|------------------|----------------|
| 28 d | | | | | | |
| All chords | 2.7±0.6 | 8.0±0.4 | 3.5±0.6 | 5.2±0.9 | 3.0±0.7 | 4.6±0.6 |
| Chords < 1 mm | 1.4±0.2 | 7.5±0.5 | 2.2±0.5 | 3.8±0.6 | 1.7±0.3 | 3.6±0.5 |
| Ratio (%) | 52 | 93 | 63 | 73 | 57 | 78 |
| 91 d | | | | | | |
| All chords | 3.1±0.5 | 7.6±0.5 | 3.4±0.6 | 4.5±0.8 | 3.1±0.9 | 4.4±0.5 |
| Chords < 1 mm | 1.7±0.3 | 7.0±0.4 | 2.2±0.5 | 3.3±0.1 | 1.8±0.3 | 3.2±0.2 |
| Ratio (%) | 55 | 92 | 65 | 73 | 58 | 73 |
| Air content (%) | | | | F(1)50A-2 | F(2)50A-2 | |
| 28 d | | | | | | |
| All chords | | | | 7.2±0.7 | 7.9±0.2 | |
| Chords < 1 mm | | | | 6.1±0.6 | 7.2±0.1 | |
| Ratio (%) | | | | 85 | 91 | |
| 91 d | | | | | | |
| All chords | | | | 6.7±0.8 | 7.4±0.6 | |
| Chords < 1 mm | | | | 6.2±0.4 | 6.8±0.8 | |
| Ratio (%) | | | | 93 | 92 | |

Regarding the HVFA compositions, air entrainment resulted in an increase of the air content, though the values obtained were lower than 6-7%. Compared to F(1)50 and F(2)50, the average hardened air contents of F(1)50A and F(2)50A were increased by only 1.8% and 1.5%, respectively. The air contents in hardened state were more or less in accordance with the measured air contents in the fresh state (F(1)50A: 5.2%, F(2)50A: 4.9%). When looking at the ratio between the air contents calculated from the traversed chords < 1 mm and those calculated from all chords traversed, the following conclusions can be drawn. With the use of fly ash F(1), adding 5.0 ml AEA/kg binder to the concrete resulted in an increase of this ratio from 63-65% to only 73%. With the use of fly ash F(2) and the same AEA dosage, this ratio increased from 57-58% to 73-78%. Thus, in contrast with the 92-93% air content ratio of

mixture T(0.45)A, the corresponding values of the two air entrained HVFA mixtures are considerably lower. From both the differences in total air content and entrained-entrapped air content proportioning, it can already be observed that the artificial air entrainment of mixtures F(1)50A and F(2)50A was less successful despite an AEA dosage of 5.0 ml/kg B.

Not only sufficient total air content is of importance, but also an adequate distribution of the artificial air bubbles. In other words, their spacing should be close enough to prevent the development of pressures from freezing which would fracture the concrete. The fulfillment of this requirement is usually evaluated through the calculation of a spacing factor L_S for the concrete. This is the maximum distance from any point within the concrete matrix to the edge of the nearest air bubble. A L_S of 200 μm is recommended as the maximum for concrete exposed to freeze/thaw attack [NBN B15-001 (2004), ACI 201.2R (2008)]. The spacing factors of all air entrained concrete compositions (T(0.45)A, F(1)50A, F(2)50A) do not exceed this maximum value after both 28 and 91 d of curing, although the HVFA mixtures are characterized by somewhat higher values (Figure 7.4b: 100-200 μm) when compared with the OPC reference (Figure 7.4b: $\pm 100 \mu\text{m}$). Without air entrainment, the spacing factors of T(0.45), F(1)50 and F(2)50 range between 250 and 350 μm .

Besides the spacing factor L_S , the specific surface α also characterizes the distribution of the air bubbles (Figure 7.4c). The higher the value for α , the more the air void system consists of finer pores which contribute to the salt scaling resistance. For air entrained concrete designed in accordance with ASTM C457 (2010) the specific surface α is usually in the range 25 to 45 mm^{-1} . All air entrained concrete mixtures (T(0.45)A, F(1)50A and F(2)50A) exhibited a higher specific surface than the non-air entrained compositions (T(0.45), F(1)50 and F(2)50). Since a higher value for the specific surface indicates the presence of finer pores, the air entrained concrete mixtures should have average chord lengths that are considerably lower than the ones recorded for the non-air entrained compositions. This was indeed the case (Figure 7.4d).

The increase of the AEA dosage from 5.0 ml/kg B to 7.0 ml/kg B, resulted in a more adequate air void system in hardened state for HVFA concrete. The total air contents measured for F(1)50A-2 and F(2)50A-2 (Figure 7.4a) slightly exceeded the 6-7% criterion recommended by the ACI 201.2R (2008) guideline. 85-93% of the total air content consisted of the air content calculated from traversed chord lengths $< 1\text{mm}$ (Table 7.4). Spacing factors decreased to values around 100 μm cf. T(0.45)A (Figure 7.3b). The compositions were characterized by the highest specific surfaces (Figure 7.4c: $\pm 55 \text{mm}^{-1}$) and the lowest average chord lengths (Figure 7.4d: $\pm 0.075 \text{mm}$).

With respect to the air void system of HVFA concrete, the following conclusions can be drawn. Compared to T(0.45)A, the air entrained HVFA mixtures F(1)50A and F(2)50A are characterized by a lower air content and a somewhat higher, yet still acceptable spacing factor. As a consequence, the mixtures with fly ash may be more susceptible to salt scaling. On the other hand, specific surface and average chord length recordings indicate that the air void systems of F(1)50A and F(2)50A contain more small air bubbles which may improve the resistance to salt scaling. Note that with a high value for the specific surface α , a suitable spacing factor L_S can still be obtained even when the air content is lower. However, in order to obtain an air void system that has both the volume capacity and the geometric parameters necessary to protect saturated mature cement paste during exposure to freezing, it is important

to obtain concrete with an acceptably high air content and a low enough spacing factor [Sommer (1979)]. To obtain this sufficiently high air content a further increase of the AEA dosage (from 5.0 ml/kg B to 7.0 ml/kg B) for the studied HVFA compositions was imperative. This intervention turned out to be beneficial for the four parameters characterizing the hardened air void system (air content A, spacing factor L_s , specific surface α and average chord length l_m).

The FA+SF concrete compositions were studied in the same way as the HVFA concrete mixtures. The results of the automated air void analysis are shown in Figures 7.5a to 7.5d. The experimental output of mixtures T(0.45) and T(0.45)A were included once again in the graphs to enable a more easy comparison between OPC and FA+SF concrete.

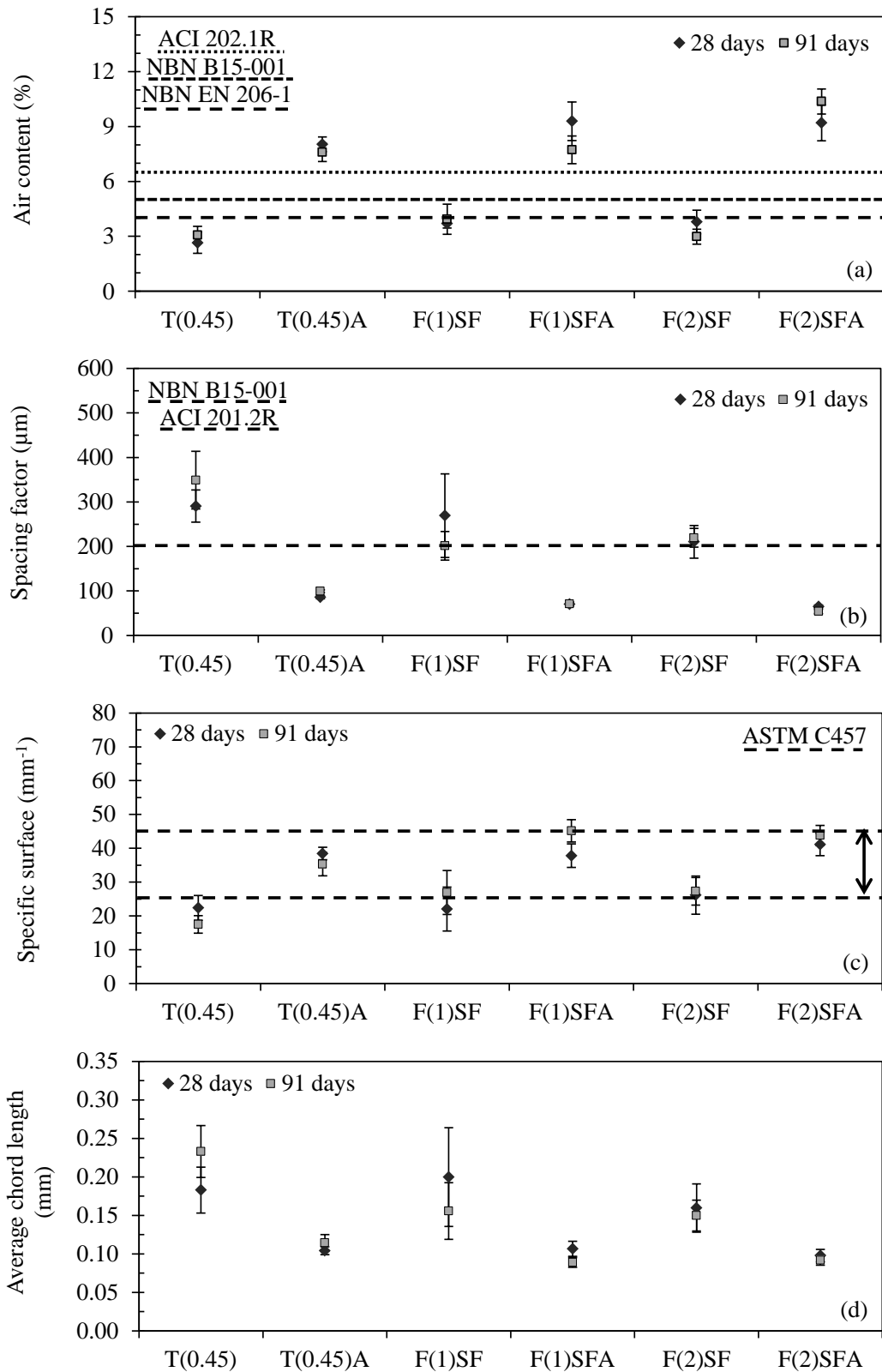
The air contents in hardened state of the air entrained FA+SF compositions F(1)SFA and F(2)SFA were found to be similar or higher than the air content of OPC reference T(0.45)A (Figures 7.5a). Their values exceeded the most strict air content criterion imposed by ACI 201.2R (2008) to achieve an acceptable salt scaling resistance. The air contents consisted of 76-88% of air voids with chord lengths < 1 mm (Table 7.5). This is somewhat less than the ratios of air contents calculated from the traversed chords < 1 mm and those from all chords traversed for the air entrained OPC reference (92-93%). Nevertheless, they still largely exceed the corresponding ratios of their non-air entrained counterparts (56-61%). Thus, based on not only the total air content (Figures 7.5a) but also on the entrained-entrapped air content proportioning (Table 7.5), artificial air entrainment of the FA+SF concrete seems to have been successful. The non-air entrained FA+SF concrete compositions do not meet the criteria of any of the standards or technical guidelines considered, although the 4% air content criterion of NBN EN 206-1 (2000) is only just not met.

Just like for the previously studied concrete compositions, the air contents in hardened state differ substantially from the initial air contents measured in the fresh state, which cannot be explained by a considerable presence of larger entrapped air voids. This issue will be discussed more in detail in Section 7.8.1.

Both mixtures F(1)SFA and F(2)SFA are characterized by spacing factors L_s that were substantially lower than 200 μm (Figure 7.5b), the maximum value allowed for concrete exposed to freeze/thaw in combination with deicing salts. Note that the spacing factors of the non-air entrained mixtures F(1)SF at 91 days and F(2)SF at 28 and 91 days do not exceed the limiting values in a significant way.

The specific surfaces α of the air-entrained FA+SF mixtures were usually rather close in value to the upper limit of 45 mm^{-1} suggested by ASTM C457 (2010) (Figure 7.5c). This suggests a well-distributed air void system consisting of a substantial quantity of finer air voids. The low average chord lengths recorded for mixtures F(1)SFA and F(2)SFA further confirm this (Figure 7.5d).

In conclusion, the air void systems of the studied FA+SF compositions with air entrainment are fully in agreement with all the existing requirements to ensure a good resistance to freeze/thaw in combination with deicing salts. This was realized with AEA dosages that did not differ too much from the dosage applied in the air entrained OPC reference (2.5 to 3.0 ml/kg B instead of 2.0 ml/kg B) with the same total binder content. Unlike during the development of a HVFA concrete with an adequate air void system, no additional FA+SF concrete manufacturing with increased AEA additions was necessary.



| | | | | | | |
|---------------------------------|-----|-----|-----|-----|-----|-----|
| B (kg/m^3) | 340 | 340 | 340 | 340 | 340 | 340 |
| AEA ($\text{ml}/\text{kg B}$) | 0.0 | 2.0 | 0.0 | 2.5 | 0.0 | 3.0 |
| Air content (%) after 15' | 2.8 | 6.8 | 2.6 | 6.3 | 2.8 | 6.5 |

Figure 7.5. Influence of AEA use on the air content (a), the spacing factor (b), the specific surface (c) and the average chord length (d) of the reference and the FA+SF mixtures as obtained from automated air void analysis after 28 and 91 d of curing.

Table 7.5. Difference between the air contents calculated from all traversed chords and the air contents calculated from the traversed chords < 1 mm during an automated air void analysis.

| Air content (%) | T(0.45) | T(0.45)A | F(1)SF | F(1)SFA | F(2)SF | F(2)SFA |
|-----------------|-----------|-----------|-----------|-----------|-----------|-----------|
| 28 d | | | | | | |
| All chords | 2.7±0.6 | 8.0±0.4 | 3.7±0.2 | 9.3±1.1 | 3.8±0.6 | 9.2±1.0 |
| Chords < 1 mm | 1.4±0.2 | 7.5±0.5 | 2.2±0.2 | 7.1±0.4 | 2.1±0.1 | 7.8±0.3 |
| Ratio (%) | 52 | 93 | 59 | 76 | 56 | 85 |
| 91 d | | | | | | |
| All chords | 3.1±0.5 | 7.6±0.5 | 3.9±0.8 | 7.7±0.8 | 3.0±0.4 | 10.4±0.7 |
| Chords < 1 mm | 1.7±0.3 | 7.0±0.4 | 2.4±0.1 | 6.8±0.5 | 1.8±0.1 | 8.8±0.5 |
| Ratio (%) | 55 | 92 | 61 | 88 | 61 | 85 |

7.7.4. Salt scaling resistance

From Figure 7.6 it is clear that ordinary Portland cement concrete does not necessarily require air entrainment to ensure limited salt scaling. After 28 d of curing, the total amount of scaled material at the end of the test is lower than 1 kg/m². After 91 d, the mean mass loss per unit area Δm is only slightly higher than the maximum value. The acceptable mass loss per unit area for T(0.45) supports the choice of this concrete composition as a reference concrete type for an XF4 environment in NBN B 15-001 (2004). Secondly, the addition of a limited amount of AEA (2.0 ml/kg B) to the same OPC concrete mixture was found to be very effective, since Δm was negligible after both 28 and 91 d of curing ($\Delta m = 0.07\text{-}0.22$ kg/m²).

In contrast with reference mixture T(0.45), the performance of the non-air entrained HVFA mixtures subjected to the same experiment was far from acceptable. On average, Δm was more than twice the maximum mass loss allowed. Again, using an AEA significantly improved the salt scaling resistance. However, the effectiveness of the admixture was less than in reference T(0.45)A. Although the AEA dosage was more than doubled (5.0 ml/kg B versus 2.0 ml/kg B), higher mass losses per unit area were recorded for the HVFA mixtures F(1)50A and F(2)50A. The mean Δm value of HVFA mixture F(1)50A slightly exceeds the 1 kg/m² criterion at ages of 28 and 91 d. On the other hand, HVFA mixture F(2)50A performed very well after 28 d since the mass loss per unit area was only 0.4 kg/m². After 91 d, this amount increased significantly to 1.4 kg/m². For all tested air entrained concrete mixtures, a small reduction in salt scaling resistance was observed between 28 and 91 d. Statistical analysis (Independent Sample T test, Significance level = 0.05) showed that only for mixture F(2)50A this difference was significant.

A reduction of the concrete's surface strength due to carbonation can be an explanation for the less than satisfactory salt scaling resistance after 91 d. Since HVFA concrete is also quite susceptible to the carbonation phenomenon, the same explanation could be valid. Now, possible carbonation of the concrete surface was not evaluated just before the salt scaling tests after 28 and 91 d of curing. This was done only afterwards for the air entrained HVFA mixtures. 10 mm thick slices were cut from 3 cubic F(2)50A concrete specimens (side length: 100 mm), and this after being stored in the curing room at 20 °C and 95% relative humidity for more than 1.5 years. Phenolphthalein was sprayed onto the slices to visualize and measure the carbonation front. The average carbonation depth equaled 2.0 ± 0.3 mm. The outcome of an additional salt scaling experiment done on the same concrete again showed that the amount

of salt scaling ($\Delta m = 1.6 \pm 0.5 \text{ kg/m}^2$) exceeded the 1 kg/m^2 . However, this does not necessarily mean that carbonation is the sole cause for increased salt scaling of this concrete. It must be said that its air content in the hardened state was below the required minimum of 6-7%, as prescribed by ACI 201.2R (2008). Logically, it is difficult to assess the effect of carbonation on the salt scaling resistance of a concrete with an inadequate air void system. Therefore, we chose to do this evaluation only for HVFA mixtures F(1)50A-2 and F(2)50A-2 with the increased AEA dosage.

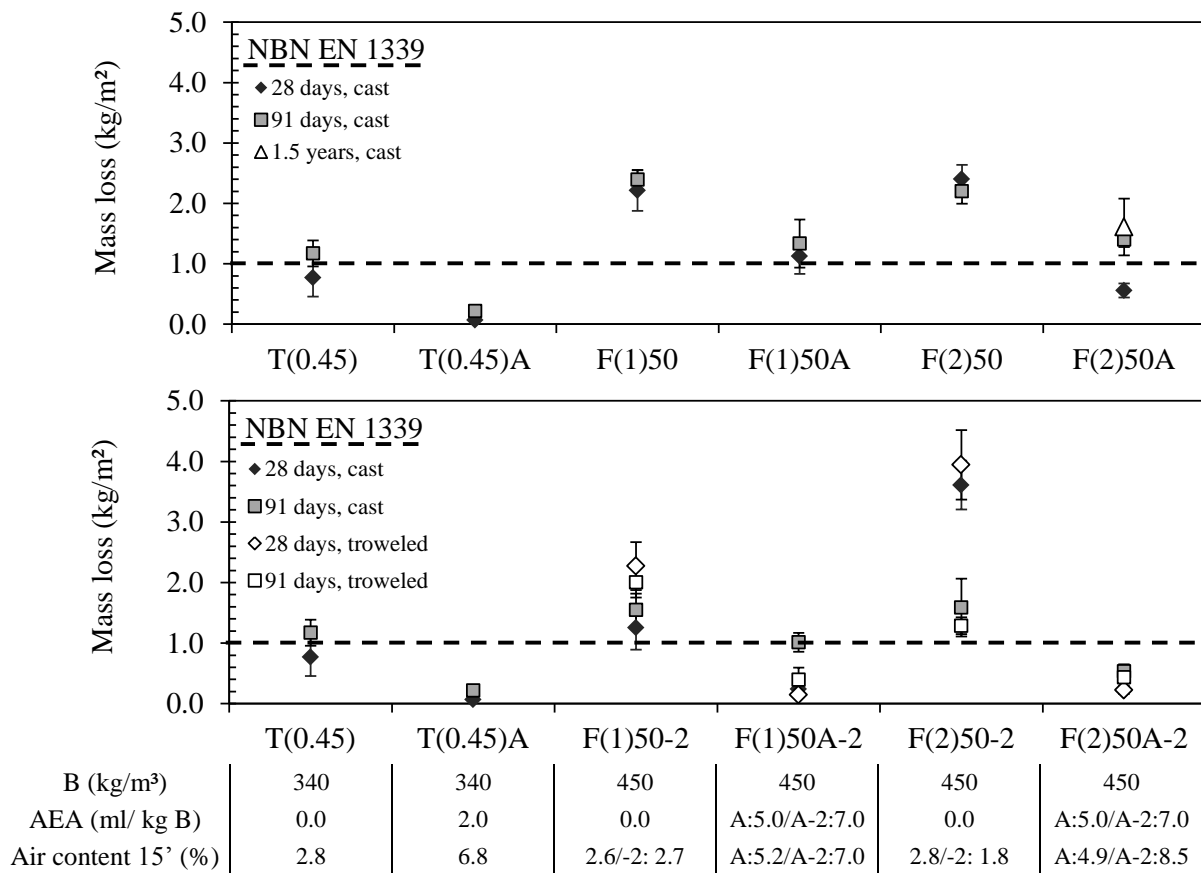


Figure 7.6. The influence of air entrainment on the salt scaling induced mass loss per unit area of OPC and HVFA concrete for different curing ages and surface finishing ($n = 6 / n = 4$).

An adequate salt scaling resistance was confirmed for cast surfaces of mixtures F(1)50A-2 and F(2)50A-2 with the higher air-to-paste ratios. For both of them, salt scaling remained far below the 1 kg/m^2 criterion after 28 d (F(1)50A-2: $\Delta m = 0.2 \pm 0.01 \text{ kg/m}^2$, F(2)50A-2: $\Delta m = 0.2 \pm 0.03 \text{ kg/m}^2$). The same goes for mixture F(2)50A-2 after 91 d ($\Delta m = 0.5 \pm 0.1 \text{ kg/m}^2$). The salt scaling resistance of mixture F(1)50A-2 after 91 d is also still acceptable, although the mass loss increased to $1.0 \pm 0.2 \text{ kg/m}^2$ (Figure 7.6). The carbonation front prior to the salt scaling test was assessed on a dummy specimen of each concrete mixture after 28 and 91 d. The measured carbonation depths were found to be rather limited (max. 1.0 mm) and no significant difference could be observed between the different mixtures and curing ages. Since limited carbonation was already observed for the specimens with very little salt scaling after 28 d (Δm : 0.2 kg/m^2), surface weakening due to carbonation can not be seen as the main cause for increased scaling at later age.

At this stage of the research troweled surfaces were also subjected to the salt scaling test to see whether the finishing of the concrete surface could have an important influence on the mass loss per unit area. Apart from mixture F(1)50A-2 after 91 days, the cast and troweled surfaces of the second series of air entrained HVFA mixtures exhibited a very similar salt scaling behaviour. In case the concrete was not air entrained, more pronounced differences could be observed. Without the incorporation of AEA troweled surfaces seem to be slightly more susceptible to salt scaling than cast surfaces. Only the recorded mass losses per unit area of mixture F(2)50-2 after 91 days do not seem to confirm this statement as their troweled surfaces showed a better performance.

Within Figure 7.7 the salt scaling resistances of non-air entrained and air entrained OPC and FA+SF concrete are compared. The applied AEA dosages in the FA+SF concrete compositions (2.0 and 2.5 ml kg/B) resulted in very limited salt scaling. This was the case for both the cast (Δm : 0.05-0.24 kg/m²) and troweled (Δm : 0.03-0.11 kg/m²) surfaces. These results are very similar to the Δm values that were recorded for OPC reference T(0.45)A (Δm : 0.07-0.22 kg/m²) which demonstrates the equivalent performance of the FA+SF concrete.

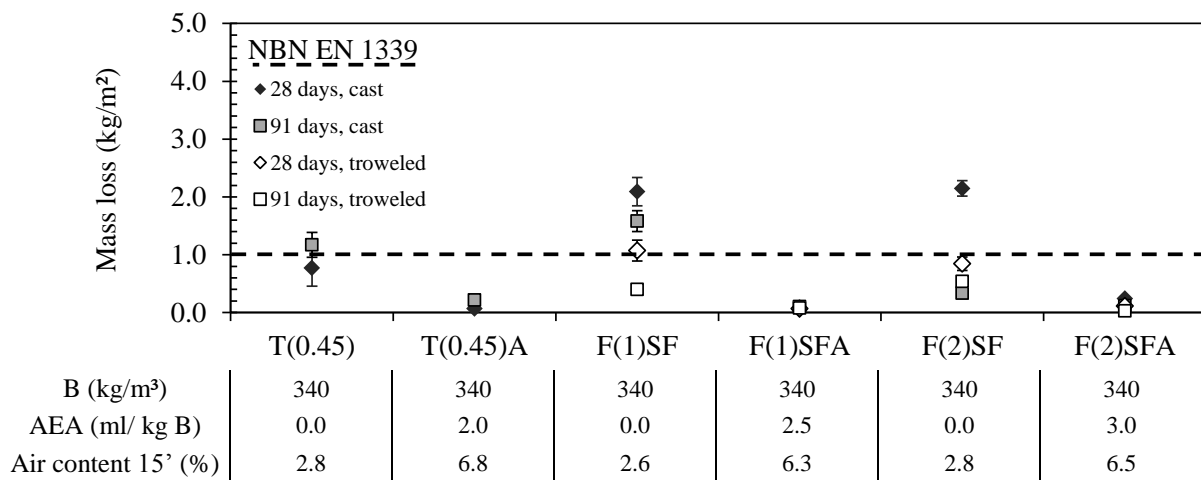


Figure 7.7. The influence of air entrainment on the salt scaling induced mass loss per unit area of OPC and FA+SF concrete for different curing ages and surface finishing (n = 4).

Without air entrainment, the amount of salt scaling increased substantially as well as the differences in performance between cast and troweled test surfaces. The troweled surfaces now seem to be the most resistant to the deterioration mechanism in most cases, sometimes even to an extent that the 1 kg/m² salt scaling criterion of NBN EN 1339 (2003) is met. This is in contrast with the salt scaling behaviour of the HVFA concrete. For the moment, the varying effect of the surface finishing of non-air entrained HVFA and FA+SF concrete cannot be explained. A concrete without a proper air void system is more susceptible to salt scaling anyway. It can easily be understood that the degree of salt scaling can vary considerably with the condition of the concrete layer just below the surface (presence of aggregates, roughness of the aggregates, etc.) and not only with the finishing of the surface (cast versus troweled). Mortar instead of concrete may need to be tested to isolate the effect of the surface finishing. However, investigating this is seen as less relevant because HVFA and FA+SF concrete should be air entrained in order to have an adequate salt scaling resistance. If done properly,

the difference in performance between a cast and a troweled surface would be negligible and would not be an issue anyway.

7.7.5. Capillary water sorption and degree of saturation

The capillary sorption behaviour of the first series HVFA concrete and the corresponding OPC references was evaluated in terms of their initial and secondary rates of water absorption and their water absorption after 14 days (at the end of the test). Table 7.6 gives a summarizing overview of those parameters obtained for the two curing periods (28 and 91 days) and pre-drying temperatures (40°C and 105°C) applied.

No clear trend could be observed with respect to the differences in rates of water absorption between the non-entrained and air entrained OPC and HVFA concrete compositions. Prolonged curing did not automatically result in an improved resistance against capillary water sorption. The initial rates of water absorption obtained after pre-drying at 105°C even seem to suggest quite the opposite. The HVFA concrete compositions are characterized by higher S_i values (71-124 mm/ \sqrt{s}) in comparison with the OPC references (34-57 mm/ \sqrt{s}) after pre-drying at 40°C. The secondary rates of absorption are rather similar for both concrete types (21-31 mm/ \sqrt{s}). This trend is not visible anymore in the capillary sorption properties obtained after pre-drying at 105°C.

Table 7.6. Influence of air entrainment, curing age and pre-drying temperature on the initial (S_i) and secondary (S_s) rate of water absorption (incl. R^2 values) and the 14 days water absorption (I) of OPC concrete and the first series of HVFA concrete.

| 28 days, 40°C | T(0.45) | T(0.45)A | F(1)50 | F(1)50A | F(2)50 | F(2)50A |
|---|-----------------|-----------------|-----------------|-----------------|------------------|-----------------|
| S_i ($\times 10^{-4}$ mm/ \sqrt{s}) | 52 | 54 | 78 | 71 | 81 | 124 |
| $R^2_{S_i}$ (-) | 0.99 | 1.00 | 1.00 | 1.00 | 0.98 | 1.00 |
| S_s ($\times 10^{-4}$ mm/ \sqrt{s}) | 21 | 21 | 28 | 27 | 30 | 31 |
| $R^2_{S_s}$ (-) | 1.00 | 1.00 | 0.99 | 1.00 | 1.00 | 1.00 |
| I_{14days} (mm) | 3.15 \pm 0.15 | 3.22 \pm 0.13 | 4.20 \pm 0.27 | 4.12 \pm 0.13 | 4.43 \pm 0.07 | 4.80 \pm 0.25 |
| 91 days, 40°C | T(0.45) | T(0.45)A | F(1)50 | F(1)50A | F(2)50 | F(2)50A |
| S_i ($\times 10^{-4}$ mm/ \sqrt{s}) | 34 | 57 | 90 | 79 | 95 | 73 |
| $R^2_{S_i}$ (-) | 1.00 | 0.99 | 0.99 | 1.00 | 1.00 | 1.00 |
| S_s ($\times 10^{-4}$ mm/ \sqrt{s}) | 20 | 27 | 25 | 27 | 24 | 22 |
| $R^2_{S_s}$ (-) | 1.00 | 0.99 | 0.99 | 1.00 | 0.96 | 0.96 |
| I_{14days} (mm) | 3.91 \pm 0.17 | 3.63 \pm 0.13 | 4.05 \pm 0.10 | 3.91 \pm 0.41 | 3.62 \pm 0.24 | 3.78 \pm 0.37 |
| 28 days, 105°C | T(0.45) | T(0.45)A | F(1)50 | F(1)50A | F(2)50 | F(2)50A |
| S_i ($\times 10^{-4}$ mm/ \sqrt{s}) | 80 | 93 | 69 | 76 | 129 | 117 |
| $R^2_{S_i}$ (-) | 0.98 | 1.00 | 1.00 | 0.99 | 1.00 | 1.00 |
| S_s ($\times 10^{-4}$ mm/ \sqrt{s}) | 63 | 52 | 36 | 51 | 79 | 67 |
| $R^2_{S_s}$ (-) | 1.00 | 1.00 | 0.99 | 1.00 | 1.00 | 1.00 |
| I_{14days} (mm) | 7.48 \pm 1.08 | 7.09 \pm 0.42 | 5.24 \pm 0.43 | 5.82 \pm 0.12 | 8.87 \pm 1.32 | 8.20 \pm 0.28 |
| 91 days, 105°C | T(0.45) | T(0.45)A | F(1)50 | F(1)50A | F(2)50 | F(2)50A |
| S_i ($\times 10^{-4}$ mm/ \sqrt{s}) | 121 | 131 | 105 | 103 | 154 | 130 |
| $R^2_{S_i}$ (-) | 1.00 | 1.00 | 1.00 | 1.00 | 1.00 | 1.00 |
| S_s ($\times 10^{-4}$ mm/ \sqrt{s}) | 57 | 75 | 71 | 61 | 106 | 88 |
| $R^2_{S_s}$ (-) | 1.00 | 1.00 | 0.96 | 0.98 | 1.00 | 1.00 |
| I_{14days} (mm) | 7.32 \pm 0.09 | 9.13 \pm 0.97 | 8.11 \pm 0.11 | 7.74 \pm 0.82 | 11.76 \pm 0.80 | 9.48 \pm 0.21 |

When looking at the recorded water absorption after 14 days, again no significant difference can be detected between the non-air entrained and the air entrained concrete mixtures after pre-drying at 40 °C. The $I_{14\text{days}}$ values of the HVFA mixtures were found to be slightly higher than the ones recorded for T(0.45) and T(0.45)A, but only after 28 days. After oven drying at 105 °C, no pronounced difference between the non-air entrained and the air entrained concrete mixtures could be observed. After 91 d of curing, mixture T(0.45)A absorbed significantly more water than mixture T(0.45). However, after pre-drying at 105 °C the recorded I values of the former composition have a rather high standard deviation and should be interpreted with caution.

Logically, increasing the pre-drying temperature to 105 °C substantially increased the water absorption. Moreover, it also somewhat changed the ranking in water absorption between the OPC concrete and the HVFA concrete made with fly ashes F(1) and F(2). However, it did not result in an important difference between the non-air entrained and the air entrained variant of each concrete type.

The second series of HVFA concrete were subjected to a capillary sorption test entirely in correspondence with the ASTM C1585 – 04e (2007). Since the sample preconditioning was different, the results obtained (Table 7.7) cannot really be compared with the capillary sorption properties of the first series (Table 7.6). The initial and secondary absorption rates of the second series air entrained HVFA concrete (with increased AEA dosage) were in most cases slightly higher than the S_i and S_s values of non-air entrained concrete. Comparison of the recorded water absorption $I_{14\text{days}}$ for F(1)50-2, F(1)50A-2, F(2)50-2 and F(2)50A-2 leads to similar conclusions. Based on this analysis the difference between non-air entrained and air entrained HVFA concrete seems even a little more obvious. No clear differences in capillary water uptake between cast and troweled concrete surfaces could be observed. Prolonged curing slightly reduced mainly the initial rate of water absorption and water absorption after 14 days. Most striking is the difference in degree of saturation at the start of the capillary sorption test between non-air entrained and air entrained HVFA concrete ($\pm 82\%$ versus $\pm 75\%$). Three days of sample preconditioning at 50 °C and 80% RH, followed by 18 days of storage in sealed containers at 20 °C and 60% RH caused the cylindrical specimens of mixtures F(1)50A-2 and F(2)50A-2 to dry out more. By the end of the capillary sorption test this difference in saturation degree had more or less disappeared as all test samples almost reached full saturation (92-100%). Note that the recorded $DoS_{\text{day}0}$ values should more or less correspond with the initial degrees of saturation of the samples that were subjected to the salt scaling test (Section 7.7.4). The less saturated condition of F(1)50A-2 and F(2)50A-2 may also to some extent have contributed to their excellent salt scaling resistance. The present air void system did not only provide the required expansion space for freezing water, but also caused that less water for freezing was present from the start.

FA+SF concrete is less susceptible to capillary water sorption than HVFA concrete (Table 7.8 versus Table 7.7). A comparison of the water absorption rates and the water absorption after 14 days of the two concrete types clearly demonstrates this. A decrease in value with more than 50% could often be observed. The differences in water absorption rate and water absorption between air entrained and non-air entrained FA+SF concrete seem rather negligible. The applied curing period and surface finishing period again do not affect the capillary sorption behaviour in a significant way. FA+SF concrete with an entrained air void

system was not characterized by a substantially lower saturation degree at the start of both the capillary sorption and salt scaling test in comparison with non-air entrained FA+SF concrete (82% versus 83%).

It was also noted that the capillary water uptake of the second series of HVFA concrete and the FA+SF concrete did not differ considerably with the fly ash used (F(1) or F(2)).

Table 7.7. Influence of air entrainment, surface finishing and curing period on the initial (S_i) and secondary (S_s) rate of water absorption (incl. R^2 values) and the 9 days water absorption (I) of the second series of HVFA concrete.

| 28 days, cast | F(1)50-2 | F(1)50A-2 | F(2)50-2 | F(2)50A-2 |
|---|-----------------|------------------|-----------------|------------------|
| S_i ($\times 10^{-4}$ mm/ \sqrt{s}) | 31 | 26 | 30 | 35 |
| $R^2_{S_i}$ (-) | 0.99 | 0.99 | 0.98 | 0.99 |
| S_s ($\times 10^{-4}$ mm/ \sqrt{s}) | 6 | 8 | 6 | 8 |
| $R^2_{S_s}$ (-) | 0.99 | 0.98 | 0.97 | 0.98 |
| $I_{9\text{days}}$ (mm) | 1.0 \pm 0.1 | 1.1 \pm 0.1 | 1.0 \pm 0.1 | 1.4 \pm 0.1 |
| DoS _{day 0} (%) | 78 \pm 1 | 71 \pm 2 | 81 \pm 1 | 75 \pm 1 |
| DoS _{day 9} (%) | 96 \pm 2 | 92 \pm 4 | 99 \pm 1 | 100 \pm 1 |
| 28 days, troweled | F(1)50-2 | F(1)50A-2 | F(2)50-2 | F(2)50A-2 |
| S_i ($\times 10^{-4}$ mm/ \sqrt{s}) | 24 | 26 | 30 | 35 |
| $R^2_{S_i}$ (-) | 0.99 | 0.98 | 0.98 | 0.99 |
| S_s ($\times 10^{-4}$ mm/ \sqrt{s}) | 7 | 9 | 5 | 9 |
| $R^2_{S_s}$ (-) | 0.99 | 0.99 | 0.96 | 0.98 |
| $I_{9\text{days}}$ (mm) | 1.0 \pm 0.1 | 1.1 \pm 0.1 | 1.0 \pm 0.1 | 1.4 \pm 0.1 |
| DoS _{day 0} (%) | 81 \pm 1 | 74 \pm 2 | 82 \pm 1 | 73 \pm 1 |
| DoS _{day 9} (%) | 99 \pm 2 | 95 \pm 2 | 99 \pm 1 | 99 \pm 1 |
| 91 days, cast | F(1)50-2 | F(1)50A-2 | F(2)50-2 | F(2)50A-2 |
| S_i ($\times 10^{-4}$ mm/ \sqrt{s}) | 16 | 19 | 17 | 21 |
| $R^2_{S_i}$ (-) | 0.99 | 0.97 | 0.98 | 0.94 |
| S_s ($\times 10^{-4}$ mm/ \sqrt{s}) | 5 | 7 | 5 | 7 |
| $R^2_{S_s}$ (-) | 0.99 | 0.99 | 1.00 | 0.99 |
| $I_{9\text{days}}$ (mm) | 0.7 \pm 0.1 | 0.9 \pm 0.1 | 0.7 \pm 0.2 | 1.0 \pm 0.2 |
| DoS _{day 0} (%) | 83 \pm 1 | 77 \pm 1 | 85 \pm 1 | 77 \pm 2 |
| DoS _{day 9} (%) | 96 \pm 1 | 95 \pm 1 | 96 \pm 1 | 93 \pm 2 |
| 91 days, troweled | F(1)50-2 | F(1)50A-2 | F(2)50-2 | F(2)50A-2 |
| S_i ($\times 10^{-4}$ mm/ \sqrt{s}) | 16 | 18 | 21 | 25 |
| $R^2_{S_i}$ (-) | 0.98 | 0.97 | 0.97 | 0.94 |
| S_s ($\times 10^{-4}$ mm/ \sqrt{s}) | 5 | 7 | 5 | 8 |
| $R^2_{S_s}$ (-) | 0.99 | 0.99 | 1.00 | 0.98 |
| $I_{9\text{days}}$ (mm) | 0.8 \pm 0.1 | 1.2 \pm 0.1 | 0.7 \pm 0.1 | 0.9 \pm 0.1 |
| DoS _{day 0} (%) | 83 \pm 1 | 79 \pm 1 | 83 \pm 1 | 75 \pm 1 |
| DoS _{day 9} (%) | 98 \pm 1 | 94 \pm 1 | 98 \pm 1 | 95 \pm 1 |

Table 7.8. Influence of air entrainment, surface finishing and curing period on the initial (S_i) and secondary (S_s) rate of water absorption (incl. R^2 values) and the 9 days water absorption (I) of FA+SF concrete.

| 28 days, cast | F(1)SF | F(1)SFA | F(2)SF | F(2)SFA |
|---|---------------|----------------|---------------|----------------|
| S_i ($\times 10^{-4}$ mm/ \sqrt{s}) | 11 | 10 | 12 | 15 |
| $R^2_{S_i}$ (-) | 0.92 | 0.94 | 0.92 | 0.92 |
| S_s ($\times 10^{-4}$ mm/ \sqrt{s}) | 2 | 3 | 3 | 3 |
| $R^2_{S_s}$ (-) | 0.92 | 0.94 | 0.90 | 0.91 |
| $I_{9\text{days}}$ (mm) | 0.5 \pm 0.1 | 0.5 \pm 0.1 | 0.5 \pm 0.1 | 0.6 \pm 0.1 |
| DoS _{day 0} (%) | 78 \pm 1 | 82 \pm 1 | 80 \pm 1 | 81 \pm 1 |
| DoS _{day 9} (%) | 93 \pm 3 | 97 \pm 1 | 99 \pm 1 | 95 \pm 1 |
| 28 days, troweled | F(1)SF | F(1)SFA | F(2)SF | F(2)SFA |
| S_i ($\times 10^{-4}$ mm/ \sqrt{s}) | 10 | 9 | 13 | 14 |
| $R^2_{S_i}$ (-) | 0.87 | 0.99 | 0.97 | 0.94 |
| S_s ($\times 10^{-4}$ mm/ \sqrt{s}) | 2 | 3 | 3 | 3 |
| $R^2_{S_s}$ (-) | 0.92 | 0.95 | 0.91 | 0.90 |
| $I_{9\text{days}}$ (mm) | 0.4 \pm 0.1 | 0.4 \pm 0.1 | 0.5 \pm 0.1 | 0.5 \pm 0.1 |
| DoS _{day 0} (%) | 82 \pm 3 | 85 \pm 1 | 83 \pm 1 | 85 \pm 1 |
| DoS _{day 9} (%) | 96 \pm 4 | 97 \pm 1 | 100 \pm 1 | 97 \pm 1 |
| 91 days, cast | F(1)SF | F(1)SFA | F(2)SF | F(2)SFA |
| S_i ($\times 10^{-4}$ mm/ \sqrt{s}) | 10 | 11 | 10 | 14 |
| $R^2_{S_i}$ (-) | 0.94 | 0.93 | 0.96 | 0.91 |
| S_s ($\times 10^{-4}$ mm/ \sqrt{s}) | 2 | 3 | 2 | 2 |
| $R^2_{S_s}$ (-) | 0.93 | 0.92 | 0.91 | 0.92 |
| $I_{9\text{days}}$ (mm) | 0.4 \pm 0.1 | 0.4 \pm 0.1 | 0.4 \pm 0.1 | 0.5 \pm 0.1 |
| DoS _{day 0} (%) | 81 \pm 1 | 84 \pm 1 | 81 \pm 2 | 82 \pm 1 |
| DoS _{day 9} (%) | 95 \pm 2 | 93 \pm 1 | 96 \pm 1 | 97 \pm 1 |
| 91 days, troweled | F(1)SF | F(1)SFA | F(2)SF | F(2)SFA |
| S_i ($\times 10^{-4}$ mm/ \sqrt{s}) | 9 | 12 | 8 | 14 |
| $R^2_{S_i}$ (-) | 0.94 | 0.94 | 0.95 | 0.91 |
| S_s ($\times 10^{-4}$ mm/ \sqrt{s}) | 2 | 3 | 2 | 2 |
| $R^2_{S_s}$ (-) | 0.94 | 0.93 | 0.91 | 0.91 |
| $I_{9\text{days}}$ (mm) | 0.4 \pm 0.1 | 0.4 \pm 0.1 | 0.3 \pm 0.1 | 0.5 \pm 0.1 |
| DoS _{day 0} (%) | 85 \pm 1 | 83 \pm 2 | 83 \pm 1 | 85 \pm 1 |
| DoS _{day 9} (%) | 97 \pm 1 | 95 \pm 2 | 96 \pm 1 | 100 \pm 1 |

7.7.6. Permeable porosity

Addition of AEA always resulted in higher permeable porosities ϕ (%) for the OPC mixture and the HVFA mixture made with fly ash F(2). This effect could not be observed for the composition containing fly ash F(1) (Figure 7.8).

After 28 d of curing, the porosities of the non-air entrained HVFA mixtures are significantly higher than the ones measured for T(0.45), and this for both drying temperatures (Figure 7.8a). The fly ash type used did not seem to have an important impact. At the age of 91 d, the differences in porosity with T(0.45) were reduced (Figure 7.8b).

Note that the order of magnitude of the porosities measured for the non-air entrained mixtures is similar to the porosities for OPC and HVFA concrete measured in Baert (2009) using the same technique. In Baert (2009) a good match could also be observed between porosities

determined as such and theoretical porosities that result from the Powers-Brownyard model updated by Baert (2009) for fly ash concrete.

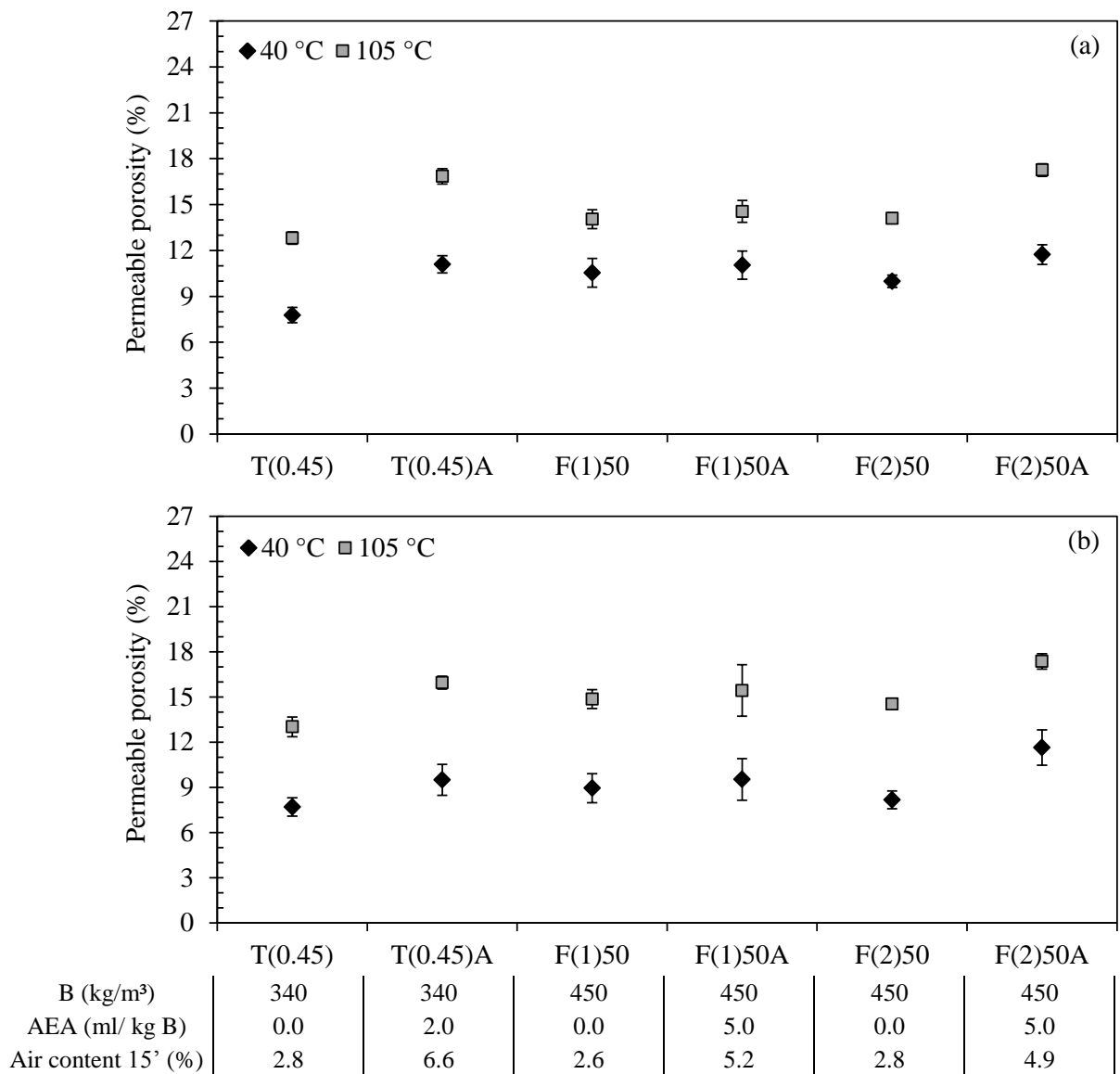


Figure 7.8. Influence of the concrete type (OPC or HVFA), the fly ash type (F(1) or F(2)) and the presence of AEA on the permeable porosity ϕ (%) after pre-drying at 40 °C and 105 °C and 28 days (a) and 91 days (b) of curing ($n = 9$).

The permeable porosities of the second series of HVFA concrete as determined on the same samples that were used for the preceding capillary sorption test are shown in Figure 7.9. When calculated from the masses under water (m_l) and the water saturated masses prior (m_s) to oven drying at 105 °C (Figure 7.9a), the porosities of air entrained HVFA concrete are very similar or just slightly higher than those of non-air entrained HVFA concrete. If on the other hand the m_l and m_s values after oven drying were used in Equation 7-7, the resulting permeable porosities of especially the air entrained HVFA concrete have increased significantly with 6.5% on average (Figure 7.9b). As a result, a substantial difference in porosity exists between non-air entrained and air entrained HVFA concrete.

Sample preconditioning may not have been the same, but a similar clear difference in permeable porosity was also observed between the T(0.45) and T(0.45)A, and F(2)50 and F(2)50A (Figure 7.8). The comparison between the porosities of F(1)50 and F(1)50A cannot be considered since the latter composition was not characterized by a well-developed air void system. For the calculation of the porosities shown in Figure 7.8 also m_s and m_l values after oven drying at 105 °C were used. These findings indicate that oven drying could damage the concrete matrix in a way that the concrete could take up more water in a subsequent vacuum saturation test. Concrete with a very pronounced entrained air void system and the resulting low strength microstructure seems to be susceptible to the phenomenon.

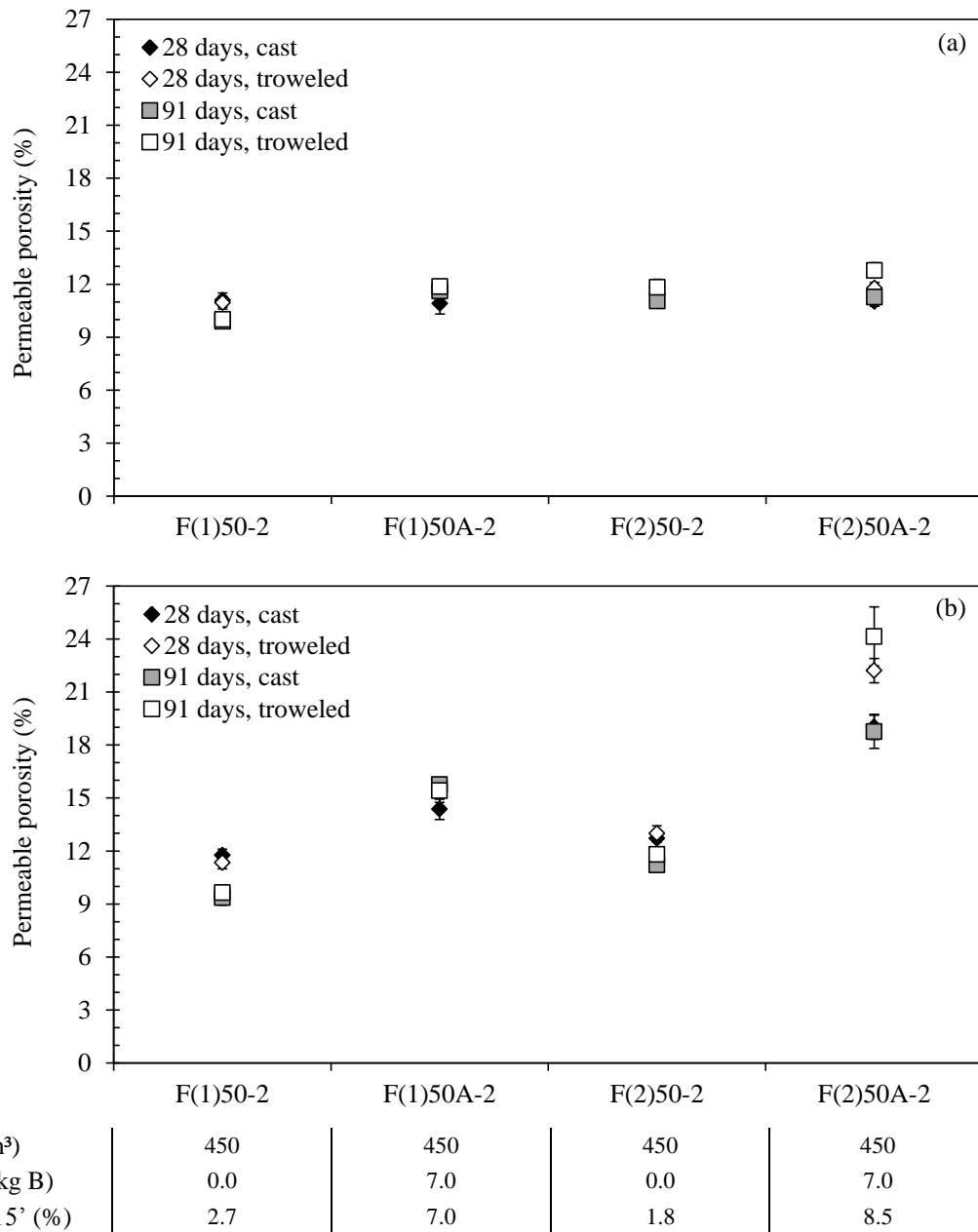


Figure 7.9. Influence of air entrainment and time of oven drying (before (b) or after (a) vacuum saturation) on the permeable porosity ϕ (%) of HVFA concrete ($n = 4$).

In contrast with the second series of HVFA concrete, the differences in permeable porosity of FA+SF concrete with and without AEA addition seems already visible when calculated from m_1 and m_s prior to oven drying (Figure 7.10a).

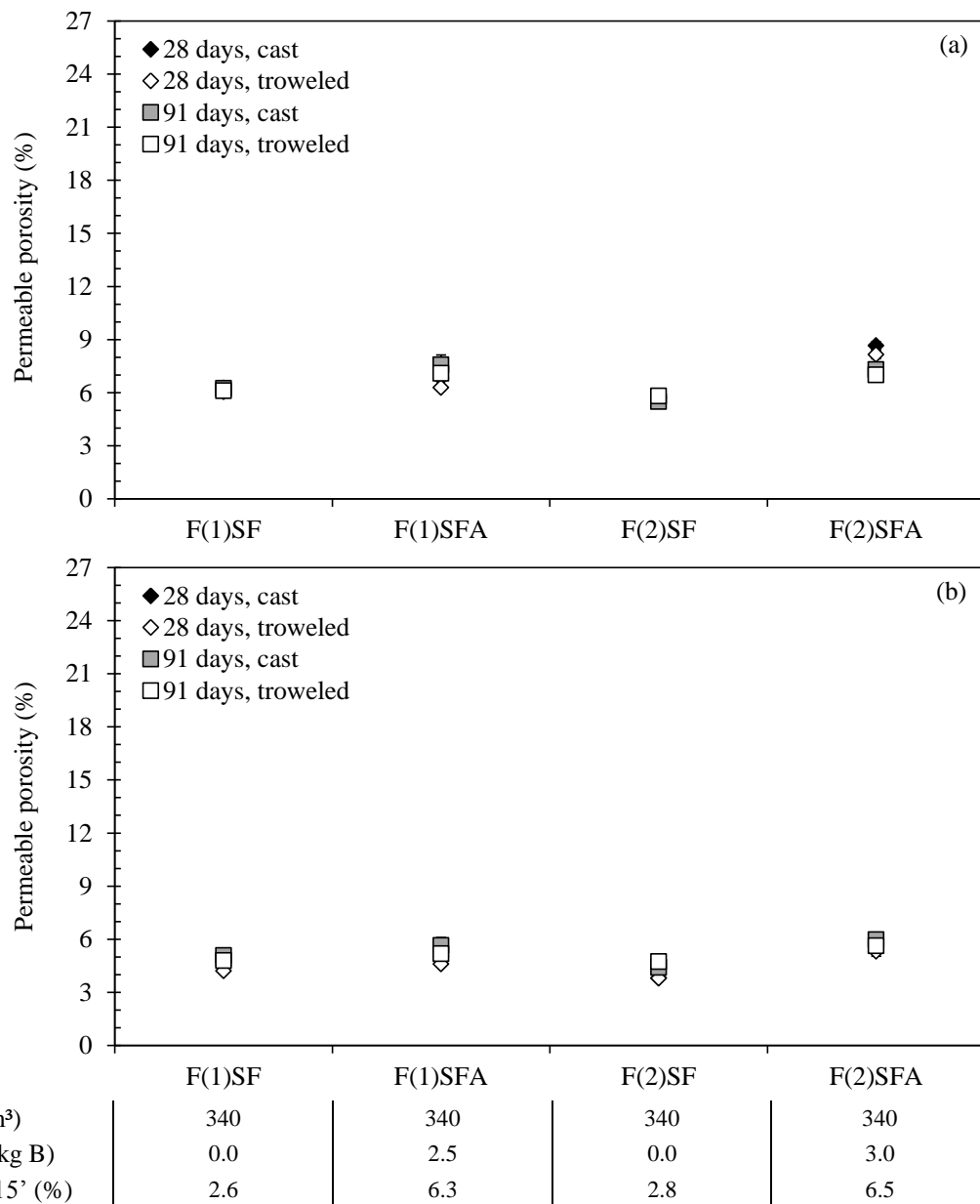


Figure 7.10. Influence of air entrainment and time of oven drying (before (b) or after (a) vacuum saturation) on the permeable porosity ϕ (%) of FA+SF concrete ($n = 4$).

An independent sample T test (Significance level = 0.05) revealed a significant difference in permeable porosity between the non-air entrained and air entrained FA+SF concrete mixtures in most cases. In case of oven drying after vacuum saturation (a), only the difference in permeable porosity between F(1)SF and F(1)SFA after 28 days was not significant for specimens with a troweled surface. In case of oven drying before vacuum saturation (b), non-significant differences were only observed between F(1)SF and F(1)SFA after 91 days, and this for both samples with cast and troweled surfaces. In general, with the addition of AEA, the permeable porosity is around 1.4 porosity percent higher. This difference did not change

substantially when m_i and m_s after oven drying were used to calculate the permeable porosity (Figure 7.10b). Then, the permeable porosities of F(1)SFA and F(2)SFA were around 1.0 porosity percent higher than those of F(1)SF and F(2)SF. Apparently oven drying at 105 °C did not induce damage to the microstructure that changed the water uptake.

For this concrete type it must be emphasized that even when air entrained it still exhibited a quite satisfactory mechanical strength performance (see Section 4.4.2). This could maybe explain the different behaviour of FA+SF in comparison with HVFA concrete.

Moreover, there is an overall reduction in porosity (−1.7 porosity percent) when choosing for vacuum saturation after oven drying (Figure 7.10a) instead of the reversed sequence (Figure 7.10b). For the moment this trend cannot be explained.

When looking at the porosity results of both concrete types (Figure 7.9 versus Figure 7.10), it is immediately clear that the porosities of all FA+SF mixtures are often only around half the porosities that were recorded for HVFA concrete. Regardless whether vacuum saturation occurred prior or after drying at 105 °C, no incontestable coherent effect of the applied curing period and surface finishing could be detected for HVFA and FA+SF concrete. The fly ash used (F(1) versus F(2)) did also not play an important role, except maybe for air entrained HVFA concrete that was dried before vacuum saturation.

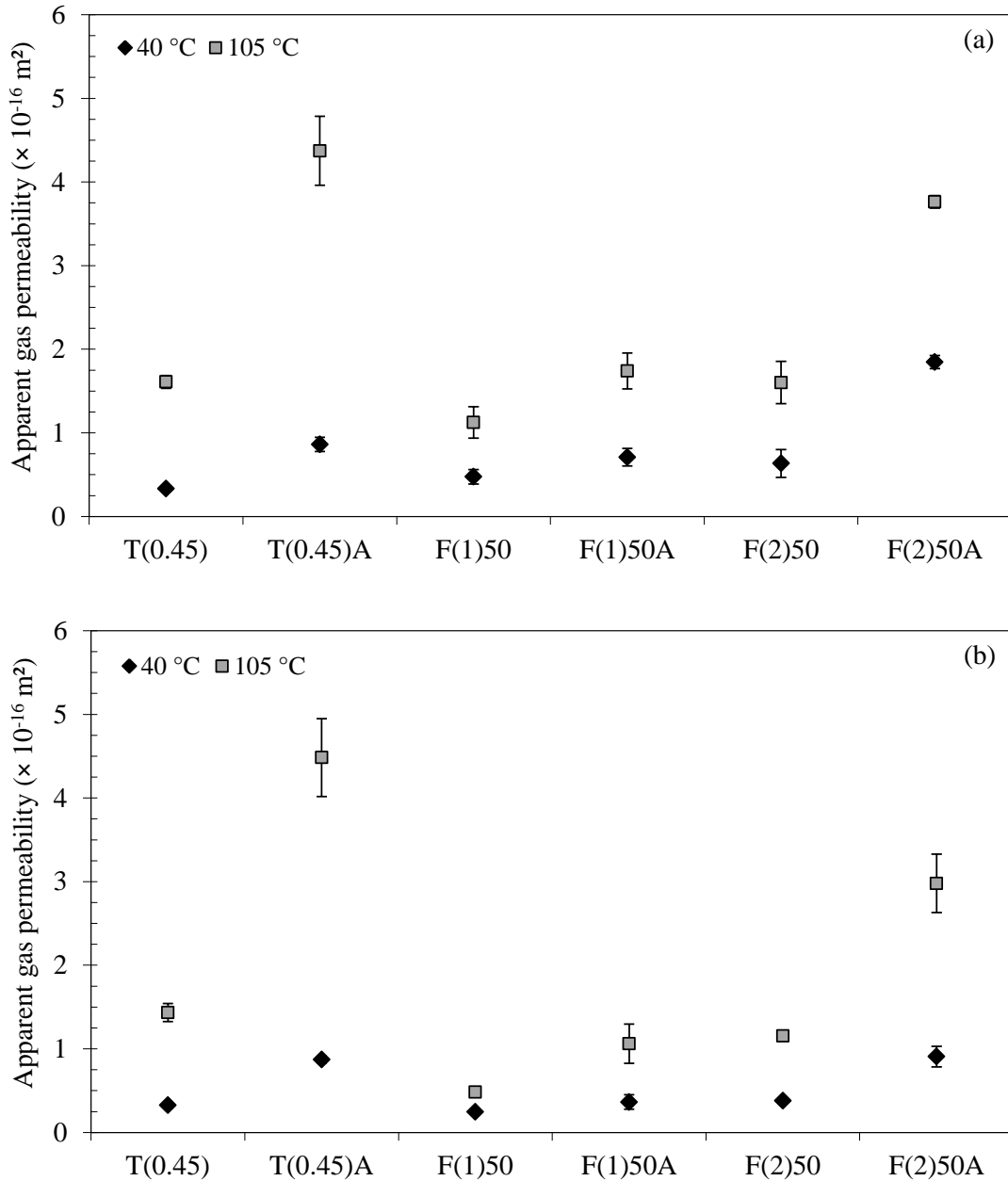
7.7.7. Gas permeability

With respect to OPC concrete and the first series of HVFA concrete, the addition of AEA resulted in higher gas permeability for all mixtures. At the age of 28 d, all air entrained concrete mixtures are clearly more permeable to gases than their non-air entrained equivalents (Figure 7.11a). After pre-drying at 40 °C, the k_a value of T(0.45)A is at least two times the value of T(0.45). The same conclusion can be drawn when F(2)50 and F(2)50A are compared with each other. A much smaller difference exists between F(1)50 and F(1)50A. Pre-drying at 105 °C makes the differences between the non-air entrained and the air entrained concrete mixtures much more pronounced. Yet again, the smallest increase in apparent gas permeability was observed between F(1)50 and F(1)50A. After 91 d of curing, the findings can be considered as similar (Figure 7.11b). Note that the k_a values of all HVFA mixtures decreased with prolonged curing.

Since already a pronounced difference in gas permeability was observed between the non-air entrained and air entrained versions of the first series of HVFA concrete, the second series of HVFA concrete characterized by an even more adequate air void system in hardened state was not evaluated anymore with respect to this transport property. It is expected that the addition of more AEA (7.0 ml/kg B instead of 5.0 ml/kg B) would result in an even higher apparent gas permeability in comparison with the k_a values that were recorded for compositions F(1)50 and F(2)50. However, this could not be verified anymore experimentally.

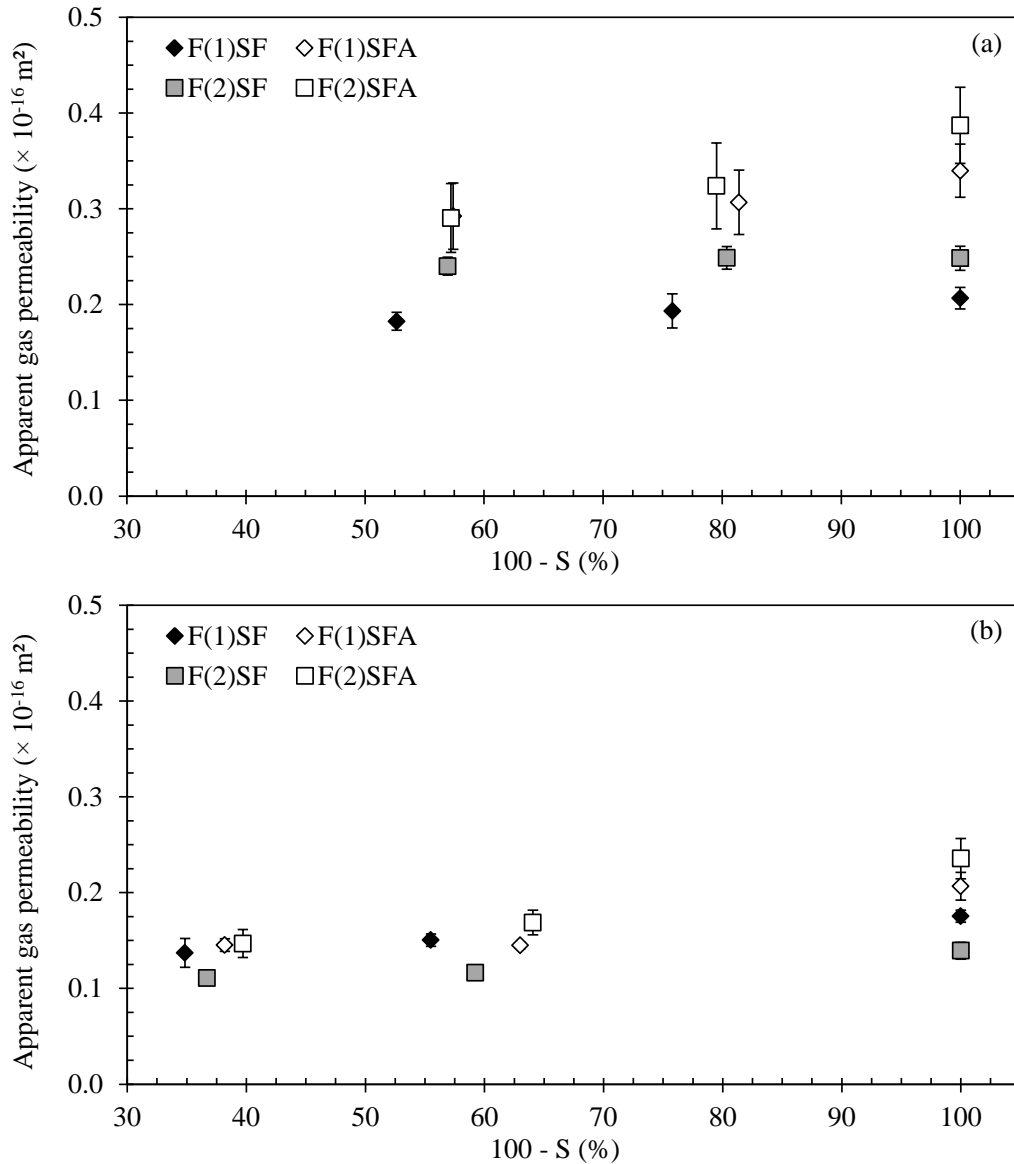
The apparent gas permeability of air entrained FA+SF concrete always exceeded the k_a value of its corresponding reference without incorporation of AEA (Figure 7.12). This was the case for almost every degree of saturation S (%) of the concrete that was considered throughout the test procedure after 28 days and 91 days of curing. The measured apparent gas permeability only very slowly increases as a function of the concrete's state of dryness ($= 100 - S$).

Sometimes subsequent drying at 80 °C and 105 °C barely seems to have an effect. Moreover, when the k_a values corresponding with the completely dry state (after drying at 105°C to constant mass) of HVFA and FA+SF concrete are compared, than the latter values turn out quite negligible ($< 0.5 \times 10^{-16} \text{ m}^2$). In correspondence with the results obtained for HVFA concrete in dry state, there is a decrease in gas permeability with prolonged curing.



| | | | | | | |
|------------------------|-----|-----|-----|-----|-----|-----|
| B (kg/m ³) | 340 | 340 | 450 | 450 | 450 | 450 |
| AEA (ml/ kg B) | 0.0 | 2.0 | 0.0 | 5.0 | 0.0 | 5.0 |
| Air content 15' (%) | 2.8 | 6.6 | 2.6 | 5.2 | 2.8 | 4.9 |

Figure 7.11. Influence of the concrete type (OPC or HVFA), the fly ash type (F(1) or F(2)) and the presence of AEA on the apparent gas permeability k_a ($\times 10^{-16} \text{ m}^2$) after 28 days (a) and 91 days (b) of curing ($n = 3$).



| | F(1)SF | F(1)SFA | F(2)SF | F(2)SFA |
|------------------------|--------|---------|--------|---------|
| B (kg/m ³) | 340 | 340 | 340 | 340 |
| AEA (ml/ kg B) | 0.0 | 2.5 | 0.0 | 3.0 |
| Air content 15' (%) | 2.6 | 6.3 | 2.8 | 6.5 |

Figure 7.12. Influence of air entrainment and concrete's degree of saturation S (%) with water on the apparent gas permeability k_a ($\times 10^{-16} \text{ m}^2$) of FA+SF concrete after 28 days (a) and 91 days (b) of curing ($n = 3$).

7.8. General discussion

7.8.1. Relation: AEA dosage, achieved air void system and salt scaling resistance

The overall results of the first series of HVFA concrete indicate that it is possible to design a HVFA concrete composition with an adequate salt scaling resistance under laboratory conditions. To achieve this, a lot of attention must be paid to the applied AEA dosage and the resulting air void system. Although the fresh air contents of the air entrained HVFA mixtures F(1)50A and F(2)50A were similar (5.2% and 4.9%, respectively), the air void system in the

hardened state was different. The automated air void analysis did not reveal important differences between the two mixtures. Yet, microscopic analysis on thin sections clearly showed a much less pronounced air void system for mixture F(1)50A. Apparently, the initially entrained air content could not be maintained everywhere in the concrete until setting. Time dependent monitoring of the air content in the first hours after mixing resulted in the following findings (Table 7.9):

(i) With an AEA dosage of 5.0 ml/kg B, the air contents of mixture F(2)50A after 15 min, 60 min and 120 min amounted to 4.0%, 7.2% and 6.6%, respectively. Thus, intermittent mixing (to simulate handling on site) resulted in an important increase of the fresh air content after 60 min. By the time of the measurement after 120 min, the air content had only gradually decreased again. A similar behaviour was observed during the time dependent air content monitoring of OPC reference T(0.45)A. Mixture F(1)50A on the other hand was characterized by a slight decrease of the air content with time (15 min: 4.6%; 60 min: 3.8%; 120 min: 4.0%).

(ii) The clearly different evolution in air content was also detected during the time dependent air content monitoring of the HVFA mixtures with the higher AEA dosage (7.0 ml/kg B). An increase in air content was recorded for mixture F(2)50A-2, while the air content of mixture F(1)50A-2 decreased as a function of time. Thus, when comparing the HVFA mixtures with the two different fly ashes, note that it is easier to obtain and maintain a high air content (6-7%) in mix F(2)50A(-2).

Table 7.9. Influence of the binder type on the evolution of the air content with time, as measured after 15, 60 and 120 min, for the applied AEA and SP dosages.

| Time | Parameter | T(0.45)A | F(1)50A | F(2)50A |
|---------|--------------------|-----------------------------------|-----------------------------------|-----------------------------------|
| | | 2.0 ml AEA/kg B 4.0 ml SP/kg B | 5.0 ml AEA/kg B 4.0 ml SP/kg B | 5.0 ml AEA/kg B 4.0 ml SP/kg B |
| 15 min | Slump ⁺ | S5 | S2 | S5 |
| | Air content | 6.8% | 4.6% | 4.0% |
| 60 min | Slump ⁺ | S3 | S1 | S1 |
| | Air content | 9.5% | 3.8% | 7.2% |
| 120 min | Slump ⁺ | S1 | S1 | S1 |
| | Air content | 7.8% | 4.0% | 6.6% |
| Time | Parameter | F(1)50A-2 | | F(2)50A-2 |
| | | 7.0 ml AEA/kg B 4.0 ml SP/kg B | | 7.0 ml AEA/kg B 4.0 ml SP/kg B |
| 15 min | Slump ⁺ | S2 | | S3 |
| | Air content | 6.1% | | 6.1% |
| 60 min | Slump ⁺ | S1 | | S1 |
| | Air content | 5.1% | | 7.7% |
| 120 min | Slump ⁺ | S1 | | S1 |
| | Air content | 4.4% | | 7.7% |

⁺ S1 (10-40 mm), S2 (50-90 mm), S3 (100-150 mm), S4 (160-210), S5 (≥ 220 mm).

All these findings point out that the initial air content in the fresh state is quite susceptible to changes with time. It immediately explains why there is almost never an exact match between the initial air content in the fresh state and the air content in the hardened state. Literature

search shows that many parameters (cement fineness, presence of finely divided materials, slump, temperature, mixer type, mixing time, transportation, consolidation, pumping,...) can influence the effectiveness of the air entrainment [Du and Folliard (2005), Dolch (1996)].

Additional mixing of the concrete normally tends to increase the fresh air content because it can induce a post-activation of the fatty acid/polyglycol based AEA (mechanism 1). An additional air entraining effect may also come from the polycarboxylic ether-based superplasticizer. This type of SP contains a defoamer to compensate for the air entraining capacities of the side chains on the comblike SP molecules. These defoamers are known to be active for only a limited period of time. As a result, they cannot prevent additional air entrainment by the SP side chains forever (mechanism 2). These two mechanisms may very well explain the evolution in air content for mixtures T(0.45)A, F(2)50A and F(2)50A-2.

The question remains why the fresh air content of F(1)50A and F(1)50A-2 decreased with time. Now, it has been reported that the presence of finely divided materials such as fly ash can be held responsible for a reduced air content. According to Dolch (1996), there is a twofold explanation for this. First of all, fine fractions tend to “bind” more of the mix water because of the fact that it coats their larger surface areas. As a consequence, the water cannot be part of the air bubble generating and stabilizing process. Secondly, increased solid surface area may adsorb molecules of the AEA and render them unusable in the air entrainment process. The results obtained in this research indicate that these findings can also hold true for HVFA concrete, especially when the fly ash is very fine. The fact that fly ash F(1) (45 μm fineness: 13.2% retained) was much finer than fly ash F(2) (45 μm fineness: 26.6% retained), can explain the better performance of the AEA in combination with fly ash F(2). According to Du and Folliard (2005), the carbon containing portions of fly ash are also thought to be highly adsorptive. Loss on ignition – an indicator for this carbon content, although sometimes questioned [Hill et al. (1997)] – was quite similar for the two studied fly ashes (Table 4.3: 4.8% and 4.4%). Thus, this phenomenon probably does not explain the difference in AEA stability between F(1)50A and F(2)50A.

Although the automated air void analysis and salt scaling test performed on air entrained FA+SF concrete confirmed that an initial air content in the fresh state of 6.3-6.5% is sufficient, it is still worthwhile investigating how this air content in the fresh state actually evolves with time. Table 7.10 gives an overview of this evolution for mixtures F(1)SFA and F(2)SFA.

Table 7.10. The evolution of the air content with time, as measured after 15, 60 and 120 min, for the applied AEA and SP dosages in air entrained FA+SF concrete.

| Time | Parameter | F(1)SFA | F(2)SFA |
|---------|--------------------|------------------------------------|------------------------------------|
| | | 2.5 ml AEA/kg B 12.0 ml SP/kg B | 3.5 ml AEA/kg B 10.0 ml SP/kg B |
| 15 min | Slump ⁺ | S4-S4 | S4 |
| | Air content | 6.3%-5.3% | 6.5% |
| 60 min | Slump ⁺ | S1-S4 | S1 |
| | Air content | 10.0%-17.0% | 17.0% |
| 120 min | Slump ⁺ | S1-S4 | S1 |
| | Air content | 7.5%-15.0% | 15.0% |

⁺ S1 (10-40 mm), S2 (50-90 mm), S3 (100-150 mm), S4 (160-210), S5 (≥ 220 mm).

For mixture F(1)SFA the time dependent monitoring of the air content was performed twice. The second time, three concrete cubes were cast at each step in the process. These cubes were tested for compressive strength at the age of 28 days. This was done for two reasons. First of all, the general appearance of the concrete with time changed as such that it became mushy (Figure 7.13).



Figure 7.13. Influence of additional intermittent mixing on the fresh state appearance of air entrained FA+SF concrete.

Moreover, the fresh state air content increased quite spectacularly due to the additional intermittent mixing of the concrete (Table 7.10). Letting the concrete rest for another hour did not cause a drop of the air content to its original level. The outcome of the compressive strength tests revealed that this phenomenon caused a substantial decrease in strength class (from C40/50 to barely C12/15). Apparently, there is an incompatibility between the applied chemical admixtures and the cement replacing materials. Nevertheless, without the intermittent mixing the applied dosages of AEA and SP in combination with fly ash and silica fume did not affect the concrete's strength performance and salt scaling resistance. Yet, this problem needs to be investigated further on to avoid problems in practice. In the future, other types of SPs and AEAs with a different chemical basis will need to be tested in combination with fly ash and silica fume.

7.8.2. Relation: AEA dosage, achieved air void system and transport properties

Adding an AEA to improve the concrete's salt scaling resistance can increase the water penetrability and gas permeability of the concrete. When looking at the capillary sorption behaviour of the first series of HVFA concrete, the use of 5.0 ml kg/B AEA did not seem to have an important effect. When water is forced into the concrete during the vacuum saturation

test, the porosities obtained for the concrete mixtures with an AEA inside are substantially higher. Mixture F(1)50A with incorporation of the finer fly ash is the only exception. Similar trends were observed during the evaluation of the concrete's gas permeability at 2 bar pressure, especially after pre-drying at 105 °C. Apparently, whenever increased (vacuum or external) pressures are applied to measure the concrete's transport properties, air entrained concrete mixtures can be considered as more accessible to water and O₂.

Similar conclusions can be drawn from the comparison of non-air entrained and air entrained HVFA concrete from the second series. Again, the permeable porosities of the latter concrete compositions were higher. The differences in porosity were even more significant for the permeable porosities calculated from the sample masses under water and the water saturated sample masses after oven drying at 105 °C. Well air entrained HVFA concrete with a low strength seems more susceptible to damage of the microstructure induced by oven drying at a high temperature. Vacuum saturation prior to oven drying is recommended for the determination of the permeable porosity of the concrete.

From the capillary sorption test entirely conforming to ASTM C1585 – 4e (2007) it could be concluded that the water absorption at the end of the test was the highest for HVFA concrete containing 7.0 ml AEA per kg binder although the differences remained small. Analysis of the rates of absorption did not reveal relevant effects of adding this dosage of AEA. Thus, the conclusion remains that only techniques involving an above normal external pressure and high drying temperature can induce large differences between HVFA concrete with and without AEA, which may not be realistic. The very same holds true for FA+SF concrete, except maybe for the fact that drying at 105 °C is not seen as a problem now. Apparently, even with an entrained air void system present its microstructure is not weakened enough to cause damage induced by oven drying.

Finally, from the comparison between non-air entrained and air entrained concrete in terms of their transport properties some tentative conclusions can also be drawn with respect to their resistance to other deterioration mechanisms. For instance, since the air permeability of concrete is key a governing factor for its carbonation resistance [Borges et al. (2010)], the increase in apparent gas permeability due to air entrainment may indicate that applying an AEA may increase the concrete's susceptibility to the carbonation phenomenon. The comparative carbonation experiments done on FA+SF concrete indeed seem to confirm this effect (Section 5.6.1).

7.9. Conclusions

- HVFA concrete with a total binder content of 450 kg/m³ and a W/B ratio of 0.35 can have an acceptable deicing salt scaling resistance ($\Delta m \leq 1 \text{ kg/m}^2$) of the cast surface when subjected to the severe accelerated salt scaling test prescribed by the applicable European standard after both 28 d and 91 d of curing. To achieve this performance, the necessary AEA dosage in presence of the specific fly ashes used in this research, must be considerably higher than for OPC concrete (7.0 ml/kg binder versus 2.0 ml/kg binder). Even then, the salt scaling resistance still tended to decrease a little bit with time. Colorimetric carbonation measurements prior to the start of every salt scaling test showed no increase in carbonation depth between 28 and 91 d. Thus, carbonation cannot explain

more salt scaling after 91 d. Given this tendency of having a little more salt scaling at later age, these HVFA compositions should also be subjected to the accelerated salt scaling tests at much later ages for further verification. To see whether this phenomenon also occurs under natural freeze/thaw conditions, additional field testing would also be needed.

- An adequate artificially induced air void system is necessary to minimize salt scaling. Especially when the fly ash is finer, it was found that it is more difficult to maintain the initially entrained air content necessary for an adequate air void system in hardened state. As a consequence, a sole measurement of the air content in the fresh state after 15 min is insufficient. It is recommended to measure the air content again after 60 and 120 min to evaluate its stability with time for the AEA-fly ash combination under investigation.
- It is also advised to design HVFA concrete compositions in accordance with the higher air content requirements (min. 6% to 7%) imposed by ACI 201.2R (2008) instead of the 4% and 5% air contents proposed by NBN EN 206-1 (2000) and NBN B 15-001 (2004), respectively. This way, the air-to-paste ratio necessary for an adequate air void system (18-20%, cf. [Pinto (2001), Mielenz (1958)]) is also ensured. Further research is needed to see whether this paste content dependency also exists for other concrete types.
- The combined implementation of the time dependent monitoring of the air content and the higher air content requirements would ensure that the amount of air entrained with an AEA in the presence of fly ash is enough. However, it remains unsure whether this rather time consuming design approach is achievable in everyday practice.
- With respect to the transport properties of the concrete, it was found that the presence of the artificial air bubbles increases the permeable porosity (as measured with water sorption under vacuum) as well as the apparent gas permeability coefficient significantly. Both properties were obtained from an accelerated test that involves an external pressure. The differences were observed both after sample preconditioning at 40 °C and 105 °C and they are applicable to the OPC and HVFA concrete mixtures that were investigated in this research. It indicates that AEA additions can affect the durability performance (e.g. resistance to steel corrosion) of these concrete mixtures in a negative way. During a natural capillary sorption test on the other hand, no significant differences in the 14 days water absorption could be observed between the non-air entrained and the air entrained batches of each concrete mixture. When the capillary sorption tests were conducted in correspondence with ASTM C1585 – 4e (2007) slight differences in water absorption do seem to exist. Yet, these differences are negligible.
- It should be noted that increasing the pre-drying temperature to 105 °C tends to change the ranking between the OPC and HVFA concrete mixtures with respect to their 14 d water absorption. Pre-drying at 105 °C also tends to amplify the difference in apparent gas permeability coefficient between the non-air entrained and the corresponding air entrained concrete mixtures. Therefore, we recommend pre-drying at 40 °C instead of at 105 °C. Regarding the permeable porosity involving a drying step at 105 °C, it is advised to calculate the value of this transport property from samples masses under water and the water saturated masses measured prior to oven drying. Therefore, the vacuum saturation should be done first.
- With respect to FA+SF concrete, it is much easier to obtain a concrete with an adequate air void system in hardened state and a salt scaling resistance that meets the 1 kg/m² criterion.

The required AEA dosages (2.5-3.0 ml kg/ B) are comparable to those needed in OPC concrete. The only problem that remains is the compatibility problem for the now considered combination of polycarboxylic ether-based SP and fatty acid/polyglycol-based AEA due to additional intermittent mixing (a practice that could occur on site). It increases the fresh air content dramatically and affects the concrete strength in a very negative way. A combination of another SP and AEA will need to be considered in the future.

- Finally, FA+SF concrete performs much better than HVFA concrete in terms of capillary water absorption, permeable porosity and gas permeability. AEA addition increases all of them, but not in a problematic manner.

PART III

SERVICE LIFE PREDICTION

Service life prediction for carbonation-induced corrosion

8.1. Choosing an appropriate prediction model and failure event

When it comes to predicting the service life of steel reinforced concrete subject to corrosion, either carbonation or chloride-induced, one has several options to consider.

According to Yuan (2009), a first important distinction can be made based on the nature of the input parameters to the prediction model. When the values of all model input parameters are fixed, the model is deterministic. If on the other hand all input parameters are treated as continuous stochastic variables, each characterized by a mean value, a standard deviation and a probabilistic density function, the model is probabilistic. Although not mentioned by Yuan (2009), a semi-probabilistic approach also exists. More details on its origin can be found in CUR guideline VC81 (2009). Filling in a mean value for each input parameter to a deterministic model will give a service life estimation that corresponds with a probability of failure of no less than 50%. For design purposes this is unacceptable. A full probabilistic approach allows for a determination of service life characterized by a much lower probability of failure. Since this method requires knowledge of all uncertainties involved and the use of specific probabilistic software, the semi-probabilistic approach has been introduced. The models used for the job originate from probabilistic analyses performed on a number of preceding case studies. This link with the probabilistic approach is necessary to determine the value of a number of partial safety factors that should ensure a sufficiently low probability of failure for the estimated service life. The models also demand characteristic values for all model input instead of mean values. The main advantage of semi-probabilistic models is that they are very straightforward and easy to use for routine design purposes. However, for more complex design cases, the full probabilistic method is still recommended.

The available prediction models can also be divided into two classes depending on their empirical or physical nature. Empirical models rely on very basic experimental concrete data and environmental parameters obtained in a relatively short period of time. These data are fitted to simple mathematical models. The resulting expressions are widely used in practice, mainly because of their simplicity. It is not surprising that most models prescribed in engineering guidelines for durability design (e.g. *fib* Bulletin 34 (2006), DuraCrete (1998-2000)) are empirical. This approach obviously has some drawbacks. The fact that early age

data are being extrapolated to predict a performance on the long term is certainly questionable. For instance, Nilsson (2002) concluded that for modelling chloride ingress this can bring along serious errors. Another main disadvantage of empirical models is that they are usually developed using data from laboratory factorial experiments and do not take into account interference of different factors [Otieno et al. (2011)].

Physical models do not have these problems. Within these expressions all occurring physical processes related to the studied deterioration mechanism are described as scientifically as possible. As a consequence, it becomes much more difficult to determine analytical solutions to these evidently more complex expressions. The necessary model input for each relevant physical process cannot easily be measured. Within the development process of a new, potentially 'green' concrete type, this aspect becomes a serious issue, especially in the early stages of the process. At that time a simple empirical approach may still be more useful, despite its drawbacks. Evidently, once the first rough empirical estimations give promising results, further verification by means of physical models is certainly recommended.

In this research, only the empirical approach was applied. Where possible, the applied models were updated with test results at different ages to reduce the errors that could result from extrapolating early age test results. This was done for the probabilistic prediction of the time to carbonation- and chloride-induced steel depassivation (= the corrosion initiation period) in accordance with *fib* Bulletin 34 (2006). A first rough estimation of the corrosion propagation period after depassivation was done using the semi-probabilistic approach suggested by DuraCrete (1998-2000). Carbonation-induced corrosion initiation and propagation have been addressed in this chapter. Service life predictions related to chloride-induced corrosion follow in Chapter 9.

8.2. First order probabilistic estimation of the corrosion initiation period

8.2.1. Limit state function

Plotting the measured carbonation depths as a function of the square root of time usually results in a fairly linear relation. As there is a direct link with Fick's first law of diffusion, this trend has a well-understood physical background. For long, this square-root-of-time relation for the carbonation rate has been considered as an effective way to estimate roughly when the carbonation front is expected to reach the reinforcing steel and trigger its depassivation. As such, a very basic limit state function can be defined for carbonation-induced steel depassivation (Equation 8-1):

$$g(d, x_c(t)) = d - x_c(t) = d - A_{\text{field}} \sqrt{t} \quad (8-1)$$

with d , the concrete cover (mm), $x_c(t)$, the carbonation depth at time t (mm), A_{field} , the carbonation rate under field conditions (mm/ $\sqrt{\text{years}}$) and t , the time (years). Nevertheless, it must be said that Equation 8-1 provides a rather simplified approach. As mentioned in Section 5.4.6 the natural carbonation rate A_{field} is obtained from Equation 5-5 which is nothing more than a simple conversion formula to go from the higher CO_2 concentration under laboratory conditions to the expected CO_2 concentration on site. For instance, it disregards the continuously changing natural environment of the concrete. Moreover, the negative effect of a

lack of curing, i.e. any measures taken to prevent premature desiccation near the concrete surface, on its effective carbonation resistance is not taken into account that way.

8.2.2. Field carbonation coefficient

The estimated A_{field} values of all studied concrete compositions, exposure conditions and curing ages can be found in Table 5.2. They were calculated from Equation 5-5 and correspond with a CO_2 concentration in the field of 0.05%. This is somewhat higher than the now observed CO_2 concentration in practice which is only around 0.03%. According to *fib* Bulletin 34 (2006), assuming a higher constant value for the atmospheric CO_2 concentration C_s of 0.00082 kg/m³ or 0.05% by volume should take into account that the current value will still increase with time (due to the greenhouse effect). According to Ehrenberg and Geiseler (1997) an increase of about 1.5 ppm per year can be expected. It should be noted that in recent literature sources more pessimistic scenarios are being mentioned. According to Stewart et al. (2011) there is the scenario of CO_2 stabilization at 550 ppm by the year 2150. It considers the effect of policy intervention. Without this intervention, much higher CO_2 concentrations (700-1000 ppm) by that time seem very well possible. CO_2 levels of this order of magnitude were not considered in his research. Evidently, it is recommended to pay attention to these worst case scenarios as well in the future.

8.2.3. Concrete cover

The value of the concrete cover d is normally chosen in perspective of the environment in which the concrete will be used. The appropriate design value for the different exposure classes is specified in Eurocode NBN EN 1992-1-1 (ANB 2010). Although strictly specified, its actual value in practice varies due to the unavoidable inaccuracies that occur in the construction stage. Therefore, this parameter has to be considered as a stochastic variable instead of as a constant value.

A normal distribution could be used to describe this variable. Yet, one has to keep in mind that this distribution does not exclude negative values for the concrete cover. Therefore, this distribution type can only be used for large concrete covers. In case of small concrete covers, distributions excluding negative concrete covers should be chosen, e.g. the Lognormal, Beta, Weibull(min)- or Neville distribution. Although the concrete covers required for the studied exposure classes in this research were always quite large, a lognormal distribution was assumed for this parameter at all time.

A typical standard deviation for the concrete cover highly depends on whether there are particular execution requirements for the concrete structure or not. Without them, the standard deviation should range between 8 and 10 mm. With assurance of an enhanced precision in the execution, the standard deviation can be decreased to 6 mm. In this research, a standard deviation of 8 mm was adopted.

NBN EN 1992-1-1 (ANB 2010) prescribes a nominal concrete cover of 25 and 30 mm for exposure classes XC3 and XC4 in case of the standard construction class S4 which corresponds with a design service life of 50 years. A design service life of 100 years implies an upgrade to construction class S6 which requires a nominal concrete cover of 35 and 40 mm, respectively. Mainly the latter two concrete covers were considered.

8.3. Second order probabilistic estimation of the corrosion initiation period

8.3.1. Original limit state function of *fib* Bulletin 34

Fib Bulletin 34 (2006) provides a more sophisticated concrete and environment specific limit state function (Equation 8-2).

$$g(d, x_c(t)) = d - x_c(t) = d - \sqrt{2 \cdot k_e \cdot k_c \cdot R_{NAC,0}^{-1} \cdot C_S} \cdot \sqrt{t} \cdot W(t) \quad (8-2)$$

with d , the concrete cover (mm), $x_c(t)$, the carbonation depth at time t (mm), k_e , the environmental function that accounts for the relative humidity in practice (–), k_c , the execution transfer parameter that deals with concrete curing (–), $R_{NAC,0}^{-1}$, the inverse effective carbonation resistance under natural carbonation conditions ((mm²/years)/(kg/m³)), C_S , the expected increased atmospheric CO₂ concentration with time without additional emissions attributed to motorized traffic (kg/m³) and $W(t)$, the weather function (–).

8.3.2. Environmental function

Environmental function k_e (Equation 8-3) takes into account that the humidity level (RH_{real}) of the actual concrete environment may differ from the reference relative humidity (RH_{ref} : 60%) imposed during the accelerated carbonation test.

$$k_e = \left(\frac{1 - \left(\frac{RH_{real}}{100} \right)^{f_e}}{1 - \left(\frac{RH_{ref}}{100} \right)^{f_e}} \right)^{g_e} \quad (8-3)$$

where f_e and g_e represent two constant parameters which are independent of the exposure conditions and management phases. As suggested by *fib* Bulletin 34 (2006) parameter RH_{real} should normally represent the relative humidity of the carbonated layer instead of relative humidity of the environment. Given the fact that these data are not readily available and that the carbonation process only takes place in the outer layer of the concrete, it is justifiable to use mean daily RH values of the ambient air. Such data for RH_{real} are normally collected from a weather station close to the location of the concrete structure. Since the main purpose of this research is an environmental evaluation of a newly developed HVFA or FA+SF concrete composition which has not been applied yet in practice, a fictitious concrete structure assumed to be located near the weather station of Zaventem, Belgium was considered. The daily mean values recorded at this weather station between 1999 and 2008 were provided by the Royal Meteorological Institute (KMI) (Table 5.1). They were used to estimate the distribution for RH_{real} . Since the lower limit of the relative humidity in Belgium is significantly different from zero and the upper limit is 100%, it is appropriate to use a distribution function with an upper and lower limit. In this research, a Beta-distribution was assumed for this parameter.

8.3.3. Execution transfer parameter

A value for the execution transfer parameter k_c (–) that accounts for the curing effect is obtained from Equation 8-4.

$$k_c = \left(\frac{t_c}{7} \right)^{b_c} \quad (8-4)$$

with b_c , the exponent of regression (–) and t_c , the period of curing (days). According to *fib* Bulletin 34 (2006), any measures taken to prevent premature desiccation of the concrete surface (water curing, air curing while covering the concrete surface with sheets, etc.) are seen as ways that guarantee proper curing. In this research, the period of curing corresponded with the period during which the samples were preconditioned at 20 °C and 95% RH. Note that the exponent b_c in Equation 8-4 may vary for different concrete types. The rather slow pozzolanic FA reaction that takes place in HVFA concrete may require longer curing than more traditional concrete in order to achieve the highest carbonation resistance possible. Accelerated carbonation tests were executed at different curing ages to evaluate this. Unfortunately, due to the observed slight increase in carbonation rate between 91 and 182 days of optimal curing (see Section 5.6.2), it was not possible to do a proper curve fitting based on only three points in time (t_c : 28, 91 and 182 days) to estimate a mix specific value of b_c for all studied concrete compositions. For now, the overall mean value (–0.567), standard deviation (0.024) and normal distribution of b_c as suggested by *fib* Bulletin 34 (2006) were adopted for all studied concrete types. As a consequence, there is for the moment no differentiation in curing behaviour between the concrete mixtures. Evidently, a more mix specific approach with respect to curing is still strongly recommended.

8.3.4. Inverse effective carbonation resistance under natural conditions

The value for $R_{NAC,0}^{-1}$ is normally calculated from the effective inverse carbonation resistance of dry concrete $R_{ACC,0}^{-1}$ (Equation 8-5), determined at a certain point in time t_0 using the accelerated carbonation test prescribed by *fib* Bulletin 34 (2006).

$$R_{NAC,0}^{-1} = k_t \cdot R_{ACC,0}^{-1} + \varepsilon_t \quad (8-5)$$

with k_t , a regression parameter which considers the influence of the test method (–) and ε_t , an error term which takes into account inaccuracies that occur conditionally when using the accelerated test method ((mm²/years)/(kg/m³)). The prescribed carbonation test consists of exposing the concrete to 2% CO₂ for 28 days after 7 days of optimal curing in water followed by 21 days of suboptimal curing (at 20°C and 65% RH). Since our accelerated carbonation test method involves exposure to no less than 10% CO₂, $R_{NAC,0}^{-1}$ cannot be calculated for the tested concrete compositions by means of Equation 8-5. Therefore, we decided to replace $\sqrt{(2 \cdot R_{NAC,0}^{-1} \cdot C_s)}$ in Equation 8-2 with A_{field} , the same load variable that was used for the simplified limit state function described in Section 8.2.1. The correspondence between $\sqrt{(2 \cdot R_{NAC,0}^{-1} \cdot C_s)}$ and A_{field} can easily be understood from the strong resemblance between

Equation 5-1 and the well-known square-root-time relation for the carbonation coefficient A_{field} (cf. Equation 8-1).

8.3.5. The weather function

By means of weather function $W(t)$ (Equation 8-6) the effect of occurring wetting events such as (driving) rain is included in the limit state function.

$$W = \left(\frac{t_0}{t} \right)^w = \left(\frac{t_0}{t} \right)^{\frac{(p_{\text{SR}} \cdot \text{ToW})^{b_w}}{2}} \quad (8-6)$$

with t_0 , the time of reference (years), w , the weather exponent (–), p_{SR} , the probability of driving rain (–), ToW , the time of wetness (–) and b_w , the exponent of regression (–). The probability p_{SR} corresponds with the average distribution of the wind direction during raining events. Its value for vertical elements was estimated from KMI weather station data measured in Zaventem, Belgium between 1998 and 2008. For the same location and time period, the average number of rainy days per year was used to calculate ToW . According to *fib* Bulletin 34 (2006), the minimum amount of precipitation for a rainy day is 2.5 mm. Based on these data, the occurrence of more realistic wet/dry cycles in exposure class XC4 can be accounted for and implemented in the limit state function. For exposure class XC3, the most critical condition exists for outdoor concrete sheltered from rain. Logically, the weather function is preferably omitted for this exposure class.

8.3.6. Applied limit state function based on *fib* Bulletin 34

Combining Equations 8-3, 8-4 and 8-6 into Equation 8-2 where A_{field} replaces $\sqrt{(2 \cdot R_{\text{NAC},0}^{-1} \cdot C_s)}$ results in an alternative limit state function (Equation 8-7) that also considers the effect of concrete curing and the varying relative humidity and weather conditions and still is to a large extent based on *fib* Bulletin 34 (2006).

$$g(d, x_c(t)) = d - x_c(t) = d - \sqrt{k_e \cdot k_c} \cdot A_{\text{field}} \cdot \sqrt{t} \cdot W(t) \quad (8-7)$$

8.3.7. Summarizing overview of the model input parameters

An overview of the applied distributions and their characterizing parameters (mean, standard deviation, lower and upper boundary) for each of the input parameters to either the simplified and advanced limit state functions are shown in Table 8.1.

The reliability indices (β) and probabilities of failure (P_f) associated with the first and second order limit state functions (Equation 8-1 and 8-7) were calculated using the First Order Reliability Method (FORM) available in the probabilistic Comrel software [RCP Consulting (1987-2013)]. Figure 8.1 gives the typical calculation output as a function of time. In compliance with the *fib* Bulletin 34 (2006), these parameters need to meet the requirements for the depassivation limit state ($\beta \geq 1.3$ and $P_f \leq 0.10$) to qualify for use.

Table 8.1. Quantification of the input parameters to the simplified 1st order and advanced 2nd order limit state functions for service life prediction.

| Parameter | Distribution | Mean | Stdv. | Lower boundary | Upper boundary |
|-----------------------------------|--------------|------------|-------|----------------|----------------|
| d_{XC3} (mm) | Lognormal | 35 | 8 | — | — |
| d_{XC4} (mm) | Lognormal | 40 | 8 | — | — |
| A_{field} (mm/ \sqrt{years}) | Normal | Table 5.2 | 0.1 | — | — |
| RH_{real} (%) | Beta | 79 | 9 | 40 | 100 |
| RH_{ref} (%) | Constant | 60 | — | — | — |
| f_e (—) | Constant | 5.0 | — | — | — |
| g_e (—) | Constant | 2.5 | — | — | — |
| b_c (—) | Normal | -0.567 | 0.024 | — | — |
| t_c (d) | Constant | 28 | — | — | — |
| t_0 (years) | Constant | 0.0767 | — | — | — |
| p_{SR} (—) | Constant | 0.16 (XC4) | — | — | — |
| ToW (—) | Constant | 0.31 (XC4) | — | — | — |
| b_w (—) | Normal | 0.446 | 0.163 | — | — |

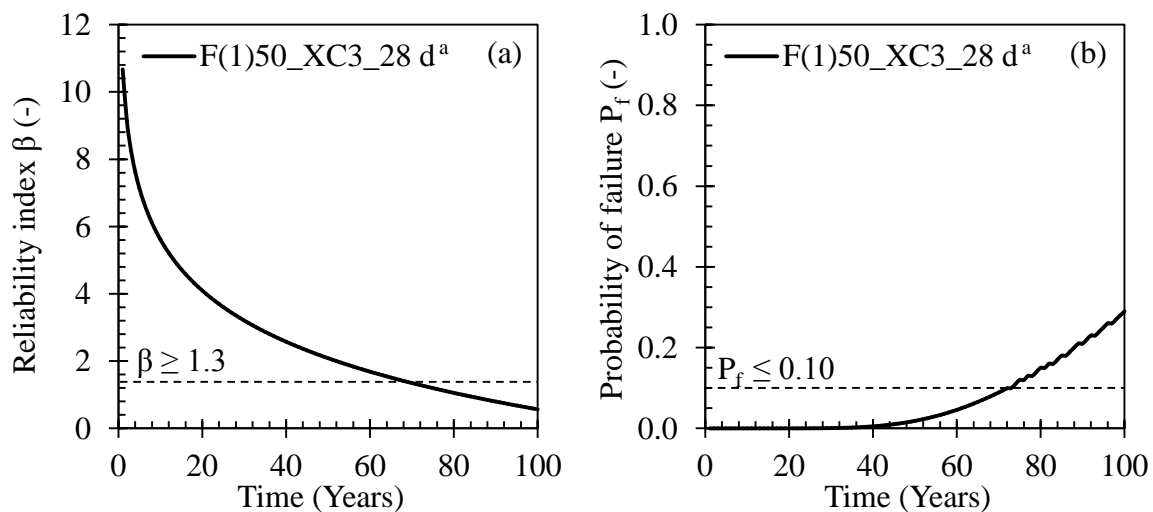


Figure 8.1. Typical evolution of the reliability index β (a) and probability of failure P_f (b) as a function of time as obtained in Comrel using the First Order Reliability Method (FORM).

8.4. Semi-probabilistic estimation of the corrosion propagation period

8.4.1. Limit state function of DuraCrete

The semi-probabilistic limit state function for the corrosion propagation period suggested by DuraCrete (1998-2000) enables an estimation of the time to unacceptable corrosion-induced cracking of the concrete cover on top of the rebar. This unacceptable cracking is associated with a critical crack width of 1.0 mm which normally marks the onset of concrete spalling. Equation 8-8 represents the as such defined limit state function in its most basic form.

$$\begin{aligned}
 g(x) &= w_{cr} - w^d \\
 &= w_{cr} - \left(w_0 + b^c \cdot \gamma_b \cdot (p^d - p_0^d) \right)
 \end{aligned}
 \tag{8-8}$$

With w_{cr} , the critical crack width of 1.0 mm, w^d , the design value of the actual crack width at a certain point in time, w_0 , the width of the initial visible crack width (0.050 mm), b^c , the characteristic value of the parameter accounting for the position of the rebar (top: 0.0086 mm/ μ m, bottom, 0.0104 mm/ μ m), γ_b , partial factor for b^c in case of a normal cost of mitigation of risk relative to the cost of repair (= 1.40), p^d , the design value of the occurring corrosion penetration (μ m) and p_0^d , the design value of the corrosion penetration necessary to produce a crack (μ m).

8.4.2. Corrosion penetration necessary to produce a crack

According to DuraCrete (1998-2000), cracking initiation mainly depends on the concrete cover/rebar diameter ratio and the tensile splitting strength of the concrete. Given this relation, parameter p_0^d can be calculated by means of Equation 8-9.

$$p_0^d = a_1 + a_2 \cdot \frac{d - \Delta d}{\Phi} + a_3 \cdot f_{c,sp}^d
 \tag{8-9}$$

With d , the concrete cover (mm), Δd , safety margin for the cover thickness (mm), Φ , the diameter of the rebar (mm), a_1 , a_2 , a_3 , three predefined regression parameters and $f_{c,sp}^d$, the design value of the tensile splitting strength (MPa).

Regarding the concrete cover d , the prescribed design values for exposure class XC3 and XC4 were used (Section 8.2.3). The safety margin for the concrete cover depends on the cost of mitigation of risk relative to the cost of repair. For a normal cost ratio a partial factor of 14 mm can be assumed. Since the duration of the propagation period was not determined for a specific steel reinforced concrete structure, the diameter of the rebar is not really fixed. A default value of 12 mm was adopted for Φ . In accordance with DuraCrete (1998-2000), the regression parameters a_1 , a_2 and a_3 amounted to 74.4 μ m, 7.3 μ m and -17.4μ m/MPa, respectively. Within Equation 8-9, parameter $f_{c,sp}^d$ is the only parameter that needs to be quantified experimentally. The necessary background regarding its experimental determination for the studied concrete mixtures is given in Section 8.4.3.

8.4.3. Tensile splitting strength

NBN EN 12390-6 (2010) indicates that the tensile splitting strength of concrete can be determined on samples with varying geometries. The standard sample geometry is a concrete cylinder. However, cubic or prismatic specimens could be used as well. DuraCrete (1998-2000) does not really specify which sample geometry should be used for quantifying $f_{c,sp}^d$. In this research, prismatic specimens were used. The test specimens originated from four 600×150×150 mm³ prisms which were first subjected to a three-point bending test cf. NBN EN 12390-5 (2009). The tensile splitting test was performed on each half of those prisms for only a selection of the concrete mixtures under investigation, i.e. OPC references T(0.45) and

T(0.55), HVFA composition F(1)50 and FA+SF composition F(1)SF. Their mean values and standard deviations on the individual values as well as the corresponding characteristic strength values are given in Table 8.2. In accordance with DuraCrete (1998-2000), the characteristic tensile splitting strength was adopted as design value $f_{c,sp}^d$.

Note that the first OPC reference T(0.45) relates to an environment involving chloride ingress and not carbonation. The corresponding $f_{c,sp}^d$ value is merely mentioned here. An estimation of the chloride-induced corrosion propagation period for composition T(0.45) in comparison with F(1)50 and F(1)SF based on their corresponding $f_{c,sp}^d$ values follows in Chapter 9.

Table 8.2. Tensile splitting strength (MPa) of OPC, HVFA and FA+SF concrete as measured in accordance with NBN EN 12390-6 (2010).

| Tensile splitting strength (MPa) | T(0.45) | T(0.55) | F(1)50 | F(1)SF |
|----------------------------------|---------|---------|--------|--------|
| Mean $f_{c,sp}$ | 5.17 | 3.52 | 4.01 | 4.97 |
| Stdv. $f_{c,sp}$ | 0.23 | 0.26 | 0.23 | 0.33 |
| $f_{c,sp}^d$ | 4.72 | 3.00 | 3.55 | 4.31 |

8.4.4. Occurring corrosion penetration

The occurring corrosion penetration is mainly controlled by the corrosion rate of the reinforcing steel once depassivated. Equation 8-10 quantifies this parameter.

$$p^d = V^d \cdot w_t \cdot (t - t_i^d) \quad (8-10)$$

With V^d , the design value of the corrosion rate ($\mu\text{m}/\text{years}$), w_t , the relative time of wetness (XC3: 0.5 / XC4: 0.75), t , the time to unacceptable corrosion-induced cracking (years) and t_i^d , the design value of the time to steel depassivation (years). Although V^d could be measured experimentally, the model relies for its quantification on a pronounced relation between corrosion rate and concrete resistivity as observed by Andrade and Arteaga (1998) and supplemented by Nilsson and Gehlen (1998) (Section 8.4.5).

8.4.5. Corrosion rate

Equation 8-11 represents the in literature reported relation between the steel corrosion rate and the concrete resistivity.

$$\begin{aligned}
 V^d &= \frac{m_0}{\rho_c} \cdot \alpha^c \cdot F_{cl}^c \cdot \gamma_v \\
 &= \frac{m_0}{\rho_0^c \cdot \left(\frac{t_{hydr}}{t_0}\right)^{n_{res}^c} \cdot k_{c,res}^c \cdot k_{T,res}^c \cdot k_{RH,res}^c \cdot k_{cl,res}^c} \cdot \alpha^c \cdot F_{cl}^c \cdot \gamma_v \\
 &= \frac{m_0}{\rho_0^c \cdot \left(\frac{t_{hydr}}{t_0}\right)^{n_{res}^c} \cdot k_{c,res}^c \cdot \frac{1}{1 + K^c(T-20)} \cdot k_{RH,res}^c \cdot k_{cl,res}^c} \cdot \alpha^c \cdot F_{cl}^c \cdot \gamma_v
 \end{aligned} \quad (8-11)$$

With m_0 , constant for corrosion rate versus resistivity ($= 882 \mu\text{m}\cdot\Omega\text{m}/\text{year}$), F_{cl}^{c} , the characteristic value of the chloride corrosion rate factor ($= 1.0$, for a chloride-free environment), α^{c} , the characteristic value of the pitting factor ($= 2.0$, in absence of chlorides), γ_{v} , the partial factor for the corrosion rate ($= 1.40$ for a normal cost mitigation of risk / cost of repair ratio), ρ^{c} , the characteristic value of the resistivity (Ωm), ρ_0^{c} , the characteristic value of the potential electrolytical resistivity (Ωm), t_0 , the age of the concrete at the time of the resistivity measurement ($= 28$ days or 0.0767 years), t_{hydr} , the age of the concrete corresponding with maximum hydration ($= 1$ year), $n_{\text{res}}^{\text{c}}$, the age factor for the electrolytical resistivity (OPC concrete: 0.23 , FA concrete: 0.62 , according to DuraCrete (1998-2000)), $k_{\text{c,res}}^{\text{c}}$, the characteristic value of the curing factor for the resistivity ($= 1.0$), $k_{\text{T,res}}^{\text{c}}$, the characteristic value of the temperature factor for the resistivity, $k_{\text{RH,res}}^{\text{c}}$, the characteristic value of the humidity factor for the resistivity (XC3: OPC, 80% RH: 3.80 , assumed idem for FA and SF), $k_{\text{cl,res}}^{\text{c}}$, the characteristic value accounting for the presence of chloride ($= 1.0$ for a chloride-free environment), K_{c} , characteristic value of the temperature dependency factor ($= 0.025^{\circ\text{C}^{-1}}$ for temperatures below $20^{\circ\text{C}}$) and T , the temperature ($= 10^{\circ\text{C}}$).

8.4.6. Potential electrolytical resistivity

The electrolytical resistivity ρ_0^{c} of the concrete is an experimental input parameter to the model. Per studied concrete composition this property should be determined by means of a standardized test method. As recommended in DuraCrete (1998-2000), the Two-Electrode Method (TEM) was used for this purpose. The procedure consists of passing an alternating current between two disc-shaped stainless steel electrodes in contact with the concrete, and measuring the resulting voltage (Figure 8.2). With both the current and the voltage known, the resistance R_{TEM} of the concrete can be quantified. The corresponding bulk resistivity ρ_{TEM} is a material property based on this resistance which is independent of the sample geometry [Polder (2001)]. As can be seen in Equation 8-12, its dimension is resistance multiplied by length (Ωm).

$$\rho_{\text{TEM}} = R_{\text{TEM}} \cdot \frac{A}{l} \quad (8-12)$$

Where A is the cross-section (m^2) and l is the length (m) of the measured specimen. DuraCrete (1998-2000) suggests cylindrical specimens with the same dimensions (H : 50 mm, \varnothing : 100 mm) as for the rapid chloride migration test for the resistivity measurements. Preferably, the specimens have been water cured for 28 days prior to the test. The characteristic value of the potential electrolytical resistivity ρ_0^{c} corresponds with the 5% fractile of the predicted (normal) distribution of the performed measurements.

In this research, the bulk resistivity of compositions T(0.45), T(0.55), F(1)50 and F(1)SF was determined with a commercially available Proceq Resipod resistivity meter (Figure 8.2) on six of the suggested concrete cylinders (H : 50 mm, \varnothing : 100 mm) per concrete mixture. The samples were not water cured for 28 days to avoid a leaching of ions which can substantially affect the recorded value of the resistivity [Weiss et al. (2013)]. Instead, concrete cubes were stored in a climatized room at $20^{\circ\text{C}}$ and 95% RH for 21 days. Next, cores were drilled from

the cubes and the appropriate cylindrical samples were sawn from the cores. After keeping them under the same climatized conditions until they were 28 days of age, they were vacuum saturated in accordance with NT Build 492 (1999). The vacuum saturation step was included to ensure thoroughly wet specimens with exclusion of very pronounced leaching phenomena. Leaching would have been much more dominant if the specimens had been cured under water for 28 days to obtain thoroughly wet specimens. The R_{meas} value ($\text{k}\Omega\text{cm}$) measured with the Proceq Resipod resistivity meter, which is in fact a modified four-point Wenner probe, can be converted to bulk resistivity by means of Equation 8-13.

$$\rho_{\text{TEM}} = \frac{R_{\text{meas}} - R_{\text{upper}} - R_{\text{lower}}}{2 \cdot \pi \cdot a_{\text{Wenner}}} \cdot \frac{A}{l} \quad (8-13)$$

With R_{upper} , Resipod reading for the foam insert of the upper electrode ($\text{k}\Omega\text{cm}$), R_{lower} , Resipod reading for the foam insert of the lower electrode ($\text{k}\Omega\text{cm}$) and a_{Wenner} , the probe spacing of the four-point Wenner probe ($= 5.0 \text{ cm}$).

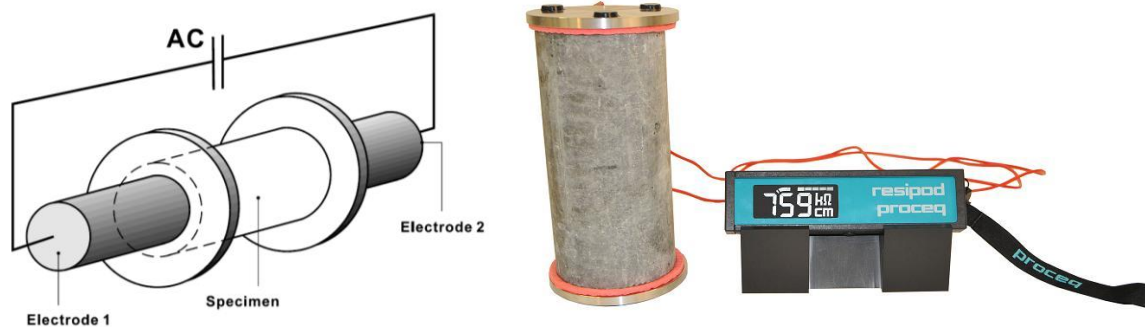


Figure 8.2. Principle of the Two Electrode Method (TEM) for measuring the electrolytical bulk resistivity cf. DuraCrete (1998-2000) and experimental setup for such a measurement using a Proceq Resipod resistivity meter.

Table 8.3 gives an overview of the measured ρ_{TEM} and ρ_0^{c} values for concrete compositions T(0.45), T(0.55), F(1)50 and F(1)SF after 28 days optimal curing. The lowest potential electrolytical resistivity was recorded for OPC reference T(0.55) with $50.02 \text{ }\Omega\text{m}$. Then, OPC reference T(0.45) and HVFA composition F(1)50 followed with ρ_0^{c} values of 81.49 and $92.27 \text{ }\Omega\text{m}$, respectively. FA+SF composition F(1)SF was characterized by the highest ρ_0^{c} value ($352.72 \text{ }\Omega\text{m}$).

The measured resistivities are all in line with resistivity values reported in literature. According to Polder (2001) and Bertolini et al. (2013) the resistivity of concrete can vary over a wide range, i.e. from 10^1 to $10^5 \text{ }\Omega\text{m}$. The main influencing parameters are the moisture content of the concrete (environment) and the concrete composition. Since sample preconditioning should have ensured a similar moisture content for all tested mixtures, the observed differences in bulk resistivity must originate from the differences in composition. The lower bulk resistivity of OPC reference T(0.55) in comparison with T(0.45) can mainly be explained by the higher W/C ratio of the former mixture (0.55 versus 0.45). A higher W/C

ratio normally implies the presence of wider pores. The imposed current will be more easily carried by the ions dissolved in the pore liquid. As a consequence, the resistivity will be lower [Polder (2001)]. The higher bulk resistivity of the HVFA and FA+SF composition can only be in part explained by their low W/B ratio (0.35). The incorporation of (porosity reducing) reactive minerals such as fly ash and silica fume are also known for increasing the concrete resistivity [Polder (2001)].

Table 8.3. Bulk resistivity (Ωm) measured for OPC, HVFA and FA+SF concrete.

| Bulk resistivity (Ωm) | T(0.45) | T(0.55) | F(1)50 | F(1)SF |
|---|----------------|----------------|---------------|---------------|
| Mean ρ_{TEM} | 86.52 | 57.00 | 102.81 | 391.56 |
| Stdv. ρ_{TEM} | 2.31 | 3.20 | 4.83 | 17.82 |
| Characteristic value ρ_0^c | 81.49 | 50.02 | 92.27 | 352.72 |

Since composition T(0.45) is not a reference concrete type for an environment with exposure to carbonation-induced corrosion, its value was not implemented in the model that estimates the corrosion propagation period for the same exposure class. In this chapter, merely compositions T(0.55), F(1)50 and F(1)SF were compared with each other in terms of their estimated corrosion propagation period in exposure class XC3. The bulk resistivity of mixture T(0.45) was used later on in Chapter 9 for estimating the time to unacceptable corrosion-induced cracking in presence of chlorides.

8.4.7. Summarizing overview of the model input parameters

Table 8.4 gives a summarizing overview of all the input parameters needed to estimate the time to unacceptable corrosion-induced concrete cracking in a semi-probabilistic way. Such an estimation was done for concrete compositions T(0.55), F(1)50 and F(1)SF located in a XC3 environment to enable a comparison between concrete types and to see whether the time to steel depassivation differs much from the time to unacceptable cracking.

Table 8.4. Quantification of the model input parameters for the semi-probabilistic estimation of the corrosion propagation period cf. DuraCrete (1998-2000).

| Parameter | Value | Parameter | Value |
|------------------------------------|--------------|--|--------------|
| w_{cr} (mm) | 1.0 | m_0 ($\mu\text{m}\cdot\Omega\text{m}/\text{year}$) | 882 |
| w_0 (mm) | 0.05 | α^c | 2.0 |
| b^c (mm/ μm) | 0.0104 | F_{cl}^c | 1.0 |
| γ_b (-) | 1.40 | ρ_0^c (Ωm) | Table 8.3 |
| d (mm) | 35 | t_{hydr} (year) | 1.0 |
| Δd (mm) | 14 | t_0 (year) | 0.0767 |
| Φ (mm) | 12 | $n_{\text{res_OPC}}^c$ (-) | 0.23 |
| $f_{\text{c,sp}}^d$ (MPa) | Table 8.2 | $n_{\text{res_FA, SF}}^c$ (-) | 0.62 |
| a_1 (μm) | 74.4 | $k_{\text{c, res}}^c$ (-) | 1.0 |
| a_2 (μm) | 7.3 | K_c ($^{\circ}\text{C}^{-1}$) | 0.025 |
| a_3 ($\mu\text{m}/\text{MPa}$) | -17.4 | T ($^{\circ}\text{C}$) | 10 |
| w_t (-) | 0.50 | $k_{\text{RH, res}}^c$ (-) | 3.80 |
| γ_V (-) | 1.40 | $K_{\text{cl, res}}^c$ (-) | 1.0 |

For some model input parameters (n_{res}^c and $k_{RH,res}^c$), DuraCrete (1998-2000) does not give values for every type of binder system. For both the HVFA and FA+SF concrete composition the age factor n_{res}^c prescribed for FA concrete was adopted (= 0.62). With respect to the humidity factor $k_{RH,res}^c$, the prescribed value for OPC concrete (which is almost identical to the one for BFS concrete) was adopted for all three compositions. In theory, the time to steel depassivation t_i^d is also an input parameter to the model. However, since this parameter can be isolated in the limit state function, its semi-probabilistic quantification is not really necessary to determine the duration of the corrosion propagation period.

8.5. Results and discussion

8.5.1. First order estimation of the corrosion initiation period

When looking at exposure class XC3, the studied HVFA and FA+SF compositions would be characterized by a much shorter time to carbonation-induced steel depassivation (as estimated from Equation 8-1) than OPC reference T(0.55) and the k-value conforming FA references F(1)15 and F(2)15 (Table 8.5). However, for the applied colorimetric and microscopic carbonation assessment methods, the time to steel depassivation would still easily exceed the predefined service life of 100 years after 28 days (F(1)50: 132-176 years, F(2)50: 196-159 years, F(1)SF: 372-514 years, F(2)SF: 322 years) of optimal curing.

Table 8.5. Influence of the simulated exposure class, the carbonation assessment method and curing age on the first order estimation of the time to steel depassivation (years).

| 1st order/XC3 | t₀ (d) | T(0.55) | F(1)15 | F(2)15 | F(1)50 | F(2)50 | F(1)SF | F(2)SF |
|---------------------------------|--------------------------|------------------|----------------|----------------|-----------------|----------------|------------------|----------------|
| Colorimetric | 28 | +1000 | – | – | 132 | 196 | 372 | 322 |
| | | – | – | – | 71 ^a | – | 220 ^a | – |
| | | 196 ^b | – | – | 40 ^b | – | 121 ^b | – |
| | | – | – | – | 21 ^c | – | 71 ^c | – |
| Microscopic | 28 | 750 | +1000 | +1000 | 176 | 159 | 514 | 322 |
| 1st order/XC4 | t₀ (d) | T(0.50)* | F(1)15* | F(2)15* | F(1)50* | F(2)50* | F(1)SF* | F(2)SF* |
| Colorimetric | 28 | – | – | – | +1000 | +1000 | – | – |
| Microscopic | 28 | – | +1000 | +1000 | +1000 | +1000 | – | – |

* Times to depassivation were calculated with inclusion of the immersion period in water.

^a Based on A_{field} values for suboptimal curing: 7 days at 20°C and 95% RH, 21 days at 20°C and 60% RH.

^b Based on A_{field} values for optimal curing corrected for the applied CO₂ concentration.

^c A_{field} values for suboptimal curing^a after correction for the applied CO₂ concentration^b.

The very low carbonation rates for all mixtures, as obtained under the laboratory conditions that should represent exposure class XC4, were responsible for the generally applicable time to depassivation of at least 1000 years (the upper limit of the timeframe considered in Comrel). Thus, a predefined service life of 100 years would not be a problem in this simulated XC4 environment. However, this statement is not necessarily valid for exposure class XC4 in general. As already pointed out in Section 5.6.1, regular immersion of the concrete in water every two weeks considerably hindered further penetration of CO₂. Concrete carbonation rates in environments characterized by more irregular wet/dry cycles and longer drying periods, could easily be much higher and result in faster depassivation of the embedded reinforcing steel.

8.5.2. Second order estimation of the corrosion initiation period

Applying the more sophisticated limit state function (Equation 8-7) gives a different outcome of the estimated service lives. Regardless the exposure class, the concrete composition, the optimal curing period and the carbonation assessment method used for determining the carbonation coefficient, the estimated time to steel depassivation was always much higher (Table 8.6). Note that standard deviations on the regression of A_{field} were used for these calculations. The effect of using standard deviations on the individual values instead has been evaluated in Appendix B.

Table 8.6. Influence of the simulated exposure class, the carbonation assessment method and curing age on the second order estimation of the time to steel depassivation (years).

| 2nd order/XC3 | t₀ (d) | T(0.55) | F(1)15 | F(2)15 | F(1)50 | F(2)50 | F(1)SF | F(2)SF |
|---------------------------------|--------------------------|------------------|----------------|----------------|------------------|----------------|------------------|---------------|
| Colorimetric | 28 | +1000 | – | – | 452 | 672 | +1000 | +1000 |
| | | – | – | – | 244 ^a | – | 753 ^a | – |
| | | 672 ^b | – | – | 137 ^b | – | 414 ^b | – |
| | | – | – | – | 72 ^c | – | 244 ^c | – |
| Microscopic | 28 | +1000 | +1000 | +1000 | 604 | 546 | +1000 | +1000 |
| 2nd order/XC4 | t₀ (d) | T(0.50) | F(1)15* | F(2)15* | F(1)50* | F(2)50* | F(1)SF | F(2)SF |
| Colorimetric | 28 | – | – | – | +1000 | +1000 | – | – |
| Microscopic | 28 | – | +1000 | +1000 | +1000 | +1000 | – | – |

* Times to depassivation were calculated with A_{field} for exposure class XC3 in combination with the weather function $W(t)$ with $p_{\text{SR}} = 0.16$ and $\text{ToW} = 0.31$.

^a Based on A_{field} values for suboptimal curing: 7 days at 20°C and 95% RH, 21 days at 20°C and 60% RH.

^b Based on A_{field} values for optimal curing corrected for the applied CO_2 concentration.

^c A_{field} values for suboptimal curing^a after correction for the applied CO_2 concentration^b.

To see which model input parameter postpones steel depassivation the most, only one parameter at a time (k_e , k_c or $W(t)$) was considered in Equation 8-7, while the other two were temporarily removed from it. The resulting service life predictions – three in total – were performed for HVFA mixture F(1)50, cured for 28 days and then assumed to be located in a XC3 environment ($a_{\text{XC3}} = 35$ mm, A_{field} colorimetric = 2.2 mm/ $\sqrt{\text{years}}$). True, it was decided to look at the most critical condition for exposure class XC3. This means that the concrete was assumed to be sheltered from rain and thus the weather function should be omitted. Nevertheless, for this example the weather function was also considered once with $p_{\text{SR}} = 0.16$ and $\text{ToW} = 0.31$ (Table 8.1), as if the concrete was located in exposure class XC4. This was done just to see the effect of the weather function. The weather function was no longer considered for all other service life predictions regarding exposure class XC3.

When only depending on model input parameter k_e , k_c or $W(t)$, the estimated time to steel depassivation would be 206 years, 289 years and 705 years, respectively. Thus, the low k_e value due to the high relative humidity ($79 \pm 9\%$) inherent to the Belgian climate (Zaventem, 1999-2008, source: KMI) is in part causing the longer steel depassivation period when estimated with the second order limit state function (Equation 8-7). The curing factor seems to have a quite similar effect. The low $W(t)$ value that accounts for the time of wetness ($\text{ToW} = 0.31$) and the probability of driving rain ($p_{\text{SR}} = 0.16$), postpones steel depassivation the most (up to 705 years). This factor is mainly responsible for the very long corrosion initiation

periods for all mixtures in exposure class XC4 (Table 8.6). However, this effect was not considered in the calculations for exposure class XC3. Only the combined effect of k_e and k_c was still taken into account. As such, the time to depassivation for HVFA mixture F(1)50, cured for 28 days and assumed to be located in a XC3 environment sheltered from rain, amounts to 452 years (Table 8.6). In fact, based on this combined *fib* Bulletin 34 (2006) approach, one would expect that repair of structures made with either of the studied concrete compositions would not need to be feared within the first 100 years after construction. This can in part be attributed to the fact that the expected relative humidity of the sheltered concrete environment does not favor carbonation-induced steel depassivation. Also concrete curing seems to play an important role. An optimal curing period of 28 days is already quite long. In practice, this period is often much shorter. If equal to less than 7 days, which is unfortunately not uncommon, the value of the curing factor k_c would exceed 1 (Equation 8-4) and the time to steel depassivation would be considerably shorter. Now, in this research the effect of more suboptimal curing was not accounted for by means of the value of k_c . Instead, A_{field} values calculated from an accelerated carbonation test after 28 days of suboptimal curing (7 days at 20°C and 95% RH followed by 21 days at 20°C and 60% RH) were implemented in the second order limit state function (Equation 8-7) without the weather function. This was done for mixtures F(1)50 (Table 5.2^a: 3.0 mm/ $\sqrt{\text{years}}$) and F(1)SF (Table 5.2^a: 1.7 mm/ $\sqrt{\text{years}}$). Obviously, the resulting times to depassivation become shorter than in case of 28 days of optimal curing (Table 8.6^a), yet they still exceed 100 years (F(1)50: 244 years, F(1)SF: 753 years).

Apart from the above mentioned parameters, there may be another important cause for the rather long depassivation periods obtained, namely the experimental origin of the field carbonation coefficient A_{field} . This value was calculated by means of Equation 5-5 from the accelerated carbonation coefficient A_{acce} obtained after exposing the concrete to 10% CO₂. As already mentioned in Section 5.4.2, Castellote et al. (2009) believe that the maximum CO₂ concentration during an accelerated carbonation test should be no more than 3%. In Section 5.6.3.1, correction factors were proposed for concrete mixtures T(0.55), F(1)50 and F(1)SF to account for the much higher CO₂ concentration that was mainly applied in this study. The resulting corrected A_{field} values were considerably higher (Table 5.2^b: T(0.55): 1.8 mm/ $\sqrt{\text{years}}$, F(1)50: 4.0 mm/ $\sqrt{\text{years}}$, F(1)SF: 2.3 mm/ $\sqrt{\text{years}}$). After implementation of these values in the second order limit state function (Equation 8-7) without the weather function, the estimated times to steel depassivation are still more than 100 years for OPC reference T(0.55) (Table 8.6^b: 672 years), HVFA composition F(1)50 (Table 8.6^b: 137 years) and FA+SF composition F(1)SF (Table 8.6^b: 414 years).

If the correction factors for the high CO₂ concentration during carbonation testing would be applied to the A_{acce} values for suboptimally cured HVFA and FA+SF concrete, then the resulting A_{field} values would amount to 5.5 mm/ $\sqrt{\text{years}}$ and 3.0 mm/ $\sqrt{\text{years}}$, respectively (Table 5.2^c). In that case, the estimated times to steel depassivation are only higher than 100 years for the FA+SF composition (Table 8.6^c: F(1)50: 72 years, F(1)SF: 244 years).

Finally, it must be recognized that the service life predictions were conducted under the assumption that the applied concrete cover was always in agreement with the limiting values imposed by NBN EN 1992-1-1 (ANB 2010) for a service life of 100 years (a_{XC3} : 35 mm, a_{XC4} : 40 mm) and that the concrete was entirely free of defects (cracks, etc.). As a

consequence, the studied HVFA and FA+SF mixtures, which are obviously more susceptible to carbonation than OPC concrete and FA concrete conforming to the k-value concept, may indeed be characterized by a time to carbonation-induced steel depassivation < 100 years due to the presence of flaws. Careful interpretation of theoretical service life predictions is therefore still advised. Insufficient concrete cover or cracking could cancel out the dominance of the beneficial effects inherent to the concrete environment and curing actions. In that perspective, the first order non-environment specific prediction approach for scenarios ^(a), ^(b) and ^(c) is also worth considering (Table 8.5). Then, each of the three scenarios gives a time to steel depassivation of less than 100 years for the HVFA mixture. In case of the FA+SF mixture only scenario ^(c) seems to be a problem.

8.5.3. Influence of the selected failure event

Table 8.7 indicates that after carbonation-induced steel depassivation it should still take quite a while before cracks 1 mm in width will occur. The time to unacceptable corrosion-induced cracking ($t_{\text{crack}_1 \text{ mm}}$) amounts to 31 years for OPC reference T(0.55). For the concrete mixtures with high cement replacement levels even longer corrosion propagation periods were estimated (F(1)50: 52 years, F(1)SF: 169 years).

Table 8.7. Estimated time to unacceptable corrosion-induced cracking (years) after depassivation of the reinforcing steel due to carbonation.

| 1st order / XC3 | T(0.55) | F(1)50 | F(1)SF |
|-----------------------------------|----------------|---------------|---------------|
| $t_{\text{crack}_1 \text{ mm}}$ | 31 | 52 | 169 |

Their high $t_{\text{crack}_1 \text{ mm}}$ values are a direct consequence of mainly the significantly higher bulk resistivities that were measured for the HVFA and especially the FA+SF concrete. Their higher experimental tensile splitting strengths also contributed to some extent. An additional positive effect originates from the higher age factor $n_{\text{res}}^c (= 0.62)$ that was assumed for these two concrete compositions. For the OPC reference an age factor of only 0.23 was defined.

Given the results shown in Table 8.7, it is clear that a mere focus on the corrosion initiation period in a carbonation exposed environment underestimates the total service life of the concrete significantly. This is most definitely the case when the concrete has a low W/B ratio and a high content of supplementary cementitious materials. Both properties contribute to a high concrete resistivity (100-400 Ωm). The steel corrosion rate (in $\mu\text{m}/\text{year}$) which is believed to be inversely proportional to this concrete property is then low. As a consequence, it takes longer before the corrosion penetration is capable of inducing cracks. This behaviour is quite in contrast with the lower carbonation resistance of the HVFA and FA+SF concrete and thus the shorter time to steel depassivation. Inclusion of the corrosion propagation period in service life calculations could often solve the problem of an insufficient time to steel depassivation. Thus, in environments with exposure to carbonation both the corrosion initiation and propagation period need to be considered to get a proper idea of the concrete's entire service life.

8.6. Conclusions

The time to carbonation-induced depassivation of steel embedded in HVFA and FA+SF concrete is considerably shorter than for reinforcing steel applied in an OPC or k-value conforming FA reference concrete. This statement holds true for simulated XC3 and XC4 exposure conditions. The estimated duration of the corrosion initiation period seems to depend a lot on the prediction model used. A general shift from a simplified first order to a more advanced second order probabilistic service life assessment can have the following consequences.

- (i) As observed in Chapter 5, the more accurate microscopically assessed carbonation depth is often higher than the corresponding colorimetric carbonation depth after prolonged exposure to 10% CO₂. The resulting difference in field carbonation rate certainly affects the time to steel depassivation when using the first order limit state function for prediction of the corrosion initiation period. Nevertheless, the estimated service life remains higher than the predefined 100 years if the concrete was optimally cured for at least 28 days at 20 °C and 95% RH. When using field carbonation rates obtained after 28 days of suboptimal curing as input, the predefined design service life of 100 years is not met for the HVFA concrete. Under these conditions still no problems are expected for the proposed FA+SF concrete composition.
- (ii) A second order estimation that takes into account the concrete's curing behaviour and expected meteorological conditions (cf. *fib* Bulletin 34 (2006)), indicated that the time to steel depassivation for the studied HVFA and FA+SF concrete compositions would always exceed 100 years regardless of the underlying (colorimetric or microscopic) carbonation assessment method. This can mainly be attributed to the unfavorable weather conditions (e.g. relative humidity: 79±9% (XC3, XC4), time of wetness: 0.31 (XC4)) for carbonation inherent to the Belgian climate. Suboptimal curing of the HVFA and FA+SF concrete certainly has an adverse effect on this, but not to an extent that it can compensate for the meteorological effects. In addition, the model does not account for the sometimes improper execution of the structure in practice and the practically unavoidable presence of flaws in the concrete (cracks, etc.). This also partially explains the often long corrosion initiation periods that follow from the considered second order prediction.
- (iii) In Chapter 5 it was found that the field carbonation rates that resulted from exposing the proposed HVFA and FA+SF concrete to 10% CO₂ at 20 °C and 60% RH are only 55% and 57% of the field carbonation rates that were obtained after its exposure to 1% CO₂ at 20 °C and 60% RH. As a consequence, the former test procedure results in an important underestimation of the actual field carbonation rate and thus an overestimation of the time to depassivation. When this phenomenon is taken into account during a second order service life prediction, the estimated time to steel depassivation of the HVFA and FA+SF concrete decreases, yet still exceeds 100 years. In case of a first order prediction, the duration of the corrosion initiation period of the HVFA concrete would be less than 50 years. When the correction factor for the applied high CO₂ concentration (10% CO₂) would be considered for suboptimally cured HVFA and FA+SF concrete, a time to steel depassivation of at least 100 years could not be guaranteed anymore for both

compositions. In that case, depassivation would already be expected after 21 and 71 years, respectively. A second order prediction indicates that this is only problematic for the HVFA mixture (time to depassivation: 72 years).

A first rough semi-probabilistic estimation of the time to unacceptable corrosion-induced cracking (critical crack width: 1.0 mm) shows that the duration of an as such defined corrosion propagation period cannot be neglected. In exposure class XC3 this period would last no less than 31, 52 and 169 years for the OPC reference, the HVFA concrete and the FA+SF concrete, respectively. Despite the higher susceptibility of HVFA and FA+SF to carbonation, service life of at least 100 years seems achievable if the corrosion propagation period would also be part of this service life.

The longer propagation periods for the latter two concrete compositions, are a direct consequence of the substantially higher bulk resistivities that were measured for the concrete mixtures with a large portion of the cement replaced by fly ash (and silica fume). This concrete property is known to be inversely related to the corrosion rate of the embedded reinforcing steel once onset of active corrosion has occurred. The higher tensile splitting strength and age factor for resistivity of the HVFA and FA+SF concrete in comparison with OPC reference T(0.55) also contributed to some extent to the longer corrosion propagation period.

Service life prediction for chloride-induced corrosion

9.1. Choosing an appropriate prediction model and failure event

Similar to carbonation-induced corrosion, the applied prediction models for chloride-induced corrosion (both for the chloride initiation and propagation period) belong to the category of the empirical models. The model for chloride ingress is to a large extent based on Fick's second law of diffusion. The model that quantifies the time to unacceptable corrosion-induced cracking relies on a proven relationship between the electrical resistivity of concrete and the corrosion rate of embedded reinforcing steel (see Chapter 8). Both models require a minimum experimental input, e.g. the chloride migration coefficient, the bulk resistivity and the tensile splitting strength at the age of 28 days. Apart from that, they rely on a series of previously quantified default input parameters that may not always be applicable to the concrete compositions under investigation. When this is the case, an experimental determination of mix specific input parameters is recommended. This was attempted for the most relevant input parameters in the model for prediction of the time to chloride-induced steel depassivation, in particular the experimental transfer parameter, the ageing exponent and the critical chloride content. The outcome of these first and second order predictions based on default and mix specific input parameters were compared to see whether the time consuming additional experimental work automatically results in a significantly different time to steel depassivation or not. This comparison is seen as relevant because in the early stages of concrete mixture development only limited experimental data are available that allow for a preliminary service life prediction. An important under- or overestimation of the actual corrosion initiation period will obviously have its consequences. An initially promising concrete mix design in terms of service life and sustainability might turn out not so promising after all. On the other hand, a mixture with an initially doubtful performance might not be developed any further, although it might perform just fine in a model with mix specific input. The model that quantifies the duration of the corrosion propagation was only applied with its default input parameters. The main aim was to see whether the total service life of the concrete structure (= corrosion initiation + propagation period) is underestimated to a significant extent when only the time to steel depassivation is considered. Evidently, further development of a mix specific corrosion propagation model would also be of value.

9.2. First order probabilistic estimation of the corrosion initiation period

9.2.1. Limit state function of *fib* Bulletin 34

Equation 9-1 represents the probabilistic limit state function for chloride-induced steel depassivation as defined in *fib* Bulletin 34 (2006).

$$C_{\text{crit}} = C_0 + (C_{S,\Delta x} - C_0) \cdot \left[1 - \operatorname{erf} \frac{d - \Delta x}{2 \cdot \sqrt{D_{\text{app},C} \cdot t}} \right] \quad (9-1)$$

with C_{crit} : the critical chloride content (m%/binder), C_0 : the initial chloride content (m%/binder), $C_{S,\Delta x}$: chloride content at depth Δx (m%/binder), d : concrete cover (mm), Δx : depth of the convection zone (mm), t : time (years), $\operatorname{erf}(\cdot)$: error function and $D_{\text{app},C}$: apparent coefficient of chloride diffusion through concrete (mm^2/years). The latter coefficient can be obtained from the experimentally derived non-steady state migration coefficient using Equation 9-2:

$$D_{\text{app},C} = k_e \cdot D_{\text{RCM},0} \cdot k_t \cdot W(t) = \exp \left(b_e \left(\frac{1}{T_{\text{ref}}} - \frac{1}{T_{\text{real}}} \right) \right) \cdot D_{\text{RCM},0} \cdot k_t \cdot \left(\frac{t_0}{t} \right)^a \quad (9-2)$$

with k_e : the environmental transfer variable (–), b_e : a regression variable (K), T_{ref} : the standard test temperature (K), T_{real} : the temperature of the structural element or the ambient air (K), $D_{\text{RCM},0}$: the non-steady state chloride migration coefficient (mm^2/years), k_t : the experimental transfer parameter, $W(t)$: the subfunction that considers ageing (–), t_0 : a reference point of time (years), t : time (years) and a : the ageing exponent (–). A combination of Equations 9-1 and 9-2 enables a probabilistic estimation of the time to chloride-induced steel depassivation.

9.2.2. Chloride migration coefficient

In its original form, the limit state function of *fib* Bulletin 34 (2006) uses a rapid chloride migration coefficient as basic experimental input because the test method for its determination is considered to be theoretically clear, experimentally simple, precise and repeatable. Its value follows from the chloride migration test described by NT Build 492 (1999). Thus, this rapid chloride migration coefficient $D_{\text{RCM},0}$ corresponds with the non-steady state chloride migration coefficients that were determined in Chapter 6. Only its original unit (in m^2/s) needs to be converted to mm^2/year . $D_{\text{RCM},0}$ is assumed to be a normally distributed variable.

As already mentioned in the same chapter, chloride migration involves the presence of a significant external electrical field which is not present in practice. The natural chloride transport mechanism for water saturated concrete is mainly diffusion controlled. Moreover, the exposure solution has a much higher chloride concentration than sea water. Also the temperature of the exposure solution is considerably different. Therefore, the derived chloride migration coefficient needs to be converted to a realistic apparent chloride diffusion coefficient $D_{\text{app},C}$ using Equation 9-2.

9.2.3. Apparent chloride diffusion coefficient

Apart from its indirect estimation calculated by means of Equation 9-2, the apparent chloride diffusion coefficient can also be measured directly from a chloride profile taken from the concrete structure under natural exposure conditions. The term ‘apparent’ refers to the fact that diffusion is only one of the transport mechanisms involved in chloride penetration. As a consequence, a ‘true’ diffusion coefficient cannot be measured that way [Costa and Appleton (1999a)]. According to Tang et al. (2012), the term ‘apparent’ refers to the fact that the measured diffusivity is assumed constant over the entire exposure period. Evidently, this is not the case in reality. Therefore, the $D_{app,C}$ value that results from chloride profiling is identified as an apparent diffusion coefficient.

The experimentally determined $D_{app,C}$ value is an average value representing the period from start of exposure to the moment of inspection. According to *fib* Bulletin 34 (2006) these chloride profiles can either be taken from existing concrete structures or from laboratory test samples stored under the conditions that are expected in practice. Because this approach is very time consuming, *fib* bulletin 34 (2006) suggests to use the indirect method based on chloride migration testing. Nevertheless, the output of this method of convenience should always be calibrated against the output of the chloride profiling method after exposure to natural conditions for a sufficiently long time.

9.2.4. Environmental transfer variable

The environmental transfer variable k_e relates to the temperature dependency of the chloride diffusion coefficient. The influence of temperature of the structural element or the ambient air (T_{real} , in K) in relation to the test temperature (T_{ref} , in K) is described by means of the Arrhenius function. T_{real} is seen as a normal distributed variable which can be estimated from weather station data. CUR guideline VC81 (2009) mentions a mean value of 283 K (or 10 °C) for the Netherlands. For Belgium a very similar value can be expected. T_{ref} on the other hand is considered as a constant parameter and amounts to 293 K (or 20 °C). Parameter b_e is a regression variable that follows a normal distribution. When based on a dataset of chloride ion diffusivities at different temperatures published by Page et al. (1981), the estimated mean value and standard deviation of b_e amount to 4800 K and 700 K, respectively. Preferably, a mix specific value of b_e is to be determined for each concrete composition. This requires chloride profiling of the concrete after exposure to chloride solutions at different temperatures. Since this could not be done within the framework of this PhD research, the default values from literature were used for all concrete compositions.

9.2.5. Experimental transfer parameter and ageing exponent

Because the apparent diffusion coefficient $D_{app,C}$ is subject to considerable scatter and tends to decrease with increasing exposure time, a transfer parameter k_t in combination with an ageing exponent a were included in Equation 9-2. Nevertheless, it must be said that *fib* bulletin 34 (2006) focuses much more on the ageing exponent than on the transfer parameter. It merely mentions that the transfer parameter should be set to 1. The guideline does not mention a value for k_t to go from a given chloride migration coefficient to its corresponding apparent diffusion coefficient at the reference temperature (= 20 °C). Now, its value cannot always

simply be equal to 1. Intuitively, it can be understood that k_t must have been originally included as parameter in Equation 9-2 to account for any differences between the rapid migration coefficient and corresponding apparent diffusion coefficient not attributable to differences in temperature of the exposure solution or ageing phenomena. Thus, the value of k_t can roughly be estimated from the ratio between the apparent diffusion coefficient and the migration coefficient measured at the same exposure temperature and concrete age. DuraCrete (1998-2000) suggests a similar estimation method for a very similar limit state function. Based on this methodology the guideline proposes a normal distributed k_t value with a mean value and standard deviation of 0.832 and 0.024, respectively. In section 9.3.1 a similar approach was adopted to estimate a mix specific experimental transfer parameter k_t for each tested concrete composition.

The ageing exponent is more documented in *fib* Bulletin 34 (2006). It includes a statistical quantification of this parameter for different binder systems which is said to be valid for the splash zone, the tidal zone and the submerged zone (Table 9.1).

Table 9.1. Ageing exponents proposed by *fib* Bulletin 34 (2006) for different binder systems.

| Ageing exponent a (–) (Beta distribution) | Mean | Stdv. | Lower boundary | Upper boundary |
|---|------|-------|----------------|----------------|
| Portland cement concrete (CEM I: $0.40 \leq W/C \leq 0.60$) | 0.30 | 0.12 | 0.0 | 1.0 |
| Portland fly ash cement concrete (FA $\geq 0.20 \cdot C$; $k = 0.50$; $0.40 \leq W/(C+k \cdot FA) \leq 0.62$) | 0.60 | 0.15 | 0.0 | 1.0 |
| Blast-furnace slag cement concrete (CEM III/B; $0.40 \leq W/C \leq 0.60$) | 0.45 | 0.20 | 0.0 | 1.0 |

These ageing exponents reflect a functional relationship between the exposure time and the apparent diffusion coefficient. Its estimation requires chloride profiling at different exposure times followed by regression analysis forced through the initial value of $D_{RCM,0}$ at the reference point in time $t_0 = 0.0767$ years (= 28 days). It is also mentioned in the guideline that an ageing exponent estimated from rapid chloride migration coefficients obtained at different ages will not lead to the same result. Ageing quantified that way will only represent a certain portion of the total ageing effect. This portion corresponds with the increase of the concrete's chloride penetration resistance due to the ongoing hydration of the concrete. Other porosity reducing effects induced by prolonged exposure (see Chapter 6) are not reflected in its value. Thus, it seems that the latter approach will lead to an underestimation of the concrete's actual ageing exponent. Service life predictions based on such exponents will be rather on the safe side. The same probably goes for an ageing exponent estimated from chloride diffusion tests performed at different curing ages, each time followed by the same exposure period. Since all experiments to characterize the chloride resistance of OPC, FA, HVFA and FA+SF concrete in this research were performed at different curing ages and not at different exposure times, all ageing exponents estimated from the data reported in Chapter 6 belong to this category. More details on their calculation can be found in Section 9.3.2.

Note that Table 9.1 only gives a limited set of ageing exponents per binder type, seemingly independent of the exposure condition. This is in contrast with the more extensive list of ageing exponents provided by DuraCrete (1998-2000). Depending on whether the concrete is

located in the submerged, tidal+splash or atmospheric zone, the ageing exponent of the concrete can vary considerably (Table 9.2). There seems to be no logic trend between the value of the ageing exponent and the exposure condition. Both *fib* Bulletin 34 (2006) and DuraCrete (1998-2000) give the same value for the ageing exponent of submerged OPC concrete (0.30). The values mentioned for FA concrete are also quite similar (0.60 and 0.69, respectively). This is not the case for BFS concrete (0.45 versus 0.71). There was no ageing exponent mentioned for SF concrete in *fib* Bulletin 34 (2006). According to DuraCrete (1998-2000) the ageing exponent of SF concrete should amount to 0.62. This value is very similar to the one derived for FA concrete.

Table 9.2. Ageing exponent per binder type and exposure condition cf. DuraCrete (1998-2000).

| Binder | Environment | Distribution | Mean | Stdv. | Lower boundary | Upper boundary |
|--------|---------------------------|--------------|------|-------|----------------|----------------|
| OPC | Submerged ⁺ | Beta | 0.30 | 0.05 | 0.0 | 1.0 |
| | Tidal+Splash ⁺ | Beta | 0.37 | 0.07 | 0.0 | 1.0 |
| | Athmospheric | Beta | 0.65 | 0.07 | 0.0 | 1.0 |
| FA | Submerged | Beta | 0.69 | 0.05 | 0.0 | 1.0 |
| | Tidal+Splash | Beta | 0.93 | 0.07 | 0.0 | 1.0 |
| | Athmospheric | Beta | 0.66 | 0.07 | 0.0 | 1.0 |
| BFS | Submerged | Beta | 0.71 | 0.05 | 0.0 | 1.0 |
| | Tidal+Splash | Beta | 0.80 | 0.07 | 0.0 | 1.0 |
| | Athmospheric | Beta | 0.85 | 0.07 | 0.0 | 1.0 |
| SF | Submerged ⁺ | Beta | 0.62 | 0.05 | 0.0 | 1.0 |
| | Tidal+Splash ⁺ | Beta | 0.39 | 0.07 | 0.0 | 1.0 |
| | Athmospheric | Beta | 0.79 | 0.07 | 0.0 | 1.0 |

⁺ Quantified from field data, others from 'expert opinion'.

9.2.6. Concrete cover

All assumptions made regarding the distribution function and standard deviation for the concrete cover have already been mentioned in Section 8.2.3. They remain valid for the case study of chloride-induced steel depassivation. NBN EN 1992-1-1 (ANB 2010) prescribes a nominal concrete cover of 40 mm for the standard construction class S4 which corresponds with a design service life of 50 years. A design service life of 100 years implies an upgrade to construction class S6 which requires a nominal concrete cover of 50 mm. In this study, the focus was on a design service life of 100 years. It was assumed that the proposed nominal concrete cover corresponded with the mean concrete cover.

9.2.7. Initial chloride content

The chloride content of concrete not only originates from external chloride ingress but also from concrete constituents that were to some extent contaminated with chlorides already. CUR guideline VC81 (2009) advises to consider a normally distributed initial chloride content with a mean value and standard deviation of 0.10 m%/binder and 0.025 m%/binder, respectively. In this research the experimental determination of the total initial chloride

content of all studied concrete compositions revealed that the initial chloride content amounted to 0.18 ± 0.03 m%/binder on average (Table 9.3). This value is only just in correspondence with the strictest maximum allowed chloride content (chloride content class Cl 0.20: 0.20 m%/binder) for concrete containing steel reinforcement or embedded metal cf. NBN EN 206-1 (2000). In practice, the contamination of the concrete constituents with chlorides should be kept very much under control, especially when the concrete is to be used in a marine environment. In this research, it was assumed from the start that this contamination with chlorides was very low and in range with the suggested 0.10 m%/binder. The actual initial chloride content of the tested concrete was only verified later on (after 1-3 years). Only then, it was found out that the initial chloride content was somewhat higher than expected. Preferably, the selection of concrete constituents in the design phase should have been as such that the suggested literature value could have been met. Therefore, it was decided to use the C_i value suggested by CUR guideline VC81 (2009) anyway, also for the second order service life predictions based on mix specific input. This choice is considered justified because normally a slightly higher value for C_i will not change the prediction outcome very much in comparison with other model input parameters such as the ageing exponent or the critical chloride content. Nevertheless, the limited effect of using the measured C_i value was verified in Appendix C.

Table 9.3. Initial total chloride content of the tested concrete compositions ($n = 3$).

| Composition | Initial total chloride content C_0 (m%/binder) |
|-------------|--|
| T(0.45) | 0.19 ± 0.01 |
| F(1)15 | n.a. |
| F(2)15 | 0.17 ± 0.02 |
| F(1)50 | 0.15 ± 0.01 |
| F(2)50 | 0.14 ± 0.01 |
| F(1)SF | 0.21 ± 0.01 |
| F(2)SF | 0.20 ± 0.01 |
| mean | 0.18 ± 0.03 |

9.2.8. Chloride content at the substitute surface

It is clear that the limit state function for chloride-induced corrosion is very much based on Fick's second law of diffusion. However, as the model also intends to be applicable for exposure conditions not exclusively governed by diffusion, e.g. exposure to frequent wetting followed by subsequent evaporation, Equation 9.1 differs from the solution of Fick's second law of diffusion in a way that it not merely depends on the chloride concentration at the surface. When the moisture flow varies over time, both in magnitude and direction (due to wetting and drying) a convection of ions in the pore solution and in and out of the concrete occurs [Tang et al. (2012)]. Obviously, this is not a diffusion controlled process. In order to deal with this phenomenon, the prediction model of *fib* Bulletin 34 (2006) does not consider the actual transport mechanism in the convection zone. It simply assumes that Fick's second law of diffusion is valid starting at depth Δx with a substitute surface concentration $C_{s,\Delta x}$. This depth Δx marks the inner boundary of the convection zone. According to *fib* Bulletin 34 (2006), applying Fick's second law of diffusion for chloride penetration depths exceeding

depth Δx is justified. It should give a good approximation of the chloride distribution from this point on. The quantification of Δx and $C_{s,\Delta x}$ may be less straightforward in case of intermittent exposure, for continuously submerged concrete this is not a problem. For this exposure condition, parameter Δx can simply be set to 0 mm. The chloride saturation concentration $C_{s,0}$ then corresponds with the chloride surface concentration C_s which can be estimated directly from chloride profiles. However, the fact that the first layer often needs to be excluded from analysis because its chloride content deviated from the overall profile curvature, may indicate that Δx is not equal to 0 mm. Moreover, the question arises whether assuming the chloride surface concentration really makes sense in case its value is measured at a rather young age. The *fib* Bulletin 34 (2006) acknowledges the existence of a non-negligible time dependency for C_s , be it mainly in case of a non-continuous exposure to chlorides. Under a continuous chloride impact of constant concentration, the chloride saturation concentration should be reached in a relatively short time. The use of a constant value for C_s is therefore seen as a simplification on the safe side. Still, as already pointed out in Chapter 6, several researchers also observed a considerable surface chloride build-up in the submerged zone. Tang et al. (2012) agree with this time-dependency for C_s , yet have to admit that the phenomenon cannot yet be explained with current knowledge. For the concrete compositions that were tested in this research, it was also concluded that the time-dependent surface chloride build-up probably exists and that it is different for different concrete types. It must be emphasized though that this conclusion was drawn indirectly (see Section 6.5.5) since no chloride profiles were determined at different exposure times. Nevertheless, despite the probably non-negligible time dependency of the surface concentration for the submerged condition, a time independent normal distributed value for this parameter was assumed for now. According to DuraCrete (1998-2000) such a surface concentration varies with the binder type and W/B ratio of the concrete. On the other hand, CUR guideline VC81 (2009) assumes a normal distributed value of 3.0 ± 0.8 m%/binder for seawater (both exposure class XS2 and XS3), regardless of the binder type and the W/B ratio of the concrete, and this for simplicity reasons. The same value was adopted as default input parameter to the model of *fib* Bulletin 34 (2006) for the time being. Obviously, it is recommended to adapt the model in perspective of the time dependency of the surface concentration as soon as the phenomenon is better understood and quantifiable.

9.2.9. Critical chloride content

Basically, there are two different definitions for the critical chloride content. Both definitions are mentioned in DuraCrete (1998-2000).

- (i) According to the first definition, the critical chloride content corresponds with the chloride concentration at which steel depassivation and iron dissolution begins, regardless whether this already leads to visible corrosion damage on the concrete surface. It is this definition that marks the end of the corrosion initiation period.
- (ii) The second definition covers the chloride concentration leading to actual damage of the reinforced concrete. This event occurs in the course of the corrosion propagation period.

Obviously, the latter critical chloride content is higher than the former because not only steel depassivation, but also a sufficient presence of oxygen and moisture around the rebar, are

required for damage. The latter two criteria are not immediately met at the moment of steel depassivation. This takes some time. In the meantime, a further chloride content build-up will occur at the surface of the rebar. For constantly dry or water-saturated concrete the critical chloride content according to the two definitions will be substantially different. On the other hand, for permanently humid or fluctuating environmental conditions, the critical chloride contents according to definition (i) and (ii) will be much more similar [DuraCrete (1998-2000)].

The *fib* Bulletin 34 (2006) adopted the first definition for the critical chloride content. In accordance with this definition, it specifies a C_{crit} value of 0.60 ± 0.15 m%/binder. The parameter is assumed to be Beta distributed with a lower and upper boundary of 0.20 and 2.0 m%/binder, respectively. It is also mentioned that the specified value is applicable to ordinary mild steel.

Now, from literature survey it can immediately be concluded that one single value for the critical chloride content may not be valid for every steel, cement type, concrete and exposure condition. Apart from the effect of the test method used to determine the critical chloride content, Angst et al. (2009) mention the following relevant, often interrelated influencing factors that relate to either steel condition, concrete and binder properties or external factors:

- Steel-concrete interface
- Concentration of hydroxide ions in the pore solution
- Electrochemical potential of the steel
- Binder type
- Surface condition of the steel
- Moisture content of the concrete
- Oxygen availability at the steel surface
- W/B ratio
- Electrical resistivity of the concrete
- Degree of hydration
- Chemical composition of the steel
- Temperature
- Chloride source (mixed in initially or penetrated into hardened concrete)
- Type of cation accompanying the chloride ion
- Presence of other species, e.g. inhibiting substances

Given this quite extensive list of influencing factors, it is not surprising that the total critical chloride content under outdoor exposure conditions in real structures can range between 0.10-1.96 m%/binder. When measured under laboratory conditions, the possible range for the total critical chloride content is even much broader (0.04-8.34 m%/binder). The corresponding range for the free critical chloride content amounts to 0.07 to 1.16 m%/binder [Angst et al. (2009)]. According to Gaal et al. (2003), the critical chloride content measured in laboratory experiments can vary between 0.2-2.0 m%/binder. Thus, a single value for the critical chloride content seems very doubtful.

When looking at the different influencing factors, several of them are of relevance in perspective of the studied concrete compositions, e.g. the binder type and W/B ratio.

Binder type

The type of binder affects both the pH and free chloride content of the pore solution. If the binder type can ensure a high pH value and bind a substantial portion of the free chlorides on a permanent basis, it will take longer before the protective steel passivation layer breaks down. The influence of using mineral additions (e.g. fly ash, silica fume) as partial cement replacement on the critical chloride content should be evaluated in perspective of these two mechanisms [Angst et al. (2009)]. The pozzolanic hydration reactions inherent to fly ash and silica fume consume the Portlandite that is responsible for the high pH of the concrete. In combination with carbonation phenomena this can result in a pH drop that can cause depassivation of the reinforcing steel over time. On the other hand, the presence of fly ash and silica fume enhances the formation of more C–S–H gel. As a consequence, larger surface areas are available for the adsorption of chlorides (physical binding) [Tang and Nilsson (1993)]. Moreover, calcium aluminate hydrates, hydration products of fly ash, also react with the chlorides from the pore solution to form Friedel's salt (chemical binding) [Justnes (1998)]. One can conclude that the pH and the chloride binding capacity in presence of mineral additions can have quite an adverse effect on the value of the critical chloride content. The question arises which effect has the upperhand. Extensive literature study conducted by Angst et al. (2009) shows that the critical chloride content for alternative binder systems is still subject of a lot of discussion. Some authors state that the presence of fly ash lowers the critical chloride content [Thomas (1996), Oh et al. (2003)] while others claim exactly the opposite [Schiessl and Breit (1996)]. On the other hand, a non-significant effect was reported by Alonso et al. (2002).

On the effect of incorporating silica fume there seems to be more agreement. Its presence usually implies that its critical chloride content will be lower [Manera et al. (2008)]. In this context, a lower chloride binding capacity of cement in combination with SF is mentioned as possible explanation. The partial replacement of OPC with SF may indeed reduce the amount of aluminate phases needed for chemical binding. The occurrence of more physical adsorption promoted by the substantial pore refinement induced by the SF addition may compensate for this. However, it has been reported that C–S–H produced by its pozzolanic reaction has lower chloride sorption capacity than C–S–H that results from cement hydration [Larsen (1998)]. This in combination with the reduced alkalinity of concrete containing SF [Byfors (1987)], contributes to the lower critical chloride content of SF concrete. It is a little strange that the very same explanation is not valid for concrete containing the other pozzolan, fly ash. All the same conditions seem present, except maybe for the fact that fly ash contains more aluminate phases. Thus, further research on the effect of the binder type is still imperative. For this reason, an attempt was made to measure the critical chloride content for OPC concrete and concrete with a 50% fly ash replacement. Therefore, specimens with embedded rebars were manufactured for corrosion potential monitoring of the reinforcing steel as a function of the Cl^- concentration near the steel surface. The details regarding the experimental determination of the critical chloride content are given in Section 9.3.3.

W/B ratio

Angst et al. (2009) also studied literature on the influence of the W/B ratio on the critical chloride content. According to several sources (e.g. in Poupard et al. (2004)] the critical chloride content should increase with a decreasing W/B ratio. In this perspective, Angst et al. (2009) mentions the well-known relation between the applied W/B ratio, the resulting porosity of the paste and the material's accessibility to moisture and oxygen. DuraCrete (1998-2000) acknowledges a link between the W/B ratio of the concrete and C_{crit} , yet only for the critical chloride content in accordance with definition (ii). The guideline also gives C_{crit} values for OPC concrete with different W/B ratios, when located in the submerged zone and the tidal or splash zone (Table 9.4). The values are ought to be valid for macro-crack free concrete (crack width ≤ 0.10 mm) and for a minimum concrete cover of 25 mm.

No significant relation between concrete technological parameters (e.g. the W/B ratio) and the critical chloride concentration in accordance with definition (i) could be observed until now. For this single value critical chloride content DuraCrete (1998-2000) assumes a normal distribution with a mean value and standard deviation of 0.48 m%/binder and 0.15 m%/binder, respectively. Nevertheless, DuraCrete (1998-2000) is not in favor of the critical chloride content according to definition (i) because its value is difficult to measure by means of non-destructive test methods. Upon initiation, corrosion first has to proceed at very low rates until a certain corrosion rate is achieved that is detectable, for instance by means of embedded corrosion sensors. At that moment, the chloride content at the location of the corroding rebar is already higher than the minimum value needed for steel depassivation (Figure 9.1).

Table 9.4. Critical chloride content C_{crit} (m%/cement) according to definition (ii) for OPC concrete as function of the W/B ratio and the exposure condition, cf. DuraCrete (1998-2000).

| W/B ratio | Submerged zone | Tidal/splash zone |
|------------------|-----------------------|--------------------------|
| 0.50 | N(1.60, 0.20) | N(0.50, 0.10) |
| 0.40 | N(2.10, 0.20) | N(0.80, 0.10) |
| 0.30 | N(2.30, 0.20) | N(0.90, 0.15) |

Note that *fib* bulletin 34 (2006) and DuraCrete (1998-2000) mention a different distribution function (Beta versus Normal) for the critical chloride content. Literature findings on this subject were evaluated more in-depth in CUR Guideline VC81 (2009). According to Breit (2001) there is a lower boundary for the critical chloride content (0.25-0.30 m%/binder). To take into account that there is a sharp lower boundary, CUR guideline VC 81 (2009) adopted a lognormal distribution. However, this approach is stricter because the probability for corrosion in case of chloride contents below 0.25 m%/binder is not equal to zero that way. On the other hand, Gehlen (2000) assumes that the critical chloride content follows a Beta distribution (mean: 0.48 m%/binder, stdv.: 0.15 m%/binder, a: 0.20 m%/binder, b: 2.0 m%/binder). Because the exposure temperature in practice (± 10 °C) is lower than under laboratory conditions (± 20 °C), it is justified according to Gehlen (2000) to use a higher mean value (0.60 m%/binder), while keeping the values of the other parameters of the Beta distribution the same. This probabilistic characterization of the critical chloride content is

fully in agreement with the one that is imposed by *fib* Bulletin 34 (2006). CUR guideline VC81 (2009) only adopted the same mean value. The applied distribution remained lognormal with a standard deviation of 0.20 m%/binder. Nevertheless, the guideline acknowledges that their approach may be too conservative, especially with respect to concrete compositions with a W/B ratio lower than 0.50. As all studied concrete compositions belong to this category, it seems appropriate to stick to the critical chloride content defined by *fib* Bulletin 34 (2006) for estimating the corrosion initiation period.

In addition, the higher W/B and exposure condition dependent critical chloride content according to definition (ii) of DuraCrete (1998-2000) also deserves attention, since this property is easier to measure for different concrete compositions. This definition was not considered for the first order prediction of the corrosion initiation period mainly based on default input from *fib* Bulletin 34 (2006), but only for the second order prediction (see Section 9.3.3 and 9.3.4). Although DuraCrete (1998-2000) assigned a normal distribution to this parameter, a Beta distribution could also be adopted for this critical chloride content. Given the fact that a W/B dependent critical chloride content is only available for OPC concrete and that there is still a lot of discussion on the effect of mineral additions, the critical chloride content for submerged OPC reference (1.9 m%/binder for a W/B ratio of 0.45, Table 9.4, interpolated value) was also adopted for the FA (and SF) containing concrete mixtures with a lower W/B ratio. The reason for choosing definition (ii) of C_{crit} for the second order prediction originated from the conclusions drawn from the preliminary experimental determination of C_{crit} (see Section 9.3.3).

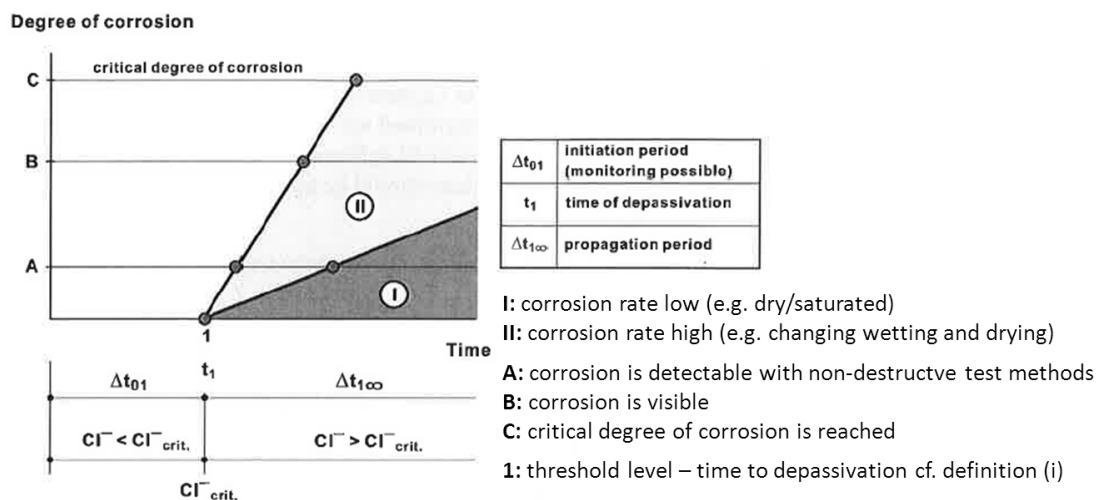


Figure 9.1. Visual representation of the critical chloride content C_{crit} according to DuraCrete (1998-2000).

9.2.10. Summarizing overview of the default model input parameters

Table 9.5 gives a summarizing overview of all the default input parameters which were used for first order service life prediction in the probabilistic Comrel software [RCP Consulting Software (1987-2013)] using the First Order Reliability method. These input parameters cannot really be considered as specifically applicable for the studied concrete compositions. The majority of the values shown are the ones suggested by *fib* bulletin 34 (2006). When not

mentioned for a particular concrete type or exposure condition, the values were obtained from other model codes (e.g. DuraCrete (1998-2000)) or guidelines (e.g. CUR guideline VC81 (2009)). The mean concrete cover simply corresponds with the required minimum values prescribed by NBN EN 1992-1-1 (ANB 2010) for exposure class XS2 and a design service life of 100 years. Just like for carbonation-induced depassivation, the corrosion initiation period was set to end when the probability of failure P_f reached 0.10 or when the reliability index β dropped below 1.3.

Table 9.5. Default input parameters for first order service life prediction.

| Parameter | Distribution | Mean | Stdv. | Lower boundary | Upper boundary |
|------------------------------------|--------------|---|-------|----------------|----------------|
| C_{crit} (m%/binder) | Beta | 0.60 | 0.15 | 0.2 | 2.0 |
| C_0 (m%/binder) | Normal | 0.10 | 0.025 | – | – |
| $C_{S,\Delta x}$ (m%/binder) | Normal | 3.0 | 0.8 | – | – |
| d (mm) | Lognormal | 50 (t_{SL} : 100 years) | 8 | – | – |
| Δx (mm) | Constant | 0 | – | – | – |
| b_e (K) | Normal | 4800 | 700 | – | – |
| T_{ref} (K) | Constant | 293 | – | – | – |
| T_{real} (K) | Normal | 283 | 5 | – | – |
| $D_{RCM,0}$ (mm ² /yrs) | Normal | Figure 6.3 (after unit conversion: m ² /s to mm ² /years) | | | |
| k_t (–) | Normal | 0.832 | 0.024 | – | – |
| t_0 (yrs) | Constant | 0.0767 (28d) | – | – | – |
| a (–) | Beta | 0.30 (OPC) | 0.12 | 0.0 | 1.0 |
| | | 0.60 (FA) | 0.15 | 0.0 | 1.0 |
| | | 0.62 (SF) | 0.05 | 0.0 | 1.0 |

9.3. Second order probabilistic estimation of the corrosion initiation period

Within the framework of this research, it was not possible to determine an experimental mixture specific value for all input parameters to the prediction model. This was only attempted for the ones that affect the outcome of the prediction the most, i.e. the experimental transfer parameter k_t , the ageing exponent a and the critical chloride concentration C_{crit} . The resulting estimations may not always be fully representative for the studied exposure conditions and concrete compositions. However, they certainly give a first good indication whether the different default input parameters that were used until now are justifiable for different binder systems.

9.3.1. Determination of the experimental transfer parameter

As already pointed out in Section 9.2.5, *fib* Bulletin 34 (2006) stays very vague on how to estimate this parameter. Therefore, a formula suggested by the DuraCrete (1998-2000) guideline was used for this purpose (Equation 9-3).

$$D_{app,C}(t_0) = k_t \cdot D_{RCM,0}(t_0) \quad (9-3)$$

With $D_{app,C}(t_0)$, the apparent ‘natural’ chloride diffusion coefficient (in mm^2/years) at a reference point of time t_0 (years), k_t , the experimental transfer / test method translation factor (–) and $D_{RCM,0}(t_0)$, the rapid chloride migration coefficient (in mm^2/years) at the same reference point of time t_0 .

Per tested concrete composition, both the above mentioned apparent diffusion and migration coefficients were determined at three different curing ages (28, 91 and 273 or 364 days). Each of these curing ages can be considered as a reference point of time (0.0767, 0.2493 and 0.7479 or 1.000 year) for which Equation (9-3) can be filled in. Table 9.6 shows the resulting estimated values of parameter k_t for the studied concrete mixtures per curing age.

From statistical analysis (Levene’s homogeneity of variance test, significance level: 0.01, followed by a One-way ANOVA test, significance level: 0.05) it was concluded that the variances and mean values for the three testing ages of the different concrete mixtures were not significantly different from each other.

Table 9.6. Mix specific experimental transfer parameters k_t at different curing ages as estimated in accordance with DuraCrete (1998-2000).

| k_t at t_0 | T(0.45) | F(1)15 | F(2)15 | F(1)50 | F(2)50 | F(1)SF | F(2)SF |
|-----------------------------|---------|--------|--------|--------|--------|--------|--------|
| 28 days | 0.32 | 0.24 | 0.27 | 0.18 | 0.19 | 0.28 | 0.40 |
| 91 days | 0.45 | 0.42 | 0.32 | 0.34 | 0.45 | 0.83 | 0.54 |
| 273 / 364 days | 0.42 | 0.42 | 0.64 | 0.35 | 0.36 | 0.51 | 0.57 |
| Mean _{91-273/364d} | 0.44 | 0.42 | 0.48 | 0.34 | 0.40 | 0.67 | 0.55 |
| Stdv _{91-273/364d} | 0.02 | 0.001 | 0.23 | 0.001 | 0.07 | 0.22 | 0.02 |

Comparison of the three estimated k_t values per concrete mixture indicates that the experimental transfer parameter obtained at 28 days was always the lowest in value. Another Levene’s test (significance level: 0.01), followed by a One-way ANOVA test (significance level: 0.05) and a subsequent Tukey Post-hoc test with t_0 as grouping variable indeed reveals that although the variances can be considered as homogenous, the mean values at 28 days were significantly different from those at 91 and 273 or 364 days. Between 91 and 273 or 364 days, the differences were non-significant. The explanation for this phenomenon relates to an important difference between an apparent diffusion coefficient and a rapid chloride migration coefficient at time t_0 . Although exposure started at time t_0 , the apparent diffusion coefficient is not really measured for this reference point of time. It is not an instantaneous value but an average value for the entire exposure period of 125 days that started at time t_0 . On the other hand, the exposure time inherent to a rapid chloride migration test is much shorter (1-4 days). Therefore, it can be seen as an almost instantaneous property. Because each test reflects the properties of concrete at a different age ($t_0 + 125$ days versus $t_0 + 1$ to 4 days), the suitability of Equation 9-3 becomes an issue, especially in case of young concrete that has not fully hydrated yet. Therefore, it was decided to only consider the k_t values corresponding with t_0 equal to 91 days and 273 or 364 days for the calculation of a mean value and standard deviation per concrete mixture (Table 9.6). This approach has the disadvantage that a homogeneity of variance check can no longer be performed because of too few data per group ($n = 2$). A tentative comparison of the mean values still reveals a non-significant difference in k_t value between the different concrete compositions (One-way ANOVA test, significance

level: 0.05). Nevertheless, not an overall value was adopted for all concrete compositions. Instead the mean k_t values obtained per mixture were used for the time being. In accordance with DuraCrete (1998-2000) it was assumed that the estimated parameter k_t follows a normal distribution.

Still, it should be emphasized that this procedure clearly deviates from *fib* Bulletin 34 (2006) where k_t is assumed to be equal to 1 at all time. Some additional service life estimations with $k_t = 1$ and alternative values for the ageing exponent (see Section 9.3.2) have been performed as well. The results of these calculations have been included in Appendix D.

9.3.2. Determination of the ageing exponent

Although not recommended in *fib* Bulletin 34 (2006), the age dependence of chloride diffusivity has been estimated in the past by using only input from chloride migration coefficients. For instance, Tang (1996) proposed the following equation (Equation 9-4) for this purpose:

$$\frac{D_{RCM}(t)}{D_{RCM}(t_0)} = \left(\frac{t_0}{t}\right)^b \quad (9-4)$$

With t , the age of the concrete, t_0 , the age of the concrete when the chloride diffusivity has reached a constant value (usually 6 months for OPC concrete) and b , a parameter expressing the age dependence. According to Tang (1996) Equation 9-4 is only valid for $t \leq t_0$. Given the available experimental data, a similar ‘ageing exponent’ can easily be calculated for each concrete composition under investigation while assuming that t_0 is equal to either 273 or 364 days. The resulting ‘ageing exponents’ obtained with linear regression analysis are shown in Table 9.7. From these results, it is clear that all fly ash (and silica fume) containing concrete mixtures are characterized by a much higher b value (= 0.45-0.78) than the OPC reference T(0.45) (= 0.11). This obvious difference in ageing exponent between OPC and FA containing concrete is in agreement with literature findings (see Section 9.2.5).

Table 9.7. Estimation of the ‘ageing exponent’ b based on the migration coefficients obtained at different curing ages.

| ‘Ageing exponent’ b | Mean | Stdv. | R^2 |
|-----------------------|------|-------|-------|
| T(0.45) | 0.11 | 0.03 | 0.87 |
| F(1)15 | 0.45 | 0.07 | 0.95 |
| F(2)15 | 0.78 | 0.06 | 0.99 |
| F(1)50 | 0.63 | 0.07 | 0.98 |
| F(2)50 | 0.71 | 0.08 | 0.98 |
| F(1)SF | 0.39 | 0.21 | 0.64 |
| F(2)SF | 0.52 | 0.04 | 0.99 |

However, according to *fib* Bulletin 34 (2006), these values cannot be used for service life prediction because they only represent a certain portion of the total ageing effect (increase of chloride penetration resistance due to ongoing hydration of concrete). Therefore, the general

age dependence of chloride diffusivity in accordance with Fick's second law is more appropriate (Equation 9-5).

$$D(t) = D(t_0) \cdot \left(\frac{t_0}{t} \right)^a \quad (9-5)$$

According to Tang et al. (2012) this equation for the determination of an ageing exponent a is applicable for ages beyond t_0 for which there are no experimental data. It justifies an early reference point of time t_0 (28 days < 6 months) for service life prediction according to *fib* Bulletin 34 (2006). Tang et al. (2012) also emphasize that the diffusivities used in this equation are point-wise or instantaneous. Thus, these diffusivities cannot simply be replaced with apparent diffusion coefficients that are assumed constant over the entire exposure period. At best, the apparent diffusion coefficient may probably only be comparable to the instantaneous diffusion coefficient that is expected around halfway the exposure period t_{ex} (in our case 125 days divided by 2). Now, this assumption can obviously not be valid for the early time of reference t_0 (= 28 days = 0.0767 years) that is normally used in the prediction model. This would mean that the measured apparent diffusion coefficient after 28 days of curing is an estimation of the instantaneous diffusion coefficient at time $t_0 + t_{ex}/2$. Given the quite extended exposure period of 125 days in case of our 'natural' diffusion test, this estimation corresponds with a concrete age at which most of the (even secondary) hydration reactions have already taken place. Using this value for the instantaneous diffusion coefficient at time t_0 will most definitely disregard some important hydration related ageing effects occurring between time t_0 and time $t_0 + t_{ex}/2$. As a result, the estimated ageing exponents will be misleadingly low. This issue can be resolved if an instantaneous diffusion coefficient would be available for $t_0 = 28$ days = 0.0767 years. The only more or less instantaneous value for t_0 is the chloride migration coefficient. By using the experimental mix specific transfer parameters k_t estimated from results obtained after prolonged curing (91 and 273 or 364 days) (Section 9.3.1), this instantaneous migration coefficient can be converted to a value that represents an instantaneous diffusion coefficient. As such, the following alternative equation for the ageing exponent can be obtained (Equation 9-6):

$$D_{app,C}(t) = D_{RCM,0}(t_0) \cdot k_t \cdot \left(\frac{t_0}{t} \right)^a \quad (9-6)$$

This equation was used to estimate the value of ageing exponent a mentioned in *fib* Bulletin 34 (2006). However, it must be said that the resulting ageing exponents shown in Table 9.8 may still be somewhat too low because the apparent diffusion coefficients were derived at different curing ages followed by a fixed exposure period and not at different exposure times starting from one curing age. As a consequence, the porosity reducing effects inherent to prolonged exposure in seawater (Section 6.5.6) were not completely taken into account.

When comparing the ageing exponent estimates shown in Table 9.7 and 9.8 it can be observed that the values are quite comparable. The substantial difference in ageing behaviour between OPC and FA (and SF) concrete is once more confirmed. The differentiation suggested by *fib*

Bulletin 34 (2006) and DuraCrete (1998-2000) for different binder systems appears to be valid. Thus, it is indeed justified to use a higher ageing exponent for the k-value conforming FA references (F(1)15, F(2)15)), the HVFA mixtures (F(1)50, F(2)50) and the FA+SF mixtures (F(1)SF, F(2)SF). While estimated values for concrete containing FA (and SF) are more or less in range with the literature values, the one for the OPC concrete is clearly not. The estimated ageing exponent is only half of literature value. Applying the mix specific ageing exponent for OPC concrete will definitely shorten the estimated time to chloride-induced steel depassivation. The magnitude of this effect will be discussed more in detail in Section 9.5.

Table 9.8. Estimation of the ageing exponent by means of Equation 9-6.

| Ageing exponent a | Mean | Stdv. | R ² |
|-------------------|------|-------|----------------|
| T(0.45) | 0.15 | 0.03 | 0.93 |
| F(1)15 | 0.50 | 0.02 | 0.99 |
| F(2)15 | 0.57 | 0.02 | 0.99 |
| F(1)50 | 0.65 | 0.03 | 0.99 |
| F(2)50 | 0.74 | 0.04 | 0.99 |
| F(1)SF | 0.65 | 0.05 | 0.99 |
| F(2)SF | 0.45 | 0.05 | 0.98 |

As mentioned in Section 9.3.2, some additional service life predictions were done with $k_t = 1$ and alternative values for the ageing exponents. For one set of calculations, the ageing exponents based on the chloride migration test results at different curing ages were used as input. For another set of calculations, ageing exponents were estimated from the ‘natural’ diffusion tests at different curing ages. The latter estimation approach was in correspondence with Gulikers (2014). The outcome of these extra calculations has been reported and discussed in Appendix D.

9.3.3. Determination of the critical chloride content

Mainly because of the still ongoing discussion on the effect of fly ash additions on the critical chloride threshold level, C_{crit} was determined experimentally for two concrete compositions with a varying binder content: one OPC mixture (C: 300 kg/m³, W/C: 0.55, cf. mix T(0.55)) and one HVFA mixture containing (C: 150 kg/m³, FA: 150 kg/m³, FA/B: 50%, W/B: 0.55, mix F(0.55)). True, given the rather low total binder content and high W/B ratio, neither of these compositions can be used in environments classified as exposure class XS2. However, since it usually takes a very long time before onset of active steel corrosion can be observed, even with reduced concrete cover on top of the rebar, it was decided to test concrete compositions with a higher W/B ratio than allowed. The resulting higher porosity and permeability of the concrete will ensure that the duration of the monitoring period for initial testing remains acceptable. Evidently, the critical chloride concentration C_{crit} of the concrete compositions intended for use in this environment (T(0.45), F(1)15, F(2)15, F(1)50, F(2)50, F(1)SF and F(2)SF) should also be determined. This investigation is still ongoing. Within the framework of this thesis, conclusions regarding the effect of fly ash additions will merely be drawn based on the comparison of the above mentioned two concrete compositions.

Onset of active corrosion normally corresponds with an important drop in corrosion potential $E(\text{corr})$ of the rebar (= working electrode) in concrete versus a common standard reference electrode (e.g. SCE: Saturated Calomel Electrode) placed in a sodium chloride solution. For the monitoring and registration of this corrosion potential as a function of exposure time a potentiostat can be used. Several PGSTAT 101 potentiostat/galvanostat (Metrohm Autolab, Ecochemie, the Netherlands) instruments are available at the Department of Analytical Chemistry of Ghent University. The monitoring of the corrosion potential was done in close collaboration with Prof. Dr. Annemie Adriaens, Dr. Alice Elia and Michel De Keersmaecker from the same department. After observing the potential drop, the chloride concentration of concrete powder collected at rebar depth can be determined. The measured concentration should correspond well with C_{crit} . The experimental procedure followed was based on still ongoing research of the RILEM Technical Committee 235 CTC.

Sample geometry, preconditioning and experimental setup for corrosion monitoring

Prismatic concrete samples ($200 \times 160 \times 140 \text{ mm}^3$) with embedded rebar were cast for measuring the critical chloride content. Prior to concrete manufacturing 340 mm long pieces of reinforcing steel ($\text{Ø} 10 \text{ mm}$) were chemically cleaned by immersing them in an aqueous solution consisting of HCl 1:1 + 3 g/l urotropine for 5 minutes. Then, while still immersed in the cleaning solution the rebars were placed in an ultrasonic bath for 2-3 minutes. If no rust stains remained after this, the cleaning step can be considered terminated. If not, the whole procedure was repeated until this was the case. Next, the rebars were alternately immersed in water and stored in a climate room at 20°C and 95% RH until the surface showed a homogeneous superficial corrosion. As such, the surface condition of the rebars in practice is simulated. After this step, part of each rebar (20 mm) was coated at the location where the bar will stick out of the concrete specimen (10 mm in the concrete, 10 mm out of concrete) to avoid defects in coating finishing at the interface concrete-rebar. Finally, the partially coated rebars were implemented in the moulds and concrete was cast (Figure 9.2).

After 28 days of optimal curing at 20°C and 95% RH part of the rebar sticking out of the prism was cut off and a prismatic portion was sawn out of the original concrete specimen to reduce the concrete cover on top of the rebar to 7-10 mm. The cantilever roof (thickness: 20 mm) created by this sawing procedure should prevent that salt from the exposure solution can crystallize near the rebar sticking out at the upper surface of the concrete specimen (Figure 9.3). For the same reason the entire upper surface of the specimen including the concrete surface-rebar interface was treated with an impermeable coating. Once coated, the samples were pre-dried at 40°C for one week before putting them in the 3.3 m% aqueous NaCl exposure solution. The pre-drying step was included to stimulate faster chloride ingress through capillary suction.

During exposure only the specimen area underneath the cantilever roof was in contact with the aqueous NaCl solution. Evaporation of the exposure solution was prevented by covering the solution surface with floating anti-evaporation spheres. Connections between the wire clamps of the potentiostat and the working and reference electrodes were carefully covered with Parafilm tape to prevent any contact with chlorides during the monitoring period. During monitoring, the corrosion potential was registered every half hour until a sudden clear drop in potential ($\geq 150 \text{ mV}$) occurred. This event was assumed to correspond with onset of active

corrosion. From then on, the monitoring continued a little longer (around 1 week) to verify whether the potential remained stable after the drop. Next, the specimen was removed from the exposure solution and rinsed with water. At a distance of around 10 mm from the rebar, a core with diameter 100 mm was drilled perpendicular to the exposed surface with the reduced concrete cover (Figure 9.3). The cover on top of the rebar was removed as well to determine the exact cover thickness by means of a dial gauge. Using the profile grinder, concrete powder was collected from the core at the depth that corresponded with the exact concrete cover on top of the embedded rebar. The total chloride content of this powder was determined using the potentiometric titration method described in Section 6.4.2.



Figure 9.2. Sample geometry and experimental setup for monitoring of the corrosion potential of a rebar embedded in concrete versus a SCE reference electrode.

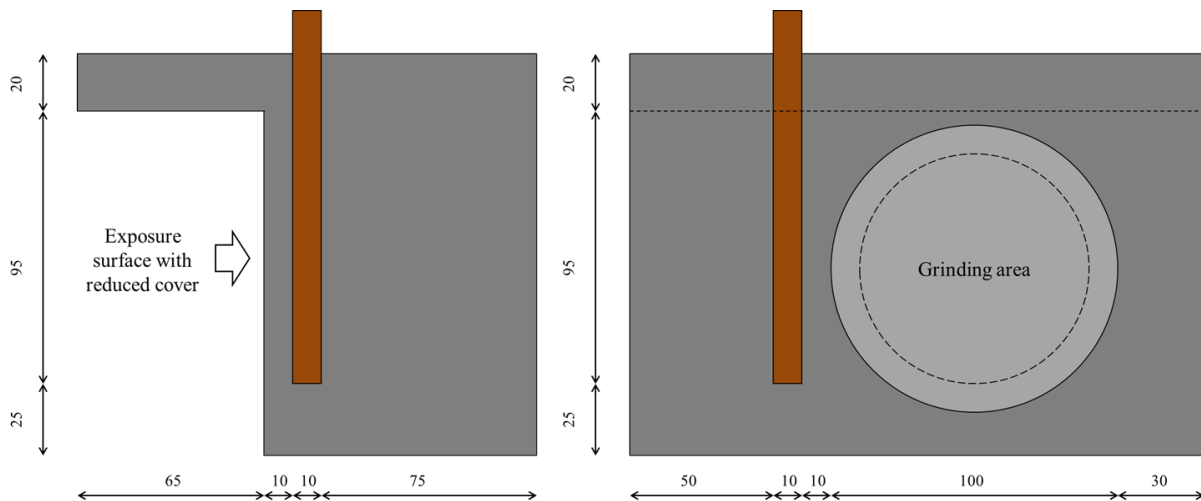


Figure 9.3. Schematic overview of the sample geometry and the position of the rebar.

Observed drop in electrochemical potential and critical chloride concentration

Figure 9.4 shows the observed potential drops and corresponding critical chloride concentrations (C_{crit} , in m%/binder) for each of the two specimens that were tested (OPC composition T(0.55) and HVFA composition F(0.55)). The duration of exposure (t_{ex} , in days) and the measured cover depths (d , in mm) have been indicated in the same figure. At the start of the experiment, the steel reinforcements embedded in OPC concrete T(0.55) (Figure 9.4a) showed a corrosion potential $E(\text{corr})$ of around -100 mV. As this value is more positive than -250 mV vs. SCE the criterion for passivated steel mentioned by Izquierdo et al. (2004) is met.

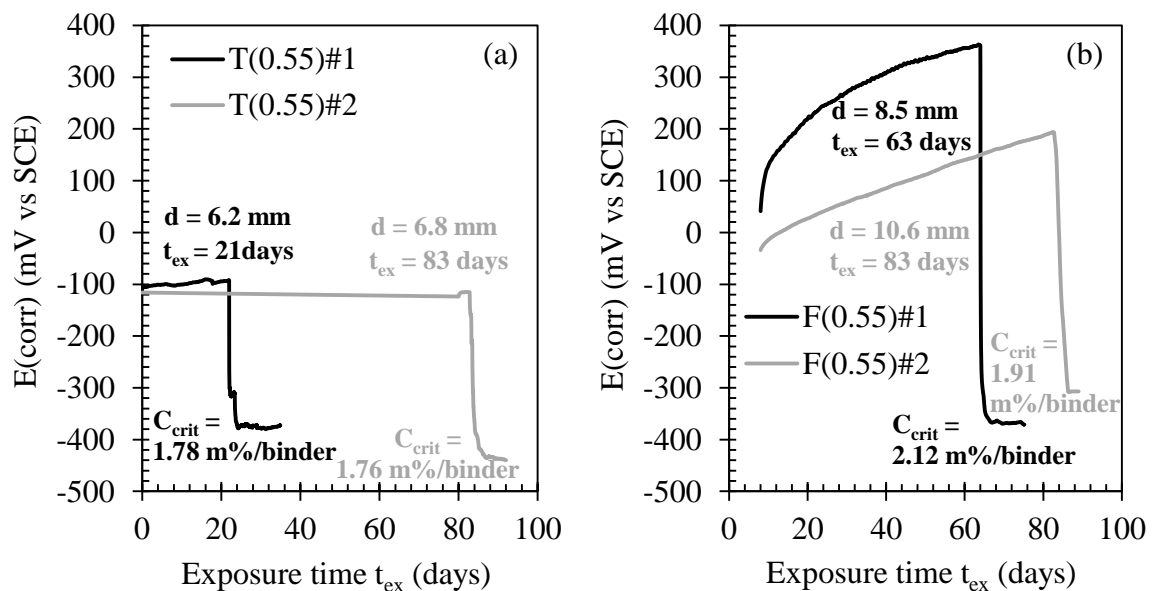


Figure 9.4. Typical drop in corrosion potential $E(\text{corr})$ marking the onset of active corrosion for OPC concrete T(0.55) (a) and HVFA concrete F(0.55) (b).

Thus, it is clear that the highly alkaline environment of the surrounding concrete provided the necessary conditions for the establishment of a fully protective passivation layer on top of the

steel surface. As long as the chlorides from the exposure solutions were not able to reach the location of the rebar at cover depth 6.2-6.8 mm in the required (critical) amount for depassivation, the corrosion potential remained more or less constant at its initial value. The observed potential drop in the course of the exposure time was very distinct. A very sudden decrease from around -100 to -400 mV was observed for both specimens whereafter the $E(\text{corr})$ value again stabilized. Very similar sudden drops in $E(\text{corr})$ were also observed by Choi et al. (2006) for steel embedded in OPC concrete with varying W/C ratios. According to ASTM C876 (1991), there is a greater than 90% probability that steel corrosion is occurring when the half-cell potential is more negative than -350 mV vs SCE. With final corrosion potentials against the same reference electrode in the range of -400 mV, onset of active corrosion indeed seems to have taken place. It is quite remarkable that the sudden potential drop was recorded at very different exposure times (21 versus 83 days) for the two specimens, although both were characterized by a very comparable concrete cover (d : 6.2-6.8 mm). It must be said that several large entrapped voids could be observed in the exposure surface of specimen T(0.55)#1, probably due to inadequate compacting. These holes most likely served as preferential pathways for the chlorides penetrating the concrete. As a result, the critical chloride concentration at rebar location must have been reached much sooner. Nevertheless, the critical total chloride concentrations C_{crit} determined by means of potentiometric titration were very similar for both specimens (1.76-1.78 m%/binder). In comparison with the values mentioned in DuraCrete (1998-2000) for OPC concrete with a W/B ratio of 0.50 (Table 9.4: 1.60 ± 0.20 m%/binder), the measured values are definitely within the same range. True, the W/C ratio of mixture T(0.55) was higher indicating that the critical chloride concentration should normally be lower than 1.60 ± 0.20 m%/binder. Additional testing on more specimens may thus still be needed.

The steel rebars embedded in the specimens of HVFA composition F(0.55) also showed a very substantial drop in $E(\text{corr})$ after prolonged immersion (t_{ex} : 64-83 days; d : 8.5-10.6 mm) in the 33 g/l aqueous NaCl solution (Figure 9.4b). After the potential drop, the stabilized $E(\text{corr})$ values amounted to -300 to -350 mV. Only one of the two specimens (F(0.55)#1) seems to meet the 90% corrosion probability criterion of ASTM C876 (1991). However, the final potentials of both specimens are within the -275 to -350 mV vs. SCE range mentioned by Ha et al. (2007) indicating 90% probability of steel depassivation. The critical chloride concentrations that correspond with the observed potential drops amounted to 1.91-2.12 m%/binder. Thus, for a given (high) W/B ratio, a 50% replacement of the cement with fly ash resulted in a considerably higher C_{crit} value.

A rather striking observation with respect to the HVFA concrete composition is the steady increase in (positive) $E(\text{corr})$ prior to the potential drop. At the start of the monitoring campaign, the potentials of both specimens were still close to 0 mV vs. SCE. From then on, the $E(\text{corr})$ increased steadily with time to values of 194 to 363 mV vs. SCE. Now, it must be said that positive $E(\text{corr})$ values are seldomly reported in literature. According to Li and Sagüés (2001), reinforcing steel in dry, aerated concrete can be characterized by potential up to 200 mV. Specimens F(0.55)#1 and F(0.55)#2 may have been dry at the beginning of the test due to the predrying at 40 °C. Yet, once immersed the specimens could hardly be considered as dry anymore, especially after prolonged exposure. Further research on this matter is certainly imperative. Despite the initial potential increase, the subsequent potential

drop remains very distinct and from an order of magnitude that probably still marks the onset of active corrosion. The corresponding C_{crit} values seem valid.

However, given the limited number of experimental data so far, it is not yet possible to use a mix specific critical chloride content as input to the prediction model for chloride-induced depassivation. The main conclusion that can be drawn from these preliminary results is that the measurable critical chloride content for the submerged condition is probably within the range of values suggested by DuraCrete (1998-2000) and that the general value of 0.6 m%/binder prescribed by *fib* Bulletin 34 (2006) can be abandoned. Although the first results indicated that the presence of fly ash had a beneficial effect on critical chloride content and thus the time to steel depassivation, it was decided to take this benefit not yet into account. Since the effect of the other binder material silica fume could not yet be experimentally verified, no differentiation between different binder systems was made. The additional beneficial effect inherent to the lower W/B ratio of the FA (and SF) containing concrete mixtures was also not considered. Instead, the C_{crit} value deduced from DuraCrete (1998-2000) for submerged OPC concrete with a W/B ratio of 0.45 was applied for all studied concrete compositions. As a consequence, all service life calculations done for the FA (and SF) containing mixtures will be rather on the safe side until more experimental C_{crit} data become available.

9.3.4. Summarizing overview of the default and mix specific input parameters

Table 9.9 gives an overview of all the model input parameters, involving both default and mix specific values, that were used for a second order estimation of the corrosion initiation period.

Table 9.9. Default and mix specific input parameters for second order service life prediction.

| Parameter | Distribution | Mean | Stdv. | Lower boundary | Upper boundary |
|------------------------------------|--------------|---|-------|----------------|----------------|
| C_{crit} (m%/binder) | Beta | 1.90 | 0.15 | 0.2 | 2.0 |
| C_0 (m%/binder) | Normal | 0.10 | 0.025 | – | – |
| $C_{S,\Delta x}$ (m%/binder) | Normal | 3.0 | 0.8 | – | – |
| d (mm) | Lognormal | 50 (t_{SL} : 100 years) | 8 | – | – |
| Δx (mm) | Constant | 0 | – | – | – |
| b_e (K) | Normal | 4800 | 700 | – | – |
| T_{ref} (K) | Constant | 293 | – | – | – |
| T_{real} (K) | Normal | 283 | 5 | – | – |
| $D_{RCM,0}$ (mm ² /yrs) | Normal | Figure 6.3 (after unit conversion: m ² /s to mm ² /years) | | | |
| k_t (–) | Normal | Table 9.6 | | – | – |
| t_0 (yrs) | Constant | 0.0767 (28d) | | | |
| a (–) | Beta | Table 9.8 | | 0.0 | 1.0 |

This table differs from Table 9.5 in the following ways:

- The critical chloride concentration prescribed by *fib* Bulletin 34 (2006) was replaced by the one suggested by DuraCrete (1998-2000) for submerged OPC concrete with a W/B ratio of 0.45. The same value was adopted for all concrete mixtures. This choice has been justified in Section 9.3.3.

- An experimentally determined mix specific transfer parameter k_t was adopted for each concrete mixture.
- An experimentally determined mix specific ageing exponent was assumed for each concrete composition.

The second order estimation of the corrosion initiation period was also done using the same probabilistic software Comrel as mentioned in Section 9.2.10.

9.4. Semi-probabilistic estimation of the corrosion propagation period

9.4.1. Limit state function of DuraCrete

To estimate the time to the occurrence of corrosion-induced cracks exceeding 1 mm in width, the same limit state function was used as in Chapter 8. The general outline of the equation suggested by DuraCrete (1998-2000) remained the same (Equation 8-8). Only several of the model input parameters were different in value for the submerged zone with exposure to chlorides, i.e. the relative time of wetness w_t (= 1.0), the characteristic pitting factor α^c (= 9.28), the characteristic chloride corrosion rate factor F_{cl}^c (= 2.63) and the characteristic value accounting for the presence of chloride $k_{cl,res}^c$ (= 0.72), cf. DuraCrete (1998-2000). The basic experimental input again comprised the potential electrolytical resistivity ρ_0^c and the tensile splitting strength $f_{c,sp}^d$ of the concrete mixtures under investigation.

9.4.2. Summarizing overview of the model input parameters

Table 9.10 summarizes the characteristic values of all model input parameters for the semi-probabilistic estimation of the time to unacceptable corrosion-induced cracking (= the end of the corrosion propagation period).

Table 9.10. Quantification of the model input parameters for the semi-probabilistic estimation of the corrosion propagation period cf. DuraCrete (1998-2000).

| Parameter | Value | Parameter | Value |
|------------------------------------|-----------|--|-----------|
| w_{cr} (mm) | 1.0 | m_0 ($\mu\text{m}\cdot\Omega\text{m}/\text{year}$) | 882 |
| w_0 (mm) | 0.05 | α^c (-) | 9.28 |
| b^c (mm/ μm) | 0.0104 | F_{cl}^c (-) | 2.63 |
| γ_b (-) | 1.40 | ρ_0^c (Ωm) | Table 8.4 |
| d (mm) | 50 | t_{hydr} (year) | 1.0 |
| Δd (mm) | 14 | t_0 (year) | 0.0767 |
| Φ (mm) | 12 | $n_{res_OPC}^c$ (-) | 0.23 |
| $f_{c,sp}^d$ (MPa) | Table 8.2 | $n_{res_FA, SF}^c$ (-) | 0.62 |
| a_1 (μm) | 74.4 | $k_{c,res}^c$ (-) | 1.0 |
| a_2 (μm) | 7.3 | K_c ($^{\circ}\text{C}^{-1}$) | 0.025 |
| a_3 ($\mu\text{m}/\text{MPa}$) | -17.4 | T ($^{\circ}\text{C}$) | 10 |
| w_t (-) | 1.0 | $k_{RH,res}^c$ (-) | 1.0 |
| γ_V (-) | 1.40 | $k_{cl,res}^c$ (-) | 0.72 |

The corrosion propagation periods estimated with the model input from Table 9.10 were compared for OPC reference T(0.45), HVFA composition F(1)50 and FA+SF composition F(1)SF, all assumed to be located in a XS2 environment. In addition, it was evaluated whether

the estimated time to steel depassivation differs much from the time to unacceptable corrosion-induced cracking.

9.5. Results and discussion

9.5.1. First order estimation of the corrosion initiation period

Combining the measured chloride migration coefficients with the default model input parameters of *fib* Bulletin 34 (2006) gives a first estimation of the corrosion initiation period for exposure class XS2 and construction class S6 (with extra concrete cover for a design service life of 100 years) (Table 9.11). Standards NBN EN 206-1 (2000) and NBN B15-001 (2004) both state that composition T(0.45) should guarantee a 50 years service life in this exposure class for a normal concrete cover. Moreover, its service life should amount to at least 100 years when assuming the extra concrete cover for construction class S6. The first order prediction clearly indicates otherwise. After 28 days of optimal curing, the estimated time to chloride-induced steel depassivation is not even 5 years. Given the deemed-to-satisfy status of the OPC reference for a 50 years time span, this prediction outcome seems unrealistic. The k-value conforming FA references F(1)15 and F(2)15 show a better performance (t_{SL} : 31-27 years). The same goes for HVFA mixtures F(1)50 and F(2)50 (t_{SL} : 17-19 years). On the other hand, a time to depassivation of more than 1000 years was found for the FA+SF compositions F(1)SF and F(2)SF. The better service life performance of all fly ash (and silica fume) containing concrete mixtures can mainly be attributed to the higher ageing exponents assumed for these types of binder systems (FA, SF: 0.60, 0.62 versus OPC: 0.3). The very low migration coefficients that were measured for these mixtures after prolonged curing sometimes had an additional beneficial effect.

Table 9.11. First order probabilistic estimation of the time to steel depassivation (years) with the default model input parameters of *fib* Bulletin 34 (2006) as input.

| 1 st order / XS2 | t_0 (d) | T(0.45) | F(1)15 | F(2)15 | F(1)50 | F(2)50 | F(1)SF | F(2)SF |
|-----------------------------|-----------|---------|--------|--------|--------|--------|--------|--------|
| Default input | 28 | 4 | 31 | 27 | 17 | 19 | +1000 | +1000 |

Thus, the first order estimation approach is most certainly in favor of the alternative binder systems. However, the question remains whether this estimation approach is justifiable given the unrealistically low prediction outcome for the applicable OPC reference. Mainly for this reason, the validity of several relevant input parameters to the model (the experimental transfer parameter k_t , the ageing exponent a and the critical chloride threshold level C_{crit}) was verified experimentally as described in Section 9.3. Their estimated values served as input to the second order probabilistic estimation of the corrosion initiation period (Section 9.5.2).

Finally, it should perhaps be highlighted why the limit state function of *fib* Bulletin 34 (2006) with default input was used for the first order estimation. This approach is in contrast with the very basic limit state function that was used for the first order estimation of the time to carbonation-induced steel depassivation (Equation 8-1). The latter equation contained only one load variable (= the time dependent carbonation depth) and one resistance variable (= the applied concrete cover). A similar very basic limit state function could be defined for chloride-induced depassivation. The chloride content at the location of the rebar and the

critical chloride content would be the only load and resistance variables. For reasons of simplification, the time and location dependent chloride content is then assumed to be only function of the measured surface concentration and the apparent diffusion coefficient after a 'natural' diffusion test. Temperature effects and ageing behaviour would not be accounted for. This approach was attempted for all concrete compositions and curing ages. It practically always resulted in a time to depassivation of less than 1 year. Therefore, the simplified limit state function was no longer considered for the first order estimation.

9.5.2. Second order estimation of the corrosion initiation period

Before implementing the alternative values for the experimental transfer parameter (k_t), the ageing exponent (a) and the critical chloride content (C_{crit}) into the model all at once, the modifications were done in steps to evaluate their individual effect (Table 9.12).

- Modification M1: use of the mix specific k_t values given in Table 9.6.
- Modification M2: use of the mix specific a values given in Table 9.8.
- Modification M3: use of 1.9 m%/binder as C_{crit} value cf. DuraCrete (1998-2000).
- Modification M1+2+3: use of the alternative values for k_t , a and C_{crit} .

Table 9.12. Second order probabilistic estimation of the time to steel depassivation (years) with default and mix specific model input parameters as input.

| 2nd order / XS2 | t_0 (d) | T(0.45) | F(1)15 | F(2)15 | F(1)50 | F(2)50 | F(1)SF | F(2)SF |
|-----------------------------------|-----------------------------|----------------|---------------|---------------|--------------------|---------------|--------------------|---------------|
| M1 (k_t) | 28 | 9 | 101 | 60 | 79 | 67 | +1000 | +1000 |
| M2 (a) | 28 | 0 | 38 | 89 | 180 | +1000 | +1000 | 231 |
| M3 (C_{crit}) | 28 | 42 | 855 | 747 | 464 | 532 | +1000 | +1000 |
| M1+2+3 | 28 | 47 | +1000 | +1000 | +1000 | +1000 | +1000 | +1000 |
| | 28 | – | – | – | +1000 ^a | – | +1000 ^a | – |

^a Based on $D_{RCM,0}$ values for suboptimal curing: 7 days at 20°C and 95% RH, 21 days at 20°C and 60% RH.

An increase of the critical chloride content C_{crit} from 0.6 m%/binder to 1.9 m%/binder prolonged the time to steel depassivation the most. The use of the estimated k_t values also always resulted in a longer corrosion initiation period. However, the effect of a lower value for this parameter (from the default 0.832 value to 0.34-0.67 cf. Table 9.6) was somewhat less pronounced.

Applying a mix specific value of the ageing exponent could result in a longer or shorter corrosion initiation period depending on whether or not the estimated value was higher or lower than the prescribed default value. Since their ageing exponents decreased in comparison with default value, modification M2 resulted in a shorter time to steel depassivation for mixtures T(0.45), F(1)15, F(2)15 and F(2)SF, respectively. The opposite trend was observed for the HVFA compositions and mixture F(1)SF.

Combining the alternative values for all three parameters still revealed an important difference between the OPC reference on the one hand and the k-value conforming FA, HVFA and FA+SF mixtures on the other hand. Although the time to depassivation of reference T(0.45) had increased in comparison with the first order approach, the estimated corrosion initiation period is barely 50 years. Keeping in mind that the required extra concrete

cover for a 100 years service life was applied, this is rather short. With incorporation of fly ash (and silica fume) the time to depassivation would increase to more than 1000 years.

Very high service life estimates should be interpreted with caution. The very positive output of the service life prediction can to some extent be explained by the optimal curing conditions that were maintained for no less than 28 days. To evaluate the magnitude of this effect, the chloride migration coefficient of mixtures F(1)50 and F(1)SF measured after 28 days of suboptimal curing (7 days at 20°C and 95% RH, 21 days at 20°C and 60% RH) were also implemented in the second order prediction model. As demonstrated in Section 6.5.1, suboptimal curing could cause a 50% increase of the 28-day chloride migration coefficient. Nevertheless, implementation of such an increased value in the prediction model still resulted in a time to steel depassivation of more than 1000 years. The same holds true for the FA+SF concrete composition. This was rather expected for that mixture because it was shown in Section 6.5.1 that suboptimal curing only caused a 10% increase in migration coefficient.

Since the optimal curing conditions cannot really be held responsible for the long time to steel depassivation, the main causes must be sought elsewhere. The fact that the model unrealistically assumes that the concrete is at all time free of flaws (cracks, etc.) could be one of the explanations. The occurrence of cracks is as good as unavoidable in practice. Nevertheless, the DuraCrete (1998-2000) guideline on which *fib* Bulletin 34 (2006) is based, states that concrete in compliance with the applicable criteria for maximum crack width could be treated as uncracked. This is in sharp contrast with some of the findings reported in Chapter 6. There, it was observed that concrete representative mortar specimens containing an artificially induced 0.1 mm wide crack cannot be seen as uncracked in terms of their chloride migration resistance. Thus, further improvement of the empirical prediction model of *fib* Bulletin 34 (2006) is imperative. A more realistic model will require an equivalent chloride migration/diffusion coefficient for cracked concrete as input.

As indicated in Sections 9.3.1 and 9.3.2 some additional second order service life predictions were done while using $k_t = 1$ (cf. *fib* Bulletin 34 (2006)) and ageing exponents estimated from either chloride migration tests or ‘natural’ diffusion tests at different curing ages. The results of these extra calculations have been discussed in Appendix D.

9.5.3. Influence of the selected failure event

The time to unacceptable corrosion-induced concrete cracking (Table 9.13: $t_{\text{crack}_{1 \text{ mm}}}$) estimated by means of the semi-probabilistic method suggested by DuraCrete (1998-2000) was found to be much shorter than the time to chloride-induced steel depassivation (Table 9.12). The difference is so substantial that the duration of the corrosion propagation period becomes negligible in comparison with the initiation period. Thus, only considering the corrosion initiation period does not lead to an important underestimation of the actual service life.

Table 9.13. Estimated time to unacceptable corrosion-induced cracking (years) after depassivation of the steel due to the presence of chlorides.

| 1st order / XS2 | T(0.45) | F(1)50 | F(1)SF |
|---|----------------|---------------|---------------|
| $t_{\text{crack}_{1 \text{ mm}}} \text{ (years)}$ | 0.4 | 1.4 | 4.8 |

The longest corrosion propagation period was recorded for the FA+SF composition. Still, this is less than 5 years. For the HVFA mixture and the OPC reference the time spans were even lower, i.e. 1.4 and 0.4 years, respectively. The better performance of the concrete mixtures with fly ash (and silica fume) can be attributed to their higher bulk resistivity and age factor (n_{res}^c) for resistivity.

The short propagation period after the chloride-induced depassivation (Table 9.13) is in contrast with the rather long propagation period after carbonation-induced depassivation (Table 8.7). This can be mainly explained by the higher pitting factor α_c (= 9.28 versus 2.0) and corrosion rate factor F_{cl}^c (= 2.63 versus 1.0) and the lower resistivity chloride factor $k_{cl,res}^c$ (= 0.72 versus 1.0) that are assumed in environments with presence of chlorides. Since chloride-induced corrosion is known for being very localized and fast, the use of higher values for α^c and F_{cl}^c can be agreed upon intuitively. However, their values could not yet be verified experimentally.

9.6. Conclusions

Both the first and second order probabilistic estimation of the time to chloride-induced steel depassivation indicate that the corrosion initiation period is considerably longer for the fly ash (and silica fume) containing concrete mixtures destined for exposure class XS2. This is a direct consequence of the lower apparent diffusion coefficients and the better ageing behaviour of the latter. A general shift from the first order approach with default model input to the second order approach with more mix specific model input revealed some important differences.

- (i) The applicable OPC reference T(0.45) is characterized by an unrealistically low depassivation period of less than 5 years when using default input for the experimental transfer parameter k_t (= 0.832), the ageing exponent a (= 0.30) and the critical chloride threshold level C_{crit} (= 0.6 m%/binder). The implementation of measured mix specific k_t and a values and the verified higher value for C_{crit} under submerged exposure conditions, postpones steel depassivation to 47 years. The higher value for C_{crit} (1.9 m%/binder) was the main contributor to this increase. It completely compensated for the fact that the measured ageing exponent (= 0.15) was much lower than the default value (= 0.30). This is still rather short because the estimation was done while assuming the required concrete cover for a service life of 100 years.
- (ii) With default model input, the k-value conforming FA references and the HVFA mixtures are characterized by a longer time to depassivation than the OPC concrete. The better performance can mainly be attributed to the higher default value for the ageing exponent (= 0.60). Nevertheless, the estimated corrosion initiation period is still less than 100 years. This is not the case anymore with the use of mix specific model input. The higher value for C_{crit} , which was assumed to be equal to the value for OPC concrete (1.9 m%/binder) for all concrete mixtures, is the main contributor to the increased service life of more than 1000 years. Since first corrosion experiments indicate that the critical chloride content of HVFA concrete is probably higher than for OPC concrete, the observed benefit inherent to the second order service life estimation approach is

even underestimated. The effect of using a mix specific ageing exponent is lower, because the measured values were very similar to the default values.

- (iii) A corrosion initiation period of more than 1000 years was estimated with both the first and second order approach for the FA+SF compositions. The very low chloride migration coefficients that were used as experimental input to the model can be held responsible for this.
- (iv) The implementation of migration coefficients measured after 28 days of suboptimal curing still resulted in corrosion initiation periods of more than 1000 years for HVFA and FA+SF concrete.
- (v) The unrealistically long depassivation periods can probably be explained by the fact that concrete in practice is never free of flaws (cracks, etc.) while the chloride migration tests for service life prediction were performed on uncracked specimens. Migration tests performed on concrete representative mortar specimens with an artificial crack showed that the presence of 0.1 mm wide cracks do have a negative effect on the chloride migration resistance. Thus, concrete with cracks smaller than 0.3 mm in width – the criterion for reinforced concrete according to Eurocode 2 – cannot be treated as uncracked. This means that prediction models should take into account the presence of cracks. For the moment this is not the case.

The semi-probabilistically assessed duration of corrosion propagation period was found to be very short (less than 5 years), even negligible in comparison with the corrosion initiation period. The high pitting and corrosion rate factors in presence of chlorides are mainly responsible for this behaviour. The longest time to unacceptable corrosion-induced cracking (= 4.8 years) was recorded for FA+SF concrete, mainly due to the high bulk resistivity of the material (= 353 Ωm versus 81 Ωm for the OPC reference), the concrete property that is inversely proportional to the steel corrosion rate.

PART IV

LIFE CYCLE ASSESSMENT

Literature review on life cycle assessment of traditional and ‘green’ concretes

10.1. Introduction

Concrete is one of the most widely used building materials in roads, buildings, bridges and other infrastructures. On average, approximately 1 ton of concrete is produced each year for every human being in the world [Lippiatt and Ahmad (2004)]. Because of this global extensive use, it is imperative to evaluate the environmental impact of this material correctly. Nowadays, a material’s environmental impact is often equated with its effect on greenhouse gas emissions (GHGs) and climate change. From this point of view, a great variance of so-called ‘green’ concrete concepts has been developed over the years. Very often these concepts focus on partially replacing the cement, the concrete constituent responsible for the highest CO₂ emissions, by other materials [Meyer (2009)]. Worldwide, the cement industry alone was estimated to be responsible for 5-7% of all anthropogenic CO₂ generated [Malhotra (2000), Humphreys and Mahasenan (2002), Bernstein et al. (2007)]. Since this branch of industry emits almost no other GHGs, it is held accountable for only about 3% of the total GHG emissions generated by human activities [Damtoft et al. (2008)].

However, the implementation of these ‘green’ concepts implies that certain parameters in the mix design need to be changed to obtain a sufficiently workable, strong and durable concrete. Moreover, the specific application and the environment in which the concrete will be used, needs to be considered. A more correct environmental evaluation takes into account all differences between the ‘green’ and traditional concrete. Therefore, it is necessary to adopt a LCA approach as generally defined in Chapter 2. This methodology compares the environmental impact of a strength and durability/service life related functional unit (FU) of traditional and ‘green’ concrete over its entire life cycle (production, use and end-of-life phase) for predefined system boundaries.

This literature review addresses the concrete properties that influence the environmental impact significantly. Life cycle inventory (LCI) data on concrete were collected from literature and compared with each other. Finally, it was investigated how these inventory data are assigned to the impact categories of different impact assessment methods and how the environmental score obtained can be affected by important input parameters, such as the FU choice, the system boundaries assumed and the applied allocation rules.

10.2. Environmental impact of concrete

10.2.1. Composition

10.2.1.1. Cement

Environmental impacts of cement manufacturing can be global, regional or local in scale [Huntzinger and Eatmon (2009)].

Global scale – Over the last decades, the emphasis has clearly shifted towards a global focus on climate change. Table 10.1 presents a summary of values found in literature for the cement related CO₂ emissions [Humphreys and Mahasanen (2002), Damtoft et al. (2008), Hendriks et al. (2011), Josa et al. (2004), Febelcem (2006), Malhotra (2004), Price et al. (1999), Flower and Sanjayan (2007), ATILH (2002), Gartner (2004)]. They are usually the sum of the CO₂ emitted during the calcination process (raw material CO₂: RM-CO₂ [Gartner (2004)]) and the CO₂ associated with energy use. With respect to the latter, a distinction can be made between indirect and direct energy bound CO₂ (IEB- and DEB-CO₂). IEB emissions comprise the CO₂ emissions associated with the generation of electrical power to operate the cement plant, while the direct energy bound emissions are associated with the fuel combustion in the cement kiln.

Regarding DEB-CO₂, the efficiency of the cement kiln plays an important role. A clinkering energy efficiency of about 3 GJ/ton is not far above the real thermodynamic limit [Gartner (2004)]. Under optimum conditions heat consumption can be reduced to less than 2.9 GJ/ton clinker. A typical modern rotary cement kiln with a specific heat consumption of 3.1 GJ/ton clinker emits approximately 0.31 kg DEB-CO₂ per kg clinker when burning traditional carbon based fuels such as coal, oil or petroleum coke, while this amount equals about 0.60 kg/kg clinker for an inefficient long rotary kiln burning wet raw materials with a heat consumption of around 6 GJ/ton clinker [Damtoft et al. (2008)].

Possibilities to reduce RM-CO₂ emissions are rather limited. Partially replacing the traditional raw materials by blast-furnace slag (BFS) or class C fly ash (FA) with a higher calcium content is one option. In practice, replacement levels of about 10% are commonly reported. For a limestone replacement of 10%, the total CO₂ reductions can in theory be as high as 25%. This is due to a concomitant reduction in fuel consumption because less heat is needed to decarbonate the remaining limestone [Damtoft et al. (2008)].

To reduce the emissions any further, alternative clinker chemistries need to be considered. Low energy belite cements seem a valuable alternative. If all the alite in cement could be substituted with belite, RM-CO₂ emissions can be reduced with about 8%. Because of the lower burning temperature, DEB-CO₂ emissions can also be lowered with about 8%. However, due to its slow setting and hardening, the successful implementation of this cement is doubtful. A more promising material is sulphoaluminate cement. Although quite expensive, this cement type has a much lower embodied RM-CO₂ content than Portland cement due to its significantly lower CaO contents (30% lower than a modern OPC clinker). Moreover, the raw materials can be burned at lower temperatures [Morbi et al. (2010)].

The greatest potential to reduce CO₂ emissions lies in the replacement of conventional carbon based fuels by alternative low fossil carbon based fuels, e.g. carbon neutral biomass [Damtoft et al. (2008)], non-carbon neutral scrap tyres [Davies and Worthington (2001)], etc.

Table 10.1. CO₂ (inclusive its distribution over RM-CO₂, IEB-CO₂ and DEB-CO₂), SO_x, NO_x and CKD emissions for Portland cement expressed in g/kg cement⁺ or g/kg clinker⁺⁺.

| Reference | RM-CO ₂ | IEB-CO ₂ | DEB-CO ₂ | Total |
|----------------------------------|-----------------------------|----------------------------|-----------------------|------------------------------|
| [Humphreys and Mahasenan (2002)] | – | – | – | 870 g/kg ⁺ |
| [Damtoft et al. (2008)] | 530 g/kg ⁺⁺ | 310-600 g/kg ⁺⁺ | | 840-1130 g/kg ⁺⁺ |
| [Hendriks et al. (2011)] | 50% | | 50% | 810 g/kg ⁺ |
| [Josa et al. (2004)] | 59% | 6% | 35% | 800 g/kg ⁺ |
| [Febelcem (2006)] | 57% | 6% | 37% | – |
| [Malhotra (2004)] | 50% | 0-10% | 40-50% | – |
| [Price et al. (1999)] | – | 80 g/kg ⁺ | – | – |
| [Flower and Sanjayan (2007)] | – | – | – | 820 g/kg ⁺ |
| [ATILH (2002)] | – | – | – | 810 g/kg ⁺ |
| [Gartner (2004)] | 425 g/kg ⁺ | 80 g/kg ⁺ | 390 g/kg ⁺ | 815 + 80 g/kg ⁺ |
| | | | Mean value | 860 g/kg⁺ |
| Reference | SO ₂ | | | |
| [Josa et al. (2004)] | 0.40-0.60 g/kg ⁺ | | | |
| [Chen et al. (2010a)] | 0.82 g/kg ⁺ | | | |
| [ATILH (2002)] | 0.58 g/kg ⁺ | | | |
| [Van Oss and Padovani (2003)] | 0.27 g/kg ⁺⁺ | | | |
| [Jacott et al. (2003)] | 0.54 g/kg ⁺⁺ | | | |
| | | | Mean value | 0.53 g/kg⁺ |
| Reference | NO _x | | | |
| [Josa et al. (2004)] | 2.40 g/kg ⁺ | | | |
| [Malhotra (2004)] | 10.00 g/kg ⁺⁺ | | | |
| [Chen et al. (2010a)] | 1.20 g/kg ⁺ | | | |
| [ATILH (2002)] | 1.50 g/kg ⁺ | | | |
| | | | Mean value | 3.65 g/kg⁺ |
| Reference | CKD/PM | | | |
| [Chen et al. (2010a)] | 0.49 g/kg ⁺ | | | |
| [ATILH (2002)] | 0.04 g/kg ⁺ | | | |
| [Van Oss and Padovani (2003)] | 150-200 g/kg ⁺⁺ | | | |
| | | | Mean value | 83.3 g/kg⁺ |

Note: Mean values were calculated for a cement consisting for 95% of Portland clinker.

Regional scale – Regional environmental impacts include SO₂ and NO_x emissions which contribute to acid rain. Table 10.1 includes an overview of the estimated SO₂ and NO_x emissions for Portland cement according to literature [Josa et al. (2004), Malhotra (2004), Chen et al. (2010a), ATILH (2002), Van Oss and Padovani (2003), Jacott et al. (2003)].

The majority of SO₂ emitted is derived from the fuel combustion and the processing of raw materials in the kilns. Around 70-95% of the fraction not attributable to energy production is absorbed due to the high alkalinity of clinker [Houghton et al. (1996)]. Thus, the majority of the SO₂ leaves the kiln with the clinker [Schuhmacher et al. (2004)].

The NO_x values refer to both NO₂ and NO emitted to the air. These are mainly an output from fuel usage during clinker production and energy consumption throughout the process chain.

Local scale – Cement kiln dust (CKD) emissions are the main contributors to the local impact. The size of CKD (0.05 to 5 µm) is within the size range of respirable particles [Schuhmacher et al. (2004)]. Since the diameter is smaller than 10 µm, CKD is classified as PM₁₀. According to the EPA [EPA (1994), EPA (1999)], these fine particulates of unburned and partially burned raw materials present in the combustion gases of the cement kiln, are considered as a potential hazardous waste due to their caustic and irritative nature. As mentioned in Table 10.1, the amount of CKD generated per kg of clinker produced equals about 15-20% (by

mass) [Van Oss and Padovani (2003)]. However, it must be said that the latter estimation was based on only very limited, informal data and conversations with plant personnel. The discontinuous nature of CKD measurements is another reason that could explain the large variability in the reported emission values. It is also not always clear which are the CKD emissions that are included in the reported values. This could be the fraction that is initially captured by the electrostatic precipitators or the baghouse filters, the fraction that is returned to the kiln, or only the fraction that is landfilled. Nowadays, both the environmental and health risks associated with CKD can be reduced significantly by means of mineral carbonation. As observed in the carbonation of other industrial wastes, sequestering carbon may yield additional benefits by stabilizing the waste (reducing the pH) which reduces health risks and the generation of harmful leachate [Huntzinger and Eatmon (2009)]. In addition, the utilization of CKD for carbon sequestration by means of mineral carbonation appears to have its advantages on the global scale, since about 7% of the carbon emissions can be captured this way [Huntzinger and Eatmon (2009)].

On the local scale, attention should also be paid to the emission of metals and polychlorinated dibenzo-p-dioxins and dibenzofurans (PCDD/Fs). After emission into the atmosphere, these chemicals can be transmitted to humans through direct (air) and indirect (groundwater, soil, vegetation) pathways. Health risks turned out to be quite low [Schuhmacher et al. (2004)]. When located in an urban area, non-carcinogenic and cancer risks derived from exposure to metal and PCDD/Fs coming from a cement plant were within the ranges acceptable according to national and international regulations, with the exception of only a few elements (e.g. As and Cr) [Rovira et al. (2010)]. In addition, no significant increases in the environmental levels of metals and PCDD/Fs were detected when comparing a conventional fossil kiln fuel with an alternative fuel (15% on average partial substitution of fossil fuel by refuse-derived fuel from municipal solid waste). Also, no changes in airborne particulate matter were noted, while significant reductions were found for a number of pollutants (PCDD/Fs, Co, Cr, Mn and Ni) in vegetation, as well as in soil (Ni) and air (Sn) [Rovira et al. (2011)].

Quite some attention is also being paid to the chromium content of cement. For instance, the sale of cement containing more than 2 ppm of soluble Cr(VI) when hydrated, is prohibited by European directive 2003/53/EC [European Union (2003)]. Hexavalent chromium or Cr(VI) is not stable. When dissolved, Cr(VI) can penetrate the unprotected skin and be transformed into Cr(III) which combines with epidermal proteins to form the allergen that causes sensitivity to certain individuals. The Cr(VI) content can originate from (i) raw materials and fuel entering the system, (ii) magnesia-chrome refractory blocks, (iii) wear metal from crushers containing chromium alloys and (iv) additions of gypsum, pozzolans, ground granulated BFS, mineral components, CKD and set regulators [Hills and Johansen 2007)].

Variability and quality of the data – An important issue regarding all cement related emission data as found in literature is the aspect of variability and quality of the reported data. The varying CO₂, NO_x, SO_x and CKD emissions as shown in Table 10.1, are a clear proof of this. Obviously, assuming constant emission values will not lead to an accurate environmental evaluation. Until now, only few sources have reported standard deviations on their average values, e.g. Chen et al. (2010a) and ATILH (2002). Von Bahr et al. (2003) investigated the data variability and quality problem by analysing the monthly dust, NO_x and SO₂ emissions of

6 Nordic cement plants for a period of 7 years (1993-1997). Significant differences were observed between cement plants and with time. These differences may depend on raw materials, production processes (including stability in the process) and varying performance of/investments in air pollution control systems. Von Bahr et al. (2003) aimed for the highest possible data quality through a close cooperation with the cement plants and through internal and external review. The resulting comparable data quality indicates that the variability of emissions remains. This conclusion should also hold true for other concrete constituents.

10.2.1.2. Cementitious materials

Table 10.2 gives an overview of the consumption of raw materials and energy in steel production, coal fired electrical power generation and Si-metal manufacturing [Chen et al. (2010b), Chen (2009)]. The use of transport and infrastructure has also been mentioned. Depending on the allocation principle adopted (Section 10.3.2.2) part of this input should be attributed to the production of the forthcoming industrial by-products BFS, FA and SF.

Table 10.2. Use of raw materials and energy in steel production, coal fired power generation and Si-metal manufacturing, plus the amounts attributable to 1 kg of the corresponding by-products through mass and economic allocation (see Section 10.3.2.2, Table 10.7).

| [Chen et al. (2010b)] | | 1 kg pig iron | 1 kg BFS (mass allocation) | 1 kg BFS (economic allocation) |
|------------------------|--------------------|--------------------------------------|--------------------------------------|---------------------------------------|
| <u>Raw materials:</u> | Sinter | 1.05 kg | 0.85 kg | 0.10 kg |
| | Pellets | 0.40 kg | 0.32 kg | 0.04 kg |
| | Lump ore | 0.15 kg | 0.12 kg | 0.01 kg |
| <u>Energy:</u> | Hard coal | 0.49 kg | 0.40 kg | 0.05 kg |
| | Electricity | 0.10 kWh | 0.08 kWh | 0.01 kWh |
| <u>Transport:</u> | Boat | 1.50 tkm | 1.21 tkm | 0.144 tkm |
| | Train | 0.25 tkm | 0.20 tkm | 0.024 tkm |
| | Truck | 0.01 tkm | 0.008 tkm | 0.001 tkm |
| <u>Infrastructure:</u> | Blast furnace | 1.33×10^{-11} unit | 1.08×10^{-11} unit | 1.27×10^{-12} unit |
| [Chen et al. (2010b)] | | 1 kWh electricity | 1 kg FA (mass allocation) | 1 kg FA (economic allocation) |
| <u>Raw materials:</u> | Water | 0.035 kg | 0.083 kg | 0.007 kg |
| <u>Energy:</u> | Hard coal | 0.432 kg | 1.030 kg | 0.083 kg |
| | Diesel | 1.56×10^{-4} m ³ | 3.72×10^{-4} m ³ | 0.300×10^{-4} m ³ |
| <u>Transport:</u> | Train | 5.09×10^{-3} tkm | 1.21×10^{-2} tkm | 9.79×10^{-4} tkm |
| <u>Infrastructure:</u> | Coal thermal plant | 1.33×10^{-11} unit | 3.17×10^{-11} unit | 2.56×10^{-12} unit |
| [Chen (2009)] | | 1 kg Si-metal | 1 kg SF (mass allocation) | 1 kg SF (economic allocation) |
| <u>Raw materials:</u> | Quartz | 2.70 kg | 2.340 kg | 0.864 kg |
| | Oxygen | 0.02 kg | 0.017 kg | 0.0064 kg |
| <u>Energy:</u> | Hard coal | 0.91 kg | 0.79 kg | 0.29 kg |
| | Electricity | 11 kWh | 9.53 kWh | 3.52 kWh |
| | Petroleum coke | 0.50 kg | 0.43 kg | 0.16 kg |
| | Charcoal | 0.17 kg | 0.15 kg | 0.05 kg |
| | Wood chips | 1.58 kg | 1.37 kg | 0.51 kg |
| <u>Infrastructure:</u> | Electric arc oven | 1.00×10^{-11} unit | 8.67×10^{-12} unit | 3.20×10^{-12} unit |

Table 10.3 summarizes the emissions to air and waste production associated with the above mentioned primary industrial processes as reported by Chen et al. (2010b) and Chen (2009).

Table 10.3. Emissions and waste production in steel production, coal fired power generation and Si-metal manufacturing, plus the amounts attributable to 1 kg of the corresponding by-products through mass and economic allocation (see Section 10.3.2.2, Table 10.7).

| [Chen et al. (2010b)] | | 1 kg pig iron | 1 kg BFS (mass allocation) | 1 kg BFS (economic allocation) |
|--------------------------|------------------|--------------------------------------|--------------------------------------|--------------------------------------|
| <u>Emissions to air:</u> | CO ₂ | 0.85 kg | 0.69 kg | 0.08 kg |
| | Dust | 3.20×10^{-5} kg | 2.59×10^{-5} kg | 0.31×10^{-5} kg |
| | SO _x | 1.33×10^{-4} kg | 1.08×10^{-4} kg | 0.13×10^{-4} kg |
| | NO _x | 7.98×10^{-5} kg | 6.45×10^{-5} kg | 0.76×10^{-5} kg |
| | Pb | 6.91×10^{-8} kg | 5.59×10^{-8} kg | 0.66×10^{-8} kg |
| | Ni | 1.60×10^{-8} kg | 1.29×10^{-8} kg | 0.15×10^{-8} kg |
| | Mn | 7.45×10^{-8} kg | 6.02×10^{-8} kg | 0.71×10^{-8} kg |
| | H ₂ S | 1.05×10^{-5} kg | 0.85×10^{-5} kg | 0.10×10^{-5} kg |
| | CO | 1.34×10^{-3} kg | 1.08×10^{-3} kg | 0.13×10^{-3} kg |
| | Dioxins | 2.66×10^{-15} kg | 2.15×10^{-15} kg | 0.25×10^{-15} kg |
| | Heat | 0.49 MJ | 0.40 MJ | 0.05 MJ |
| <u>Waste:</u> | Sludge | 2.50×10^{-2} kg | 2.02×10^{-2} kg | 0.24×10^{-2} kg |
| | Waste water | 1.81×10^{-3} m ³ | 1.46×10^{-3} m ³ | 0.17×10^{-3} m ³ |
| | Ashes | 1.28×10^{-2} kg | 1.03×10^{-2} kg | 0.12×10^{-2} kg |
| [Chen et al. (2010b)] | | 1 kWh electricity | 1 kg FA (mass allocation) | 1 kg FA (economic allocation) |
| <u>Emissions to air:</u> | CO ₂ | 0.95 kg | 2.27 kg | 0.18 kg |
| | Dust | 3.38×10^{-4} kg | 8.06×10^{-4} kg | 0.65×10^{-4} kg |
| | SO _x | 4.45×10^{-3} kg | 10.61×10^{-3} kg | 0.86×10^{-3} kg |
| | NO _x | 1.96×10^{-3} kg | 4.67×10^{-3} kg | 0.38×10^{-3} kg |
| | HCl | 1.26×10^{-4} kg | 3.00×10^{-4} kg | 0.24×10^{-4} kg |
| | Pb | 2.32×10^{-7} kg | 5.53×10^{-7} kg | 0.45×10^{-7} kg |
| | Ni | 1.07×10^{-7} kg | 2.55×10^{-7} kg | 0.21×10^{-7} kg |
| | Mn | 1.01×10^{-7} kg | 2.41×10^{-7} kg | 0.19×10^{-7} kg |
| | CH ₄ | 1.04×10^{-5} kg | 2.48×10^{-5} kg | 0.20×10^{-5} kg |
| | CO | 8.16×10^{-5} kg | 19.46×10^{-5} kg | 1.57×10^{-5} kg |
| | Dioxins | 7.14×10^{-14} kg | 17.03×10^{-14} kg | 1.37×10^{-14} kg |
| Heat | 5.62 MJ | 13.40 MJ | 1.08 MJ | |
| <u>Waste:</u> | Ashes | 2.88×10^{-3} kg | 6.87×10^{-3} kg | 0.55×10^{-3} kg |
| [Chen (2009)] | | 1 kg Si-metal | 1 kg SF (mass allocation) | 1 kg SF (economic allocation) |
| <u>Emissions to air:</u> | CO ₂ | 5.20 kg | 4.51 kg | 1.66 kg |
| | Dust | 7.81×10^{-3} kg | 6.77×10^{-3} kg | 2.50×10^{-3} kg |
| | SO _x | 1.23×10^{-2} kg | 1.07×10^{-2} kg | 0.39×10^{-2} kg |
| | NO _x | 9.82×10^{-3} kg | 8.51×10^{-3} kg | 3.14×10^{-3} kg |
| | Pb | 3.46×10^{-7} kg | 3.00×10^{-7} kg | 1.11×10^{-7} kg |
| | H ₂ S | 5.00×10^{-4} kg | 4.33×10^{-4} kg | 1.60×10^{-4} kg |
| | CO | 2.00×10^{-3} kg | 1.73×10^{-3} kg | 0.64×10^{-3} kg |
| <u>Waste:</u> | Ashes | 2.50×10^{-2} kg | 2.17×10^{-2} kg | 0.80×10^{-2} kg |

Again, they can be partially assigned to the corresponding by-products BFS, FA and SF while using a well-defined allocation principle (e.g. allocation by mass or economic value). More

details regarding the necessary allocation of impacts when dealing with an industrial by-product can be found in Section 10.3.2.2. The environmental implications that an allocation of impacts gives for BFS, FA and SF have been discussed there as well.

Once the by-products are collected during the primary industrial process, they still require some basic treatment before they can be applied as secondary cementitious material. For BFS, this treatment comprises granulating, drying and grinding of the produced slags before they can be stored. In case of FA, the basic treatment before storage consists of drying the ashes that have been captured from the flue gases. After being collected, SF can almost directly be stored. Evidently, the basic treatment operations (granulation, drying, grinding and storage) also have an environmental impact. Since these actions are not an essential part of the primary industrial process, their impacts need to be assigned fully to the industrial by-products BFS, FA and SF. Chen et al. (2010b) and Chen (2009) provided inventory data for this basic treatment. They have been summarized in Table 10.4. The allocated inventory data from Table 10.3 and the treatment data from Table 10.4 need to be summed to get the full inventory for BFS, FA and SF.

Table 10.4. Use of raw materials and energy, emissions to air and waste production inherent to the basic treatment of BFS, FA and SF.

| [Chen et al. (2010b), Chen (2009)] | | 1 kg BFS | 1 kg FA | 1 kg SF |
|------------------------------------|------------------|-----------------------------------|-----------------------------------|-----------------------------------|
| <u>Raw material:</u> | Water | $1.00 \times 10^{-2} \text{ m}^3$ | $3.50 \times 10^{-2} \text{ m}^3$ | – |
| <u>Energy:</u> | Electricity | $7.22 \times 10^{-3} \text{ kWh}$ | $6.82 \times 10^{-3} \text{ kWh}$ | $3.17 \times 10^{-3} \text{ kWh}$ |
| | Gas | $3.16 \times 10^{-1} \text{ MJ}$ | $2.90 \times 10^{-1} \text{ MJ}$ | – |
| | Diesel | $1.14 \times 10^{-6} \text{ m}^3$ | $1.03 \times 10^{-6} \text{ m}^3$ | – |
| <u>Transport:</u> | Train | $3.00 \times 10^{-3} \text{ tkm}$ | – | – |
| | Truck | $5.30 \times 10^{-3} \text{ tkm}$ | $3.00 \times 10^{-3} \text{ tkm}$ | – |
| <u>Emissions to air:</u> | Dust | $1.37 \times 10^{-4} \text{ kg}$ | $3.23 \times 10^{-5} \text{ kg}$ | $2.16 \times 10^{-5} \text{ kg}$ |
| | SO _x | $2.08 \times 10^{-4} \text{ kg}$ | $9.13 \times 10^{-8} \text{ kg}$ | – |
| | NO _x | $2.17 \times 10^{-5} \text{ kg}$ | $1.75 \times 10^{-5} \text{ kg}$ | – |
| | CH ₄ | $1.20 \times 10^{-6} \text{ kg}$ | – | – |
| | H ₂ S | $2.43 \times 10^{-4} \text{ kg}$ | – | – |
| | CO | $4.90 \times 10^{-5} \text{ kg}$ | $9.05 \times 10^{-6} \text{ kg}$ | – |
| <u>Waste:</u> | Sludge | $1.50 \times 10^{-3} \text{ kg}$ | $8.48 \times 10^{-5} \text{ kg}$ | $8.48 \times 10^{-5} \text{ kg}$ |
| | Waste water | $3.00 \times 10^{-3} \text{ m}^3$ | – | – |

Despite some limited emissions of metals to air (Pb, Ni and Mn) during the primary industrial processes, some toxic metals remain also present in the eventually obtained by-products. The presence of these metals in slags and fly ashes is not really seen as a problem. Mehta (2000) suggested that the concrete industry offers ideal conditions for the use of these by-products, since the metals can be immobilized and safely incorporated in the hydration products of cement. Leaching tests conforming to NEN 7345 (1995) showed that paving concretes made with CEM III/A 42.5 LA, only leach heavy metals at very low concentrations, significantly lower than the parametric values given in European Directive 98/83/EC (1998), which defines the quality of water intended for human consumption. Thus, the partial replacement of clinker with BFS, within the limits defined in NBN EN 197-1 (2011) for CEM III/A type cements (36% to 65% of slag), has no effect on the leaching behaviour of the concrete [Marion et al. (2005)]. Specific data on the leaching behaviour of FA and SF in concrete could not be found.

Another problem might be the potential Radon exhalation. Most building materials contain naturally occurring radioactive elements. Building inhabitants may be externally exposed to gamma rays originating from these radio-isotopes. As the presence of Radon is responsible for the largest fraction of the natural radiation dose to the population, the tracking of this Radon concentration is of great importance. The Radon in FA originates from the coal burned in the electrical power plants. Kovler et al. (2005) found that despite the higher ^{226}Ra content of FA (more than 3 times, compared to OPC), Radon emanation from cement-FA pastes is significantly lower (7.65% for cement versus 0.52% only for FA). However, note that little information is currently available on the emanation behaviour of FA in concrete during the use phase of the structure and after demolition.

10.2.1.3. Water

A low water-to-cement (W/C) ratio is advised especially in more demanding applications. To make sure that the water does not contain organic substances, chlorides or alkalies, drinkable water is usually applied in practice. Apart from in agriculture, the demands for freshwater in industry are causing groundwater resources to be depleted and surface waters to be abstracted in ways which compromise the freshwater ecosystem health [Smakhtin (2008)]. This impact can be assessed by calculating the water footprint of a product. This is typically the sum of all water consumed in the various stages of production and therefore the same as its virtual water content [Hoekstra et al. (2011)]. Lafarge uses approximately 343 litres of water to manufacture 1 ton of cement. In addition, about 284 liters of water are needed on average to produce 1 m³ of concrete [Lafarge (2011)]. According to Chen (2009) around 350 l water is consumed per cubic meter of concrete. Around one third of this amount corresponds with the mixing water needed to manufacture the concrete, while the other two third is the required amount of water to clean the concrete mixing trucks upon return from the construction site. Evidently, within this whole process a reduced use of ground water and surface water, the so-called blue water according to Ridoutt and Pfister (2010), would be beneficial.

Nowadays, concrete plants are already recycling the water that is used to clean the installations of the plant and the concrete mixing trucks. The water content of the concrete remaining in the mixing trucks upon return can also be recycled and reused as mixing water. Evidently, the quality of the water collected from the infrastructure for recycling (decantation reservoirs, filter installations,...) needs to be verified on a regular basis. A key parameter is the remaining content of fines in the recycled water. In practice, this content can be checked indirectly by monitoring its density. To qualify for recycling this density should be no more than 1.01 kg/l [Chen (2009)].

Apart from the benefits that can be achieved with the recycling of water, the practice of concrete mixture proportioning should simply aim at minimizing the portion of water in a concrete composition. Nevertheless, the increased use of superplasticizers to achieve this low water content without losing workability cannot be neglected.

10.2.1.4. Admixtures

The European Federation of Concrete Admixture Associations (EFCA), has published an eco-profile on superplasticizers [EFCA (2006)]. It is valid for the four main groups of

superplasticizers: sulphonated naphthalene formaldehyde, sulphonated melamine formaldehyde, vinyl copolymers and polycarboxylic ethers. All of them are dissolved in water and typically contain 30-45% active matter. Table 10.5 gives an overview of this eco-profile.

Table 10.5. Eco-profile for 1 kg of superplasticizer [EFCA (2006)].

| Raw materials input | Value | Unit | Emissions to water | Value | Unit |
|----------------------------|--------------|----------------|---------------------------|--------------|-------------|
| Coal, hard | 82 | g | Chemical oxygen demand | 2.6 | g |
| Coal, brown | 51 | g | PAHs | 67 | µg |
| Crude oil | 0.16 | kg | Oils, unspecified | 0.63 | g |
| Natural gas | 0.22 | m ³ | Barite | 51 | mg |
| Emissions to air | Value | Unit | Nickel (Ni) | 3.9 | mg |
| CO ₂ | 0.72 | kg | Emissions to soil | Value | Unit |
| CO | 0.55 | g | Chromium VI (Cr) | 0.22 | mg |
| NO _x | 1.8 | g | Oils, unspecified | 0.66 | g |
| SO _x | 3.6 | g | Solid waste | Value | Unit |
| N ₂ O | 67 | mg | Non-hazardous waste | 21 | g |
| Methane | 1.2 | g | Hazardous waste | 0.45 | g |
| Butane | 11 | mg | Total energy | Value | Unit |
| Pentane | 14 | mg | Total energy | 18.3 | MJ |
| Methanol | 60 | mg | | | |
| Ethene | 8.9 | mg | | | |
| Benzene | 7.4 | mg | | | |
| Non-methane VOC | 0.29 | g | | | |
| PAH | 39 | µg | | | |
| Acetic acid | 63 | mg | | | |
| Ammonia | 2.1 | g | | | |
| Arsenic (As) | 58 | µg | | | |
| Chromium VI (Cr) | 16 | µg | | | |
| Mercury (Hg) | 94 | µg | | | |
| Nickel (Ni) | 0.46 | mg | | | |
| Vanadium (V) | 1.2 | mg | | | |
| Dioxins | 43 | ng | | | |
| CFC-10 | 2.0 | µg | | | |
| CFC-114 | 1.8 | µg | | | |
| Halon-1211 | 4.1 | µg | | | |
| Halon-1301 | 5.0 | µg | | | |

It is worth noticing that the amount of CO₂ (720 g/kg) emitted for the production of 1 kg of superplasticizer is only a little bit lower than the CO₂ emissions associated with the production of cement (860 g/kg). Superplasticizer related NO_x emissions are also lower (1.8 g/kg versus 3.65 g/kg). On the other hand, the amount of SO_x emitted to manufacture the superplasticizer is significantly higher (3.6 g/kg versus 0.53 g/kg). However, as the amount of superplasticizer used in concrete is almost negligible when compared with its cement content, these emissions should not contribute significantly to the overall environmental impact.

10.2.1.5. Fine and coarse aggregates

A distinction must be made between naturally rounded alluvial aggregates and crushed aggregates. Rounded aggregates are the result of weathering and erosion and do not require any processing once collected from their valley or sea or river bed of origin. Crushed aggregates are exploited from quarries and require mechanical crushing. The required main equipment for the exploitation of these two aggregate types differs. While alluvial aggregates

basically need infrastructure for washing operations that remove all impurities from the collected material, crushed aggregates require a rock crusher to reduce the collected material to an appropriate size range [Chen (2009)]. A more detailed overview on the energy use of all the equipment needed to exploit aggregates from a quarry can be found in Martaud (2008).

Over the years, a lot of research has been done on the recycling of construction and demolition waste [Vyncke and Vrijders (2010)]. However, the use of recycled aggregates in structural concrete is still lacking confidence [Vrijders and Desmyter (2008)].

To date, few reliable data exist on the environmental impact of sand and aggregates consumption. Habert et al. (2010) stated that the indicators currently available to assess resource consumption in Life Cycle Impact Assessment (LCIA) are not fully adapted to the concrete industry. Since concrete and its constituents are not transported over long distances, the regional scale is a more relevant scale upon which resource extraction policies should be based. Since the price per ton aggregates transported doubles every 30 km, the reason for this is clear. The assessment approach of Habert et al. (2010) confirmed that depending on the size of the studied territory the depletion of bulk resources is different. At a world scale, depletion of bulk resources is negligible [Guinée (2002)], at a country scale, depletion is low and at a regional scale, depletion is clear.

Besides the regional availability and accessibility, the aggregate type is of importance. According to Steen (1999) the extra cost for crushing rock to a size as small gravel is about 2 Euro/ton. Emissions and energy consumption per metric ton of glacier rock produced by a Nordberg HP400 SX rock crusher [Landfield (2000)] are shown in Table 10.6.

Table 10.6. Emissions and Energy consumption to produce 1 metric ton of crushed glacier rock with the Nordberg HP400 SX rock crusher [Landfield (2000)].

| | | |
|------------------|------------------------------------|-----------------------------|
| Emissions | CO ₂ , fossil | 6.5×10^{-1} kg/ton |
| | NO _x as NO ₂ | 2.1×10^{-3} kg/ton |
| | SO _x as SO ₂ | 3.6×10^{-3} kg/ton |
| | Particulates (unspecified) | 3.8×10^{-3} kg/ton |
| Energy | Total primal energy | 9.8 MJ/ton |

Flower and Sanjayan (2007) found that for granite/hornfels and basalt aggregates, GHG emissions amount to 45.9 kg CO₂ equivalents/tonne and 35.7 kg CO₂ equivalents/tonne, respectively. These figures include the average contribution of transport from the quarry to the concrete batching plants. The amount of CO₂ released during the production and subsequent transport of concrete-sand was found to be 13.9 kg CO₂ equivalents/tonne. The production process included the strip-mining of raw sand by excavators, the subsequent loading into haulers, the washing into pumpable slurry, the piping to the grading plant and the filtering into standard grades. The lack of a crushing step explains the difference between the fine and coarse aggregate related emissions [Flower and Sanjayan (2007)].

Schuermans et al. (2005) conducted an LCA study for 21 finer sands exploited from land and marine sources in the Netherlands to be used in 1 m³ of concrete. They found that using finer sands has a lower environmental impact than the use of coarse sands from quarries in terms of land use, while other environmental effects (impacts on global warming, acidification, photochemical oxidant formation, energy use and waste production) did not change in an

important way. Unfortunately, this LCA study did not provide detailed inventory data (emission values,...) on the exploitation of the different sands.

10.2.2. Workability

The required workability of the fresh concrete highly depends on its specific application field. In road construction, where fast setting after casting is desirable, concrete with rather low consistency is needed, e.g. roller compacted concrete [Vahedifard et al. (2010)]. In case of complex formworks or a high density of steel reinforcements, a much higher consistency is necessary. The same goes when the implementation of the concrete on site involves pumping. When adequate mechanical compaction is not possible, it is advised to use self-compacting concrete (SCC). De Schutter et al. (2010) estimated that a pipe factory can save annually about 1 GWh of energy when the shift is made from traditional concrete to SCC. This substantial reduction in energy use is about 60% of the energy consumption for the production of concrete pipes.

10.2.3. Strength and mechanical loading

The dimensioning of reinforced concrete structures subjected to a given mechanical load is traditionally based upon the concrete's 28 day characteristic compressive strength and the characteristic tensile strength of the steel reinforcements [NBN EN 1992-1-1 (ANB 2010)]. When using a concrete with a high mechanical strength, this could decrease the amount of concrete needed to build a given structural element [Habert and Roussel (2009)]. Of course, the dimensions highly depend on the type of structural element. Habert and Roussel (2009) evaluated the impact of a higher strength for a horizontal element carrying only itself, a horizontal element carrying an external load and a vertical element carrying an external load. In all three cases, the total CO₂ production was found to be less when a stronger concrete was used. The vertical element turned out to be the most environment friendly structural element. According to Habert and Roussel (2009), a doubling of the strength of commonly used concretes, would result in 30% less CO₂ emissions. When a certain high strength concrete is also characterised by a high cement replacement level, an additional CO₂ reduction of about 15% could be obtained.

Increasing the compressive strength is seen as one of the key options to increase the efficiency of cement use [Damtoft et al. (2008)]. Therefore, Damineli et al. (2010) proposed the binder intensity index which measures the total amount of binder per m³ of concrete necessary to deliver 1 MPa of strength. This approach is very useful within the LCA framework, as it defines a unit of functional performance (cf. the functional unit FU, see also Section 10.3.1.1) instead of a unit of concrete volume or weight.

Note that a general shift towards high-strength concrete for every application will require a revision of NBN EN 206-1 (2000) where an indicative minimum strength class is given per concrete exposure class.

Revisions may also be necessary with respect to the age at which this minimum strength is specified. For instance, the relatively slow strength development of FA concrete is a disadvantage in applications where high early strength is required. However, in many situations, especially those involving mass concrete structures such as dams and heavy

foundations, which are not loaded to their design values until months if not years after their placement, it is quite common to specify 90-day strengths instead of the conventional 28-day strength [Meyer (2009)]. In contrast with NBN EN 206-1 (2000), the Canadian standard CSA A23.1-09/A23.2-09 (2009) already specifies a 56-day strength for some exposure classes.

10.2.4. Durability, environment and service life prediction

10.2.4.1. Environment specific durability based design approaches

Prescription based design, European school – When looking at the NBN EN 206-1 (2000), six main exposure classes can be identified (X0: No risk of corrosion or attack, XC: Corrosion induced by carbonation, XD: Corrosion induced by chlorides other than from seawater, XS: Corrosion induced by chlorides from seawater, XF: Freeze-thaw attack with or without de-icing agents, XA: Chemical attack).

Prescription based design, American school – Only four main exposure categories are defined in the American standard ACI 318-08 (2008) (F: Freezing and thawing, S: Sulfate, P: Requiring low permeability, C: Corrosion protection of reinforcement). In contrast with the European approach, the risk of carbonation-induced corrosion is not specifically covered in a separate exposure class.

Prescription based design, Considerations – Since concrete structures are easily catalogued in a different way depending on the applicable standard, it is of importance to look at the minimum concrete requirements per exposure class for the different standards. In Europe, limiting values are mentioned for the minimum cement content, the maximum W/C ratio and the minimum indicative compressive strength class. In North America, there are no requirements regarding the minimum cement content. The mix design of a concrete is only governed by a maximum W/B ratio and a minimum compressive strength.

Another important difference between the European and the North-American approach involves the performance attributed to mineral by-products. Within the European framework this performance is not considered as equivalent to Portland cement. The k-value concept strictly limits the amount of exposure classes in which concretes with a significant by-product content can be used. In the North-American standards, much less limitations are imposed on the FA and slag content.

Evidently, fixing the minimum cement content has its consequences when choosing an appropriate reference for evaluation of new concrete types. For less demanding applications this cement content may already be quite low. Applying a high cement replacement level with mineral by-products can result in a poor performance, especially at early age. To avoid this, an increase in total binder content (cement + by-product) may be necessary. As a consequence, the environmental benefit will not simply equal the percentage of by-products used. When only the maximum W/B ratio and the minimum strength are being limited, the choice of reference will be somewhat different. For a given maximum W/C ratio, the minimum strength required highly influences the cement content and thus the composition of the reference.

Performance based design – For a given deterioration process, this design approach describes the involved mechanisms using mathematical models and predicts the induced degradation

extent (as described in *fib* Bulletin 34 (2006), DuraCrete (2000), etc.). This degradation should remain acceptable within the predefined service life of the structure (see Section 10.2.4.2). Although seemingly more universal than the prescriptive design approach, some problems remain, e.g. the definition of the critical chloride concentration threshold level when evaluating concrete's resistance to chloride-induced corrosion. A wide range of values can be found in literature [Song et al. (2009)], but a reliable value is still not available.

Recommendations – Li et al. (2008) point out that both design methods are complementary and not opposite to one another. Therefore, a combined methodology may be advised when assessing the environmental impact of concrete in which the choice of reference is prescription based and the calculation of service life is performance based.

10.2.4.2. Service life prediction

For service life prediction, the DuraCrete (2000) methodology requires the definition of the desired structure performance, usually by setting a required target service life and by specifying the event which corresponds with the end of this service life. With respect to corrosion, four different events can be seen as the end of service life: depassivation of the reinforcement, cracking, spalling or collapse of the concrete structure.

The first event limits service life to the initiation period of the corrosion process. When corrosion is chloride induced, the initiation phase ends when the chloride concentration at the reinforcement reaches a critical threshold value. For carbonation-induced corrosion, the initiation period comes to an end when the carbonation front reaches the reinforcement. In both cases, the depassivation event does not represent structural failure. However, since from then on the actual corrosion process begins, the end of the initiation period is often equated with the end of service life. The propagation period for chloride-initiated corrosion is usually very short compared to the initiation period. As a consequence, it is sufficiently accurate to assume that the sum of the initiation period and the propagation period is simply equal to the initiation period [DuraCrete (2000)].

The other three events are all situated in the propagation period of the corrosion process. Val and Stewart (2003) see spalling as the most influential failure mode for the estimation of life cycle cost, because corrective actions such as repair or replacement usually are made to the structure almost immediately after spalling. When the aim of the study is a quantification of the environmental impact instead of the monetary cost, the same reasoning should be valid. Obviously, it is the additional concrete manufacturing for repair or replacement after concrete spalling that will result in a substantial extra environmental load.

Once the failure event is set, the applicable environmental actions and degradation mechanisms need to be identified. DuraCrete (2000) defines a limit state function for chloride and carbonation-induced corrosion.

A similar but updated design approach can be found in *fib* Bulletin 34 (2006). The required safety levels associated for the different limit states are usually expressed in terms of a reliability index β . Depending on the type of limit state – Service Limit State (SLS) or Ultimate Limit State (ULS) – and the consequences of failure, values for β are specified in Eurocode 0. For instance, depassivation will be classified as a SLS as there is no immediate

consequence on structural safety. β -values in the range of 1.0-1.5 may be appropriate for depassivation.

It should be noted that the currently available models to predict carbonation- and chloride-induced corrosion assume that the concrete is uncracked during the initiation period. In practice, this is often not the case. It is known that the presence of cracks accelerates the penetration of CO₂ and chlorides inside concrete [Song et al. (2009), Audenaert et al. (2009)] and therefore, shortens the initiation period. This observation suggests that an update of the existing models is needed to include the cracking aspect. Also, both the cracking resistance and the healing capacity of potentially ‘green’ concrete mix designs should be verified and improved if necessary.

Besides the design methods for carbonation- and chloride-induced corrosion, *fib* Bulletin 34 (2006) also provides a probabilistic design approach for frost induced internal damage and for salt-frost induced surface scaling. However, the models are less straightforward as the ones used for chloride- and carbonation-induced corrosion. For environments where chemical attack is at risk, the necessary models for adequate service life prediction are not yet available. With a notion of the concrete’s service life based on durability tests representative for its environment, it would be possible to expand the definition of the binder intensity proposed by Damineli et al. (2010) (see Section 10.2.3) as follows: the total amount of binder per m³ concrete necessary to deliver one 1 MPa of strength and 1 year of service life. This way, the unit of functional performance is obtained on two levels – strength and durability/service life – which is ideal for LCA of concrete.

10.3. Life cycle assessment of concrete

LCA is defined as ‘the compilation and evaluation of the inputs, outputs and potential environmental impacts of a product system throughout its life cycle [ISO 14040 (2006)]’. In other words, LCA is a tool for the analysis of the environmental burden of products at all stages in their life cycle. According to this definition, the impact of a product is studied from “the cradle to the grave”.

Within the construction industry, LCA studies can be performed at many different levels. First of all, there is the cradle-to-gate approach that only considers the impact of raw material extraction, the production of materials and product parts until the end product leaves the gate of the factory. However, a simple cradle-to-gate analysis cannot be used when evaluating the environmental benefit of potential ‘green’ concrete types. On this level, only the influencing parameters workability (Section 10.2.2) and strength (Section 10.2.3) can be considered, durability (Section 10.2.4) not. The demolition and waste phase are also not taken into account. Therefore, it may neglect the impacts of heavy metal leaching from industrial by-products contributing to human toxicity and ecotoxicity. The same is true for the processing steps taken to make the material recyclable or even reusable.

A cradle-to-grave approach on the other hand, can take the latter aspect into account, since the LCA looks at the material’s impact over its entire life cycle. However, in contrast with the well-known concrete production process, representative data related to the use phase and end-of-life phase for a specific concrete structure, are not always known.

To include all influencing parameters – workability, strength and durability – into the LCA without knowing all the details, a modified cradle-to-gate approach can be adopted. This methodology intends to quantify the environmental impact of the total amount of concrete that the manufacturer will need to produce and maintain a specific structure during its predefined service life.

As the aim for sustainability should stimulate profound recycling and reuse, the cradle-to-cradle concept [Braungart and McDonough (2002)] is gaining importance today. Products should be designed in such a way that at the end of the life cycle the materials can be recycled as raw material for production. Completely recyclable concrete is an example of this concept. Its mix design is adjusted in such a way that after demolition the concrete debris can simply be reused as raw materials for cement production [De Schepper et al. (2011)].

In view of the different above mentioned approaches for life cycle assessment (cradle-to-gate, modified cradle-to-gate, cradle-to-grave, cradle-to-cradle), the different scales for life cycle assessment of concrete considered by Chen (2009) are also worth mentioning.

- (i) Laboratory scale: An LCA study on this level only considers the environmental impacts associated with the production of the different concrete constituents. The transport of the constituents to the concrete plant and the operation of the plant are not taken into account. This seems the ideal scale for comparing the environmental impact of concrete compositions with a different proportioning of the constituents. However, this scale excludes by definition the so relevant strength and durability aspects.
- (ii) Industrial scale: At this stage the transport of the constituents as well as the operation of the plant are included in the LCA. Yet, the strength and durability aspects are still not part of the study
- (iii) Structure scale: This is the largest scale possible for LCA of concrete. It incorporates the production of the different constituents, their transport, the operation of the concrete plant, casting of the concrete on site, the use and maintenance of the structure during its life span and the end-of-life scenarios (demolition, recycling,...). The advantage of this scale is that the LCA study will account for environmental effects inherent to differences in strength and durability. However, since so many items are included in the LCA, specific effects that relate with the mixture proportioning (e.g. high cement replacement levels) might be partially masked by other effects. This can make it difficult to evaluate whether a concrete composition is 'green' in terms of composition. In that perspective, the laboratory scale most certainly still has its value.

Most ideally, a full environmental assessment of a concrete mixture should be based on an aggregated LCA that subsequently addresses all three of the above mentioned scales.

Either way, ISO 14040-14044 (2006) specify a four step LCA methodology for each approach: definition of goal and scope, inventory analysis, impact analysis and interpretation.

10.3.1. Definition of goal and scope

Obviously, the goal of LCA here is to accurately compare the overall environmental impact of traditional and 'green' concrete. Regarding the scope of the LCA, system boundaries must be described clearly using a flow diagram or process tree.

10.3.1.1. Functional unit choice

Of great importance is the definition of the functional unit (FU). This unit is seen as the reference unit of the product system for which the environmental impact will be calculated [ISO 14040 (2006), Desmyter and Martin (2001)]. Literature review shows that the scale of this FU for LCA can vary significantly from the material level (i) on to the structure level (ii):

- (i) When comparing the environmental impact of different concrete mix designs, a small scale FU on the material level can be appropriate. An efficiency indicator similar to the one proposed by Damineli et al. (2010) (see Section 10.2.3.) is seen as a first example, although it should not only be expressed in terms of a compressive strength unit, but also relate to a unit of service life (see Section 10.2.4.2.). Another possible functional unit choice is the amount of concrete needed in a simple structural element (column, beam, slab,...) with a given mechanical load and a predefined service life in a given environment. This way, additional concrete manufacturing due to replacement or repair over time, is included in the LCA. The same goes for differences in strength. The use of a high strength concrete implicates that structure dimensions and thus the overall concrete amount needed can often be reduced considerably. The resulting environmental benefit will be visible in the LCA output.
- (ii) When LCA is used to evaluate the environmental impact of a specific structure, the FU usually corresponds with the structure itself. For a LCA study on pavements, Sayagh et al. used a 1 km pavement with a lane width of 3.5 m as FU. The service life was set at 30 years with a traffic load of 9.4 million trucks per lane within this period [Sayagh et al. (2010)]. Both durability and mechanical load aspects are included in the study that way. Park et al. (2003) calculated environmental impacts for 1 km of a four lane highway with a predefined service life of 20 years and repair once every 7 years. However, construction activities and maintenance are not always included. For instance, Chowdhury et al. (2010) chose a road section with a thickness, width and length of 600 mm, 2.5 m and 1000 m, respectively, as FU. The focus of the study was simply on the material level with no specification of a service life.

Besides road structures, entire buildings can be the object of an environmental evaluation. Xing et al. (2008) studied the difference in impact between steel and concrete construction office buildings with a use life of 50 years. Both the construction and use phase were taken into account. One m² of building area was adopted as FU. For the assessment of wood and steel reinforced housing construction, Gerilla et al. (2007) expressed the FU in kilogram emission per year and per m². It was assumed that the detached houses had a 150 m² floor space and a design life of 35 years. The whole life cycle of the houses was considered. Specifying a 1 m² area is not always correct [López-Mesa et al. (2009)]. When comparing the construction related impact of in situ cast floors with precast floors, the smallest precast hollow core slabs on the market performed much better than a normally dimensioned in situ cast floor regarding structural strength. As a consequence, the spans achievable with precast concrete slabs are higher and this reduces the number of columns and spread footings. Therefore, the FU comprised the whole building, although the main goal of the study was only an evaluation of the floor type used.

In conclusion, regardless the scale of the FU for a LCA study comparing the environmental impact of traditional and 'green' concrete, the unit should be able to deal with strength and durability/service life differences between the two concrete types.

10.3.1.2. Other system boundaries

Note that even for a strength and durability related FU, it often remains difficult to decide what to and what not to include in the system. For instance, transport of materials can be incorporated in different ways. First of all, one can decide to attribute the impact of transport between systems to the system under investigation or not. In case of inclusion, the partial transport impact associated with the transported material or good has to be specified [Peuportier (2001)]. Since railway carriages, ships and aircraft normally return with other goods after delivery, the impacts of the return travel do not have to be considered. Trucks transport other goods only on a part of the return travel to limit empty tours. This observation suggests including the impact of half of the return travel in the LCA. Another issue is the status of capital goods. Certainly, production processes require the appropriate infrastructure of which the construction has a certain environmental impact. Peuportier (2001) states that the effects of making the infrastructure available for use are in general negligible. ISO 14044 (2006) provides several cut-off criteria to decide which inputs are to be included in the assessment, such as mass, energy and environmental significance.

10.3.1.3. Data quality

Finally, the necessary criteria regarding LCA data quality need to be set. The following data requirements should be addressed: time-related coverage, geographical coverage, technology coverage, precision, completeness, representativeness, consistency, reproducibility and (un)certainty of the information [ISO 14044 (2006)].

A distinction can be made between primary and secondary data [PréConsultants bv (2008)]. Primary data are required for the key constituents of a product (e.g. cement), meaning that they should be as accurate and representative as possible. Therefore, they should be obtained from the manufacturer directly. Note that the IPCC provides three methods to calculate the cement related CO₂ emissions depending on the information available: (i) the estimated clinker production data through use of cement production data, (ii) the available clinker production data or (iii) the original carbonate input data of the cement manufacturer [Hanle et al. (2006)]. Obviously, (iii) gives the most accurate results and is recommended when primary data are required. On the other hand, inventory data regarding transport can be treated as secondary data. It means that the more general data available in LCA databases, such as Ecoinvent [Frischknecht and Jungbluth (2007)] can be used for this.

10.3.2. Inventory analysis

10.3.2.1. Data collection

The necessary information can be obtained directly from the industries involved using detailed questionnaires or from publicly available annual environmental reports (ERs) and environmental product declarations (EPDs). Obviously, data from questionnaires will result in

a more reliable life cycle inventory (LCI) because ERs and EPDs will always hold a certain risk of misinterpretation and double counting. However, first hand data are not always provided by the companies because of confidentiality issues. As a consequence, the larger part of the LCIs is based on data from ERs, EPDs and LCA related journals. Therefore, it is understandable that ISO 14044 (2006) requires detailed documentation referencing for all public sources used. A sensitivity analysis is also very useful. For instance, Josa et al. (2004) made an extensive comparative analysis of the available life cycle inventories of cement in the EU to obtain a general trend in CO₂, NO_x, SO_x and dust emissions. LCA databases (e.g. Ecoinvent [Frischknecht and Jungbluth (2007)]) are seen as another important data source. As data availability and quality affect all four LCA phases, there is still a need for more peer-reviewed, standardized LCA inventory databases [Reap et al. (2008)].

10.3.2.2. Allocation

While collecting the inventory data, attention needs to be paid to allocation. Problems occur whenever a system produces more than one product. Somehow, the environmental impacts have to be divided over the different end products. Although this allocation of impacts is preferably avoided, it is often impossible. When this is the case, the inputs and outputs of the system should be partitioned between its different products or functions in a way that reflects the underlying relationships between them, e.g. allocation by mass or by economic value [ISO 14044 (2006)].

Allocation is of particular importance when industrial by-products like BFS, FA or SF are in play. Whenever these materials are used as a cement replacing material, attention needs to be paid to their allocated environmental impact. When no impact is attributed to them, they are considered as wastes of the primary industrial processes. The environmental load is at expense of its producer, i.e. the steel, electricity or Si-metal producer. However, BFS, FA and SF are no longer considered as merely waste, but as useful by-products. All three of them meet the necessary requirements imposed by the European Union directive 2008/98/EC (2008) to qualify for the by-product status: (i) further use of the substance is certain, (ii) the substance or object is produced as an integral part of a production process, (iii) the substance or object can be used directly without any further processing other than normal industrial practice, and (iv) further use is lawful. Moreover, sometimes the use of these by-products is even highly recommended to obtain a sufficient performance. For instance, the use of slag in concrete has been proven beneficial to increase the concrete's resistance to acid attack [Gruyaert et al. (2009)]. As a consequence, the question rises whether it would not be more appropriate to allocate a part of the environmental load to the concrete producer. Sayagh et al. (2010) studied two extreme allocation procedures for BFS. Firstly, the BFS is considered as a waste with no steel plant environmental loads allocated to it. Secondly, the BFS is seen as a by-product with 20% of the steel plant environmental flows allocated to the BFS. This percentage is in correspondence with the BFS/steel mass ratio. The environmental indicator results were found to be highly sensitive to the adopted allocation hypothesis. A 20% allocation by mass resulted in a contribution increase to the greenhouse effect of roughly 60%. Acidification and eutrophication potentials were found to be around 25% higher. Ecotoxicity potentials on the other hand almost doubled.

Chen et al. (2010b) and Chen (2009) evaluated the influence of three allocation procedures on the environmental impacts of BFS, FA and SF: no allocation, allocation by mass and allocation by economic value. The latter two approaches resulted in the calculation of a mass allocation coefficient C_m and an economic allocation coefficient C_e (Table 10.7) using Equations 10-1 and 10-2, respectively.

$$C_m = \frac{m_{\text{by-product}}}{m_{\text{main product}} + m_{\text{by-product}}} \quad (10-1)$$

$$C_e = \frac{(\text{€} \cdot m)_{\text{by-product}}}{(\text{€} \cdot m)_{\text{main product}} + (\text{€} \cdot m)_{\text{by-product}}} \quad (10-2)$$

Chen et al. (2010b) collected the required steel, BFS, electricity and FA data for these calculations from Althaus (2003), Sokka et al. (2005), Dones et al. (2007), Dahlström and Ekins (2006), Metal Bulletin (2011), Ecocem (2008), EDF (2008). The required Si-metal and SF data come from Chen (2009). The resulting allocation coefficients were used to determine the amount of raw material use, energy use, emissions and waste production attributable to the by-products BFS, FA and SF (Table 10.2 and 10.3).

Table 10.7. Allocation percentages by mass and economic value for FA, granulated BFS and SF as calculated by Chen et al. (2010b) and Chen (2009).

| Product | Mass produced | Market price | Mass allocation | Economic allocation |
|-------------|--------------------|--------------------------------|-----------------|-----------------------------|
| Steel | 1 kg | 400 €/t | 80.6% | 97.7% |
| BFS | 0.24 kg | 40 €/t | 19.4% | 2.3% |
| Electricity | 1 kWh ⁺ | 0.1 / 0.06 ⁺⁺ €/kWh | 87.6% | 99.0 / 97.1 ⁺⁺ % |
| FA | 0.052 kg | 20 / 35 ⁺⁺ €/t | 12.4% | 1.0 / 2.9 ⁺⁺ % |
| Si-metal | 1 kg | 1200 / 1729 ⁺⁺ €/t | 87.0% | 95.2 / 93.9 ⁺⁺ % |
| Silica fume | 0.15 kg | 400 / 750 ⁺⁺ €/t | 13.0% | 4.8 / 6.1 ⁺⁺ % |

⁺ Equivalent to 0.367 kg of hard coal used to produce electricity. The remaining produced FA and bottom ash.

⁺⁺ (based on) more recent main product and by-product prices from 2012-2014.

Each of these two allocation principles has its advantages and disadvantages. Mass allocation imposes enormous environmental impacts to the industrial by-products which may discourage the concrete industry to continue applying them as cement replacement [Chen et al. (2010b)]. When comparing the mass allocated emission values for BFS, FA and SF (Table 10.2-10.3) with the corresponding cement related emissions (Table 10.1), it is for instance clear that considerably more CO₂ (FA: 2.27 kg/kg; cement: ± 0.86 kg/kg), SO_x (FA: 10.61 g/kg; cement: ± 0.53 g/kg) and NO_x (FA: 4.67 g/kg; cement: 3.65 g/kg) are emitted for 1 kg of FA. In fact most of the mass allocated environmental impacts attributed to FA are high. This is mainly caused by the fact that very little FA (0.052 kg) is produced per kWh of electricity. As a consequence, the mass allocation coefficient of 12.4% needs to be applied to the impacts of about 19.2 kWh of electricity to obtain the impact of 1 kg of FA. Since a lot more BFS is produced per kg of steel (0.24 kg), the mass allocated impact of 1 kg BFS is much lower than the mass allocated impact of 1 kg FA. The same holds true for SF, with 0.15 kg of the

material produced per kg Si-metal. There is one exception though. Because high amounts of CO₂ emissions are inherent to the Si-metal production process, the CO₂ emissions assigned to silica fume through mass allocation remain huge (4.51 kg/kg).

When adopting the economic allocation principle, the impacts imposed onto 1 kg of BFS, FA and SF are much lower. Yet, for the latter by-product the CO₂ emissions remain higher than for cement production (SF: 1.66 kg/kg; cement 0.86 kg/kg). Economic allocation is sensitive to price instability which can make the LCA outcome fluctuate considerably. To see the effect of price fluctuations, the economic allocation coefficient was recalculated based on more recent prices for FA and SF, and their corresponding main products (sources: pers. comm with suppliers of FA and SF (2012), Metalprices.com (2013), Testaankoop (2014)). As can be seen from Table 10.7, the use of these more recent prices increases the economic allocation coefficients for both by-products (FA: 2.9%, SF: 6.1%). These were the values that were mainly used in this research for the LCA calculations of HVFA and FA+SF concrete.

When attributing an environmental load to BFS, FA or SF through mass allocation, the corresponding allocation coefficient will remain more or less constant over a long period of time [Chen et al. (2010b)].

10.3.3. Impact analysis

The main aim of the impact analysis is to connect each LCI result to the corresponding environmental impacts. Usually, this approach results into a classification of impact categories, each with a category indicator. Two main schools of methods can be distinguished [Jolliet et al. (2003)].

- (i) The first school comprises classical life cycle impact assessment (LCIA). Its category indicator is located right in between the LCI results and the category end points (where the environmental effect or damage occurs). The corresponding methods restrict quantitative modeling to relatively early stages in the cause-effect chain to limit uncertainties and group LCI results related to a certain environmental problem, into midpoint categories. Therefore, these methods (e.g. CML 2001) are considered to be problem oriented. For example, a material's impact on climate change can be expressed in kilograms CO₂ equivalents. Obviously, this is merely a quantification of an emission that contributes to the problem of climate change and not a quantification of the actual environmental damage.
- (ii) The second school focuses much more on the actual effect. So-called damage oriented impact methods (e.g. Eco-indicator 99) try to model the cause-effect chain up to the endpoint, or the actual environmental damage, sometimes with high uncertainties. With respect to climate change, the damage on human health is quantified in terms of disability adjusted life years (DALYs). This unit counts as a measure for the Years Lived Disabled (YLD) and the Years of Life Lost (YLL) due to this damage.

According to Benetto et al. (2004) the problem related approach provides reliable results, although it is sometimes difficult to compare them with each other. On the other hand, damage oriented impact analysis, allows for a much easier interpretation of the LCA output, but is considered to be not so reliable.

10.3.3.1. The IPCC approach

When the aim of the LCA study is a quantification of the concrete related GHG emissions only, it is justified to use the IPCC 2007 GWP impact method. According to this method, the corresponding Global Warming Potential (GWP) index is calculated for every emitted GHG. The index is based on the time-integrated global mean radiative forcing of a pulse emission of 1 kg of some compound relative to that of 1 kg of the reference gas CO₂ [Houghton et al. (1990)]. Logically, the GWP value for CO₂, the main GHG associated with cement production, equals 1 for the 3 commonly used time horizons, i.e. 20, 100 and 500 years [Forster and Ramaswamy (2007)]. The GWP index proposed by the IPCC is a problem oriented indicator because it merely quantifies GHG emissions (in kilograms CO₂ equivalents) and not the resulting climate change related damage (in DALYs) induced by them (see Section 10.3.3). The same indicator is used within the CML impact method for the impact category Climate change (see Section 10.3.3.3).

10.3.3.2. The Eco-indicator 99 approach

Eco-indicator 99 combines a series of scores representative for different environmental impacts into one single score through weighing by a panel of specialists [Goedkoop and Spriensma (2001)]. Naturally, the weighing part to obtain an aggregated indicator is the most critical and controversial step in the impact method. A panel was asked to weigh three types of environmental damages (Table 10.8), namely damages to human health (i), ecosystem quality (ii) and resources extraction (iii).

Table 10.8. Link between the LCI data and the damage categories of the Eco-indicator 99 methodology, cf. Goedkoop and Spriensma (2001).

| Life cycle inventory (LCI) | Effect | Damage category |
|---|--|--|
| Extraction of minerals and fossil fuels | Surplus energy for future extraction | Damage to mineral and fossil resources (MJ surplus energy) |
| Land use: occupation and transformation | Occurrence of vascular plant species (POO) | Damage to ecosystem quality (% vascular plant species · km ² · yr) |
| NO _x , SO _x , NH ₃ | Acidification/eutrophication (PDF) | |
| Pesticides, heavy metals | Ecotoxicity: toxic stress (PAF) | Damage to human health (DALY) |
| CO ₂ , Hydrochlorofluorocarbons (HCFC) | Climate change | |
| Hydrochlorofluorocarbons (HCFC) | Ozone layer depletion | |
| Nuclides | Ionizing radiation | |
| Suspended Particulate Matter (SPM), Volatile Organic compounds (VOC), NO _x , SO _x | Respiratory effects | |
| Polycyclic Aromatic Hydrocarbons (PAH) | Carcinogenics | |

- (i) The first damage type combines respiratory and carcinogenic effects, the effects on climate change, ozone layer depletion and ionizing radiation into one value expressed in DALY.
- (ii) The damage to ecosystem quality is expressed in terms of the percentage of species that have disappeared in a certain area due to the environmental load (% vascular plant

species · km² · yr). With respect to ecotoxicity, this definition covers the percentage of all species present in the environment living under toxic stress (PAF: Potentially Affected Fraction). Regarding acidification/eutrophication, the damage to a specific target species (vascular plants) in natural areas is modelled (PDF: Potentially Disappeared Fraction). Land use and land transformation on the other hand are based on empirical data regarding the occurrence of vascular plants as a function of the land use type and the area size (POO: Probability Of Occurrence).

- (iii) The damage category dealing with resource extraction gives a value expressed in MJ surplus energy to indicate the quality of the remaining mineral and fossil resources. Logically, further extraction of mineral resources will result in a decreased ore grade and increased energy requirements for future mining. For fossil resources, a shift towards exploitation of unconventional resources can also induce an increase in extraction energy. The mining of resources such as sand or gravel are adequately covered by the effects on land use, not by the damage category on extraction of resources.

10.3.3.3. The CML 2001 approach

The list of best available practice impact categories drawn up by the SETAC (Society of Environmental Toxicology and Chemistry) Working Group on LCIA served as a basic list for the problem oriented impact method CML 2001 [Guinée (2002)]. For LCA on concrete, we will mainly look at the baseline impact categories. For each category, a category indicator can be calculated based on the applicable characterization model and the characterization factors derived from the underlying model. The applicable characterization factors and indicator units per impact category are summarized in Table 10.9.

Table 10.9. Characterization factors and indicator units of the CML 2001 impact method, cf. Guinée (2002).

| Impact category | Characterization factor | Indicator unit |
|--------------------------------|--|---------------------------------------|
| Abiotic depletion | Abiotic depletion potential (ADP) | kg (Sb eq) |
| Climate change | Global warming potential (GWP) | kg (CO ₂ eq) |
| Ozone layer depletion | Ozone depletion potential (ODP) | kg (CFC-11 eq) |
| Human toxicity | Human toxicity potential (HTP) | kg (1,4-DB eq) |
| Freshwater aquatic ecotoxicity | Freshwater aquatic ecotoxicity potential (FAETP) | kg (1,4-DB eq) |
| Marine aquatic ecotoxicity | Marine aquatic ecotoxicity potential (MAETP) | kg (1,4-DB eq) |
| Terrestrial ecotoxicity | Terrestrial ecotoxicity potential (TETP) | kg (1,4-DB eq) |
| Photochemical oxidation | Photochemical ozone creation potential (POCP) | kg (C ₂ H ₄ eq) |
| Acidification | Acidification potential (AP) | kg (SO ₂ eq) |
| Eutrophication | Eutrophication potential (EP) | kg (PO ₄ eq) |

10.3.4. Interpretation

One of the key parts of the interpretation phase is the identification of the significant issues based on the results of the LCI and LCIA phases. The literature review conducted in this chapter allows not only for their identification starting from each phase, but also for revealing the link between the phases. Table 10.10 shows this link between the most important OPC, BFS, FA and SF related LCI results and the appropriate problem (cf. CML 2001 [Guinée (2002)]) or damage oriented (cf. Eco-indicator 99 [Goedkoop and Spriensma (2001)]) LCIA categories.

Table 10.10. Link between the most relevant LCI data of OPC, BFS, FA and SF, and the LCIA categories (CML 2001 and Eco-indicator 99) to which they are assigned.

| LCI | Problem oriented LCIA (CML 2002) | Damage oriented LCIA (Eco-indicator 99) |
|--|---|--|
| 1 kg CO ₂ | <u>Climate Change:</u> 1 kg CO ₂ eq | <u>Damage to human health:</u> 2.10×10^{-7} DALY |
| 1 kg SO _x (as SO ₂) | <u>Human toxicity:</u> 0.096 kg 1,4-DB eq <u>Acidification:</u> 1 kg SO ₂ eq | <u>Damage to human health:</u> 5.46×10^{-5} DALY <u>Damage to ecosystem quality:</u> 1.041 PDF·m ² ·yr |
| 1 kg NO _x (as NO ₂) | <u>Photochemical oxidation:</u> 0.028 kg C ₂ H ₄ eq <u>Acidification:</u> 0.70 kg SO ₂ eq <u>Eutrophication:</u> 0.13 kg PO ₄ eq | <u>Damage to human health:</u> 8.87×10^{-5} DALY <u>Damage to ecosystem quality:</u> 5.713 PDF·m ² ·yr |
| 1 kg PM ₁₀ | <u>Human toxicity:</u> 0.82 kg 1,4-DB eq | <u>Damage to human health:</u> 3.75×10^{-4} DALY |
| 1 MJ energy | <u>Abiotic depletion:</u> 4.57×10^{-4} kg Sb eq (coal) 5.34×10^{-4} kg Sb eq (gas) 4.90×10^{-4} kg Sb eq (oil) | <u>Damage to mineral and fossil resources:</u> 0.00859 MJ surplus energy (coal) 0.15000 MJ surplus energy (gas) 0.14400 MJ surplus energy (oil) |

Table 10.11 gives the problem oriented CML output associated with the LCI data for BFS, FA and SF cf. Chen et al. (2010b) and Chen (2009). The reported impacts apply for their status as supplementary cementitious materials. They do not account for other scenarios, such as the landfilling of BFS, FA and SF when not recycled as binder material in concrete. For each of these alternative binder materials, a schematic overview of the considered system boundaries is shown in Figure 10.1.

Compared to the CML output of 1 kg OPC, substantially higher values were recorded for BFS, FA and SF when applying mass allocation, and this for every studied impact category.

When applying an economic allocation of impacts for BFS, there are only important benefits in comparison with OPC in terms of GWP, ODP, TETP, AP and EP. Chen et al. (2010b) attribute the high impacts related to abiotic depletion, human toxicity, freshwater and marine ecotoxicity and photochemical oxidation to the fact that the extraction of raw materials in the iron industry is causing much more water pollution than cement production.

In case of FA, economic allocation assigns important environmental effects to abiotic depletion, human toxicity, marine aquatic ecotoxicity, photochemical oxidation and acidification. Chen et al. (2010b) attribute the substantial effect on acidification to the large quantities of NO₂ and SO₂ emissions which are inherent to coal fired electrical power plants. As a consequence, even a small impact allocation will still significantly affect the value of the corresponding category indicators. The effect on human toxicity, marine aquatic ecotoxicity is not explained by the authors. It is probably due to the abundant use of coal in the process. When fossil fuels are in play, the CML method assigns a lot of (eco)toxicity related impact to the disposal of the waste produced during coal mining and the emissions related to the combustion coal in the power plant.

Note that both the mass and economic allocated impacts of FA are clearly much higher than for BFS. As already stated in Section 10.3.2.2, this is mainly attributed to the fact that very

little FA (0.052 kg) is produced per kWh of electricity, while more BFS is produced per kg of steel (0.24 kg).

Table 10.11. Problem/damage oriented LCIA of 1 kg of OPC, BFS, FA and SF (cf. Chen et al. (2010b) and Chen (2009)).

| LC1 | Problem oriented LCIA (CML) | | | |
|----------------|--|-----------------------|-----------------------|---------------------|
| 1kg OPC | Abiotic depletion potential (kg Sb _{eq}) | 1.59×10^{-3} | | |
| | Global warming potential (kg CO _{2eq}) | 8.44×10^{-1} | | |
| | Ozone depletion potential (kg CFC-11 _{eq}) | 2.28×10^{-8} | | |
| | Human toxicity potential (kg 1,4-DB _{eq}) | 4.02×10^{-2} | | |
| | Freshwater aquatic ecotoxicity potential (kg 1,4-DB _{eq}) | 4.14×10^{-3} | | |
| | Marine aquatic ecotoxicity potential (kg 1,4-DB _{eq}) | 19.44 | | |
| | Terrestrial ecotoxicity potential (kg 1,4-DB _{eq}) | 1.17×10^{-3} | | |
| | Photochemical ozone creation potential (kg C ₂ H _{4eq}) | 4.26×10^{-5} | | |
| | Acidification potential (SO _{2eq}) | 1.15×10^{-3} | | |
| | Eutrophication potential (PO _{4eq}) | 1.73×10^{-4} | | |
| LC1 | Problem oriented LCIA (CML) | | Mass allocation | Economic allocation |
| 1kg BFS | Abiotic depletion potential (kg Sb _{eq}) | 1.21×10^{-2} | 1.41×10^{-3} | |
| | Global warming potential (kg CO _{2eq}) | 1.25 | 1.34×10^{-1} | |
| | Ozone depletion potential (kg CFC-11 _{eq}) | 2.45×10^{-8} | 6.05×10^{-9} | |
| | Human toxicity potential (kg 1,4-DB _{eq}) | 4.00×10^{-1} | 4.53×10^{-2} | |
| | Freshwater aquatic ecotoxicity potential (kg 1,4-DB _{eq}) | 2.01×10^{-1} | 2.08×10^{-2} | |
| | Marine aquatic ecotoxicity potential (kg 1,4-DB _{eq}) | 520.72 | 58.41 | |
| | Terrestrial ecotoxicity potential (kg 1,4-DB _{eq}) | 3.36×10^{-3} | 4.47×10^{-4} | |
| | Photochemical ozone creation potential (kg C ₂ H _{4eq}) | 8.40×10^{-4} | 1.15×10^{-4} | |
| | Acidification potential (SO _{2eq}) | 4.86×10^{-3} | 7.74×10^{-4} | |
| | Eutrophication potential (PO _{4eq}) | 6.77×10^{-4} | 7.37×10^{-5} | |
| 1kg FA | Abiotic depletion potential (kg Sb _{eq}) | 1.95×10^{-2} | 1.78×10^{-3} | |
| | Global warming potential (kg CO _{2eq}) | 2.50 | 2.10×10^{-1} | |
| | Ozone depletion potential (kg CFC-11 _{eq}) | 2.43×10^{-8} | 5.06×10^{-9} | |
| | Human toxicity potential (kg 1,4-DB _{eq}) | 5.00×10^{-1} | 4.24×10^{-2} | |
| | Freshwater aquatic ecotoxicity potential (kg 1,4-DB _{eq}) | 3.17×10^{-2} | 2.75×10^{-3} | |
| | Marine aquatic ecotoxicity potential (kg 1,4-DB _{eq}) | 2964.07 | 244.91 | |
| | Terrestrial ecotoxicity potential (kg 1,4-DB _{eq}) | 4.47×10^{-3} | 3.82×10^{-4} | |
| | Photochemical ozone creation potential (kg C ₂ H _{4eq}) | 6.59×10^{-4} | 5.59×10^{-5} | |
| | Acidification potential (SO _{2eq}) | 1.92×10^{-2} | 1.60×10^{-3} | |
| | Eutrophication potential (PO _{4eq}) | 1.05×10^{-3} | 9.10×10^{-5} | |
| 1 kg SF | Abiotic depletion potential (kg Sb _{eq}) | 3.43×10^{-2} | 1.32×10^{-2} | |
| | Global warming potential (kg CO _{2eq}) | 4.12 | 1.58 | |
| | Ozone depletion potential (kg CFC-11 _{eq}) | 2.59×10^{-7} | 9.95×10^{-8} | |
| | Human toxicity potential (kg 1,4-DB _{eq}) | 1.74 | 6.69×10^{-1} | |
| | Freshwater aquatic ecotoxicity potential (kg 1,4-DB _{eq}) | 5.69×10^{-2} | 2.19×10^{-2} | |
| | Marine aquatic ecotoxicity potential (kg 1,4-DB _{eq}) | 1.80×10^4 | 6.91×10^3 | |
| | Terrestrial ecotoxicity potential (kg 1,4-DB _{eq}) | 1.38×10^{-2} | 5.33×10^{-3} | |
| | Photochemical ozone creation potential (kg C ₂ H _{4eq}) | 2.26×10^{-3} | 8.68×10^{-4} | |
| | Acidification potential (SO _{2eq}) | 2.42×10^{-2} | 9.30×10^{-3} | |
| | Eutrophication potential (PO _{4eq}) | 1.87×10^{-3} | 7.21×10^{-4} | |

Silica fume has a higher impact than cement, BFS and FA for all category indicators, even when applying the less severe economic allocation principle. The consumption of large amounts of fossil fuels (Table 10.2) and the resulting emissions (Table 10.3) when producing Si-metals can again be held responsible for this. The calculated global warming potential clearly indicates that 1 kg of SF has a much higher environmental burden than 1 kg of OPC cement. Since silica fume is being applied in concrete in rather small amounts (usually 5-15%

of the total binder content), this may not be an issue. However, this finding proves that from an environmental viewpoint this industrial by-product can only be used on a limited basis. Thus, although the economic allocation coefficients for BFS, FA and SF are much smaller than their corresponding mass allocation coefficients, the environmental impacts assigned to them as such can still be substantial. Chen et al. (2010b) acknowledged this problem. According to them, the key solution lies in defining what would be an acceptable by-product/main product selling price ratio ensuring an acceptable environmental impact. The acceptable environmental impact should be regulated by the policymakers that still want to stimulate the further use of supplementary cementitious materials in the concrete industry. The maximum by-product/main product selling price ratios should be set accordingly. This is with no doubt an interesting allocation approach. Still, it remains a challenge how to determine what an acceptable environmental impact is.

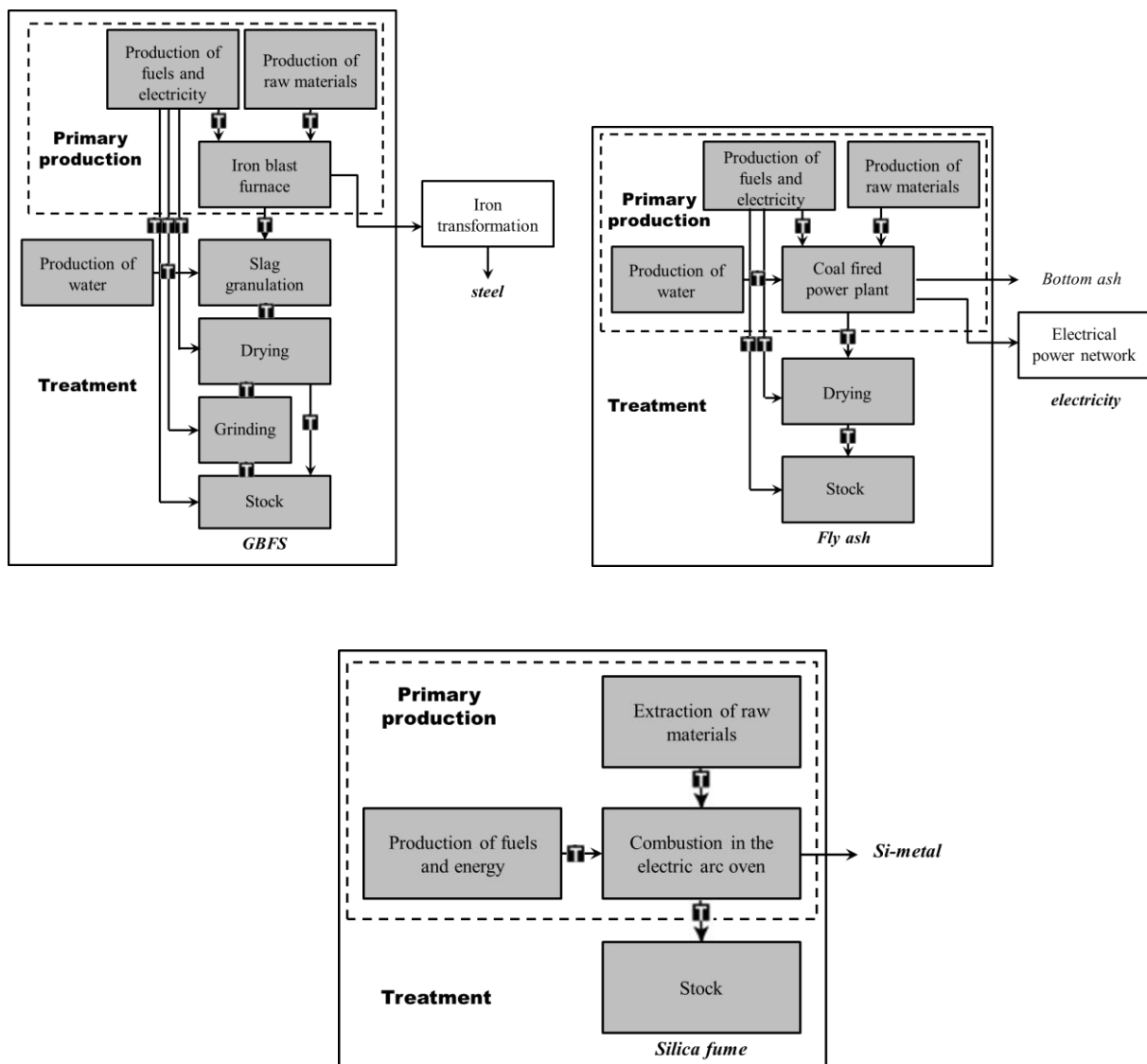


Figure 10.1. System boundaries considered by Chen et al. (2010b) and Chen (2009) for BFS, FA and SF.

It should be noted that the reported impact for OPC and the alternative binder materials in accordance with Chen et al. (2010b) and Chen (2009) is specifically valid for the French context. A search was conducted for a similar environmental assessment that represents the Belgian context.

The required information could to some extent be found for cement in an Environmental Product Declaration (EPD). This information is available for an Ordinary Portland cement CEM I 52.5 N, but also for two blended cements, i.e. a CEM II B/M 32.5 and a CEM III/A 42.5 N LA [Febelcem (2012)]. It must be emphasized that these EPDs were compiled in accordance with the Cembureau method. EPDs that fully meet the criteria of the more recent European standard NBN EN 15804 (2014) are still being developed for the moment.

A summarizing overview of the most relevant problem oriented category indicators mentioned in the EPDs of the three cement types can be found in Table 10.12. Figure 10.2 shows which processes have been included in the EPDs of the three cements. Note that the impacts on (eco)toxicity are not shown in the Cembureau conforming EPDs provided by Febelcem (2012) because there are no internationally recognised models for the assessment of the (eco)toxicity impact for the moment. As a consequence, an in-depth study of all CML 2001 baseline impact categories mentioned in Table 10.9 is not possible for the Belgian cements.

Table 10.12. Problem oriented impact categories reported in Cembureau conforming EPDs for three Belgian cements [Febelcem (2012)].

| | CEM I 52.5 N | CEM II B/M 32.5 | CEM III/A 42.5 N LA |
|-------------------------|---|---|---|
| Global warming | 9.09×10^{-1} kg CO ₂ eq | 7.14×10^{-1} kg CO ₂ eq | 4.74×10^{-1} kg CO ₂ eq |
| Acidification | 2.49×10^{-3} kg SO ₂ eq | 2.00×10^{-3} kg SO ₂ eq | 1.29×10^{-3} kg SO ₂ eq |
| Ozone depletion | 0.00 kg CFC-11 eq | 0.00 kg CFC-11 eq | 0.00 kg CFC-11 eq |
| Photochemical oxidation | 2.60×10^{-4} kg C ₂ H ₄ eq | 2.10×10^{-4} kg C ₂ H ₄ eq | 1.30×10^{-4} kg C ₂ H ₄ eq |
| Eutrophication | 4.90×10^{-4} kg PO ₄ eq | 4.20×10^{-4} kg PO ₄ eq | 3.20×10^{-4} kg PO ₄ eq |

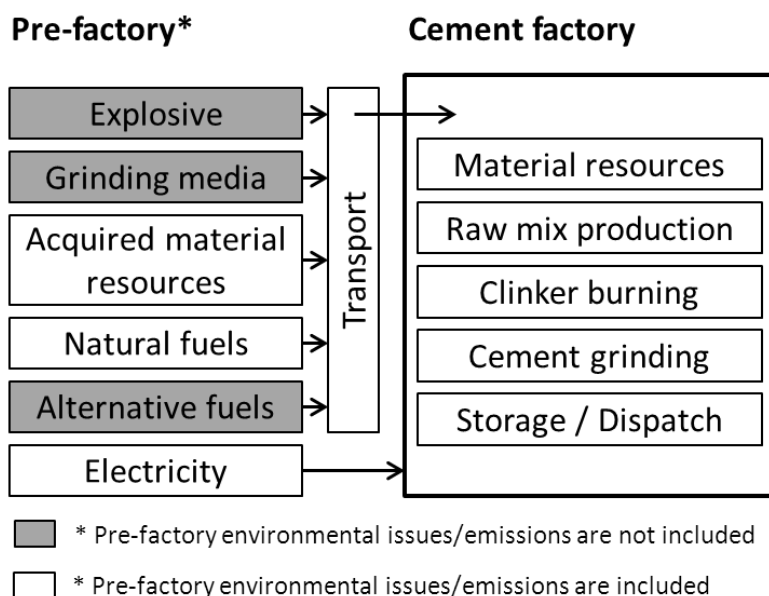


Figure 10.2. System boundaries of the Cembureau conforming EPDs for Belgian cements [Febelcem (2012)].

Of all three cement types, the pure Portland cement CEM I 52.5 N has the highest environmental burden in terms of the effect on global warming. This statement also holds true for acidification, photochemical oxidation and eutrophication. It indicates that only small impacts were assigned to the by-products present in the blended cements. The specific allocation principle applied for these materials remains uncertain as it was not indicated in the EPDs. In comparison with the Ordinary Portland cement mentioned by Chen et al. (2010b), the impacts of the Belgian CEM I 2.5 N are substantially higher. This aspect most certainly needs to be taken into consideration when evaluating the potential 'greenness' of a concrete composition with high cement replacement levels in Belgium. The allocated impacts of the alternative binders should also be verified for the Belgian context. Unfortunately, these data have not been made public yet. Therefore, the outcome of the LCA calculations performed for HVFA and FA+SF concrete in Chapter 12 has mainly been verified in perspective of the LCI and LCIA data reported by Chen et al. (2010b) and Chen (2009) for OPC, FA and SF.

For the aggregates and admixtures used in concrete published results of problem/damage oriented impact assessment or excerpts from EPDs could also have been reported here. Yet, they were not included for the following reasons. As mentioned in Section 10.2.1.5, the energy use and air emissions associated with crushed aggregates (which are more labour-intensive than natural aggregates) are quite low compared to the values recorded for cementitious materials (Tables 10.1, 10.2, 10.3). Since superplasticizers are usually used in small amounts, their contribution to the impact of a concrete mix is also considered to be very small (Section 10.2.1.4).

Note that the impact of the mixing water can not be calculated with either of the impact methods mentioned in this review. The term water footprint has evolved independently from the discipline of LCA and accordingly there is no clear relationship between a water footprint and potential environmental harm [Ridoutt and Pfister (2010)].

Finally, it should be noted that this chapter mainly focused on the environmental impact associated with the material concrete. It is known that the embodied energy of building materials is normally much less than the energy required to operate building facilities (energy for heating, air conditioning,...) during their service life [Goggins et al. (2010)]. In this sense, it would be interesting to include the thermal efficiency of the material within comparative LCA studies of traditional and 'green' concrete.

10.4. Conclusions

Within LCA, small variances in the definition of goal and scope (i), the inventory analysis (ii) and the impact analysis (iii) may induce important differences in the environmental score eventually obtained in the interpretation phase.

Within step (i), the definition of goal and scope, the functional unit (FU) choice is seen as one of the most influencing factors. Preferably, this unit includes all relevant concrete aspects, being its strength, its durability and to some extent its workability. To take into account both strength and durability, it should comprise the concrete amount needed to manufacture a structural element or even a whole building with a given mechanical load and a predefined service life. The concrete's life span should be evaluated in relation to the latter, using probabilistic service life prediction models based on experimental durability tests

representative for the application field. As LCA usually involves a comparison of impacts, the choice of the reference concrete, characterized by a minimum cement content and strength according to the applicable standards, is also extremely important. This is because the environmental benefit of a potential 'green' concrete is mainly due to its reduced cement content and strength governed structure dimensions in comparison with the reference. Besides material aspects, LCA system boundaries (cradle-to-gate, cradle-to-grave,...) play an important role. Since concrete durability is an important issue, at least the amount of concrete needed (including repairs and replacements) to maintain the structure during its predefined service life (modified cradle-to-gate) should be considered as system boundary.

Within step (ii), the inventory analysis, the inventory data used can obviously influence the LCA outcome. The preference goes to first hand data to ensure correctness and technological, geographical and time related representativeness of the LCA. Of importance is also the allocation approach used (none, by mass or by economic value) on the inventory results associated with by-products. Economic allocation is advised to guarantee an enduring use of BFS, FA and SF as cement replacing materials. Nevertheless, it still can impose important impacts to the by-products. Mass allocation results in environmental impacts of BFS, FA and SF that are about an order of a magnitude higher. As a consequence, their environmental burdens, especially when considering FA, become much higher than the burden of traditional cement.

Within step (iii), the impact analysis, the choice of the impact assessment method, which aggregates the relevant concrete related LCI results, should be carefully considered. The method used preferably covers more than only the impact on climate change and should be problem oriented.

Applied LCA methodology

11.1. Definition of goal and scope

11.1.1. Functional unit choice

The previous chapter revealed that a proper functional unit (FU) for LCA of a potentially ‘green’ concrete composition should account for the material’s strength and service life. In addition, it is not sufficient to consider only the environmental score for the particular concrete composition under investigation. Instead, a proper reference concrete should also be assessed in the same way. The forthcoming results are preferably interpreted in comparison with each other to evaluate the environmental benefit of the former in relation to the latter. In this perspective, several functional units were chosen for environmental impact quantification of the proposed HVFA and FA+SF concrete in environments with exposure to carbonation- or chloride-induced corrosion.

11.1.1.1. One m³ of concrete

Although clearly not suitable as functional unit for LCA purposes, the calculation for one m³ of concrete was done anyway to see what the environmental consequences can be of not taking into account the concrete’s strength and service life performance. By considering just 1 m³ of concrete as FU only the differences in total binder content and composition, as well as some other differences (sand, aggregate and water content as well as chemical admixture dosage) relative to the reference composition are accounted for.

11.1.1.2. Concrete amount per unit of strength and service life

By dividing 1 m³ of the studied concrete composition by its overall characteristic cubic strength defining its strength class and by its estimated service life, an environmental score can be calculated for the concrete amount needed to achieve 1 N/mm² of strength and 1 year of service life (= the corrosion initiation period or the sum of the corrosion initiation and propagation period). This way, the necessary strength and durability aspects are taken into account.

This definition is very similar to the concept of the binder intensity index proposed by Damineli et al. (2010) (Section (10.2.3)). There, the unit measures the total amount of binder per m^3 of concrete to deliver 1 N/mm^2 of strength. Only the durability aspect is missing. Also the impacts of all the other concrete constituents besides the binder materials are not considered in the functional unit of Damineli et al. (2010). Therefore, the earlier mentioned definition is seen as more appropriate.

The suggested strength and durability related approach is certainly straightforward and easy to use. However, it assumes that every benefit in terms of strength and durability can always be valorized. In practice, this is not always the case. Depending on the loading conditions and other functionalities, a higher mechanical strength does not always automatically result in smaller dimensions of a structural element. It also does not address the varying impacts of different repair intervals in the course of time. To cover these aspects a certain structural element with a predefined mechanical load and service life can be chosen as functional unit. Two such functional units have been defined in the following sections.

11.1.1.3. Concrete column with a given load and service life

The amount of concrete needed to construct and maintain an axially loaded column (height: 3.0 m, cross-section: rectangular) carrying a design load of 1500 kN for 100 years is an example of a functional unit that relates to a specific structural element. The experimental strength classes given in Tables 4.8, 4.9, 4.12 and 4.16 were used for the column design. Ribbed steel bars with a diameter of 12 mm and steel quality 500 were used as reinforcements. All calculations regarding concrete and steel reinforcement dimensioning were done in accordance with NBN EN 1992-1-1 (ANB 2010). In case service life is believed to be less than 100 years, additional concrete manufacturing necessary to repair the column is included as well. It was assumed that a full column repair consisted of a replacement of the entire 35 mm (d_{XC3}), 40 mm (d_{XC4}) or 50 mm (d_{XS2}) concrete cover. The proposed concrete covers are in agreement with the guidelines of NBN EN 1992-1-1 (ANB 2010) for a construction class upgrade to achieve a service life of 100 years.

11.1.1.4. Concrete slab with a given load and service life

A concrete slab (span: 5 m, width: 1 m) carrying a variable load of 5 kN/m^2 for 100 years can also be chosen as functional unit. Dimensioning of this structural element was again based on the experimental strength classes of the different concrete compositions mentioned in Tables 4.8, 4.9, 4.12 and 4.16. Ribbed steel bars with a diameter of 16 mm and steel quality 500 were used as reinforcements. All design calculations were done in accordance with NBN EN 1992-1-1 (ANB 2010). This functional unit was also considered since the mechanical loading conditions (i.e. bending mode) totally differed from the axial loading of a column (i.e. compression mode). Time dependent repair was assumed to consist of an entire replacement of the concrete cover on top of the rebars in the tensile zone of the slab.

Another reason for choosing a concrete slab relates to the fact that this type of structural element allows for a crack controlled design. As a result, it can be calculated how much extra reinforcing steel would be needed to obtain a slab where the concrete in the tensile zone would behave as uncracked cf. the drawing in Figure 6.1c. Only for a slab designed as such,

service life prediction based on tests performed on uncracked concrete samples would be valid. Thus, a quantification of the additional environmental impact attributed to the crack-controlling efforts would be very useful. These effects were assessed in particular for OPC reference T(0.45) and FA+SF concrete F(2)SF subject to chloride-induced corrosion. The characteristic crack width w_k (mm) of the slabs with different contents of reinforcing steel was verified in accordance with NBN EN 1992-1-1 (ANB 2010). Equation 11-1 shows the applicable formula.

$$w_k = \left(3.4 \cdot (d + 10) + 0.425 \cdot k_1 \cdot k_2 \cdot \frac{\Phi}{A_{c,eff}} \right) \cdot \left(\frac{\sigma_s}{E_s} - k_t \cdot \frac{f_{ct,eff}}{A_s \cdot E_s} \cdot \left(1 + \alpha \cdot \frac{A_s}{A_{c,eff}} \right) \right) \quad (11-1)$$

with d : concrete cover (mm), factor k_1 : coefficient accounting for the bond properties of the reinforcing steel (= 0.8 in case of high bond), factor k_2 : coefficient accounting for the strain distribution (= 0.5 in bending mode), Φ : diameter of the rebar, A_s : cross-sectional area of the steel (mm²), $A_{c,eff}$: effective cross-sectional area of the concrete in the tensile zone (mm²), σ_s : steel stress (N/mm²), E_s : design value for the steel's modulus of elasticity (N/mm²), k_t : factor accounting for the load duration (= 0.4 for a long-term mechanical load), $f_{ct,eff}$: concrete's effective tensile strength (N/mm²), α : effective ratio of the moduli of elasticity for the steel (E_s) and the concrete (E_{cm}).

11.1.2. System boundaries

In this study, a modified cradle-to-gate approach was mainly aimed for. Figure 11.1 gives a schematic overview of the general system boundaries for this approach.

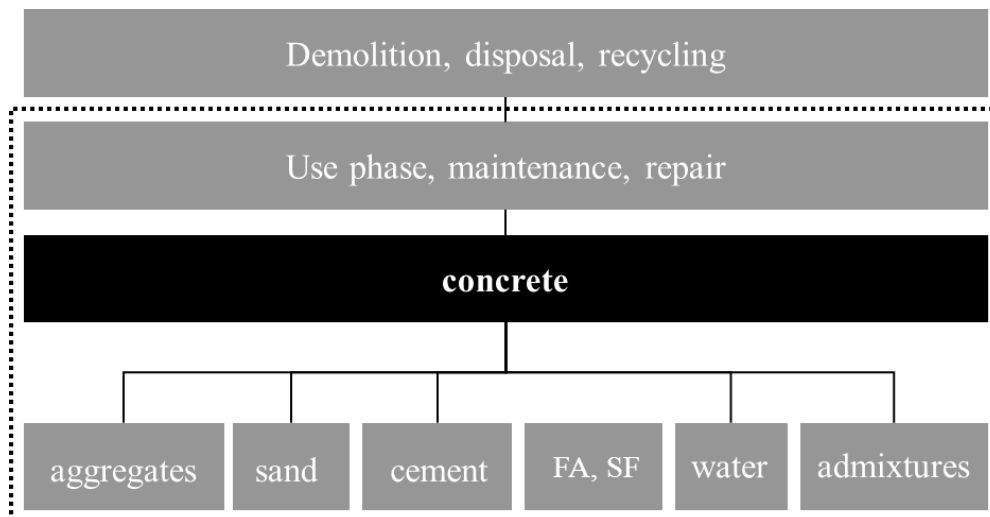


Figure 11.1. General system boundaries for a modified cradle-to-gate approach

Note that the focus is mainly on the material level. Since it comprises only the production of the constituents and not their transport and the operation of the concrete plant, this approach is

very comparable to the LCA study on laboratory scale suggested by Chen (2009). However, by considering the strength of the material and additional concrete manufacturing for replacement or repair, the modified cradle-to-gate approach adds an extra dimension to the LCA study on laboratory scale. In a way, the modified cradle-to-gate approach includes two items that would normally only be accounted for by Chen (2009) in an LCA study on structure scale. In perspective of evaluating new concrete compositions with a varying strength and durability performance, the modified cradle-to-gate approach seems to have its advantages. The laboratory scale of the study is maintained to a large extent which minimizes masking effects of other impacts (e.g. transport). On the other hand, the aspects of strength and durability which can alter the environmental score significantly are not neglected. Note that other functionalities of structures made with the concrete (e.g. the thermal performance, etc.) are excluded from the system boundaries of this LCA study.

Apart from the aggregated impact of all constituents per concrete composition, the impact of transporting all raw materials to the concrete plant and mixing them should also be included at least once. This would give a first indication on what to expect when the LCA study for HVFA and FA+SF concrete would shift to the industrial scale. Therefore, transport of each applied concrete constituent to a fictitious ready mixed concrete plant located at the Magnel Laboratory for Concrete Research was included in the system boundaries. The same goes for the operation of the mixing equipment to manufacture the concrete.

An overview of the transport distances for each constituent is given in Table 11.1. In contrast with Peuportier (2001) always the one-way distance of transport was incorporated in the system, regardless whether it was transport by ship or truck (see Section 10.3.1.2). This was done because we believe that the impact of transport should always be equally divided among the supplier and the consumer of the materials. The location of the Magnel Laboratory for Concrete Research may not be ideal to achieve minimal transport distances for the majority of the concrete constituents. Yet, finding the most ideal location for a concrete plant in terms of logistics is a complex study on its own which was not addressed any further here. Making the shift to the industrial scale in this study mainly aimed at getting a first impression on how the environmental score could be affected by it.

Table 11.1. Transport distances for the concrete constituents from the manufacturer to the fictitious concrete plant (Magnel Laboratory for Concrete Research in Ghent).

| Constituent | Transport means | One-way distance (km) |
|------------------|-----------------|-----------------------|
| CEM I 52.5 N | Truck | 112 |
| Fly ash F(1) | Truck | 34 |
| Fly ash F(2) | Truck | 196 |
| Silica fume | Freight ship | 954 |
| | Truck | 78 |
| Sand, aggregates | Barge | 193 |
| | Truck | 25 |
| Superplasticizer | Truck | 118 |

It is certain though that the transport distances for some constituents cannot easily be reduced in a significant way. For instance, since Belgian electricity production is depending less and less on coal fired electrical power plants. Fly ash will need to be imported from our

neighbouring countries on a more regular basis. As can be seen in Table 11.1, using fly ash F(2) instead of fly ash F(1) makes the one-way transport distance increase with more than four times. As a consequence, the transport related impacts of HVFA and FA+SF concrete are bound to increase in the future.

A similar problem arises for silica fume. This concrete constituent is not produced in Belgium. It needed to be imported from Norway. The majority of the transport distance may be covered by freight ship which normally has a lower environmental impact than transport by road. Nevertheless, the huge overall transport distance for SF cannot be neglected. Thus, an increased use of HVFA and FA+SF concrete in Belgium may not be so feasible after all, unless the benefits inherent to the use of the material can cancel out the negative effects that relate with transport. A comparative LCA study with and without the inclusion of the transport related environmental impacts will bring clarity on this issue.

11.2. Inventory analysis

For life cycle assessment of HVFA and FA+SF concrete in comparison with the applicable OPC and/or k-value conforming FA references, inventory data were mainly collected from the renowned Ecoinvent database [Frischknecht and Jungbluth (2007)]. True, most of the data in Ecoinvent are specifically applicable for Switzerland or represent a European average and may not be completely valid for Belgium. Therefore, the available Ecoinvent inventory data for each concrete constituent were carefully analysed to see whether the involved production processes deviated much from what is common practice in Belgium. Where possible, the necessary changes were made to make them more representative for the Belgian situation. When changes could not be made due to a lack of detailed quantitative data, it was highlighted in what way the Ecoinvent data should be adapted to fully represent the current practice in Belgium.

11.2.1. Inventory data for cement CEM I 52.5

Table 11.2 gives an overview of the Ecoinvent life cycle inventory data for the production of 1 kg of Portland cement CEM I 52.5 produced at a cement plant in Switzerland. It is immediately clear that practically all underlying data to this process are either unit (U) processes representative for Switzerland (CH) or Europe (RER). The actions that can be taken to make the process more representative for the Belgian situation are rather limited since the database contains few Belgian processes.

Table 11.2. Ecoinvent inventory data for the production of 1 kg Portland cement CEM I 52.5.

| Products | Amount | Unit |
|--|-----------------------|-------------|
| Portland cement, strength class Z 52.5, at plant/CH U | 1 | kg |
| Materials/fuels | Amount | Unit |
| Clinker, at plant/CH U | 0.912 | kg |
| Electricity, medium voltage, at grid/CH U ⁺ | 4.85×10^{-2} | kWh |
| Ethylene glycol, at plant/RER U | 3.5×10^{-4} | kg |
| Steel, low-alloyed, at plant/RER U | 6.0×10^{-5} | kg |
| Emissions to air | Amount | Unit |
| Heat, waste | 1.75×10^{-1} | MJ |

⁺ replaced by 'Electricity, medium voltage, at grid/BE U'

Table 11.3. Ecoinvent inventory data for the production of 0.912 kg Portland Clinker.

| Products | Amount | Unit |
|--|------------------------|----------------|
| Clinker, at plant/CH U | 0.912 | kg |
| Resources | Amount | Unit |
| Water, unspecified natural origin/m ³ | 1.48×10^{-3} | m ³ |
| Materials/fuels | Amount | Unit |
| Ammonia, liquid, at regional storehouse/CH U | 8.28×10^{-4} | kg |
| Lubricating oil, at plant/RER U | 4.30×10^{-5} | kg |
| Calcareous marl, at plant/CH U | 4.25×10^{-1} | kg |
| Clay, at mine/CH U | 3.02×10^{-1} | kg |
| Limestone, milled, loose, at plant/CH U | 7.67×10^{-1} | kg |
| Sand, at mine/CH U | 8.45×10^{-3} | kg |
| Lime, hydrated, loose, at plant/CH U | 3.58×10^{-3} | kg |
| Diesel, burned in building machine/GLO U | 1.22×10^{-2} | MJ |
| Electricity, medium voltage, at grid/CH U ⁺ | 5.29×10^{-2} | kWh |
| Hard coal, at regional storage/WEU U | 3.23×10^{-2} | kg |
| Bauxite, at mine/GLO U | 1.09×10^{-4} | kg |
| Natural gas, high pressure, at consumer/CH U ⁺⁺ | 6.21×10^{-3} | MJ |
| Heavy fuel oil, at regional storage/CH U | 2.33×10^{-2} | kg |
| Light fuel oil, at regional storage/CH U | 3.41×10^{-4} | kg |
| Petroleum coke, at refinery/RER U | 3.57×10^{-3} | kg |
| Tap water, at user/RER U | 3.10×10^{-1} | kg |
| Emissions to air | Amount | Unit |
| Ammonia | 2.08×10^{-5} | kg |
| Antimony | 1.82×10^{-9} | kg |
| Arsenic | 1.09×10^{-8} | kg |
| Beryllium | 2.74×10^{-9} | kg |
| Cadmium | 6.38×10^{-9} | kg |
| Carbon dioxide, biogenic | 1.38×10^{-2} | kg |
| Carbon dioxide, fossil | 7.65×10^{-1} | kg |
| Carbon monoxide, fossil | 4.30×10^{-4} | kg |
| Chromium | 1.32×10^{-9} | kg |
| Cobalt | 3.65×10^{-9} | kg |
| Copper | 1.28×10^{-8} | kg |
| Dioxin, 2,3,7,8 Tetrachlorodibenzo-p- | 8.76×10^{-13} | kg |
| Heat, waste | 3.30 | MJ |
| Hydrogen chloride | 5.75×10^{-6} | kg |
| Lead | 7.75×10^{-8} | kg |
| Mercury | 3.01×10^{-8} | kg |
| Methane, fossil | 8.10×10^{-6} | kg |
| Nickel | 4.56×10^{-9} | kg |
| Nitrogen oxides | 9.85×10^{-4} | kg |
| NMVOC, non-methane volatile organic compounds, unspecified origin | 5.14×10^{-5} | kg |
| Particulates, < 2.5 µm | 2.20×10^{-5} | kg |
| Particulates, > 10 µm | 5.16×10^{-6} | kg |
| Particulates, > 2.5 µm, and < 10µm | 7.22×10^{-6} | kg |
| Selenium | 1.82×10^{-9} | kg |
| Sulfur dioxide | 3.24×10^{-4} | kg |
| Thallium | 1.19×10^{-8} | kg |
| Tin | 8.21×10^{-9} | kg |
| Vanadium | 4.56×10^{-9} | kg |
| Zinc | 5.47×10^{-8} | kg |
| Chromium VI | 5.02×10^{-10} | kg |
| Waste to treatment | Amount | Unit |
| Disposal, inert waste, 5% water, to inert material landfill/CH U | 7.30×10^{-5} | kg |
| Disposal, municipal solid waste, 22.9% water, to municipal incineration/CH U | 4.10×10^{-5} | kg |

⁺ replaced by 'Electricity, medium voltage, at grid/BE U'

⁺⁺ replaced by 'Natural gas, high pressure, at consumer/BE U'

One important change can be made though. The Swiss electricity production mix can be replaced with the one for Belgium ('Electricity, medium voltage, at grid/BE U') in a copy of the original Ecoinvent unit process for cement production in the LCA software SimaPro 7.3.3. This modification was made. This increases the overall impact of cement production because Belgium depends much less than Switzerland on environmentally friendly hydro-electric power generation.

Table 11.2 actually contains rather few data on raw material use and emission values for cement production. This is because the majority of these data are included in one of the underlying processes, i.e. 'Clinker, at plant/CH U'. Table 11.3 shows the Ecoinvent inventory data for 0.912 kg of clinker necessary to produce 1 kg of CEM I 52.5 N.

Note that only the use of raw materials, the emissions to air and waste treatments are shown. Inventory data that relate to the infrastructure of the cement plant and transport of the raw materials were not included in order to keep the table comprehensive. Infrastructure and transport data were excluded from practically all tabulated inventories in this chapter. Yet, they were included in the LCA calculations. For the full inventory lists we refer to the Ecoinvent database [Frischknecht and Jungbluth (2007)]. Within the LCI for clinker production, the process 'Electricity, medium voltage, at grid/CH U' was again replaced by 'Electricity, medium voltage, at grid/BE U'. 'Natural gas, high pressure, at consumer/CH U' was replaced by 'Natural gas, high pressure, at consumer/BE U'.

To see whether the adapted inventory data shown in Tables 11.2 and 11.3 for 1 kg CEM I 52.5 result in environmental impacts similar to the ones reported in the EPD for the same cement type (Table 10.11) published by Febelcem (2012), the CML 2001 baseline impact category indicators were determined for 1 kg of cement from Ecoinvent. The global warming, acidification and eutrophication potentials shown in the EPD for an average Belgian Portland cement CEM I 52.5 N are considerably higher (Table 11.4). One should keep this in mind when performing a LCA based on inventory data from Ecoinvent.

Table 11.4. CML 2001 baseline impact indicators for 1 kg CEM I 52.5 N as reported in the EPD by Febelcem (2012) and as calculated from the adapted Ecoinvent inventory data.

| | CEM I 52.5 N (Febelcem) | CEM I 52.5 (Ecoinvent) |
|--|-------------------------|------------------------|
| Abiotic depletion potential (kg Sb _{eq}) | n.a. | 1.75×10^{-3} |
| Global warming potential (kg CO _{2eq}) | 9.09×10^{-1} | 8.53×10^{-1} |
| Ozone depletion potential (kg CFC-11 _{eq}) | 0.00 | 2.41×10^{-8} |
| Human toxicity potential (kg 1,4-DB _{eq}) | n.a. | 7.01×10^{-2} |
| Freshwater aquatic ecotoxicity potential (kg 1,4-DB _{eq}) | n.a. | 2.49×10^{-2} |
| Marine aquatic ecotoxicity potential (kg 1,4-DB _{eq}) | n.a. | 5.92×10^1 |
| Terrestrial ecotoxicity potential (kg 1,4-DB _{eq}) | n.a. | 1.24×10^{-3} |
| Photochemical ozone creation potential (kg C ₂ H _{4eq}) | 2.60×10^{-4} | 4.58×10^{-5} |
| Acidification potential (SO _{2eq}) | 2.49×10^{-3} | 1.24×10^{-3} |
| Eutrophication potential (PO _{4eq}) | 4.90×10^{-4} | 2.77×10^{-4} |

11.2.2. Inventory data for fly ash

The inventory data for coal fired electricity production used by Chen et al. (2010b) and Chen (2009) to calculate an allocated impact for its by-product fly ash were to a large extent based on the Ecoinvent process: 'Electricity, hard coal, at power plant/FR U'. In accordance with this approach, an allocated impact for Belgian fly ash was determined using the Ecoinvent

process for Belgian electricity production: ‘Electricity, hard coal, at power plant/BE U’. Table 11.5 and 11.6 give the inventory data for this process (excl. infrastructure and transport).

Table 11.5. Ecoinvent inventory data for the production of 1 kWh of coal fired electricity in Belgium: Resources, material/fuels, emissions to water and waste to treatment.

| Products | Amount | Unit |
|--|-----------------------|----------------|
| Electricity, hard coal, at power plant/BE U | 1 | kWh |
| Resources | Amount | Unit |
| Water, cooling, unspecified natural origin/m ³ | 3.50×10^{-2} | m ³ |
| Materials/fuels | Amount | Unit |
| Hard coal supply mix/BE U | 4.15×10^{-1} | kg |
| Chlorine, liquid, production mix, at plant/RER U | 1.00×10^{-4} | kg |
| Light fuel oil, at regional storage/RER U | 1.70×10^{-4} | kg |
| Water, completely softened, at plant/RER U | 6.00×10^{-2} | kg |
| Water, decarbonised, at plant/RER U | 1.50 | kg |
| SO _x retained, in hard coal flue gas desulphurisation/RER U | 8.18×10^{-4} | kg |
| NO _x retained, in SCR/GLO U | 1.34×10^{-4} | kg |
| Emissions to water | Amount | Unit |
| Heat, waste | 1.44 | MJ |
| Waste to treatment | Amount | Unit |
| Disposal, hard coal ash, 0% water, to residual material landfill/BE U | 3.22×10^{-3} | kg |
| Disposal, residue from cooling tower, 30% water, to sanitary landfill/CH U | 5.00×10^{-5} | kg |

A comparison was made between some relevant emission values reported by Ecoinvent and those published in the activity and sustainability report of Electrabel [Electrabel (2011)]. According to this report, the amount of CO₂, SO₂, NO_x and particulate matter emissions for Belgian power plants using fossil fuels (including biomass) amount to 6.49×10^{-1} kg/kWh, 7.60×10^{-5} kg/kWh, 3.02×10^{-4} kg/kWh and 5.00×10^{-5} kg/kWh. All these emission values are much lower, than the corresponding ones from Ecoinvent (Table 11.6: 9.48×10^{-1} kg/kWh, 3.47×10^{-3} kg/kWh, 1.57×10^{-3} kg/kWh and 2.92×10^{-4} kg/kWh). This can mainly be explained by the fact that the figures from Electrabel represent an average of all types of power plants that consume the traditional fossil fuels and biomass. As the classic coal fired power plants are becoming scarce in Belgium, their higher emission values are to some extent compensated by those of the other types of plants (steam and gas fired power plants,...). As a consequence, the values reported in the activity and sustainability report of Electrabel (2011) do not enable an easy comparison.

A little more information could be gathered on the coal fired electrical power plant that produced fly ash F(1). This power plant did not entirely depend on the combustion of hard coal. Around 8% of the hard coal was replaced by an unknown mixture of olive pits, wood pellets and gasified wood waste. Moreover, the plant was equipped with an advanced DeSO_x and DeNO_x installation which was far more efficient than indicated in the Ecoinvent inventory. Tables 11.5 and 11.6 indicate that only around 19% of the SO_x and 7.8% of the NO_x could be retained, while the plant producing fly ash F(1) had the potential of retaining no less than 95% of the SO_x and 85% of the NO_x [Electrabel (2009)]. This indicates the actual power plant was more environmentally friendly on various levels than what Ecoinvent shows. However, due to the fact that the above mentioned values are only rough indications and that no other emission data for the alternative fuels were available, a fully correct modification of the Ecoinvent inventory was not possible. Therefore, no modifications were made for now.

Table 11.6. Ecoinvent inventory data for the production of 1 kWh of coal fired electricity in Belgium: Emissions to air.

| Emissions to air | Amount | Unit |
|---|------------------------|------|
| Heat, waste | 5.46 | MJ |
| Antimony | 3.10×10^{-9} | kg |
| Arsenic | 2.82×10^{-8} | kg |
| Barium | 3.44×10^{-7} | kg |
| Benzene | 2.17×10^{-6} | kg |
| Benzo(a)pyrene | 2.00×10^{-12} | kg |
| Boron | 3.41×10^{-6} | kg |
| Bromine | 1.53×10^{-6} | kg |
| Butane | 1.90×10^{-7} | kg |
| Cadmium | 2.14×10^{-9} | kg |
| Carbon dioxide, fossil | 9.48×10^{-1} | kg |
| Carbon monoxide, fossil | 8.00×10^{-5} | kg |
| Chromium | 3.09×10^{-8} | kg |
| Chromium VI | 3.82×10^{-9} | kg |
| Cobalt | 1.51×10^{-8} | kg |
| Copper | 4.19×10^{-8} | kg |
| Dinitrogen monoxide | 1.24×10^{-5} | kg |
| Dioxin, 2,3,7,8 Tetrachlorodibenzo-p- | 7.00×10^{-14} | kg |
| Ethane | 4.10×10^{-7} | kg |
| Formaldehyde | 5.80×10^{-7} | kg |
| Hydrocarbons, aliphatic, alkanes, unspecified | 2.19×10^{-6} | kg |
| Hydrocarbons, aliphatic, unsaturated | 2.16×10^{-6} | kg |
| Hydrogen chloride | 9.19×10^{-5} | kg |
| Hydrogen fluoride | 3.96×10^{-5} | kg |
| Iodine | 7.55×10^{-7} | kg |
| Lead | 1.02×10^{-7} | kg |
| Lead-210 | 2.55×10^{-4} | kBq |
| Manganese | 9.12×10^{-8} | kg |
| Mercury | 4.88×10^{-8} | kg |
| Methane, fossil | 1.00×10^{-5} | kg |
| Molybdenum | 5.75×10^{-9} | kg |
| Nickel | 7.46×10^{-8} | kg |
| Nitrogen oxides | 1.57×10^{-3} | kg |
| PAH, polycyclic aromatic hydrocarbons | 1.00×10^{-8} | kg |
| Particulates, < 2.5 µm | 2.06×10^{-4} | kg |
| Particulates, > 10 µm | 6.21×10^{-5} | kg |
| Particulates, > 2.5 µm, and < 10µm | 2.42×10^{-5} | kg |
| Pentane | 1.47×10^{-6} | kg |
| Polonium-210 | 4.66×10^{-4} | kBq |
| Potassium-40 | 9.14×10^{-5} | kBq |
| Propane | 3.50×10^{-7} | kg |
| Propene | 1.60×10^{-7} | kg |
| Radium-226 | 6.58×10^{-5} | kBq |
| Radium-228 | 3.80×10^{-5} | kBq |
| Radon-220 | 2.85×10^{-3} | kBq |
| Radon-222 | 5.06×10^{-3} | kBq |
| Selenium | 6.47×10^{-8} | kg |
| Strontium | 4.01×10^{-7} | kg |
| Sulfur dioxide | 3.47×10^{-3} | kg |
| Thorium-228 | 2.05×10^{-5} | kBq |
| Thorium-232 | 3.22×10^{-5} | kBq |
| Toluene | 1.09×10^{-6} | kg |
| Uranium-238 | 5.48×10^{-5} | kBq |
| Vanadium | 6.33×10^{-8} | kg |
| Xylene | 9.22×10^{-6} | kg |
| Zinc | 2.08×10^{-7} | kg |

Assigning an allocated impact of coal fired electricity production to fly ash only covers impacts associated with the initial production of the by-product. Inventory data with respect to the required basic treatment afterwards need to be considered as well. Chen et al. (2010b) and Chen (2009) provided a basic dataset for drying and storage of fly ash (Table 10.4). This inventory was compiled from the treatment data published by Construction Technology Laboratories, Inc (2003). Based on these data from literature, a similar life cycle inventory for fly ash treatment was developed in Ecoinvent (Table 11.7).

Table 11.7. Ecoinvent inventory data for the treatment of 1 kg of fly ash.

| Products | Amount | Unit |
|--|-----------------------|----------------|
| Treatment of fly ash (drying + stock) | 1 | kg |
| Materials/fuels | Amount | Unit |
| Electricity, medium voltage, at grid/BE U | 6.82×10^{-3} | kWh |
| Natural gas, high pressure, at consumer/BE U | 2.90×10^{-1} | MJ |
| Diesel, at regional storage/RER U | 8.57×10^{-4} | kg |
| Emissions to air | Amount | Unit |
| Particulates | 3.23×10^{-5} | kg |
| Sulfur oxides | 9.13×10^{-8} | kg |
| Nitrogen oxides | 1.75×10^{-5} | kg |
| Carbon monoxide | 9.05×10^{-6} | kg |
| Waste to treatment | Amount | Unit |
| Treatment, sewage, to wastewater treatment, class 3/CH U | 8.48×10^{-5} | m ³ |

Given the inventory data for coal fired electricity production and fly ash treatment, the CML 2001 category impact indicators for 1 kg fly ash can be calculated. In accordance with Chen et al. (2010b) three allocation scenarios were considered:

- (i) No allocation: Only fly ash treatment is taken into consideration.
- (ii) Mass allocation: Fly ash treatment and an allocated impact by mass value of coal fired electricity production are accounted for.
- (iii) Economic allocation: Fly ash treatment and an allocated impact by economic value are taken into account. Both the economic allocation coefficients of Chen et al. (2010b) as well as the economic allocation coefficients based on more recently collected price data (Table 10.7) were used to see the effect of price fluctuations. Table 11.8 gives all calculated impacts for 1 kg in accordance with the CML 2001 impact method.

Table 11.8. CML 2001 baseline impact indicators for 1 kg of FA.

| CML 2001 impact category indicator | No | Economic^a | Economic^b | Mass |
|--|-----------------------|-----------------------------|-----------------------------|-----------------------|
| Abiotic depletion potential (kg Sb _{eq}) | 1.91×10^{-4} | 1.74×10^{-3} | 4.69×10^{-3} | 1.94×10^{-2} |
| Global warming potential (kg CO _{2eq}) | 3.85×10^{-3} | 2.11×10^{-1} | 6.06×10^{-1} | 2.58 |
| Ozone depletion potential (kg CFC-11 _{eq}) | 1.61×10^{-9} | 3.35×10^{-9} | 6.65×10^{-9} | 2.32×10^{-8} |
| Human toxicity potential (kg 1,4-DB _{eq}) | 2.84×10^{-3} | 7.08×10^{-2} | 2.00×10^{-1} | 8.45×10^{-1} |
| Freshwater aquatic ecotoxicity potential (kg 1,4-DB _{eq}) | 6.34×10^{-4} | 9.06×10^{-2} | 2.62×10^{-1} | 1.12 |
| Marine aquatic ecotoxicity potential (kg 1,4-DB _{eq}) | 3.33 | 2.04×10^2 | 5.86×10^2 | 2.49×10^3 |
| Terrestrial ecotoxicity potential (kg 1,4-DB _{eq}) | 1.58×10^{-5} | 3.94×10^{-4} | 1.11×10^{-3} | 4.71×10^{-3} |
| Photochemical ozone creation potential (kg C ₂ H _{4eq}) | 1.09×10^{-6} | 4.57×10^{-5} | 1.30×10^{-4} | 5.54×10^{-4} |
| Acidification potential (SO _{2eq}) | 2.42×10^{-5} | 1.34×10^{-3} | 3.83×10^{-3} | 1.63×10^{-2} |
| Eutrophication potential (PO _{4eq}) | 7.66×10^{-6} | 6.16×10^{-4} | 1.77×10^{-3} | 7.55×10^{-3} |

^a based on the prices of electricity and FA reported by Chen et al. (2010b), see Table 10.7.

^b based on more recent prices of electricity and FA, see Table 10.7.

When comparing the CML 2001 impact indicators obtained for 1 kg fly ash with those for 1 kg CEM I 52.5 (Table 11.4), it is clear that fly ash is not always beneficial from an environmental perspective. Only when just the impact of fly ash treatment is assigned to the material, all impact indicators for fly ash are lower than those for cement. When including part of the impact of coal fired electricity production to the fly ash by means of the economic allocation coefficient proposed by Chen et al. (2010b), only the global warming, ozone depletion and terrestrial ecotoxicity potentials of fly ash are lower. An economic allocation coefficient calculated from more recent prices for electricity and fly ash, increases the impacts of fly ash substantially. The material still only has a lower environmental burden on global warming, ozone layer depletion and terrestrial ecotoxicity. Mass allocation eliminates all potential environmental benefits from the material. In literature, there may be a preference for economic allocation as it would assign a fair impact to the by-product. However, the demonstrated important susceptibility to price fluctuations surely questions the preference for this allocation approach. Nevertheless, going for the no allocation approach is also no option, since fly ash has lost the status of waste material. The considerable environmental impacts assigned to fly ash as by-product also implicate that the benefit of using fly ash is not in the fact that it replaces an important portion of the cement. The most important benefit of using fly ash can only result from a substantial improvement of concrete properties such as durability.

When simply looking at 1 kg fly ash, then there would only be an environmental benefit in comparison with 1 kg cement for all ten CML 2001 baseline impact categories (also the very critical one relating to marine aquatic ecotoxicity) if the economic allocation coefficient could be reduced to around 0.2%. Therefore, the selling price of fly ash would need to be reduced to around 2.3 €/ton.

11.2.3. Inventory data for silica fume

Chen (2009) assigned an allocated impact of Metallurgical Grade silicon or MG-silicon production to silica fume. The inventory data for the primary industrial process more or less corresponded with the Ecoinvent process 'MG-silicon, at plant/NO U'. The same approach was adopted in this research. Since the silica fume used for the manufacturing of the FA+SF concrete compositions also came from Norway, no changes with respect to the applied electricity mix or fuels needed to be made. Table 11.9 gives the life cycle inventory for the production of 1 kg MG-silicon with exclusion of infrastructure and transport data.

An adequate comparison between the most relevant emissions for MG-silicon production according to Ecoinvent and the emissions from Elkem Microsilica, the producer of the applied silica fume, could not be made. The most recent sustainability report from Elkem gives emission values for CO₂, NO_x and SO₂ emissions for the year 2012. They amounted to 8.7×10^5 tonnes, 5.125×10^3 tonnes and 3.233×10^3 tonnes, respectively [Elkem (2012)]. Yet, these emission values are not linked with production values. Moreover, the reported emissions cover all activities of Elkem, not only the production of MG-silicon and silica fume.

Once obtained as by-product from MG-silicon production, the silica fume only requires some very basic treatment. Only the impacts that relate with storage of silica fume need to be considered. Therefore, Chen (2009) used tabulated data for storage in silos from Construction

technologies, Inc. (2003). Based on this information a similar life cycle inventory for silica fume treatment was created from Ecoinvent data (Table 11.10).

Table 11.9. Ecoinvent inventory data for the production of 1 kg of MG-silicon in Norway.

| Products | Amount | Unit |
|--|------------------------|----------------|
| MG-silicon, at plant/NO U | 1 | kg |
| Materials/fuels | Amount | Unit |
| Electricity, medium voltage, at grid/NO U | 1.10×10^1 | kWh |
| Wood chips, mixed, u=120%, at forest/RER U | 3.25×10^{-3} | m ³ |
| Hard coal coke, at plant/RER U | 2.31×10^1 | MJ |
| Graphite, at plant/RER U | 1.00×10^{-1} | kg |
| Charcoal, at plant/GLO U | 1.70×10^{-1} | kg |
| Petroleum coke, at refinery/RER U | 5.00×10^{-1} | kg |
| Silica sand, at plant/DE U | 2.70 | kg |
| Oxygen, liquid, at plant/RER U | 2.00×10^{-2} | kg |
| Emissions to air | Amount | Unit |
| Heat, waste | 7.13×10^1 | MJ |
| Arsenic | 9.42×10^{-9} | kg |
| Aluminium | 1.55×10^{-6} | kg |
| Antimony | 7.85×10^{-9} | kg |
| Boron | 2.79×10^{-7} | kg |
| Cadmium | 3.14×10^{-10} | kg |
| Calcium | 7.75×10^{-7} | kg |
| Carbon monoxide, biogenic | 6.20×10^{-4} | kg |
| Carbon monoxide, fossil | 1.38×10^{-3} | kg |
| Carbon dioxide, biogenic | 1.61 | kg |
| Carbon dioxide, fossil | 3.58 | kg |
| Chromium | 7.85×10^{-9} | kg |
| Chlorine | 7.85×10^{-8} | kg |
| Cyanide | 6.87×10^{-6} | kg |
| Fluorine | 3.88×10^{-8} | kg |
| Hydrogen sulfide | 5.00×10^{-4} | kg |
| Hydrogen fluoride | 5.00×10^{-4} | kg |
| Iron | 3.88×10^{-6} | kg |
| Lead | 3.44×10^{-7} | kg |
| Mercury | 7.85×10^{-9} | kg |
| NMVOC, non-methane volatile organic compounds, unspecified origin | 9.60×10^{-5} | kg |
| Nitrogen oxides | 9.74×10^{-3} | kg |
| Particulates, > 10 µm | 7.75×10^{-3} | kg |
| Potassium | 6.20×10^{-5} | kg |
| Silicon | 7.51×10^{-3} | kg |
| Sodium | 7.75×10^{-7} | kg |
| Sulfur dioxide | 1.22×10^{-2} | kg |
| Tin | 7.85×10^{-9} | kg |
| Waste to treatment | Amount | Unit |
| Disposal, slag from MG silicon production, 0% water, to inert material landfill/CH U | 2.50×10^{-2} | kg |

Table 11.10. Ecoinvent inventory data for the treatment of 1 kg silica fume.

| Products | Amount | Unit |
|--|-----------------------|----------------|
| Treatment of silica fume (storage) | 1 | kg |
| Materials/fuels | Amount | Unit |
| Electricity, medium voltage, at grid/NO U | 3.17×10^{-3} | kWh |
| Emissions to air | Amount | Unit |
| Particulates | 2.16×10^{-5} | kg |
| Waste to treatment | Amount | Unit |
| Treatment, sewage, to wastewater treatment, class 3/CH U | 8.48×10^{-5} | m ³ |

From the inventory data reported in Table 11.9 and 11.10, the CML 2001 impact indicators can be calculated for 1 kg of silica fume (Table 11.11). The same three allocation approaches as for the fly ash were tested, being no allocation, mass allocation and economic allocation. In case of economic allocation, the allocation coefficients were calculated from two different price sets for Si-metal and silica fume. The first one was in agreement with the prices reported by Chen (2009). The second one was based on more recent prices of the main product and the by-product. All applied allocation coefficients as well as their basis of calculation can be found in Table 10.7.

Table 11.11. CML 2001 baseline impact indicators for 1 kg of SF.

| CML 2001 impact category indicator | No | Economic ^a | Economic ^b | Mass |
|--|------------------------|-----------------------|-----------------------|-----------------------|
| Abiotic depletion potential (kg Sb _{eq}) | 8.82×10^{-7} | 1.24×10^{-2} | 1.58×10^{-2} | 3.37×10^{-2} |
| Global warming potential (kg CO _{2eq}) | 1.47×10^{-4} | 1.59 | 2.02 | 4.30 |
| Ozone depletion potential (kg CFC-11 _{eq}) | 1.13×10^{-11} | 1.02×10^{-7} | 1.29×10^{-7} | 2.76×10^{-7} |
| Human toxicity potential (kg 1,4-DB _{eq}) | 1.66×10^{-4} | 3.82×10^{-1} | 4.85×10^{-1} | 1.03 |
| Freshwater aquatic ecotoxicity potential (kg 1,4-DB _{eq}) | 5.86×10^{-5} | 2.52×10^{-1} | 3.20×10^{-1} | 6.83×10^{-1} |
| Marine aquatic ecotoxicity potential (kg 1,4-DB _{eq}) | 1.01×10^{-1} | 6.69×10^2 | 8.50×10^2 | 1.81×10^3 |
| Terrestrial ecotoxicity potential (kg 1,4-DB _{eq}) | 4.88×10^{-6} | 5.38×10^{-3} | 6.83×10^{-3} | 1.46×10^{-2} |
| Photochemical ozone creation potential (kg C ₂ H _{4eq}) | 2.63×10^{-8} | 8.32×10^{-4} | 1.06×10^{-3} | 2.25×10^{-3} |
| Acidification potential (SO _{2eq}) | 6.33×10^{-7} | 9.55×10^{-3} | 1.21×10^{-2} | 2.59×10^{-2} |
| Eutrophication potential (PO _{4eq}) | 1.25×10^{-6} | 1.98×10^{-3} | 2.52×10^{-3} | 5.36×10^{-3} |

^a based on the prices of Si metal and SF reported by Chen (2009), see Table 10.7.

^b based on more recent prices of Si metal and SF, see Table 10.7.

Silica fume only has a better environmental performance than cement when only the basic treatment of the material is included in its impact. From the moment an economically allocated impact from Si-metal production is taken into account, the benefits completely disappear for all impact indicators. For instance, the greenhouse gas emissions associated with silica fume production are around twice as high or even higher (1.59-2.02 kg/kg), in comparison with cement (0.85 kg/kg). Substantially higher impacts are also assigned to all the other impact indicators (human toxicity, ecotoxicity, acidification, eutrophication, etc.). Increases in impacts with more than a factor 10 are no exception. This is in strong contrast with fly ash. That by-product still showed a beneficial performance in comparison with cement for several impact categories. Logically, imposing a mass allocated impact to silica fume is even more disadvantageous in terms of its impact on the environment.

Sticking to the economic allocation principle would only turn out beneficial for each of the ten CML 2001 impact categories (incl. photochemical oxidation, the most critical one) if the economic allocation coefficient and the corresponding selling price of the silica fume could be reduced to around 0.2% and 23 €/ton, respectively.

11.2.4. Inventory data for mixing water

Ecoinvent provides an inventory process for tap water. The impacts related to it can be considered as a European average. Table 11.12 gives the corresponding life cycle inventory for 1 kg tap water with exclusion of the infrastructure (water supply network, pump station,...) and the transport involved. The underlying process for electricity production in Europe was replaced by the corresponding Belgian process (Electricity, medium voltage,

production BE, at grid/BE U). Table 11.13 shows the CML 2001 impact indicators for 1 kg of this tap water. In comparison with the binder materials of concrete, very low values were obtained for all impact categories.

Table 11.12. Ecoinvent inventory data for the production of 1 kg tap water.

| Products | Amount | Unit |
|---|-----------------------|----------------|
| Tap water, at user/ RER U | 1 | kg |
| Resources | Amount | Unit |
| Water, river | 5.13×10^{-4} | m ³ |
| Water, lake | 2.05×10^{-4} | m ³ |
| Water, well, in ground | 4.10×10^{-4} | m ³ |
| Materials/fuels | Amount | Unit |
| Electricity, medium voltage, production UCTE, at grid/UCTE U ⁺ | 3.90×10^{-4} | kWh |
| Chlorine, liquid, production mix, at plant/RER U | 1.00×10^{-7} | kg |
| Hydrogen peroxide, 50% in H ₂ O, at plant/RER U | 8.80×10^{-7} | kg |
| Ozone, liquid, at plant/RER U | 3.33×10^{-6} | kg |
| Charcoal, at plant/GLO U | 4.17×10^{-6} | kg |
| Aluminium sulphate, powder, at plant/RER U | 6.33×10^{-6} | kg |
| Emissions to air | Amount | Unit |
| Heat, waste | 1.40×10^{-3} | MJ |
| Emissions to water | Amount | Unit |
| Aluminium | 1.29×10^{-6} | kg |
| Chlorine | 1.00×10^{-7} | kg |
| Chloride | 5.04×10^{-6} | kg |
| Waste to treatment | Amount | Unit |
| Disposal, wood untreated, 20% water, to municipal incineration/CH U | 4.17×10^{-6} | kg |
| Treatment, sewage, unpolluted, to wastewater treatment, class 3/CH U | 1.77×10^{-5} | m ³ |

⁺ replaced by: 'Electricity, medium voltage, production BE, at grid/BE U'

Table 11.13. CML 2001 baseline impact indicators for 1 kg of tap water.

| CML 2001 impact category indicator | Tap water |
|--|------------------------|
| Abiotic depletion potential (kg Sb _{eq}) | 1.50×10^{-6} |
| Global warming potential (kg CO _{2eq}) | 2.41×10^{-4} |
| Ozone depletion potential (kg CFC-11 _{eq}) | 1.44×10^{-11} |
| Human toxicity potential (kg 1,4-DB _{eq}) | 1.37×10^{-4} |
| Freshwater aquatic ecotoxicity potential (kg 1,4-DB _{eq}) | 8.87×10^{-5} |
| Marine aquatic ecotoxicity potential (kg 1,4-DB _{eq}) | 1.56×10^{-1} |
| Terrestrial ecotoxicity potential (kg 1,4-DB _{eq}) | 1.55×10^{-6} |
| Photochemical ozone creation potential (kg C ₂ H _{4eq}) | 7.63×10^{-8} |
| Acidification potential (SO _{2eq}) | 9.52×10^{-7} |
| Eutrophication potential (PO _{4eq}) | 3.53×10^{-7} |

However, this does not mean that the consumption of potable water in concrete production is never a problem. As discussed in Chapter 10, water use is simply not properly covered by the commonly used impact methods for life cycle assessment. For instance, the abiotic depletion potential does not account for the exploitation of water. There is also no fully developed separate impact category for the moment that quantifies the water footprint of a product.

11.2.5. Inventory data for superplasticizers

Since there is no inventory process for superplasticizers present in the Ecoinvent database, a new process had to be created. The eco-profile published by the EFCA in 2006 (Table 10.5)

served as basis for the modelling of the life cycle inventory of this process. In fact, this document contains practically all required information (raw materials, emissions to air, etc.) and thus can be implemented directly as published in Ecoinvent. Chen (2009) followed the very same procedure. No information is available though on the impacts that relate with transport and infrastructure. These could not be taken into account in the LCA calculations.

Table 11.14 presents the CML baseline impact indicators for 1 kg of superplasticizer as modeled in Ecoinvent from the EFCA eco-profile. In comparison with the impact assessment results for cement CEM I 52.5, most impact indicators give higher values. Only the global warming potential, the freshwater aquatic ecotoxicity potential and the terrestrial ecotoxicity potential are somewhat lower. However, since superplasticizers are normally applied in concrete in rather small amounts, the overall higher environmental burden of this admixture is not necessarily problematic. Still, when studying concrete compositions with low water contents and thus higher SP dosages, their environmental impact should be kept in mind.

Table 11.14. CML 2001 baseline impact indicators for 1 kg of superplasticizer.

| CML 2001 impact category indicator | Superplasticizer |
|--|-----------------------|
| Abiotic depletion potential (kg Sb _{eq}) | 8.56×10^{-3} |
| Global warming potential (kg CO _{2eq}) | 7.68×10^{-1} |
| Ozone depletion potential (kg CFC-11 _{eq}) | 8.48×10^{-8} |
| Human toxicity potential (kg 1,4-DB _{eq}) | 2.59×10^{-1} |
| Freshwater aquatic ecotoxicity potential (kg 1,4-DB _{eq}) | 1.12×10^{-2} |
| Marine aquatic ecotoxicity potential (kg 1,4-DB _{eq}) | 4.15×10^1 |
| Terrestrial ecotoxicity potential (kg 1,4-DB _{eq}) | 5.04×10^{-3} |
| Photochemical ozone creation potential (kg C ₂ H _{4eq}) | 2.29×10^{-4} |
| Acidification potential (SO _{2eq}) | 8.58×10^{-3} |
| Eutrophication potential (PO _{4eq}) | 1.03×10^{-3} |

11.2.6. Inventory data for sand and aggregates

For both sand and round gravel there are life cycle inventories available in Ecoinvent. The data include the whole manufacturing process for the digging, the internal processes (transport, etc.) and the infrastructure for the operation (machinery) in Switzerland. The land-use of the mine (incl. unpaved roads) is included directly, while the land use of the paved roads and buildings are included in a separate underlying module 'Mine, gravel/sand/CH/I U' of the inventory processes for sand and gravel. Recultivation of closed mines is taken into account. No dust emissions are included because it is mostly a wet process. The same goes for wastewater. Since the process water is not polluted, the water does not require further treatment. Table 11.15 gives the full Ecoinvent life cycle inventory for both sand and gravel (including land use, transport and infrastructure). The data were summarized in only one table, because the database assigned identical inventories to both materials on every level.

This is because the two materials are exploited simultaneously from the location. Ecoinvent sees the mining of round gravel and sand as a multi-output process. It results in a production mix of around 65% of round gravel and 35% of sand. Now, neither of the end products can be identified as main product or by-product. Thus, an allocation of impacts may not be evident. However, some kind of differentiation should at least be made to account for the different processing operations necessary to obtain sands and aggregates of different particle size ranges for use in concrete. To achieve this goal, Chen (2009) modified the existing Ecoinvent

data for crushed aggregates and sand by assuming different uses of electricity and diesel fuel as well as a different intensity of transport on site for the different particle size ranges. The applied modifications were based on field data collected by Martaud (2008) for a series of French quarries. Still, the modified inventories compiled by Chen (2009) may not be applicable for the sands and aggregates that were used within the framework of this PhD research. Applied sands and aggregates were collected alongside the rivers in the Netherlands (geological formation Kreftenheye) and the Upper Rhine River at the border of the Netherlands and Germany. The exploitation of these materials does normally not require a crushing step, so the data of Martaud (2008) on use of electricity, diesel and transport as a function of the material's particle size range could not be used.

Table 11.15. Ecoinvent inventory data for the exploitation of 1 kg of sand or gravel.

| Products | Amount | Unit |
|--|------------------------|-------------|
| Sand, at mine/ CH U / Gravel, round at mine/CH U | 1 | kg |
| Resources | Amount | Unit |
| Gravel, in ground | 1.04 | kg |
| Occupation, mineral extraction site | 2.88×10^{-4} | m^2a |
| Occupation, water bodies, artificial | 6.27×10^{-5} | m^2a |
| Transformation, to mineral extraction site | 2.88×10^{-5} | m^2 |
| Transformation, to water bodies, artificial | 6.27×10^{-6} | m^2 |
| Water, unspecified natural origin/ m^3 | 1.38×10^{-3} | m^3 |
| Transformation, from unknown | 3.50×10^{-5} | m^2 |
| Materials/fuels | Amount | Unit |
| Building, hall, steel construction/CH/I U | 5.03×10^{-7} | m^2 |
| Conveyor belt, at plant/RER/I U | 9.51×10^{-8} | m |
| Diesel, burned in building machine/GLO U | 1.47×10^{-2} | MJ |
| Electricity, medium voltage, at grid/CH U ⁺ | 2.72×10^{-3} | kWh |
| Heat, light fuel oil, at boiler 10kW, non-modulating/CH U | 2.44×10^{-3} | MJ |
| Industrial machine, heavy, unspecified, at plant/RER/I U | 1.12×10^{-5} | kg |
| Lubricating oil, at plant/RER U | 1.85×10^{-6} | kg |
| Mine, gravel/sand/CH/I U | 4.75×10^{-11} | p |
| Recultivation, limestone mine/CH U | 8.48×10^{-6} | m^2 |
| Steel, low-alloyed, at plant/RER U | 1.30×10^{-5} | kg |
| Synthetic rubber, at plant/RER U | 2.00×10^{-6} | kg |
| Tap water, at user/RER U | 1.01×10^{-2} | kg |
| Transport, lorry 3.5-20t, fleet average/CH U | 8.79×10^{-7} | tkm |
| Transport, lorry 20-28t, fleet average/CH U | 1.72×10^{-5} | tkm |
| Transport, van <3.5t/CH U | 1.55×10^{-5} | tkm |
| Emissions to air | Amount | Unit |
| Heat, waste | 9.77×10^{-3} | MJ |
| Waste to treatment | Amount | Unit |
| Disposal, municipal solid waste, 22.9% water, to municipal incineration/CH U | 2.77×10^{-6} | kg |
| Disposal, used mineral oil, 10% water, to hazardous waste incineration/CH U | 1.85×10^{-6} | kg |

⁺ replaced by: 'Electricity, medium voltage, at grid/BE U'

Since no specific inventory data on the exploitation and sieving of river sands and aggregates could be found, it was decided to simply adopt the default life cycle inventory data from Ecoinvent with no differentiation between impacts for different particle size ranges. The data were only modified for Belgian electricity production. This approach is considered justified, because the focus in this research is on concrete with alternative binder compositions. In comparison with the binder materials in concrete, the environmental impact of sands and aggregates are normally much smaller. The CML impact indicators for 1 kg sand or gravel

from Ecoinvent give a first indication of the low environmental burden associated with the inert fraction of a concrete composition (Table 11.16).

Table 11.16. CML 2001 baseline impact indicators for 1 kg of sand or gravel.

| CML 2001 impact category indicator | Sand/Gravel |
|--|------------------------|
| Abiotic depletion potential (kg Sb _{eq}) | 2.02×10^{-5} |
| Global warming potential (kg CO _{2eq}) | 2.97×10^{-3} |
| Ozone depletion potential (kg CFC-11 _{eq}) | 2.92×10^{-10} |
| Human toxicity potential (kg 1,4-DB _{eq}) | 2.48×10^{-3} |
| Freshwater aquatic ecotoxicity potential (kg 1,4-DB _{eq}) | 6.75×10^{-4} |
| Marine aquatic ecotoxicity potential (kg 1,4-DB _{eq}) | 1.27 |
| Terrestrial ecotoxicity potential (kg 1,4-DB _{eq}) | 1.20×10^{-5} |
| Photochemical ozone creation potential (kg C ₂ H _{4eq}) | 5.97×10^{-7} |
| Acidification potential (SO _{2eq}) | 1.65×10^{-5} |
| Eutrophication potential (PO _{4eq}) | 4.82×10^{-6} |

Unlike for the applied cement, there is no environmental product declaration available for the applied sands and aggregates. On the other hand, the supplier did calculate a carbon footprint for the sand with the Bilan Carbone software application of ADEME (Agence de l'Environnement et de la Maîtrise de l'Énergie). The exploitation and processing of the sand to the appropriate particle size range have a total carbon footprint of 7.80×10^{-3} kg CO_{2 eq} per kg of sand. Since the applied aggregates are actually the sieving residue of this sand which requires no further extensive processing, the same carbon footprint can be assumed for the aggregates. Based on this information from the supplier, it is justified to use an identical life cycle inventory for both the sand and aggregates. One should keep in mind though that our materials had a carbon footprint that was more than twice the Ecoinvent value for Swiss sand and gravel. Nevertheless, in comparison with cement this impact is still rather negligible.

11.2.7. Inventory data for transport

As indicated in Table 11.1, three means of transport were used for bringing the concrete constituents from their producer to the fictitious concrete plant at the Magnel Laboratory for Concrete Research: by freight ship, by barge and by truck. The following Ecoinvent inventory processes were used to model the transport from the supplier to the concrete plant.

- Freight ship: 'Transport, transoceanic freight ship/OCE U'
- Barge: 'Transport, Barge/RER U'
- Truck: 'Transport, lorry 20-28t, fleet average/CH U'

The appropriate unit for quantifying transport in a life cycle inventory is traditionally load multiplied by distance. Table 11.17 gives the CML baseline indicators for 1 tkm of each means of transport. As quite commonly known, transport over water has the lowest environmental burden. For a fixed consumption of fossil fuels and loading capacity, the action radius of a ship exceeds the action radius of a truck by far. As a consequence, the CO₂ emissions associated with the former are much lower than with the latter. The same goes for other emissions (SO_x, NO_x, dust, etc.). Unfortunately, not all concrete constituents are being transported over water today. In fact, this is perhaps only the case for sands and aggregates. In most cases, the binder materials are still being delivered to the concrete plant by trucks.

Table 11.17. CML 2001 baseline impact indicators for 1 tkm of transport by freight ship, barge and truck.

| CML 2001 impact category indicator | Freight ship | Barge | Truck |
|--|-----------------------|-----------------------|-----------------------|
| Abiotic depletion potential (kg Sb _{eq}) | 7.14×10^{-5} | 2.82×10^{-4} | 1.40×10^{-3} |
| Global warming potential (kg CO _{2eq}) | 1.07×10^{-2} | 4.63×10^{-2} | 1.94×10^{-1} |
| Ozone depletion potential (kg CFC-11 _{eq}) | 1.21×10^{-9} | 4.83×10^{-9} | 3.14×10^{-8} |
| Human toxicity potential (kg 1,4-DB _{eq}) | 7.36×10^{-3} | 9.12×10^{-3} | 4.40×10^{-2} |
| Freshwater aquatic ecotoxicity potential (kg 1,4-DB _{eq}) | 1.20×10^{-3} | 4.36×10^{-3} | 1.59×10^{-2} |
| Marine aquatic ecotoxicity potential (kg 1,4-DB _{eq}) | 3.09 | 1.02×10^1 | 3.45×10^1 |
| Terrestrial ecotoxicity potential (kg 1,4-DB _{eq}) | 2.51×10^{-5} | 8.95×10^{-5} | 3.85×10^{-4} |
| Photochemical ozone creation potential (kg C ₂ H _{4eq}) | 7.50×10^{-6} | 6.51×10^{-6} | 3.72×10^{-5} |
| Acidification potential (SO _{2eq}) | 2.36×10^{-4} | 3.37×10^{-4} | 1.07×10^{-3} |
| Eutrophication potential (PO _{4eq}) | 2.57×10^{-5} | 8.82×10^{-5} | 2.77×10^{-4} |

10.2.8. Inventory data for concrete manufacturing at a concrete plant

When the shift is made from the laboratory scale to the industrial scale, life cycle assessment of concrete not only requires inventory data on the concrete constituents and their transport, but also on the operation of the concrete plant where the constituents will be used to produce the alternative concrete compositions under investigation. Therefore, an existing Ecoinvent inventory process that covers concrete manufacturing at a typical Swiss concrete plant was modified to simulate the operation of a concrete plant that produces the studied OPC, k-value conforming FA, HVFA and FA+SF concrete compositions. Table 11.18 shows this process ('Concrete, normal, at plant/CH U') in its original form.

Table 11.18. Ecoinvent inventory data for production of 1 m³ of normal concrete at the plant.

| Products | Amount | Unit |
|--|-----------------------|----------------|
| Concrete, normal at plant/CH U | 1 | kg |
| Materials/fuels | Amount | Unit |
| Concrete mixing plant/CH/I U | 4.57×10^{-7} | p |
| Diesel, burned in building machine/GLO U | 22.7 | MJ |
| Electricity, medium voltage, at grid/CH U ⁺ | 4.36 | kWh |
| Gravel, round, at mine/CH U ⁺⁺ | 1890 | kg |
| Heavy fuel oil, burned in industrial furnace 1MW, non-modulating/CH U | 3.09 | MJ |
| Light fuel oil, burned in industrial furnace 1MW, non-modulating/CH U | 13.3 | MJ |
| Lubricating oil, at plant/RER U | 1.19×10^{-2} | kg |
| Natural gas, burned in industrial furnace low-NOx >100kW/RER U | 1.16 | MJ |
| Portland cement, strength class Z 42.5, at plant/CH U ⁺⁺ | 300 | kg |
| Steel, low-alloyed, at plant/RER U | 2.38×10^{-2} | kg |
| Synthetic rubber, at plant/RER U | 7.13×10^{-3} | kg |
| Tap water, at user/CH U ⁺⁺ | 186 | kg |
| Transport, barge/RER U ⁺⁺⁺ | 49.2 | tkm |
| Transport, freight, rail/CH U ⁺⁺⁺ | 6.82 | tkm |
| Transport, lorry 3.5-20t, fleet average/CH U | 0.998 | tkm |
| Transport, lorry 20-28t, fleet average/CH U ⁺⁺⁺ | 9.44 | tkm |
| Emissions to air | Amount | Unit |
| Heat, waste | 15.7 | MJ |
| Waste to treatment | Amount | Unit |
| Disposal, concrete, 5% water, to inert material landfill/CH U | 16.9 | kg |
| Disposal, municipal solid waste, 22.9% water, to municipal incineration/CH U | 9.51×10^{-2} | kg |
| Treatment, concrete production effluent, to wastewater treatment, class 3/CH U | 1.43×10^{-2} | m ³ |

⁺ replaced by: 'Electricity, medium voltage, at grid/BE U'.

⁺⁺ to be replaced by the constituents of our concrete compositions expressed in the appropriate proportions.

⁺⁺⁺ to be replaced by the transport of our concrete constituents expressed in the applicable tkms.

It comprises the whole process of producing 1 m³ of ready-mixed concrete, including all internal processes (transport, wastewater treatment, etc.) and infrastructure, for a composition containing 186 kg of water, 300 kg of cement and 1890 kg of gravel (and sand, with the same inventory as gravel). These concrete constituents were delivered to the plant using a combination of transport by barge, freight train and truck (20-28t). By removing the data of the original concrete constituents and their transport to replace them by the corresponding data for our concrete compositions, a life cycle inventory is obtained that could well represent the production of OPC, k-value conforming FA, HVFA and FA+SF concrete at a ready-mixed concrete plant. As usual, the electricity production mix was adapted for Belgium.

Table 11.19 gives an overview of the CML 2001 baseline impact indicators for the adapted Ecoinvent inventory process of 1 m³ of 'Concrete normal, at plant/CH U' with inclusion and exclusion of the concrete constituents and the transport of constituents. This way, one has an impression of the impacts only associated with the operation of the concrete plant. Except for the environmental burdens on human toxicity and freshwater and marine aquatic ecotoxicity (24-29% of the whole impact), the impacts for the operation of the plant with exclusion of the production and transport of the constituents, are rather small (3-9% of the whole impact).

Table 11.19. CML 2001 baseline impact indicators for a concrete plant producing 1 m³ of concrete with and without the impact related to the constituents and their transport.

| CML 2001 impact category indicator | incl. constituents | incl. constituents | excl. constituents |
|--|-----------------------|-----------------------|-----------------------|
| | incl. transport | excl. transport | excl. transport |
| Abiotic depletion potential (kg Sb _{eq}) | 5.75×10^{-1} | 5.48×10^{-1} | 4.80×10^{-2} |
| Global warming potential (kg CO _{2eq}) | 2.62×10^2 | 2.58×10^2 | 7.04 |
| Ozone depletion potential (kg CFC-11 _{eq}) | 8.75×10^{-6} | 8.20×10^{-6} | 7.66×10^{-7} |
| Human toxicity potential (kg 1,4-DB _{eq}) | 3.48×10^1 | 3.38×10^1 | 1.01×10^1 |
| Freshwater aquatic ecotoxicity potential (kg 1,4-DB _{eq}) | 1.18×10^1 | 1.14×10^1 | 3.01 |
| Marine aquatic ecotoxicity potential (kg 1,4-DB _{eq}) | 2.56×10^4 | 2.47×10^4 | 6.09×10^3 |
| Terrestrial ecotoxicity potential (kg 1,4-DB _{eq}) | 4.30×10^{-1} | 4.21×10^{-1} | 4.04×10^{-2} |
| Photochemical ozone creation potential (kg C ₂ H _{4eq}) | 1.62×10^{-2} | 1.55×10^{-2} | 1.56×10^{-3} |
| Acidification potential (SO _{2eq}) | 4.45×10^{-1} | 4.18×10^{-1} | 3.77×10^{-2} |
| Eutrophication potential (PO _{4eq}) | 1.09×10^{-1} | 1.02×10^{-1} | 1.39×10^{-2} |

Figure 11.2 presents the contribution of constituent production, constituent transport and operation of the concrete plant in terms of percentage for each CML 2001 baseline impact indicator, i.e. the abiotic depletion potential (ADP), the global warming potential (GWP), the ozone depletion potential (ODP), the human toxicity potential (HTP), the freshwater aquatic ecotoxicity potential (FAETP), the marine aquatic ecotoxicity potential (MAETP), the terrestrial ecotoxicity potential (TETP), the photochemical ozone creation potential (POCP), the acidification potential (AP) and the eutrophication potential (EP). For the Ecoinvent inventory process 'concrete, normal, at plant/CH U', the production of the constituents can be held responsible for the largest impacts in all categories (68-96%). The contribution of their transport is always very small (2-6% of the whole impact). Nevertheless, it could very well be that the transport related impact contributions in terms of percentage are somewhat higher for our mixtures because constituent transport depended much more on road transport than for normal concrete from the Ecoinvent database.

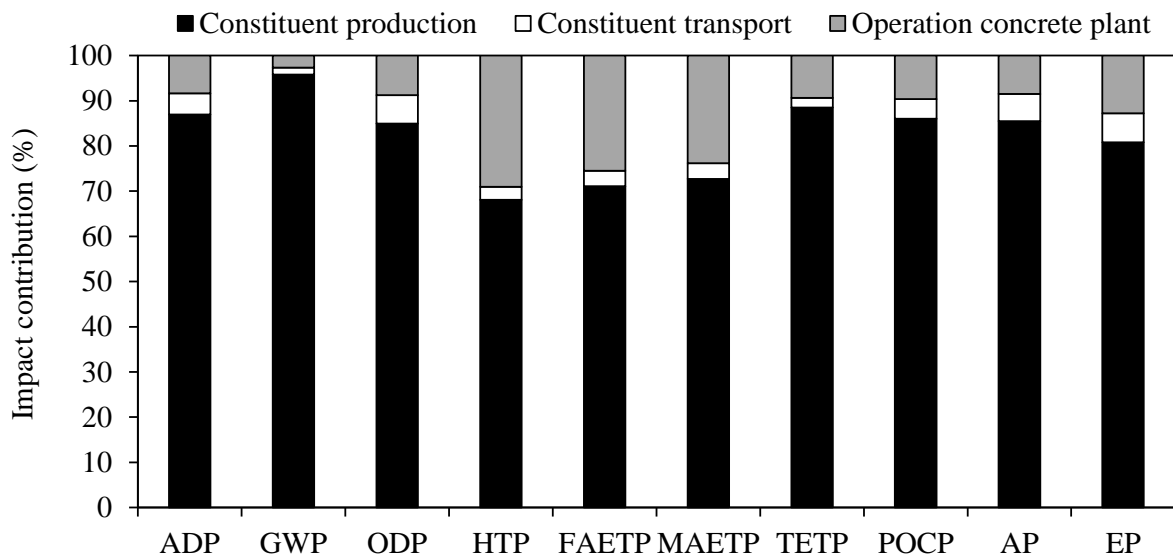


Figure 11.2. Contribution of constituent production, constituent transport and operation of the concrete plant to produce 1 m³ of normal concrete in accordance with Ecoinvent.

11.2.9. Inventory data for reinforcing steel

In this research, LCA of concrete was not only performed on the laboratory and industrial scale. Strength and durability are two concrete properties that can normally only be accounted for by means of a LCA on the structure scale. As discussed in Section 11.1, a suitable functional unit for such a study can be a very simple structural element (column, slab, etc.) with a given mechanical load and a predefined service life. Such an element is always steel reinforced. As a consequence, a life cycle inventory is also needed for reinforcing steel. The Ecoinvent database provides an inventory process that represents an average for the production of reinforcing steel in Europe, i.e. 'Reinforcing steel, at plant/RER U'. The very same inventory process was used in this research in the modelling of the columns (Section 11.1.1.3) and slabs (Section 11.1.1.4) for LCA purposes. The corresponding CML 2001 baseline impact indicators for 1 kg of this steel are shown in Table 11.20.

Table 11.20. CML 2001 baseline impact indicators for 1 kg of reinforcing steel.

| CML 2001 impact category indicator | Reinforcing steel |
|--|-----------------------|
| Abiotic depletion potential (kg Sb _{eq}) | 1.26×10^{-2} |
| Global warming potential (kg CO _{2eq}) | 1.47 |
| Ozone depletion potential (kg CFC-11 _{eq}) | 5.59×10^{-8} |
| Human toxicity potential (kg 1,4-DB _{eq}) | 8.68×10^{-1} |
| Freshwater aquatic ecotoxicity potential (kg 1,4-DB _{eq}) | 9.85×10^{-1} |
| Marine aquatic ecotoxicity potential (kg 1,4-DB _{eq}) | 1.36×10^3 |
| Terrestrial ecotoxicity potential (kg 1,4-DB _{eq}) | 2.73×10^{-2} |
| Photochemical ozone creation potential (kg C ₂ H _{4eq}) | 8.12×10^{-4} |
| Acidification potential (SO _{2eq}) | 5.21×10^{-3} |
| Eutrophication potential (PO _{4eq}) | 3.18×10^{-3} |

Clearly, the environmental impact of reinforcing steel cannot be neglected. In comparison with the impacts associated with 1 kg of Portland cement CEM I 52.5, all impact indicators for the steel give higher values. For instance, the global warming potential of 1 kg of cement

is only 58% of the GWP value for 1 kg of reinforcing steel. Moreover, given the high volumetric density of steel (around 7850 kg/m³), the nominal mass of a steel rebar with a nominal diameter of 12 or 16 mm is no less than 0.888 kg/m or 1.578 kg/m, respectively. Thus, impacts related with a single full length steel rebar of 3 or 5 m are quite a bit higher than the values for 1 kg given in Table 11.20. As a consequence, from the moment additional reinforcing steel is needed for a structural element this will with no doubt significantly contribute to its overall environmental impact. The same holds true for structural elements in which more reinforcing steel is used to limit the crack widths in the concrete. The steel related environmental consequences will in particular be of relevance for the columns and slabs described in Sections 11.1.1.3 and 11.1.1.4.

11.3. Impact analysis

11.3.1. The IPCC 2007 global warming potential impact method

The proposed HVFA and FA+SF compositions were mainly developed to reduce the cement related greenhouse emissions. Therefore, one of the priorities in the LCA calculations was a quantification of the global warming potential for the two concrete types in accordance with the IPCC 2007 impact method. This may seem narrow minded, but it must be said that nowadays there is a lot of focus on the carbon footprint of materials. This in part justifies why the calculation of the global warming potential served as leitmotiv throughout this environmental study. However, this was done while keeping an eye on the broader picture. The use of the problem oriented CML 2001 baseline impact method of which the global warming potential is just one impact category, ensured that the effect of the proposed concrete compositions on other environmental problems was not neglected.

11.3.2. The CML 2001 baseline impact method

Thus, besides the global warming potential, the use of this impact method enabled the consideration of the:

- Acidification potential
- Eutrophication potential
- Abiotic depletion potential
- Freshwater aquatic ecotoxicity potential
- Marine aquatic ecotoxicity potential
- Terrestrial ecotoxicity potential
- Human toxicity potential
- Ozone depletion potential
- Photochemical ozone creation potential

This multidisciplinary impact assessment cf. Guinée (2002) was already applied in this chapter for the environmental characterization of each individual concrete constituent, transport means, etc. The same evaluation approach was adopted for the concrete compositions in the next chapter, yet only for one functional unit definition, i.e. the required concrete volume to achieve 1 unit of strength and service life. Similar trends were expected for the other functional units. The preference for the problem oriented approach lies in the fact that the

method is more accepted in literature because the modelling of impacts involves much less uncertainties.

11.3.3. The Eco-indicator 99 impact method

Nevertheless, to have an idea on what the problem oriented impacts mean in terms of actual environmental damage, the LCA calculations were also done in accordance with the Eco-indicator 99 method of Goedkoop and Spriensma (2001), again only for one functional unit definition, i.e. the required concrete volume to achieve 1 unit of strength and service life. As such, the damage to mineral and fossil resources, human health and ecotoxicity was also determined.

11.4. Interpretation

The interpretation of all LCA calculations done in the LCA software SimaPro 7.3.3 to compare the environmental impacts of OPC, k-value conforming FA, HVFA and FA+SF concrete follows in the next chapter. The main question there was how the different strength and durability properties of the proposed HVFA and FA+SF concrete compositions in comparison with more traditional concrete can affect their environmental score. This question was answered considering the different functional units proposed in Section 11.1. The quantitative definitions of these functional units can differ considerably depending on the underlying experimental and mathematical assessment technique for characterizing the durability and service life in environments with exposure to either carbonation or chloride-induced corrosion. In Chapters 8 and 9 of this thesis, it was shown that the shift from a simplified first order to a more complex second order service life estimation of the concrete can result in a significantly different outcome. In the next chapter, it will be shown how the potential environmental benefit of a concrete composition can be affected by this.

Environmental impact of HVFA and FA+SF concrete

12.1. Impact of 1 m³ of concrete

12.1.1. Summary of the LCA input in SimaPro

LCA calculations were performed for all concrete compositions that were tested for use in an environment with exposure to carbonation- and chloride-induced corrosion. This includes the OPC references T(0.55) (XC3), T(0.50) (XC4) and T(0.45) (XS2), the k-value conforming FA references F(1)15_{XC4}, F(2)15_{XC4}, F(1)15_{XS2} and F(2)15_{XS2}, the HVFA mixtures F(1)50 and F(2)50 as well as the FA+SF mixtures F(1)SF and F(2)SF. Their mixture proportions as shown Tables 4.7, 4.9, 4.11 and 4.15 were modelled in SimaPro 7.3.3 by linking the concrete constituents of the mixtures in their proper amounts to one of the life cycle inventories defined in Chapter 11. Table 12.1 establishes this link by mentioning a brief description of the applicable inventory process per constituent and a reference to the tables where the full life cycle inventories can be found.

Table 12.1. Link between the applied concrete constituents and the corresponding life cycle inventories serving as input for the LCA calculations in SimaPro.

| Constituent | Short description LCI | Overview LCI |
|------------------|--|------------------|
| Sand 0/4 | Sand, at mine | Table 11.15 |
| Aggregate 2/8 | Gravel, round at mine | Table 11.15 |
| Aggregate 8/16 | Gravel, round at mine | Table 11.15 |
| CEM I 52.5 N | Portland cement, strength class Z 52.5, at plant | Table 11.2, 11.3 |
| Fly ash | Electricity, hard coal, at power plant (allocated) | Table 11.5, 11.6 |
| | Treatment of fly ash (drying + storage) | Table 11.7 |
| Silica fume | MG-silicon, at plant (allocated) | Table 11.9 |
| | Treatment of silica fume (storage) | Table 11.10 |
| Water | Tap water, at user | Table 11.12 |
| Superplasticizer | Superplasticizer EFCA (2006) | Table 10.5 |

The applicable inventory processes were in most cases slightly modified inventories from the Ecoinvent database (Version 2.2). Only the processes covering the treatment of the industrial by-products FA and SF and the production of superplasticizer had to be implemented

completely in the software. Note that always the highest dosage of superplasticizer used in each mixture was considered for the LCA calculations (see Tables 4.8, 4.9, 4.12 and 4.16). Although 1 m³ of concrete is definitely not a suitable functional unit for LCA of concrete, the calculations for this FU were performed anyway to show how the more accurate strength and service life related environmental performance of the concrete can deviate from these calculations. Now, the use of considerable portions of fly ash as cement replacement in concrete is often being justified in literature by the potential of this practice to reduce greenhouse gas emissions significantly. Therefore, only the global warming potential was reported for this FU. Evidently, for the more appropriate required concrete volume per unit of strength and service life, the mere focus on the greenhouse gas effect was abandoned. For this FU, more impact categories were considered, i.e. those of the problem oriented CML 2001 impact method and those of the damage oriented Eco-indicator 99 impact method.

12.1.2. Global warming potential per m³

By simply comparing global warming potentials for 1 m³ of each studied concrete composition, quite different impacts can already be obtained for the fly ash (and silica fume) containing mixtures depending on the allocation principles adopted for the by-products. In case only the basic treatment of the fly ash and silica fume after production is taken into account (scenario (i): no allocation), there is a pronounced environmental benefit of using a HVFA concrete (GWP -16-28%) or a FA+SF concrete (GWP -29-39%) instead of the applicable OPC reference (T(0.55), T(0.50) or T(0.45)) for the exposure classes under investigation (XC3, XC4 or XS2). When the k-value conforming FA references F(1,2)15_{XC4} and F(1,2)15_{XS2} are identified as the appropriate reference concrete types, the benefit slightly changed (HVFA: GWP -17-23%, FA+SF: GWP -29-35%). As expected, the main contributor to the GWP of each concrete turned out to be its cement content. The impact of all other constituents present in each composition was negligible (Figure 12.1).

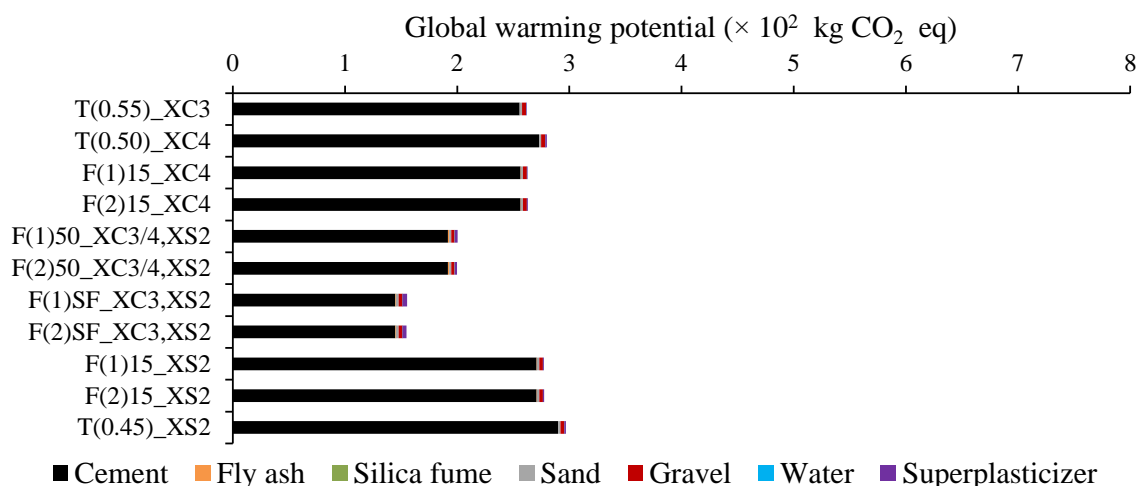


Figure 12.1. Global warming potential per m³ of concrete, no allocation.

With almost no impacts assigned to the by-products fly ash and silica fume, the positive outcome of this very rudimentary LCA calculation approach is not very surprising. Moreover,

it does not represent the current material status of fly ash and silica fume. The sole consideration of their basic treatment after production by the responsible industries would be appropriate for waste products, yet not for the by-products that can be valorized by the cement and concrete industry. As described in Chapters 10 and 11 an allocated impact of coal-fired electricity and Si-metal/MG-silicon production needs to be added to the impact of drying and storing the fly ash and silica fume to get an impact that is more worthy to their current material status. Now, mass allocation (scenario (ii)) is probably the most straightforward way of attributing an impact to an industrial by-product. A mass allocation coefficient is rather easy to determine. Its value is also stable in time because the mass proportioning of main product (or fuel to produce the main product) and by-product is not subject to important changes. However, given the mass ratios mentioned in Table 10.7, this calculation approach imposes a huge global warming potential to both fly ash and silica fume. As a consequence, choosing for a HVFA or FA+SF concrete composition instead of a OPC or k-value conforming FA reference holds no benefit anymore, at least not in view of reducing greenhouse gas emissions associated with 1 m³ of concrete (Figure 12.2).

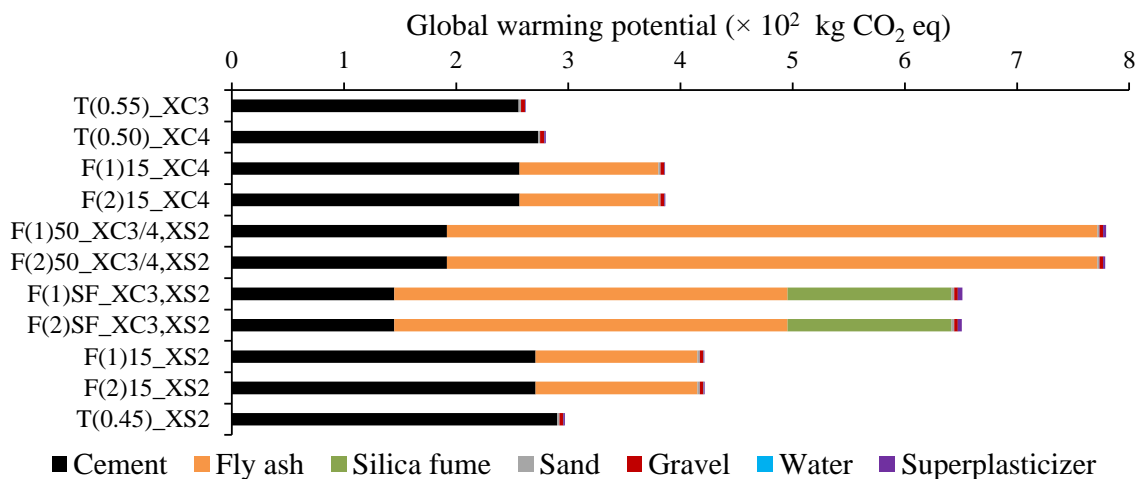


Figure 12.2. Global warming potential per m³ of concrete, mass allocation.

Since this approach would discourage concrete producers of still using industrial by-products as partial cement replacement, it is quite commonly accepted that allocation by mass value is not a useful principle. Allocation by economic value (scenario (iii)) is believed to be a more justifiable alternative. Although the economic allocation coefficients calculated by Chen et al. (2010) and Chen (2009) (Table 10.7: FA: 1%, SF: 4.8%) are much lower than the formerly applied mass allocation coefficients (Table 10.7: FA: 12.4%, SF: 13%), this still increases the global warming potentials of all fly ash (and silica fume) containing concrete compositions considerably. For HVFA concrete there is only a small benefit which ranges between 6-17% depending on the exposure class and the reference concrete type. The same holds true for the FA+SF concrete compositions as their GWP values are 4-15% lower (Figure 12.3). However, as can be seen from Figure 12.4, these benefits disappear when the economic allocation coefficients are calculated from more recent prices of the main products and the by-products (Table 10.7: FA: 2.9%, SF: 6.1%). Only exceptions are the FA+SF concrete compositions when compared with the k-value conforming FA references for exposure class XS2. The

comparison of the Figures 12.3 and 12.4 clearly demonstrates the non-negligible effects of the price fluctuations inherent allocation by economic value.

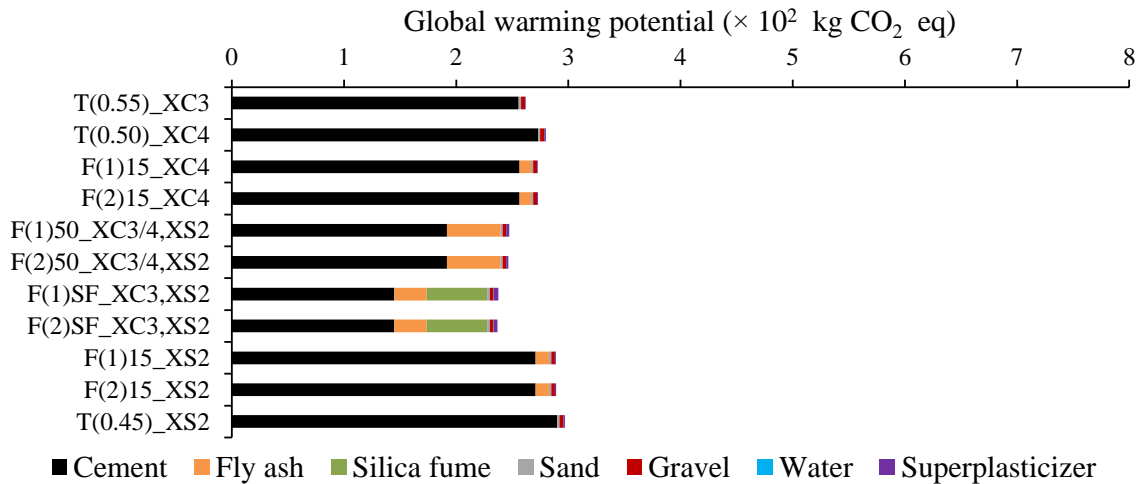


Figure 12.3. Global warming potential per m³ of concrete, economic allocation (FA: 1.0%, SF: 4.8%).

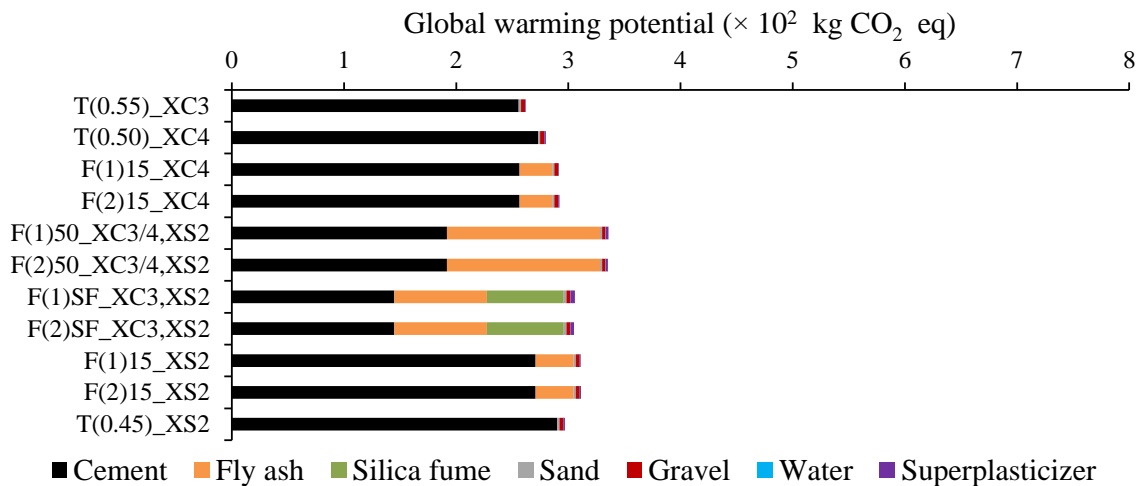


Figure 12.4. Global warming potential per m³ of concrete, economic allocation (FA: 2.9%, SF: 6.1%).

Some increases in GWP due to the higher economic allocation coefficients are remarkable. For instance, the effect of using 10% silica fume is substantial. It contributes more or less to the same extent to the overall GWP of FA+SF concrete as the presence of 40% fly ash.

Thus, given the still important effects of the more accepted economic allocation approach, it is evident that the benefit of partially replacing cement with industrial by-products does totally not correspond with the cement replacement level of the concrete. A 50% cement replacement does not lead to a 50% reduction in greenhouse gas emissions. This is simply due to the fact that the responsible industries have to emit huge amounts of CO₂ to produce 1 kg of fly ash (18.27 kg) and silica fume (34.67 kg). Even when using a low allocation coefficient, still a considerable portion of GHG emissions are assigned to the by-products. In case of silica

fume these CO₂ emissions are more than twice the emissions associated with the production of 1 kg ordinary Portland cement (0.85 kg).

12.2. Impact of the concrete volume per unit of strength and service life

12.2.1. Summary of the LCA input in SimaPro

One m³ of concrete does not account for any of the relevant functionalities of the material, i.e. the strength and service life. This can be done by dividing the 1 m³ concrete volume by the minimum characteristic cube strength as indicated by its strength class, and the service life of the material in an environment with exposure to carbonation or chloride-induced corrosion. These concrete properties were quantified in Chapters 4, 8 and 9. Tables 12.2 and 12.3 summarize these data and give the corresponding value of the FU in m³/(N/mm² · yr).

Table 12.2. Quantification of the concrete volume per 1 N/mm² of strength and 1 year of service life for each composition exposed to carbonation-induced corrosion.

| Composition | Strength class (-) | Strength (N/mm ²) | Prediction approach | Service life (years) | FU (m ³ /(N/mm ² · yr)) |
|--------------|--------------------|-------------------------------|--|------------------------------------|---|
| T(0.55)_XC3 | C30/37 | 37 | t _{ini} (1 st order) | 100 ^{a, b} | 2.70 × 10 ^{-4 a, b} |
| | | | + t _{crack_1mm} | 100 ^{a, c} | 2.70 × 10 ^{-4 a, c} |
| | | | t _{ini} (2 nd order) | 100 ^{a, b} | 2.70 × 10 ^{-4 a, b} |
| | | | + t _{crack_1mm} | 100 ^{a, c} | 2.70 × 10 ^{-4 a, c} |
| T(0.50)_XC4 | C45/55 | 55 | t _{ini} (1 st order) | 100 ^a | 1.82 × 10 ^{-4 a} |
| | | | t _{ini} (2 nd order) | 100 ^a | 1.82 × 10 ^{-4 a} |
| F(1)15_XC4 | C45/55 | 55 | t _{ini} (1 st order) | 100 ^a | 1.82 × 10 ^{-4 a} |
| | | | t _{ini} (2 nd order) | 100 ^a | 1.82 × 10 ^{-4 a} |
| F(2)15_XC4 | C45/55 | 55 | t _{ini} (1 st order) | 100 ^a | 1.82 × 10 ^{-4 a} |
| | | | t _{ini} (2 nd order) | 100 ^a | 1.82 × 10 ^{-4 a} |
| F(1)50_XC3/4 | C35/45 | 45 | t _{ini} (1 st order) | 100 ^a / 21 ^b | 2.22 × 10 ^{-4 a} / 1.06 × 10 ^{-3 b} |
| | | | + t _{crack_1mm} | 100 ^a / 73 ^c | 2.22 × 10 ^{-4 a} / 3.04 × 10 ^{-4 c} |
| | | | t _{ini} (2 nd order) | 100 ^a / 72 ^b | 2.22 × 10 ^{-4 a} / 3.09 × 10 ^{-4 b} |
| | | | + t _{crack_1mm} | 100 ^{a, c} | 2.22 × 10 ^{-4 a, c} |
| F(2)50_XC3/4 | C30/37 | 37 | t _{ini} (1 st order) | 100 ^a | 2.70 × 10 ^{-4 a} |
| | | | t _{ini} (2 nd order) | 100 ^a | 2.70 × 10 ^{-4 a} |
| F(1)SF_XC3 | C50/60 | 60 | t _{ini} (1 st order) | 100 ^a / 71 ^b | 1.67 × 10 ^{-4 a} / 2.35 × 10 ^{-4 b} |
| | | | + t _{crack_1mm} | 100 ^{a, c} | 1.67 × 10 ^{-4 a, c} |
| | | | t _{ini} (2 nd order) | 100 ^{a, b} | 1.67 × 10 ^{-4 a, b} |
| | | | + t _{crack_1mm} | 100 ^{a, c} | 1.67 × 10 ^{-4 a, c} |
| F(2)SF_XC3 | C55/67 | 67 | t _{ini} (1 st order) | 100 ^a | 1.49 × 10 ^{-4 a} |
| | | | t _{ini} (2 nd order) | 100 ^a | 1.49 × 10 ^{-4 a} |

^a t_{ini} without correction for the applied CO₂ concentration and curing conditions.

^b t_{ini} after correction for the applied CO₂ concentration and curing conditions (only XC3).

^c t_{ini} + t_{crack_1mm} after correction for the applied CO₂ concentration and curing conditions (only XC3).

As the estimated life span of the material could vary considerably with the applied prediction approach, not just one value is obtained for the functional unit per concrete mixture. For each environment, there was a first and second order approach for determining the duration of the corrosion initiation period (t_{ini}). The former relied on either simplified empirical prediction

models or on default input values to these models, while the latter used more advanced models with experimentally determined or verified model input. For some mixtures the time to unacceptable cracking ($t_{\text{crack}_1 \text{ mm}}$) after depassivation of the steel was also estimated. As a result, their service life could also be quantified as the sum of t_{ini} (1st/2nd order) and $t_{\text{crack}_1 \text{ mm}}$. This gives another set of functional unit values for these mixtures.

In chapters 8 and 9, the second order predictions of the corrosion initiation periods often resulted in very long time spans. Because the values obtained often seemed unrealistically high, the maximum time span considered was only 100 years, the design service life of important concrete structures, such as bridges, etc. The service lives used for determining the FU value were always based on the prediction outcome for time of reference $t_0 = 28$ days.

For all concrete compositions exposed to carbonation-induced corrosion, the duration of t_{ini} or the sum of t_{ini} and $t_{\text{crack}_1 \text{ mm}}$ exceeded 100 years after 28 days optimal curing and without correction for the applied high CO_2 concentration during the accelerated carbonation test. In Chapter 5 the obtained field carbonation coefficients for mixtures T(0.55), F(1)50 and F(1)SF were corrected for the high CO_2 concentration during carbonation testing. In addition, correction factors were determined for mixtures F(1)50 and F(1)SF to consider suboptimal curing conditions (7 days at 20°C and 95% RH, 21 days at 20°C and 60% RH) prior to carbonation testing. The combined effect of these corrections can reduce the estimated service life of the concrete significantly. First and second order prediction sometimes resulted in service lives lower than the desired 100 years, especially with respect to HVFA concrete. The corresponding alternative FU values for these mixtures were calculated accordingly.

Table 12.3. Quantification of the concrete volume per 1 N/mm² of strength and 1 year of service life for each composition exposed to chloride-induced corrosion.

| Composition | Strength class (-) | Strength (N/mm ²) | Prediction approach | Service life (years) | FU (m ³ /(N/mm ² · years)) |
|-------------|--------------------|-------------------------------|--|----------------------|--|
| T(0.45)_XS2 | C45/55 | 45 | t_{ini} (1 st order) | 4 | 4.55×10^{-3} |
| | | | + $t_{\text{crack}_1 \text{ mm}}$ | 4.4 | 4.13×10^{-3} |
| | | | t_{ini} (2 nd order) | 47 | 3.87×10^{-4} |
| | | | + $t_{\text{crack}_1 \text{ mm}}$ | 47.4 | 3.84×10^{-4} |
| F(1)15_XS2 | C40/50 | 40 | t_{ini} (1 st order) | 31 | 6.45×10^{-4} |
| | | | t_{ini} (2 nd order) | 100 | 2.00×10^{-4} |
| F(2)15_XS2 | C45/55 | 45 | t_{ini} (1 st order) | 27 | 6.73×10^{-4} |
| | | | t_{ini} (2 nd order) | 100 | 1.82×10^{-4} |
| F(1)50_XS2 | C35/45 | 35 | t_{ini} (1 st order) | 17 | 1.31×10^{-3} |
| | | | + $t_{\text{crack}_1 \text{ mm}}$ | 18.4 | 1.21×10^{-3} |
| | | | t_{ini} (2 nd order) | 100 | 2.22×10^{-4} |
| | | | + $t_{\text{crack}_1 \text{ mm}}$ | 100 | 2.22×10^{-4} |
| F(2)50_XS2 | C30/37 | 30 | t_{ini} (1 st order) | 19 | 1.42×10^{-3} |
| | | | t_{ini} (2 nd order) | 100 | 2.70×10^{-4} |
| F(1)SF_XS2 | C50/60 | 50 | t_{ini} (1 st order) | 100 | 1.67×10^{-4} |
| | | | + $t_{\text{crack}_1 \text{ mm}}$ | 100 | 1.67×10^{-4} |
| | | | t_{ini} (2 nd order) | 100 | 1.67×10^{-4} |
| | | | + $t_{\text{crack}_1 \text{ mm}}$ | 100 | 1.67×10^{-4} |
| F(2)SF_XS2 | C55/67 | 55 | t_{ini} (1 st order) | 100 | 1.49×10^{-4} |
| | | | t_{ini} (2 nd order) | 100 | 1.49×10^{-4} |

In environments classified as exposure class XS2, a first order prediction of the corrosion initiation period always resulted in service lives that were substantially lower than 100 years except for the FA+SF concrete compositions. Inclusion of the time to unacceptable concrete cracking after depassivation (when available) did not change this finding significantly for OPC and HVFA concrete because this adds only 0.4 and 1.4 years to the service life. After a shift to the second order prediction approach, life spans amounted to at least 100 years for all compositions, except for the OPC reference. The use of mix specific input parameters to the model increased the service life of mixture T(0.45) substantially. Yet, it still remained below 50 years. Evidently, service lives lower than 100 years will impose a higher environmental impact to the required concrete volume per unit of strength and service life.

12.2.2. Global warming potential of the required concrete volume

In all LCA calculations for FA (and SF) containing concrete, the strictest economic allocation coefficients based on the most recent prices of main products and by-products were used (FA: 2.9%, SF: 6.1%). In exposure class XS2 always $t_{ini} + t_{crack_1mm}$ was considered if t_{crack_1mm} was determined.

12.2.2.1. In exposure class XC3/4

Figure 12.5 gives the global warming potentials for the FUs that resulted from the first order prediction of t_{ini} , combined with t_{crack_1mm} when quantified.

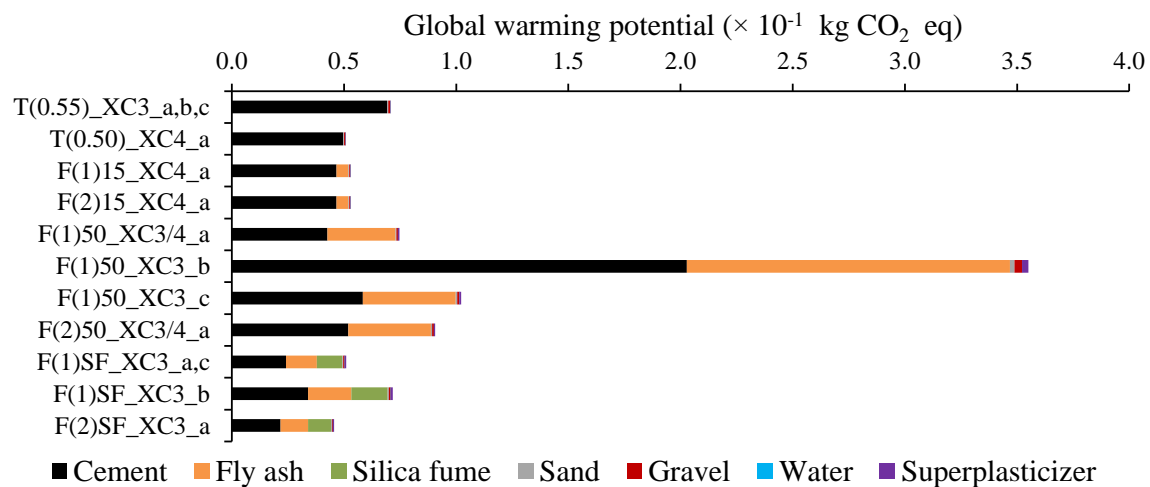


Figure 12.5. Global warming potential of the concrete volume per N/mm² of strength and year of t_{ini} (1st order) (+ t_{crack_1mm}) (XC3/4), economic allocation (FA: 2.9%, SF: 6.1%).

Even when assuming a 100 year service life for HVFA mixtures F(1)50 and F(2)50 (option a: no correction for the applied CO₂ concentration and curing conditions), its GWP exceeds the corresponding value of the reference mixtures. This is definitely the case for exposure class XC4, because references T(0.50), F(1)15 and F(2)15 are all characterized by a much higher strength class (C45/55). The lower strength classes of the HVFA concrete (C35/45, C30/37) resulted in substantially higher concrete volumes per unit of strength and service life. On the other hand, with a strength class equal or higher than C30/37, the strength class of OPC

reference T(0.55) for exposure class XC3, one would expect a slightly better environmental performance of the HVFA concrete because of its somewhat lower cement content. However, the economically allocated impact assigned to the fly ash cancels out this benefit completely. When the estimated corrosion initiation period is corrected for the applied CO₂ concentration during carbonation testing and the curing conditions (Table 12.2: option b), there is not only the disadvantage of a lower strength, but also the negative effect of a lower service life. This causes an enormous increase of the global warming potential. Inclusion of the considerably long time to unacceptable cracking for HVFA mixture F(1)50 ($t_{\text{crack}_1 \text{ mm}}$: 52 years) cannot completely compensate for this (Table 12.2: option c).

When a concrete composition with a high cement replacement level meets the design service life of 100 years just like its corresponding reference, it is of importance to achieve a (much) higher strength to reach a low global warming potential. The FA+SF concrete compositions F(1)SF and F(2)SF meet this criterion. Their high strength classes (C50/60, C55/67) resulted in environmental benefits of 28 and 36%, when compared with OPC reference T(0.55). However, option b shows that this benefit can easily be lost from the moment the corrosion initiation period drops below 100 years.

The second order prediction of the initiation period always resulted in service life estimations of at least 100 years, except for option b of HVFA mixture F(1)50 in exposure class XC3. With a service life of 72 years, the corresponding FU value increases. The GWP values are affected by it accordingly. For the other mixtures, all previously observed trends for a 100 year service life remained valid. In other words, still only the use of FA+SF compositions can cause a pronounced reduction in greenhouse gas emissions in comparison with the OPC reference for exposure class XC3.

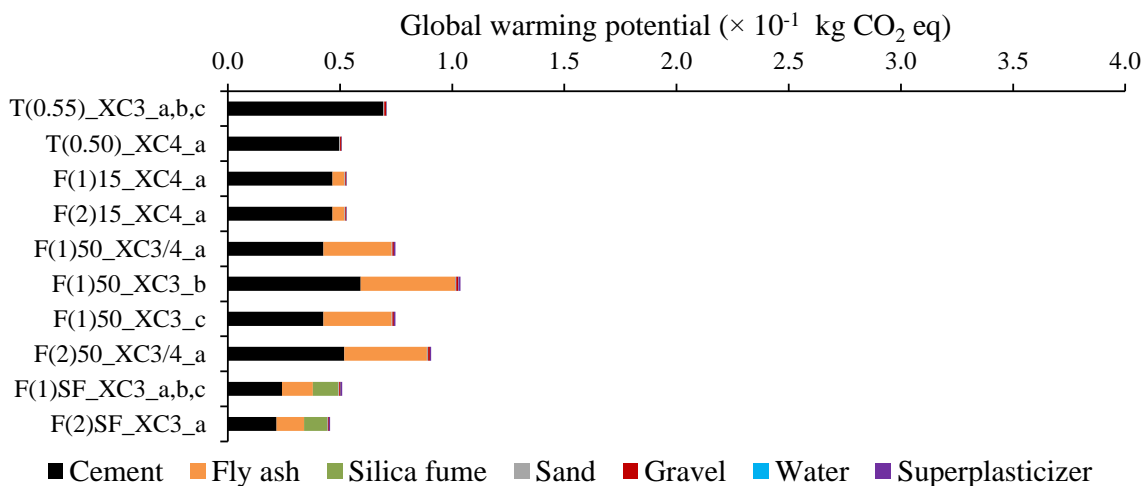


Figure 12.6. Global warming potential of the concrete volume per N/mm² of strength and year of t_{ini} (2nd order) (+ $t_{\text{crack}_1 \text{ mm}}$) (XC3/4), economic allocation (FA: 2.9%, SF: 6.1%).

12.2.2.2. In exposure class XS2

Because the life span ($t_{\text{ini}} + t_{\text{crack}_1 \text{ mm}}$) of OPC reference T(0.45) in a XS2 environment is expected to be very short (< 5 years) when based upon a first order prediction, a high concrete volume per unit of strength and service life is obtained as FU for this mixture. As a result,

both the HVFA and the FA+SF compositions are characterized by a much lower global warming potential (Figure 12.7: GWP $-61-67\%$ and $-95-96\%$). When the k-value conforming FA mixtures with a longer service life (27-31 years) are considered as reference, then only the FA+SF compositions seem useful from an environmental perspective (GWP $-75-78\%$).

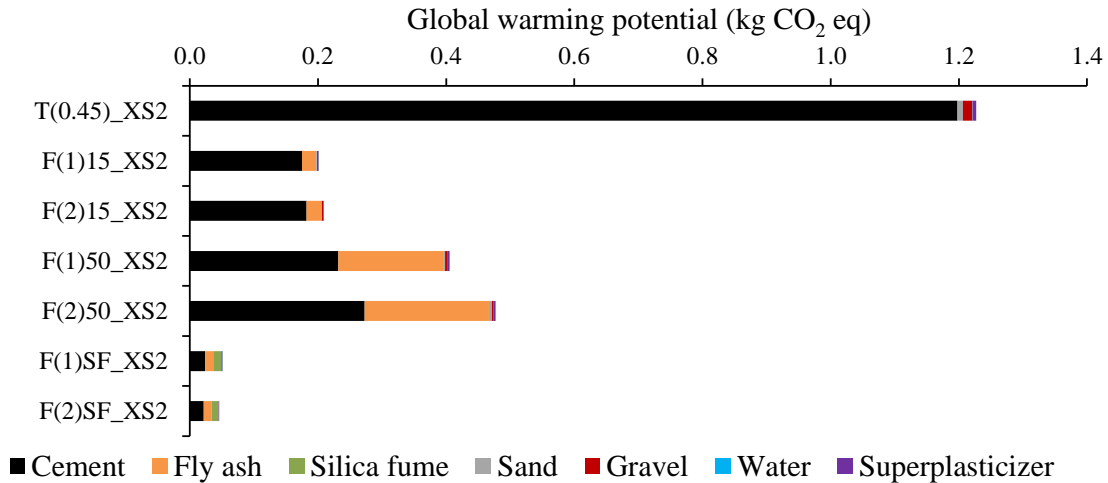


Figure 12.7. Global warming potential of the concrete volume per N/mm² of strength and year of t_{ini} (1st order) ($+ t_{crack_1mm}$) (XS2), economic allocation (FA: 2.9%, SF: 6.1%).

Second order estimations of $t_{ini} + t_{crack_1\text{ mm}}$ make the GWP values of all mixtures decrease, because this prediction approach always resulted in longer service lives. Basically the same trends can still be observed, although the differences have become smaller (Figure 12.8). Both the HVFA and FA+SF compositions show a better performance in comparison with the OPC reference (GWP $-20-35\%$ and $-55-60\%$), while in comparison with F(1)15 and F(2)15 only the FA+SF compositions are still advantageous (GWP $-19-21\%$). Also note that mixtures F(1)15 and F(2)15 turned out much more beneficial than T(0.45) (GWP $-45-50\%$).

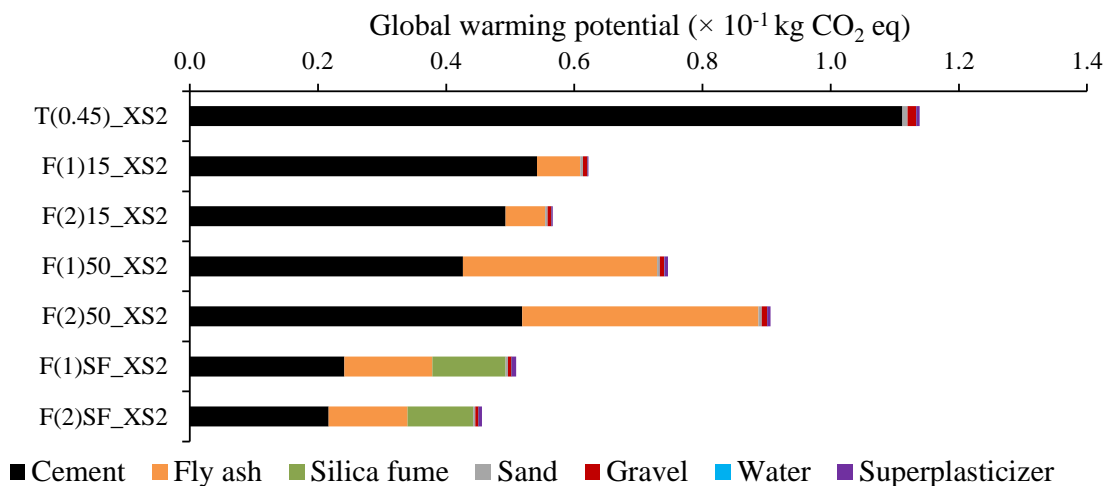


Figure 12.8. Global warming potential of the concrete volume per N/mm² of strength and year of t_{ini} (2nd order) ($+ t_{crack_1mm}$) (XS2), economic allocation (FA: 2.9%, SF: 6.1%).

12.2.3. Global warming potential including transport and production

Until now only the greenhouse gas emissions related to the production of the concrete constituents per mixture were taken into consideration for a LCA on laboratory scale with inclusion of strength and service life aspects. In practice, the constituents need to be transported to the concrete plant and mixed in order to produce the actual concrete compositions. Obviously, constituent transport and operation of the concrete plant also contribute to the global warming potential. Figures 12.9 and 12.10 give an indication of their contribution for the concrete volumes of each mixture per unit of strength and service life in exposure classes XC3/4 and XS2. A second order prediction approach for the corrosion initiation period was assumed.

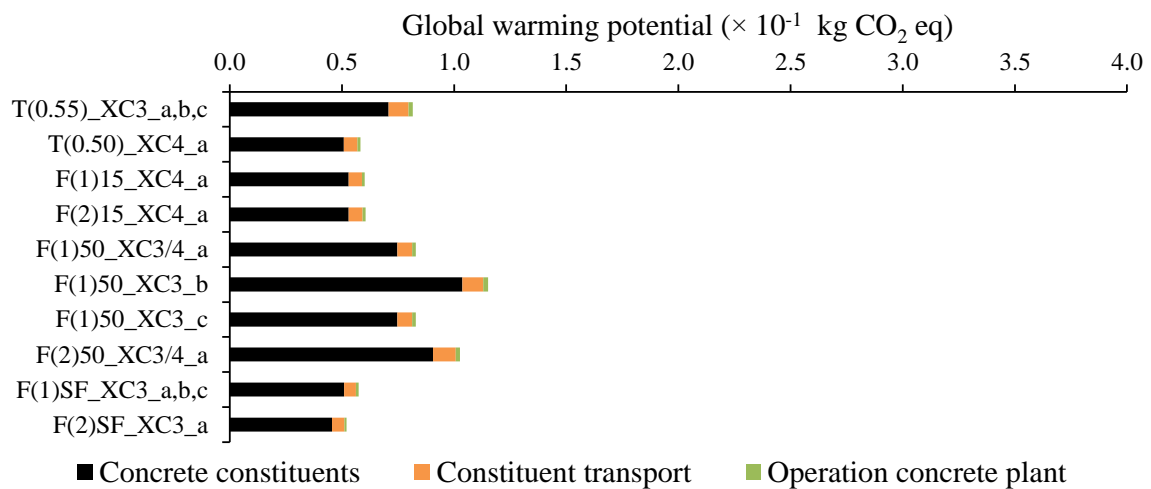


Figure 12.9. Global warming potential of the concrete volume per N/mm² of strength and year of t_{ini} (2nd order) (+ t_{crack_1mm}) (XC3/4), produced at a concrete plant, economic allocation (FA: 2.9%, SF: 6.1%).

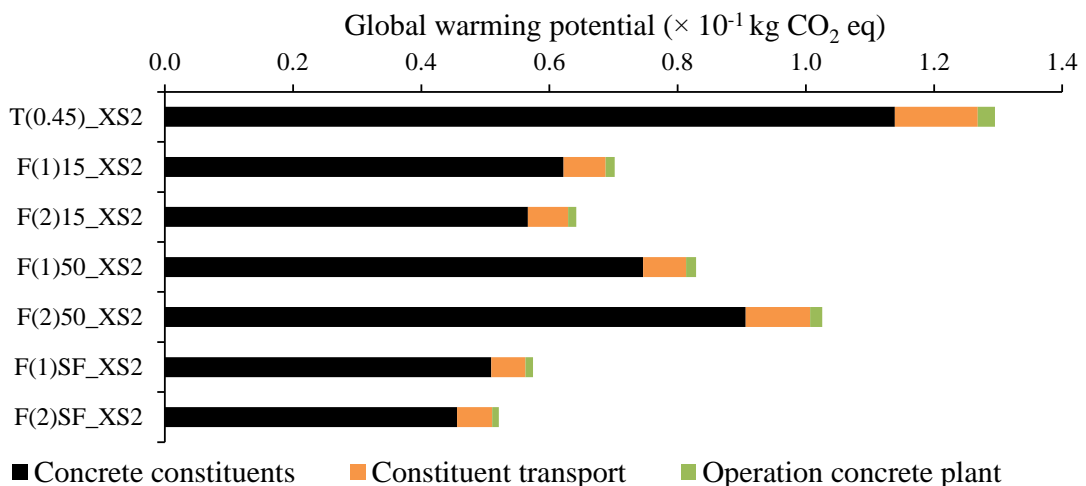


Figure 12.10. Global warming potential of the concrete volume per N/mm² of strength and year of t_{ini} (2nd order) (+ t_{crack_1mm}) (XS2), produced at a concrete plant, economic allocation (FA: 2.9%, SF: 6.1%).

Clearly, the recorded GWP values are dominated by the GHGs emitted during the production of the concrete constituents. This comprises around 85 to 90% of the total global warming potential for each mixture. Thus, constituent transport and especially operation of the concrete plant are only minor contributors. Moreover, as the location of the (fictitious) concrete plant was now far from ideal to achieve minimal transport distances and more sustainable transport over water for all constituents, the already limited impact of transport can probably still be reduced even more. However, this latter aspect was not investigated any further because this research mainly aimed at investigating the effect of the concrete composition and its relevant material properties. Mainly for this reason, transport and operation of the concrete plant were not included anymore in the outcome of all further LCA calculations.

12.2.4. Other problem oriented impacts of the required concrete volume

Today, the concrete industry focuses perhaps a little too much on reducing cement related GHG emissions to achieve a higher sustainability. However, as shown in Chapter 10, other environmental issues are of importance as well. Figures 12.11-12.16 give the other 9 baseline impact indicators of the CML 2001 impact method for the concrete volumes per unit of strength and service life in exposure class XC3/4 and XS2 per composition.

Apparently, there is seldomly an environmental benefit to gain by replacing considerable portions of the ordinary Portland cement by fly ash (and silica fume) in exposure class XC3/4 and XS2. The economically allocated impacts assigned to the by-products are often much higher than the impacts of cement (see also Chapter 11). As a consequence, the recorded values per indicator are mainly governed by the by-products, even when present in rather small amounts (10-15%).

Acidification potential – For fly ash, the burning of hard coal at the power plant (0.415 kg/kWh) as well as the operation of the transoceanic freight ship that transports the imported hard coal to Belgium are responsible for the largest portion of acidifying pollutant emissions per kg of this by-product. For silica fume, the production of the main product MG-silicon also relies to a large extent on the combustion of hard coal (23.1 MJ/kg or ± 0.91 kg/kg). Since 19.23 kWh of coal fired electricity and 6.67 kg of MG-silicon need to be produced to obtain 1 kg of FA and 1 kg SF it is not surprising that more of these sulphur and nitrogen containing fossil fuels need to be burned than the amount needed to produce of 1 kg ordinary Portland cement (3.23×10^{-2} kg/kg). The acidifying emissions may only be partially assigned to the fly ash and silica fume through economic allocation. Yet, they still remain higher than for cement.

Eutrophication potential – For this impact indicator there is again a strong relation with the the use of hard coal by the main industries. The disposal of spoil from coal mining to surface landfill is accountable for no less than 85% of the eutrophication potential for 1 kg of fly ash. In case of silica fume, the disposal of spoil from coal and lignite mining together with the production process of the MG-silicon itself cause the largest portion (> 80%) of pollutant emissions (e.g. NO_x) that contribute to the eutrophication potential. In the manufacturing process of OPC, mainly the clinkering process is the main pollutor followed by the disposal of spoil from coal and lignite mining. Together, they comprise over 80% of the EP value. Again, the low by-product/main product production ratios for the supplementary cementitious

materials explain why the economically allocated impacts of FA and SF still exceed those for cement production.

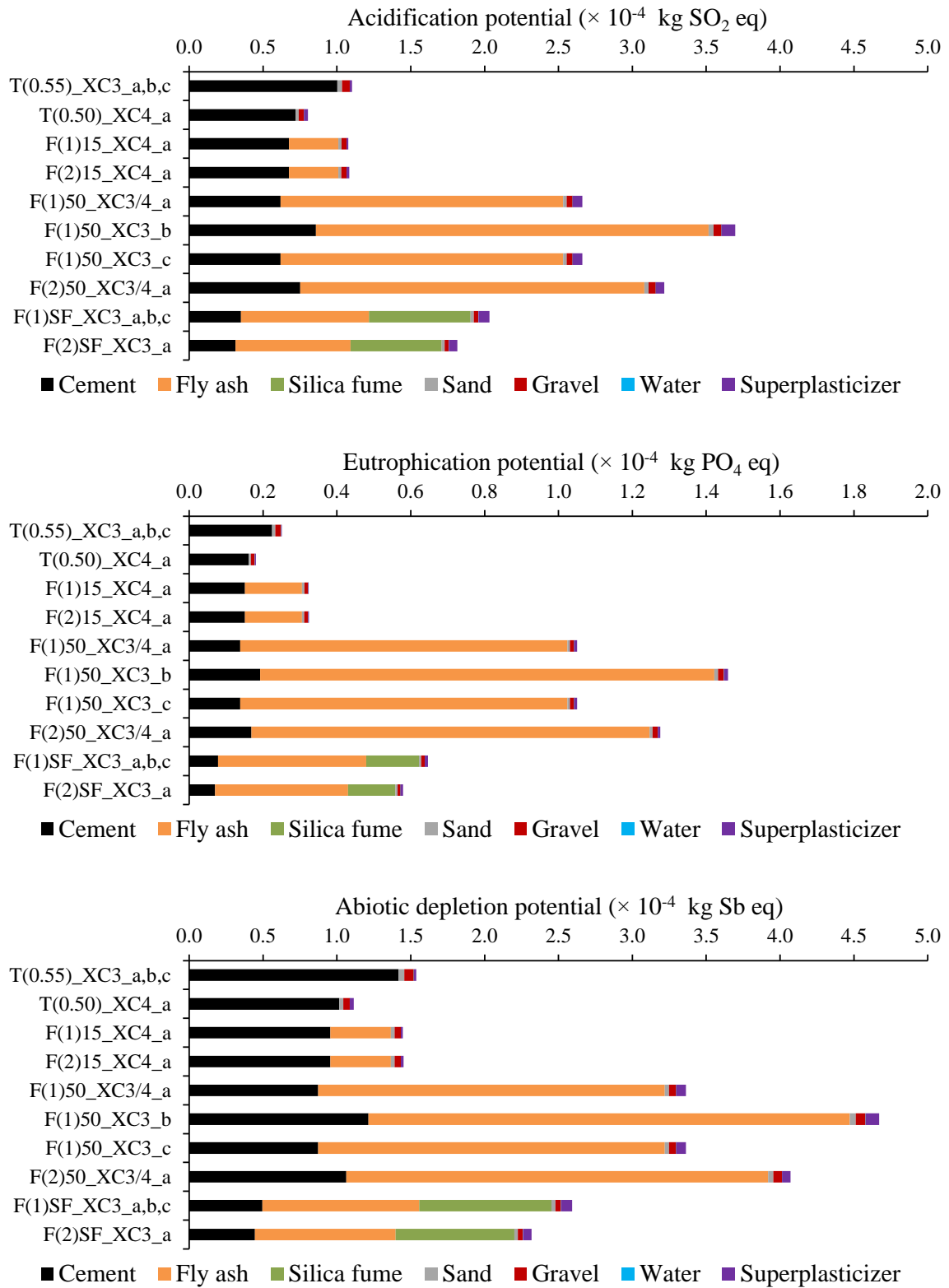


Figure 12.11. Acidification, eutrophication and abiotic depletion potentials of the concrete volume per N/mm^2 of strength and year of t_{ini} (2^{nd} order) ($+ t_{\text{crack}_{1\text{mm}}}$) (XC3/4), economic allocation (FA: 2.9%, SF: 6.1%).

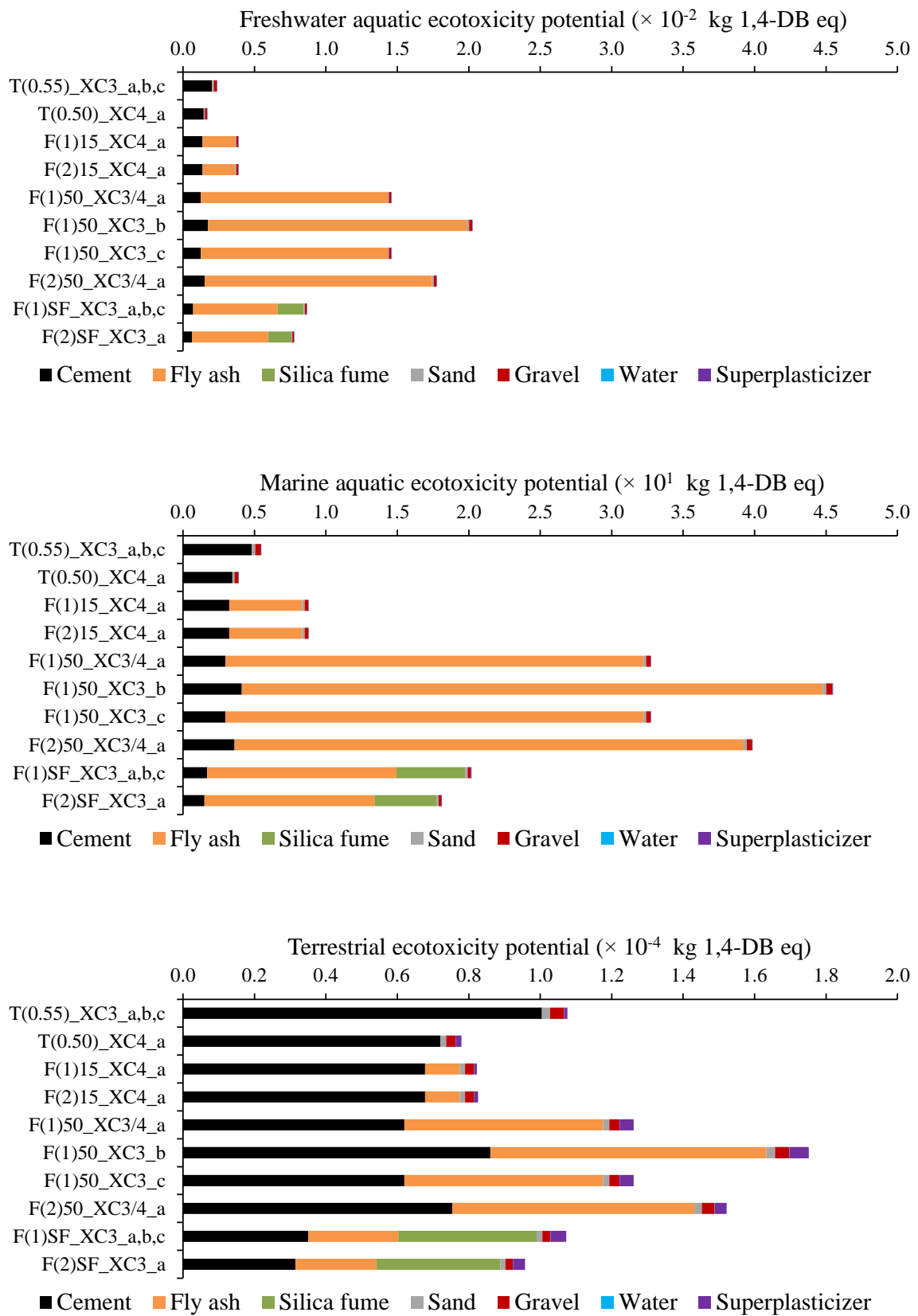


Figure 12.12. Freshwater and marine aquatic ecotoxicity and terrestrial ecotoxicity potentials of the concrete volume per N/mm² of strength and year of t_{ini} (2nd order) (+ t_{crack_1mm}) (XC3/4), economic allocation (FA: 2.9%, SF: 6.1%).

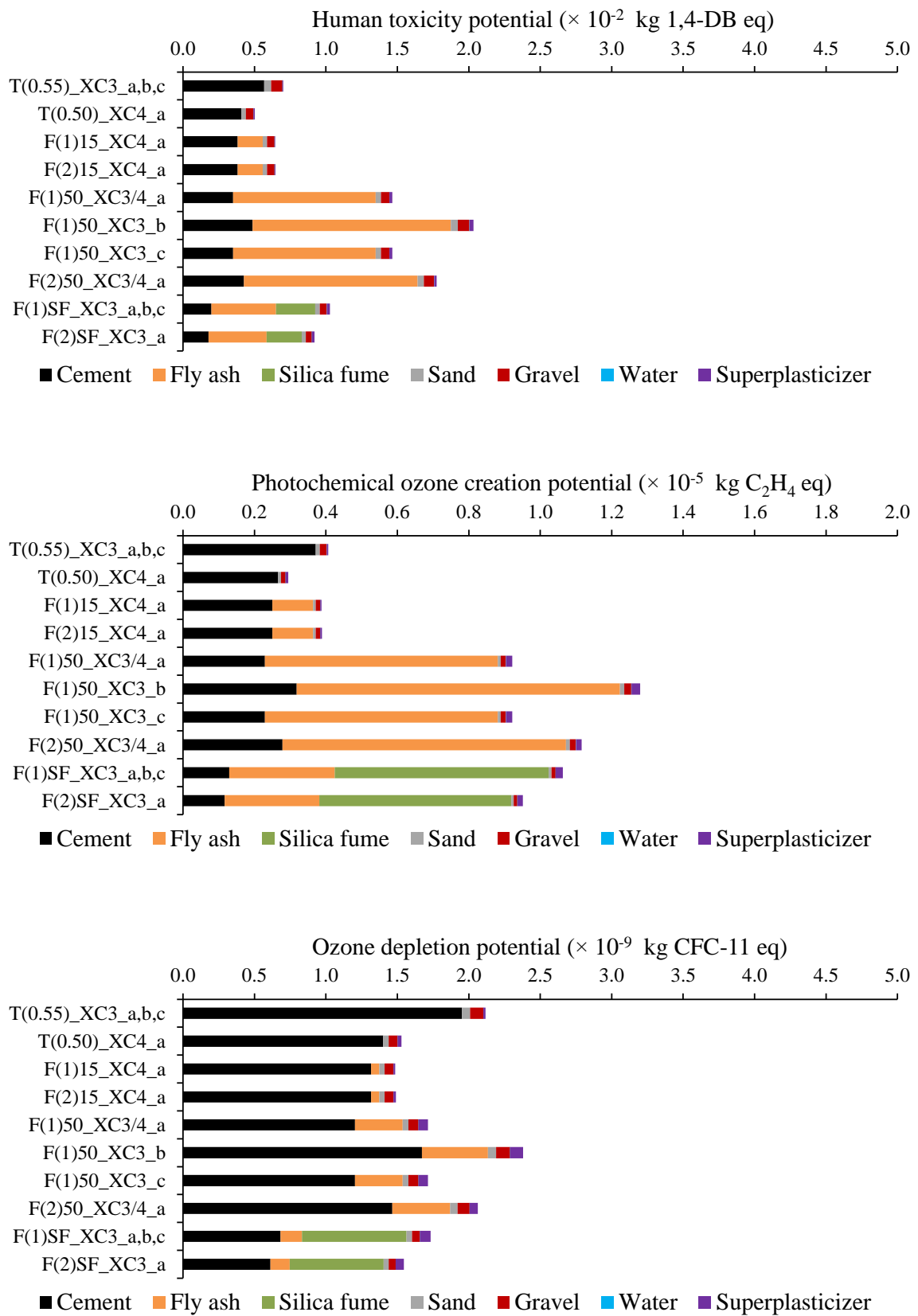


Figure 12.13. Human toxicity, photochemical ozone creation and ozone depletion potentials of the concrete volume per N/mm² of strength and year of t_{ini} (2nd order) (+ t_{crack_1mm}) (XC3/4), economic allocation (FA: 2.9%, SF: 6.1%).

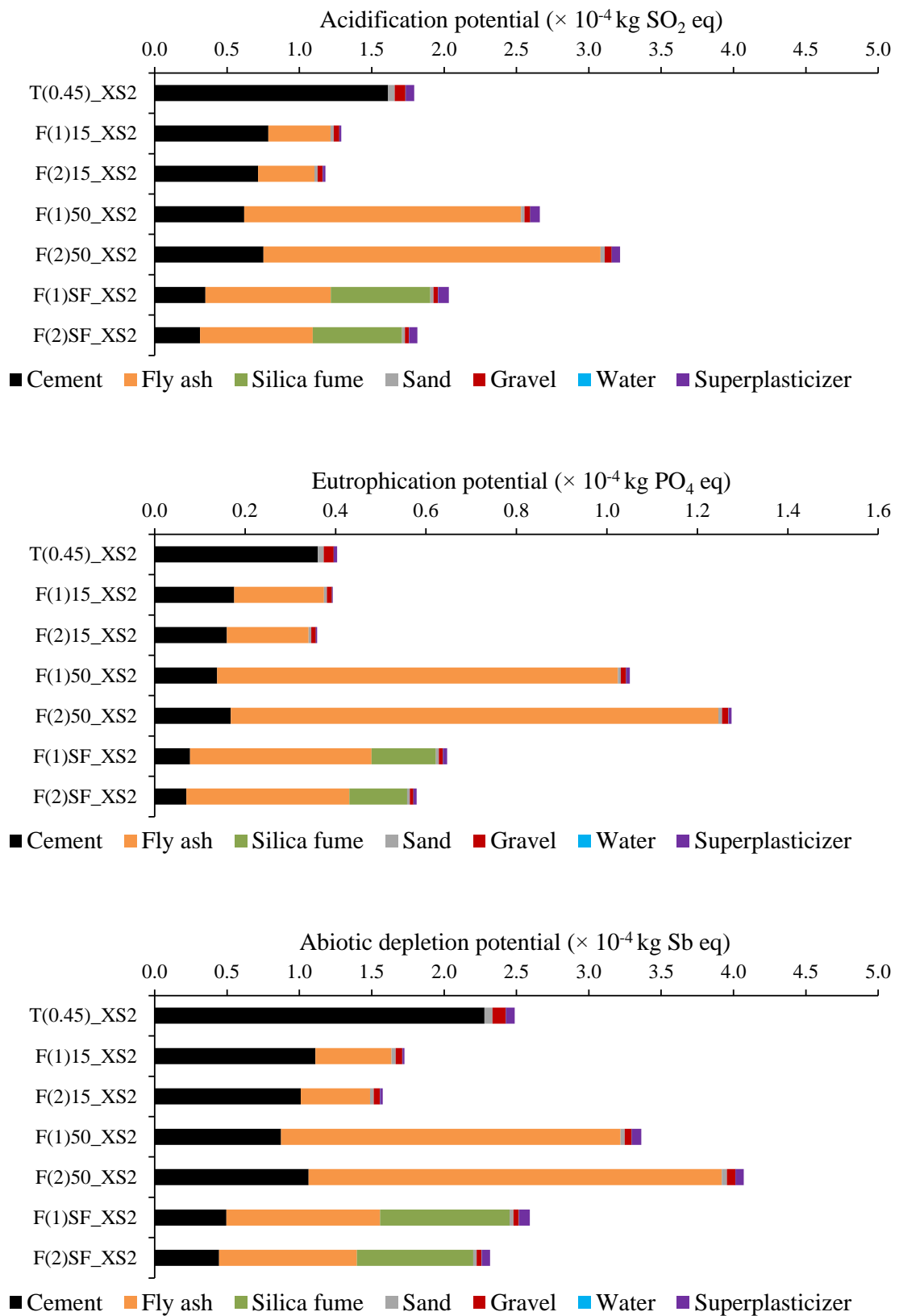


Figure 12.14. Acidification, eutrophication and abiotic depletion potentials of the concrete volume per N/mm² of strength and year of t_{ini} (2nd order) (+ t_{crack_1mm}) (XS2), economic allocation (FA: 2.9%, SF: 6.1%).

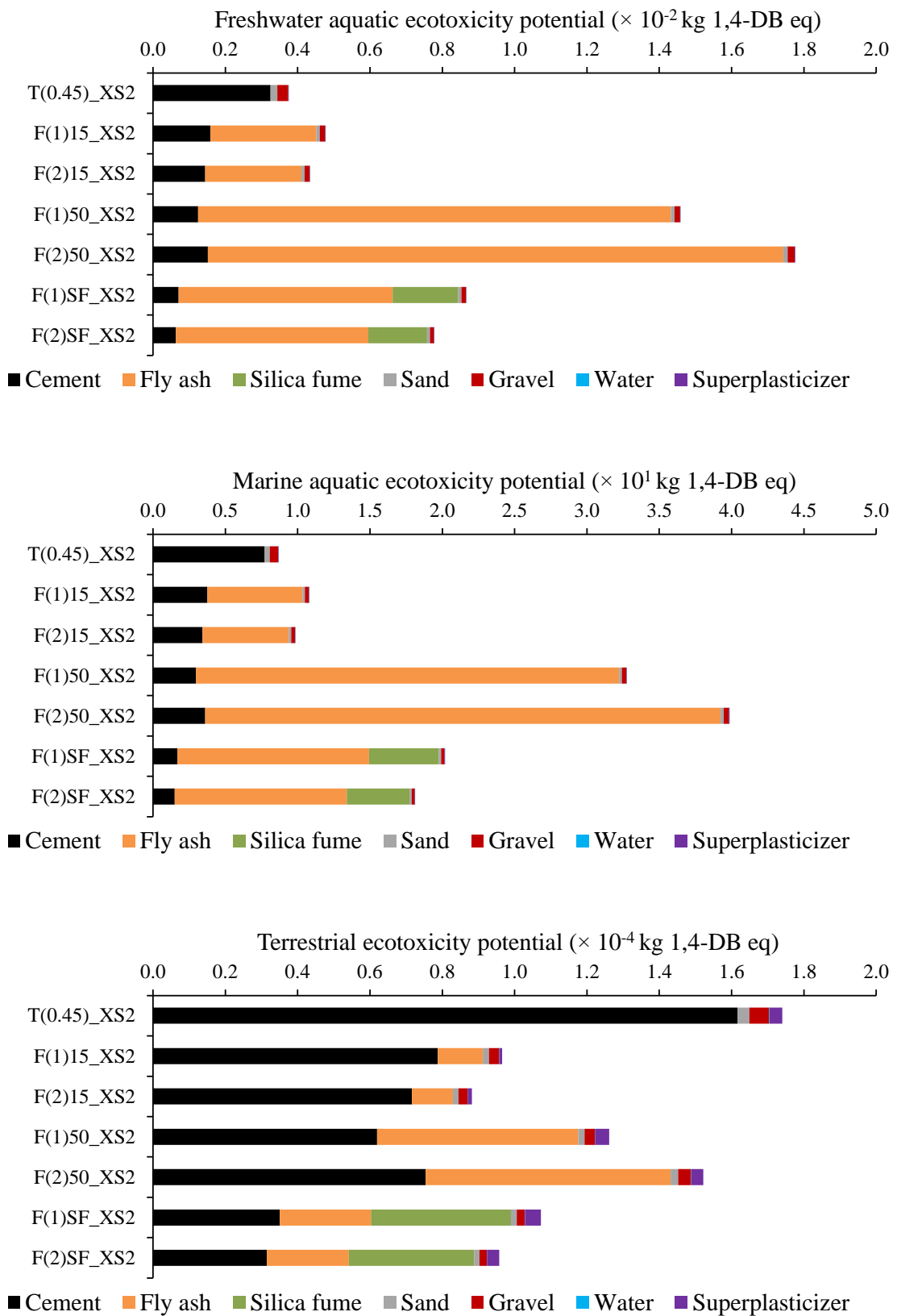


Figure 12.15. Freshwater and marine aquatic ecotoxicity and terrestrial ecotoxicity potentials of the concrete volume per N/mm² of strength and year of t_{ini} (2nd order) (+ t_{crack_1mm}) (XS2), economic allocation (FA: 2.9%, SF: 6.1%).

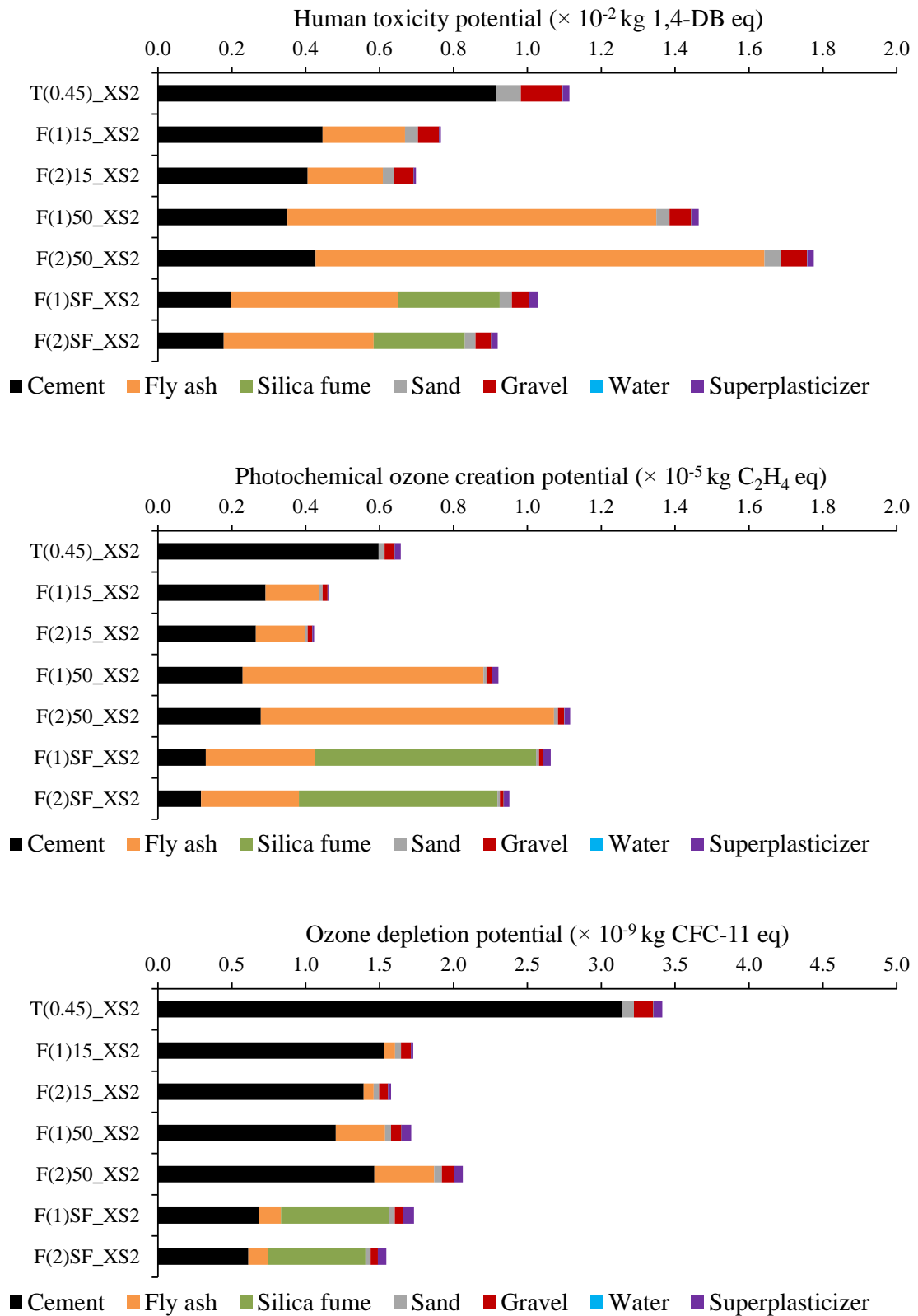


Figure 12.16. Human toxicity, photochemical ozone creation and ozone depletion potentials of the concrete volume per N/mm² of strength and year of t_{ini} (2nd order) (+ t_{crack_1mm}) (XS2), economic allocation (FA: 2.9%, SF: 6.1%).

Abiotic depletion potential – The exploitation of fossil fuels is the main cause for depletion of abiotic resources here. The economically allocated impact of fly ash originates for almost 90% from the mining of hard coal. In case of silica fume, the combined exploitation of hard coal, lignite and crude oil is for more than 95% responsible, while for cement this is the consumption of hard coal, crude oil and natural gas, be it in much smaller amounts per kg.

Freshwater aquatic ecotoxicity potential – For this impact indicator there is again a direct link with the abundant use of hard coal in electricity and MG-silicon production. For fly ash, over 90% of the FAETP value is attributable to the disposal of spoil from coal and lignite mining to surface landfill and the disposal of the tailings from hard coal milling to impoundment storage. It accounts for the leachate to groundwater induced by these practices. The FAETP value of silica fume is governed by the same types of waste treatment. They account for around 85% of the total. For OPC there is an additional contribution of sulfidic tailings disposal besides the disposal of spoil and tailings from coal/lignite mining and coal milling. Together, they comprise around 79% of the total impact. In comparison with the industrial by-products with a low by-product/main product mass ratio this is again much lower.

Marine aquatic ecotoxicity potential – Very similar conclusions can be drawn as for the previous indicator. For fly ash, the disposal of spoil and tailings from coal mining and milling account for more than 90% of the MAETP value. For silica fume, there are few additional important contributions, i.e. the production process of MG-silicon itself, the disposal of sulfidic tailings and the offshore well for marine exploration of fossil fuels. Together, they account for over 90% of the total economically allocated impact. Cement production has the same major impact contributions. They represent a little more than 80% of the total impact.

Terrestrial ecotoxicity potential – Terrestrial ecotoxicity is mainly affected by the disposal of of spoil from hard coal mining and the burning of this hard coal at the power plant. The economically allocated impact of the fly ash is affected accordingly. Around 85% of the TETP value is determined by these practices. This is not the case for silica fume production where around 78% of the TETP value appears to be at the expense of the transmission network for electricity production. With respect to the manufacturing of cement, the clinkering process is the main contributor (72%).

Human toxicity potential – Under the economic allocation principle, fly ash has a human toxicity potential governed by the toxic emissions (e.g. heavy metals) to groundwater due to the disposal of spoil from coal and lignite mining and the disposal of tailings from hard coal milling (68%). In addition, toxic substances emitted (e.g. heavy metals, particulate matter) during the burning of hard coal at the power plant and operation of the freight ship transporting the coal account for 13% and 9% of the total impact. For silica fume production, impact of the disposal of hard coal mining is again the major contributor. However, it only accounts for 23% of the overall human toxicity potential per kg. Apart from that, there are a wide range of small contributions, among which the production process of MG-silicon itself (7%). In cement production, 22% of the HTP value per kg is at the expense of the clinkering process (e.g. particulate matter emissions), again followed by several minor contributions, e.g. disposal of spoil from hard coal mining, disposal of sulfidic tailings, etc.

Photochemical ozone creation potential – Over 90% of POCP value of fly ash is attributable to the emissions to air that result from burning hard coal, operating the transoceanic freight ship that transports the hard coal and mining the hard coal. For silica fume production, the

emissions during the production of charcoal, hard coal coke, natural gas and petroleum coke which are used as fuel at the MG-silicon plant as well as emissions during their transport and those during the MG-silicon production process itself are the main contributors. The emissions during the clinkering process and the production of fossil fuels for heating the cement kiln determine to a large extent (78%) the POCP value of 1 kg OPC.

Ozone depletion potential – The ozone depletion potentials for 1 kg FA, SF and OPC are all very small. Still, the reported ODP values differ considerably for all three materials. Fly ash barely has an impact on this category. The highest contributions result from the production of crude oil and transport of natural gas used in secondary processes indirectly related with coal fired electricity production (e.g. the transoceanic transport of coal). For silica fume, the impacts are obviously much higher because the production process of MG-silicon involves the direct use of crude oil derived petroleum cokes as combustible. Over 90% of the impact originates from the production of crude oil. This also holds true for cement production. Still, the overall value for the cement related ozone depletion potential is smaller than the one for silica fume, yet higher than the one for fly ash.

All in all, it can be concluded that the other baseline impact indicators besides the global warming potential are substantially higher for fly ash and silica fume than for cement. The main cause for this lies in the fact that main industries responsible for producing these by-products also rely to large extent on fossil fuels, even more than the cement industry. The use of resources and emissions related to the exploitation and combustion of these fuels still have a non-negligible effect on abiotic depletion, acidification, eutrophication, freshwater and marine aquatic ecotoxicity, terrestrial ecotoxicity, human toxicity, photochemical oxidation and ozone depletion when using the economic allocation approach. In addition, the low by-product/main product mass ratios amplify the environmental effects assigned to fly ash and silica fume even more. As a consequence, there is seldomly an environmental benefit with respect to these impact categories from the moment large amounts of these materials are being applied in concrete. This is especially true for exposure class XC3/4. In exposure class XS2 a considerable reduction in impact in comparison with the OPC reference is sometimes possible (e.g. with respect to terrestrial ecotoxicity and ozone layer depletion). This is mainly due to the poor service life performance of the OPC reference (< 50 years) which is considered in the functional unit definition. It should also be noted that within exposure class XS2 the k-value conforming FA references show a much better environmental performance than the OPC reference for quite some baseline impact categories (acidification, abiotic depletion, terrestrial ecotoxicity, human toxicity, photochemical oxidation and ozone depletion). Thus, instead of aiming for a concrete with high cement replacement levels in this environment, it might be better to stick to small fly ash additions and use concrete compositions that are in agreement with the k-value concept of NBN B15-001 (2004).

The global warming potential seems a less problematic impact category, yet only when the strength and service life of the alternative concrete compositions are taken into account in exposure class XS2. In exposure class XC3/4, the substantial amount of greenhouse gases assigned to the by-products can only be compensated for in case of a FA+SF composition. A reduced global warming potential in comparison with the applicable references for exposure classes XC3/4 is not possible for HVFA concrete.

12.2.5. Damage oriented impacts of the required concrete volume

Eco-indicator 99 was used to estimate the damage oriented impact for the concrete volume per unit of strength and service life (t_{ini} (2nd order) (+ $t_{crack_1\text{ mm}}$)) in exposure class XC3/4 (Figure 12.17) and XS2 (Figure 12.18).

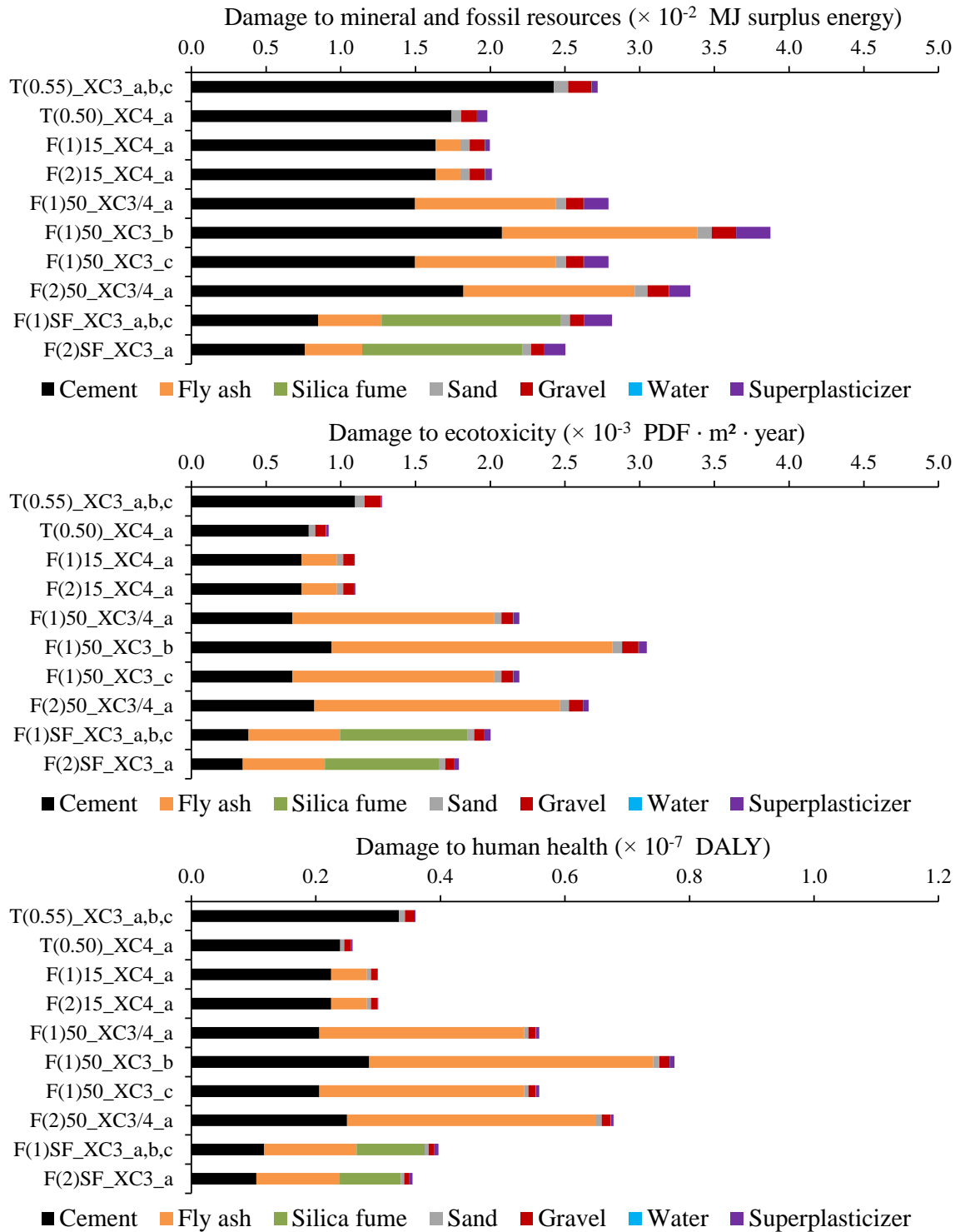


Figure 12.17. Damage to mineral and fossil resources, ecotoxicity and human health of the concrete volume per N/mm² of strength and year of t_{ini} (2nd order) (+ $t_{crack_1\text{mm}}$) (XC3/4), economic allocation (FA: 2.9%, SF: 6.1%).

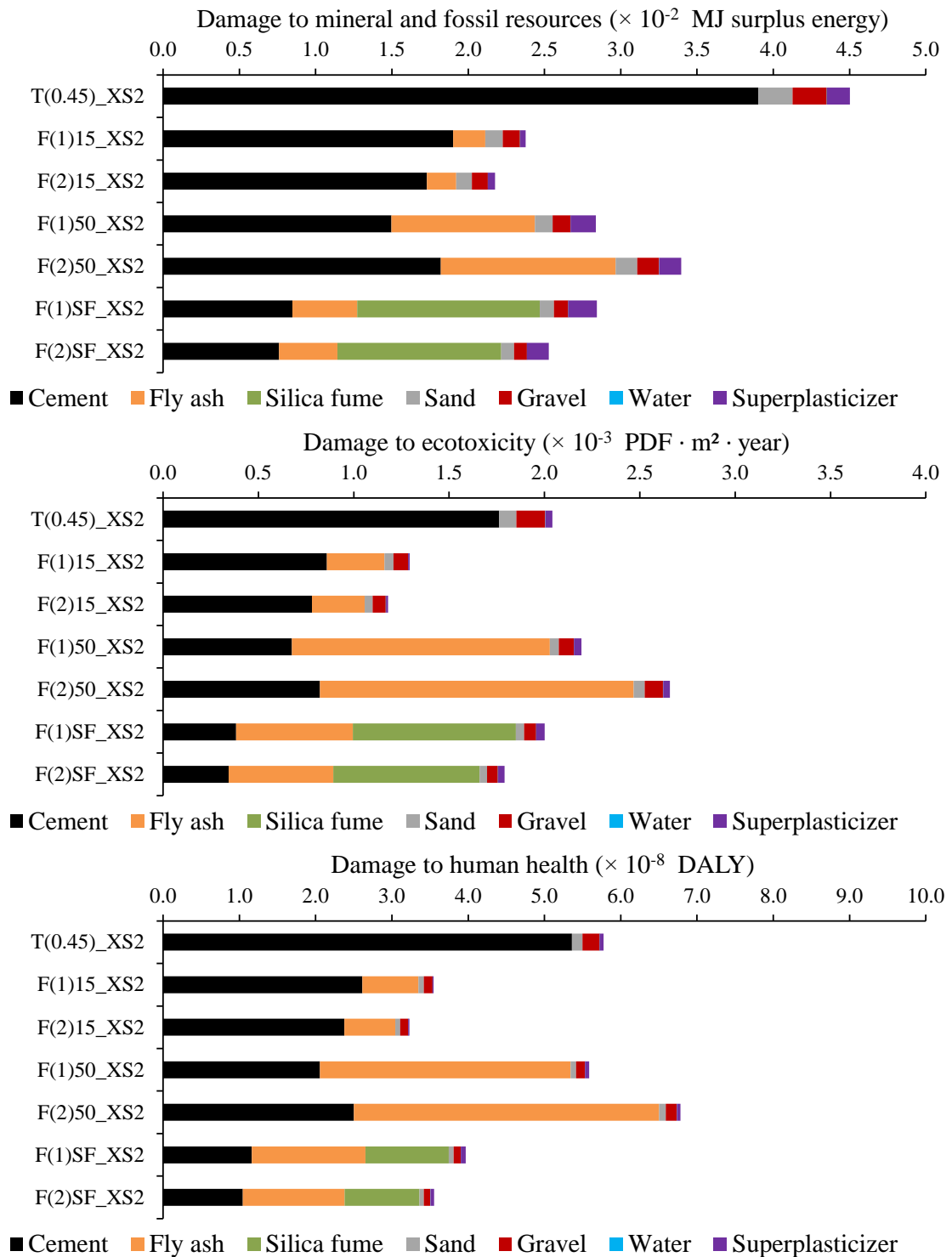


Figure 12.18. Damage to mineral and fossil resources, ecotoxicity and human health of the concrete volume per N/mm² of strength and year of t_{ini} (2nd order) (+ t_{crack_1mm}) (XS2), economic allocation (FA: 2.9%, SF: 6.1%).

This damage oriented impact assessment more or less confirmed the trends that were observed for exposure class XC3/4 using the problem oriented CML 2001 impact method. In comparison with OPC reference T(0.55), the HVFA and FA+SF compositions would cause more damage to mineral and fossil resources, ecotoxicity and human health. The damage

oriented impact assessment gives a more positive outlook for at least the use of FA+SF and k-value conforming FA concrete in exposure class XS2. This is mainly due to the poor service life performance and lower strength of OPC reference T(0.45) and thus the corresponding higher concrete volume per unit of strength and service life. As a consequence, FA+SF and k-value conforming FA concrete impose less damage to all three impact categories, although the benefit may be negligible in terms of the ecotoxicity related impact of the former. In fact, the overall environmental burden seems less critical than after a problem oriented impact assessment for this exposure class.

12.3. Impact of a concrete column with a given load and service life

12.3.1. Summary of the LCA input in SimaPro

Tables 12.4 and 12.5 give the required concrete volumes needed to produce and maintain an axially loaded column for 100 years in exposure classes XC3/4 and XS2.

Table 12.4. Required concrete volume for an axially loaded column with a design service life of 100 years in an environment with exposure to carbonation-induced corrosion.

| Composition | Strength class (-) | Dimensions (mm ²) | Prediction approach | # repairs (-) | FU (m ³) |
|--------------|--------------------|-------------------------------|--|---------------------------------|---|
| T(0.55)_XC3 | C30/37 | 300 × 295 | t _{ini} (1 st order) | 0 ^{a, b} | 2.64 × 10 ^{-1 a, b} |
| | | | + t _{crack_1mm} | 0 ^{a, c} | 2.64 × 10 ^{-1 a, c} |
| | | | t _{ini} (2 nd order) | 0 ^{a, b} | 2.64 × 10 ^{-1 a, b} |
| | | | + t _{crack_1mm} | 0 ^{a, c} | 2.64 × 10 ^{-1 a, c} |
| T(0.50)_XC4 | C45/55 | 300 × 197 | t _{ini} (1 st order) | 0 ^a | 1.76 × 10 ^{-1 a} |
| | | | t _{ini} (2 nd order) | 0 ^a | 1.76 × 10 ^{-1 a} |
| F(1)15_XC4 | C45/55 | 300 × 197 | t _{ini} (1 st order) | 0 ^a | 1.76 × 10 ^{-1 a} |
| | | | t _{ini} (2 nd order) | 0 ^a | 1.76 × 10 ^{-1 a} |
| F(2)15_XC4 | C45/55 | 300 × 197 | t _{ini} (1 st order) | 0 ^a | 1.76 × 10 ^{-1 a} |
| | | | t _{ini} (2 nd order) | 0 ^a | 1.76 × 10 ^{-1 a} |
| F(1)50_XC3/4 | C35/45 | 300 × 253 | t _{ini} (1 st order) | 0 ^a / 4 ^b | 2.27 × 10 ^{-1 a} / 6.33 × 10 ^{-1 b} |
| | | | + t _{crack_1mm} | 0 ^a / 1 ^c | 2.27 × 10 ^{-1 a} / 3.28 × 10 ^{-1 c} |
| | | | t _{ini} (2 nd order) | 0 ^a / 1 ^b | 2.27 × 10 ^{-1 a} / 3.28 × 10 ^{-1 b} |
| | | | + t _{crack_1mm} | 0 ^{a, c} | 2.27 × 10 ^{-1 a, c} |
| F(2)50_XC3/4 | C30/37 | 300 × 295 | t _{ini} (1 st order) | 0 ^a | 2.64 × 10 ^{-1 a} |
| | | | t _{ini} (2 nd order) | 0 ^a | 2.64 × 10 ^{-1 a} |
| F(1)SF_XC3 | C50/60 | 300 × 178 | t _{ini} (1 st order) | 0 ^a / 1 ^b | 1.59 × 10 ^{-1 a} / 2.44 × 10 ^{-1 b} |
| | | | + t _{crack_1mm} | 0 ^{a, c} | 1.59 × 10 ^{-1 a, c} |
| | | | t _{ini} (2 nd order) | 0 ^{a, b} | 1.59 × 10 ^{-1 a, b} |
| | | | + t _{crack_1mm} | 0 ^{a, c} | 1.59 × 10 ^{-1 a, c} |
| F(2)SF_XC3 | C55/67 | 300 × 162 | t _{ini} (1 st order) | 0 ^a | 1.44 × 10 ^{-1 a} |
| | | | t _{ini} (2 nd order) | 0 ^a | 1.44 × 10 ^{-1 a} |

^a t_{ini} without correction for the applied CO₂ concentration and curing conditions.

^b t_{ini} after correction for the applied CO₂ concentration and curing conditions (only XC3).

^c t_{ini} + t_{crack_1 mm} after correction for the applied CO₂ concentration and curing conditions (only XC3).

The reported volumes for the functional unit value comprise the concrete volume needed to initially construct the column as well as the volumes needed to replace the entire concrete

cover on top of the rebars in the course of the 100 year time period when service life is expected to end. In an environment with exposure to carbonation-induced corrosion, the repair volumes only needed to be included for both HVFA composition F(1)50 and FA+SF composition F(1)SF when service life in exposure class XC3 was obtained from a first order prediction of the corrosion initiation period and after correction for the applied CO₂ concentration during carbonation testing and the curing conditions prior to these tests. A second order service life prediction only indicated repair for the HVFA concrete.

Table 12.5. Required concrete volume for an axially loaded column with a design service life of 100 years in an environment with exposure to chloride-induced corrosion.

| Composition | Strength class (-) | Dimensions (mm ²) | Prediction approach | # repairs (-) | FU (m ³) |
|-------------|--------------------|-------------------------------|--|---------------|-------------------------|
| T(0.45)_XS2 | C45/55 | 300 × 197 | t _{ini} (1 st order) | 24 | 3.04 |
| | | | + t _{crack_1mm} | 22 | 2.80 |
| | | | t _{ini} (2 nd order) | 2 | 4.14 × 10 ⁻¹ |
| | | | + t _{crack_1mm} | 2 | 4.14 × 10 ⁻¹ |
| F(1)15_XS2 | C40/50 | 300 × 222 | t _{ini} (1 st order) | 3 | 5.78 × 10 ⁻¹ |
| | | | t _{ini} (2 nd order) | 0 | 1.98 × 10 ⁻¹ |
| F(2)15_XS2 | C45/55 | 300 × 197 | t _{ini} (1 st order) | 3 | 5.34 × 10 ⁻¹ |
| | | | t _{ini} (2 nd order) | 0 | 1.76 × 10 ⁻¹ |
| F(1)50_XS2 | C35/45 | 300 × 253 | t _{ini} (1 st order) | 5 | 9.06 × 10 ⁻¹ |
| | | | + t _{crack_1mm} | 5 | 9.06 × 10 ⁻¹ |
| | | | t _{ini} (2 nd order) | 0 | 2.27 × 10 ⁻¹ |
| | | | + t _{crack_1mm} | 0 | 2.27 × 10 ⁻¹ |
| F(2)50_XS2 | C30/37 | 300 × 295 | t _{ini} (1 st order) | 5 | 1.01 |
| | | | t _{ini} (2 nd order) | 0 | 2.64 × 10 ⁻¹ |
| F(1)SF_XS2 | C50/60 | 300 × 178 | t _{ini} (1 st order) | 0 | 1.59 × 10 ⁻¹ |
| | | | + t _{crack_1mm} | 0 | 1.59 × 10 ⁻¹ |
| | | | t _{ini} (2 nd order) | 0 | 1.59 × 10 ⁻¹ |
| | | | + t _{crack_1mm} | 0 | 1.59 × 10 ⁻¹ |
| F(2)SF_XS2 | C55/67 | 300 × 162 | t _{ini} (1 st order) | 0 | 1.44 × 10 ⁻¹ |
| | | | t _{ini} (2 nd order) | 0 | 1.44 × 10 ⁻¹ |

In exposure class XS2, a first order prediction of the corrosion initiation period requires the inclusion of concrete repair volumes for all mixtures except for the FA+SF compositions. The number of repair volumes is particularly high for OPC reference T(0.45). A second order prediction of the corrosion initiation period eliminates the repair volumes for all concrete compositions except for the same OPC reference. For this mixture still two repair volumes needed to be considered.

12.3.2. Global warming potential of the concrete column

12.3.2.1. In exposure class XC3/4

Figures 12.19 and 12.20 give GWP values for the columns made from each studied concrete composition with inclusion of the impacts associated with four reinforcement bars (Ø 12 mm, length 3.0 m) and the required repair volumes over time.

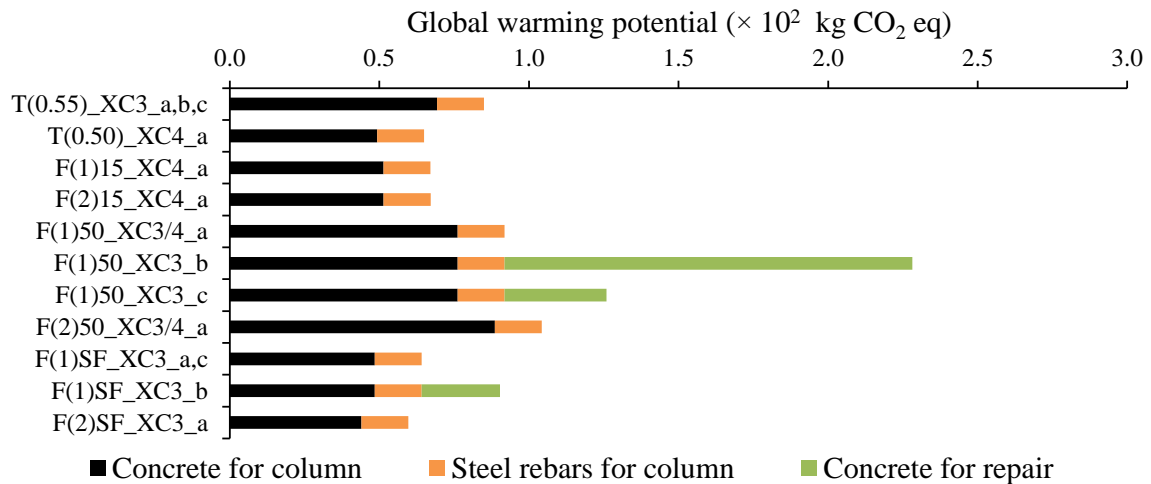


Figure 12.19. Global warming potential of an axially loaded column with a 100 year design service life (t_{ini} (1st order) (+ t_{crack_1mm})) in exposure class XC3/4, economic allocation (FA: 2.9%, SF: 6.1%).

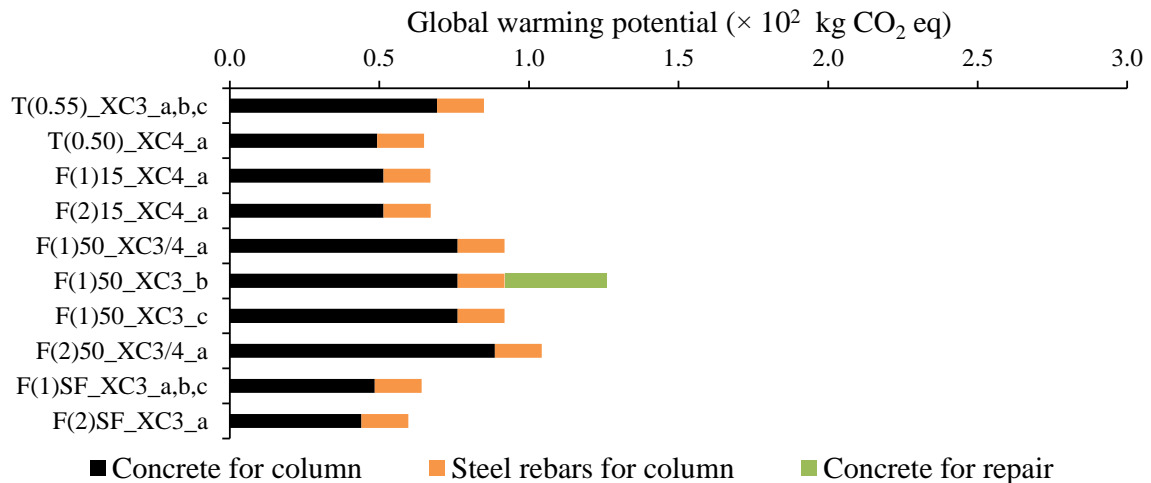


Figure 12.20. Global warming potential of an axially loaded column with a 100 year design service life (t_{ini} (2nd order) (+ t_{crack_1mm})) in exposure class XC3/4, economic allocation (FA: 2.9%, SF: 6.1%).

More or less the same trends are observed as for the previously considered functional unit, i.e. the required concrete volume per unit of strength and service life (Section 12.2.2.1). When no repair is believed to be necessary based on a first or second order prediction of the corrosion initiation period, all or not in combination with the time to unacceptable concrete cracking, only the proposed FA+SF concrete compositions have a reduced global warming potential in comparison with the OPC reference for exposure class XC3 (GWP -25-30%). The HVFA mixtures have a pronounced higher impact on the greenhouse gas effect than this reference. Note that the four reinforcement bars used to manufacture the column contribute substantially (15 to 27% of the overall GWP value) to the overall GWP value per concrete column. This demonstrates that concrete is not the only commonly used construction material with a negative impact on global warming.

12.3.2.2. In exposure class XS2

As can be seen in Figures 12.21 and 12.22, the differences between mixtures in exposure class XS2 are comparable to those obtained when considering the concrete volume per unit of strength and service life as functional unit (Section 12.2.2.2).

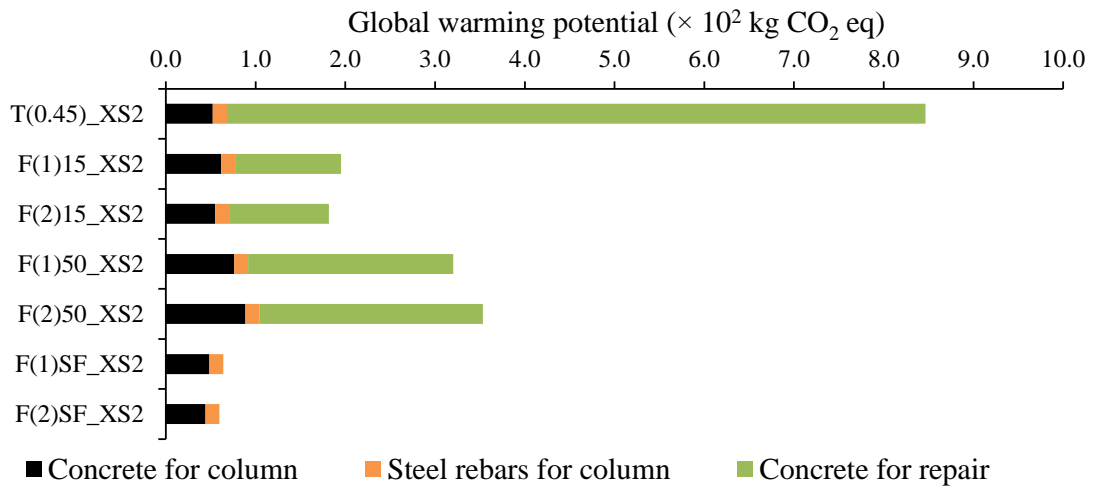


Figure 12.21. Global warming potential of an axially loaded column with a 100 year design service life (t_{ini} (1st order) (+ t_{crack_1mm})) in exposure class XS2, economic allocation (FA: 2.9%, SF: 6.1%).

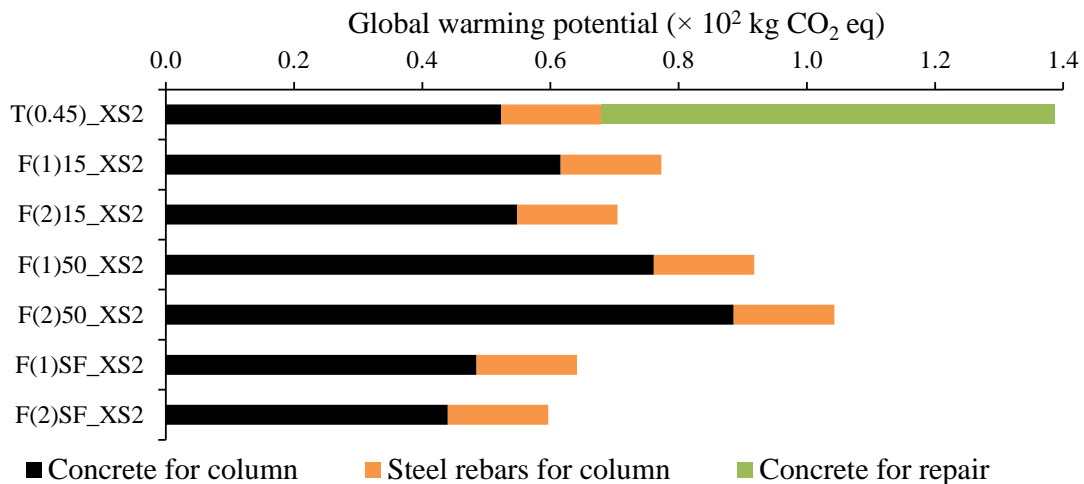


Figure 12.22. Global warming potential of an axially loaded column with a 100 year design service life (t_{ini} (2nd order) (+ t_{crack_1mm})) in exposure class XS2, economic allocation (FA: 2.9%, SF: 6.1%).

The large number of repairs (22) expected within the 100 year life span for the column made with OPC reference T(0.45) when based upon a first order prediction approach, imposes a huge global warming potential on the composition (Figure 12.21). Since the repair frequency is much lower for the columns made with HVFA concrete, there is a substantial environmental benefit for this concrete type (GWP -58-62%) when compared with the column made with the OPC reference. On the other hand, when the k-value conforming FA references with an even lower repair frequency are seen as the appropriate reference, there is

no benefit. The FA+SF columns, which require no repair at all, turn out beneficial when compared with the columns made with compositions T(0.45) (GWP -92-93%), F(1)15 (GWP -77%) or F(2)15 (GWP -79%).

The second order prediction of t_{ini} reduces number of repairs for the column made with the OPC reference from over 20 to only 2. This results in an important decrease in environmental benefit for the HVFA and FA+SF columns (Figure 12.22). Yet, reduced GWP values remain substantial for both concrete types (HVFA: GWP -25-34%, FA+SF: GWP -54-57%). With mixtures F(1)15 or F(2)15 as reference composition, there is no advantage of using HVFA concrete for the construction of the considered column. There still is for FA+SF concrete (GWP -15-17%). The benefit of using mixtures F(1)15 and F(2)15 instead of the OPC reference in exposure class XS2 is also worth mentioning (GWP -44-49%).

12.4. Impact of a concrete slab with a given load and service life

12.4.1. Summary of the LCA input in SimaPro

Tables 12.6 and 12.7 give the required concrete volumes for the initial construction of a slab with a uniformly distributed load and its maintenance for 100 years.

Table 12.6. Required concrete volume for a slab with a uniformly distributed load and a service life of 100 years in an environment with exposure to carbonation-induced corrosion.

| Composition | Strength class (-) | Dimensions (mm ²) | Prediction approach | # repairs (-) | FU (m ³) |
|-------------|--------------------|-------------------------------|-----------------------------------|----------------------------------|---|
| T(0.55)_XC3 | C30/37 | 1000 × 165 5 × Ø 16 mm | t_{ini} (1 st order) | 0 ^{a, b} | $8.20 \times 10^{-1 a, b}$ |
| | | | + t_{crack_1mm} | 0 ^{a, c} | $8.20 \times 10^{-1 a, c}$ |
| | | | t_{ini} (2 nd order) | 0 ^{a, b} | $8.20 \times 10^{-1 a, b}$ |
| | | | + t_{crack_1mm} | 0 ^{a, c} | $8.20 \times 10^{-1 a, c}$ |
| T(0.50)_XC4 | C45/55 | 1000 × 150 6 × Ø 16 mm | t_{ini} (1 st order) | 0 ^a | $7.44 \times 10^{-1 a}$ |
| | | | t_{ini} (2 nd order) | 0 ^a | $7.44 \times 10^{-1 a}$ |
| F(1)15_XC4 | C45/55 | 1000 × 150 6 × Ø 16 mm | t_{ini} (1 st order) | 0 ^a | $7.44 \times 10^{-1 a}$ |
| | | | t_{ini} (2 nd order) | 0 ^a | $7.44 \times 10^{-1 a}$ |
| F(2)15_XC4 | C45/55 | 1000 × 150 6 × Ø 16 mm | t_{ini} (1 st order) | 0 ^a | $7.44 \times 10^{-1 a}$ |
| | | | t_{ini} (2 nd order) | 0 ^a | $7.44 \times 10^{-1 a}$ |
| F(1)50_XC3 | C35/45 | 1000 × 155 6 × Ø 16 mm | t_{ini} (1 st order) | 0 ^{a / 4} ^b | $7.69 \times 10^{-1 a} / 1.47$ ^b |
| | | | + t_{crack_1mm} | 0 ^{a / 1} ^c | $7.69 \times 10^{-1 a} / 9.44 \times 10^{-1 c}$ |
| | | | t_{ini} (2 nd order) | 0 ^{a / 1} ^b | $7.69 \times 10^{-1 a} / 9.44 \times 10^{-1 b}$ |
| | | | + t_{crack_1mm} | 0 ^{a, c} | $7.69 \times 10^{-1 a, c}$ |
| F(2)50_XC3 | C30/37 | 1000 × 165 5 × Ø 16 mm | t_{ini} (1 st order) | 0 ^a | $8.20 \times 10^{-1 a}$ |
| | | | t_{ini} (2 nd order) | 0 ^a | $8.20 \times 10^{-1 a}$ |
| F(1)SF_XC3 | C50/60 | 1000 × 140 6 × Ø 16 mm | t_{ini} (1 st order) | 0 ^a or 1 ^b | $6.94 \times 10^{-1 a} / 8.69 \times 10^{-1 b}$ |
| | | | + t_{crack_1mm} | 0 ^{a, c} | $6.94 \times 10^{-1 a, c}$ |
| | | | t_{ini} (2 nd order) | 0 ^{a, b} | $6.94 \times 10^{-1 a, b}$ |
| | | | + t_{crack_1mm} | 0 ^{a, c} | $6.94 \times 10^{-1 a, c}$ |
| F(2)SF_XC3 | C55/67 | 1000 × 135 6 × Ø 16 mm | t_{ini} (1 st order) | 0 ^a | $6.69 \times 10^{-1 a}$ |
| | | | t_{ini} (2 nd order) | 0 ^a | $6.69 \times 10^{-1 a}$ |

^a t_{ini} without correction for the applied CO₂ concentration and curing conditions.

^b t_{ini} after correction for the applied CO₂ concentration and curing conditions (only XC3).

^c $t_{ini} + t_{crack_1 mm}$ after correction for the applied CO₂ concentration and curing conditions (only XC3).

Depending on the underlying service life prediction approach, these concrete volumes can vary per mixture. Unlike for a column, the dimensioning of a slab is influenced by the exposure class dependent concrete cover criteria (XC3: 35 mm, XC4: 40 mm and XS2: 50 mm). As a result, for a fixed strength class of concrete, the slab dimensioning can still vary with the exposure class. The concrete volumes reported in Table 12.6 for mixtures T(0.55), F(1)50, F(2)50, F(1)SF and F(2)SF refer to slabs designed in accordance with the 35 mm criterion cf. their corresponding exposure class. For mixtures T(0.50), F(1)15 and F(2)15, the required 40 mm concrete cover for exposure class XC4 was adopted. Although mixtures F(1)50 and F(2)50 were also tested in the simulated XC4 environment, the resulting service life performance turned out much less critical than in the simulated XC3 environment. There, repairs over time can be necessary when using first order prediction of the corrosion initiation period with correction for the applied high CO₂ concentration during carbonation testing and for suboptimal curing conditions in practice. For this reason, the focus remained on exposure class XC3 and the slabs were designed accordingly. In table 12.7, all reported concrete volumes relate to slabs with a 50 mm concrete cover on top the rebars as required for exposure class XS2. These concrete volumes vary again with the underlying service life prediction approach (1st order versus 2nd order).

Table 12.7. Required concrete volume for a slab with a uniformly distributed load and a service life of 100 years in an environment with exposure to chloride-induced corrosion.

| Composition | Strength Class (-) | Dimensions (mm ²) | Prediction approach | # repairs (-) | FU (m ³) |
|-------------|--------------------|-------------------------------|--|---------------|-------------------------|
| T(0.45)_XS2 | C45/55 | 1000 × 160 6 × Ø 16 mm | t _{ini} (1 st order) | 24 | 6.79 |
| | | | + t _{crack_1mm} | 22 | 6.29 |
| | | | t _{ini} (2 nd order) | 2 | 1.29 |
| | | | + t _{crack_1mm} | 2 | 1.29 |
| F(1)15_XS2 | C40/50 | 1000 × 165 6 × Ø 16 mm | t _{ini} (1 st order) | 3 | 1.57 |
| | | | t _{ini} (2 nd order) | 0 | 8.19 × 10 ⁻¹ |
| F(2)15_XS2 | C45/55 | 1000 × 160 6 × Ø 16 mm | t _{ini} (1 st order) | 3 | 1.54 |
| | | | t _{ini} (2 nd order) | 0 | 7.94 × 10 ⁻¹ |
| F(1)50_XS2 | C35/45 | 1000 × 175 6 × Ø 16 mm | t _{ini} (1 st order) | 5 | 2.12 |
| | | | + t _{crack_1mm} | 5 | 2.12 |
| | | | t _{ini} (2 nd order) | 0 | 8.69 × 10 ⁻¹ |
| | | | + t _{crack_1mm} | 0 | 8.69 × 10 ⁻¹ |
| F(2)50_XS2 | C30/37 | 1000 × 185 5 × Ø 16 mm | t _{ini} (1 st order) | 5 | 2.17 |
| | | | t _{ini} (2 nd order) | 0 | 9.20 × 10 ⁻¹ |
| F(1)SF_XS2 | C50/60 | 1000 × 155 6 × Ø 16 mm | t _{ini} (1 st order) | 0 | 7.69 × 10 ⁻¹ |
| | | | + t _{crack_1mm} | 0 | 7.69 × 10 ⁻¹ |
| | | | t _{ini} (2 nd order) | 0 | 7.69 × 10 ⁻¹ |
| | | | + t _{crack_1mm} | 0 | 7.69 × 10 ⁻¹ |
| F(2)SF_XS2 | C55/67 | 1000 × 150 7 × Ø 16 mm | t _{ini} (1 st order) | 0 | 7.43 × 10 ⁻¹ |
| | | | t _{ini} (2 nd order) | 0 | 7.43 × 10 ⁻¹ |

Apart from the effect of the applied concrete cover, there is another difference with column design. Considering a different strength class for the concrete not only affects the thickness of the slab. It can also result in a higher or lower number of rebars in the tensile zone of the slab.

This means that the impact of these rebars needs to be included in the LCA study. Besides those rebars, there is evidently more reinforcing steel present in each slab (upper reinforcements, shear reinforcements, etc.). Since this steel content is more or less the same in all slabs, only the rebars in the tensile zone were considered in the calculation of the global warming potential.

12.4.2. Global warming potential of the concrete slab

12.4.2.1. In exposure class XC3/4

When calculated for a concrete slab, the differences in GWP between mixtures seem to have become smaller (Figures 12.23-12-24).

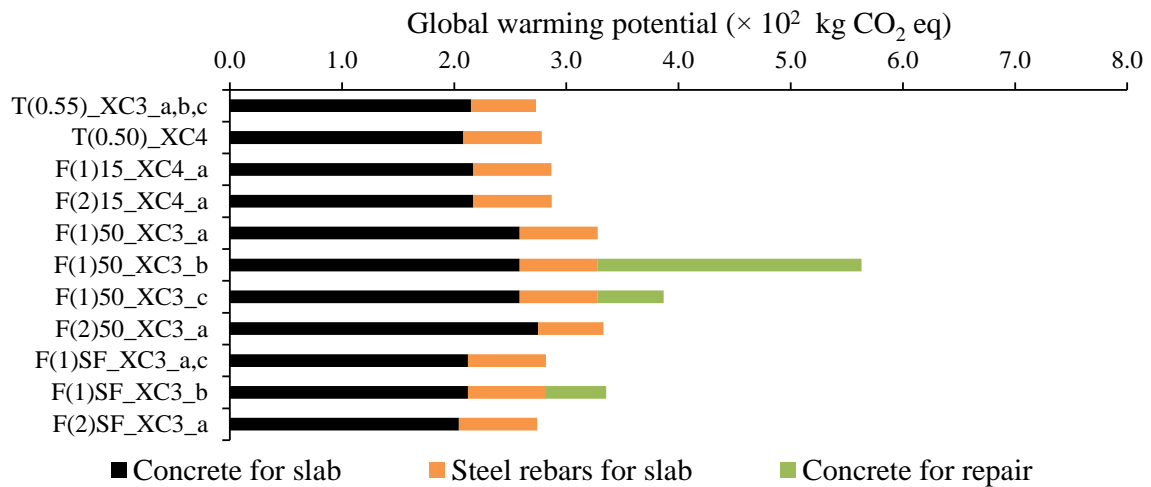


Figure 12.23. Global warming potential of a uniformly loaded slab with a 100 year design service life (t_{ini} (1st order) (+ t_{crack_1mm})) in exposure class XC3/4, economic allocation (FA: 2.9%, SF: 6.1%).

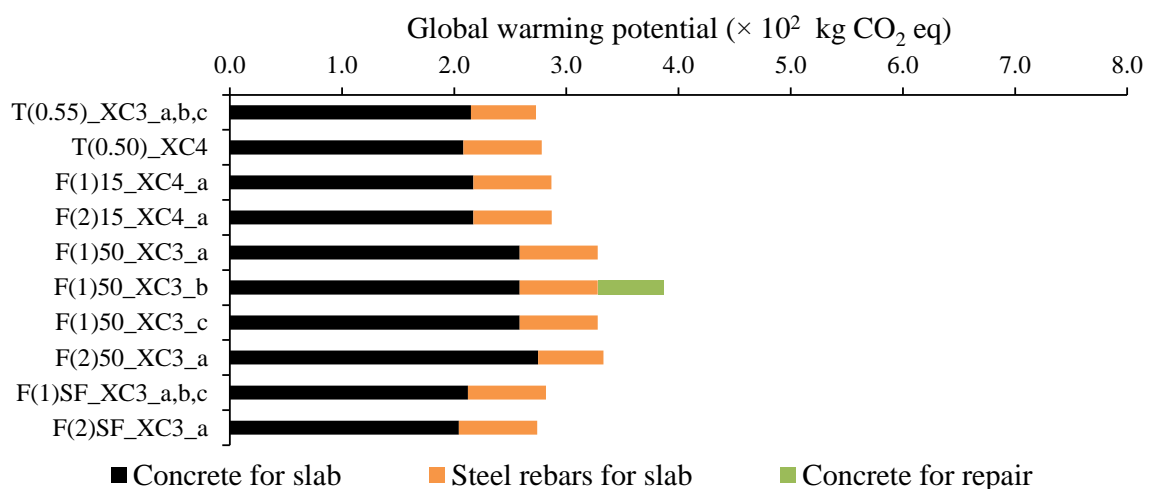


Figure 12.24. Global warming potential of a uniformly loaded slab with a 100 year design service life (t_{ini} (2nd order) (+ t_{crack_1mm})) in exposure class XC3/4, economic allocation (FA: 2.9%, SF: 6.1%).

This is mainly due to the fact that under the given uniformly distributed load the slab is subject to bending. As a consequence the structural height of the element is of importance. This implies that an increase in concrete strength does not automatically result in an important reduction of the slab thickness. When reduced too much by using a high strength concrete, the use of more reinforcing steel becomes necessary to compensate for the reduced structural height of the slab. When looking at GWPs associated with a first and second order service life prediction (Figure 12.23 and 12.24, respectively), the environmental benefit of the repair-free FA+SF compositions is negligible in comparison with OPC reference T(0.55). This is in sharp contrast with the previously considered functional units. For the concrete volume per unit of strength and service life as well as for the concrete column, still pronounced reductions in global warming potential could be recorded for repair-free FA+SF concrete. In slab design, the high strength of this concrete type cannot be sufficiently valorized. For the repair-free HVFA compositions, conclusions drawn from studying the other functional units remain valid. Mixtures F(1)50 and F(2)50 do not have the potential to reduce concrete related greenhouse gas emissions in this particular environment.

12.4.2.2. In exposure class XS2

With a slab as functional unit, a first order prediction of $t_{ini} + t_{crack_1\text{ mm}}$ in exposure class XS2 results in GWP values for HVFA and FA+SF concrete that are much lower than for OPC reference T(0.45) (Figure 12.25). The GWP reductions that are achieved that way amount to 60% and 84% respectively. In comparison with the k-value conforming FA references F(1)15 and F(2)15 there is only an environmental benefit for the FA+SF concrete (GWP –44-45%).

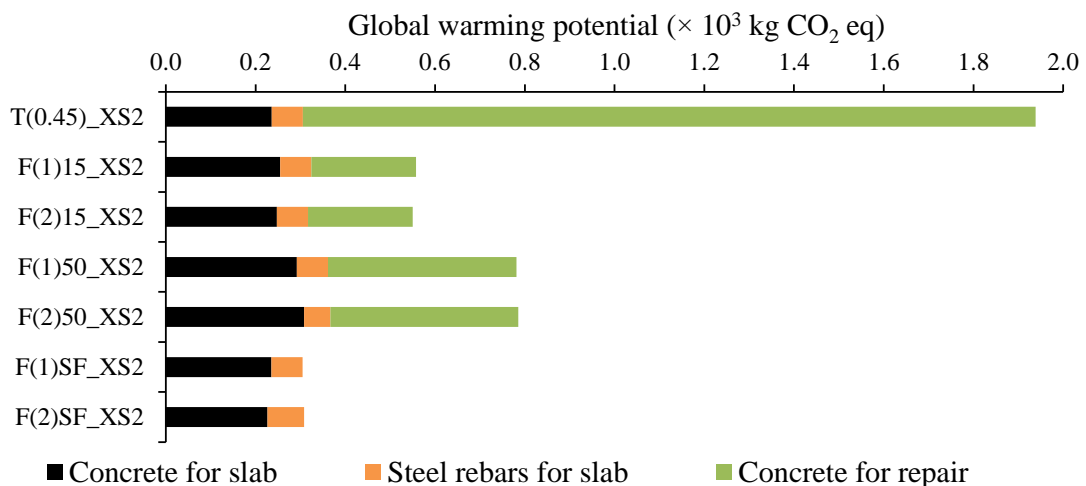


Figure 12.25. Global warming potential of a uniformly loaded slab with a 100 year design service life (t_{ini} (1st order) (+ t_{crack_1mm})) in exposure class XS2, economic allocation (FA: 2.9%, SF: 6.1%).

Since the second order prediction approach indicated that much less repairs are needed for the OPC reference within a timeframe of 100 years, both alternative concrete types turn out much less advantageous in comparison with the OPC reference (Figure 12.26: HVFA: GWP –19-20%, FA+SF: GWP –32-33%). The benefit of the FA+SF compositions in comparison with

mixtures F(1)15 and F(2)15 has become rather negligible (GWP $-3-6\%$). The relatively small benefits obtained for FA+SF concrete are again mainly attributable to the fact that the high strengths of these mixtures cannot really be valorized in slab design. Thus, depending on the specific loading conditions, not every strength gain can be accounted for in the environmental score.

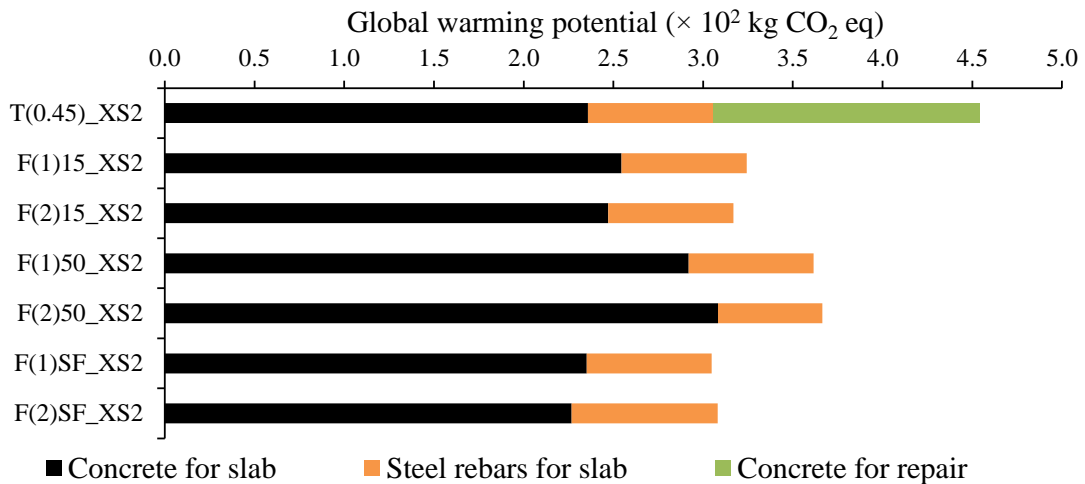


Figure 12.26. Global warming potential of a uniformly loaded slab with a 100 year design service life (t_{ini} (2nd order) (+ t_{crack_1mm})) in exposure class XS2, economic allocation (FA: 2.9%, SF: 6.1%).

12.4.3. Influence of active crack width control

In Section 6.5.7 it was concluded that MBE mortar specimens representing concrete mixtures T(0.45) and F(2)SF and containing an artificial 0.3 mm wide crack, could not really be treated as uncracked. Despite the fact that such a crack is in agreement with the maximum allowable crack width specified in Eurocode 2, increased chloride ingress could be observed in the vicinity of the artificial crack after a chloride migration test. Moreover, reducing the artificial crack width to only 0.1 mm, could still not guarantee a seemingly uncracked condition of the material. Apparently, even stricter crack width criteria need to be imposed to avoid that the cracks offer direct pathways for the penetrating chlorides. A 0.05 mm wide crack which could probably be healed in an autogenous way, was suggested as alternative crack width criterion in Section 6.5.7.3. When designed accordingly, the seemingly uncracked condition may exist. Under these conditions, the outcome of the applied empirical service life prediction models specifically developed for uncracked concrete still makes sense. Evidently, this design approach will have its implications on the amount of reinforcing steel needed and therefore on the global warming potential of the slab. To evaluate the effect of the additional reinforcing steel, the slabs made with compositions T(0.45) and F(2)SF were once redesigned for exposure class XS2. With the initial 6 or 7 rebars (\varnothing : 16 mm), the characteristic crack widths for the two slabs in the tensile zone amounted to 0.21 mm and 0.18 mm, respectively. To meet the 0.05 mm crack width criterion, the required number of rebars would need to be no less than 16 and 17, respectively. Figure 12.27 gives a comparison of the global warming

potentials for the slabs with the initial and increased number of rebars. Their values are based on a second order prediction of the corrosion initiation period.

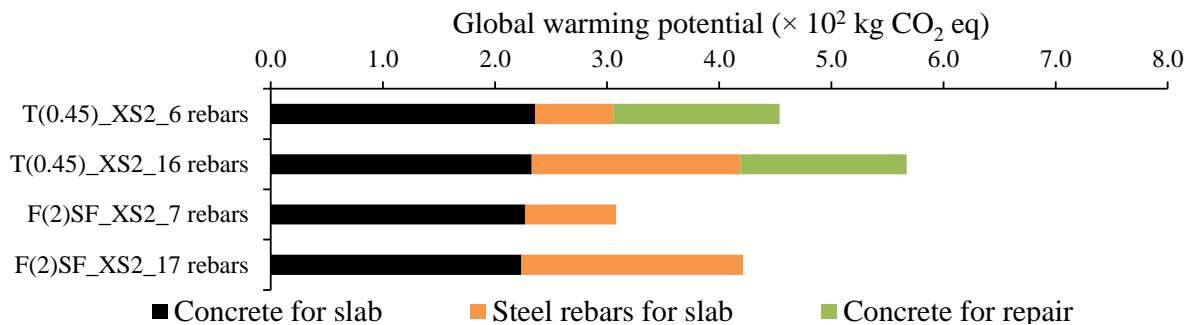


Figure 12.27. Effect of using additional reinforcing steel on the global warming potential of slabs made with compositions T(0.45) and F(2)SF having a 100 year design service life (t_{ini} (2nd order) + t_{crack_1mm}) in exposure class XS2, economic allocation (FA: 2.9%, SF: 6.1%).

The extra reinforcing steel makes the GWP values of the slabs increase with 25% and 37%, respectively. One should be aware of this when doing LCA calculations based on service life predictions for uncracked concrete.

For practical and economical reasons structure design in accordance with a very strict crack width criterion may not be feasible. If so, the currently available service life prediction models for uncracked concrete seem not very useful. In other words, there is a real need for improving these models to make them account for the unavoidable cracking phenomena that occur in practice.

12.5. Conclusions

In conclusion, the environmental benefit achievable with the proposed HVFA and FA+SF concrete compositions depends a lot on the functional unit choice, the applicable reference concrete, the allocation principles applied, the exposure class and the considered environmental effects.

- When focussing on the global warming potential per m³ of concrete, there is only a substantial reduction in GWP value for both concrete types possible when only the impact of the basic by-product treatment (drying + storage) after production is accounted for. With no impact of the main industries allocated to them, the HVFA compositions have GWP values which are 16 to 28% lower than the corresponding values of the OPC references. In comparison with the k-value conforming FA references the benefits are rather similar (GWP -17-23%). The greenhouse gas emissions related to the FA+SF compositions are even lower (-29-39%).
- With a mass allocated impact of coal fired electricity and MG-silicon production assigned to the fly ash and the silica fume, both alternative concrete types are characterized by a much higher environmental burden than the reference concrete types. This is mainly due to the low by-product/main product production ratios, especially with respect to the fly ash. Allocation by economic value, which is the more commonly accepted allocation principle, results in little or no benefit for 1 m³ of HVFA or FA+SF concrete. The

increasing prices of the by-products are mainly responsible for a higher allocation coefficient and thus a higher impact of concrete compositions containing considerable portions of these by-products. Obviously, the prices of by-products depend very much on the local context. For instance, in countries like China and India where fly ash is abundantly available, the selling prices of fly ash are probably much lower than 35 €/ton. As a result, the applicable economic allocation coefficients for these countries are probably much lower, perhaps even lower than the 1% suggested by Chen et al. (2010b). The resulting impacts for concrete containing large portions of fly ash may be much more acceptable.

- Choosing the amount of concrete needed to achieve one unit of strength and service life as functional unit, still results in reduced global warming potentials for the HVFA and FA+SF concrete under the assumption of the economic allocation principle. Still, a lot depends on the considered exposure class.
- In exposure class XC3/4 where practically all considered concrete mixtures can have an adequate service life performance (100 years or more) the strength of the concrete is the determining factor for the global warming potential of the concrete. HVFA concrete is the only exception. In case first or second order prediction of the corrosion initiation period for this composition is done with correction for the applied high CO₂ concentration during carbonation testing and the optimal curing conditions, time spans lower than 100 years are possible. This in combination with the equal or lower strength of HVFA concrete in comparison with the references, is responsible for the fact that no reduction in GWP value can be achieved for this mixture in this particular environment. This remains possible for the high strength FA+SF concrete, yet only when compared with the OPC reference for exposure class XC3 (GWP -28-36%).
- In exposure class XS2, more substantial benefits (HVFA: GWP -20-35%, FA+SF: GWP -55-60%) can be obtained because of the rather poor service life performance of the OPC reference (< 50 years, even when based upon a second order prediction). In comparison with the k-value conforming FA references, there is only a small GWP reduction possible for FA+SF concrete (GWP -19-21%). Moreover, the k-value conforming FA references with a fly ash content of only 15% seem actually a better alternative to the OPC reference (GWP -45-50%) than the concrete compositions with high cement replacement levels.
- The impacts associated with the production of the concrete constituents govern the overall global warming potential of a concrete composition. Transport of the concrete constituents to the concrete plant and the operation of the plant only contribute to a minor extent (10-15%).
- The incorporation of fly ash and silica fume in concrete has a very negative effect on other environmental problems when the impacts assigned to the by-products are economically allocated. In comparison with cement, both by-products are characterized by substantially higher acidification, eutrophication, abiotic depletion, freshwater/marine aquatic ecotoxicity, terrestrial ecotoxicity, human toxicity, ozone depletion and photochemical ozone creation potentials. This is mainly due to the fact that coal fired electricity and Si-metal/MG-silicon production depend even more than cement on the exploitation and combustion of fossil fuels which have an adverse effect on all these impact categories. Similar conclusions can be drawn from a damage oriented impact assessment. Clearly, the

current focus of the concrete industry on reducing greenhouse gas emissions most definitely needs to be broadened in the near future. The question may also rise whether the now applied economic allocation coefficients for fly ash and silica fume are not too high. In Chapter 11, it was mentioned that lowering the economic allocation coefficient to only 0.2% for both by-products could guarantee that the impacts assigned to each of the ten CML 2001 baseline impact categories per kg by-product would be equal or lower than the corresponding impacts of ordinary Portland cement. These allocation coefficients correspond with selling prices for fly ash and silica fume of only 2.3 €/ton and 23 €/ton, respectively. These are much lower than the currently reported prices (FA: 20-35 €/ton, SF: 400-750 €/ton) for France and Belgium. It is not certain whether policymakers can impose such strict price criteria in order to further stimulate the enduring use of fly ash and silica fume in the concrete industry when aiming at the replacement of large portions of the cement. If achievable, then a better strength and service life performance of the concrete with high cement replacement levels would automatically imply an additional environmental benefit for every CML 2001 baseline impact category. However, one should remain aware of the fact that deliberately aiming for very low allocation coefficients just to prove that fly ash and silica fume are 'green' materials, may not be in terms with the concept of sustainability. If there is indeed an important environmental burden to be assigned to fly ash and silica fume, this should be done. If this means that considerably less of these materials can be used in concrete for environmental reasons, so be it.

- An axially loaded concrete column as functional unit gives a very similar reduction in global warming potential as the required concrete volume per unit of strength and service life. On the other hand, a slab subject to bending as functional unit gives a lower GWP reduction for FA+SF concrete because its high strength cannot fully be valorized in the slab design. In exposure class XC3, there is no benefit anymore, while in exposure class XS2, the benefit in comparison with the OPC reference has reduced to only 32-33% under the assumption of the more correct second order service life prediction approach.
- The currently applied service life prediction models need to be improved to account for the unavoidable presence of cracks in concrete. The application of more reinforcing steel to reduce the characteristic crack width to a seemingly uncracked condition makes the global warming potential of a slab increase with 25 to 37%.

PART V

CONCLUSIONS

Main research findings

13.1. HVFA and FA+SF concrete

In literature, replacing large portions of cement by industrial by-products in concrete is often recommended because cement related CO₂ emissions can be reduced significantly that way. The development of High-Volume Fly Ash concrete in the 1980s is seen as an extreme example of this premise. With at least 50% of the cement replaced by pozzolanic fly ash, CO₂ emissions could in theory be reduced with a percentage comparable to the cement replacement level. In this perspective, the material has been applied in mainly less demanding concrete applications such as foundations, etc.

In this research, it was investigated whether HVFA concrete could also be used in more demanding concrete environments, for instance as reinforced concrete susceptible to carbonation- or chloride-induced steel corrosion or in outdoor concrete applications subject to freeze/thaw attack in combination with deicing salts. A sustainable use of the material under these exposure conditions requires that the material shows at least a comparable performance in terms of strength and durability with more traditional concrete. The experimental characterization of the OPC and k-value conforming FA references for exposure classes XC3, XC4, XS2 and XF4 cf. NBN B15-001 (2004) and NBN EN 206-1 (2000) showed that it may not be evident to achieve the same experimental strength class with ordinary HVFA concrete containing 50% fly ash. Increasing the total binder content to 450 kg/m³ and lowering the W/B ratio to 0.35 could only in part compensate for the slow strength development of HVFA concrete. Thus, a sustainable use of such a HVFA concrete composition could only result from an excellent durability performance which should compensate for its high total binder content and moderate early age strength performance.

To cope with this problem, it was decided to introduce 10% silica fume as third powder. In combination with 40% fly ash and 50% OPC a total binder content of only 340 kg/m³ could be maintained without a strength loss at the age of 28 days. With a strength class of C50/60 up to C55/67, the FA+SF concrete shows even a better experimental strength performance than the OPC reference with the highest cement content and lowest W/C ratio, i.e. T(0.45) (C45/55). Thus, in case of FA+SF concrete, there is a strength benefit that could contribute to the sustainability of the material as well. In combination with an excellent durability

performance in the studied environments, the proposed FA+SF concrete could be more sustainable than the HVFA concrete.

13.2. Resistance to carbonation

Equivalent performance in terms of carbonation resistance cf. NBN B15-100 (2008) could not be confirmed for the HVFA and the FA+SF concrete.

In exposure class XC3, both concrete types were characterized by field carbonation rates which exceeded those of the OPC reference. This conclusion remained valid regardless whether the carbonation rate was determined colorimetrically or microscopically. The field carbonation coefficients estimated from an accelerated carbonation test at 10% CO₂ after 28 days of optimal curing amounted to 2.2 mm/√years. The FA+SF concrete showed a lower carbonation coefficient of 1.4 mm/√years. Still, this remains higher than the corresponding value of the applicable OPC reference (0.7-0.9 mm/√years). Moreover, the carbonation resistance of HVFA and FA+SF concrete is susceptible to suboptimal curing in the first 28 days after manufacture. It increases their field carbonation coefficients to 3.0 mm/√years and 1.7 mm/√years, respectively. The use of a simple CO₂ concentration based conversion formula to go from accelerated carbonation rates to more natural carbonation rates, also tends to underestimate the actual carbonation rate in the field. Exposure to only 1% CO₂ after 28 days of optimal curing resulted in field carbonation coefficients for OPC, HVFA and FA+SF concrete of 1.8, 4.0 and 2.3 mm/years, respectively.

Intermittent immersion in water and exposure to 10% CO₂ to simulate exposure class XC4, logically results in much lower carbonation rates. It takes time for the concrete to dry out before the CO₂ can steadily penetrate again. Although reduced with more than half, the HVFA concrete still showed a carbonation rate higher than the ones of the applicable OPC and k-value conforming FA references. Nevertheless, the estimated field carbonation rates still remained very low in comparison with those expected in exposure class XC3.

13.3. Resistance to chloride ingress

HVFA and FA+SF concrete do meet the equivalent performance criterion for chloride resistance cf. NBN B15-100 (2008) when compared with the applicable OPC and k-value conforming FA references. Comparative migration tests, accelerated and 'natural' diffusion tests confirm this statement. After 28 days of optimal curing, the HVFA concrete only just meets the criterion in terms of migration coefficient. From then on, the concrete showed a very positive ageing effect with prolonged curing. Migration coefficients after 1 year amounted to only $2.0-3.0 \times 10^{-12}$ m²/s which is less than one third of the corresponding values for the OPC reference. FA+SF concrete obtains this very low migration coefficient already after 28 days. Suboptimal curing in the first 28 days after manufacture does not seem to affect this value much. A higher susceptibility to suboptimal curing was noted for HVFA concrete.

From the results of the comparative diffusion tests more or less the same conclusions can be drawn with respect to the optimally cured HVFA and FA+SF concrete. Only the positive ageing effect is less pronounced because the long exposure periods prior to chloride profiling implicate that the concrete can only be tested at later age when most of the secondary hydration reactions have already taken place.

Accurate chloride profiling implies that the initial chloride content of the concrete really needs to be considered to achieve a proper fit. The acid-soluble chloride content as determined by means of potentiometric titration does not differ much from the corresponding value that is obtained with the RCT method. The water soluble chloride content is very different depending on whether its value is determined with the potentiometric titration or the RCTW method.

For the submerged exposure condition, the chloride surface concentration cannot be considered as constant. It differs with the tested concrete type and applied curing period. There is probably a mix specific surface chloride build-up with prolonged exposure.

Reducing the width of an artificial crack in concrete representative mortar from 0.3 mm to only 0.1 mm does not diminish the chloride ingress around the crack. To achieve the seemingly uncracked condition of the material, the crack width should be reduced even more to a crack width that can easily be healed autogenously.

13.4. Resistance to freeze/thaw with deicing salts

An air entrained HVFA and FA+SF concrete may not exactly meet the equivalent performance criterion of NBN B15-100 (2008) in terms of salt scaling resistance. Nevertheless, their mass loss per unit area after an accelerated scaling test cf. NBN EN 1339 (2003) does not exceed the prescribed 1 kg/m² limiting value.

To achieve such an adequate salt scaling resistance for the proposed HVFA concrete, special attention must be paid to its artificial air entrainment. The HVFA concrete requires a much higher AEA dosage than the applicable OPC reference (7.0 ml/kg binder versus 2.0 ml/kg binder). Maintaining the initially entrained air content as a function of time is not easy with AEA dosages lower than 7.0 ml/kg binder, especially when incorporating large portions of finer fly ashes in the concrete. Time dependent monitoring of the air content in the fresh state showed that with incorporation of a fine fly ash (45 µm fineness: 13.2% retained), the initially measured air content after 15 min gradually decreases until the last measurement after 120 min, probably due to adsorption phenomena. A reduced air content in the fresh state can result in an inadequate air content in hardened state as observed microscopically on thin sections and by means of automated air void analysis. To compensate for any possible adsorption of the applied fatty acid/polyglycol based AEA, the dosage should be increased to achieve an initial air content after 15 min of around 6-7%. This air content range is in agreement with the criteria of the American standard ACI 201.2R (2008) for the applied maximum nominal aggregate size (16 mm) in combination with severe exposure involving deicing salts. It is advised to stick to these criteria, and not to the less strict design rules of the corresponding European and Belgian standards. As such, the necessary air-to-paste ratio of 18-20% for an adequate air void system in hardened state can more easily be guaranteed.

Air entrainment affects the porosity and transport properties of the HVFA concrete, at least when their experimental characterization involves external pressures. The presence of a well developed artificially induced air void system results in a substantially higher permeable porosity of the concrete as determined with a vacuum saturation test. It also increases the apparent gas permeability at 2 bar pressure significantly. These trends could be observed both after sample preconditioning at 40°C and 105°C. On the other hand, natural capillary sorption

tests indicated no important differences in water absorption between non-air entrained and air entrained HVFA concrete. Thus, depending on the underlying assessment technique, the effect of air entrainment on the porosity and transport properties can be substantial. Hence, the deterioration mechanisms governed by these properties (e.g. the concrete's resistance to corrosion of embedded reinforcing steel) may also be affected.

Salt scaling of well air entrained FA+SF concrete with a total binder content of 340 kg/m³ can be kept below 1 kg/m² in a much easier way. The required dosage of AEA (2.5-3.0 ml/kg binder) for an initial air content of 6-7% is more similar to the corresponding dosage (2.0 ml/kg binder) needed for the OPC reference with the same total binder content. This initial air content resulted in an adequate air void system in hardened state (air content: > 7%, spacing factor: < 200 μm, specific surface: 25-45 mm⁻¹ and average chord length: ~ 0.100 mm). However, the applied combination of a polycarboxylic ether-based superplasticizer and fatty acid/polyglycol-based air entraining agent in a binder system consisting of 50% Portland cement, 40% fly ash and 10% silica fume still has an important drawback. The air content in the fresh state can increase dramatically due to intermittent mixing in the first hour after the initial mixing process has ended. This can cause an important loss of the concrete's strength in hardened state. Without this intermittent mixing, the mixture performs well, also in terms of porosity and transport properties. Addition of AEA increases the capillary water absorption, permeable porosity and gas permeability, but not much. Moreover, the FA+SF concrete turns out much less porous and permeable than the proposed HVFA concrete.

13.5. Service life prediction

13.5.1. Carbonation-induced corrosion

Given the higher field carbonation rates of HVFA and FA+SF concrete in comparison with the applicable OPC and k-value conforming FA references, the time to carbonation-induced steel depassivation of the alternative concrete types is evidently shorter. However, corrosion initiation periods of at least 100 years, the normal design service life of important concrete infrastructure, still seem possible. Nevertheless, a lot depends on the underlying carbonation assessment approach and the applied prediction model.

When using a simplified first order probabilistic model with the estimated field carbonation coefficient and the applicable concrete cover as only load and resistance variables, a predicted life span of more than 100 years can be achieved for both concrete types. This prediction assumes that the field carbonation coefficients were estimated from accelerated carbonation experiments at 10% CO₂ during which the carbonation depths at different time intervals were evaluated colorimetrically with phenolphthalein. A microscopic assessment of the carbonation depth often tends to result in shorter times to depassivation. Still the remaining corrosion initiation period in exposure class XC3 lasted for more than 100 years after 28 days of optimal curing at 20°C and 95% RH. Suboptimal curing in the first 28 days after manufacture turned out problematic for the HVFA composition. In that case, the duration of the initiation period was only 71 years. Additional correction for the applied high CO₂ concentration during carbonation testing which normally considerably underestimates the actual carbonation rate in the field due to the use of an oversimplified conversion formula can result in an initiation

period of only 21 years for HVFA concrete. For FA+SF concrete this corrected value is also less than 100 years. Yet, it still remains 71 years.

Consideration of the curing behaviour and the meteorological conditions in a more advanced second order probabilistic prediction cf. *fib* Bulletin 34 can postpone the time to carbonation-induced steel depassivation considerably in exposure class XC3 and XC4. This is mainly due to the unfavourable Belgian weather conditions for carbonation (e.g. relative humidity: $79\pm 9\%$ RH, time of wetness: 0.31). Accelerated carbonation tests involving exposure to 10% CO₂ and subsequent colorimetric or microscopic carbonation depth assessment again indicate no problems after 28 days of optimal curing in a sheltered outdoor environment (exposure class XC3). In case of suboptimal curing, steel depassivation for the HVFA concrete still takes more than 100 years. After correction for the applied high CO₂ concentration during carbonation testing, the duration of the initiation period would only be 72 years anymore. On the other hand, a 100 year life span is expected for FA+SF concrete under all of the above mentioned circumstances.

The time from corrosion initiation until the occurrence of unacceptable corrosion-induced cracks (crack width: 1.0 mm) is believed to be non-negligible (HVFA concrete: 52 years, FA+SF concrete: 169 years) when based on the semi-probabilistic prediction model of DuraCrete for the corrosion propagation period. This model requires concrete resistivity as basic experimental input. Thus, for the alternative concrete types characterized by a resistivity of around 100 Ωm or more, the sole consideration of the corrosion initiation period underestimates the actual service life (= corrosion initiation + propagation period) of the concrete substantially.

13.5.2. Chloride-induced corrosion

Estimating the time to chloride-induced steel depassivation from chloride migration coefficients using the *fib* Bulletin 34 model with a default experimental transfer parameter ($k_t = 0.832$), ageing exponent and critical chloride content (the first order approach), turned out positive for the HVFA and FA+SF concrete. The applicable OPC reference for a submerged marine environment (exposure class XS2) was characterized by a corrosion initiation period of less than 5 years while this was around 30, 20 and +1000 years for k_t -value conforming FA, HVFA and FA+SF concrete after 28 days of optimal curing. In view of a design service life of 100 years, only the FA+SF concrete type is complying. The very short corrosion initiation period of the OPC reference is mainly caused by the low default ageing exponent ($a = 0.30$) for OPC binder systems and the low critical chloride threshold level ($C_{crit} = 0.6$ m%/binder) which is independent of the binder system. The better service life performance of the alternative concrete types is mainly due to higher default ageing exponent for concrete with fly ash ($a = 0.60$) and silica fume ($a = 0.62$). For the FA+SF concrete there is an additional contributor to the very long depassivation period, namely the very low chloride migration coefficient of the concrete after already 28 days.

A more mix specific second order prediction approach required the experimental determination or verification of the experimental transfer parameter, the ageing exponent and the critical chloride threshold level. Comparative chloride migration and natural diffusion tests revealed an experimental transfer parameter of around 0.4-0.5 on average for all concrete

types. Chloride diffusion tests after 28, 91 and 273 or 364 days of optimal curing resulted in mix specific ageing exponents for the OPC reference ($a = 0.15$), the k-value conforming FA reference ($a = 0.53$), the HVFA concrete ($a = 0.70$) and the FA+SF concrete ($a = 0.55$). The monitoring of the corrosion potential of a rebar embedded in chloride exposed concrete until onset of active corrosion and the subsequent determination of the chloride content near the rebar, indicated that the critical chloride content is probably much higher than the default value of 0.6 m%/binder. The preliminary C_{crit} values measured were more in range with 1.9 m%/binder as suggested by the DuraCrete guideline. When assuming the alternative values for all three model input parameters, the duration of the corrosion initiation period increased to around 50 years for the OPC reference. All other mixtures were characterized by times to steel depassivation of more than 1000 years. The use of chloride migration coefficients obtained after 28 days of suboptimal curing as model input did not change this conclusion for the HVFA and FA+SF concrete.

Adding the time to corrosion-induced cracking to the estimated corrosion initiation periods does not increase the total service life in a substantial way. The corrosion propagation period estimated from concrete resistivity measurements amounted to maximum 4.8 years for the FA+SF concrete.

Note that all the above mentioned service life estimations should still be interpreted with caution. An important drawback of the currently considered empirical models is that they do not account for the presence of flaws in the concrete. For instance, cracks are difficult to avoid in practice. They offer direct pathways for harmful substances such as CO_2 , chloride, O_2 and H_2O to penetrate which obviously reduces the service life of steel reinforced concrete.

13.6. Life cycle assessment

It is of importance to include the strength and service life properties of concrete in the functional unit definition for life cycle assessment. The current by-product status of fly ash and silica fume also implies that not only their basic treatment after production (drying + storage) needs to be accounted for in environmental impact calculations, but also an allocated impact of the primary production processes, i.e. coal fired electricity and Si-metal production. The preference normally goes to economic allocation. Given the by-product / main product mass and price ratios, the economic allocation coefficient for fly ash and silica fume should amount to 2.9% and 6.1%, respectively in Belgium. These coefficients are higher than the 1.0% and 4.8% from literature based on older prices of by-products and main products in France. Given the use of the above mentioned allocation coefficients for Belgium, it should be noted that the conducted LCA calculations specifically represent the Belgian situation where fly ash and silica fume are less and less readily available. The outcome of the LCA study can be very different for countries like China and India. There, by-products like fly ash are still being produced in large amounts at coal fired electrical power plants. To prevent stockpiling of this by-product and stimulate its use in concrete, the selling price is kept low. Hence, the resulting economic allocation coefficients will be much lower and thus also the fly ash related environmental impact.

The required concrete volume per unit of strength and service life is seen as a better functional unit than 1 m^3 of concrete to account for the functionalities of the material. With an

economically allocated impact assigned to the by-products the possible reduction in GHG emissions depends a lot on the studied exposure class. In exposure class XC3/4 no benefits are possible for the HVFA mixture mainly because of its moderate strength performance in comparison with the references. Moreover, first and second order service life prediction indicate that its service life could be less than 100 years which results in an even higher required concrete volume per unit of strength and service life. The use of the high-strength FA+SF composition enables a reduction in GWP of 28-36%, yet only in comparison with the OPC reference for exposure class XC3. In exposure class XS2, the use of the HVFA and FA+SF concrete is advantageous, mainly due to the poor service life performance of the OPC reference. Their global warming potentials are easily 25-35% and 55-60% lower. In comparison with the k-value conforming FA references for which a 100 year service life is very well possible, only the global warming potential of the FA+SF concrete is lower (GWP – 19-21%). In fact, the k-value conforming FA references themselves with a fly ash content of only 15% count as a better alternative to OPC concrete (GWP –45-50%) than the concrete mixtures with high cement replacement levels.

Consideration of other environmental issues, such as the effects on acidification, eutrophication, abiotic depletion, freshwater/marine aquatic ecotoxicity, terrestrial ecotoxicity, human toxicity, ozone layer depletion and photochemical oxidation, indicates problematic impacts for both alternative concrete types. Coal fired electricity and Si-metal production rely very much on the exploitation and combustion of fossil fuels which has a very negative effect on all these impact categories. Adopting even small (economic) allocation coefficients for the by-products results in impacts higher than those associated with cement production. As such, the suitability of the economic allocation principle for the concrete industry can most certainly be questioned.

Apart from the required concrete volume per unit of strength and service life, simple structural elements with a given mechanical design load and service life can also be used as proper functional units for life cycle assessment. Considering a concrete column as FU leads to similar conclusions, while the reduction in GWP for a concrete slab is considerably less. In case of FA+SF concrete, the high strength of the material cannot be fully valorized in the slab design. Moreover, the extra reinforcing steel needed to reduce the crack width to a seemingly uncracked condition can make the GWP go up with 25-37%.

Future research perspectives

14.1. Resistance to carbonation

Assessing the carbonation resistance of a potentially ‘green’ concrete in the design phase usually involves accelerated carbonation testing at a higher CO₂ concentration than the normal concentration observed in the field (around 0.03% CO₂). As a consequence, a conversion is required to go from an accelerated to a field carbonation rate for service life prediction purposes. Literature mentions a simple conversion formula relying only on the ratio of the CO₂ concentrations applied and the CO₂ concentration in the field. Depending on the literature source, this formula could be valid for an experimental CO₂ concentration up to 10%. Other sources indicate that the CO₂ concentration during carbonation testing should not exceed 3% to avoid important changes in the carbonation mechanism. From this research it was clear that the use of the simple conversion formula to go from a carbonation coefficient obtained after exposure to 10% CO₂ to a carbonation coefficient representing exposure to only 1% CO₂, results in an important underestimation of the actual carbonation rate at 1% CO₂. For a pure OPC binder system this could only partially be explained by a porosity reduction and pore refinement of the microstructure as observed with MIP. For binder systems with 50% of the cement replaced by fly ash (and silica fume) this was not the case. Moreover, combined TGA and XRD analyses showed that the most important differences in carbonation behaviour (portion of C–S–H carbonation, total amount of Calcite, Vaterite and Aragonite) existed between exposure to 0.03% and 1% CO₂. Thus, a correct conversion formula should account for much more than the ratio of the CO₂ concentrations in play, even when the applied experimental CO₂ concentration is lower than the 3% criterion from literature. An improvement of the conversion formula should definitely be the subject of future research. One of the items that should be addressed in the process is the abundant production of water during highly accelerated carbonation. If this water cannot steadily be evacuated in time, it could induce pore blocking, hence slow down the carbonation rate unrealistically.

14.2. Resistance to chloride ingress

Although literature mentions that for the submerged exposure condition a constant chloride surface concentration can be assumed, the results obtained in this research seem to indicate

otherwise. A build-up in chloride surface concentration is expected with prolonged curing until a concentration is reached that exceeds the original chloride concentration of the exposure solution. To find further confirmation for this chloride build-up, additional chloride diffusion tests are needed with chloride profiling at various exposure times. They would provide a better understanding of the mechanisms behind the chloride build-up. As such, the phenomenon could be taken into account in the prediction models that estimate the time to chloride-induced depassivation of reinforcing steel embedded in concrete.

In this research the focus was on exposure class XS2. Reinforced concrete in a permanently submerged marine environment is normally less susceptible to chloride-induced steel corrosion than concrete located in the tidal, splash or spray zone. Still, the durability performance of HVFA and FA+SF concrete was only determined for the former condition because the effects of realistic intermittent exposure to chlorides are difficult to understand without prior knowledge of the effects inherent to continuous exposure. Evidently, it would be interesting to develop a chloride test that adequately simulates intermittent exposure. This would allow for a durability and service life assessment of HVFA and FA+SF concrete in the more critical exposure class XS3.

The exposure liquid used for the ‘natural’ diffusion tests was an aqueous NaCl solution with the same chloride concentration as seawater. As a consequence, porosity reducing effects with prolonged exposure induced by the other ions present in the actual seawater (e.g. magnesium and sulfate ions) are not accounted for in the determination of the ageing exponent for HVFA and FA+SF concrete. Therefore, it might be interesting to do chloride profiling after immersion in realistic seawater solutions in the future as well.

14.3. Resistance to freeze/thaw with deicing salts

Air entrained FA+SF concrete showed an excellent salt scaling resistance in exposure class XF4. However, time dependent monitoring of the concrete in the fresh state revealed a compatibility problem for the now considered combination of polycarboxylic-ether based superplasticizer and fatty acid/polyglycol-based air entraining agent. Further research is needed to evaluate which combination of superplasticizer and air entraining agent would be more suitable for the binder system of FA+SF concrete.

In contrast with carbonation- and chloride-induced steel corrosion, deterioration of the concrete surface due to freeze/thaw in combination with deicing salts, cannot really be predicted as a function of time. The few empirical models available are rather vague and not straightforward in use. A future challenge lies in the further development of these models.

14.4. Service life prediction

The second order empirical models for estimating the carbonation- or chloride-induced corrosion initiation period often resulted in very long time spans. This was in part attributed to the fact the models of *fib* Bulletin 34 do not account for the presence of cracks in concrete. Since it is difficult to avoid the occurrence of cracks in practice, this is an important shortcoming in the models. Further research efforts are needed to include the aspect of cracking in the models.

Semi-probabilistic assessment of the corrosion propagation period cf. DuraCrete shows that the time from onset of active corrosion to unacceptable concrete cracking is far from negligible for HVFA and FA+SF concrete when carbonation-induced. This means that the actual service life is in fact much longer than the time to steel depassivation. The model used is based on the in literature observed relation between an experimentally determined concrete resistivity and the corrosion rate of reinforcing steel, as well as a series of material and environment characterizing input parameters. The validity of the model for alternative concrete types such as HVFA and FA+SF concrete still requires further experimental verification in the future. This can be done by performing combined resistivity and linear polarization corrosion rate measurements.

14.5. Life cycle assessment

A life cycle assessment methodology was proposed specifically for concrete in which 50% of the cement was replaced by fly ash (and silica fume). This methodology required a strong connection with the experimental strength, durability and service life characterization of the concrete. A modified cradle-to-gate approach served this purpose well. Apart from that, the importance of allocated impacts associated with the industrial by-products fly ash and silica fume was highlighted. Now, most of these principles remain applicable for other alternative concrete types such as high-volume blast-furnace slag concrete, ultra-high performance concrete, self-compacting concrete, completely recyclable concrete and self-healing concrete. Still, the overall LCA methodology can still be improved. Ideally, it should consider the environmental impact from the cradle-to-the-grave. To include end-of-life related impacts in the study, one must fully understand the environmental consequences of landfilling each concrete type after demolition (e.g. the impacts of leaching on (eco)toxicity) and the avoided impacts inherent to a complete recycling of the concrete in high-value applications (e.g. recycled aggregates, cement manufacture). Specifically with respect to self-healing concrete, one of the future challenges will lie in compiling adequate life cycle inventories for the production of the non-traditional concrete constituents (e.g. production of the polymer-based healing agents, the capsules, the bacterial spores, etc.) involved. Moreover, the underlying prediction models for defining a service life related functional unit for self-healing concrete should account for crack occurrence and their subsequent healing.

**BIBLIOGRAPHY, APPENDICES,

CURRICULUM VITAE**

Bibliographical references

- ACI 201.2R (2008). Guide to durable concrete, Reported by ACI Committee 201. Farmington Hills: American Concrete Institute.
- ACI 318-08 (2008). Building code requirements for structural concrete and commentary. Farmington Hills: American Concrete Institute.
- Adamson AW, Gast AP (1997). Physical chemistry of surfaces, Sixth edition. New York: Wiley.
- AFPC-AFREM (1997). Recommended test methods for measuring the parameters associated with durability (in French). In: Proceedings of Journées Techniques AFPC-AFREM Durabilité des Bétons, Toulouse, France, December 11-12, 1997. Toulouse: INSA.
- Afrani I, Rogers C (1993). The effect of different cementing materials and curing regimes on the scaling resistance of concrete. In: Proceedings of the 3rd Canadian Symposium on Cement and Concrete, Ottawa, Canada, August 3-4, 1993. Ottawa: National Research Council of Canada, Institute for Research in Construction, 149-166.
- Aitcin PC, Pigeon M (1986). Performance of condensed silica fume concrete used in pavements and sidewalks. *Durab Build Mater*;3(4):353-368.
- Akhavan A, Shafaatian SMH, Rajabipour F (2012). Quantifying the effects of crack width, tortuosity, and roughness on water permeability of cracked mortars. *Cem Concr Res*;42(2):313-320.
- Alonso C, Castellote M, Andrade C (2002). Chloride threshold dependence of pitting potential of reinforcement. *Electrochim Acta*;47(21):3469-3481.
- Althaus HJ (2003). Life cycle inventories of metals, Final reportecoinvent 2000, No. 10. Dübendorf: Swiss Centre for Life Cycle Inventories.
- Andrade C (1993). Calculation of chloride diffusion coefficients in concrete from ionic migration measurements. *Cem Concr Res*;23(3):724-742.
- Andrade C, Arteaga A (1998). Statistical quantification of the propagation period, BE95-134/TG4, Sub-task 4.1 Report. Madrid: Institute 'Eduardo Torroja' (IET) of Construction Science of the CSIC of Spain.
- Andrade C, Castellote M, Alonso C, González C (2000). Non-steady-state chloride diffusion coefficients obtained from migration and natural diffusion tests, Part I: Comparison between several methods of calculation. *Mater Struct*;33(1):21-28.
- Angst U, Elsener B, Larsen CK, Vennesland O (2009). Critical chloride content in reinforced concrete – A review. *Cem Concr Res*;39(12):1122-1138.

- Ann KY, Ahn JH, Ryou JS (2009). The importance of chloride content at the concrete surface in assessing the time to corrosion of steel in concrete structures. *Constr Build Mater*;23(1):239-245.
- Assies JA (1992). Introduction paper to SETAC-Europe workshop on environmental life cycle analysis of products. In: *Life Cycle Assessment, Proceedings of a SETAC-Europe workshop on Environmental Life Cycle Assessment of Products*, Leiden, the Netherlands, December 2-3, 1991. Brussels: SETAC-Europe.
- ASTM C 1585 – 04^e (2007). Standard test method for measurement of rate of absorption of water by hydraulic-cement concretes. West Conshohocken: ASTM International.
- ASTM C457 – 10a (2010). Standard test method for microscopical determination of parameters of the air-void system in hardened concrete. West Conshohocken: ASTM International.
- ASTM C618-12a (2012). Standard specification for coal fly ash and raw or calcined natural pozzolan for use in concrete. West Conshohocken: ASTM International.
- ASTM C642 – 06 (2006). Standard test method for density, absorption, and voids in hardened concrete. West Conshohocken: ASTM International.
- ASTM C672 – 03 (2003). Standard test method for scaling resistance of concrete surfaces exposed to deicing chemicals. West Conshohocken: ASTM International.
- ASTM C876 (1991). Standard test method for corrosion potentials of uncoated reinforcing steel in concrete. West Conshohocken: ASTM International.
- ATILH (2002). Environmental inventory of French cement production. Paris: Association Technique des Liants Hydrauliques (Hydraulic Binder Industries Union).
- Audenaert K (2006). Transport mechanisms of self-compacting concrete related to carbonation and chloride penetration (in Dutch). PhD thesis. Ghent: Ghent University.
- Audenaert K, Marsavina L, De Schutter G (2009). Influence of cracks on the service life of concrete structures in a marine environment. *Key Eng Mat*;399:153-160.
- Baert (2009). Physico-chemical interactions in Portland cement – (high volume) fly ash binders. PhD thesis. Ghent: Ghent University.
- Baroghel-Bouny V (2007). Water vapour sorption experiments on hardened cementitious materials, Part I: Essential tool for analysis of hygral behaviour and its relation to pore structure. *Cem Con Res*;37(3):414-437.
- Baroghel-Bouny V, Belin P, Maultzch M, Henry D (2007a). AgNO₃ spray tests: advantages, weaknesses, and various applications to quantify chloride ingress into concrete, Part 1: Non-steady-state diffusion tests and exposure to natural conditions. *Mater Struct*;40(8):759-781.
- Baroghel-Bouny V, Belin P, Maultzch M, Henry D (2007b). AgNO₃ spray tests: advantages, weaknesses, and various applications to quantify chloride ingress into concrete, Part 2: Non-steady-state migration tests and chloride diffusion coefficients. *Mater Struct*;40(8):783-799.
- Benetto E, Rousseaux P, Blondin J (2004). Life cycle assessment of coal by-products based electric power plants. *Fuel*;83(7-8):957-970.
- Bernstein L, Roy J, Delhotal KC, Harnisch J, Matsushashi R, Price L, Tanaka K, Worrell E, Yamba F, Fengqi Z (2007). Industry. In: Metz B, Davidson OR, Bosch PR, Dave R, Meyer LA (Eds.), *Climate change 2007: Mitigation, Contribution of Working Group III to the Fourth Assessment Report of the IPCC*. Cambridge and New York: Cambridge University Press, 447-496.
- Bertolini L, Elsener B, Pedefferri P, Redaelli E, Polder R (2013). Corrosion of steel in concrete, Prevention, diagnosis, repair, Second, completely revised and enlarged edition. Weinheim: Wiley-VCH Verlag GmbH & Co. KgaA.

- Bilodeau A, Carette GG, Malhotra VM (1991). Influence of curing and drying on salt scaling resistance of fly ash concrete. In: Malhotra VM (Ed.), ACI Special Publication SP-126. Detroit: American Concrete Institute, 201-228.
- Bilodeau A, Malhotra VM (1992). Concrete incorporating high volumes of ASTM class F fly ashes: Mechanical properties and resistance to deicing salt scaling and to chloride-ion penetration. In: Malhotra VM (Ed.), ACI Special Publication SP-132. Detroit: American Concrete Institute, 319-349.
- Boel V (2006). Microstructure of self-compacting concrete related to gas permeability and durability aspects (in Dutch). PhD thesis. Ghent: Ghent University.
- Boel V, Audenaert K, De Schutter G (2008). Gas permeability and capillary porosity of self-compacting concrete. *Mater Struct*;41(7):1283-1290.
- Borges PHR, Costa JO, Milestone NB, Lynsdale CJ, Streatfield RE (2010). Carbonation of CH and C-S-H in composite cement pastes containing high amounts of BFS. *Cem Concr Res*;40(2):284-292.
- Braungart M, McDonough W (2002). *Cradle to cradle: Remaking the way we make things*. New York: North Point Press.
- Breen LC, Yarwood J, Garbev K, Stemmermann P (2007). Structural features of C-S-H (I) and its carbonation in air – a Raman spectroscopy study, Part II: carbonated phases. *J Am Ceram Soc*;90(3):908-917.
- Breit W (2001). Critical corrosion inducing chloride content – State of the art and new investigation of results. *VDZ BB*:145-148.
- Browne RD (1980). Mechanisms of corrosion of steel in concrete in relation to design, inspection, and repair of offshore and coastal structures. In: Malhotra VM (Ed.), *Proceedings of the International Conference on Performance of Concrete in Marine Environment*, St. Andrews by the Sea, Canada, August, ACI Special publication SP-65. Detroit: American Concrete Institute, 169-203.
- Byfors K (1987). Influence of silica fume and fly ash on chloride diffusion and pH values in cement paste. *Cem Concr Res*;17(1):115-130.
- Castellote M, Andrade C (2001a). Round-Robin test on chloride analysis in concrete – Part I: Analysis of total chloride content. *Mater Struct*;34(9):532-549.
- Castellote M, Andrade C (2001b). Round-Robin test on chloride analysis in concrete – Part II: Analysis of water-soluble chloride content. *Mater Struct*;34(10):589-596.
- Castellote M, Andrade C, Alonso C (1999). Chloride binding isotherms in concrete submitted to non-steady state migration experiments. *Cem Concr Res*;29(11):1799-1806.
- Castellote M, Fernandez L, Andrade C, Alonso C (2009). Chemical changes and phase analysis of OPC pastes carbonated at different CO₂ concentrations. *Mater Struct*;42(4):515-525.
- Chang CF, Chen JW (2006). The experimental investigation of concrete carbonation depth. *Cem Concr Res*;36(9):1760-1767.
- Chatterji S, Kawamura M (1992). Electrical double layer, ion transport and reactions in hardened cement paste. *Cem Concr Res*;22(5):774-782.
- Chaussadent T, Arliguie G (1999). AFREM test procedures concerning chlorides in concrete: Extraction and titration methods. *Mater Struct*;32(3):230-234.
- Chen C (2009). A study of traditional and alternative structural concretes by means of the life cycle assessment method (in French). PhD thesis. Troyes: UTT.
- Chen C, Habert G, Bouzidi Y, Jullien A (2010a). Environmental impact of cement production: detail of the different processes and cement plant variability evaluation. *J Clean Prod*;18(5):478-485.

- Chen C, Habert G, Bouzidi Y, Jullien A, Ventura A (2010b). LCA allocation procedure used as an incitative method for waste recycling: An application to mineral additions in concrete. *Resour Conserv Recy*;54(12):1231-1240.
- Chen JJ, Thomas JJ, Jennings HM (2006). Decalcification shrinkage of cement paste. *Cem Concr Res*;36(5):801-809.
- Choi YS, Kim JG, Lee KM (2006). Corrosion behavior of steel bar embedded in fly ash concrete. *Corros Sci*;48(7):1733-1745.
- Chowdhury R, Apul D, Fry T (2010). A life cycle based environmental impacts assessment of construction materials used in road construction. *Resour Conserv Recy*;54(4):250-255.
- Coelho AA (2007). Topas Academic Version 4.1 [computer software]. Brisbane: Coelho Software.
- Consoli F, Allen D, Boustead I, Oude N, de Fava J, Franklin W, Quay B, Parrish R, Perriman R, Postlethwaite D, Seguin J, Vignon B (Eds.) (1993). *Guidelines for life cycle assessment: A code of practice*, 1st Ed. Brussels: SETAC-Europe.
- Construction Technology Laboratories, Inc. (2003). *Life cycle inventory of slag cement inventory process: Project CTL, No 312012*. Illinois: Construction Technology Laboratories, Inc.
- Copuroglu O (2006). *The characterization, improvement and modelling aspects of frost salt scaling of cement-based-materials with a high slag content*. PhD thesis. Delft: TU Delft.
- Costa A, Appleton J (1999a). Chloride penetration into concrete in marine environment – Part I: Main parameters affecting chloride penetration. *Mater Struct*;32(5):252-259.
- Costa A, Appleton J (1999b). Chloride penetration into concrete in marine environment – Part II: Prediction of long term chloride penetration. *Mater Struct*;32(5):354-359.
- Cox K, De Belie N (2007). Durability behavior of high-volume fly ash concrete. In: Claisse P, Sadeghi-Pouya H, Naik TR, Chun Y (Eds.), *Proceedings of the International Conference on Sustainable Construction Materials and Technologies*, Coventry, Great Britain, June 11-13, 2007. Coventry: Coventry University and University of Wisconsin Milwaukee Centre for By-Products Utilization, 45-53.
- CSA A23.1-09/A23.2-09 (2009). *Concrete materials and methods of concrete construction/Test methods and standard practices for concrete*. Ontario: CSA.
- CUR recommendation 48 (1999). *Feasibility study of new cements for application in concrete (in Dutch)*. Gouda: CUR.
- CUR report 100 (1981). *Durability maritime structures (in Dutch)*. Gouda: CUR-VB.
- CUR VC81 (2009). *Guideline 1: Durability of structural concrete with respect to chloride-induced corrosion, Guideline for the formulation of performance criteria, Background report (in Dutch)*. Gouda: CUR Bouw & Infra.
- da Silva FG, Helene P, Castro-Borges P, Liborio JBL (2009). Sources of variations when comparing concrete carbonation results. *J Mater Civ Eng*;21(7):333-342.
- Dahlström K, Ekins P (2006). Combining economic and environmental dimensions: Value chain analysis of UK iron and steel flows. *Ecol Econ*;58(3):507-519.
- Damineli BL, Kemeid FM, Aguiar PS, John VM (2010). Measuring the eco-efficiency of cement use. *Cem Concr Compos*;32(8):555-562.
- Damtoft JS, Lukasik J, Herfort D, Sorrentino D, Gartner EM (2008). Sustainable development and climate change initiatives. *Cem Concr Res*;38(2):115-127.
- De Ceukelaire L, Van Nieuwenburg D (1993). Accelerated carbonation of a blast-furnace cement concrete. *Cem Concr Res*;23(2):442-452.

- De Schepper M, Van den Heede P, Windels C, De Belie N (2011). Life cycle assessment of completely recyclable concrete. In: Bilek V, Keršner Z (Eds.), Proceedings of the 4th International Conference Non-Traditional Cement & Concrete, Brno, Czech Republic, June 27-30, 2011. Brno: Brno University of Technology, 67-76.
- De Schutter G, Feys D, Verhoeven R (2010). Ecological profit for a concrete pipe factory due to self-compacting concrete technology. In: Zachar J, Claisse P, Naik TR, Ganjian E (Eds.), Proceedings of the Second International Conference on Sustainable Construction Materials and Technologies, Volume Two of Three, Ancona, Italy, June 28-30, 2010. Milwaukee: University of Wisconsin Milwaukee Center for By-Products Utilization, 1281-1287.
- Delagrave A, Marchand J, Ollivier JP, Julien S, Hazrati K (1997). Chloride binding capacity of various hydrated paste systems. *Adv Cem Based Mater*;6(1):28-35.
- Desmyter J, Martin Y (2001). The environmental impact of building materials and buildings (in Dutch). WTCB Bulletin. Limelette: WTCB.
- Dolch WL (1996). Air-entraining Admixtures. In: Ramachandran VS (Ed.), Concrete admixtures handbook, 2nd Edition: Properties, science, and technology. Ottawa: National Research Council Canada, 518-557.
- Dones R, Bauer C, Bollinger R, Burger B, Faist Emmenegger M, Frischknecht R, et al. (2007). Life cycle inventories of energy systems: results for current systems in Switzerland and other UCTE countries. Ecoinvent report no. 5. St-Gallen: Swiss Centre for Life Cycle Inventories.
- Du L, Folliard KJ (2005). Mechanisms of air entrainment in concrete. *Cem Concr Res*;35(8):1463-1471.
- DuraCrete (1998). Probabilistic performance based durability design of concrete structures: Compliance testing for probabilistic design purposes – Evaluation report. Document BE95-1347/R7. Gouda: CUR.
- DuraCrete (1999). Probabilistic performance based durability design of concrete structures: Compliance testing for probabilistic design purposes. Document BE95-1347/R8. Gouda: CUR.
- DuraCrete (2000). Probabilistic performance based durability design of concrete structures: Statistical quantification of the variables in the limit state functions. Document BE95-1347/R9. Gouda: CUR.
- DuraCrete (2000). Probabilistic performance based durability design of concrete structures: General guidelines for durability design and redesign. Document BE95-1347/R15. Gouda: CUR.
- DuraCrete (2000). Probabilistic performance based durability design of concrete structures: DuraCrete Final technical report. Document BE95-1347/R17. Gouda: CUR.
- Ecocem (2008). Producer of ground granulated blast-furnace slag (GGBS).
- EDF (2008). Leading the energy change. *Changer l'énergie ensemble*. 2008 Sustainable development report. Paris: EDF.
- Edvardsen C (1999). Water permeability and autogenous healing of cracks in concrete. *ACI Mater J*;96(4):448-454.
- EFCA (2006). European Federation of Concrete Admixtures Associations. EFCA environmental declaration superplasticizing admixtures (2006), EFCA doc 325 ETG [updated 2006 Apr; cited 2013 May 26]. Available from: <http://www.efca.info/publications.html>.
- Ehrenberg A, Geiseler J (1997). Ecological properties of blast-furnace cement: Life cycle production: Energy consumption, CO₂ emission and greenhouse gas effect (in German). *Beton-Informationen*;37(4):51-63.
- Electrabel (2009). Welcome to the power plant of Ruien (in Dutch). Powerpoint presentation. Brussels: Electrabel GDF Suez.
- Electrabel (2011). Activity and sustainable development report 2011. Brussels: Electrabel GDF Suez.
- Elkem (2012). Elkem sustainability report 2012. Oslo: Elkem A Blue Star Company.

- EN 1097-6 (2000). Tests for mechanical and physical properties for aggregates – Part 6: Determination of particle density and water absorption. Brussels: CEN.
- EPA (1994). Emission factor documentation for AP-42, section 11.6: Portland Cement Manufacturing, Final report, EPA Contract 68-D2-0159, MRI Project No. 4601-01. Washington D.C.: U.S. Environmental Protection Agency.
- EPA (1999). Management standards proposed for cement kiln dust waste. Environmental Fact Sheet, EPA 530-F-99-023. Washington D.C.: U.S. Environmental Protection Agency.
- European Union (1998). Directive 1998/83/EC of the European parliament and the council of 3 November 1998 on the quality of water intended for human consumption. Off J Eur Union;L330:32–54.
- European Union (2003). Directive 2003/53/EC of the European parliament and the council of 18 June 2003 relating to restrictions on the marketing and use of certain dangerous substances and preparations (nonylphenol, nonylphenol ethoxylate and cement). Off J Eur Union;L178:24-27.
- European Union (2008). Directive 2008/98/EC of the European parliament and the council of 19 November 2008 on waste and repealing certain directives. Off J Eur Union;L312:3-20.
- Fagerlund G (1977). The critical degree of saturation method of assessing the freeze/thaw resistance of concrete. Mater Struct;10(4) :217-229.
- Febelcem (2012a). Environmental Product Declaration for Belgian cement – Cembureau EPD format. Cement CEM I 52.5 N. Brussels: Febelcem v.z.w.
- Febelcem (2012b). Environmental Product Declaration for Belgian cement – Cembureau EPD format. Cement CEM II B/M 32.5. Brussels: Febelcem v.z.w.
- Febelcem (2012c). Environmental Product Declaration for Belgian cement – Cembureau EPD format. Cement CEM III/A 42.5 N LA. Brussels: Febelcem v.z.w.
- Febelcem v.z.w (2006). Environmental report of the Belgian cement industry 2006 (in Dutch). Brussels: Febelcem v.z.w.
- Fernández Bertos MF, Simons SJR, Hill CD, Carey PJ (2004). A review of accelerated carbonation technology in the treatment of cement-based materials and sequestration of CO₂. J Hazard Mater;112(3):193-205.
- fib* Bulletin 34 (2006). Model code for service life design. Lausanne: *fib*.
- Flower DJM, Sanjayan JG (2007). Green house gas emissions due to concrete manufacture. Int J LCA;12(5):282-288.
- Forster P, Ramaswamy V (2007). Changes in atmospheric constituents and in radiative forcing. In: Solomon S, Qin D, Manning M, Chen Z, Marquis M, Averyt KB, Tignor M, Miller HL (Eds.), Climate Change 2007: The Physical Science Basis: Contribution of Working Group I to the Fourth Assessment Report of the IPCC. Cambridge and New York: Cambridge University Press, 129-234.
- Friedmann H, Amiri O, Ait-Mokhtar A (2008). Physical modeling of the electrical double layer effects on multispecies ions transport in cement-based materials. Cem Concr Res;38(12):1394-1400.
- Frischknecht R, Jungbluth N (Eds.) (2007). Overview and methodology, Final report ecoinvent v2.0, No. 1. St-Gallen: Swiss Centre for Life Cycle Inventories.
- Gaal GCM, Polder RB, Walraven JC, van der Veen C (2003). Critical chloride content – State of the art. In: Forde MC (Ed.), Proceedings of the 10th International Conference on Structural Faults and Repair, London, Great Britain, July 1-3, 2003. Edinburgh: Engineering Technics Press.
- Gagne R, Pigeon M, Aitcin PC (1991). Deicer salt scaling resistance of high strength concretes made with different cements. In: Malhotra VM (Ed.), ACI Special Publication SP-126. Detroit: American Concrete Institute, 185-199.
- Gartner E (2004). Industrially interesting approaches to low-CO₂ cements. Cem Concr Res;34(9):1489-1498.

- Gebler SH, Klieger P (1983). Effect of fly ash on the air void stability of concrete. In: Malhotra VM (Ed.), ACI Special Publication SP-79. Detroit: American Concrete Institute, 103-142.
- Gehlen C (2000). Probabilistic service life determination of reinforced concrete structures – Reliability analyses for the prevention of reinforcement corrosion (in German). DAFStb-Heft 510. Berlin: Beuth.
- General Chemistry Online (2014). Senese F. Frostburg: Frostburg State University, Dept. of Chemistry; c1997-2010 [updated 2010 Feb 15; cited 2014 Jan 2]. Available from: <http://antoine.frostburg.edu/chem/senese/101/acidbase/indicators.shtml>.
- Gerilla GP, Teknomo K, Hokao K (2007). An environmental assessment of wood and steel reinforced concrete housing construction. *Build Environ*;42(7):2778-2784.
- Giaccio GM, Malhotra VM (1988). Concrete incorporating high-volumes of ASTM class F fly ash. *ASTM J Cem Concr Aggr*;10(2):88-95.
- Glass GK, Buenfeld NR (1997). The presentation of the chloride threshold level for corrosion of steel in concrete. *Corros Sci*;39(5):1001-1013.
- Glass GK, Buenfeld NR (2000). The influence of chloride binding on the chloride induced corrosion risk in reinforced concrete. *Corros Sci*;42(2):324-344.
- Glass GK, Wang Y, Buenfeld NR (1996). An investigation of experimental methods used to determine free and total chloride contents. *Cem Concr Res*;26(9):1443-1449.
- Goedkoop M, Spriensma R (1999). The Eco-indicator 99 – A damage oriented method for life cycle impact assessment. Amersfoort: PRé Consultants bv.
- Goedkoop M, Spriensma R (2001). The Eco-indicator 99. A damage oriented method for life cycle impact assessment, Methodology report, Third Edition. Amersfoort: PRé Consultants bv.
- Goggins J, Keane T, Kelly A (2010). The assessment of embodied energy in typical reinforced concrete building structures in Ireland. *Energ Buildings*;42(5):735-744.
- Groves GW, Brough A, Richardson IG, Dobson CM (1991). Progressive changes in the structure of hardened C₃S cement pastes due to carbonation. *J Am Ceram Soc*;74(11):2891-2896.
- Gruyaert E (2011). Effect of blast-furnace slag as cement replacement on hydration, microstructure, strength and durability of concrete. PhD thesis. Ghent: Ghent University.
- Gruyaert E, De Belie N, Van den Heede P (2009). Acid resistance of concrete containing blast-furnace slag: influence of the pore structure and hydration process. In: Alexander MG, Bertron A (Eds.), *Proceedings of the International RILEM TC211-PAE final conference on Concrete in Aggressive Aqueous Environments, Performance, Testing and Modeling*, Toulouse, France, June 3-5, 2009. Bagnex: RILEM Publications, 389-396.
- Gruyaert E, Van den Heede P, De Belie N (2013). Carbonation of slag concrete: Effect of the cement replacement level and curing on the carbonation coefficient – Effect of carbonation on the pore structure. *Cem Concr Compos*;35(1):39-48.
- Gulikers J (2014). Quantification of the instantaneous chloride diffusion coefficient from short-term bulk diffusion tests. Technical Note. Utrecht: Rijkswaterstaat GPO.
- Guinée JB (Ed.) (2002). *Handbook on Life Cycle assessment, Operational Guide to the ISO Standards*. Dordrecht: Kluwer Academic Publishers.
- Guinée JB, Heijungs R, Huppes G, Zamagni A, Masoni P, Ekvall T, Rydberg T (2011). Life cycle assessment: Past, present, and future. *Environ Sci Technol*;45(1):90-96.
- Ha TH, Muralidharan S, Bae JH, Ha YC, Lee HG, Park KW, Kim DK (2007). Accelerated short-term techniques to evaluate the corrosion performance of steel in fly ash blended concrete. *Build Environ*;42(1):78-85.

- Habert G, Bouzidi Y, Chen C, Jullien A (2010). Development of a depletion indicator for natural resources used in concrete. *Resour Conserv Recy*;54(6):364-376.
- Habert G, Roussel N (2009). Study of two concrete mix design strategies to reach carbon mitigation objectives. *Cem Concr Compos*;31(6):397-402.
- Hanle L, Maldonado P, Onuma E, Tichy M, van Oss HG (2006). Mineral industrial emissions. In: Eggleston HS, Buendia L, Miwa K, Ngara T, Tanabe K (Eds.), 2006 IPCC Guidelines for National Greenhouse Gas Inventories, Volume 3: Industrial processes and product use. Hayama: Institute for Global Environmental Strategies.
- Hansen WC (1963). Crystal growth as a source of expansion in Portland cement concrete. *Am Soc Testing Mats, Proc*, 63:932-945.
- Heijungs R, Guinée JB, Huppes G, Lankreijer RM, Udo de Haes HA, Wegener Sleeswijk A, Ansems AMM, Eggels PG, van Duin R, de Goede HP (1992). Environmental life cycle assessment of products. Guide & backgrounds – October 1992. Leiden: Centre for Environmental Science, Leiden University.
- Hendriks CA, Worrell E, de Jager D, Block K, Riemer P (2011). Emission reduction of greenhouse gases from the cement industry [updated 2004 Aug 23; cited 2011 Aug 18]. Available from: <http://www.wbcscement.org/pdf/tf1/prghgt42>.
- Hill RL, Sarkar SL, Rathbone RF, Hover JC (1997). An examination of fly ash carbon and its interactions with air entraining agent. *Cem Concr Res*;27(2):193-204.
- Hills L, Johansen VC (2007). Hexavalent chromium in cement manufacturing: Literature Review. PCA R&D Serial No. 2983. Skokie: Portland Cement Association.
- Hoekstra AY, Chapagain AK, Aldaya MM, Mekonnen MM (2011). The water footprint assessment manual: Setting the global standard. London: Earthscan.
- Houghton JT, Jenkins GJ, Ephraums JJ (Eds.) (1990). Climate Change. The IPCC Scientific Assessment. Cambridge and New York: Cambridge University Press.
- Houghton JT, Meira Filho LG, Lim B, Tréanton K (Eds.) (1996). Revised 1996 IPCC Guidelines for National Greenhouse Gas Inventories, Greenhouse Gas Inventory Reference Manual (Volume 3). Bracknell: Meteorological Office.
- Houst YF, Wittman FH (1994). Influence of porosity and water content on the diffusivity of CO₂ and O₂ through hydrated cement. *Cem Concr Res*;24(6):1165-1176.
- Houst YF, Wittman FH (2002). Depth profiles of carbonates formed during natural carbonation. *Cem Concr Res*;32(12):1923-1930.
- Humphreys K, Mahasanen M (2002). Toward a sustainable cement industry. Substudy 8: Climate change. Geneva: WBCSD.
- Hunt RG, Franklin WE, Welch RO, Cross JA, Woodal AE (1974). Resource and environmental profile analysis of nine beverage container alternatives. Washington D.C.: U.S. Environmental Protection Agency.
- Huntzinger DN, Eatmon TD (2009). A life-cycle assessment of Portland cement manufacturing: comparing the traditional process with alternative technologies. *J Clean Prod*;17(7):668-675.
- ISO 14040 (1997). Environmental management – Life cycle assessment – Principles and framework. Geneva: ISO.
- ISO 14040 (2006). Environmental management – Life cycle assessment – Principles and framework. Geneva: ISO.
- ISO 14041 (1998). Environmental management – Life cycle assessment – Goal and scope definition and inventory analysis. Geneva: ISO.

- ISO 14042 (2000). Environmental management – Life cycle assessment – Life cycle impact assessment. Geneva: ISO.
- ISO 14043 (2000). Environmental management – Life cycle assessment – Interpretation. Geneva: ISO.
- ISO. ISO 14044 (2006). Environmental management – Life cycle assessment – Requirements and guidelines. Geneva: ISO.
- Izquierdo D, Alonso C, Andrade C, Castellote M (2004). Potentiostatic determination of chloride threshold values for rebar depassivation. Experimental and statistical study. *Electrochim Acta*;49(17-18):2731-2739.
- Jacobsen S, Farstad T, Gran HC, Sellevold EJ (1991). Frost scaling of no slump concrete: effect of strength. *Nord Concr Res*;11(1):57-71.
- Jacott M, Comunes F, Reed C, Taylor A, Whinfield M (2003). Energy use in the cement industry in North America: Emissions, waste generation and pollution control, 1999-2001. In: Proceedings of the Second North American symposium on assessing the environmental effects of trade, Mexico City, Mexico, March 24-26, 2003. Montreal: Commission for Environmental Cooperation.
- Jakobsen UH, Pade C, Thaulow N, Brown D, Sahu S, Magnusson O, De Buck S, De Schutter, G (2006). Automated air void analysis of hardened concrete – a round robin study. *Cem Concr Res*;36(8):1444-1452.
- Janeva D, Beslac J, Sekulic D, Mavar K (2002). The influence of hydraulic additions to cement on frost and de-icing salt scaling resistance of concrete. In: Setzer MJ, Auberg R, Keck HJ (Eds.), Proceedings of the 2nd International RILEM Workshop on Frost Resistance of Concrete from Nano-Structure and Pore Solution to Macroscopic Behavior and Testing, Essen, Germany, April 18-19, 2002. Bagnaux: RILEM Publications, 343-350.
- Jaroenratanapirom D, Sahamitmongkol R (2011). Self-crack closing ability of mortar with different additives. *J Met Mater Miner*;21(1):9-17.
- Jennings HM (2000). A model for the microstructure of calcium silicate hydrate in cement paste. *Cem Concr Res* 2000;30(1):101-116.
- Johannesson B, Utgenannt P (2001). Microstructural changes caused by carbonation of cement mortar. *Cem Concr Res*;31(6):925-931.
- Jolliet O, Margni M, Charles R, Humbert S, Payet J, Rebitzer G, Rosenbaum R (2003). IMPACT 2002+: a new life cycle assessment methodology. *Int J LCA*;10(6):324-330.
- Josa A, Aguado A, Heino A, Byars E, Cardim A (2004). Comparative analysis of available life cycle inventories of cement in the EU. *Cem Concr Res*;34(8):1313-1320.
- Justnes H (1998). A review of chloride binding in cementitious systems. *Nord Concr Res*;21(1):48-63.
- Kayyali OA, Haque MN (1995). The Cl⁻/OH⁻ ratio in chloride contaminated concrete – a most important criterion. *Mag Concr Res*;47(172):235-242.
- Klieger P, Gebler SH (1987). Fly ash and concrete durability. In: Scanlon J (Ed.), ACI Special Publication SP-100. Detroit: American Concrete Institute, 1043-1069.
- Klinkenberg LJ (1941). The permeability of porous media to liquids and gases. *Drilling and Production Practice*. API:200-213.
- KMI (2010). Personal communication with Debontridder L, Reference R100666. Brussels: Royal Meteorological Institute (KMI).
- Kobayashi K, Suzuki K, Uno Y (1994). Carbonation of concrete structures and decomposition of C–S–H. *Cem Concr Res*;24(1):55-61.

- Manera M, Vennesland O, Bertolini L (2008). Chloride threshold for rebar corrosion in concrete with addition of silica fume. *Corros Sci*;50(2):554-560.
- Marion AM, De Lanève M, De Grauw A (2005). Study of the leaching behaviour of paving concretes: quantification of heavy metal content in leachates issued from tank test using demineralized water. *Cem Concr Res*;35(5):951-957.
- Martaud T (2008). Environmental evaluation of the production of natural aggregates exploited from a quarry: Indicators, models and tools (in French). PhD thesis. Orléans: University of Orléans.
- McGrath P, Hooton RD (1996). Influence of voltage on chloride diffusion coefficients from chloride migration tests. *Cem Concr Res*;26(8):1239-1244.
- Mehta PK (1998). Role of pozzolanic and cementitious materials in sustainable development of the concrete industry. In: VM Malhotra (Ed.), *ACI Special Publication SP-178*. Detroit: American Concrete Institute, 1-20.
- Mehta PK, Monteiro PJM (2001). *Concrete microstructure, properties and materials*, 2nd edition. Berkeley: University of California.
- Metal Bulletin (2011). Ferrous and non-ferrous market prices 2004-2008 [cited 2011 Aug 18]. Available from: <http://www.metalbulletin.com>.
- MetalPrices.com (2014). Silicon prices [updated 2013 Mar 1; cited 2014 Apr 7]. Available from: <http://www.metalprices.com/metal/silicon>.
- Meyer C. The greening of the concrete industry. *Cem Concr Compos* 2009;31(8):601-605.
- Mielenz RC, Wolkodoff VE, Backstrom JE, Burrows RH (1958). Origin, evolution, and effects of the air void system in concrete, Part 4 – The air void system in job concrete. *ACI J Proc*; 55(10):507-517.
- Morbi A, Cangiano S, Borgarello E (2010). Cement-based materials for sustainable development. In: Zachar J, Claisse P, Naik TR, Ganjian E (Eds.), *Proceedings of the Second International Conference on Sustainable Construction Materials and Technologies, Proceedings of Sessions in Honor of: Dr. Enrico Borgarello, Professor Theodore W. Bremner, Professor David W. Fowler, Professor Konstantin Kovler, Professor Koji Sakai, Ancona, Italy, June 28-30, 2010*. Milwaukee: University of Wisconsin Milwaukee Center for By-Products Utilization, 1-10.
- Mu S (2012). Chloride penetration and service life prediction of cracked self-compacting concrete. PhD thesis. Ghent: Ghent University.
- Nagataki S, Otsuki N, Wee TH, Nakashita K (1993). Condensation of chloride ion in hardened cement matrix materials and on embedded steel bars. *ACI Mater J*;90(4):323-332.
- NBN B05-201 (1976). Resistance of materials to freezing – water absorption by capillarity (in Dutch). Brussels: BIN.
- NBN B15-001 (2004) Supplement to NBN EN 206-1, Concrete – specification, performance, production and conformity (in Dutch). Brussels: BIN.
- NBN B15-100 (2008). Methodology for assessment and the validation of fitness for use of cements or additions of type II for concrete (in Dutch). Brussels: BIN.
- NBN B15-220 (1990) Concrete Testing: Determination of compressive strength (in Dutch). Brussels: BIN.
- NBN EN 12350-2 (2009). Testing fresh concrete – Part 2: Slump-test. Brussels: BIN.
- NBN EN 12350-7 (2009). Testing fresh concrete – Part 7: Air content – Pressure methods. Brussels: BIN.
- NBN EN 12390-5 (2009). Testing hardened concrete – Part 5: Flexural strength of test specimens. Brussels: BIN.
- NBN EN 12390-6 (2010). Testing hardened concrete – Part 6: Tensile splitting strength of test specimens. Brussels: BIN.

- NBN EN 13263-1+A1 (2009). Silica fume for concrete – Part 1: Definitions, requirements and conformity criteria. Brussels: BIN.
- NBN EN 1339 (2003). Concrete paving flags – Requirements and test methods. Brussels: BIN.
- NBN EN 15804+A1 (2014). Sustainability of construction works – Environmental product declarations – Core rules for the product category of construction products. Brussels: BIN.
- NBN EN 196-1 (2005). Methods of testing cement – Part 1: Determination of strength. Brussels: BIN.
- NBN EN 196-2 (2005). Methods of testing cement – Part 2: Chemical analysis of cement. Brussels: BIN.
- NBN EN 196-6 (2010). Methods of testing cement – Part 6: Determination of fineness. Brussels: BIN.
- NBN EN 197-1 (2011). Cement – Part 1: Composition, specifications and conformity criteria for common cement. Brussels: BIN.
- NBN EN 1990 (2002). Eurocode – Basis of structural design. Brussels: BIN.
- NBN EN 1992-1-1 (ANB 2010). Eurocode 2: Design of concrete structures – Part 1-1: General rules and rules for buildings (+AC: 2008)(+AC: 2010). Brussels: BIN.
- NBN EN 206-1 (2000). Concrete – Part 1: Specification, performance, production and conformity. Brussels: BIN.
- NBN EN 450-1 (2012). Fly ash for concrete – Part 1: Definitions, specifications and conformity criteria. Brussels: CEN.
- NBN EN 451-2 (1995). Method of testing fly ash – Part 2: Determination of fineness by wet sieving. Brussels: BIN.
- NEN 7345 (1995). Leaching characteristics of solid earthy and stony building and waste materials, Leaching tests, Determination of the leaching of inorganic components from building and monolithic waste materials with the diffusion test. Delft: NEN.
- Neuwald A, Krishnan A, Weiss J, Olek J, Nantung TE (2003). Concrete Curing and its relationship to measured scaling in concrete containing fly ash. In: Proceedings of the 82nd Annual Meeting Indiana Transportation Research Board, Washington DC, USA, January 12-16, 2003. West Lafayette: TRB.
- Neville AM (1995). Properties of Concrete. New York: John Wiley and Sons, Inc.
- Nilsson LO (2002). Concepts in chloride ingress modelling. In: Andrade C, Kropp J (Eds.), Proceedings of the Third RILEM Workshop on Testing and Modelling the Chloride Ingress into Concrete, 9-10 September 2002, Madrid, Spain. Bagneux: RILEM Publications, 29-48.
- Nilsson LO, Gehlen C (1998). Summary of the statistical quantification of the DuraCrete resistivity corrosion rate model, BE95-134/TG4, Sub-Task 4.1 Report. Gothenborg and Aachen: Chalmers University of Technology, Sweden and Institute of Building Research, Technical University of Aachen (ibac).
- NT Build 357 (1989). Concrete, repairing materials and protective coating: carbonation resistance. Espoo: Nordtest.
- NT Build 443 (1995). Concrete, Hardened: Accelerated chloride penetration. Espoo: Nordtest.
- NT Build 492 (1999). Concrete, mortar and cement-based repair materials: Chloride migration coefficient from non-steady state migration experiments. Espoo: Nordtest.
- Oh BH, Jang SY, Shin YS (2003). Experimental investigation of the threshold chloride concentration for corrosion initiation in reinforced concrete structures. *Mag Concr Res*;55(2):117-124.
- Ollivier JP, Arsenault J, Truc O, Marchand J (1997). Determination of chloride binding isotherms from migration tests. In: Mehta PK (Ed.), Proceedings of the Mario Collepardi Symposium on Advances in Concrete Science and Technology, Rome, Italy, October 7-10, 1997. Rome: the Organizing Committee of the Conference, 198-217.

- Otieno MB, Beushausen HD, Alexander MG (2011). Modelling corrosion propagation in reinforced concrete structures – A critical review. *Cem Concr Compos*;33(2):240-245.
- Oxford Instruments (2014). AztecEnergy, EDS software for SEM [computer software]. Oxfordshire: Oxford Instruments.
- Page CL, Short NR, El Tarras A (1981). Diffusion of chloride ions in hardened cement pastes. *Cem Concr Res*;11(3):395-406.
- Pane I, Hansen W (2005). Investigation of blended cement hydration by isothermal calorimetry and thermal analysis. *Cem Concr Res* 35(6):1155-1164.
- Papadakis VG, Vayenas CG, Fardis MN (1991). Fundamental modeling and experimental investigation of concrete carbonation. *ACI Mater J*;88(5):363-373.
- Park K, Hwang Y, Seo S, Seo H (2003). Quantitative assessment of environmental impacts of life cycle of highways. *J Constr Eng Manage*;129(1):25-31.
- Parrot LJ (1987). A review of carbonation in reinforced concrete. Wexham Springs: Cement and Concrete Association.
- Pavlik V (2000). Water extraction of chloride, hydroxide and other ions from hardened cement pastes. *Cem Concr Res*;30(6):895-906.
- Petersson PE (2004). A service life model for scaling resistance of concrete – reflections. Contribution to *fib* task group 5.6. Lund.
- Peupartier BLP (2001). Life cycle assessment applied to the comparative evaluation of single family houses in the French context. *Energ Buildings*;33(5):443-450.
- Pietersen HS (1993). Reactivity of fly ash and slag in cement. PhD thesis. Delft: TU Delft.
- Pinto RCA, Hover KC (2001). Frost and scaling resistance of high-strength concrete, RD122. Skokie : Portland Cement Association.
- Pistilli MF (1983). Air void parameters developed by air-entraining admixtures, as influenced by soluble alkalis from fly ash and Portland cement. *J Am Concr Inst*;80(3):217-222.
- Plummer LN, Busenberg E (1982). The solubilities of calcite, aragonite and vaterite in CO₂-H₂O solutions between 0 and 90°C, and an evaluation of the aqueous model for the system CaCO₃-CO₂-H₂O. *Geochim Cosmochim Acta*;46(6):1011-1040.
- Polder RB (2001). Test methods for on site measurement of resistivity of concrete – a RILEM TC-154 technical recommendation. *Constr Build Mater*;15(2-3):125-131.
- Poupard O, Aït-Mokhtar A, Dumargue P (2004). Corrosion by chlorides in reinforced concrete: Determination of chloride concentration threshold by impedance spectroscopy. *Cem Concr Res*;34(6):991-1000.
- Powers TC (1965). The mechanisms of frost action in concrete. Stanton Walker Lecture Series on the Material Science.
- PRé Consultants bv (2011). SimaPro, Version 7.3.3 [computer software]. Amersfoort: PRé Consultants bv.
- PRé Consultants bv: De Schryver A, Goedkoop M, Alvarado C, Vieira M (2008). SimaPro Training – Effective LCA with SimaPro. Amersfoort: PRé Consultants bv.
- Price L, Worrell E, Phylipsen D (1999). Energy use and carbon dioxide emissions in energy-intensive industries in key developing countries. In: Proceedings of the 1999 Earth Technologies Forum, Washington DC, September 27-29, 1999. Berkeley: Lawrence Berkeley National Laboratory, Environmental Energy Technologies Division.
- Ravina D (1986). Properties of fresh concrete containing large amounts of fly ash. *Cem Concr Res*;16(2):227-238.

- RCP Consulting Software (1987-2013). Comrel, TI, Version 8.10 [computer software]. Munich: RCP Consulting Software.
- Reap J, Roman F, Duncan S, Bras B (2008). A survey of unresolved problems in life cycle assessment, Part 2: impact assessment and interpretation. *Int J LCA*;13(5):374-388.
- Reddy B, Glass GK, Lim PJ, Buenfeld NR (2002). On the corrosion risk presented by chloride bound in concrete. *Cem Concr Compos*;24(1):1-5.
- Ridoutt BG, Pfister S (2010). A revised approach to water footprinting to make transparent the impacts of consumption and production on global freshwater scarcity. *Glob Environ Chang*;20(1):113-120.
- RILEM CPC-18 (1988). CPC-18 Measurement of hardened concrete carbonation depth. *Mater Struct*;21(126):453-455.
- RILEM TC 116-PCD (1999). Permeability of concrete as a criterion of its durability. *Mater Struct*;32(217):174-179.
- RILEM TC 178-TMC (2002a). Analysis of total chloride content in concrete – Recommendation. *Mater Struct*;35(9):583-585.
- RILEM TC 178-TMC (2002b). Analysis of water soluble chloride content in concrete – Recommendation. *Mater Struct*;35(9):586-588.
- Rougeau P. (1997). AFREM Round-robin test results “The accelerated carbonation test” (in French). In: Proceedings of Journées Techniques AFPC-AFREM Durabilité des Bétons, Toulouse, France, December 11-12, 1997. Toulouse: INSA.
- Rovira J, Mari M, Nadal M, Schuhmacher M, Domingo JL (2010). Partial replacement of fossil fuel in a cement plant: Risk assessment for the population living in the neighborhood. *Sci Total Environ*;408(22):5372-5380.
- Rozière E, Loukili A, Cussigh F. A performance based approach for durability of concrete exposed to carbonation. *Constr Build Mater* 2009;23(1):190-199.
- Saetta AV, Vitaliani RV (2004). Experimental Investigation and numerical modeling of carbonation process in reinforced concrete structures, Part I: Theoretical formulation. *Cem Concr Res*;34(4):571-579.
- Sandberg P, Tang L, Andersen A (1998). Recurrent studies of chloride ingress in uncracked marine concrete at various exposure times and elevations. *Cem Concr Res*;28(10):1489-1503.
- Sauman Z (1971). Carbonation of porous concrete and its main binding components. *Cem Concr Res*;1(6):645-662.
- Sayagh S, Ventura A, Hoang T, François D, Jullien A (2010). Sensitivity of the LCA allocation procedure for BFS recycled into pavement structures. *Resour Conserv Recy*;54(6):348-358.
- Schiessl P, Breit W (1996). Local repair measures at concrete structures damaged by reinforcement corrosion – Aspects of durability. In: Page C, Bamforth P, Figg J (Eds.), Proceedings of the 4th International Symposium on Corrosion of Reinforcement in Concrete Construction, Cambridge, July 1-4, 1996. Cambridge: The Royal Society of Chemistry.
- Schuhmacher M, Domingo JL, Garreta J (2004). Pollutants emitted by a cement plant: health risks for the population living in the neighborhood. *Environ Res*;95(2):198-206.
- Schuermans A, Rouwette R, Vonk N, Broers JW, Rijnsburger HA, Pietersen HS (2005). LCA of finer sand in concrete. *Int J LCA*;10(2):131-135.
- Schwartzentruber A, Catherine C (2000). Method of the concrete equivalent mortar (CEM) – A new tool to design concrete containing admixtures (in French). *Mater Struct*;33(232):475-482.
- Sellevoid EJ, Farstad T (1991). Frost/salt testing of concrete: Effect of test parameters and concrete moisture history. *Nord Concr Res*;10:121-138.

- Sisomphon K, Copuroglu O, Fraaij ALA (2010). Development of blast-furnace slag mixtures against frost salt attack. *Cem Concr Compos*;32(8):630-638.
- Sisomphon K, Franke L (2007). Carbonation rates of concretes containing high volume of pozzolanic materials. *Cem Concr Res*;37(12):1647-1653.
- Slegers PA, Rouxhet PG (1976). Carbonation of the hydration products of tricalcium silicate. *Cem Concr Res*;6(3):381-388.
- Smakhtin V (2008). Basin closure and environmental flow requirements. *Int J Water Resour D*;24(2):227-233.
- SN 505 262/1 (2003). Construction with concrete– Complementary specifications (in French). Zurich : Société des ingénieurs et des architectes.
- Snyder (Ed.) (1965). Protective coatings to prevent deterioration of concrete by deicing chemicals. National Cooperative Highway Research Program Report 16. Washington DC: Transportation Research Board.
- Sokka L, Koskela S, Seppälä J (2005). Life cycle inventory analysis of hard coal based electricity generation. The Finnish environment 797. Helsinki: Finnish Environment Institute.
- Sommer H (1979). The precision of the microscopical determination of the air-void system in hardened concrete. *Cem Concr Aggr*;1(2):49-55.
- Song HW, Kwon SJ, Byun KJ, Park CK (2006). Predicting carbonation in early aged cracked concrete. *Cem Concr Res*;36(5):979-989.
- Sorensen EG (1983). Freezing and thawing resistance of condensed silica fume (microsilica) concrete exposed to deicing chemicals. In: Malhotra VM (Ed.), *ACI Special Publication SP-79*. Detroit: American Concrete Institute, 709-718.
- St John D, Poole AW, Sims I (1998). *Concrete petrography, A handbook of investigative techniques*. London: Arnold Publishers.
- Stark J, Ludwig HM (1997). Freeze-thaw and freeze-deicing salt resistance of concretes containing cement rich in blast-furnace slag. In: Justness H (Ed.), *Proceedings of the 10th International Congress on Chemistry of Cement, Vol. 4.*, Gothenborg, Sweden, June 2-6, 1997. Trondheim: SINTEF.
- Steen B (1999). A systematic approach to environmental priority strategies in product development (EPS). 2000-general system characteristics and 2000-models and data. CPM Report: 1999, 4-5. Gothenburg: Chalmers University of Technology, Technical Environmental Planning, Centre for Environmental Assessment of Products and Material Systems.
- Stewart MG, Wang X, Nguyen MN (2011). Climate change impact and risks of concrete infrastructure deterioration. *Eng Struct*;33(4):1326-1337.
- Sturup VR, Hooton RD, Clendenning TG (1983). Durability of fly ash concrete. In: Malhotra VM (Ed.), *ACI Special publication SP-79*. Detroit: American Concrete Institute, 71-86.
- Suryavanshi AK, Scantlebury JD, Lyon SB (1998). Corrosion of reinforcement steel embedded in high water-cement ratio concrete contaminated with chloride. *Cem Concr Compos*;20(3):263-269.
- Suzuki K, Nishikawa T, Ito S (1985). Formation and carbonation of C–S–H in water. *Cem Concr Res*;15(2):213-224.
- Swamy RN, Hamada H, Laiw JC (1994). A critical evaluation of chloride penetration into concrete in marine environment. In: Swamy RN (Ed.), *Proceedings of the International Conference on Corrosion and Corrosion Protection of Steel in Concrete*, Sheffield, England, July 24-28, 1994. Sheffield: Sheffield Academic Press, 404-419.
- Taerwe L, De Schutter G (1996-2006). *Concrete technology + additional course notes (in Dutch)*. Course notes. Ghent: Ghent University.

- Takemoto K, Uchikawa H (1980). Hydration of pozzolanic cement. In: Proceedings of the 7th International Congress on the Chemistry of Cement, IV-2, Paris, France, 1980. Paris: Editions Septima, 1-29.
- Tang (1996). Chloride transport in concrete: Measurement and prediction. Doctoral thesis, Publication P-96:6. Gothenborg: Department of Building materials, Chalmers University of Technology.
- Tang L, Nilsson LO (1992). Rapid determination of the chloride diffusivity in concrete by applying an electrical field. *ACI Mater J*;89(1):49-53.
- Tang L, Nilsson LO (1993). Chloride binding capacity and binding isotherms of OPC pastes and mortars. *Cem Concr Res*;23(2):247-253.
- Tang L, Nilsson LO (2001). Discussion on the paper 'AFREM test procedures concerning chlorides in concrete: Extraction and titration methods', by T Chaussadent and G Arliguie. *Mater Struct* 34(2):128.
- Tang L, Nilsson LO, Basheer PAM (2012). Resistance of concrete to chloride ingress, Testing and modelling. New York: Spon Press.
- Testaankoop (2014). Koopwijzer gas en elektriciteit. Electrabel FixOnline. [cited 2014 Apr 7]. Available from: <http://www.test-aankoop.be/woning-energie/energie/bereken-zelf/energie-wie-wordt-uw-leverancier>.
- Thermo Fisher Scientific Inc. (2011). SOL.I.D., Solver of Intrusion Data Software for PASCAL 140/240/440 Series Mercury Porosimeters [computer software]. Rodano-Milan: Thermo Fisher Scientific Inc.
- Thiery M, Villain G, Dangla P, Platret G (2006). Investigation of the carbonation front shape on cementitious materials: Effects of the chemical kinetics. *Cem Concr Res* 2007;37(7):1047-1058.
- Thomas JJ, Jennings HM, Allen AJ (1999). The surface area of hardened cement pastes as measured by various techniques. *Concr Sci Eng*;1(1):45-64.
- Thomas M (1996). Chloride thresholds in marine concrete. *Cem Concr Res*;26(4):513-519.
- Tuutti K (1982). Corrosion of steel in concrete. Stockholm: Swedish Cement and Concrete Research Institute.
- Utgenannt P (1999). Influence of carbonation on the scaling resistance OPC concrete. In: Janssen DJ, Setzer MJ, Snyder MB (Eds.), Proceedings of the International Workshop on Frost Damage in Concrete, Minneapolis, USA, June 28-30, 1999. Bagnaux: RILEM Publications, 103-113.
- Vahedifard F, Nili M, Meehan CL (2010). Assessing the effects of supplementary cementitious materials on the performance of low-cement roller compacted concrete pavement. *Constr Build Mater*;24(12):2528-2535.
- Val DV, Stewart MG (2003). Life-cycle cost analysis of reinforced concrete structures in marine environments. *Struct Saf*;25(4):343-362.
- Valenza II JJ, Scherer GW (2007a). A review of salt scaling: I. Phenomenology. *Cem Concr Res*;37(7):1007-1021.
- Valenza II JJ, Scherer GW (2007b). A review of salt scaling: II. Mechanisms. *Cem Concr Res*;37(7):1022-1034.
- Van den Heede P (2008). Porosity and transport properties of 'green' concrete types (in Dutch). Master thesis. Ghent: Ghent University.
- Van den Heede P, De Belie N (2012). Environmental impact and life cycle assessment (LCA) of traditional and 'green' concretes: Literature review and theoretical calculations. *Cem Concr Compos*;34(4):431-42.
- Van den Heede P, De Belie N (2014). A service life based global warming potential for high-volume fly ash concrete exposed to carbonation. *Constr Build Mater*;55(3):183-193.
- Van den Heede P, Furniere J, De Belie N (2013). Influence of air entraining agents on deicing salt scaling resistance and transport properties of high-volume fly ash concrete. *Cem Concr Compos*;37(3):293-303.

- Van den Heede P, Gruyaert E, De Belie N (2010). Transport properties of high-volume fly ash concrete: Capillary water Sorption, water sorption under vacuum and gas permeability. *Cem Concr Compos*;32(10):749-756.
- Van den Heede P, Maes M, De Belie N (2014). Influence of active crack width control on the chloride penetration resistance and global warming potential of concrete slabs made with fly ash + silica fume concrete. *Constr Build Mater*;67(Part A):74-80.
- Van den Heede P, Maes M, Gruyaert E, De Belie N (2012). Full probabilistic service life prediction and life cycle assessment of concrete with fly ash and blast-furnace slag in a submerged marine environment: A parameter study. *Int J Environ Sust Dev*;11(1):32-49.
- Van der Sloot HA, Cnubben PAJP (2000). Exploratory evaluation on the effects of co-combustion of biomass at a pulverized coal fired power plant and the mixing of biomass ash with coal fly ash on the quality of pulverized coal fly ash (in Dutch). ECN-C—00-058. NOVEM.
- Van Oss HG, Padovani AC (2003). Cement manufacture and the environment, Part II: environmental challenges and opportunities. *J Ind Ecol*;7(1):93-127.
- Virtanen J (1990). Field study on the effects of additions on the salt scaling resistance of concrete. *Nord Concr Res*;9:197-212.
- Visser JHM (2002). Salt scaling resistance of concrete (in Dutch). *Cement*;2:99-105.
- Visser JHM (2009). Predicting the durability of marine structures in the Netherlands: Assessing the migration coefficient. In: Kovler K (Ed.), *Proceedings of the 2nd International Workshop on Concrete Durability and Service Life Planning (ConcreteLife '09)*, Haifa, Israel, September 7-9, 2009. Bagnoux: RILEM Publications, 221-228.
- Visser JHM (2012). Accelerated carbonation testing of mortar with supplementary cementing materials: Limitation of the acceleration due to drying. *Heron*;57(3):231-246.
- Visser JHM, Gaal GCM, Rooij MR (2002). Time dependency of chloride diffusion coefficients in concrete. In: Andrade C, Kropp J (Eds.), *Proceedings of the Third International RILEM Workshop on Testing and Modelling the Chloride Ingress into Concrete*, Madrid, Spain, September 9-10, 2002. Bagnoux: RILEM Publications, 423-433.
- Visser JHM, Siemes T (2010). Service life calculations for concrete structures (in Dutch). Delft: TNO.
- von Bahr B, Hanssen OJ, Vold M, Pott G, Stoltenberg-Hansson E, Steen B (2003). Experiences of environmental performance evaluation in the cement industry, Data quality of environmental performance indicators as a limiting factor for benchmarking and rating. *J Clean Prod*;11(7):713-725.
- Vrijders J, Desmyter J (2008). Stimulating a high-quality use of recycled aggregates (in Dutch). PA/AVP-AD/0702. A study conducted by the Belgian Building Research Institute (WTCB) for the Public Waste Agency of Flanders (OVAM), September 2008. Limelette: WTCB.
- Vyncke J, Vrijders J (2010). Recycling of C & D waste in Belgium: State-of-the-art and opportunities for technology transfer. In: Zachar J, Claisse P, Naik TR, Ganjian E (Eds.), *Proceedings of the Second International Conference on Sustainable Construction Materials and Technologies, Proceedings of Sessions in Honor of: Dr. Enrico Borgarello, Professor Theodore W. Bremner, Professor David W. Fowler, Professor Konstantin Kovler, Professor Koji Sakai*, Ancona, Italy, June 28-30, 2010. Milwaukee: University of Wisconsin Milwaukee Center for By-Products Utilization, 191-201.
- Weiss J, Snyder K, Bullard J, Bentz D (2013). Using a saturation function to interpret the electrical properties of partially saturated concrete. *J Mater Civ Eng*;25(8):1097-1106.
- Whiting D (1989). Deicer scaling resistance of lean concretes containing fly ash. In: Malhotra VM (Ed.), *ACI Special Publication SP-114*. Detroit: American Concrete Institute, 349-372.

- Wiens U, Schiessl P (1997). Chloride binding of cement paste containing fly ash. In: Justness H (Ed.), Proceedings of the 10th International Conference on the Chemistry of Cement, Gothenborg, Sweden, June 2-6. Trondheim: SINTEF, 4-10.
- World Commission on Environment and Development (1987). Our common future. Oxford: Oxford University Press
- Xiantuo C, Ruizhen Z (1994). Kinetic study of ettringite carbonation reaction. *Cem Concr Res*;24(7):1383-1389.
- Xing S, Xu Z, Jun G (2008). Inventory analysis of LCA on steel- and concrete-construction office buildings. *Energ Buildings*;40(7):1188-1193.
- Yuan Q (2009). Fundamental studies on test methods for the transport of chloride ions in cementitious materials. PhD thesis. Ghent: Ghent University.
- Zhang DS (1996). Air entrainment in fresh concrete with PFA. *Cem Concr Compos*;18(6):409-416.
- Zhou Q, Glasser FP (2000). Kinetics and mechanism of the carbonation of ettringite. *Adv Cem Res*;12(3):131-136.

Appendix A

Effect of the applied CO₂ concentration as evaluated by Visser (2012)

According to Visser (2012) there is another way to see whether accelerating the carbonation test by increasing the CO₂ concentration may lead to unwanted effects, such as an important over- or underestimation of the concrete's service life when based upon these kinds of tests. The evaluation procedure follows directly from Equation 5-1. When plotting the measured carbonation depths during the accelerated carbonation tests at 1% and 10% CO₂ as a function of $\sqrt{(2 \cdot c_s \cdot t)}$, the slope of the linear trends obtained should be equal to $\sqrt{(1/R_{carb})}$ (Figure A-1).

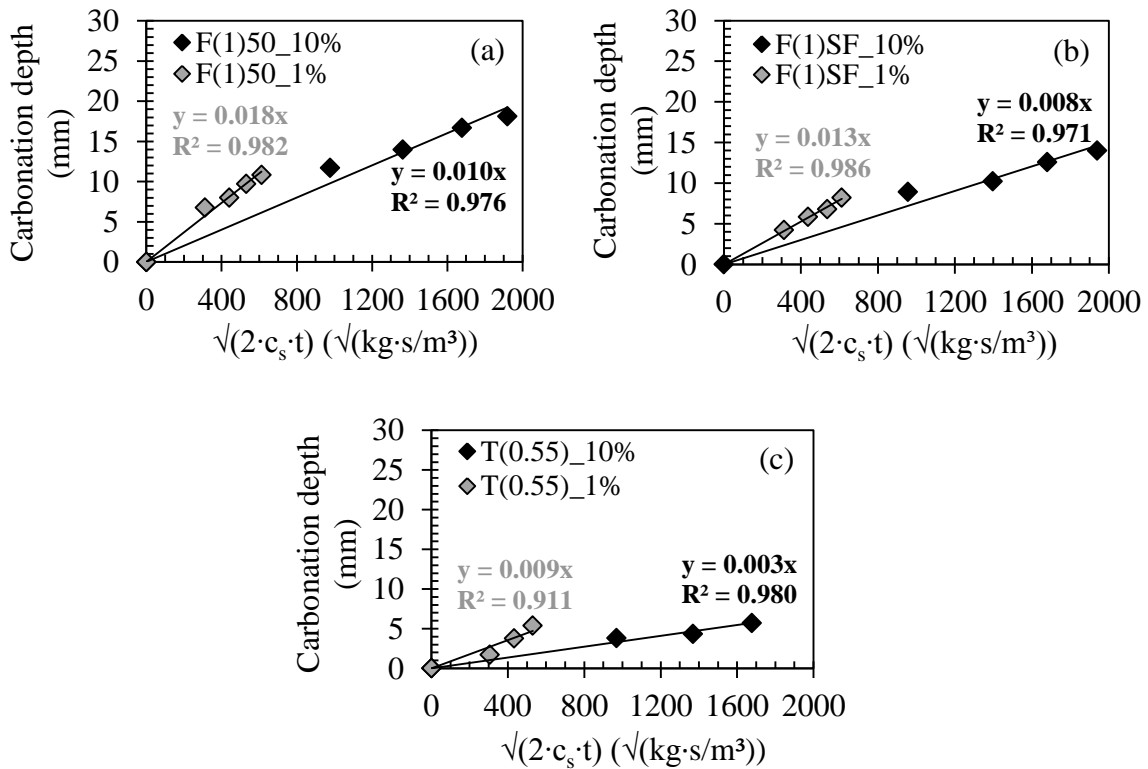


Figure A-1. Difference between the carbonation test at 1% and 10% CO₂ in terms of the slope $1/\sqrt{(R_{carb})}$ for the linear trend observed when plotting the carbonation depth x_c as a function of $\sqrt{(2 \cdot c_s \cdot t)}$.

Since R_{carb} is a material variable which is normally independent of the applied CO_2 concentration, the slopes should be similar for the two carbonation tests. If not, some other unwanted effects must have occurred. Figure A-1 clearly indicates that the slope corresponding with a carbonation test at 10% CO_2 significantly differs from the one obtained at only 1%. Thus, increasing the CO_2 concentration to 10% indeed induces non-negligible changes. It can be seen as a further confirmation of the observed differences between the carbonation rate at 1% CO_2 as estimated from a carbonation experiment at 10% CO_2 and the carbonation rate which was actually measured at 1% CO_2 (Figure 5.7).

Appendix B

Second order prediction of the time to carbonation-induced depassivation with the standard deviations on the individual values of A_{field} as input.

In chapter 8, the estimation of the time to carbonation-induced depassivation was based on the standard deviation on the regression for the measured accelerated carbonation coefficients. The corresponding standard deviations for the field carbonation rate A_{field} were calculated from these values and implemented in the limit state function for carbonation (Equation 8-7) with omission of the weather function. These standard deviations were in the range of 0.1 mm/ $\sqrt{\text{years}}$ or less for all studied concrete mixtures. More critical conditions in terms of service life prediction outcome would be reached if the standard deviations on the individual values would be used. Table B.1 gives an overview of the mean values and the standard deviations on the individual values for A_{field} after 28 days.

Table B.1. A_{field} values (mm/ $\sqrt{\text{years}}$) incl. standard deviations on the individual values after 28 days as input for second order prediction of the initiation period in exposure class XC3.

| $A_{\text{field}}/\text{XC3}$ | t_0 (d) | T(0.55) | F(1)15 | F(2)15 | F(1)50 | F(2)50 | F(1)SF | F(2)SF |
|-------------------------------|-----------|----------------------|---------|---------|----------------------|---------|----------------------|---------|
| Colorimetric | 28 | 0.7±0.4 | – | – | 2.2±0.3 | 1.8±0.3 | 1.3±0.6 | 1.4±0.4 |
| | | – | – | – | 3.0±0.4 ^a | – | 1.7±0.8 ^a | – |
| | | 1.8±0.9 ^b | – | – | 4.0±0.5 ^b | – | 2.3±1.0 ^b | – |
| | | – | – | – | 5.5±0.6 ^c | – | 3.0±1.3 ^c | – |
| Microscopic | 28 | 0.9±0.3 | 0.4±0.1 | 0.1±0.1 | 1.9±0.2 | 2.0±0.4 | 1.1±0.3 | 1.4±0.3 |

^a Based on A_{field} values for suboptimal curing: 7 days at 20°C and 95% RH, 21 days at 20°C and 60% RH.

^b Based on A_{field} values for optimal curing corrected for the applied CO₂ concentration.

^c A_{field} values for suboptimal curing^a after correction for the applied CO₂ concentration^b.

The as such reported A_{field} values and the corresponding standard deviations on the individual values after 28 days were also once implemented in the second order limit state function (Equation 8-7) with omission of the weather function. The resulting estimations of the carbonation-induced corrosion initiation period per concrete mixture are shown in Table B.2.

Table B.2. Second order prediction of the corrosion initiation period (years) in exposure class XC3 with A_{field} incl. standard deviations on the individual values after 28 days as input.

| 2 nd order/XC3 | t_0 (d) | T(0.55) | F(1)15 | F(2)15 | F(1)50 | F(2)50 | F(1)SF | F(2)SF |
|---------------------------|-----------|------------------|--------|--------|------------------|--------|------------------|--------|
| Colorimetric | 28 | +1000 | – | – | 425 | 616 | 818 | 884 |
| | | – | – | – | 229 ^a | – | 472 ^a | – |
| | | 405 ^b | – | – | 129 ^b | – | 270 ^b | – |
| | | – | – | – | 68 ^c | – | 159 ^c | – |
| Microscopic | 28 | +1000 | +1000 | +1000 | 585 | 481 | +1000 | 965 |

^a Based on A_{field} values for suboptimal curing: 7 days at 20°C and 95% RH, 21 days at 20°C and 60% RH.

^b Based on A_{field} values for optimal curing corrected for the applied CO₂ concentration.

^c A_{field} values for suboptimal curing^a after correction for the applied CO₂ concentration^b.

In comparison with the times to depassivation reported in Table 8.6, the ones given Table B.2 were somewhat lower. This can be expected because the standard deviations on the individual values are larger than the standard deviations on the regression. This means that more variation on the values of A_{field} is possible. Higher values than the mean value of A_{field} will occur more frequently which means that the time to depassivation will also be shorter.

However, although these additional calculations based on the standard deviation on the individual values represent a more critical condition, they do not have an important effect on the life cycle assessment presented in Chapter 12. Since the maximum service life considered in the functional unit definition for LCA amounted to no more than 100 years, not much has changed. As shown in Table B.2, the corrosion initiation periods still easily exceeded 100 years for most mixtures. Thus, the functional unit definitions and corresponding environmental impact calculations were not affected by this change in calculation approach.

Only in case the A_{field} values of composition F(1)50 were corrected for the curing conditions and the CO₂ concentration during carbonation testing, the initiation period was less than 100 years. When using the standard deviation on the individual values of A_{field} as input, depassivation is expected after 68 years, while this was 72 years when using the standard deviations on the regression as input. Nevertheless, the difference is small.

When assuming a concrete column or slab as functional unit for LCA (see Section 12.3 and 12.4), the number of repairs necessary in a 100 year timeframe remains the same. Only one repair would be necessary in both cases. The environmental impact calculations expressed in global warming potential would not have a different outcome.

In case the required concrete volume per unit of strength and service life would be considered as functional unit (see Section 12.2), then the functional unit value and corresponding global warming potential will change a bit when just the corrosion initiation period is considered in the service life. The functional unit would increase from $3.09 \times 10^{-4} \text{ m}^3/(\text{N}/\text{mm}^2 \cdot \text{yr})$ (see Table 12.2: F(1)50^b) to $3.27 \times 10^{-4} \text{ m}^3/(\text{N}/\text{mm}^2 \cdot \text{yr})$. The resulting global warming potential would only rise from $1.04 \times 10^{-1} \text{ kg CO}_2 \text{ eq}$ (see Figure 12.6: F(1)50_XC3_b) to $1.10 \times 10^{-1} \text{ kg CO}_2 \text{ eq}$.

All in all, the use of the standard deviation on the individual values instead of the standard deviation on the regression of A_{field} for service life prediction results in a rather negligible increase in impact.

Appendix C

Second order prediction of the time to chloride-induced depassivation with the measured initial chloride content as input.

In chapter 9, a literature value of the initial chloride content suggested by CUR Guideline VC81 (2009) was used for the second order prediction of the time to chloride-induced depassivation. This initial chloride content has a normal distribution with a mean value and standard deviation of 0.10 m%/binder and 0.025 m%/binder, respectively. In a final phase of the research, the total chloride contents of remaining concrete samples (age: 1 to 3 years) that were never exposed to chlorides were measured. These initial chloride contents for the different concrete compositions were shown in Table 9.3 without being used further on for service life prediction. In this appendix, an additional second order prediction of the corrosion initiation period was conducted while using the model input mentioned in Table 9.9 in combination with the measured values for C_i (Table 9.3). The outcome of this prediction is shown in Table C.1 for time of reference $t_0 = 28$ days. The results obtained need to be compared with the ones presented in Table 9.12.

Table C.1. Second order prediction of the time to chloride-induced steel depassivation (years) with the measured initial chloride content per concrete mixture as input.

| 2nd order / XS2 | t_0 (d) | T(0.45) | F(1)15 | F(2)15 | F(1)50 | F(2)50 | F(1)SF | F(2)SF |
|-----------------------------------|-----------------------------|----------------|---------------|---------------|--------------------|---------------|--------------------|---------------|
| M1+2+3 | 28 | 43 | n.a. | +1000 | +1000 | +1000 | +1000 | +1000 |
| | 28 | – | – | – | +1000 ^a | – | +1000 ^a | – |

^a Based on $D_{RCM,0}$ values for suboptimal curing: 7 days at 20°C and 95% RH, 21 days at 20°C and 60% RH.

This comparison shows that the implementation of measured C_i values that were slightly higher than the general value suggested by CUR Guideline VC81 (2009) does not cause important changes in prediction outcome. For the OPC reference T(0.45), the time to chloride-induced steel depassivation decreases from 47 years to 43 years. This is a decrease of only 4 years. For the fly ash (and silica fume) containing concrete compositions the corrosion initiation period still was equal to more than 1000 years when the measured C_i values were used in the calculation. Clearly, the consequences for the functional unit definitions and the corresponding environmental impacts presented in Chapter 12 would be negligible. For the

columns and slab as functional unit the required number of repairs for all mixtures would remain the same, hence also the corresponding global warming potentials. The other functional unit, i.e. the required concrete volume per unit of strength and service life, would only increase for OPC reference T(0.45) from $3.84 \times 10^{-4} \text{ m}^3/(\text{N}/\text{mm}^3 \cdot \text{years})$ (Table 12.3) to $4.19 \times 10^{-4} \text{ m}^3/(\text{N}/\text{mm}^3 \cdot \text{years})$. The global warming potentials for the same composition would go up from $1.14 \times 10^{-1} \text{ kg CO}_2 \text{ eq}$ (Figure 12.8) to $1.24 \times 10^{-1} \text{ kg CO}_2 \text{ eq}$. For all other fly ash (and silica fume) containing concrete mixtures the global warming potentials would remain the same.

Appendix D

Considerations regarding the experimental transfer parameter and the ageing exponent

In Sections 9.3.1 and 9.3.2 the suggested procedures for estimating the experimental transfer parameter k_t and the ageing exponent a , may seem a bit unusual as these procedures differ from what is mentioned in *fib* Bulletin 34 (2006).

First of all, k_t is not considered to be a parameter with a constant value equal to 1. Instead, it is seen as a factor that quantifies the difference between the apparent diffusion coefficient and the migration coefficient (cf. Equation 9-3), and this mainly at later ages (91 and 273 or 364 days) to cancel out additional ageing effects.

Secondly, the ageing exponent was estimated from the apparent diffusion coefficients that were derived at different curing ages. Now, apparent diffusion coefficients as determined by the 'natural' bulk diffusion test are known to be non-instantaneous. Given the quite long exposure period of 125 days employed in this research for each diffusion test, important ageing effects due to ongoing hydration between 28 and 91 days may not be noted when estimating the ageing exponent from apparent diffusion coefficients at early age. Moreover, also during exposure the diffusion coefficient gradually decreases. An apparent diffusion coefficient counts as a time-averaged value between the start and end of exposure. Especially at young age this time-averaged value will deviate considerably from the instantaneous value that corresponds with the starting age. Therefore, it was decided to replace the apparent diffusion coefficient for time t_0 (= 28 days) by the instantaneous migration coefficient at the same age, multiplied with k_t in order to obtain an estimated instantaneous diffusion coefficient for 28 days (Equation 9-6). The fact that apparent diffusion coefficients are being combined with migration coefficients for the estimation of the ageing exponent may not be a very convenient way of working. It is more practical to stick either to the migration coefficients or to the apparent diffusion coefficients alone. It must be mentioned that Visser (2002) also considered these two approaches separately for the estimation of the ageing exponent.

When working with migration coefficients only, one has the advantage that they represent instantaneous values. On the other hand, there is the disadvantage that an ageing exponent derived as such only considers ageing induced by the ongoing hydration of the concrete.

Other aspects which may affect transport properties due to prolonged immersion in seawater are not being considered. Binding of chloride ions is also not accounted for.

In that perspective the use of apparent diffusion coefficients could be more interesting. According to Gulikers (2014), chloride diffusion tests are considered as a more realistic alternative because in practice it is mainly diffusion that acts as the driving force for the transport of chlorides. Moreover, binding of the chloride ions is included in the transport mechanism. Yet, the problem remains that the apparent diffusion coefficient does not reflect an instantaneous value. In other words, its magnitude depends on both the age of the concrete specimen at the start of exposure as well as on the duration of the exposure. Thus, the diffusion coefficient that results from chloride profiling will present a time-averaged value. As a result, it is not evident to estimate ageing exponents from apparent diffusion coefficients. Nevertheless, in this appendix it has been attempted to estimate ageing exponents from both migration and apparent diffusion coefficients obtained at multiple testing ages. It should be noted that there are still other calculation approaches. For instance, sometimes a migration or diffusion coefficient at time infinity is being included in mathematical expressions dealing with the time dependency of chloride transport. This is done because it is considered unrealistic that the migration or diffusion coefficients will decrease over time until infinity according to the trend presented by the typical power law expression for ageing (Equation 9-5). Eventually, they may attain a limiting value. Examples of such an approach can be found in Visser (2009) and Visser and Siemes (2010). Another example is the Life-365 service life prediction model which is commonly used in US [Life-365 (2000-2013)]. In accordance with this model no decrease in apparent diffusion coefficient is taken into account anymore after 25 years. From then on, the apparent diffusion coefficient is assumed to remain equal to the one after 25 years. However, since no migration or diffusion coefficients were experimentally determined at a late age (e.g. after several years) it is difficult to have an idea on their value at time infinity. Therefore, this alternative approach was not studied further in this research.

Second order prediction of the time to chloride-induced depassivation with $k_t = 1$ and an ageing exponent calculated from migration coefficients as input.

For this additional second order prediction the experimental transfer parameter was set to 1 cf. *fib* Bulletin 34 (2006). The ageing exponent, denoted by α_1 , was quantified by performing linear regression analysis on the migration coefficients measured after 28, 91 and 273 or 364 days of curing while assuming that t_0 is equal to the more commonly used 28 days (Table D.1). Note that this calculation approach does not result in exactly the same ageing exponents as the ones shown in Table 9.7 for $t_0 = 273$ or 364 days (cf. Tang (1996) with $t_0 > t$). The other model input was the same as the input shown in Table 9.9. Table D.2 summarizes the prediction outcome in terms of time to depassivation.

Table D.1. Ageing exponents α_1 estimated from chloride migration coefficients at different curing ages with $t_0 = 28$ days.

| $t_0 = 28$ d | | T(0.45) | F(1)15 | F(2)15 | F(1)50 | F(2)50 | F(1)SF | F(2)SF |
|----------------|-------|---------|--------|--------|--------|--------|--------|--------|
| α_1 (-) | mean | 0.15 | 0.55 | 0.68 | 0.74 | 0.84 | 0.69 | 0.59 |
| | stdv. | 0.03 | 0.08 | 0.07 | 0.08 | 0.09 | 0.18 | 0.03 |

Table D.2. Second order prediction of the time to chloride-induced steel depassivation (years) with $k_t = 1$ and an ageing exponent calculated from migration coefficients as input.

| 2 nd order / XS2 | t_0 (d) | T(0.45) | F(1)15 | F(2)15 | F(1)50 | F(2)50 | F(1)SF | F(2)SF |
|-----------------------------|-----------|---------|--------|--------|--------------------|--------|--------------------|--------|
| | 28 | 18 | +1000 | +1000 | +1000 | +1000 | +1000 | +1000 |
| | 28 | – | – | – | +1000 ^a | – | +1000 ^a | – |

^a Based on $D_{RCM,0}$ values for suboptimal curing: 7 days at 20°C and 95% RH, 21 days at 20°C and 60% RH.

In comparison with the prediction outcome shown in Table 9.12 the following observations can be made: (i) the predicted time to depassivation of the OPC reference has decreased from 47 years to only 18 years, (ii) the time to depassivation of all fly ash (and silica fume) containing concrete compositions remains at a level of more than 1000 years. In that perspective there is no difference with the calculation approach that was adopted in Chapter 9.

Second order prediction of the time to chloride-induced depassivation with $k_t = 1$ and an ageing exponent calculated from apparent diffusion coefficients as input.

In order to derive an ageing exponent from the apparent diffusion coefficients, denoted by α_2 , obtained at three different curing ages (28, 91 and 273 or 364 days) followed by a fixed exposure period of 125 days, some additional calculations need to be done. The applied calculation approach was in agreement with the method proposed by Gulikers (2014). Once it is understood that the result of a bulk diffusion test represents a time-averaged value of the diffusion coefficient, the following mathematical relation is valid (Equation D-1).

$$D_a = \frac{\int_{t_{start}}^{t_{end}} D_{ai,0} \cdot \left(\frac{t_0}{t}\right)^{\alpha_2} dt}{(t_{end} - t_{start})} \quad (D-1)$$

With D_a : the apparent chloride diffusion coefficient as quantified from the chloride profile (= $D_{e,nat}$ in Chapter 6), $D_{ai,0}$: the unknown instantaneous apparent chloride diffusion coefficient at time of reference t_0 (= 28 days), α_2 : the unknown ageing exponent to be estimated from the apparent diffusion coefficients, t_{end} : end of the exposure period (28 + 125, 91 + 125 or 273 / 364 + 125 days) and t_{start} : start of the exposure period (28, 91 or 273 / 364 days). Complete elaboration of Equation D-1 results in Equation D-2.

$$D_a = \frac{1}{1 - \alpha_2} \cdot D_{ai,0} \cdot t_0^{\alpha_2} \cdot [t_{end}^{(1-\alpha_2)} - t_{start}^{(1-\alpha_2)}] \quad (D-2)$$

Equation D-2 has to be employed three successive times with the results of the ‘natural’ bulk diffusion tests (= D_a or $D_{e(nat)}$) obtained at the three different curing ages (see Chapter 6). Next, the two unknown parameters $D_{ai,0}$ and α_2 can be fitted using non-linear regression analysis in the statistical software SPSS. The output of this analysis for each concrete composition is shown in Table D.3.

Table D.3. The estimated instantaneous diffusion coefficients $D_{ai,0}$ and the corresponding ageing exponents as obtained from employing Equation D-2 three times with the apparent diffusion coefficients at three curing ages followed by non-linear regression.

| $t_0 = 28 \text{ d}$ | | T(0.45) | F(1)15 | F(2)15 | F(1)50 | F(2)50 | F(1)SF | F(2)SF |
|---|-------|----------------|---------------|---------------|---------------|---------------|---------------|---------------|
| $D_{ai,0} (\times 10^{-12} \text{ m}^2/\text{s})$ | mean | 4.46 | 4.49 | 6.51 | 6.16 | 6.25 | 1.38 | 2.01 |
| | stdv. | 0.22 | 0.53 | 0.48 | 0.34 | 0.73 | 0.25 | 0.57 |
| $\alpha_2 (-)$ | mean | 0.07 | 0.48 | 0.60 | 0.73 | 0.76 | 0.44 | 0.63 |
| | stdv. | 0.02 | 0.08 | 0.05 | 0.04 | 0.09 | 0.12 | 0.21 |

Note that parameter $D_{ai,0}$ is a parameter that cannot be determined directly. A test method that enables a direct quantification of an instantaneous apparent diffusion coefficient simply does not exist. The parameter $D_{ai,0}$ can only be quantified indirectly from a series of apparent diffusion coefficients obtained from tests having a duration of several weeks. When comparing the ageing exponents α_2 with α_1 , it turns out that for all concrete compositions the former are always lower than the latter. Still, the clear difference in ageing behaviour between OPC and fly ash (and silica fume) containing concrete remains. In that perspective the two different calculation approaches do not differ.

$D_{ai,0}$ and α_2 now need to be implemented in a proper limit state function for service life prediction. Therefore, the original limit state function of *fib* Bulletin 34 (2006) needs to be modified to account for the instantaneous level of the diffusion coefficient. Equation D-3 complies with this criterion. It is in agreement with the more general formula proposed by Gulikers (2014).

$$C_{\text{crit}} = C_0 + (C_{S,\Delta x} - C_0) \cdot \left[1 - \text{erf} \frac{d - \Delta x}{2 \cdot \sqrt{k_e \cdot k_t \cdot \frac{D_{ai,0}}{1 - \alpha_2} \cdot \left(\frac{t_0}{t}\right)^{\alpha_2} \cdot t}} \right] \quad (\text{D-3})$$

with C_{crit} : the critical chloride content (m%/binder), C_0 : the initial chloride content (m%/binder), $C_{S,\Delta x}$: chloride content at depth Δx (m%/binder), d : concrete cover (mm), Δx : depth of the convection zone (mm), $\text{erf}(\cdot)$: error function, k_e : the environmental transfer variable (-), k_t : the experimental transfer parameter (-), $D_{ai,0}$: the instantaneous apparent chloride diffusion coefficient (mm^2/years) at time of reference t_0 (= 28 days), α_2 : the ageing exponent estimated from the apparent diffusion coefficients obtained from bulk diffusion tests, and t : time (years).

When using the results of the diffusion tests as a basis for service life predictions, the experimental transfer parameter can be taken equal to 1. All other model input was the same as shown in Table 9.9. The times to depassivation obtained with this second order prediction for $t_0 = 28$ days are shown in Table D.4. Compared to the second order prediction shown in Chapter 9 (Table 9.12), the time to depassivation for the OPC reference is a bit lower (32 years instead of 47 years). For the fly ash (and silica fume) containing concrete compositions, again very long times to depassivation exceeding 100 years by far were estimated.

Table D.4. Second order prediction of the time to chloride-induced steel depassivation (years) with $k_t = 1$ and an ageing exponent calculated from apparent diffusion coefficients as input.

| 2nd order / XS2 | t₀ (d) | T(0.45) | F(1)15 | F(2)15 | F(1)50 | F(2)50 | F(1)SF | F(2)SF |
|-----------------------------------|--------------------------|----------------|---------------|---------------|---------------|---------------|---------------|---------------|
| | 28 | 32 | 751 | +1000 | +1000 | +1000 | +1000 | +1000 |

In conclusion, it can be stated that the two alternative calculation approaches yield a very similar outcome for the concrete compositions containing fly ash (and silica fume). In view of the environmental impact calculations presented in Chapter 12, this will not lead to different conclusions because 100 years was the maximum service life that was taken into account. However, the much lower service life of the OPC reference has implications in terms of environmental impact when looking at the benefit of fly ash (and silica fume) concrete in comparison with the OPC reference. With the OPC reference having a shorter time to depassivation, these benefits will become higher. By keeping the second order service life prediction outcome of Chapter 9, the comparison needs to be made with a OPC reference having a time to depassivation of 47 years. This gives a more critical comparison when evaluating the environmental benefit of the alternative concrete types relative to the OPC reference. Therefore, it was decided to stick with that calculation approach.

Curriculum vitae

Personalialia

Name Philip Van den Heede
Date of birth 04/03/1985
Place of birth Gent
Address Oude Dorpsweg 14, 9750 Zingem/Ouwegem
E-mail philip.vandenheede@ugent.be

Education

2003-2008 Master of Engineering: Architecture – Main Subject: Architectural Design and Construction Techniques – Ghent University
Graduated *magna cum laude*
Master thesis: Porosity and Transport Properties of ‘Green’ Concrete Types (in Dutch), Supervisor: Prof. dr. ir. Nele De Belie

1997-2003 General Secondary Education:
Latin-Mathematics (6 hours mathematics)
Sint-Barbaracollege, Gent

Employment

2008-2014 Full-time research assistant at the Department of Structural Engineering, Magnel Laboratory for Concrete Research, Ghent University

2008 PhD scholar at the Department of Structural Engineering, Magnel Laboratory for Concrete Research, Ghent University

PhD research:

Durability and Sustainability of Concrete with High Volumes of Fly Ash

Teaching activities:

Exercises *Statistics and Data Processing* (2008-2014)

Practical courses *Sustainability of Materials and Structures* (2010-2014)

Practical courses *Materials Technology: Basic Concepts and Project* (2008-2014)

Services:

Responsible for calibrations of testing machines and measurement equipment for the Magnel Laboratory for Concrete Research / companies and editing of calibration certificates

Responsible for non-standard tests for companies and editing of the test reports

Doctoral training

DTU – RILEM doctoral course *Durability of Concrete* (DTU – Lyngby, Denmark), Seminar *Carbon Footprinting* (KVIV), Seminar *Research Methodology* (UGent), Seminar *Basic Assistant Training* (UGent), Seminar *Effective Scientific Communication* (UGent), TU Delft course *Concrete Microscopy* (TU Delft – Delft, the Netherlands), Research meeting *Waste = A Valuable Resource* (Innovation Center East Flanders), Course *Instrumental Methods, Physical Mineral Research and Geological Applications* (UGent), SimaPro course: *Effective LCA with SimaPro and Advanced Modelling with SimaPro* (PRé Consultants bv – Amsterdam, the Netherlands)

Scientific publications

- A1** **Van den Heede P**, Maes M, De Belie N. Influence of active crack width control on the chloride penetration resistance and global warming potential of concrete slabs made with fly ash + silica fume concrete. *Constr Build Mater* 2014;67(Part A):74-80.
- Van den Heede P**, De Belie N. A service life based global warming potential for high-volume fly ash concrete exposed to carbonation. *Constr Build Mater* 2014;55(3):183-193.
- Van den Heede P**, Furniere J, De Belie N. Influence of air entraining agents on deicing salt scaling resistance and transport properties of high-volume fly ash concrete. *Cem Concr Compos* 2013;37(3):293-303.
- Van den Heede P**, De Belie N. Environmental impact and life cycle assessment (LCA) of traditional and “green” concretes: Literature review and theoretical calculations. *Cem Concr Compos* 2012;34(4):431-442.
- Van den Heede P**, Gruyaert E, De Belie N. Transport properties of high-volume fly ash concrete: capillary water sorption, water sorption under vacuum and gas permeability. *Cem Concr Compos* 2010;32(10):749–56.
- Gruyaert E, **Van den Heede P**, De Belie N. Carbonation of slag concrete: Effect of the cement replacement level and curing on the carbonation coefficient – Effect of carbonation on the pore structure. *Cem Concr Compos* 2013;35(1):39-48.
- Gruyaert E, **Van den Heede P**, Maes M, De Belie N. Investigation of the influence of blast-furnace slag on the resistance of concrete against organic acid or sulphate attack by means of accelerated degradation tests. *Cem Concr Res* 2012;42(1):173-185.
- A2** **Van den Heede P**, Maes M, De Belie N. Full probabilistic service life prediction and life cycle assessment of concrete with fly ash and blast-furnace slag in a submerged marine environment: A parameter study. *Int J Environ Sust Dev* 2012;11(1):32-49.
- A3** **Van den Heede P**, De Belie N. Concrete with fly ash durable? Porosity and transport properties investigated (in Dutch). *Cement* 2009;3:46-49.
- P1** De Schepper M, **Van den Heede P**, De Belie N. The use of fly ash in completely recyclable concrete. In: Brameshuber W (Ed.), *Proceedings of the International RILEM Conference on Material Science, Volume III*, Aachen, Germany, September 6-8, 2010. Bagnaux: RILEM Publications, 35-43.

Gruyaert E, **Van den Heede P**, De Belie N. A comparative study of the durability of ordinary Portland cement concrete and concrete containing (high) percentages of blast-furnace slag. In: Brameshuber W (Ed.), Proceedings of the International RILEM Conference on Material Science, Volume III, Aachen, Germany, September 6-8, 2010. Bagnex: RILEM Publications, 241-251.

Baert G, **Van den Heede P**, Audenaert K, De Belie N. Microstructure of high-volume fly ash concrete. In: Sun W, van Breugel K, Miao C, Ye G, Chen H (Eds.), Proceedings of the First International Conference on Microstructure Related Durability of Cementitious Composites, Nanjing, China, October 13-15, 2008. Bagnex: RILEM Publications, 207-215.

C1 **Van den Heede P**, De Belie N. Service life based assessment of the global warming potential of concrete with supplementary cementitious materials. In: Stephan D, von Daake H, Märkl V, Land G (Eds.), Proceedings of the 1st International Conference on the Chemistry of Construction Materials, Berlin, Germany, October 7-9, 2013. Frankfurt am Main: Gesellschaft Deutscher Chemiker (GDCh), 5-8.

Van den Heede P, Maes M, De Belie N. Influence of crack width limitation on the chloride penetration resistance and global warming potential of concrete slabs. In: Sakata K, Naik TR (Eds.), Proceedings of the 3rd International Conference on Sustainable Construction Materials & Technologies, Kyoto, Japan, August 18-21, 2013, 1-10.

Van den Heede P, Maes M, Caspeele R, De Belie N. Chloride diffusion tests as experimental basis for full probabilistic service life prediction and life cycle assessment of concrete with fly ash in a submerged marine environment. In: Strauss A, Frangopol DM, Bergmeister K (Eds.), Proceedings of the 3rd International Symposium on Life Cycle Civil Engineering (IALCCE 2012), Vienna, Austria, October 3-6, 2012. Leiden: CRC Press, 913-920.

Van den Heede P, De Belie N. Strength related global warming potential of fly ash (+ silica fume) concrete with(out) mass/economic allocation of the by-products' impact. In: Ventura A, de la Roche C (Eds.), Proceedings of the International Symposium on Life Cycle Assessment and Construction, Proceedings, Nantes, France, July 10-12, 2012. Bagnex: RILEM Publications, 336-343.

Van den Heede P, Maes M, Gruyaert E, De Belie N. Full probabilistic service life prediction and life cycle assessment of concrete with industrial by-products in a submerged marine environment: A parameter study. In: Ban M, Duic N, Guzovic Z (Eds.), Proceedings of 6th Dubrovnik Conference on Sustainable Development of Energy, Water and Environment Systems, Dubrovnik, Croatia, September 25-29, 2011. Zagreb, Faculty of Mechanical Engineering and Naval Architecture, 1-13.

Van den Heede P, De Belie N. The "Greenness" of high-volume fly ash (HVFA) concrete when exposed to carbonation. In: Leung C, Wan K (Eds.), Proceedings of the International Conference on Advances in Construction Materials through Science and Engineering, Hong Kong, September 5-7, 2011. Bagnex, RILEM Publications, 1-7.

Van den Heede P, Furniere J, De Belie N. Influence of air entraining agents (AEAs) on deicing salt scaling resistance of high-volume fly ash concrete (HVFA concrete). In: Peixoto de Freitas V, Corvacho H, Lacasse M (Eds.), Proceedings of 12th International Conference on Durability of Building Materials and Components. Porto, Portugal, April 12-15, 2011. Porto: FEUP, 1585-1592.

Van den Heede P, Gruyaert E, Robeyst N, De Belie N. Life cycle assessment of a column supported isostatic beam in high-volume fly ash concrete (HVFA concrete). In: van Breugel K, Ye G, Yuan Y (Eds.), Proceedings of the 2nd International Symposium on Service Life Design for Infrastructure, Delft, the Netherlands, October 4-6, 2010. Bagnex: RILEM Publications, 437-444.

Van den Heede P, De Belie N. Durability related functional units for life cycle assessment of high-volume fly ash concrete. In: Zachar J, Claisse P, Naik TR, Ganjian E (Eds.), Proceedings of the Second International Conference on Sustainable Construction Materials and Technologies, Ancona, Italy, June 28-30, 2010. Milwaukee: University of Wisconsin Milwaukee Center for By-Products Utilization, 583-594.

Maes M, Caspeele R, **Van den Heede P**, De Belie N. Influence of sulphates on chloride diffusion and the effect of this on service life prediction of concrete in a submerged marine environment. In: Strauss A, Frangopol DM, Bergmeister K (Eds.), Proceedings of the 3rd International Symposium on Life Cycle Civil Engineering (IALCCE 2012), Vienna, Austria, October 3-6, 2012. Leiden, CRC Press, 899-906.

De Schepper M, **Van den Heede P**, Windels C, De Belie N. Life cycle assessment of completely recyclable concrete. In: Bilek V, Keršner Z (Eds.), Proceedings of the 4th International Conference Non-Traditional Cement & Concrete, Brno, Czech Republic, June 27-30, 2011. Brno: Brno University of Technology, 67-76.

De Schepper M, **Van den Heede P**, Windels C, De Belie N. The resistance of completely recyclable concrete to carbonation, chloride penetration and freeze-thaw attack with deicing agents. In: Peixoto de Freitas V, Corvacho H, Lacasse M (Eds.), Proceedings of the 12th International Conference on Durability of Building Materials and Components, Porto, Portugal, April 12-15, 2011. Porto: FEUP, 2061-2068.

Gruyaert E, **Van den Heede P**, De Belie N. Chloride ingress for concrete containing blast-furnace slag, related to microstructural parameters. In: Kovler K (Ed.), Proceedings of the 2nd International RILEM Workshop on Concrete Durability and Service Life Planning (ConcreteLife '09), Haifa, Israel, September 7-9, 2009. Bagnoux, RILEM Publications, 440-448.

Gruyaert E, De Belie N, **Van den Heede P**. Acid resistance of concrete containing blast-furnace slag: influence of the pore structure and hydration process. In: Alexander MG, Bertron A (Eds.), Proceedings of the International RILEM TC211-PAE final conference on Concrete in Aggressive Aqueous Environments, Performance, Testing and Modeling, Toulouse, France, June 3-5, 2009. Bagnoux: RILEM Publications, 389-396.

